# Gas Phase Chemical Physics Program

DOE Principal Investigators'
Abstracts

May 31 – June 2, 2023

Chemical Sciences, Geosciences, and Biosciences Division
Office of Basic Energy Sciences
Office of Science
U.S. Department of Energy

The research grants and contracts described in this document are supported by the U.S. DOE Office of Science, Office of Basic Energy Sciences, Chemical Sciences, Geosciences and Biosciences Division.

# Foreword

The 42nd Annual Gas Phase Chemical Physics (GPCP) Principal Investigators' Meeting sponsored by the U. S. Department of Energy (DOE), Office of Basic Energy Sciences (BES) provides a forum for GPCP principal investigators (PIs) to discuss cutting-edge research supported by the program. This meeting will facilitate scientific interchange among PIs and afford opportunities for research collaboration.

The GPCP program seeks to understand energy flow and reaction mechanisms in complex, nonequilibrium, gas-phase environments. This is accomplished by focusing on fundamental research that explores chemical reactivity, kinetics, and dynamics at the level of electrons, atoms, molecules, and nanoparticles. The expertise, approaches, and capabilities of the GPCP program provide foundational knowledge and tools to address scientific challenges important for Department of Energy's mission, including the Earthshots Initiative which aims to accelerate breakthroughs towards more abundant, affordable, and reliable clean energy solutions.

This collection of abstracts presents innovative state-of-the-art research that is advancing gas phase chemical physics and that aligns with the research objectives of the Department of Energy's Office of Basic Energy Sciences (BES). We thank all the researchers whose dedication and innovation have advanced DOE BES research. We look forward to our assembly in 2024 for our 43rd annual meeting.

Wade Sisk
Tom Settersten

# Table of Contents

# Nanoparticle Surface Kinetics and Dynamics by Single Nanoparticle Mass Spectrometry

Scott L. Anderson, Chemistry Department, University of Utah
315 S. 1400 E. Salt Lake City, UT 84112 anderson@chem.utah.edu

## Program Scope

This project is focused on reaction kinetics and emission spectroscopy for individual nanoparticles (NPs) at high temperatures ($T_{NP}$), using a single NP mass spectrometry (NPMS) technique. During the current grant period, work has included studies of the high $T_{NP}$ sublimation and oxidation of carbon, silicon, silica, and hafnium carbide NPs, and on growth chemistry of carbon NPs by reaction with $C_2H_2$. For carbon, NPs of graphite, graphene, graphene oxide, carbon black, diamond, and nano-onion morphology were studied. We also have continued to refine and extend NPMS for new materials and temperature ranges. In addition to measuring temperature-dependent reaction kinetics, we are interested in understanding structure-reactivity relationships, and probing the effects of three different kinds of heterogeneity on NP kinetics and optical properties: 1. NPs feedstocks have significant NP-to-NP variation in size, shape, and structure, all of which affect reaction kinetics and spectroscopy. 2. *Individual NPs* have distributions of surface sites that control reactivity. 3. NP surfaces evolve under reaction conditions, resulting in evolution of reactivity. The single NPMS method complements NP ensemble kinetics methods, which allow more detailed (and faster) experiments, but are unable to observe the heterogeneity effects mentioned above, and may also have lower upper temperature limits.

## Methodology

Details of the methodology for measuring kinetics are in papers 6 and 7 below, and the approach to measuring NP temperature ($T_{NP}$) is discussed in papers 9 and 10. Briefly, a single NP of the material of interest is injected into an electrodynamic trap and held at reduced pressure (to slow reaction kinetics). The NP is laser heated with $T_{NP}$ determined by fitting its blackbody-like emission spectrum, and the NP mass is determined with 0.1% precision from the frequency of NP motion in the trap. By monitoring the NP mass vs. time when the NP is held at elevated $T_{NP}$ in either inert or reactive atmosphere, the kinetics for mass-changing processes, such as sublimation, pyrolysis, oxidation, or growth, can be determined with high sensitivity. In addition to being used to determine $T_{NP}$, the emission spectra and laser heating power provide information about changes in the emissivity and absorptivity of the NP caused by the chemical process being studied.

The single NP approach avoids ensemble averaging, thus providing unique insights into heterogeneity and structure-reactivity relationships, but it is a slow method. Therefore, the experiments are highly automated, allowing operation with just occasional operator input, which can be done remotely. Current improvements in methodology are aimed at reaching higher temperatures to allow studies of refractory NPs of interest from both biofuels and high temperature materials applications.

## Recent Progress

Highlights of this research include:

- Measurement of the effects of NP-to-NP variations on reactivity, and on the evolution of reactivity under reaction conditions, for many different NP types and several reactions, including sublimation, oxidation by $O_2$ and $N_2O$, and growth by $C_2H_2$ addition.
- Use of $O_2$ etching kinetics to monitor changes in the numbers of reactive surface sites for NPs under active etching, allowing correlations with other chemistry, e.g. growth by $C_2H_2$ addition.
- Characterization of the effects of carbon NP feedstock structure on initial reactivity toward growth, etching, and sublimation reactions.
- Measurement of the kinetics for transformation of different structured carbon NPs to form surface layers that are inert to further attack by $O_2$, $N_2O$, and $C_2H_2$ in the 1200 to 1800 K range. Inertness implies transformation of the NP surfaces to have near-zero uncoordinated sites that would be reactive under these conditions. The passivation kinetics were complex, and found to depend strongly on initial NP structure, with particularly complex behavior for graphitic NPs.

- Observation that passivation during NP growth by $C_2H_2$ addition (but not etching or sublimation) varied qualitatively for NPs of different sizes, even for NPs of the same feedstocks, attributed to size-dependent differences in the mesoscale structure of the larger aggregate NPs.
- Measurements for the etching and sublimation kinetics of Si NPs for $T_{NP}$ ranging from well below to well above the Si bulk $T_{melt}$ (1687 K).
- Observation that Si NPs passivate under low $O_2$ pressure/high temperature conditions where passivation has not been observed for bulk Si.
- Development of a modeling approach that identified oxygen saturation of the limited core volume as being critical to Si NP passivation under conditions where large Si particles or bulk Si do not passivate.
- Comparison of etching and passivation kinetics for Si NPs with and without melting, with the analogous kinetics for surface-reduced silica NPs (Si surface/$SiO_x$ core), confirming the importance of core oxygen in Si NP passivation.
- Development of T-pulse methods to study chemistry at ultra-high $T_{NP}$, above the range where steady state kinetics measurement methods can be used, due to fact NP sublimation/decomposition. One approach was used in our study of Si NPs to examine the stability of passivation layers at temperatures to 2700 K, i.e., near $T_{boil,}$ and ***far*** above $T_{melt}$ for both Si and silica, under conditions where substantial mass loss occurs on the few second time scale. A related approach was used to create surface-reduced silica NPs.
- Observation of correlations between evolution of sublimation or etching rates and thermal emission spectral properties for carbon, Si, and $SiO_x$ NPs.
- Preliminary measurements of the $O_2$ etching and passivation behavior of SiC NPs, and comparison to the behavior for carbon and silicon NPs. As expected, SiC passivates at low $T_{NP}$ (<~1600 K) but for $T_{NP}$ >1700 K, it actively etches because the $SiO_2$ surface layer reacts with underlying SiC.
- Preliminary measurements of the etching and passivation behavior for NPs of HfC, an ultrahigh temperature ceramic material. HfC was found to be stably passivated once an $HfO_2$ surface layer formed, however, under some conditions the NPs etched for many hours without passivating.
- Improvement to our emission spectral measurement setup and calibration to allow kinetics measurements at higher $T_{NP}$.

**Recent (not yet published) examples:**

**1. Growth and passivation of carbon NPs by $C_2H_2$ addition**

Papers 1, 3, and 5-8 listed below discuss reactions (sublimation, $O_2$ and $N_2O$ etching) that removed material from different types of carbon NPs, silicon NPs, and silicon surface/silica core NPs. Interpretation of these experiments was informed by a large surface science literature for etching of silicon and carbon surfaces. In the case of carbon NPs, where a stable surface oxide layer cannot form, initial rapid etching led to eventual passivation, which was attributed to complex structural transformations to generate NPs with fully-coordinated nano-onion (fullerene-like) surface layers. The obvious questions are whether the same structure-reactivity relationships observed for etching would hold for the much less studied process of carbon addition by reaction with hydrocarbons, whether passivation would occur under growth conditions, and if the kinetics of the passivation process would be different. Paper 2 below reports a study of carbon addition to graphite, graphene, graphene oxide, carbon black, diamond, and nano-onion NPs via reactions with $C_2H_2$ at temperatures between 1200 and 1700 K. Except possibly at 1200 K, the

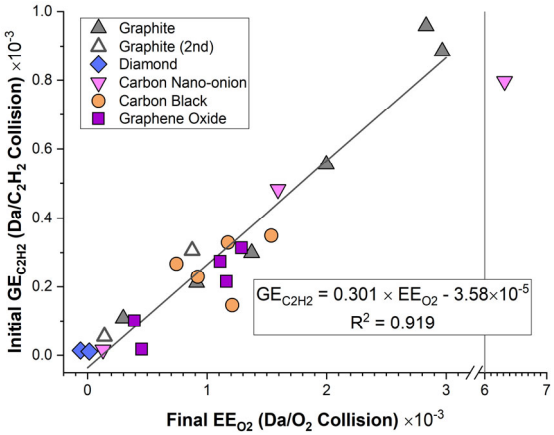


Figure 1. Correlation between back-to-back $EE_{O2}$ and $GE_{C2H2}$ measurements. The nano-onion NP with $EE_{O2}$ larger than $6 \times 10^{-3}$ is an outlier and is not included in the linear fit.

lifetime of surface C-H bonds with respect to H desorption is short enough that under our conditions, the steady state H coverage would remain low, i.e., if passivation by C-H termination is not possible.

The connection between the structure-reactivity relationships for $O_2$ etching and $C_2H_2$ addition (with H loss) was explored by back-to-back $O_2$ and $C_2H_2$ exposures, comparing $EE_{O2}$ with the analogous growth efficiencies ($GE_{C2H2}$ = Da mass gain/$C_2H_2$ collision). As shown in Fig. 1, $GE_{C2H2}$ and $EE_{O2}$ varied by orders of magnitude for different NPs, but $EE_{O2}/GE_{C2H2} \approx 3.3$ for all NPs of all feedstocks. The exception was the nano-onion NP at the far right of the figure, where $EE_{O2}/ GE_{C2H2} \approx 10$. Nano-onions have highly variable reactivity due to the presence of non-onion carbon contamination, and passivate quickly during $O_2$ etching as this contaminant etches away. In this experiment, the NP partially passivated during the $O_2$ etching period, resulting in the low $GE_{C2H2}$ value. Indeed, there was a systematic tendency for the $EE_{O2}/GE_{C2H2}$ ratio to increase as NPs began to passivate, suggesting that the few reactive sites remaining on nearly-passivated carbon NPs retained higher reactivity toward $O_2$ than $C_2H_2$.

The other interesting aspect of the $C_2H_2$ growth experiments was that the passivation dynamics was correlated with NP mass in way not seen for etching. The lightest NPs passivated monotonically in the course of adding less than a few percent of mass. The most massive NPs never passivated even after adding up to 300% to the mass, and intermediate mass NPs grew in multiple waves. The difference was attributed to the large NPs being aggregates of smaller particles, thus tentatively to mesoscale structure.

**2. Ultra-high temperature ceramic NPs**

Many technologies, including turbine engines and hypersonic/re-entry vehicles, require thermal protection layers, and there is considerable interest in materials that can survive at high temperatures in reactive atmospheres. Because NPMS can measure kinetics at temperatures only limited by the sublimation properties of the material, it can easily work under conditions difficult to reach with surface science methods. We chose HfC (m.p. = 4170 K, oxide m.p. = 3300 K) as our initial system to explore the use of NPMS in this context. The expectation from known vapor pressures, was that HfC would react with $O_2$ to generate CO gas, quickly forming a passivating $HfO_2$ layer. The reality is far more complex. For example, Fig. 2 shows an HfC NP with $M_{initial}$ corresponding to ~61 nm nominal diameter, etching with increasing rates over the 1100 to 1400 K range, with no sign of passivating. The total mass loss was ~2/3rd of $M_{initial}$, corresponding to removing ~20 nm from the NP nominal diameter, or ~60 HfC monolayers. Such large mass loss implies desorption of some Hf-containing product, most likely HfO, and we speculate that the mechanism that results in etching at such low temperatures involves volatilization of carbon as CO, formation of $HfO_x$, which is, however, unstable respect to reaction with underlying HfC to generate CO and HfO.

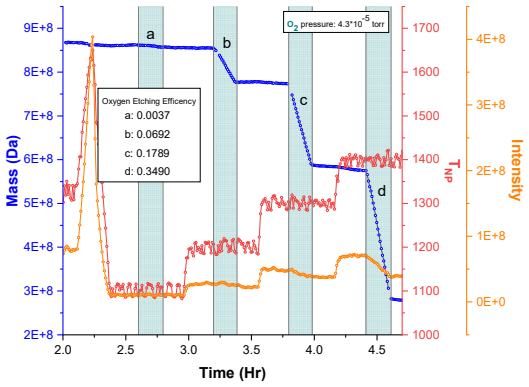

Fig. 2. $O_2$ etching of HfC

HfC NPs eventually do passivate toward $O_2$ attack after substantial etching, presumably due to formation of an $HfO_2$ surface layer thick enough to act as a diffusion barrier for O and C atoms. Once passivated, the NPs remain passivated even after brief heating in both inert and oxidizing atmospheres to temperatures of at least 2500 K. Sublimation from oxidized/passivated HfC NPs is, however, much faster than from unoxidized HfC, i.e., the passivating layer is unstable at high temperatures. To complete this story, we will do additional experiments on sublimation and etching of HfC NPs, but also of $HfO_2$ NPs, $HfO_2$ NPs with reduced (Hf-rich) surface layers, and of Hf NPs, with and without surface oxide layers. By studying NPs with these various core/surface properties (which can be prepared *in situ* by appropriate thermal/reactant treatments), we can address questions both about the surface chemistry, but also about the effects of solid-state diffusion on the stability of the surface layers.

**Plans for the coming year:**

The current grant period expires in August, and during the remaining time, I anticipate finishing the study of HfC, $HfO_2$, and Hf NPs. In the process, we will refine pulsed methods to study chemistry at ultra-high $T_{NP}$. The plan after than is to use our methods to examine two types of high and ultra-high $T_{NP}$ chemistry. One is reactions of volatile Si-containing species with siliceous NPs, relevant to biogas utilization. The other is to examine oxidation chemistry of $MoSi_2$ NPs. For both thrusts we hope to acquire a thermal O atom source that also can be used as a radical source.

**Publications 2020-2023 acknowledging support from the DOE GPCP program**

*Published or in press:*

1. "High Temperature Reaction of Individual Graphite Nanoparticles with $N_2O$: Etching, Passivation, Sublimation, and Comparison to $O_2$", Chris Y. Lau, Abigail M. Friese, and Scott L. Anderson, J. Phys. Chem. (submitted). Published on Chemrxiv (DOI: 10.26434/chemrxiv-2023-6894f)
2. "Growth and Passivation of Individual Carbon Nanoparticles by $C_2H_2$ addition at High Temperatures: Dependence of Growth Rate and Evolution on Material and Size", Chris Y. Lau, Daniel J. Rodriguez, Abigail M. Friese, and Scott L. Anderson, J. Chem. Phys. (in press). Also ChemRxiv (DOI: 10.26434/chemrxiv-2023-g9sm2).
3. "High Temperature Transformation, $O_2$ Etching, and Passivation of Single $SiO_x$ Nanoparticles: Kinetics and Optical Properties as Structure Probes", Daniel J. Rodriguez, Chris Y. Lau, Abigail M. Friese, and Scott L. Anderson, Mol. Phys. (2023) p. e2184652 DOI: 10.1080/00268976.2023.2184652, and ChemRxiv DOI: 10.26434/chemrxiv-2023-cs6vh.
4. "Methods for Non-Destructive, High Precision Mass/Charge Determination for Single, Trapped, GigaDalton Nanoparticles", David M. Bell, Collin R. Howder, Bryan A, Long, Scott L. Anderson, ChemRxiv (December 2022) DOI: 10.26434/chemrxiv-2022-1n56p Note: this is a "how-to" article which we decided to make available online to help others get started with NP mass measurements.
5. "$O_2$ Oxidation and Sublimation Kinetics of Single Silicon Nanoparticles at 1200 to 2050 K: Variation of Reaction Rates, Evolution of Structural and Optical Properties, and the Active-to-Passive Transition", Daniel J. Rodriguez, Chris Y. Lau, Abigail M. Friese, Bryan A. Long, and Scott L. Anderson, J. Phys. Chem. C (2023)126, 18716–18733, DOI: 10.1021/acs.jpcc.2c05985. Also ChemRxiv DOI: 10.26434/chemrxiv-2022-2ll5c
6. "High Temperature Oxidation of Single Carbon Nanoparticles: Dependence on Surface Structure, and Probing Real-Time Structural Evolution via Kinetics", Daniel J. Rodriguez, Chris Y. Lau, Abigail M. Friese, Alexandre Magasinski, Gleb Yushin, and Scott L. Anderson*, J. Am. Chem. Soc. (2022), 144, 4897–4912, DOI: 10.1021/jacs.1c12698. Also ChemRxiv: 10.26434/chemrxiv-2022-3b3h8
7. "$O_2$-Oxidation of Individual Graphite and Graphene Nanoparticles in the 1200 – 2200 K Range: Particle-to-Particle Variations and the Evolution of the Reaction Rates and Optical Properties", Daniel J. Rodriguez, Chris Y. Lau, Bryan A. Long, Susanna An Tang, Abigail M. Friese, and Scott L. Anderson*, Carbon 173 (2021) 286-300, DOI: 10.1016/j.carbon.2020.10.053. Also at arXiv DOI: 10.48550/arXiv.2008.05078
8. "Sublimation Kinetics for Individual Graphite and Graphene Nano-particles (NPs): NP-to-NP Variations and Evolving Structure-Kinetics and Structure-Emissivity Relationships", Bryan A. Long, Chris Y. Lau, Daniel J. Rodriguez, Susanna An Tang, and Scott L. Anderson, J. Am. Chem. 142 (2020) 14090–14101. DOI:10.1021/jacs.0c01720, Also at arXiv, DOI: 10.48550/arXiv.2002.07835
9. "Thermal Emission Spectroscopy of Single, Isolated Carbon Nanoparticles: Effects of Particle Size, Material, Charge, and Thermal History", Bryan A. Long, Daniel J. Rodriguez, Chris Y. Lau, Madeline Schultz, and Scott L. Anderson, J. Phys. Chem. C 124 (2020) 1704-1716. DOI: 10.1021/acs.jpcc.9b10509. Also at arXiv, DOI: 10.48550/arXiv.2001.05594
10. "Thermal Emission Spectroscopy for Single Nanoparticle Temperature Measurement: Optical System Design and Performance", Bryan A. Long, Daniel J. Rodriguez, Chris Y. Lau, and Scott L. Anderson, Applied Optics 58 (2019) 642-649; DOI: 10.1364/AO.58.000642, Also arXiv, DOI: 10.48550/arXiv.1812.11858

## Chemical Dynamics in the Gas Phase at Argonne: Chemical Dynamics Subtask

Ahren W. Jasper (ajasper@anl.gov), Stephen T. Pratt (stpratt@anl.gov),
and Kirill Prozument (prozument@anl.gov)
*Chemical Sciences and Engineering Division, Argonne National Laboratory*

### Program Scope

Complementary experimental and theoretical studies of gas phase dynamics are performed to explore unimolecular and bimolecular reactivity, energy flow within molecules and between collision partners, and the detailed mechanisms through which chemistry takes place. The studies produce improved theoretical methods and new fundamental descriptions of chemical dynamics at the molecular scale and are carried out in close coordination with work in the Thermochemistry, Kinetics, and Methods and Modeling Subtasks of the Chemical Dynamics in the Gas Phase Group at Argonne. The theoretical component is supplied by Jasper who emphasizes methods development and applications for collisional energy transfer, rovibrational anharmonicity, and electronically nonadiabatic chemistry, with recent studies taking advantage of high-performance computing. The experimental component is supplied by Pratt and Prozument. Pratt uses photoionization and photodissociation experiments to elucidate the spectroscopy and dynamics of highly excited molecules and radicals and to characterize the photoionization cross sections of reactive species, with future work focusing on inner- and outer-valence shell processes as well as new experiments using ultrafast free-electron laser sources. Prozument develops and applies chirped-pulse millimeter-wave spectroscopy to probe chemical dynamics and kinetics as well as artificial intelligence methods to assign rotational spectra. His future work involves a multi-experiment approach to understanding dynamical phenomena at different energy scales and in varied environments through the quantification of time- and vibrational-state-dependent branching ratios. Solving the inverse problem in rotational spectroscopy using artificial intelligence methods will also be pursued.

### Recent Progress

*Theory.* In ongoing work, we are developing transition state theories (TSTs) for describing nonthermal and nonequilibrium kinetics. The key choice defining these methods is their prescription for the state populations at the transition state. In conventional (thermal/canonical or microcanonical) TST, transition state populations are assumed to be governed by the same distributions as the reactants, and the good accuracy of this so-called "local equilibrium" assumption has been repeatedly demonstrated via comparisons with trajectories, quantum dynamics, and experiment. For nonthermal and nonequilibrium systems, the application of the local equilibrium assumption is inherently ambiguous. We derived a set of useful expressions for nonthermal and nonequilibrium cases and tested their accuracies via comparisons with quasiclassical trajectories (QCTs) for several of systems: H,O,OH + $CH_4$, H,O + $H_2O$, OH + CO, and OH + $CH_3OH$. For example, the rate constant for a nonthermal reaction involving two reactants initially prepared at different temperatures, A($T_A$) + B($T_B$) $\rightarrow$ products, can be written as the product of a conventional thermal rate constant evaluated at an effective temperature $T$ (defined assuming equipartition of $T_A$ and $T_B$) and a correction term involving the partition functions of A and B evaluated at $T$ and $T_A$ and $T_B$, respectively. This expression is shown to predict the QCT results within a factor of two and is generally more accurate than simply using the effective temperature approach and ignoring the correction term. Furthermore, we showed that the method could be improved via short-time dynamical corrections designed to quantify nonequilibrium effects that project reactant energies onto transition state vibrational modes (in the same spirit as the sudden vector projection (SVP) model of Guo).

Many of the full-dimensional potential energy surfaces required for in the QCT studies were developed using automation and validation strategies developed in the past few years and in collaboration with Davis. Supported by an ASCR Leadership Computing Challenge (ALCC) computer time award, a strategy for symmetrizing permutationally invariant polynomial (PIP) expansions for systems of any stoichiometry was presented. Systems with up to 15 atoms and 39 degrees of freedom were considered, and permutational invariance was enforced in expansions with 30 million terms and 13 atom types. Later, we demonstrated a

reduction in the number of terms needed for accurate PIP expansions using multi-pass greedy subset selection, a strategy borrowed from the statistics and signal processing literature, which is a kind of machine learning. The size of the reduced basis sets scaled ~linearly with dimensionality. Recently, we demonstrated dramatic speedups in PIP evaluations using GPUs.

Another major goal of this work is to develop, apply, and demonstrate the accuracy of a priori predictions of collisional energy transfer (CET) and pressure dependent kinetics. In a recent study, low-pressure-limit microcanonical (collisional activation) and thermal rate constants were predicted using a combination of ab initio potential energy surfaces, classical trajectories, transition state theory, and a detailed kinetic model for systems where experimental information was available for validation. The a priori approach involved no adjustable parameters and employed a detailed "two-dimensional" (in both *E*, the total energy of the reactant, and *J*, its total angular momentum) description of CET. The predicted rate constants were found to be in excellent agreement with experiment (to better than ~25%) and performed equally well for atomic, diatomic, and polyatomic baths.

We also carried out many CET applications and kinetics studies in collaboration with modelers and experimentalists, including $O_3$(+M), $NH_3$(+M), and $N_2H_4$(+M) with Glarborg and co-workers, QOOH(+M) with Lester and co-workers, third $O_2$ and ozone-assisted chemistry with Hansen, several astrochemical systems with Galvão and Kaiser, several nonthermal and radical-radical studies with Tranter and Sivaramakrishnan, and a trajectory study of $CO_2$ superrotors with Kliewer.

*Experimental Photoionization and Photodissociation.* Pratt is performing photoabsorption and photoionization experiments to highlight and elucidate specific intramolecular energy conversion processes among the rotational, vibrational, and electronic degrees of freedom in small molecules. New work includes time-resolved studies using free electron laser (FEL) facilities to complement and extend the frequency domain work performed in the laboratory and at synchrotron facilities.

Over the past year, we analyzed high-resolution absorption data obtained using the vacuum ultraviolet (VUV) Fourier transform spectrometer (FTS) at the SOLEIL Synchrotron. We focused on the analysis of photoabsorption cross sections for ammonia recorded between ~60,000 and 95,000 $cm^{-1}$ in both a room-temperature cell and a jet-cooled molecular beam (~70 K) at a resolution of 0.23 $cm^{-1}$. This work is a collaboration with de Oliveira (SOLEIL), Jacovella and Boyé-Péronne (ISMO), Holland (STFC, UK), and Ashfold (Bristol). The combination of such high resolution and well-calibrated intensities makes this a particularly useful data set, and a manuscript on this work is nearing completion. In the coming year, we hope to record comparable spectra for $ND_3$ and, if possible, the mixed isotopomers $NH_2D$ and $NHD_2$.

In collaboration with Bozek (SOLEIL), Powis (Nottingham), and Holland, we performed new experiments on the resonant Auger-Meitner decay of $CH_3I$ and iodobenzene in the region of the I $4d^{-1}$ edges (~50 eV). The pre-edge features in this region can decay by autoionization processes that involve only the core electrons (spectator decay) or that involve the resonantly excited electron (participator decay). In $CH_3I$ the latter processes tend to access the same electronic states of the $CH_3I^+$ ion as are observed in non-resonant photoionization but with different branching ratios and photoelectron angular distributions. We recorded photoelectron spectra and angular distribution data for a number of pre-edge features. Focusing on the lowest energy (I $4d^{-1}$)$\sigma^*$ resonance, we find that participator decay into the two spin orbit components of the $CH_3I^+$ X $^2E$ ground state leads to a long progression in the C–I stretching vibration. This observation is consistent with autoionization during the dissociation of the $CH_3I$ (I $4d^{-1}$)$\sigma^*$ state. One interesting aspect of this dissociation and decay is that the hole is localized on the I atom in the initial state, while the ground state ion dissociates to $CH_3^+$ + I. Thus, at some C–I distance in the dissociation process, the charge transfer process must become slow. We are in the process of analyzing the data in more detail and extending this analysis to the decay of other electronic states of $CH_3I^+$.

Pratt has been involved in several collaborations using ultrafast FEL sources to study excited state chemical dynamics. As part of a large collaboration led by K. Ueda (Tohoku University) and K. Prince (Elettra) at the FERMI FEL, we analyzed an extension of our earlier study on $N_2$ in which we used pump-probe techniques to create and manipulate Rydberg wavepackets in $N_2$. A second set of experiments on the manipulation of Rydberg wavepackets in atomic He, which greatly simplifies the analysis of the results, has also been analyzed. We are now preparing manuscripts on these two experiments. In addition, we are continuing to analyze the results of another experiment at FERMI on the excited state dynamics of acetylene. In these experiments, the molecule was excited at ~200 nm by an ultrafast pump pulse and was

probed in the vacuum ultraviolet by the FERMI FEL. Time-resolved photoelectron spectroscopy shows how the excited state evolves on a sub-picosecond timescale. Theoretical electronic structure and trajectory calculations are currently being performed by N. Doslic (Ruđer Bošković Institute) and coworkers in an attempt to analyze these results.

Finally, experimental results from a collaboration led by Argonne's Atomic, Molecular, and Optical Physics Group at the LCLS some years ago were analyzed and published in *Nature Communications*. In these experiments, an ultrafast pump was used to create a 1s hole on the oxygen atom in CO, and a second probe pulse was used to probe the electronic distribution around the carbon atom through the ejection of a C 1s electron. Changes in the binding energy were monitored by using high resolution photoelectron spectroscopy. The combination of site-selective excitation and detection provided new insight into ultrafast changes in the chemical bonding induced by core-shell excitation.

*Chirped-Pulse Rotational Spectroscopy: Oxidation of Ethylene.* Oxidation of hydrocarbons is being studied using the newly developed $SiO_2$/SiC microreactor and chirped-pulse (CP) millimeter-wave spectroscopy. The $SiO_2$/SiC microreactor is a modification of the SiC microreactor that is fitted with a quartz insert to prevent the degradation of heated SiC by oxygen. The oxidation products are detected by the CP spectrometer in the continuous flow supersonic expansion cooled to rotational temperatures of 7–12 K. The E-band (60–90 GHz) CP spectrometer has been modified with a fast digitizer with 14-bit vertical resolution, a 10 GS/s sampling rate, and 3 GHz analogue bandwidth. The digitizer acquires and averages $10^8$ free induction decay traces in under 15 minutes. An E-band low noise amplifier with a protective fast switch has been installed before the down-converting balanced mixer for an additional factor of 3 in the signal-to-noise ratio. Detection of the $4_{04}$–$3_{03}$ transition of $^{13}CH_2DCCH$ in natural abundance in a 5% propyne mixture in argon using a 30-MHz chirp and averaging 100M FIDs demonstrates the sensitivity of the redesigned E-band spectrometer.

The spectra in Fig. 1 were obtained with the new setup to demonstrate transitions for three isomers of $C_2H_4O$ (acetaldehyde, vinyl alcohol, and oxirane) that result from the oxidation of ethylene in the $SiO_2$/SiC microreactor heated to 1700 K. Oxirane is currently not included in detailed mechanisms of ethylene oxidation, and Prozument is working with Sivaramakrishnan to use experimental branching ratios to complete the mechanism.

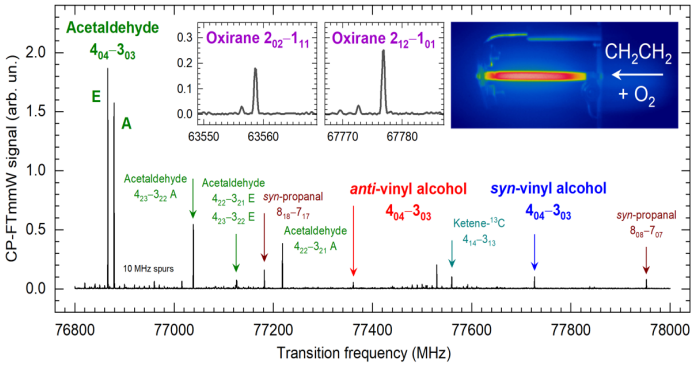


Figure 1. $C_2H_4O$ spectra identifying three isomers (acetaldehyde, vinyl alcohol, and oxiraine) produced from $C_2H_4$ oxidation.

*Chirped-Pulse Rotational Spectroscopy: Photodissociation of Formamide.* The time-resolved kinetic chirped-pulse (TReK-CP) experiment has been upgraded for work in the 260–290 GHz spectral range, which improves its sensitivity by a factor of 10 to 100 compared to the 75–110 GHz spectrometer. This is because the precursor molecules in this experiment flow in a tubular reactor at room temperature and the photolysis products are observed as they rotationally cool from thousands of Kelvin to 300 K upon collisional thermalization. The Boltzmann distribution of the rotational level population dictates that near-THz frequency ranges are favored for detection of rotationally hot molecules. The schematic of the current TReK-CP setup is shown in Fig. 2. An important advantage of this experiment is that products are detected *in situ*, within the reactor, unlike in the oxidation experiment described above. That limits the pressure within the TReK-CP reactor to ~10 μbar due to the onset of collisional broadening. There is, however, a class of

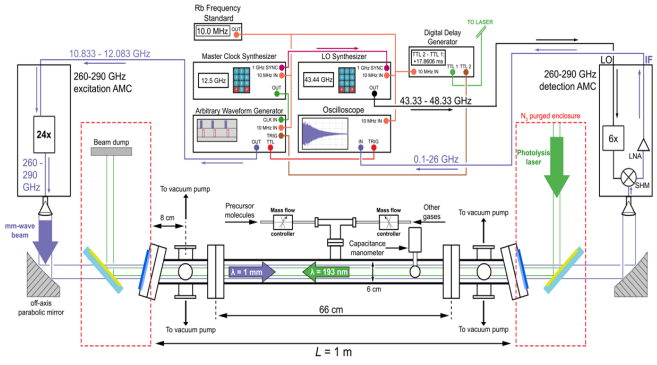


Figure 2. Schematic of the TReK-CP setup.

molecules with lower vapor pressure, amides, that presents a challenge for molecular beam studies but is ideally suitable for TReK-CP. We have investigated the 193 nm photodissociation of formamide and observed the HCN, HNC, HNCO, and HCO products. The branching ratios of these photodissociation products will be compared with the predictions of TST and molecular dynamics (Jasper).

**Future Work**

*Theory.* We will further generalize our TST models for predicting nonthermal and nonequilibrium kinetics, including methods for predicting microcanonical low-pressure-limit rate constants. The methods will require TST to be generalized to include energy- (momentum-) dependent dividing surfaces. Although described in foundational TST papers from Wigner and Keck, generalizations of the usual coordinate-only dividing surfaces have not found widespread use. When reactants and products are distinguished from one another by their internal energies, as in CET, TST dividing surfaces can be defined as a constraint on this energy. Such a simple constraint provides a valid dividing surface but surely features significant recrossing, and more accurate dividing surfaces likely involve more complex constraints on the momenta. Trajectories will be analyzed to develop useful momentum-dependent dividing surfaces that minimize recrossing with the goal of exploring whether or not transition state dividing surfaces for CET that are simple enough to be useful can be identified. Closely related to CET applications are intramolecular vibrational energy redistribution (IVR) applications, where one wishes to follow the flow of energy within a molecule to test statistical assumptions central to conventional TST, and IVR applications will also be pursued.

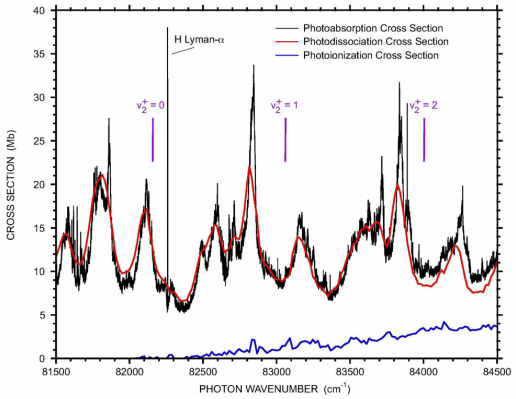


Figure 3. Our new room-temperature absorption (black) spectrum of $NH_3$ recorded from just below the ionization threshold to just above the $NH_3^+$ $\tilde{X}^+$ $^2A_2''$, $\nu_2^+ = 2$ ionization threshold. The $\nu_2^+ = 0 - 2$ ionization thresholds are indicated in purple. Also shown are the absolute photodissociation (red) and photoionization (blue) cross sections from Edvardsson et al., *J. Phys. B* **32**, 258–2609 (1999).

*Experimental Photoionization and Photodissociation.* We are planning to complete our analysis of the $NH_3$ spectra (see Fig. 3) in the near future, and we are hoping to receive new beamtime for the FTS to record the high-resolution absorption spectra of the isotopomers of ammonia. In principle, such data would allow us to extend the analysis of the $NH_3$ spectrum to higher energy and provide a unified description of the spectrum. We will also continue to analyze our new data on resonant Auger-Meitner decay in $CH_3I$ and extend this analysis to our new iodobenzene data. Finally, we will return to our double resonance experiments on molecular nitrogen and to the analysis of the corresponding VUV absorption spectrum of the first three ionization thresholds. This region is particularly interesting as it contains contributions from rotational, vibrational, and electronic autoionization.

Pratt is scheduled to lead an experimental run to study two-photon excitation of Xe and $XeF_2$ at the FERMI FEL in early June. (This beamtime was delayed by over a year due to facility closures resulting from both COVID and energy-related issues.) These experiments will be performed in collaboration with Bozek, Holland, Minns (Southhampton), Vozzi (Politecnico di Milano), and the FERMI staff. The goal of these experiments is to characterize the region near the Xe $4p^{-1}$ absorption edge. This region is particularly interesting because the energy of this edge is almost exactly twice that of the Xe $4d^{-1}$ edge. As a result, there is strong configuration interaction between the $4p^{-1}$ and $4d^{-2}$np and nf configurations. In the single-photon spectrum, this configuration completely distorts the $4p^{-1}$ photoelectron spectrum. By accessing this region via two-photon excitation, we hope to influence the contribution of the $4d^{-1}n$p and $n$f configurations to the spectrum and provide new insight into these interactions. For $XeF_2$, a significant "$4p^{-1}$"$\sigma_u$* resonance is also expected about 10 eV below the corresponding Xe $4p^{-1}$ threshold. This resonance is parity forbidden in single-photon excitation but allowed in two-photon excitation. We hope to characterize this resonance as well. In particular, we will explore how Xe $4d^{-2}n\ell n\ell'$ configurations influence the nature of the resonance.

Lan Cheng (Johns Hopkins University) and Phay Ho (Argonne) are also working to address these processes though quantum chemical calculations.

The high-intensity, ultrafast VUV laser system that we ordered last year is due to be installed in July 2023. This system will be shared with Tranter. We will use it to perform UV-pump, VUV-probe experiments using velocity map ion imaging at selected VUV energies, which will allow detailed exploratory measurements for future FEL work. Longer term developments will include the extension to time-dependent photodissociation and photoionization studies with photoion and photoelectron detection.

*Chirped-Pulse Rotational Spectroscopy.* We plan additional studies of oxidation chemistry using our newly designed heated microreactor. We will follow up on our preliminary observations of the Criegee intermediate $CH_2OO$ in the oxidation of ethane and ethylene. These results are interesting because it would be the first observation of this transient species in a combustion-relevant environment. At the same time, it is surprising to see this very unstable intermediate in a reactor at 1700 K. We plan to investigate the mechanism of $CH_2OO$ formation in these preliminary experiments using both the theory and additional experiments. We plan to continue our time-resolved photodissociation experiments with nitrogen-containing species such as methyl carbamate ($CH_3OC(O)NH_2$), urethane ($CH_3CH_2OC(O)NH_2$), and benzamide ($C_6H_5C(O)NH_2$). Competition between the various product channels in highly energized molecules will be investigated including: H-atom scrambling; H-atom transfer; HCN, HNC, and HNCO elimination via tight transition states; H-N and H-C simple bond fissions.

## Publications supported by this project since 2020


1. T. Y. Chen, S. A. Steinmetz, B. D. Patterson, A. W. Jasper, and C. J. Kliewer, Direct observation of coherence transfer and rotational-to-vibrational energy exchange in optically centrifuged $CO_2$ super-rotors. *Nature Comm.*, accepted (2023).
2. T. M. Selby, F. Goulay, S. Soorkia, A. Ray, A. W. Jasper, S. J. Klippenstein, A. N. Morozov, A. M. Mebel, J. D. Savee, C. A. Taatjes, and D. L. Osborn, Radical-radical reactions in molecular weight growth: The phenyl + propargyl reaction. *J. Phys. Chem. A* 127, 2577–2590 (2023).
3. A. C. R. Gomes, A. C. Souza, A. W. Jasper, and B. R. L. Galvão, The $P(^4S) + NH(^3\mathbf{\Sigma}^-)$ and $N(^4S) + PH(^3\mathbf{\Sigma}^-)$ reactions as sources of interstellar phosphorus nitride. *Pub. Astron. Soc. Aus.* 40, e011 (2023).
4. D. E. Couch, A. W. Jasper, G. Kukkadapu, M. M. San Marchi, A. J. Zhang, C. A. Taatjes, and Nils Hansen, Molecular weight growth by the phenyl + cyclopentadienyl reaction: Well-skipping, ring-opening, and dissociation. *Combust. Flame*, 112502 (2022).
5. J. Cho, A. W. Jasper, Y. Georgievskii, S. J. Klippenstein, and R. Sivaramakrishnan, The role of energy transfer and competing bimolecular reactions in characterizing the unimolecular dissociations of allylic radicals. *Combust. Flame*, online (2022).
6. D. E. Couch, G. Kukkadapu, A. J. Zhang, A. W. Jasper, C. A. Taatjes, and Nils Hansen, The role of radical-radical chain propagating pathways in the phenyl + propargyl reaction. *Proc. Combust. Inst.*, online (2022).
7. J. Cho, Y. Tao, Y. Georgievskii, S. J. Klippenstein, A. W. Jasper, and R. Sivaramakrishnan, The role of collisional energy transfer on the thermal and prompt dissociation of 1-methyl allyl. *Proc. Combust. Inst.*, online (2022).
8. Z. Wang, H. Zhao, C. Yan, Y. Lin, A. D. Lele, W. Xu, B. Rotavera, A. W. Jasper, S. J. Klippenstein, and Yiguang Ju, Methanol oxidation up to 100 atm in a supercritical pressure jet-stirred reactor. *Proc. Combust. Inst.*, online (2022).
9. A. W. Jasper, D. R. Moberg, Y. Tao, S. J. Klippenstein, and R. Sivaramakrishnan, Inefficient intramolecular vibrational energy redistribution for the $H + HO_2$ reaction and negative internal energy dependence for its rate constant. *Frontiers Phys.* **10**, 1003010 (2022).
10. Z. Yang, S. Doddipatla, C. He, S. J. Goettl, R. I. Kaiser, A. W. Jasper, A. C. R. Gomes, and B. R. L. Galvão, Can third-body stabilization of bimolecular collision complexes in cold molecular clouds happen? *Mol. Phys.* **120**, e2134832 (2022).
11. A. C. R. Gomes, C. M. R. Rocha, A. W. Jasper, and B. R. L. Galvão, Formation of phosphorus monoxide through the $P(^4S) + O_2(^3\Sigma^-) \rightarrow O(^3P) + PO(^2\Pi)$ reaction. *J. Molec. Model.* **28**, 259 (2022).
12. J. Jian, H. Hashemi, H. Wu, A. W. Jasper, and P. Glarborg, A reaction mechanism for ozone dissociation and reaction with hydrogen at elevated temperature. *Fuel* 322, 124138 (2022).
13. A. W. Jasper, Predicting third-body collision efficiencies for water and other polyatomic baths. *Faraday Discuss.* **238**, 68–86 (2022).
14. C. Yan, H. Zhao, Z. Wang, G. Song, Y. Lin, C. R. Mulvihill, A. W. Jasper, S. J. Klippenstein, and Y. Ju, Low- and intermediate-temperature oxidation of dimethyl ether up to 100 atm in a supercritical pressure jet-stirred reactor. *Combust. Flame* **243**, 112059 (2022).
15. A. Al-Haddad, S. Oberli, J. González-Vázquez, M. Bucher, G. Doumy, P. Ho, J. Krzywinski, T. J. Lane, A. Lutman, A. Marinelli, T. J. Maxwell, S. Moeller, S. T. Pratt, D. Ray, R. Shepard, S. H. Southworth, A. Vazquez-Mayagoitia, P. Walter, L. Young, A. Picón, and C. Bostedt, Observation of site-selective chemical bond changes via ultrafast chemical shifts, *Nature Comm.* **13**, 7170 (2022).
16. R. Forbes, P. Hockett, I. Powis, J. D. Bozek, S. T. Pratt, and D. M. P. Holland, Auger electron angular distributions following excitation or ionization from the Xe 3d and F 1s levels in xenon difluoride, *Phys. Chem. Chem. Phys.* **24**, 1367-1379 (2022).
17. I. Fischer and S. T. Pratt, Photoelectron spectroscopy in molecular physical chemistry, *Phys. Chem. Chem. Phys.* **24**, 1944-1959 (2022).
18. N. A. Seifert, K. Prozument, and M. J. Davis, Computational optimal transport for molecular spectra: The semi-discrete case, *J. Chem. Phys.* **156**, 134117 (2022).

19. D. R. Moberg, A. W. Jasper, and M. J. Davis, Parsimonious potential energy surface expansions using dictionary learning with multi-pass greedy selection. *J. Phys. Chem. Lett.* **12**, 9169–9174 (2021).
20. A. R. Conrad, N. Hansen, A. W. Jasper, N. K. Thomason, L. Hidaldo-Rodrigues, S. Treshock, and D. M. Popolan-Vaida, Identification of the acetaldehyde oxide Criegee intermediate reaction network in the ozone-assisted low-temperature oxidation of trans-2-butene. *Phys. Chem. Chem. Phys.* **23**, 23554–23566 (2021).
21. D. R. Moberg and A. W. Jasper, Permutationally invariant polynomial expansions with unrestricted complexity, *J. Chem. Theory Comput.* **17**, 5440–5455 (2021).
22. A. S. Hansen, T. Bhagde, K. B. Moore III, D. R. Moberg, A. W. Jasper, Y. Georgievskii, M. F. Vansco, S. J. Klippenstein, and M. I. Lester, Watching a hydroperoxyalkyl radical (•QOOH) dissociate. *Science* **373**, 679–682 (2021).
23. P. Glarborg, H. Hashemi, S. Cheskis, and A. W. Jasper, On the rate constant for $NH_2$ + $HO_2$ and third body collision efficiencies for $NH_2$ + H (+M) and $NH_2$ + $NH_2$ (+M). *J. Phys. Chem. A* **125**, 1505–1516 (2021).
24. J. A. Miller, R. Sivaramakrishnan, C. F. Goldsmith, M. P. Burke, A. W. Jasper, J. Zádor, N. Hansen, N. J. Labbe, and P. Glarborg, Combustion chemistry in the twenty-first century: Developing theory-informed chemical kinetics models. *Prog. Energy Combust. Sci.* **83**, 100886 (2021).
25. Y. Tao, A. W. Jasper, Y. Georgievskii, S. J. Klippenstein, and R. Sivaramakrishnan, Termolecular chemistry facilitated by radical-radical recombinations and its impact on flame speed predictions. *Proc. Combust. Inst*. **31**, 515–522 (2021).
26. N. Hansen, G. Kukkadapu, B. Chen, S. Dong, H. J. Curran, C. A. Taatjes, A. J. Eskola, D. L. Osborn, L. Sheps, W. J. Pitz, K. Moshammer, A. W. Jasper, W. Chen, J. Yang, and Z. Wang, The impact of the third $O_2$ addition reaction network on ignition delay times of neo-pentane. *Proc. Combust. Inst*. **31**, 299–307 (2021).
27. M. Fushitani, S. T. Pratt, D. You, S. Saito, Y. Luo, K. Ueda, H. Fujise, A. Hishikawa, H. Ibrahim, F. Légaré, P. Johnsson, J. Peschel, E. R. Simpson, A. Olofsson, J. Mauritsson, P. A. Carpeggiani, Praveen K. Maroju, M. Moioli, D. Ertel, R. Shah, G. Sansone, T. Csizmadia, M. Dumergue, N. G. Harshitha, S.Kühn, C. Callegari, O. Plekan, M. Di Fraia, M. Danailov, Luca Giannessi, L. Raimondi, M. Zangrando, G. De Ninno, P. Rebernik Ribic, and K. C. Prince, Time-resolved photoelectron imaging of complex resonances in molecular nitrogen, *J. Chem. Phys.* **154**, 144305 (2021).
28. R. Forbes, P. Hockett, I. Powis, J. D. Bozek, D. M. P. Holland, and S. T. Pratt, Photoionization from the Xe 4d orbitals of $XeF_2$, *J. Chem. Phys.* **155**, 194301 (2021).
29. M. Patanen, A. R. Abid, S. T. Pratt, A. Kivimäki, A. B. Trofimov, A. D. Skitnevskay, E. K. Grigoricheva, E. V. Gromov, I. Powis, and D. M. P. Holland, Valence shell photoelectron angular distributions and vibrationally resolved spectra of imidazole: A combined experimental-theoretical study, *J. Chem. Phys.* 155, 054304 (2021).
30. R. Lambo, C. -Y. Xu, S. T. Pratt, H. Xu, J. C. Zappala, K. G. Bailey, Z. -T. Lu, P. Mueller, T. P. O'Connor, B. B. Kamorzin, D. S. Bezrukov, Y. Xie, A. A. Buchachenko, and J. T. Singh, High resolution spectroscopy of neutral Yb atoms in a solid Ne matrix, *Phys. Rev. A*, **104**, 062809 (2021).
31. D. P. Zaleski, R. Sivaramakrishnan, H. R. Weller, N. A. Seifert, D. H. Bross, B. Ruscic, K. B. Moore III, S. N. Elliott, A. V. Copan, L. B. Harding, S. J. Klippenstein, R. W. Field, and K. Prozument, Substitution reactions in the pyrolysis of acetone revealed through a modeling, experiment, theory paradigm, *J. Am. Chem. Soc.* **143**, 3124–3142 (2021).
32. N. A. Seifert, K. Prozument, and M. J. Davis, Computational optimal transport for molecular spectra: The fully discrete case, *J. Chem. Phys.* **155**, 184101 (2021).
33. A. C. Rousso, A. W. Jasper, Y. Ju, and N. Hansen, Extreme low temperature combustion chemistry: Ozone-initiated oxidation of methyl hexanoate, *J. Phys. Chem. A* **124**, 9897–9914 (2020).
34. J. B. Randazzo, A. W. Jasper, R. Sivaramakrishnan, T. Sikes, P. T. Lynch, and R. S. Tranter, An experimental and theoretical study of the high temperature reactions of four butyl radical isomers, *Phys. Chem. Chem. Phys.* **22**, 18304–18319 (2020).
35. Z. Wang, N. Hansen, A. W. Jasper, B. Chen, S. M. Popolan-Vaida, K. K. Yalamanchi, A. Najjar, P. Dagaut, and S. M. Sarathy, Cool flame chemistry of diesel surrogate compounds: n-decane, 2-methylnonane, 2,7-dimethyloctane, and n-butylcyclohexane. *Combust. Flame* **219**, 384–392 (2020).
36. A. W. Jasper, "Third-body" collision parameters for hydrocarbons, alcohols, and peroxides and an effective internal rotor approach for estimating them. *Int. J. Chem. Kinet.* **52**, 387–402 (2020).
37. A. W. Jasper, Microcanonical rate constants for unimolecular reactions in the low-pressure limit. *J. Phys. Chem. A* **124**, 1205–1226 (2020).
38. R. Forbes, S. T. Pratt, A. De Fanis, A. R. Milosavljević, C. Nicolas, J. D. Bozek, N. A. Besley, and D. M. P. Holland, Photoabsorption, photoionization, and auger processes at the carbon K-edge in $CH_3I$, *Phys. Rev.* A **101**, 023408 (2020).
39. R. Forbes, A. De Fanis, D. Rolles, S. T. Pratt, I. Powis, N. A. Besley, A. R. Milosavljević, C. Nicolas, J. D. Bozek, and D. M. P. Holland, Photoionization of the I 4d and valence orbitals of methyl iodide, *J. Phys.* B **53**, 155101 (2020).
40. S. Hartweg, J. -C. Loison, S. Boyé-Péronne, B. Gans, D. M. P. Holland, G. A. Garcia, L. Nahon, and S. T. Pratt, Photoionization of the $C_4H_5$ isomers, *J. Phys. Chem.* A **124**, 6050-6060 (2020).
41. H. R. Hrodmarsson, B. Gans, S. Boyé-Péronne, G. A. Garcia, L. Nahon, S. T. Pratt, D. M. P. Holland, The effect of autoionization on the $HBr^+$ $^2\Pi_{3/2,1/2}$ state photoelectron angular distributions *Chem. Phys.* 539, 110961 (2020).
42. V. Makhija, K. Véyrinas, A. E. Boguslavskiy, R. Forbes, I. Wilkinson, R. Lausten, S. P. Neville, S. T. Pratt, M. S. Schuurman, and A. Stolow, Ultrafast molecular frame electronic coherences from lab frame scattering anisotropies, *J. Phys. B* **53**, 114001 (2020).
43. K. Prozument, J. H. Baraban, P. B. Changala, G. B. Park, R. G. Shaver, J. S. Muenter, S. J. Klippenstein, V. Y. Chernyak, and R. W. Field, Photodissociation transition states characterized by chirped pulse millimeter wave spectroscopy, *Proc. Nat. Acad. Sci.* **117**, 146–151(2020).
44. K. Prozument, B. G. Sartakov, and A. F. Vilesov, Mixed ortho-$H_2$ and para-$H_2$ clusters studied by vibrational coherent anti-Stokes Raman spectroscopy, *Phys. Rev. B* **101**, 184507 (2020).

## Chemical Dynamics in the Gas Phase at Argonne: Chemical Kinetics Subtask

Rebecca L. Caravan, Stephen J. Klippenstein, Robert S. Tranter
*Chemical Sciences and Engineering Division, Argonne National Laboratory, Lemont, IL, 60439

caravarl@anl.gov; sjk@anl.gov; tranter@anl.gov

### Program Scope

The goal of this program is to explore foundational problems in gas phase chemical kinetics through a combination of experimental studies and *ab initio* chemical kinetics calculations. We use these methods to explore reactions on complex potential energy surfaces (PESs), which includes assessments of the reaction rates, the role of incomplete thermalization in kinetics, the potential importance of novel classes of reactions, and the role of all aspects of the global PES. The close linkage of experimental and theoretical studies of prototypical reactions allows us to deeply explore key kinetic questions, while generating kinetic data of relevance to a variety of complex, chemically reactive, non-equilibrium systems such as combustion, atmospheric chemistry, and atomic layer deposition. Our efforts to address these key science questions will benefit from continued development of unique experimental and theoretical methods. The experimental approach spans a wide range of reaction conditions using a combination of shock tube and flow reactor methods. A suite of optical and mass spectrometric diagnostics allow in-depth interrogation of reactions. Extensive use of synchrotron (VUV and x-ray) techniques enhance the laboratory capabilities.

### Recent Progress

*Criegee intermediate reactivity:* We have continued our collaborative work on Criegee intermediate (CI) reactivity with Lester (Penn), Taatjes, Osborn, and Sheps (Sandia), and our collaborators outside of the program including Percival and Winiberg (NASA JPL), and Shallcross (Bristol). We have focused our efforts on unimolecular and bimolecular studies of the methyl ethyl Criegee intermediate (MECI). MECI is the saturated, non-resonance stabilized analogue of methyl vinyl ketone oxide, an isoprene-derived CI that we have studied previously.

In a collaborative multi-institute study led by Lester we examined product formation in the unimolecular decay of methyl-ethyl CI (MECI) through a combination of experimental measurements and theoretical predictions. The decay process begins with an H transfer to yield a vinylhydroperoxide, whose OO bond fission is generally presumed to produce OH and a vinoxy radical. However, a prior direct experimental study of dimethyl CI decay observed significant formation of hydroxyacetone, with a subsequent theoretical effort by Kuwata demonstrating that this product arises from OH roaming. In multiplexed photoionization mass spectrometry experiments at the Advanced Light Source, we identified the formation of hydroxybutanone on timescales consistent with the unimolecular decay of MECI, indicating that a roaming mechanism is operative for this CI. We used complementary multireference electronic structure calculations to map the unimolecular decay pathways for both *anti*- and *syn*-MECI. The process starts with a 1,4 H-atom transfer from a methyl or methylene group to the terminal oxygen, transiently forming a hydroperoxybutene intermediate, followed by roaming of the separating OH and butanonyl radicals in the long-range region of the potential. The latter roaming sequence occurs over barriers that are submerged by about 4-5 kcal mol$^{-1}$ relative to OH

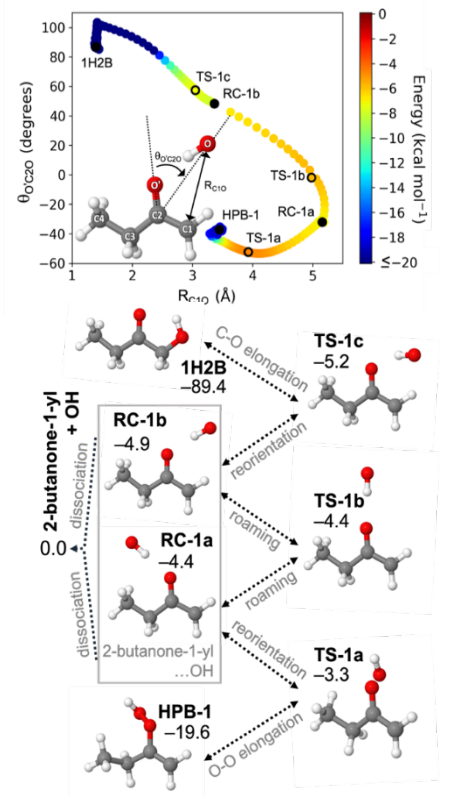


***Figure 1:*** *(Top) Minimum energy path for the roaming mechanism from 2-hydroperoxy-but-1-ene (HPB-1) to 1-hydroxy-2-butanone (1H2B). (Bottom): Molecular configurations at the labeled points.*

+ butanonyl. An illustrative plot of the minimum energy path potential for the overall roaming sequence in the *anti*-MECI decay is provided in Fig. 1.

A comprehensive theoretical kinetic analysis was conducted to evaluate rate constants and branching yields for thermal unimolecular decay of MECI to conventional and roaming products under laboratory and atmospheric conditions, demonstrating a significant yield of roaming products under both conditions. The predicted branching to hydroxybutanone is in reasonable agreement with that estimated experimentally. Meanwhile subsequent C-O elongation and H-transfer can lead to MVK (methyl vinyl ketone), which is also observed. Furthermore, the lowest bond fissions of the hydroxybutanones, which are also below the threshold for OH formation, could yield a second stage of roaming to produce a bewildering array of roaming products.

Our initial experiments on MECI bimolecular reactivity have revealed that it reacts more quickly (e.g., with $SO_2$) than its resonance-stabilized analog, MVK-oxide. Continued experimental and theoretical investigations will help to reveal the effects of structure vs. conjugation on CI reactivity.

*Hydroxy-functionalized peroxy radical reactions:* Recently, the Beauchamp (Caltech) and Wilson (LBNL) groups found compelling evidence for the conversion of β-hydroxyfunctionalized peroxy radicals (HO-$RO_2$) to CIs in heterogeneous environments. Following on from the exquisite work of Wilson's group, with Wilson, Percival, Winiberg, Osborn and Taatjes, we have conducted direct gas-phase studies to examine if this facile conversion is operative in the gas phase, and the mechanism by which it proceeds. Our initial experiments on HO-$RO_2$ formed from the reaction of OH and $O_2$ with ethene, cis-2-butene, and isoprene have indicated that this pathway is minor in the gas phase, highlighting the interesting differences in reactivity of intermediates in purely gas-phase vs heterogenous environments. Through our experiments, we have also examined the self-reaction products of these various HO-$RO_2$. Recent reexamination of $RO_2$ self- and cross-reactions in the atmospheric chemistry community have indicated the possible role that one product channel, ROOR+ $O_2$, may play in aerosol formation. While the reaction kinetics and product branching for $RO_2$ self-reactions are strongly influenced by the R functional group (and temperature and pressure), previous extensive investigations of small, alkyl-functionalized $RO_2$, concluded that the ROOR formation channel was negligible. However, more recent experimental efforts have revealed that ROOR formation may be much more significant for functionalized $RO_2$; for example, for $CH_3C(O)CH_2OO$, Berndt et al. assigned a ROOR yield of 16%, and very recently, Murphy et al. assigned a yield of 23% for the ROOR formed in the ethene-derived HO-$RO_2$ self-reaction. We are examining the self-reaction products, including evidence for ROOR, in the reaction of HO-$RO_2$ from our recent data.

*Review of theory of unimolecular reactions:* As part of the Spiers memorial lecture at a recent Faraday discussion meeting celebrating 100 years since the Lindemann mechanism, we provided a comprehensive review of the theory of unimolecular reaction kinetics. The review first considered the progress from the Lindemann mechanism to the master equation, which now provides the cornerstone for most theoretical analyses. The current status of ab initio transition state theory based implementations of the master equation was then reviewed, beginning with a discussion of the energy resolved chemical conversion rates, followed by a review of the pressure dependence of the thermal kinetics. The latter discussion focused on the collisional energy and angular momentum transfer rates as well as the complexities of non-thermal effects and of multi-well multiple channel reactions. The synergy with recent state-of-the-art experiments was used to motivate these discussions. Attempts to automate the calculations were also briefly reviewed. Throughout the discussion, we provided our perspective on current understanding and continuing challenges and opportunities. One such key challenge relates to the coupling of sequences of reactions, which frequently leads to deviations from the classic presumption of thermal reactants.

*Special Issues*: During the past year we organized three separate special journal issues, each of which may be of some interest to the gas phase chemical physics community. First, a memorial issue honoring Jim Miller was organized together with Judit Zádor for publication in Combustion and Flame. Next, together

with Katharina Kohse-Hoeinghaus, we guest edited a virtual special issue of J. Phys. Chem. A on "Combustion in a Sustainable World: From Molecules to Processes". Finally, together with Nathan Kidwell, Julia Lehman, and Anne McCoy we are guest editing a Festschrift issue of J. Phys. Chem. A honoring Marsha Lester.

*X-ray fluorescence:* We have completed work on measuring temperatures in a heavily sooting ethylene diffusion flame using the krypton x-ray fluorescence method. This study is built on a prior study of sooting methane flames where the fluorescent agent was seeded into all the burner gases, which consumed a significant amount of krypton. In the ethylene work only the fuel gas was seeded with krypton, reducing consumption to 0.5% of the methane study. Seeding only one gas stream complicates measuring temperatures accurately by XRF. However, the temperatures obtained are in very good agreement with 2D CFD simulations and a variety of literature measurements. A rigorous error analysis of the XRF data was developed. Other notable features of this work are that the XRF temperature measurements are not perturbed by particles and the high spatial resolution resolves temperatures in areas of large gradients. In a related study we have also applied the XRF method to the measurement of temperatures in premixed non-sooting flames. Part of the goal was to determine the degree to which a thermocouple perturbs the flame. A type R (Pt:Pt/Rh) 125 micron thermocouple was placed in the flame at various locations and raster scans made around the Tc junction. Within a couple of hundred microns of the thermocouple the flame temperature is unperturbed. Two significant challenges were encountered in these experiments. First, Pt has a fluorescence line close to that of Kr-Kα, the XRF probe and it was necessary to develop a deconvolution method to recover the desired signal. Secondly, the thermocouple is non-uniform, and the lead wires enter the measurement volume. To accurately locate the thermocouple junction required developing an image processing method. Despite these challenges measurements could be made within 200 μm of the thermocouple junction. The XRF data are in excellent agreement with simulations of the flame. However, the thermocouple measurements are only in good agreement near the burner surface but become increasingly lower at larger heights above the burner. The source of this deviation is under investigation.

*Difluoromethane pyrolysis*: We have previously reported results from an experimental, theory and modeling investigation with Sivaramakrishnan and Jasper on the dissociation of difluoromethane (DFM). The initial study probed the dissociation of DFM to CHF + HF and the subsequent bimolecular reactions of CHF. While fair agreement was obtained between the theoretical predictions of key rate coefficients and laser schlieren (LS) shock tube data the experiments consistently showed much less pressure dependency than the master equation simulations predicted, particularly for pressures less than 100 torr. Additional LS experiments at low temperatures (T < 1000 K), where dissociation of DMF does not occur, have revealed that DMF exhibits slow IVR. Careful examination of the LS dissociation experiments at P < 100 torr indicates that they are impacted by slow IVR and in a few cases relaxation and dissociation may be observable in the same signal. Accounting for IVR and the associated incubation delays prior to dissociation bring the experimental and theoretical results into good agreement. Analysis of the low temperature LS experiments is ongoing.

*Isopropyl alcohol dissociation:* In collaboration with Wooldridge (U. Michigan), we have performed LS studies on the dissociation of isopropyl alcohol (IPA). IPA dissociates by two channels, dehydration to propene and water, and bond scission giving methyl and the 1-hydroxy ethyl radical ($CH_3CHOH$). Experimental and theoretical studies of IPA dissociation are sparse and kinetic models have mainly been developed by drawing analogies with butanols. Simulations with these models fail to capture the LS experiments, Fig. 2. The LS results are in fair agreement with an experimental value for the dehydration channel and a theoretical value for the radical path. However, after several microseconds there are indications that our kinetic model is

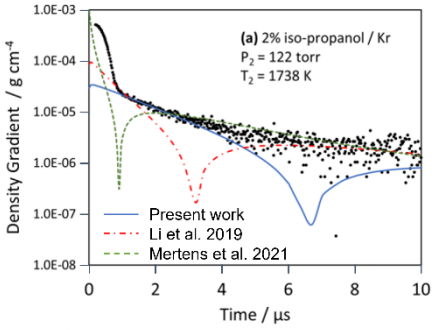


***Figure 2:*** *IPA: comparison of experiment and simulations.*

producing too many methyl radicals. Recombination of these radicals begins to dominate the simulated LS signal driving it negative in contrast to the actual signal, which remains positive. The reason for this discrepancy is being investigated, but it is likely that consumption of IPA by reaction with H-atoms is underestimated and that the reactions of the abstraction products require further theoretical and experimental study.

*Broad band UV-Visible time resolved absorption experiment*: The final construction of the new broadband UV-Visible time-resolved absorption experiment is well underway in a newly renovated state-of-the-art laser laboratory. The experiment comprises a glass reactor (2" diameter, 1 m length) fitted with removable window flanges bearing AR-coated windows for the UV-Vis region. Gas is delivered to the reactor via a newly constructed mixing manifold comprising 6 mass flow controllers for the delivery of various reactant, precursor, and bath gases over different flow rate ranges. A second mixing manifold, equipped with new high accuracy baratrons and an Edwards RV8 pump, has been constructed in one of the laboratory's two fume hoods for the preparation of dilute gas mixtures. The reactor pressure (~1-760 Torr) will be controlled by a feedback butterfly valve. The vapor of low vapor pressure liquid precursors (e.g., $CH_2I_2$ for $CH_2OO$ production) will be entrained into the gas phase using custom glass bubblers (Argonne Glassblowing Studio). Further reactors of different dimensions are currently under design and production. The reactor is evacuated by an oil free pump set (Edwards GV80/EH500) located outside of the laboratory to minimize noise and vibrations. A new stainless steel vacuum line (4" diameter) connects the pump to the laboratory, with two ports located over two optical tables servicing the current apparatus and allowing for future expansion. Photolytic experiments will be initiated by a newly installed and commissioned Coherent COMPex 205F excimer laser, which is being aligned along the length of the reactor. The excimer laser is currently configured for easy switching between operation at 248 nm (up to ~750 mJ/pulse) and 351 nm (up to ~350 mJ/pulse) to enable generation of different reactive intermediates from photolytic precursors. A new fiber-coupled laser driven light source (Energetiq EQ-99X-FC) has been tested. The stable, CW, collimated, broadband (190- 2500 nm) output of a fiber-coupled Energetiq EQ-99X-FC LDLS is single or multipassed through a glass reactor, the latter using a set of custom broadband UV-Vis mirrors that are being mounted externally to the reactor in a White Cell configuration. The broadband light is being aligned into a Teledyne Princeton IsoPlane 320 aberration-free spectrograph that is fitted with three diffraction gratings mounted on a computer-controlled turret. Each grating is blazed for UV-Vis light diffraction but at different grove densities. This facilitates the capture of finer- or coarser-resolution spectra, over narrower or broader spectral ranges, respectively. The diffracted light is imaged onto a Teledyne Princeton PI-Max 4 1024-F intensified charged-coupled device (iCCD) detector that has a 1024 × 1024 array. The fast-gating capabilities of the iCCD enables full spectra to be captured over an integration window as short as 2 ns. The experiment will be run in one of two modes, depending on the time-scale of the chemistry to be studied: (1) *Kinetics mode*. A full kinetic profile over the whole spectral window for every excimer laser pulse is captured at ~60 μs increments (at typical operating conditions where 10 rows of the iCCD are illuminated). The full wavelength vs. kinetic time dataset is captured following a single excimer laser pulse. The data is signal averaged over ~100s of laser pulses to improve the signal to noise ratio. (2) *Stepped-delay-time mode*. The whole spectral range is measured at a fixed delay time after the first excimer pulse. At each sequential excimer pulse, the delay time between the excimer pulse and absorption measurement will be stepped by user-selected increments, and the absorption over the whole spectral range will be measured at each stepped delay time. This process will be repeated to build up a kinetic profile across the whole spectral range at fine time increments, and then to improve the signal-to-noise ratio at each delay time. The DAQ code has been written using LabVIEW and is being tested with the spectrograph and iCCD, and the experimental timing will be controlled by a delay generator. The first absorption spectra (of $CH_2I_2$ and then $NO_2$) will be recorded in the coming weeks. The first photolytic experiment (of $CH_2OO$ production from $CH_2I_2$ photolysis in the presence of $O_2$) will be recorded thereafter. Initial kinetics work will focus on CIs and peroxy radicals, complementing our collaborative ALS experiments and theoretical efforts.

## Future Work

Our theoretical and experimental investigations of CI reactivity will continue with our collaborators, with a theme of understanding the influence of CI structure on their reactivity. We are in the process of extending our theoretical analysis of OH roaming in MECI to a study of the related processes arising from the ozonolysis of α-pinene. Our experimental studies on HO-$RO_2$ will continue, and will be complimented by our AutoMech investigations to predict the stability of a variety of $RO_4R$ species, which are an interesting intermediate arising in the self-reaction of $RO_2$ radicals.

We will perform VUV-PIMS studies of IPA to directly determine the reaction products and their time dependencies. These data will help refine the pyrolysis mechanism. Additionally, we will perform VUV-PIMS and LS studies of IPA + H to develop a more in-depth understanding of what appears to be a key part of the mechanism. We are also continuing work on the reactions of aromatic radicals with a focus on determining rate coefficients and reaction paths. A particular immediate focus is on the phenoxy radical over a broad range of experimental conditions.

## DOE Supported Publications 2020 - present


1. **Photodissociation Transition States Characterized by Chirped Pulse Millimeter Wave Spectroscopy,** K. Prozument, J. H. Baraban, P. B. Changala, G. B. Park, R. G. Shaver, J. S. Muenter, S. J. Klippenstein, V. Y. Chernyak, R. W. Field, *Proc. Nat. Acad. Sci*. **117**, 146-151 (2020).
2. **Reaction Profiles and Kinetics for Radical-Radical Hydrogen Abstraction via Multireference Coupled Cluster Theory,** C.-H. Wu, D. B. Magers, L. B. Harding, S. J. Klippenstein, W. D. Allen, *J. Chem. Theory Comp.* **16***,* 1511-1525 (2020).
3. **Experimental and Theoretical Studies of the Doubly-Substituted Methyl-Ethyl Criegee Intermediate: Infrared Action Spectroscopy and Unimolecuar Decay to OH Radical Products,** V. P. Barber, A. S. Hansen, S. J. Klippenstein, M. I. Lester**,** *J. Chem. Phys.* **152***, 094301* (2020).
4. **Direct Kinetic Measurements and Theoretical Predictions of an Isoprene-Derived Criegee Intermediate,** R. L. Caravan, M. F. Vansco, K. Au, M. A. H. Khan, Y.-L. Li, F. A. F. Winiberg, K. Zuraski, Y.-H. Lin, W. Chao, N. Trongsiriwat, P. J. Walsh, D. L. Osborn, C. J. Percival, J. Jr-M. Lin, D. E. Shallcross, L. Sheps, S. J. Klippenstein, C. A. Taatjes, M. I. Lester**,** *Proc. Nat. Acad. Sci.* **117**, 9733-9740 (2020).
5. **Formic Acid Catalyzed Isomerization and Adduct Formation of an Isoprene-Derived Criegee Intermediate: Experiment and Theory,** M. F. Vansco, R. L. Caravan, S. Pandit, K. Zuraski, F. A. F. Winiberg, K. Au, T. Bhagde, N. Trongsiriwat, P. J. Walsh, D. L. Osborn, C. J. Percival, S. J. Klippenstein, C. A. Taatjes, M. I. Lester**,** *Phys. Chem. Chem. Phys*. **22***,* 26796-26805 (2020).
6. **An Experimental and Theoretical Study of the High Temperature Reactions of All Four Butyl Radical Isomers,** J. B. Randazzo, R. Sivaramakrishnan., A. W. Jasper, T. Sikes, P. T. Lynch, R. S. Tranter, *Phys. Chem. Chem. Phys*, **22**, 18304 -18319 (2020).
7. **Experimental Evidence of Dioxole Unimolecular Decay Pathway for Isoprene-Derived Criegee Intermediates** M.F. Vansco, R.L. Caravan, K. Zuraski, F.A.F. Winiberg, K. Au, N. Trongsiriwat, P.J. Walsh, D.L. Osborn, C.J. Percival, M.A.H. Khan, D.E. Shallcross, C.A. Taatjes and M.I. Lester, *J. Phys. Chem. A* **124**, 3542-3554 (2020).
8. **Insertion Products in the Reaction of Carbonyl Oxide Criegee Intermediates with Acids: Chloro(Hydroperoxyl)Methane Formation from Reaction of $CH_2OO$ with HCl and DCl**. C. A. Taatjes, R. L. Caravan. F. A. F. Winiberg, K. Zuraski, K. Au, L. Sheps, D. L. Osborn, L. Vereecken, C. J. Percival*. Mol. Phys*. e1975199 (2021).
9. **Absolute Photoionization Cross Section of the Simplest Enol, Vinyl Alcohol,** D. Rösch, R. L. Caravan, C. A. Taatjes, K. Au, R. Almeida and D. L. Osborn, *J. Phys. Chem. A* 125, 7920-7928 (2021).
10. **Automated Theoretical Chemical Kinetics: Exploring the Initial Stages of Pyrolysis,** S. N. Elliott, K. B. Moore, A. V. Copan, M. Keceli, C. Cavallotti, Y. Georgievskii, H. F. Schaefer III, S. J. Klippenstein**,** *Proc. Combust. Inst.* **38**, 375-384 (2021).
11. **Functionalized Hydroperoxide Formation from the Reaction of Methacrolein-Oxide, an Isoprene-Derived Criegee Intermediate, with Formic Acid: Experiment and Theory** M. F. Vansco, K. Zuraski, F. A. F. Winiberg, K. Au, N. Trongsiriwat, P. J. Walsh, D. L. Osborn, C. J. Percival, S. J. Klippenstein, C. A. Taatjes, M. I. Lester, R. L. Caravan, *Molecules*, **26**, 3058 (2021).
12. **Entanglement Effect and Angular Momentum Conservation in a Non-separable Tunneling Treatment**, Y. Georgievskii, S. J. Klippenstein, *J. Chem. Theo. Comp*. **17**, 3863-3885 (2021).

13. **Watching a Hydroperoxyalkyl Radical (•QOOH) Dissociate**, A. S. Hansen, T. Bhagde, K. B. Moore III, Daniel R. Moberg, A. W. Jasper, Y. Georgievskii, M. F. Vansco, S. J. Klippenstein, M. I. Lester, *Science*, **373**, 679-682 (2021).
14. **Initiation Reactions in the High Temperature Decomposition of Styrene,** T. Sikes, C. B. Banyon, R. A. Schwind, P. T Lynch., A. Comandini, R. Sivaramakrishnan, R. S. Tranter, *Phys. Chem. Chem. Phys*, **23**, 18432-18448 (2021).
15. **Editorial Joe V. Michael Memorial Issue** R. S. Tranter, N. Chaumeix, M. S. Wooldridge, *Int. J. Chem. Kinet.,* https://doi.org/10.1002/kin.21481 (2021).
16. **Ring Opening in Cycloheptane and Dissociation of 1-Heptene at High Temperatures,** T. Sikes, K. Bell Burdett., R. L. Speth, C. F. Goldsmith, R. Sivaramakrishnan, R. S. Tranter, *Proc. Combust. Inst.*, **38**, 929-937 (2021).
17. **Open Questions on the Reactivity of Criegee Intermediates** R. L. Caravan, M. F. Vansco, M. I. Lester, *Comm. Chem.***4**, 44 (2021).
18. **Theoretical Kinetics Predictions for $NH_2 + HO_2$,** S. J. Klippenstein, P. Glarborg, *Combust. Flame*, **236**, 111787 (2022).
19. **Dramatic Conformer-Dependent Reactivity of Acetaldehyde Oxide Criegee Intermediate with Dimethylamine via a 1,2-Insertion Mechanism,** M. F. Vansco, M. Zou, I. O. Antonov, K. Ramasesha, B. Rotavera, D. L. Osborn, Y. Georgievskii, C. J. Percival, S. J. Klippenstein, C. A. Taatjes, M. I. Lester, R. L. Caravan, *J. Phys. Chem. A*, **126**, 710-719 (2022).
20. **Infrared Spectroscopic Signature of a Hydroperoxyalkyl Radical (•QOOH),** A. S. Hansen, T. Bhagde, Y. Qian, A. Cavazos, R. M. Huchmala, M. A. Boyer, C. F. Gavin-Hanner, S. J. Klippenstein, A. B. McCoy, M. I. Lester**,** *J. Chem. Phys*., **156**, 014301 (2022).
21. **Rapid Allylic 1,6 H-Atom Transfer in an Unsaturated Criegee Intermediate,** A. S. Hansen, Y. Qian, C. A. Sojdak, M. Kozlowski, V. J. Esposito, J. S. Francisco, S. J. Klippenstein, M. I. Lester, *J. Am. Chem. Soc*., **144**, 5945-5955 (2022).
22. **Energy-Resolved and Time-Dependent Unimolecular Dissociation of Hydroperoxyalkyl Radicals (•QOOH),** T. Bhagde, A. S. Hansen, S. Chen, P. J. Walsh, S. J. Klippenstein, M. I. Lester**,** *Faraday Disc*., **238**, 575-588 (2022).
23. **In Situ Temperature Measurements in Sooting Methane/Air Flames Using Synchrotron X-Ray Fluorescence of Seeded Krypton Atoms,** M. J. Montgomery, H. Kwon, A. L. Kastengren, L. D. Pfefferle, T. Sikes, R. S. Tranter, Y. Xuan, C. S. McEnally, *Sci. Adv.,* **8**, eabm7947 (2022).
24. **Spiers Memorial Lecture: Theory of Unimolecular Reactions**, S. J. Klippenstein, *Faraday Disc*., **238**, 11-67 (2022).
25. **Automated Identification and Calculation of Prompt Effects in Kinetic Mechanisms using Statistical Models,** L. Pratali Maffei, K. B. Moore III, Y. Georgievskii, C. R. Mulvihill, S. N. Elliott, J. Cho, R. Sivaramakrishnan, T. Faravelli, S. J. Klippenstein**,** *Combust. Flame*, 112422 (2022). https://doi.org/10.1016/j.combustflame.2022.112422. *Jim Miller memorial issue*
26. **Formation of Organic Acids and Carbonyl Compounds in n-Butane Oxidation via ɣ-Ketohydroperoxide Decomposition**, D. M. Popolan-Vaida, A. J. Eskola, B. Rotavera, J. F. Lockyear, Z. Wang, S. M. Sarathy, R. L. Caravan, J. Zádor, L. Sheps, A. Lucassen, K. Moshammer, P. Dagaut, D. L. Osborn, N. Hansen, S. R. Leone, C. A. Taatjes, *Angew. Chem. Int. Ed.* 61, e202209168 (2022).
27. **Temperature Measurements in Heavily-Sooting Ethylene/Air Flames Using Synchrotron X-Ray Fluorescence of Krypton,** C. Banyon, M. J. Montgomery, H. Kwon, A. L. Kastengren, L. D. Pfefferle, T. Sikes, Y. Xuan. C. S. McEnally, R. S. Tranter, *Combust. Flame*. 112494 (2022) https://doi.org/10.1016/j.combustflame.2022.112494. *Jim Miller memorial issue*
28. **A Wide Range Experimental Study and Further Development of a Kinetic Model Describing Propane Oxidation,** L. Zhu, S. Panigraphy, S. N. Elliott, S. J. Klippenstein, M. Baigmohammadi, A. Abd El-Sabor Mohamed, J. W. Hargis, S. Alturaifi, O. Mathieu, E. L. Petersen, K. A. Heufer, A. Ramalingam, Z. Wang, Henry J. Curran**,** *Combust. Flam*e, 248, 112562 (2023).
29. **Conformer-Dependent Chemistry: Experimental Product Branching of the Vinyl Alcohol + OH + $O_2$ Reaction,** D. Rösch, G. H. Jones, R. Almeida, R. L. Caravan, A. Hui, A. W. Ray, C. J. Percival, S. P. Sander, M. D. Smarte, F. A. F. Winiberg, M. Okumura, D. L. Osborn, *J. Phys. Chem. A*, 127, 3221-3230 (2023).
30. **Radical-Radical Reactions in Molecular Weight Growth: The Phenyl + Propargyl Reaction** T. M. Selby, F. Goulay, S. Soorkia, A. Ray, A. W. Jasper, S. J. Klippenstein, A. N. Morzov, A. M. Mebel, J. D. Savee, C. A. Taatjes, D. L. Osborn, *J. Phys. Chem. A*, 127, 2577-2590 (2023). *Virtual issue on "Combustion in a Sustainable World: From Molecules to Processes"*

**Chemical Dynamics in the Gas Phase at Argonne: Theory, Modeling, and Methods Subtask**

Ron L. Shepard[1], Raghu Sivaramakrishnan[2], and Michael J. Davis[3]
Chemical Sciences and Engineering Division
Argonne National Laboratory
Lemont, IL 60439
Email:[1]shepard@tcg.anl.gov, [2]raghu@anl.gov,[3]davis@tcg.anl.gov

The Theory, Modeling, and Methods Subtask focuses on the development of three research areas corresponding to: electronic structure methods; the generation and analysis of chemical kinetic mechanisms for simulating complex systems; and the exploration of chemically reactive systems, including isolated chemical reactions, complex chemical kinetic mechanisms, and spectroscopy, through the methods of novel numerical analysis. These efforts are closely connected to the goals of the other three subtasks and result in substantial cross-fertilization.

**Theoretical Studies of Potential Energy Surfaces and Computational Methods: Ron Shepard**

**Program Scope**: This project involves the development, implementation, and application of theoretical methods for the calculation and characterization of potential energy surfaces (PES) and other molecular properties involving species that occur in combustion, atmospheric, and general gas-phase chemistry. An accurate and balanced treatment of reactants, intermediates, and products for both ground and excited electronic states is required. This difficult challenge is met with general multiconfiguration self-consistent field (MCSCF) and multireference configuration interaction (MRCI) methods [see *Chem. Rev.* **112**, 108 (2012) and *J. Chem. Phys.* **152**, 134110 (2020)]. More recently, the *graphically contracted function* (GCF) method has been developed to address some of the practical limitations of the traditional MCSCF and MRCI approaches, including the number of active electrons that may be accommodated and the overall expense associated with the study of larger molecular systems [see *J. Chem. Phys.* **141**, 064105 (2014) and references therein]. These methods are developed and maintained within the COLUMBUS Program System.

**Recent Progress:** The COLUMBUS Program System is now an open-source distribution through the GitLab repository [https://gitlab.com/columbus-program-system/columbus]. The distribution includes the source code, documentation, validation runs, tutorials, and various programmer tools. One component of this distribution is the COLUMBUS Library (colib), which includes common utilities that are shared by the entire program system. In the past year, this library has been restructured and various site-dependent codes have been merged into a common source. Part of the restructuring effort has included the introduction of shared modules. By moving the code into shared modules, the compiler provides explicit interfaces for all the member subprograms. These explicit interfaces in turn allow the compiler to identify many programmer mistakes at compile time, including type, kind, and rank mismatches of subprogram arguments. In the legacy library codes, these errors could only be found at runtime, sometimes a tedious process; thus, the new structure allows the programmer working within COLUMBUS to be much more productive. Furthermore, many of the shared routines have been simplified and modernized using new features of the Fortran language. This rewrite of the low-level library codes is a first step toward modernizing the individual computational codes within COLUMBUS over the next months.

***CSF TO GCF INTERCONVERSION***: In COLUMBUS, an electronic wave function may be represented as a linear expansion in configuration state functions (CSF), $|\psi\rangle = \sum_{m=1}^{N_{\mathrm{CSF}}} x_m |\tilde{m}\rangle$, or as a linear expansion of GCFs, $|\psi\rangle = \sum_{P=1}^{N_{\mathrm{GCF}}} c_P |P\rangle$. Both representations are based on the Graphical Unitary Group Approach (GUGA). We have recently developed algorithms and initial computer codes to perform transformations between these two representations. The GCF to CSF transformation proceeds by computing the $x_m$ from the matrix-product state (MPS) expression with matrices of arc factors $\boldsymbol{\alpha}_{jk}^{P}$. A straightforward computation of the full set of CSF coefficients from a GCF expansion requires $\sim 2n\bar{f}^2 N_{\mathrm{CSF}} N_{\mathrm{GCF}}$ floating point operations where $\bar{f}$ is an average

facet count. A Depth-First Search (DFS) algorithm reuses intermediate arrays to eliminate redundant computations and reduces the total effort to only $O\left(\bar{f}^2 N_{\mathrm{CSF}} N_{\mathrm{GCF}}\right)$.

Two different algorithms have been developed for the CSF to GCF transformation. The first is based on the property that two GCFs may be merged together into a single GCF. This merge procedure is applied recursively, first on pairs of individual CSFs, then on these merged GCFs, and so on until the entire expansion is converted into a single GCF. An early merge convention was adopted that reduces the total storage requirements from $N_{\mathrm{CSF}}$ intermediate GCFs to only $\mathrm{floor}\left((\log_2(N_{\mathrm{CSF}}) + 1)\right)$ GCFs. The second algorithm is based on minimization of the least-squares error $\mathcal{E} = \sum_{m=1}^{N_{\mathrm{CSF}}} (x_m - y_m)^2$ with $x_m \equiv x_m(\boldsymbol{\alpha})$ with respect to the arc factors $\alpha_{j\mu,k\nu}^P$ and for the reference CSF coefficients $y_m$; this algorithm uses a DFS to make maximal reuse of intermediate quantities. The merge algorithm scales as $O\left(n\bar{f}^3 N_{\mathrm{CSF}}\right)$ while the least-squares optimization scales as $O\left(\bar{f}^2 N_{\mathrm{CSF}}\right)$ each iteration step.

These transformations will allow properties most easily computed with one wave function form to be applied to wave functions represented in the other form. The GCF form may also be used as a lossy data compression representation of the linear CSF expansion form.

**Mechanisms and Models for Simulating Gas Phase Chemical Reactivity: Raghu Sivaramakrishnan**

The scope of this program involves the development and analysis of detailed chemical kinetics mechanisms and models used for predictive simulations of gas phase reactivity in complex systems. Kinetics modeling has been used predominantly as an engineering tool for making predictions for practical applications in combustion and chemical conversions. However, within the context of the chemical physics BES program we have utilized a concerted Modeling-Experiment-Theory (MET) approach to further our understanding of the chemical kinetics of gas phase reactions.

**Recent Progress**

***Competition between Radical and Molecular Channels in Methylformate Dissociation***

Methylformate has received considerable attention in the combustion and kinetics community particularly over the past 15 years since the methylester functional group forms the backbone of the molecular structure of biodiesel fuel components. The thermal dissociation of this molecule has been characterized by numerous experimental and theoretical studies that all seem to agree that the lowest energetically accessible process is a 3-center H-atom transfer that leads to the molecular products $CH_3OH$ + CO. However, these literature studies seem to be at odds with regards to the role of other competing molecular elimination and bond-fission processes and therefore a complete and resolved mechanistic picture of methylformate thermal dissociation still eludes us. Methylformate is also a classic example where one might anticipate a strong competition between a lower-energy tight molecular elimination process and a higher energy direct bond-fission process, a common scenario typically encountered in high-temperature (or high energy) dissociations.

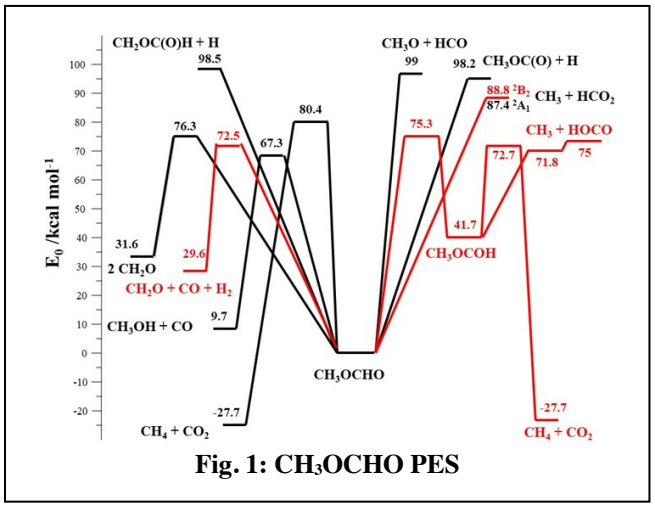


**Fig. 1: $CH_3OCHO$ PES**

In this work, we have performed high-level electronic structure theory calculations to characterize the energetics of other overlooked molecular and radical processes (red channels in Fig. 1) that can originate on this complex $CH_3OC(O)H$ potential energy surface (PES). The present

calculations do indeed confirm that the lowest energy process accessible on this PES is the molecular elimination to form $CH_3OH + CO$. However, unlike prior theoretical studies, the present calculations reveal that the second lowest energy process is a 5-center concerted elimination process that leads to the direct formation of $H_2 + CH_2O + CO$. We also find that the barrier for H-atom migration to form the carbene ($CH_3OC(OH)$) is similar to the direct 4-center elimination process leading to $CH_2O + CH_2O$ characterized in prior literature studies. Radical and molecular pathways to $CH_3 + HOCO$ and $CH_4 + CO_2$ can also be facilitated from the carbene, and they are all lower in energy than the other proposed molecular ($CH_4 + CO_2$) and bond-fission channels ($CH_3 + OCHO$) in the literature. Master equation calculations were performed to characterize the competition between these various molecular and radical processes on this more elaborate $CH_3OC(O)H$ PES. The results of the present theoretical analyses were used to resolve outstanding questions on the role of secondary radical-initiated reactions in characterizing prior literature experimental studies.

***Bimolecular Peroxy Radical Reactions Impact Ozone Initiated Oxidation of Hydrocarbons***

In collaboration with Klippenstein, we have initiated theory and modeling studies on the role of poorly characterized bimolecular peroxy radical reactions in auto-ignition and oxidation of hydrocarbons. Peroxy radicals + OH are a class of radical-radical reactions that are of current topical interest in atmospheric chemistry. Recent studies indicate that these are fast reactions at room temperature with potentially multiple competing product channels. Despite being such fast reactions, the lack of kinetics studies (rate constants and product branching) at higher temperatures has precluded the inclusion of this class of reactions in detailed kinetics models developed for combustion applications. In this work, kinetics simulations using such detailed kinetics models showed that the inclusion of $RO_2 + OH$ reaction significantly retards the auto-ignition delay predictions for $C_2H_6$ (Fig. 2) and dimethyl ether (DME) in the negative temperature coefficient (NTC) regime, and its relevance was more pronounced under $O_3$ enriched oxidation. Further analysis of the consumption pathway of the $RO_2$ radical revealed that $RO_2 + OH$ acts as a sink of OH radical at the early stage of $O_3$ enriched combustion. The $C_2H_6$ simulations revealed sensitivity to the $RO_2 + OH$ product branching ratios, while DME showed marginal sensitivity to the assumed product branching. This is attributed to the difference in the role of $HO_2$ in the low-temperature chemistry of each fuel. A parametric study was carried out to understand the relevance of $RO_2 + OH$ reactions under a broader range of conditions. It revealed that the inclusion of the $RO_2 + OH$ reaction is more important for simulations at the leaner fuel/air ratio or higher $O_3$ concentration. The relevance of the $RO_2 + OH$ reaction to the other small hydrocarbons ($CH_4$, $C_2H_4$, and $C_3H_8$) was smaller than for $C_2H_6$ and DME, and further study is required to understand the structural effects of the $RO_2 + OH$ class of reactions in auto-ignition and oxidation.

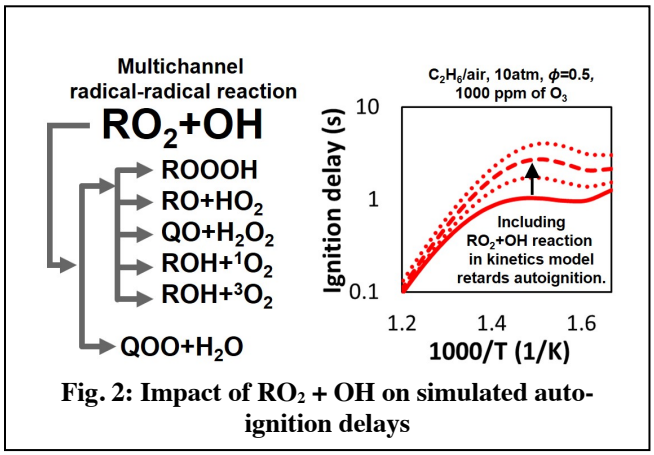


**Fig. 2: Impact of $RO_2 + OH$ on simulated auto-ignition delays**

***Exploration of chemical reactivity and spectroscopy using novel numerical analysis: Michael J. Davis***

This work involves the exploration of chemically reactive systems, including isolated chemical reactions and complex chemical-kinetics mechanisms, as well as molecular spectroscopy. The work relies on modern-day numerical analysis. The analysis is generally applicable, and we have been able to use it in work with other subtasks, as well as for projects outside our group.

**Recent Progress**

Work on fitting potential energy surfaces has continued. It is a collaboration with Jasper. The focus in the present year has been on improving the sampling technique, which is a combination of basis-set sampling and optimal experimental design. The program for optimal experimental design has been completed and we are improving the basis-set sampling portion of the procedure so that it can be scaled to larger molecular systems. In addition, initial explorations testing the use of unsupervised learning techniques have begun. Two projects have been completed on applying computational optimal transport to continuous molecular spectra, completing the fundamental investigations of its utility for comparing molecular spectra in a quantitative manner following the work in Refs. [13] and [19]. Based on past and current work, it was shown that computational optimal transport is a useful tool for tuning theoretical models of experimental spectra and for pattern recognition.

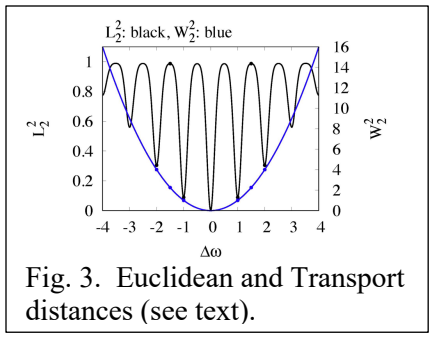

Fig. 3. Euclidean and Transport distances (see text).

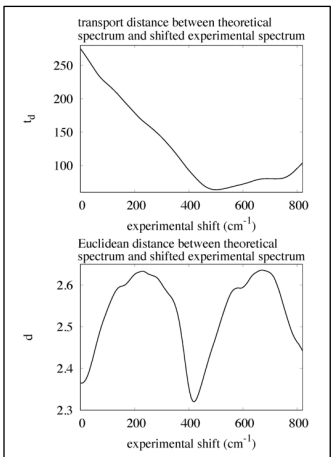

Fig. 4. See text.

The first completed project in the present period [27] demonstrated how optimal transport distances were superior to standard Euclidean distances for comparing two continuous spectra and developed the techniques to implement them. Figure 3 demonstrates the difficulty in using standard Euclidean distances. The oscillatory nature of most spectra means that a Euclidean distance measured between a spectrum and its translated versions will go through a set of local minima, as shown with the black curve in Fig. 3, whereas the optimal transport distance in blue has a well-defined minimum which is smoothly approached. A similar behavior is observed in Fig. 4 which compares displaced versions of an experimental electronic absorption spectrum of $SO_2$ with its theoretical estimate [27].

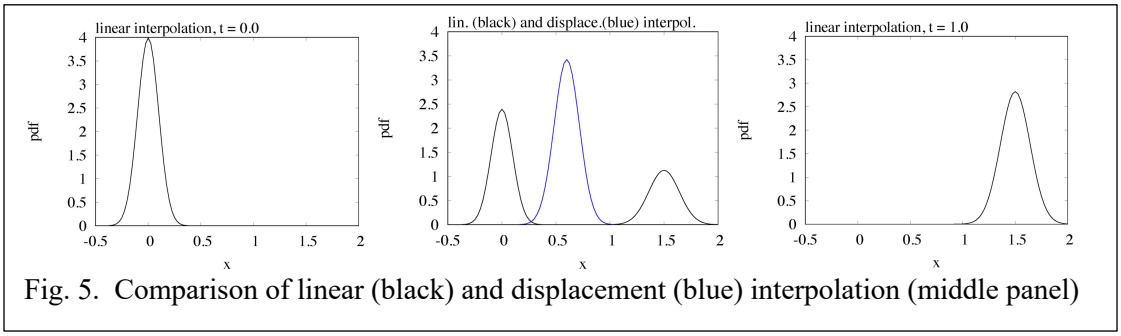

Fig. 5. Comparison of linear (black) and displacement (blue) interpolation (middle panel)

Optimal-transport geometry is fundamentally different than Euclidean geometry. In the middle panel of Fig. 5 the black curves show a linear combination of the two functions plotted on the end panels, whereas the optimal transport geometry leads to "displacement interpolation" shown with the blue curve [28]. Figure 6 shows a geodesic between two continuous molecular spectra extending the use of transport geometry in Fig. 5. Computational optimal transport is successful

because it uses a non-Euclidean geometry which is appropriate for probabilities and this geometry can be adapted to study geodesics for density matrices. These geodesics have been incorporated into an ongoing collaboration with Stephen Gray (CNM, ANL) on quantum information applications. A very simple test case was studied so far, two coupled two-level systems coupled to a resonator. Figure 7 shows the actual propagation (black) versus the geodesic (blue) between two density matrices for this system.

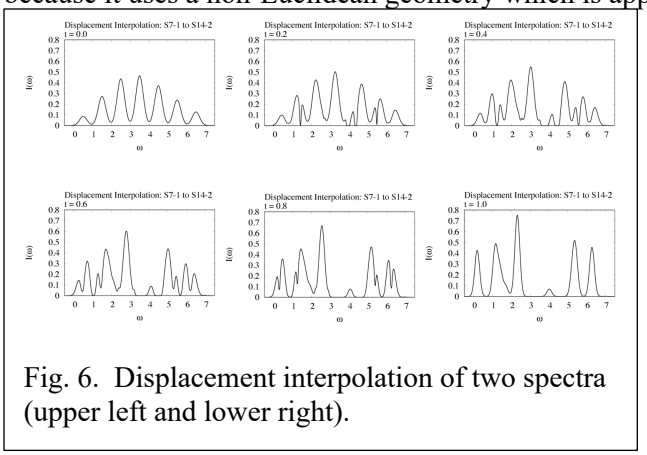


Fig. 6. Displacement interpolation of two spectra (upper left and lower right).

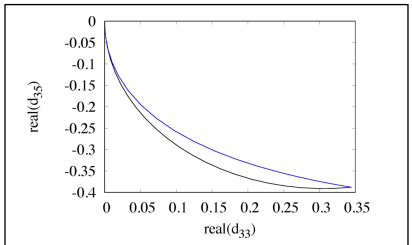


Fig. 7. Geodesic for a density matrix (blue) vs. dynamics.

**Future Plans**

We expect that the full implementation of unsupervised learning techniques will be undertaken in the potential energy fitting project. We plan on using greedy column subset selection to reduce the number of quantum chemistry calculations necessary for accurately fitting a potential energy surface. The work on computational optimal transport will continue. Geodesics in the optimal transport space will be used to design new basis functions. In the quantum-information project with Gray we will use the geodesic in a quantum control project connecting the two states on two ends of the optimal-transport geodesic with suitable laser pulses.

**Publications (2020-2023)**


1. H. Lischka, R. Shepard, T. Müller, P. G. Szalay, R. M. Pitzer, A. J. A. Aquino, M. M. A. do Nascimento, M. Barbatti, L. T. Belcher, J.-P. Blaudeau, I. Borges Jr., S. R. Brozell, E. A. Carter, A. Das, G. Gidofalvi, L. Gonzalez, W. L. Hase, G. Kedziora, M. Kertesz, F. Kossoski, F. B. C. Machado, S. Matsika, S. A. do Monte, D. Nachtigallova, R. Nieman, M. Oppel, C. A. Parish, F. Plasser, R. F. K. Spada, E. A. Stahlberg, E. Ventura, D. R. Yarkony, and Z. Zhang, "The Generality of the GUGA MRCI Approach in COLUMBUS for Treating Complex Quantum Chemistry", J. Chem. Phys. **152**, 134110 (2020). DOI: 10.1063/1.5144267.

2. R. Shepard, S. R. Brozell, J. Larson, P. Hovland, and S. Leyffer, "An Arc Density Maximum Flow Algorithm", 60th Sanibel Symposium Abstracts (2020).

3. R. Shepard, S. R. Brozell, and G. Gidofalvi, "Representations of Shavitt Graphs Within the Graphical Unitary Group Approach", J. Computational Chem. **41**, 129-135 (2020). DOI: 10.1002/jcc.26080.

4. J. B. Randazzo, R. Sivaramakrishnan, A. W. Jasper, T. Sikes, P. T. Lynch, R. S. Tranter, "An Experimental and Theoretical Study of the High Temperature Reactions of the Four Butyl Radical Isomers", Phys. Chem. Chem. Phys. **22** (2020) 18304-18319.

5. A. Mannodi-Kanakkithodi, M. Y. Toriyama, F. G. Sen, M. J. Davis, R. F. Klie, and M. K. Y. Chan, "Machine-Learned Impurity Level Prediction for Semiconductors: The Example of Cd-Based Chalcogenides", NPJ Comput. Mater. **6** (2020) Article No. 39, 14 pages.

6. R. Shepard, S. R. Brozell, J. Larson, P. Hovland, and S. Leyffer, "Wave Function Analysis with a Maximum Flow Algorithm", Mol. Phys. **119**, e1861351 (2021). DOI: 10.1080/00268976.2020.1861351.

7. S. R. Brozell and R. Shepard, "Edge Counts for the Auxiliary Pair Graph Within the Graphical Unitary Group Approach", Mol. Phys. **119**, e1950858 (2021). DOI: 10.1080/00268976.2021.1950858.

8. R. Sivaramakrishnan, J. R. Barker, "A Pioneer of Direct Measurements to Advance Modern Gas-Phase Chemical Kinetics", Editorial, Int. J. Chem. Kin. **53** (2021) 3-6.

9. T. Sikes, K. B. Burdett, R. L. Speth, C. F. Goldsmith, R. Sivaramakrishnan, R. S. Tranter, "Ring Opening in Cycloheptane and Dissociation of 1-heptene at High Temperatures", Proc. Combust. Inst. **38** (2021) 929.

10. D. P. Zaleski, R. Sivaramakrishnan, H. R. Weller, N. A. Seifert, D. H. Bross, B. Ruscic, K. B. Moore III, S. N. Elliott, A. V. Copan, L. B. Harding, S. J. Klippenstein, R. W. Field, K. Prozument, "Substitution Reactions in the Pyrolysis of Acetone Revealed through a Modeling, Experiment, Theory Paradigm", J. Am. Chem. Soc. **143** (2021) 3124-3142.
11. T. Sikes, R. Sivaramakrishnan, C. Banyon, R. A. Schwind, P. T. Lynch, A. Comandini, R. S. Tranter, "Initiation Reactions in the High Temperature Decomposition of Styrene", Phys. Chem. Chem. Phys. **23** (2021) 18432-18448.
12. D. R. Moberg, A. W. Jasper, and M. J. Davis. "Parsimonious Potential Energy Surface Using Dictionary Learning with Multipass Greedy Selection", J. Phys. Chem Lett. **12** (2021) 969-974.
13. N. A. Seifert, K. Prozument, and M. J. Davis, "Computational Optimal Transport for Molecular Spectra: The Fully Discrete Case", J. Chem. Phys. **155** (2021) 184101, 18 pages.
14. R. Shepard, "The Cosine-Sine Decomposition with Different-Orbitals-for-Different-Spins Determinants", Mol. Phys. (2022). DOI: 10.1080/00268976.2022.2077853.
15. R. F. K. Spada, M. P. Franco, R. Nieman, A. J. A. Aquino, R. Shepard, F. Plasser, and H. Lischka, "Spin-Density Calculation via the Graphical Unitary Group Approach", Mol. Phys. (2022). DOI: 10.1080/00268976.2022.2091049.
16. R. Shepard, "Some Comments on Different-Orbitals-for-Different-Spins Determinants," The 10th OpenMolcas Developers' Workshop Abstracts (2022).
https://enccs.github.io/openmolcas-2022/posters/
17. A. Al-Haddad, S, Oberli, J, González-Vázquez, M. Bucher, G. Doumy, P. Ho, J. Krzywinski, T. J. Lane, A. Lutman, A. Marinelli, T. J. Maxwell, S. Moeller, S. T. Pratt, D. Ray, R. Shepard, S. H. Southworth, Á. Vázquez-Mayagoitia, P. Walter, L. Young, A. Picón, and C. Bostedt, "Observation of Site-Selective Chemical Bond Changes via Ultrafast Chemical Shifts," *Nature Communications* (2022). DOI: 10.1038/s41467-022-34670-2.
18. C. L. Cortes, P. Lefebvre, N. Lauk, M. J. Davis, S. K. Gray, N. Sinclair, and D. Oblak,"Adaptive Calibration of Photon Indistinguishability in Quantum Networks Using Bayesian Optimization", Phys, Rev. Appl. **17** (2022) 034067, 17 pages
19. N. A. Seifert, K. Prozument, and M. J. Davis "Computational Optimal Transport for Molecular Spectra: The Semi-Discrete Case", J. Chem. Phys. **156** (2022) 134117, 16 pages.
20. R. Shepard, "The Efficient Conversion Between Linear Wave Function Expansions and Nonlinear Graphically Contracted Function Expansions," 62nd Sanibel Symposium Proceedings (2023). http://qtp.ufl.edu/sanibel/abstracts.html.
21. Giovanni Li Manni, R. Shepard, *et al*., "The OpenMolcas Web: A Community-Driven Approach to Advancing Computational Chemistry," *J. Chem. Theory Comput*., (*in press*) (2023).
22. Rosa Di Felice, Maricris L. Mayes, Ryan M. Richard, David B. Williams-Young, Garnet Kin-Lic Chan, Wibe A. de Jong, Niranjan Govind, Martin Head-Gordon, Matthew R. Hermes, Karol Kowalski, Xiaosong Li, Hans Lischka, Karl T. Mueller, Erdal Mutlu, Anders M.N. Niklasson, Mark R. Pederson, Bo Peng, Ron Shepard, Edward F. Valeev, Mark van Schilfgaarde, Bess Vlaisavljevich, Theresa L. Windus, Sotiris S. Xantheas, Xing Zhang, and Paul M. Zimmerman, "A Perspective on Sustainable Computational Chemistry Software Development and Integration," *J. Chem. Theory Comput*., (*submitted, 2023*).
23. R. Shepard, "The Efficient Conversion Between Linear Wave Function Expansions and Nonlinear Graphically Contracted Function Expansions," *Mol. Phys*. (*submitted, 2023*).
24. J. Cho, C. R. Mulvihill, S. J. Klippenstein, R. Sivaramakrishnan, "Bimolecular Peroxy Radical ($RO_2$) Reactions and Their Relevance in Radical Initiated Oxidation of Hydrocarbons," J. Phys. Chem. A 127 (2023) 300-315.
25. R. Sivaramakrishnan, N. J. Labbe, L. B. Harding, S. J. Klippenstein, "Molecular and Radical Channels in the High Temperature Decomposition of Methylformate", In Preparation, J. Phys. Chem. A (2023).
26. R. Sivaramakrishnan, A. W. Jasper, R. A. Shaik, P. T. Lynch, and R. S. Tranter, "Radical Chain Propagation Induced by Secondary Reactions in the Thermal Dissociation of $CH_2F_2$", In Preparation, (2023).
27. N. A. Seifert, K. Prozument, and M. J. Davis, "Computational Optimal Transport for Continuous Molecular Spectra with an Application to an Electronic Absorption Spectrum of $SO_2$", to be submitted (2023).
28. M. J. Davis, "Computational Optimal Transport for Continuous Molecular Spectra: Advanced Analysis", preprint (2023).

## Chemical Dynamics in the Gas Phase

## Thermochemistry Subtask

Branko Ruscic and Stephen J. Klippenstein
Chemical Sciences and Engineering Division, Argonne National Laboratory,
9700 South Cass Avenue, Lemont, IL 60439
ruscic@anl.gov, sjk@anl.gov

### Program Scope

The *spiritus movens* of the Thermochemistry Subtask of the Chemical Dynamics in the Gas Phase Program at Argonne is the need to provide the scientific community with accurate and reliable thermochemical information on chemical species that are relevant in energy-generating chemical processes or play prominent roles in subsequent environmental chemistry. Detailed knowledge of thermodynamic parameters for a broad array of stable and ephemeral chemical species is pivotal to chemistry and essential in many industries. In particular, the availability of accurate, reliable, and internally consistent thermochemical values is a *conditio sine qua non* in kinetics, reaction dynamics, formulation of plausible reaction mechanisms, and construction of predictive models of complex chemical environments. In addition, the availability of accurate thermochemical values has historically been the prime driver for steady improvements in fidelity of increasingly sophisticated electronic structure theories.

The focus of this program is on bringing substantial innovations to the thermochemical field through development of new methodologies, and utilizing them to systematically improve both the quality and quantity of available thermochemical data relevant to the DOE mission. In order to achieve the stated goals, this program has developed a novel approach that is centered on analyzing and optimally utilizing the information content of *all available* thermochemically relevant determinations, both from theory and experiments. The aim is not only to dynamically produce the best currently possible thermochemical parameters for the targeted chemical species, but also to allow efficient updates as new knowledge becomes available, properly propagating its consequences through all affected chemical species, as well as providing critical tests of new experimental or theoretical data and, when possible, generating pointers to new determinations that are most likely to efficiently improve the overall thermochemical knowledge base. In order to provide a broad perspective of this area of science, the effort of this Subtask is synergistically coordinated with related experimental and theoretical efforts within other Subtasks of the Chemical Dynamics in the Gas Phase Group at Argonne.

### Recent Progress

Over the past year we have continued the development of Active Thermochemical Tables (ATcT). The ATcT approach is the long-term centerpiece development of the Thermochemistry Subtask. The distinguishing feature of the ATcT approach is the capability of producing accurate, reliable, and internally consistent enthalpies of formation, which are arguably the central thermochemical quantities, for both stable and ephemeral chemical species. ATcT is currently capable of delivering the thermochemistry of species in a variety of aggregate states, including gas phase, condensed phases (both solids and liquids), aqueous solutions, and - as of recently - also species that are adsorbed on various substrates, such as catalysts. In general, thermochemically-relevant determinations (such as reaction enthalpies, equilibrium constants, bond dissociation energies, etc.) by definition involve several chemical species, and thus help define (within the limitations of the associated error bars) the enthalpy of formation of the target chemical species only *relative* to other reactants and products in the underlying chemical reaction. Consequently, enthalpies of formation generally do not correspond to directly measured quantities; rather, they are indirectly defined via complex manifolds of thermochemical dependencies. The extraction of enthalpies of formation from intertwined (and frequently mutually inconsistent) dependencies among multiple species was historically an intractable proposition, resulting in a simplified *sequential* approach of inferring the relevant quantities one at the time (A begets B, B begets C, etc.),

producing static sets of values that contain hidden progenitor-progeny relationships and cannot be updated with new knowledge without introducing new inconsistencies. In contrast, the ATcT approach relies on a unique paradigm that is rooted in assembling all relevant thermochemical determinations into complex Thermochemical Networks (TN). The TN effectively represent a set of qualified constrains that must be simultaneously satisfied to the maximum degree possible by the resulting thermochemistry. Categorizing the TN as a set of conditional constraints allows its detailed analysis using mathematical and statistical manipulations (enabling, for example, the isolation and remediation of internal inconsistencies). Once self-consistency is achieved across the TN, ATcT solves it simultaneously for the optimal enthalpies of formation of all included chemical species.

The most significant vehicle for disseminating the ATcT results is the ATcT website, ATcT.anl.gov. The website enjoys high popularity in the chemical community (steadily attracting 20,000 – 30,000 visitors each month) and continues to be hyped in the scientific literature as the most reliable source of accurate enthalpies of formation for species relevant in combustion and atmospheric chemistry, as well as other areas. Some time ago, DOE Office of Science (SC) has initiated a detailed scrutiny of ATcT as a potential SC Public Reusable Research (PuRe) Data Resource. The examination was very recently successfully completed, culminating in a public announcement of the prestigious designation for ATcT in late March 2023.[1-3] In order to ascend to this category, the candidate resource has to satisfy a set of stringent requirements,[4] such as being generally recognized by the scientific community as an authoritative provider of data, being publicly available and easily discoverable, maintaining detailed documentation on the provenance of data and providing adequate metadata, preserving strict versioning that maintains journal-like archival quality of published data, observing high standards for data management, curation, long-term preservation, etc. Pleasingly, the vast majority of these requirements were automatically satisfied by virtue of the original conceptual design of ATcT, allowing its ascension to SC PuRe status.

During the last year, we have publicly released three new versions of ATcT results, 1.122v, 1.122x, and 1.124. ATcT TN ver. 1.122v is an expansion of the previous version to include species relevant to the study of acetone pyrolysis (Zaleski et al.), ver. 1.122x was additionally expanded to include species relevant to the study of bond dissociation enthalpies of representative aromatic aldehydes (Ren et al.), and ver. 1.124 was essential in our recent study of thermophysical and thermochemical properties of $CH_2$ and $CH_3$ using nonrigid rotor anharmonic oscillator (NRRAO) partition functions (Ruscic and Bross), in the development and benchmarking of a state-of-the-art computational approach that aims to reproduce total atomization energies of small molecules within 10–15 $cm^{-1}$ (Thorpe et al.), as well as in the study of the reversible reaction $C_2H_3 + H_2 \rightleftarrows C_2H_4 + H \rightleftarrows C_2H_5$ (Nguyen et al.).

It should be noted that the latest public version contains nearly 2800 species, interconnected by > 30,000 determinations. The current developmental version of the TN (ver. 1.156, the ontogenesis of which is still in progress) has just surpassed 3100 species, for a growth of ~150 new species within the last year.

Besides publishing updated versions of results on the ATcT website and steadfastly expanding the developmental ATcT TN, we have also continued a broad range of collaborations that resulted in five peer-reviewed papers. A significant amount of collaboration involves researchers formally organized as the ATcT Task Force One (J. Stanton and T. L. Nguyen and their groups at UF, B. Ellison, UColorado, B. Changala, Harvard-Smithsonian, J. Baraban and his group at Ben-Gurion, and D. H. Bross, ANL). This Task Force continues to be very active, maintaining weekly teleconference meetings, and has a number of currently ongoing projects. In the past year, the collaborations within this group resulted in three papers.

One paper was a detailed high-level analysis of the mechanism, thermochemistry, and kinetics of the reversible reactions $C_2H_3 + H_2 \rightleftarrows C_2H_4 + H \rightleftarrows C_2H_5$, which play an important role in the combustion of hydrocarbons. In the set of radical/radical reactions leading to soot formation in flames, the addition of H-atoms to alkenes is likely a common reaction, triggering the isomerization of complex hydrocarbons to aromatics. The study resulted in a paper published in *Faraday Discussions* which combined state-of-the-art electronic structure computations (HEAT) with the ATcT approach, the latter also using - in addition to the TN analysis - fully corrected NRRAO thermophysical properties of all involved species.

A second paper, published in *J. Am. Chem. Soc.*, combined synchrotron-based photoelectron spectroscopy of cyclopropyl radical with state-of-the-art theoretical approaches and ATcT-based analyses, to study the ring-opening dynamics of cyclopropyl and of the corresponding cation. Cyclopropylium has an unusual transition-state nature. Thus, the related photoelectron spectrum of cyclopropyl radical is a rare example of directly accessing a transition state cation by photoionization of an ephemeral neutral species.

The third paper emanating from the ATcT Task Force One collaboration is a continuation of work on HF, CO, $N_2$, $H_2O$, that probed the current limits of state-of-the-art electronic structure methods, aiming to achieve uncertainties of the order of ± 8–15 $cm^{-1}$, and using very large basis sets (up to aug–cc–pV8Z, which were specifically constructed to enable these studies). Exploration and benchmarking of theoretical limits at this level of accuracy is possible only in conjunction with ATcT, which can provide total atomization enthalpies with uncertainties under ± 5 $cm^{-1}$. The collaboration resulted in a paper published in *Phys. Chem. Chem. Phys.* that uncovered a systematic error in previous high-level computations of the bond dissociation energy of CH, caused by ignoring the role of the rotational angular momentum in the spin-orbit coupling.

A second ATcT Task Force (K. Peterson, WSU and his group, and D. H. Bross, ANL, in collab. with G. Bacskay at U. Sidney) applied state-of-the-art electronic structure computations (FPD) in combination with the ATcT approach and existing experimental data to obtain accurate thermochemistry of 38 key bromides and iodides. Organic bromides and iodides are not only favorite precursors for generating by photolysis radicals for laboratory spectroscopic and kinetic studies, but are also of considerable wider interest because of their roles in atmospheric chemistry and in numerous industrially relevant processes as solvents, refrigerants, fire retardants, etc. However, their thermochemistry historically suffered from both experimental and theoretical inaccuracies. In particular, ab initio calculations involving heavier halogens are significantly more difficult not only on account of their larger number of electrons but also on account of the increasing importance of relativistic effects. This collaboration resulted in an extensive paper in *J. Phys. Chem A*, which was accompanied by ATcT-related cover art that depicts a portion of the ATcT TN.

In collaboration with D. H. Bross and the ECC project (led by J. Zador, Sandia CRF), we have continued exploring and further developing various approaches that would allow a sensible and accurate description of partition function-based thermophysical properties of adsorbates, focusing in particular on the modes responsible for diffusion on the surface and libration of the adsorbates, resulting in a paper in *ACS Catalysis*.

With respect to other activities within the Thermochemistry Subtask, our collaborative work with Curran (NUI Galway) exploring the thermochemistry of alkane oxidation came to fruition this year with the publication of five papers. The first paper focused on predictions of the 0 K heat of formation for a set of 194 alkane oxidation related species. This set includes alkanes and hydroperoxides, and alkyl, peroxy, and hydroperoxyalkyl radicals with up to 8 C atoms and varying degrees of branching. The challenge of obtaining high accuracy predictions for such large species was met by coupling the connectivity based hierarchical (CBH) scheme of Raghavachari with the ANL scheme for calculating energies. This CBH-ANL approach, automated in the AutoMech software suite, combines high level reference species energies (from ANL calculations) with chemistry conserving balanced chemical equations (from the CBH scheme) to obtain a high level of error cancellation. At the CBH2 level, the reference species contain up to five heavy atoms, exactly the size manageable by the ANL0 approach. For these reference species, the high-level ANL values are further refined with a novel laddering of the ANL0 and ANL1 values. The estimated uncertainty in our final CCSD(T)-F12/cc-pVTZ-F12/B2PLYP-D3/cc-pVTZ based predictions of $\Delta H_f$ (0 K) for the 194 alkane oxidation species is $2\sigma$ = 0.2–0.5 kcal $mol^{-1}$. Notably, predictions based on inexpensive ωB97X-D/cc-pVTZ reaction energies differ from these predictions by only −0.19 ± 0.74 kcal $mol^{-1}$, while those based on the doubly hybrid B2PLYP-D3/cc-pVTZ reaction energies differ by −0.04 ± 0.38 kcal $mol^{-1}$. This work was published in a virtual issue of J. Phys. Chem. A on *"Combustion in a Sustainable World: From Molecules to Processes.* It was selected as an ACS Editors Choice article, and the companion artwork was chosen for the cover of the Feb. 16, 2023 issue.

The second paper focused on a systematic procedure for evaluating the temperature dependent thermodynamic properties for the same set of hydrocarbons. The procedure, termed STAR-1D, combines conformer sampling to find the minimum geometry, B2PLYP-D3/cc-pVTZ harmonic frequency evaluations, and ωB97X-D/cc-pVTZ one-dimensional torsional mapping. It includes two physically-based scaling routines: a frequency-dependent scaling to B2PLYP-D3/cc-pVTZ anharmonic frequencies and a scaling of one-dimensional ωB97X-D/cc- pVTZ torsional profiles to reproduce the product of the B2PLYP-D3/cc-pVTZ frequencies in the harmonic limit. Substantive comparisons with existing experimental databases, together with careful examinations of key theoretical assumptions, were used to explore the accuracy of the predictions. These computationally intensive explorations of 195 species were facilitated by the AutoMech software suite.

The third and fourth papers were led by Curran and involved updates to their standard group theory methods for predicting thermochemical and thermodynamic parameters. A set of 58 group additivity values (GAV) for the calculation of the heat of formation, the entropy and the heat capacity were derived from fits to the CBH-ANL and STAR-1D values for our alkane oxidation set of species. The GAV and ab initio based 298 K enthalpies for this dataset show excellent agreement, with a 2σ deviation of 0.9 kcal $mol^{-1}$. The 2σ deviations in the GAV results relative to the STAR-1D data set are 2.4 cal $K^{-1}$ $mol^{-1}$ for the entropies and at most 2.0 cal $K^{-1}$ $mol^{-1}$ for the heat capacities in the temperature range 500–800 K. The 2σ deviations in the heat capacity gradually reduce at higher temperatures reaching a value of 0.8 cal $K^{-1}$ $mol^{-1}$ at 2000 K. Among the 58 GAV terms, 40 are refinements of previously reported terms, while 18 are newly developed. These new GAV terms are mainly non-next-nearest neighbor interactions (NNI) and β-corrections. The inclusion of these new groups significantly improves the accuracy of the GAV estimates of the thermochemistry. The updated GAVs provide increased confidence in estimates for the thermodynamic properties of combustion relevant hydrocarbons and oxygenated hydrocarbons and their corresponding radicals, which are important to predicting low-temperature chemistry.

The last paper explored the influence of thermochemistry on the reactivity of fuels at low temperatures (600–1000 K). Experimentally measured ignition delay times for propane, the pentane isomers, and n-heptane were simulated using NUIGMech1.2 and replacing the thermochemistry of the low temperature species with different sets of calculated values. Three different calculated sets were used, namely CCSD(T)-F12/TZ-F12//B2PLYP-D3/TZ///B2PLYP-D3/TZ (QM1), CCSD(T)-F12/TZ-F12//B2PLYP-D3/TZ///ωB97X-D/TZ (QM2) and B2PLYP-D3/TZ/ωB97X-D/6-31G*///ωB97X-D/6-31G* (QM3), while a fourth set consisted of the newly optimized group additivity (NGA) values.

## Future Plans

Future plans of this program pivot around further development and expansion of the Active Thermochemical Tables approach, continuing to provide accurate thermochemistry to the scientific community and driving targeted thermochemically-relevant theoretical and experimental investigations of radicals and transient species that are intimately related to chemical processes of relevance to the DOE mission. A significant part of the effort will be focused on continued 'finalization' and dissemination of the resulting ATcT thermochemistry, typically involving groups of related chemical species. One important component of this process, focused on their enthalpies of formation, consists of testing and analyzing the TN dependencies, using tools such as the variance/covariance decomposition approach and analyses of the influence of relevant determinations via the hat-matrix, followed by improving the connectivity within the TN and adding new high-quality results (either virtual, i.e. computational, or actual, i.e. experimental) to coerce the resulting thermochemistry toward stable, 'release quality' values. This iterative process unavoidably results in additional expansion of the TN with new related chemical species, which is an added benefit. Another equally important component focuses on enhancing the accuracy of the thermophysical properties derived from the partition functions, typically by upgrading RRHO partition functions to NRRAO partition functions, which is also a currently ongoing effort.

The ascension of ATcT to the DOE SC PuRe Resource status provides a strong additional impetus for steadfast curation, aggressive expansion, and unfaltering long-term stewardship and maintenance. It also

entails a careful evaluation of various suggestions proposed by users at large, as well as serious consideration of any and all requests for inclusion of particular additional species in ATcT. Thus, for example, we plan to expand the pages that provide additional details for each species with additional metadata that would further enhance discoverability via internet search engines, as well as an expansion of ATcT coverage to other interesting areas of chemistry (catalysis, energy storage, etc.)

Our theoretical thermochemistry work will continue with further developments and applications of the AutoMech code. This work will involve the expanded application of the CBH-2 schemes to additional sets of molecules, including molecules with other elements (e.g., N, S, and halogens), charges (e.g., cations), and molecular structures (e.g., kethohydroperoxides, polycyclic aromatic hydrocarbons, and $RO_xR$; x=2,3,4). We will also dig more deeply into the role of low frequency motions for the partition functions of large molecules such as large alkanes and bioesters. Finally, we will explore the utility of the databases we generate for machine learning based representations of the properties.

*This work is supported by the U.S. Department of Energy, Office of Basic Energy Sciences, Division of Chemical Sciences, Geosciences, and Biosciences, under Contract No. DE–AC02–06CH11357.*

**References**

[1] For the DOE announcement, see: https://www.energy.gov/science/articles/active-thermochemical-tables-atct-advance-chemistry-pure-data-resource

[2] Argonne press release: https://www.anl.gov/article/department-of-energy-recognizes-two-decades-worth-of-argonnes-highquality-thermochemical-data

[3] For a list of current PuRe Resources, see: https://science.osti.gov/Initiatives/PuRe-Data/Resources-at-a-Glance

[4] For DOE SC PuRe Resource requirements, see: https://science.osti.gov/Initiatives/PuRe-Data

## Publications resulting from DOE sponsored research (2020 – present)

- *Active Thermochemical Tables: Enthalpies of Formation of Bromo- and Iodo-Methanes, Ethenes and Ethynes*, D. H. Bross, G. B. Bacskay, K. A. Peterson, and B. Ruscic, *J. Phys. Chem. A* **127**, 704-723 (2023); DOI: 10.1021/acs.jpca.2c07897 (with cover art)
- *Sub 20 $cm^{-1}$ Computational Prediction of the CH Bond Energy – A Case of Systematic Error in Computational Thermochemistry*, J. H. Thorpe, D. Feller, D. H. Bross, B. Ruscic, and J. F. Stanton, *Phys. Chem. Chem. Phys.* **25**, Advance Article (2023); DOI: 10.1039/D2CP03964H (selected as *PCCP Hot Article*; also part of thematic issue: *Benchmark Experiments for Numerical Quantum Chemistry*)
- *High Accuracy Heats of Formation for Alkane Oxidation: From Small to Large via the CBH-ANL Method,* S. N. Elliott, M. Keçeli, M. K. Ghosh, K. P. Somers, H. J. Curran, and S. J. Klippenstein*, J. Phys. Chem. A* **127***,* 1512-1531 (2023); DOI: 10.1021/ac/jpca.2c07248 (with cover art, part of virtual issue *Combustion in a Sustainable World: From Molecules to Processes*; *ACS Editors' Choice Article*)
- *Systematically Derived Thermodynamic Properties for Alkane Oxidation*, S. N. Elliott, K. B. Moore III, A. V. Copan, Y. Georgievskii, M. Keceli, K. P. Somers, M. K. Ghosh, H. J. Curran, and S. J. Klippenstein, *Comb. Flame* 112487 (2023); DOI: 10.1016/j.combustflame.2022.112487 (*Jim Miller Memorial Issue*)
- *Group Additivity Values for Entropies and Heat Capacities of C2-C8 Alkanes, Alkyl Hydroperoxides, and their Radicals*, M. K. Ghosh, S. N. Elliott, K. P. Somers, S. J. Klippenstein, and Henry J. Curran*, Combust. Flame* 112706 (2023); DOI: 10.1016/j.combustflame.2023.112706
- *Ring-Opening Dynamics of the Cyclopropyl Radical and Cation: The Transition State Nature of the Cyclopropyl Cation*, N. Genossar, P. B. Changala, B. Gans, J.-C. Loison, S. Hartweg, M.-A. Martin-Drumel, G. A. Garcia, J. F. Stanton, B. Ruscic, and J. H. Baraban, *J. Am. Chem. Soc.* **144**, 18518-18525 (2022); DOI: 10.1021/jacs.2c07740
- *Configuration Space Integration for Adsorbate Partition Functions: The Effect of Anharmonicity on the Thermophysical Properties of CO–Pt(111) and $CH_3OH$–Cu(111)*, K. Blöndal, K. Sargsyan, D. H. Bross, B. Ruscic, and C. F. Goldsmith, *ACS Catalysis* **13**, 19-32 (2022); DOI: 10.1021/acscatal.2c04246
- *Mechanism, Thermochemistry, and Kinetics of the Reversible Reactions: $C_2H_3 + H_2 \rightleftarrows C_2H_4 + H \rightleftarrows C_2H_5$*, T. L. Nguyen, D. H. Bross, B. Ruscic, G. B. Ellison, and J. F. Stanton, *Faraday Discuss.* **238**, 405-430 (2022); DOI: 10.1039/D1FD00124H
- *Group Additivity Values for the Heat of Formation of C2-C8 Alkanes, Alkyl Hydroperoxides, and their*

*Radicals,* M. K. Ghosh, S. N. Elliott, K. P. Somers, S. J. Klippenstein, and H. J. Curran, *Combust. Flame* 112492 (2022); DOI: 10.1016/j.combustflame.2022.112492

- *Influence of Thermochemistry on the Reactivity of Propane, the Pentane Isomers, and n-Heptane in the Low Temperature Regime*, M. K. Ghosh, S. Panigraphy, S. Dong, S. N. Elliott, S. J. Klippenstein, and H. J. Curran, *Proc. Combust. Inst.* 39 *(in press)* (2022); DOI: 10.1016/j.proci.2022.08.086
- *Active Thermochemical Tables (ATcT) Enthalpies of Formation Based on Version 1.124 of the Thermochemical Network*, B. Ruscic and D. H. Bross, Argonne National Laboratory, Lemont, Ill. (2022), https://atct.anl.gov/Thermochemical%20Data/version%201.124/index.php; DOI: 10.17038/CSE/1885923
- *Active Thermochemical Tables (ATcT) Enthalpies of Formation Based on Version 1.122x of the Thermochemical Network*, B. Ruscic and D. H. Bross, Argonne National Laboratory, Lemont, Ill. (2022), https://atct.anl.gov/Thermochemical%20Data/version%201.122x/index.php; DOI: 10.17038/CSE/1885922
- *Active Thermochemical Tables (ATcT) Enthalpies of Formation Based on Version 1.122v of the Thermochemical Network*, B. Ruscic and D. H. Bross, Argonne National Laboratory, Lemont, Ill. (2022), https://atct.anl.gov/Thermochemical%20Data/version%201.122v/index.php; DOI: 10.17038/CSE/1885921
- *Elaborated Thermochemical Treatment of HF, CO, $N_2$, and $H_2O$: Insight into HEAT and Its Extensions*, J. H. Thorpe, J. L. Kilburn, D. Feller, P. B. Changala, D. H. Bross, B. Ruscic, and J. F. Stanton, *J. Chem. Phys.* **155**, 184109/1-13 (2021); DOI: 10.1063/5.0069322
- *Active Thermochemical Tables: The Thermophysical and Thermochemical Properties of Methyl, $CH_3$, and Methylene, $CH_2$, Corrected for Nonrigid Rotor and Anharmonic Oscillator Effects*, B. Ruscic and D. H. Bross, *Mol. Phys.* **119**, e1969046/1-17 (2021); DOI: 10.1080/00268976.2021.1969046 (*J. F. Stanton Festschrift*)
- *Active Thermochemical Tables (ATcT) Enthalpies of Formation Based on Version 1.122q of the Thermochemical Network*, B. Ruscic and D. H. Bross, Argonne National Laboratory, Lemont, Ill. (2021), https://atct.anl.gov/Thermochemical%20Data/version%201.122q/index.php; DOI: 10.17038/1821118
- *Active Thermochemical Tables (ATcT) Enthalpies of Formation Based on Version 1.122r of the Thermochemical Network*, B. Ruscic and D. H. Bross, Argonne National Laboratory, Lemont, Ill. (2021), https://atct.anl.gov/Thermochemical%20Data/version%201.122r/index.php; DOI: 10.17038/CSE/1822363
- *Reactions of $NO_3$ with Aromatic Aldehydes: Gas Phase Kinetics and Insights into the Mechanism of the Reaction*, Y. Ren, L. Zhou, A. Mellouki, V. Daële, M. Idir, S. S. Brown, B. Ruscic, R. S. Paton, M. R. McGillen, and A. R. Ravishankara, *Atmos. Chem. Phys.* **21**, 13537-13551 (2021); DOI: 10.5194/acp-21-13537-2021
- *Adsorbate Partition Functions via Phase Space Integration: Quantifying the Effect of Translational Anharmonicity on Thermodynamic Properties*, K. Blöndal, K. Sargsyan, D. H. Bross, B. Ruscic, and C. F. Goldsmith, *J. Phys. Chem. C* **125**, 20249-20260 (2021); DOI: 10.1021/acs.jpcc.1c04009
- *Substitution Reactions in the Pyrolysis of Acetone Revealed through a Modeling, Experiment, Theory Paradigm*, D. P. Zaleski, R. Sivaramakrishnan, H. R. Weller, N. A. Seifert, D. H. Bross, B. Ruscic, K. B. Moore III, S. N. Elliott, A. V. Copan, L. B. Harding, S. J. Klippenstein, R. W. Field, and K. Prozument, *J. Am. Chem. Soc.* **143**, 3124-3142 (2021); DOI: 10.1021/jacs.0c11677
- *Automated theoretical chemical kinetics: Predicting the kinetics for the initial stages of pyrolysis*, S.N. Elliott, K. B. Moore III, A. V. Copan, M. Keçeli, C. Cavallotti, Y. Georgievskii, H. F. Schaefer III, and S. J. Klippenstein, *Proc. Combust. Inst.* **38**, 375-384 (2021); DOI: 10.1016/j.proci.2020.06.019
- *Active Thermochemical Tables (ATcT) Enthalpies of Formation Based on Version 1.122p of the Thermochemical Network*, B. Ruscic and D. H. Bross, Argonne National Laboratory, Argonne, Ill. (2020); URL: https://atct.anl.gov/Thermochemical%20Data/version%201.112p/
- *Active Thermochemical Tables (ATcT) Enthalpies of Formation Based on Version 1.122o of the Thermochemical Network*, B. Ruscic and D. H. Bross, Argonne National Laboratory, Argonne, Ill. (2020); URL: https://atct.anl.gov/Thermochemical%20Data/version%201.112o/
- *Active Thermochemical Tables (ATcT) Enthalpies of Formation Based on Version 1.122n of the Thermochemical Network*, B. Ruscic and D. H. Bross, Argonne National Laboratory, Argonne, Ill. (2020); URL: https://atct.anl.gov/Thermochemical%20Data/version%201.112n/
- *Active Thermochemical Tables (ATcT) Enthalpies of Formation Based on Version 1.122h of the Thermochemical Network*, B. Ruscic and D. H. Bross, Argonne National Laboratory, Argonne, Ill. (2020); URL: https://atct.anl.gov/Thermochemical%20Data/version%201.112h/

## ARGONNE-SANDIA CONSORTIUM ON PRESSURE-DEPENDENT CHEMISTRY

Stephen J. Klippenstein, Ahren W. Jasper, Raghu Sivaramakrishnan, Robert S. Tranter
**Chemical Sciences and Engineering Division, Argonne National Laboratory, Lemont, IL, 60439*

Leonid Sheps, Craig A. Taatjes
*[#]Combustion Research Facility, MS 9055, Sandia National Laboratories Livermore, CA 94551-0969*
sjk@anl.gov; lsheps@sandia.gov

### Program Scope

This project explores fundamental aspects of collisional energy transfer and chemical kinetics with the goal of developing accurate models for gas-phase chemistry at the high pressures of practical devices. We design and implement novel experiments, theory, and modeling to probe high-pressure kinetics from elementary reactions to comprehensive chemical mechanisms. We focus on sensitive time-resolved experimental probes of reaction intermediates, which enable direct pressure-dependent studies of chemical systems of interest to DOE energy missions. We apply novel master equation and stochastic simulation methods to accurately predict the kinetics of key processes. The theoretical predictions and experimental observations are employed in high fidelity non-empirical chemical models for combustion processes, and, importantly, identifies departures from standard chemical kinetics assumptions. Recently, we have been pursuing detailed understandings of non-equilibrium effects and of radical oxidation chemistry. We are currently integrating modeling, experiment, and theory (MET) through feedback loops at all levels of chemical complexity for small alkanes, alcohols, and ethers (including cyclic variants) as key prototype fuels. The consortium expands and enhances collaborations between Argonne's Chemical Dynamics Group and the Gas-Phase Chemical Physics Group in Sandia's Combustion Research Facility.

### Recent Progress

***Nonstatistical kinetics in H + $HO_2$***: Quasiclassical trajectories (QCT) and global potential energy surfaces (PESs), constructed using new strategies, were used to compute thermal and nonthermal rate constants for the H + $HO_2$ reaction. The thermal QCT rate constants were up to 50% smaller than transition state theory (TST) rate constants due to inefficient intramolecular vibrational energy redistribution (IVR). A significant fraction of trajectories that reach the $H_2O_2$ well promptly dissociate back to reactants instead of via the heavily statistically favored 2OH channel. This effect increases with the vibrational energy of $HO_2$* such that nonthermal H + $HO_2$ rate constants depend inversely on the initial vibrational excitation of $HO_2$.

***PES Expansions:*** Two strategies for PES construction were developed. First, a method and a code for generating permutationally invariant polynomial (PIP) expansions for chemical systems of any stoichiometry were developed. Demonstrations were made for three categories of gas-phase dynamics and kinetics: collisional energy-transfer trajectories for predicting pressure-dependent kinetics, three-body collisions for describing transient van der Waals adducts relevant to atmospheric chemistry, and nonthermal reactivity via quasi-classical trajectories. The quality of the PIP expansions was demonstrated through the convergence of in-sample and out-of-sample errors with respect to both the number of training data and the order of the expansion, and these errors are shown to predict errors in the dynamics for both reactive and nonreactive applications. Then, a dictionary learning strategy for achieving linear scaling of the PES expansions with system size was demonstrated. Subsets of the full set of conventional basis functions were optimized using a newly developed multipass greedy regression method inspired by forward and backward selection methods from the statistics, signal processing, and machine learning literatures.

***Automated prompt effects in kinetic mechanisms:*** The importance of prompt dissociations in various reactive environments led us to develop a fully automated methodology for the calculation of prompt effects of a chosen species in a kinetic mechanism. This methodology, which takes full advantage of the AutoMech environment, includes (i) reaction selection; (ii) theoretical calculation of rate constants and prompt branching fractions; and (iii) final rate constant fitting. The energy partition between hot fragments can be estimated using a variety of statistical models, including a new physically sound microcanonical statistical model based on the rovibrational density of states of the fragments. The methodology was validated against

literature data for the prompt dissociations of HCO and $C_3H_7$ radicals. The microcanonical statistical model is in better agreement with trajectory simulations for larger species than the tradition thermal model and is thus applicable for practical systems that typically involve large molecules, for which direct dynamics calculations are impractical. The full automated workflow was demonstrated through a study of the effects of prompt dissociation for two isomeric radicals $C_4H_7$1-3 (1-methylallyl) and $C_4H_7$1-4 (3-buten-1-yl).

***Automated stereochemistry in kinetic mechanisms:*** Our study of the stereochemical aspects of diethyl ether (DEE) oxidation sparked our interest in better understanding the general effects of stereochemistry on chemical reactivity. To this end, we developed an automated methodology for adding stereochemical features to an existing mechanism. This effort (again taking full advantage of the AutoMech environment) scans the mechanism to enumerate all species with stereochemical sites, expands the reaction list to include all stereochemically related reactions, and reduces that list to remove degenerate reactions (e.g., ones that just differ at one chiral site). The automated rate prediction methodologies within AutoMech can then be used to populate the expanded mechanism with stereospecific reaction rates. The process of implementing this methodology led to the realization that SMILES and the available implementations of InChI's do not properly distinguish cis and trans versions of resonantly stabilized radicals. Notably, 9% of the species and 13% of the reactions in a pyrolysis mechanism from Galway have such incomplete InChIs. To account for this limitation, we developed a generalized form of InChIs, which we call the "AutoMech Chemical Identifier" (AMChI), as an integral part of the AutoMech suite.

***Roaming Radical Reactions (RRRs):*** We conducted a study of neopentanol decomposition using the high-repetition rate shock tube (HRRST) coupled to VUV photoionization (PIMS) mass spectrometry detection. Neopentanol is predicted to have two RRR with saddle points several kcal/mol lower than the lowest of three radical channel asymptotes. Preliminary laser schlieren experiments at P ~ 100 Torr indicate significant branching to the RRRs, yet the HRRST experiments at 1100-1400 K and P > 5.5 bar found no evidence of either methanol or isobutane, which are unique products of the RRRs. It was determined that dissociation occurs almost exclusively via C-C scission yielding tert-butyl and hydroxymethyl radicals, which rapidly eliminate H-atoms to give isobutene and formaldehyde. At similar temperatures and 1.1 bar a branching fraction of 0.2 to roaming was observed by Sivaramakrishnan *et al*. in neopentane. The possible structure- and pressure-dependent kinetics of RRRs will be further explored in future work.

**i$^2$PEPICO studies of PAH formation:** In collaboration with Comandini and Chaumeix (CNRS-Orleans), we have continued investigations of PAH (polyaromatic hydrocarbon) by HRRST/i$^2$PEPICO experiments at the SOLEIL synchrotron. Previous work on toluene pyrolysis was extended to a broader range of reaction conditions and studies of pyrolysis were conducted. From both studies mass spectra with identifiable peaks up to around m/z 450 were observed and repeating patterns in the mass spectra corresponding to the addition of various subunits (e.g., $C_2H_2$, $C_4H_2$, $C_6H_5$ etc.) followed by H-eliminations were identified. From both studies photoelectron spectra that contain features from many isomers and concentration/time profiles for stable and radical species were obtained. Theoretical photoelectron spectra for discrete isomers were calculated by Jasper and enabled simulating the experimental spectra. In Fig. 1 experimental concentration profiles, corrected for pressure changes during HRRST experiments by a new external calibration method, are compared with simulations using an unmodified chemical kinetic model for PAH formation (CNRS-ICARE model).

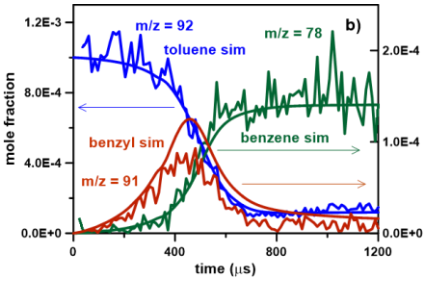


Figure 1. Concentration profiles for stable and radical species from HRRST/i$^2$PEPICO experiments with toluene. Smooth lines are simulations with CNRS-ICARE model for PAH growth from aromatics.

***Role of Collisional Energy Transfer in the Thermal and Prompt Dissociation of Allylic radicals:*** Prior studies in this program established that prompt dissociations are a universal feature of the thermal dissociation of radicals. It is important to understand the relevance of prompt dissociations to global observables (e.g., flame speeds) for various classes of radicals. We have characterized the thermal and

prompt dissociation of a series of allylic radicals in flame simulations, including their competition with corresponding radical-radical recombinations. We selected $C_3$ – $C_5$ allylic radicals: allyl ($C_3H_5$-A), 1-methylallyl (1MA), 2-methylallyl (2MA), 1,1-dimethylallyl (11DMA), 1,2-dimethylallyl (12DMA), and 1,3-dimethylallyl (13DMA). We compared the thermal dissociation rate coefficients ($k_{therm}$), where the dissociation kinetics of 11DMA/12DMA were determined from *ab initio* calculations. $k_{therm}$ was smallest for $C_3H_5$-A, followed by 2MA, and then 1MA, which is comparable to those for 11DMA, 12DMA, and 13DMA, revealing the sensitivity of $k_{therm}$ to methyl substitution. The non-equilibrium factor ($f_{ne}$), which correlates with a lower limit for the prompt dissociation, was sensitive to the dissociation energy and the molecular size, with 1MA, 11DMA, 12DMA, and 13DMA all exhibiting significant prompt dissociation at $T > 1500$ K. The thermal rate constants, $k_{therm}$, for the allylic radicals were used in flame simulations with a literature kinetics model, along with the competing allylic radical + H recombination kinetics from literature or the present *ab initio* calculations. The consumption pathway analysis revealed that the allylic radical dissociation closely competes with several radical-radical recombination reactions, including radical + H, O, OH, $O_2$, $HO_2$, HCO, $CH_3$ and the self-recombination reaction, which implies the importance of prompt dissociation for the secondary chemistry of allylic radicals.

In these studies, prompt dissociation was approximated by the $f_{ne}$ model which assumes an incipient thermal distribution for the radical for ease of application in practical kinetics models. However, as depicted in Fig. 2, these RSR's can be internally excited because of exothermic hydrogen abstractions. Therefore, a statistical model was developed to calculate the energy partitioning to the excited product radical from an incipient exothermic reaction. We also developed an automated strategy for calculating and implementing prompt dissociation of any radical in a detailed kinetics model. This automated workflow was applied to the 1-MA RSR as well as its non-resonant $C_4H_7$ isomer, 3-buten-1-yl. Simulations of 1-butene and 2-butene flames depicted a noticeable effect when including the increased prompt dissociation predicted by the statistical model. The statistical model is particularly suitable for accurate predictions of prompt dissociation in larger radicals and will be tested in proposed modeling studies aimed at understanding the growth of PAH's and other large molecules that rely on radical species as their building blocks.

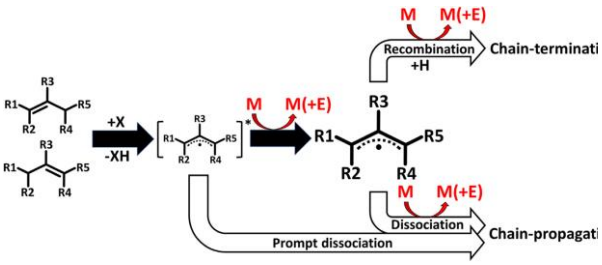

Figure 2: Dissociation and recombination of allylic radicals.

***Detailed time-resolved speciation measurements of hydrocarbon oxidation.*** We completed an experimental investigation of dimethyl ether (DME, $CH_3OCH_3$) oxidation. We measured the concentration-time profiles of DME, $CH_2O$, $RO_2$, $O_2QOOH$, methyl formate (MF), and hydroxymethyl formate (HPMF) via time-resolved photoionization mass spectrometry (PIMS) following Cl-initiated experiments at 10 bar and 450 – 575K. The reactive intermediates $RO_2$, $O_2QOOH$, and HPMF were characterized by PIMS and quantified using a global carbon balance method we recently introduced. A comparison of the experimental data to the predictions of three leading chemical models revealed consistent model deficiencies. We showed that the rate coefficients for $RO_2 \leftrightarrow$ QOOH and QOOH decomposition were significantly underestimated by literature mechanisms and demonstrated that a rapid OH + $RO_2$ reaction was likely the source of abundant MF, in contrast to model predictions, which assumed MF to come from $RO_2$ self-reaction.

We also performed a computational study of low-T cyclopentane oxidation, anchored by our time-resolved measurements of $RO_2$, $O_2QOOH$, and hydroperoxide intermediates, along with the major product cyclopentene (cy-$C_5H_8$), following photolytic initiation at 10 bar and 450 – 650 K. We ran detailed chemical simulations using a master-equation (ME) model of the primary R + $O_2$ + $O_2$ reactions, embedded in the LLNL cyclopentane combustion mechanism. By varying sensitive ME parameters via a genetic algorithm (GA) optimization loop, we determined the elementary rate coefficients with uncertainty estimates for the rate-limiting reactions $RO_2 \leftrightarrow$ γ-QOOH and $RO_2 \rightarrow$ cy-$C_5H_8$ + $HO_2$ from the final (optimized) ME parameter distributions. This study demonstrated the powerful pairing of highly detailed, quantitative

measurements of reactive intermediates with a flexible GA model optimization strategy.

We completed a multi-institution study of n-butane oxidation in jet-stirred and laser photolysis reactors, focusing on the decomposition of ketohydroperoxides (KHPs), which are formed from $O_2$QOOH. KHPs decompose to oxy-radical + OH or to carbonyl + carboxylic acid (the Korcek rearrangement), and the branching between these channels is critical to modeling combustion in the low-T and negative temperature coefficient (NTC) regime. The present study used isotopic labeling to quantify the products of the Korcek reaction and unambiguously link the timescale of their formation with that of KHP decay.

**Future Work:**

***Prompt Dissociations of Carbonyl Centered Radicals:*** We propose to continue our efforts to explore the relevance of prompt dissociation for different classes of radicals. Our completed prompt dissociation studies on RSR's led us to revisit the validity of the proposed criteria for the relevance of prompt dissociation in practical simulations. Our analysis suggests that the criteria should be expanded to also include, "The production rate of the radical should be sufficiently large". For example, in a flame simulation at any given stoichiometry the production rate of the corresponding fuel radical/radicals (i.e., those radicals produced by hydrogen abstraction from the fuel) decreases with increasing fuel molecular size. Imposing this additional constraint suggests that prompt dissociations of smaller radicals, i.e., those with 3-4 heavy atoms (C, N, O atoms) should be more relevant, at least in standard fuel-air flames. Some promising candidates are HOCO, $CH_3CO$, $C_2H_5CO$, $CH_3OC(O)$, HC(O)C(O), and $CH_3C(O)C(O)$, with these radicals formed by H-abstraction from formic acid, acetaldehyde, propanal, methyl formate, glyoxal, and methylglyoxal respectively. These radicals are expected to satisfy some of the proposed criteria; viz., being the right molecular size and with appropriate dissociation thresholds. Of course, kinetics simulations are required to gauge their production rates and competition with other reactions.

***HRRST****:* We will continue to explore the dissociation of neopentanol by reducing the reaction pressure to below 1bar, i.e., similar to the prior study on neopentane where a strong roaming channel was identified in H-ARAS experiments. Based on our low-pressure studies we expect to identify conditions where RRRs become important. We intend to continue work on the pyrolysis of aromatics and PAH formation. In particular, the HRRST/i$^2$PEPICO experiments will expand to include blends of reagents e.g., toluene/ethyl benzene + propene to examine synergistic effects on the isomer distributions in PAH growth. These may be important in practical systems where multiple reagents are present.

***AutoMech development*****:** The AutoMech code now allows us to implement two key advances (full stereochemical treatment and automated prompt dissociation branching) beyond what are generally included in traditional modeling studies. A variety of large-scale applications to both radical oxidation and pyrolysis systems are now planned. For radical oxidation, the inclusion of proper stereochemical restrictions within automated rate predictions will be particularly important for explorations of the third $O_2$ addition, where there will be multiple chiral centers. It will also be important in pyrolysis modeling, where cis and trans isomers can have quite different kinetic behavior. We will also incorporate the newly completed automated prompt dissociation methodology within global uncertainty and sensitivity analyses, which should provide novel opportunities for exploring and optimizing this key aspect of the dynamics.

***Pressure Dependent Branching and Improved Collision Kernels:*** It is of general importance to understand product branching, as competing products can feature different chemical reactivities with important ramifications for global chemical behavior. For example, HOCO can be formed as a transient intermediate, and its subsequent product branching via unimolecular dissociation to H + $CO_2$ or OH + CO can influence global properties. While these two channels have similar classical thresholds, the H + $CO_2$ channel features significant tunneling, whereas the OH + CO does not. This leads to branching that is sensitive to both the energy *E* and angular momentum *J* of the system. Furthermore, the low-pressure limit is sometimes defined as the limit where all activating collisions are reactive. The presence of tunneling confuses this limit, as "bound" states can react via tunneling, the tunneling rates depend on *E* and *J*, and this low-pressure limit is only reached at extremely low pressures. We will demonstrate that predicting accurate pressure-dependent

reactivity for this case requires the 2DME, which includes explicit consideration of both *E* and *J*.

***Stochastic Dynamics***: We propose to use a stochastic master equation strategy involving the sampling of gas phase events enabled by Argonne's high-performance computing resources to study nonthermal systems, quantify and improve our 2DME collision kernel, characterize the influence of collisions on threshold reactivity of multi-channel systems, and study the reactivity of transient van der Waals complexes at high pressures.

***Molecular structure and pressure-dependent hydrocarbon oxidation reactions.*** We will build on our recent success in quantifying reactive intermediates in cyclopentane and DME oxidation by measuring the kinetics of the main chain-branching pathways of diethyl ether, neopentane, and tetrahydrofuran over a broad T and P range. These experiments will also employ a new complementary capability for quantitative OH and $HO_2$ detection via a high-pressure Fluorescence Assay by Gas Expansion (FAGE) apparatus. The FAGE measurements will provide additional experimental constraints on chemical model development by discriminating among OH-forming and $HO_2$-forming pathways from $O_2QOOH$ in cases when mass spectrometric detection cannot distinguish the hydroperoxide co-products of OH and $HO_2$.

DEE, neopentane, and THF differ from cyclopentane and DME in the size and shape (branched vs. linear or cyclic) molecular backbone. The energetic barriers of individual reaction channels and the overall exothermicity of the $R + O_2 + O_2$ reaction in these systems vary substantially, leading to distinct product branching, temperature- and pressure-dependent kinetics, and the degree of non-thermal reactions (i.e., reactions of activated intermediates before collisional stabilization). We will characterize the detailed kinetics of the competing reaction channels in all three systems and compare them to detailed theoretical predictions, performed as part of the theory and modeling efforts under this program.

## Publications acknowledging support from this program, 2020-Present


1. **An Experimental and Theoretical Study of the High Temperature Reactions of Four Butyl Radical Isomers**, J. B. Randazzo, A. W. Jasper, R. Sivaramakrishnan, T. Sikes, P. T. Lynch, R. S. Tranter, *Phys. Chem. Chem. Phys.* **22**, 18304-18319 (2020).
2. **Direct Time-Resolved Detection and Quantification of Key Reactive Intermediates in Diethyl Ether Oxidation at T = 450 – 600 K**, M. Demireva, K. Au, L. Sheps, *Phys. Chem. Chem. Phys.* **22**, 24649-24661 (2020).
3. **Low Temperature Oxidation of Diethyl Ether: Reactions of Hot Radicals Across Coupled Potential Energy Surfaces**, A. D. Danilack, S. J. Klippenstein, Y. Georgievskii, C. F. Goldsmith, *Proc. Combust. Inst.* **38**, 671-679 (2020).
4. **Solenoid Actuated Driver Valve for High Repetition Rate Shock Tubes**, R. S. Tranter, T. Sikes, *Rev. Sci. Instrum.* **91**, 056101 (2020).
5. **Termolecular Chemistry Facilitated by Radical-Radical Recombinations and Its Impact on Flame Speed Predictions**, Y. Tao, A. W. Jasper, Y. Georgievskii, S. J. Klippenstein, R. Sivaramakrishnan, *Proc. Combust. Inst.* **38**, 515-522 (2021).
6. **"Third-Body" Collision Parameters for Hydrocarbons, Alcohols, and Peroxides and an Effective Internal Rotor Approach for Estimating Them**, A. W. Jasper, *Int. J. Chem. Kinet.* **52**, 387-402 (2020).
7. **Combustion Chemistry in the Twenty-First Century: Developing Theory-Informed Chemical Kinetics Models**, J. A. Miller, R. Sivaramakrishnan, Y. Tao, C. F. Goldsmith, M. P. Burke, A. W. Jasper, N. Hansen, N. J. Labbe, P. Glarborg, J. Zádor, *Prog. Energy Combust. Sci.* **83**, 100886 (2021).
8. **Reaction Mechanisms of a Cyclic Ether Intermediate: Ethyloxirane**. M. G. Christianson, A. C. Doner, M. M. Davis, A. L. Koritzke, J. M. Turney, H. F. Schaefer III, L. Sheps, D. L. Osborn, C. A. Taatjes, B. Rotavera, *Int. J. Chem. Kinet.* **53**, 43-59 (2021).
9. **Isomer-Dependent Reaction Mechanisms of Cyclic Ether Intermediates: Cis-2,3-dimethyloxirane and Trans-2,3-dimethyloxiran**e. A. C. Doner, M. M. Davis, A. L. Koritzke, M. G. Christianson, J. M. Turney, H. F. Schaefer III, L. Sheps, D. L. Osborn, C. A. Taatjes, B. Rotavera, *Int. J. Chem. Kinet.* **53**, 127-145 (2021).
10. **Reactions of Propyl Radicals: A Shock Tube–VUV Photoionization Mass Spectrometry Study** C. K. Banyon, T. Sikes, R. S. Tranter, *Combust. Flame*, **224**, 14-23 (2021).
11. **Temporally and Spatially Resolved X-Ray Densitometry in a Shock Tube**, R. A. Shaik, A. L. Kastengren, R. S. Tranter, P. T. Lynch, *Combust. Flame* **224**, 136-149 (2021).
12. **Pyrolysis of Ethanol Studied in a New High-Repetition-Rate Shock Tube Coupled to Synchrotron-Based Double Imaging Photoelectron/Photoion Coincidence Spectroscopy**, S. Nagaraju, R. S. Tranter, F. E. Cano Ardila, S. Abida, P. T. Lynch, G. A. Garcia, J. F. Gil, L. Nahon, N. Chaumeix, A. Comandini, *Combust. Flame* **226**, 53-68 (2021).
13. **Substitution Reactions in the Pyrolysis of Acetone Revealed through a Modeling, Experiment, Theory Paradigm,** D. P. Zaleski, R. Sivaramakrishnan, H. R. Weller, N. A. Seifert, D. H. Bross, B. Ruscic, K. B. Moore III, S. N. Elliott, A. V. Copan, L. B. Harding, S. J. Klippenstein, R. W. Field, K. Prozument, *J. Am. Chem. Soc.* **143**, 3124-3142 (2021).

14. **Entanglement Effect and Angular Momentum Conservation in a Non-separable Tunneling Treatment**, Y. Georgievskii, S. J. Klippenstein, *J. Chem. Theo. Comp.* **17**, 3863-3885 (2021).
15. **Diastereomers and Low-Temperature Oxidation**, A. D. Danilack, C. R. Mulvihill, S. J. Klippenstein, C. F. Goldsmith, *J. Phys. Chem. A*, **125**, 8064-8073 (2021).
16. **Non-Boltzmann Effects in Chain Branching** a**nd Pathway Branching for Diethyl Ether Oxidation**, C. R. Mulvihill, A. D. Danilack, C. F. Goldsmith, M. Demireva, L. Sheps, Y. Georgievskii, S. N. Elliott, S. J. Klippenstein, *Energy Fuels*, **35**, 17890-17908 (2021).
17. **Initation Reactions in the High Temperature Decomposition of Styrene,** T. Sikes, C. Banyon. R. A. Schwind, P. T. Lynch, A. Comandini, R. Sivaramakrishnan, R. S. Tranter, *Phys. Chem. Chem. Phys*. **23**, 18432-18448 (2021).
18. **The Impact of the Third $O_2$ Addition Reaction Network on Ignition Delay Times of Neo-Pentane.** N. Hansen, G.Kukkadapu, B. Chen, S. Dong, H. Curran, C. A. Taatjes, A. Eskola, D. Osborn, L. Sheps, W. Pitz, *Proc. Comb. Inst.* **38**, 299-307 (2021).
19. **Quantitative Detection of Products and Radical Intermediates in Low-Temperature Oxidation of Cyclopentane.** L. Sheps, A. L. Dewyer, M. Demireva, J. Zádor, *J. Phys. Chem. A **125***, 4467-4479 (2021).
20. **High Pressure, High Flow Rate Batch Mixing Apparatus for High Throughput Experiments,** A. Dalmiya, J. M. Mehta, R. S. Tranter, P. T. Lynch, *Rev. Sci. Instrum.* **92**, 114104 (2021).
21. **Parsimonious Potential Energy Surface Expansions using Dictionary Learning with Multi-Pass Greedy Selection**, D. R. Moberg, A. W. Jasper, and M. J. Davis, *J. Phys. Chem. Lett*. **12**, 9169–9174 (2021).
22. **Watching a Hydroperoxyalkyl Radical (•QOOH) Dissociate**, A. S. Hansen, T. Bhagde, K. B. Moore III, D. R. Moberg, A. W. Jasper, Y. Georgievskii, M. F. Vansco, S. J. Klippenstein, and M. I. Lester, *Science* **373**, 679-682 (2021).
23. **Permutationally Invariant Polynomial Expansions with Unrestricted Complexity**, D. R. Moberg and A. W. Jasper, *J. Chem. Theory Comput*. **17**, 5440–5455 (2021).
24. **Bayesian Model Calibration for Vacuum-Ultraviolet Photoionisation Mass Spectrometry**, J. Oreluk, L. Sheps, H. Najm, *Comb. Theo. Mod.* **26,** 513-540 (2022).
25. **Methanol Oxidation up to 100 Atm in a Supercritical Pressure Jet-Stirred Reactor,** Z. Wang, H. Zhao, C. Yan, Y. Lin, A. D. Lele, W. Xu, B. Rotavera, A. W. Jasper, S. J. Klippenstein, Y. Ju, *Proc. Combust. Inst.* **39**, (2022). **DOI:** 10.1016/j.proci.2022.07.068
26. **The Role of Collisional Energy Transfer in the Thermal and Prompt Dissociation of 1-Methylallyl**, J. Cho, Y. Tao, Y. Georgievskii, S. J. Klippenstein, A. W. Jasper, R. Sivaramakrishnan, *Proc. Combust. Inst.* **39**, (2022). **DOI**: 10.1016/j.proci.2022.07.155
27. **Formation of Organic Acids and Carbonyl Compounds in n-Butane Oxidation via γ-Ketohydroperoxide Decomposition**. D. M. Popolan-Vaida, A. J. Eskola, B. Rotavera, J. F. Lockyear, Z. Wang, S. M. Sarathy, R. L. Caravan, J. Zádor, L. Sheps, A. Lucassen, K. Moshammer, P. Dagaut, D. L. Osborn, N. Hansen, S. R. Leone, C. A. Taatjes, *Angew. Chem. Int. Ed.* **61,** e202209168 (2022).
28. **Quantification of Key Peroxy and Hydroperoxide Intermediates in the Low-Temperature Oxidation of Dimethyl Ether**. D. E. Couch, C. R. Mulvihill, R. Sivaramakrishnan, K. Au, C. A. Taatjes L. Sheps, *J. Phys. Chem. A* **126**, 9497-9509 (2022).
29. **Bimolecular Peroxy Radical ($RO_2$) Reactions and Their Relevance in Radical Initiated Oxidation of Hydrocarbons,** J. Cho, C. R. Mulvihill, S. J. Klippenstein, R. Sivaramakrishnan**,** *J. Phys. Chem. A* **127**, 300-315 (2022).
30. **Inefficient Intramolecular Vibrational Energy Redistribution for the H + $HO_2$ Reaction and Negative Internal Energy Dependence for its Rate Constant,** A. W. Jasper, D. R. Moberg, Y. Tao, S. J. Klippenstein, R. Sivaramakrishnan, *Front. Phys.* **10**, 1003010 (2022).
31. **Low- and Intermediate-Temperature Oxidation of Dimethyl Ether up to 100 atm in a Supercritical Pressure Jet-Stirred Reactor,** C. Yan, H. Zhao, Z. Wang, G. Song, Y. Lin, C. R. Mulvihill, A. W. Jasper, S. J. Klippenstein, Y. Ju**,** *Combust. Flame*, **236**, 112059 (2022).
32. **$HO_2$ + $HO_2$: High Level Theory and the Role of Singlet Channels**, S. J. Klippenstein, R. Sivaramakrishnan, U. Burke, K. P. Somers, H. J. Curran, L. Cai, H. Pitsch, M. Pelucchi, T. Faravelli, P. Glarborg, *Comb. Flame* **243**, 111975 (2022).
33. **Effects of Non-thermal Termolecular Reactions on Detonation Development in Hydrogen ($H_2$)/Methane ($CH_4$) - Air Mixtures** S. S. Desai, Y. Tao, R. Sivaramakrishnan, Y. Wu, T. F. Lu, J. H. Chen, *Combust. Flame* **244**, 112277 (2022).
34. **The Role of Energy Transfer and Competing Bimolecular Reactions in Characterizing the Unimolecular Dissociations of Allylic Radicals**, J. Cho, A. W. Jasper, Y. Georgievskii, S. J. Klippenstein, R. Sivaramakrishnan**,** *Combust. Flame*, 112502 (2022). **DOI**: 1016/j.combustflame.2022.112502
35. **Genetic Algorithm Optimization of a Master Equation Cyclopentane Oxidation Model against Time-Resolved Speciation Experiments**. M. Demireva, J. Oreluk, A. L. Dewyer, J. Zádor, L. Sheps, *Combust. Flame*, 112506 (2022). **DOI**: 10.1016/j.combustflame.2022.112506
36. **Automated Identification and Calculation of Prompt Effects in Kinetic Mechanisms using Statistical Models**, L. Pratali Maffei, K. B. Moore III, Y. Georgievskii, C. R. Mulvihill, S. N. Elliott, J. Cho, R. Sivaramakrishnan, T. Faravelli, S. J. Klippenstein, *Combust. Flame*, 112422 (2022). **DOI**: 1016/j.combustflame.2022.112422
37. **High-Temperature Dissociation of Neopentanol: Shock Tube Photoionization Mass Spectrometry Studies**, C. Banyon, R. S. Tranter, *J. Phys. Chem. A* 127, 1293–1301 (2023).
38. **Effect of Non-thermal Termolecular Reactions on Wedge-induced Oblique Detonation Waves,** S. S. Desai, Y. Tao, S. R. Sivaramakrishnan, J. H. Chen, *Combust. Flame*, 112681 (2023). **DOI**: 10.1016/j.combustflame.2023.112681

# Chemical Kinetic Data of Benchmark Accuracy through Multi-Scale Informatics Strategies

Michael P. Burke

*Department of Mechanical Engineering, Department of Chemical Engineering, & Data Science Institute*
*Columbia University, New York, NY 10027*
*mpburke@columbia.edu*

## Program Scope

The reliability of predictive simulations for advanced energy conversion devices depends on the availability of accurate data for thermochemistry, chemical kinetics, and transport. In that regard, accurate data are critically important for both their direct use in predictive simulations and for benchmarking improved theoretical methodologies that can similarly produce accurate data for predictive simulations. The use of informatics-based strategies for the determination of accurate thermochemical data with well-defined uncertainties, i.e. the Active Thermochemical Tables (ATcT),[1] has revolutionized the field of thermochemistry – ATcT provides thermochemical data of unprecedented accuracy for direct use in predictive simulation and has served as a key enabler of *ab initio* electronic structure methodologies of equally impressive accuracy. In this program, we are developing an analogous active database for *chemical kinetics* to establish high-accuracy kinetic data for predictive simulation and to evaluate emerging *ab initio*-based theoretical kinetics methods, using novel multiscale informatics strategies we are developing. Particular emphasis is placed on reaction systems for which non-thermal kinetic sequences arise and for which combining theoretical and experimental data is necessary to unravel complex reaction data into chemical information, where this program advances the state of the art in computational methodologies for those purposes.

## Recent Progress

There are several significant challenges in deriving high-accuracy kinetic data of relevance to the complex reactions encountered in combustion, planetary atmospheres, and interstellar environments. First, even the most "direct" experimental rate constant determinations are often influenced by uncertainties in secondary reactions – leading to a complex web of interdependences among kinetic parameters for many reactions (and an opportunity to gain more information than has been attained previously, since uncertainties are seldom at the noise floor of the measurements). Second, there is rarely enough experimental data to constrain the full temperature, pressure, and composition (*T*/*P*/$\underline{X}$) dependence of many rate constants – rendering usual rate-parameter-based uncertainty quantification approaches ineffective. Third, many reactions of interest to various application domains and gas-phase theoretical chemistry involve non-thermal kinetic sequences[2-3,iii] – posing an additional problem for rate-parameter-based approaches.

During the past several years, we have been developing a multi-scale uncertainty quantification approach, MultiScale Informatics (MSI),[4,i,ii,iv,viii] to address the challenges involved in 1) unraveling the complex web of interdependences among reactions in complex systems data (by reinterpreting the raw data from multi-reaction systems used to determine rate constants experimentally), 2) sufficiently constraining the *T*/*P*/$\underline{X}$ dependence of rate constants (by incorporating theoretical calculations to extrapolate constraints imposed by limited data), and 3) analyzing data from reaction systems involving non-thermal kinetic sequences (by leveraging the physics-based framework to account for such processes). In this program, we are applying and expanding MSI to develop a high-accuracy kinetics database through carefully chosen reaction systems that serve to both anchor the database and grow it in ways leveraging its anchored foundations – while addressing outstanding scientific questions and identifying new ones.

*$HO_2$ + $HO_2$ = products*. We have now published[viii] our analysis of the $HO_2$ + $HO_2$ reaction, for which recent high-level theoretical calculations[5] predicted a mild temperature dependence inconsistent with state-of-the-art experimental determinations[6] that upheld the stronger temperature dependence observed in early experiments. Notably, our analysis identified an alternative interpretation of the raw experimental data that uses $HO_2$ + $HO_2$ rate constants nearly identical to theoretical predictions – implying that the theoretical and experimental data are actually consistent, at least when considering the *raw* experimental data. Similar analyses of typical signals from low-temperature experiments indicated that an HOOOOH intermediate – identified by recent theory but absent from earlier interpretations – yields modest effects that are smaller than, but may have contributed to, the scatter in data among different experiments.

*$H + O_2 = O + OH$, $OH + H_2 = H_2O + H$, $O + H_2 = OH + O$, $H + HO_2$ = products, TBHP fragment kinetics, $CH_2O$ kinetics, and other reaction systems.* We have been conducting a massive simultaneous analysis of several hundred (raw) experimental and theoretical datasets spanning many dozens of reactions in order to unravel their dauntingly complex web of interdependences. The goals of this endeavor are to properly anchor the active network and to determine refined values for their rate constants and uncertainties (including for the first three reactions listed above, whose rate constants are generally well known but still hindered by uncertainties in the other reactions listed above). For example, our uncertainty-weighted sensitivity analysis for data used to determine rate constants for OH + $H_2$ indicate strong influences from several reactions involving the decomposition fragments from the common OH-precursor tert-butylhydroperoxide (TBHP) including $CH_3$ + $CH_3$, $CH_3$ + OH, and OH + $CH_3COCH_3$. The overall analysis has already yielded insights into rate constants, and discrepancies among data, for many reactions (only some of which are presented here as examples).

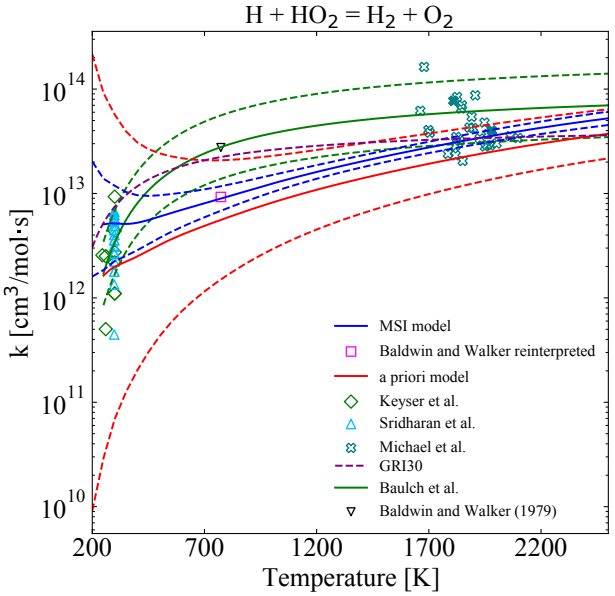

Fig. 1. Rate constants for H + $HO_2$ = $H_2$ + $O_2$ (R1).

The results shown in Figs. 1-3 demonstrate how decades of errors due to neglecting the inherent correlations among rate constant determinations propagate into even the most precise determinations of the most precisely characterized reaction (H + $O_2$ = O + OH, Fig. 3). For quite some time, the only rate constant determinations for H + $HO_2$ = $H_2$ + $O_2$ (R1) above atmospheric temperatures were at 773 K. Namely, Baldwin and Walker[7] derived a $k_1$ value (shown in the triangle symbol shown in Fig. 1) from their measured ratio of rate constants for R1, H + $O_2$ = O + OH (R2), and $HO_2$ + $HO_2$ = $H_2O_2$ + $O_2$ (R3) along with then contemporary values of $k_2$ and $k_3$. This derived rate constant along with 298 K $k_1$ determinations[8] formed the basis of static evaluations (including Baulch et al.[9]) and kinetic models (including GRI-MECH 3.0[10]), which each assigned an uncertainty of a factor of two. In GRI-MECH 3.0, the original rate constant expression was then additionally optimized to combustion property measurements, whose interpretations involved many more reactions, to reach similar values at 773 K to the originally derived values from Baldwin and Walker.

While the rate constants of Baulch et al. and GRI-MECH 3.0 are reasonably consistent with later high-temperature determinations from Michael et al.[11], they are inconsistent with later theoretical calculations[12] (corresponding to the a priori model shown in Fig. 1) and reinterpretations of the measured rate constant ratio at 773K using more recent, improved values of $k_2$ and $k_3$. In fact, the theoretical calculations and reinterpreted 773 K determinations (shown in the square symbol in Fig. 1 when using the MSI model values for $k_2$ and $k_3$) both fall outside the uncertainty bounds assigned by Baulch et al. and GRI-MECH 3.0.

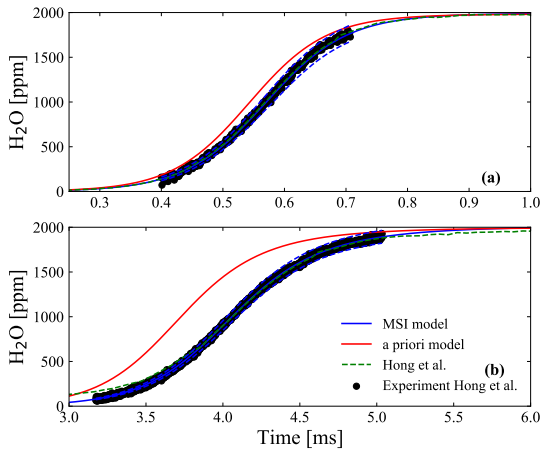


Fig. 2. Time profiles of $H_2O$ mole fraction in shock-heated $H_2/O_2/Ar$ mixtures at (a) 1472 K and 1.83 atm and (b) 1100 K and 1.95 atm.

In 2011, Hong et al.[13] presented the most precise determinations (< 4.6% to 8.8%) of $H + O_2 = O + OH$ (R2) based on adjusting $k_2$ within model predictions using GRI-MECH 3.0 to fit their measured $H_2O$ time profiles (Fig. 2). By using a highly sensitive absorption diagnostic, the uncertainties in their determinations were not due to signal noise. Rather, the uncertainties were primarily due to uncertainties in experimental temperatures and $k_1$.

Our simultaneous MSI analysis of all the above-mentioned data as well as data for many other coupled reactions indicate significantly lower rate constants for both R1 (Fig. 1) and R2 (Fig. 3). Yet, for R1, the MSI model is consistent with the theoretical calculations,[12] low-temperature determinations,[8] measured 773 K rate constant ratio,[7] and H atom time profiles used for the high-temperature determinations (not shown).[11] Likewise, the MSI model also reproduces the measured $H_2O$ time profiles of Hong et al. equally as well as the original interpretations deriving $k_2$. However, as shown in Fig. 3, the MSI interpretations instead imply a rate constant for R2 that is near the lower end of the reported uncertainty bounds from Hong et al. Given that R2 is often the most sensitive reaction under many oxidation conditions, even a 5-10% lower $k_2$ (as MSI finds) would be of immense importance for combustion predictions and other rate constant determinations.

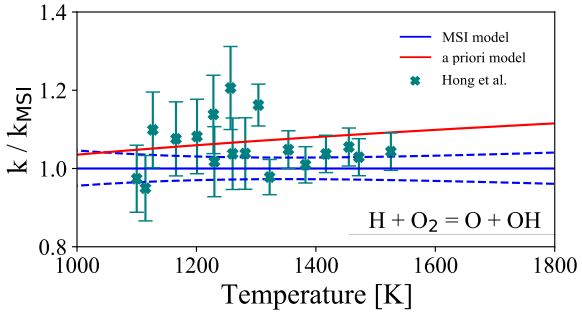


Fig. 3. Rate constants for $H + O_2 = O + OH$ relative to those in the MSI model. Symbols show the original experimental interpretations of Hong et al.

As an example of how this difference in $k_2$ then in turn propagates into differences in other rate constant determinations, the OH time profiles used for the rate constant determinations for $H + O_2 (+M) = HO_2 (+M)$ (R4) from Davidson et al.[14] are also very sensitive to R2. The MSI model, which employs a much lower $k_2$ than Davidson et al., is able to reproduce the OH time profiles from Davidson et al. with a much lower $k_4$ that is also consistent with recent a priori 2D-ME calculations.[15]

*$CH_2O$ (+M) and $CH_2O + O_2$.* Not only are the $CH_2O$ +M/$O_2$ reactions tightly entangled with many other rate constant determinations and each other, but also they are important to both combustion and atmospheric chemistry. We have continued assembling an MSI description of them under pyrolytic and photolytic initiation. Building on our master equation calculations[vi] of the $CH_2O$ photochemical system (including the recently suggested the rovibrationally excited $CH_2O^* + O_2$ reaction[16]) reported last year, we have also begun initial MSI analysis of the measured time profiles of photochemical experiments.[16]

We have also now published[vii] our description of a newly proposed mechanism for pressure dependence of even non-associative bimolecular reactions, whose rate constants are usually considered pressure-independent. Specifically, unimolecular dissociation of one or more reactants in a bimolecular reaction can preferentially deplete the high energy states that would usually contribute the most to high-activation-energy bimolecular reactions – thereby producing pressure-dependent rate constants for even non-associative bimolecular reactions at pressures below the high-pressure limit for dissociation. Our calculations indicate that this dissociation-induced non-equilibrium effect on bimolecular reactions can be substantial – even when the chemical timescales are well separated from internal energy relaxational timescales (as for $CH_2O$). These effects are much more pronounced for reactions involving HCOH, which

ceases to exist as a chemical species at intermediate temperatures. Our calculations also reveal significant problems with treatments of species merging that assume rapid equilibration among isomers.

**Future Plans**

We plan to publish our simultaneous analyses of the inextricably entangled reactions involving $H + O_2 = OH + O$, $OH + H_2 = H + H_2O$, $O + H_2 = H + OH$, $H + HO_2$ = products, $H + O_2$ (+M) = $HO_2$ (+M), and TBHP fragment kinetics and continue venturing into less characterized and more difficult-to-isolate subsystems, such as those involving $CH_2O$ and HCO, where the anchored database can be leveraged for the analysis and associated non-equilibrium kinetic sequences. Along the way, we plan to continue MSI improvements to broaden the datatypes that can be used as targets (including the abovementioned $CH_2O$ photochemical experiments[16]), enable a greater degree of data redundancy, and allow more rigorous evaluations of theoretical methodologies, particularly those for non-equilibrium kinetic sequences.

**References**


1. B. Ruscic, et al. *J Phys Chem A* 108 (2004) 9979–9997.
2. M.P. Burke, S.J. Klippenstein. *Nature Chemistry* 9 (2017) 1078-1082.
3. N.J. Labbe, et al. *J. Phys. Chem. Lett.* 7 (2015) 85–89.
4. M.P. Burke. *Int J Chem Kinet* 48 (2016) 212–235.
5. S. J. Klippenstein, et al. 11th U.S. National Combustion Meeting (2019).
6. Z. Hong, K.-Y. Lam, R. Sur, S. Wang, D.F. Davidson, R.K. Hanson. *Proc Combust Inst* 34 (2013) 565–571.
7. R.R. Baldwin, R.W. Walker, *Faraday Transactions* 75 (1979) 140–154.
8. L.F. Keyser. *J Phys Chem* 90 (1986) 2994–3003; U. Sridharan, L. Qiu, F. Kaufman, *J Phys Chem* 86 (1982) 4569–4574.
9. D.L. Baulch, et al. *J Phys Chem Ref Data* 34 (2005) 757–1397.
10. G.P. Smith et al., GRI-Mech 3.0.
11. J.V. Michael, J.W. Sutherland, L.B. Harding, A.F. Wagner. *J Phys Chem* 2 (2000) 1471–1478.
12. M.P. Burke, M. Chaos, Y. Ju, F.L. Dryer, S.J. Klippenstein. *Int J Chem Kinet* 44 (2012) 444–474.
13. Z. Hong, D.F. Davidson, E.A. Barbour, R.K. Hanson. *Proc Combust Inst* 33 (2011) 309–316.
14. D.F. Davidson, E. Petersen, M. Röhrig, R.K. Hanson, C.T. Bowman *Proc Combust Inst* 26 (1996) 481–488.
15. S.J. Klippenstein. *Proc Combust Inst* 36 (2017) 77–111.
16. B. Welsh, M. Corrigan, Assaf, M. Jordan, C.M. Fittschen, S. Kable. A181-0022. AGU Fall Meeting 2020.


**BES-supported products (2020-present)**

i. C.E. LaGrotta, M.C. Barbet, L. Lei, M.P. Burke, "Towards a High-Accuracy Kinetic Database Informed by Theoretical and Experimental Data: $CH_3 + HO_2$ as a Case Study," *Proceedings of the Combustion Institute* 38 (2021) 1043-1051.

ii. C.E. LaGrotta, L. Lei, M.C. Barbet, Z. Hong, D.F. Davidson, R.K. Hanson, M.P. Burke, "Towards Resolution of Lingering Discrepancies in the $H_2O_2$ Decomposition System: $HO_2 + HO_2$," 12th U.S. National Combustion Meeting, College Station, Texas, May 2021.

iii. L. Lei, M.P. Burke, "An Extended Methodology for Automated Calculations of Non-Boltzmann Kinetic Sequences: $H + C_2H_2 + X$ and Combustion Impact," *Proceedings of the Combustion Institute* 38 (2021) 661-669.

iv. C.E. LaGrotta, M.C. Barbet, L. Lei, M.P. Burke. MSI: A Package for MultiScale Informatics. https://github.com/TheBurkeLab/MSI.

v. L. Lei, M.P. Burke. AutoNonBoltzmann: A Code for Automated Calculations of Non-Boltzmann Kinetic Sequences.

vi. M.P. Burke, "Master Equation Calculations to Assess the Role of Non-Thermal Bimolecular Reactions in Formaldehyde Photochemistry," American Geophysical Union Fall Meeting, December 2021.

vii. M.P. Burke, Q. Meng, C. Sabaitis, "Dissociation-Induced Depletion of High-Energy Reactant Molecules as a Mechanism for Pressure-Dependent Rate Constants for Bimolecular Reactions," *Faraday Discussions* 238 (2022) 355–379.

viii. C.E. LaGrotta, Q. Meng, L. Lei, M.C. Barbet, Z. Hong, M.P. Burke, "Resolving Discrepancies Between State-of-the-Art Theory and Experiment for $HO_2 + HO_2$ via Multiscale Informatics," *Journal of Physical Chemistry A* 127 (2023) 799–816.

# Dynamics and Energetics of Elementary Reactions and Transient Species using Coincidence Spectroscopy

**Grant DE-FG03-98ER14879**

Robert E. Continetti (rcontinetti@ucsd.edu)
Department of Chemistry and Biochemistry, University of California San Diego
9500 Gilman Drive, La Jolla, CA 92093-0340

## I. Program Scope

This research program has focused on experimental studies of fundamental chemical reactions that provide benchmarks for advancing our theoretical understanding of chemical reactions, in particular the potential energy surfaces (PESs) that govern the reactions, and computational studies of the reaction dynamics. Our efforts have focused on the bimolecular reactions of the hydroxyl radical,[1] the fluorine atom,[2] and oxygenated carbon radicals.[3, 4] Over the years, these experiments have provided benchmark information on the potential energy surfaces and dynamics of important combustion systems (HOCO) and elementary reactions ($F+H_2O$), as well as insights into the photochemistry of negative ions, anion resonances and vibrational Feshbach resonances in neutral reactions. Notably, in a number of cases, these efforts have involved collaboration with leading theoretical groups.[2, 5-7] The experimental approach employs a unique photoelectron-photofragment coincidence (PPC) spectrometer equipped with a cryogenic octopole accumulator trap (COAT) for the preparation of anions thermalized below 20K.[8] These cold anions are used to load an electrostatic ion beam trap (EIBT),[9] allowing the PPC measurement to be carried out on 7 keV ions, with the fast beam enabling detection in coincidence of photoelectrons, stable photoneutrals, and photofragments. The PPC experiment is notable in that it yields a kinematically complete measurement of energy partitioning in reactions induced by photodetachment of precursor anions. During this project period, limited progress was made as detailed below, but with a renewal of support we are now preparing to resume our efforts with a focus on implementing new three-dimensional imaging detectors. The initial experiments will focus on resolving an outstanding question with anion internal excitation in a study of the propiolate anion $CH_3CCCO_2^-$ using the cold COAT ion source before returning to studies of fluoride complexes, carbon oxides, and preparing for a return to IR excitation experiments[10, 11] on the excitation and isomerization of HOCO.

## II. Recent Progress

At the beginning of this reporting period in May 2022, we had brought the apparatus back online following maintenance of the EIBT region, and we began to do further experiments. Warranty-related service issues with the Ti:Sa laser led to further delays, but finally we were able to begin optimizing the apparatus using the trapping of beams of $O^-$ and $O_2^-$. However, we faced significant difficulties in achieving the 4% resolution that we previously had obtained routinely. Some of the problems were traced to the age of the microchannel plates, so these were replaced and we achieved a resolution of 10% $\Delta E/E$ for the $O^-$ single-photon photodetachment peak at eKE = 1.75 eV using 3.20 eV photons. This resolution is just not sufficient for measurements on polyatomic molecular and cluster anions. A degradation of the performance of the peak sensing ADCs used in the obsolete CAMAC data acquisition system is the likely origin of this limited resolution. Now that project funding has been restored, we are preparing to replace both the electron and multiparticle photofragment detector with multihit time- and position-sensitive detectors based on CCD phosphor images coupled with timing information recorded with high bandwidth transient digitizers, similar to those described in an extensive body of work by Li and co-workers.[12] In addition to replacing the 30-year old data acquisition system for both the electron and multiparticle detectors, this upgrade should lead to a significant simplification of the calibration procedures for the multiparticle detector, which is composed of 4 double-hit crossed delay lines, leading to 16 linear calibration curves. In addition, the new multiparticle and photoelectron detector will not have the significant dead-time issues associated with delay line and charge division time- and position encoding methods. This will be an exciting new era for this experimental program.

## II. Future Work

With the renewal of this research grant we are now prepared to move forward with upgrading our three-dimensional imaging detectors and resuming experiments. In particular we will focus on resolving the question of internal excitation in the propiolate anion $CH_3CCO_2^-$ that was the outstanding question in an earlier joint theory-experiment study undertaken in collaboration with Stanton and co-workers. Now, using the COAT we will be able to cool the anions to less than 20K, and definitively rule out the presence of unrelaxed high-frequency vibrations in the anion. This will experimentally define the energetics in this system that represents a notable challenge for quantum chemistry given the interaction of the carbon-carbon triple bond with the carboxyl group in the neutral propiolyl radical. With that data in hand, we intend to move on to studies of the effect of solvation by examining the $F^-(H_2O)_2$ system, other halide complexes, and oxidized carbon species, including $CO_3^-$, $CO_4^-$ and $HCO_3^-$. Finally, we intend to return to our earlier studies examining the effects of IR excitation in anion complexes. Initial experiments using IR excitation will examine influencing the *cis*-$HOCO^-$/*trans*-$HOCO^-$ and $HCO_2^-$/$HOCO^-$ isomerizations and we will then pursue examination of mode-specific effects on the dissociation dynamics of HOCO by the DPD of vibrationally excited $HOCO^-$ anions. With the resumption of this research program, we look forward to continuing to produce state-of-the-art benchmark experimental results to guide the future development of quantum chemistry and dynamics theory in increasingly complex systems supporting the advance of a fundamental understanding of chemical phenomena.

## III. DOE-supported publications by this project 2020-2023

1. Y. Benitez, A.J. Parsons, K.G. Lunny and R.E. Continetti, *Dissociative photodetachment dynamics of the $OH^-(C_2H_4)$ anion complex*, J. Phys. Chem. A. **125**, 4540-4547 (2021). doi: 10.1021/acs.jpca.1c01835
2. Y. Benitez, T.L. Nguyen, A.J. Parsons, J.F. Stanton and R.E. Continetti, *Probing the exit channel of the $OH + CH_3OH \rightarrow H_2O + CH_3O$ reaction by photodetachment of $CH_3O^-(H_2O)$*, J. Phys. Chem. Lett. **13**, 142-148 (2021). doi: 10.1021/acs.jpclett.1c03568

## References


1. C. J. Johnson, R. Otto and R. E. Continetti, Phys. Chem. Chem. Phys. **16**, 19091-19105 (2014).
2. R. Otto, J. Ma, A. W. Ray, J. S. Daluz, J. Li, H. Guo and R. E. Continetti, Science **343**, 396-399 (2014).
3. A. W. Ray, B. B. Shen, B. L. J. Poad and R. E. Continetti, Chem. Phys. Lett. **592** (0), 30-35 (2014).
4. B. L. J. Poad, A. W. Ray and R. E. Continetti, J. Phys. Chem. A **117**, 12035-12041 (2013).
5. A. W. Ray, J. Agarwal, B. B. Shen, H. F. Schaefer and R. E. Continetti, Phys. Chem. Chem. Phys. **18**, 30612-30621 (2016).
6. Y. Benitez, D. Lu, K. G. Lunny, J. Li, H. Guo and R. E. Continetti, J. Phys. Chem. A **123** (23), 4825-4833 (2019).
7. Y. Benitez, T. L. Nguyen, A. J. Parsons, J. F. Stanton and R. E. Continetti, J. Phys. Chem. Lett. **13**, 142-148 (2021).
8. B. B. Shen, K. G. Lunny, Y. Benitez and R. E. Continetti, Front. Chem. **7**, 295 (2019).
9. C. Johnson, B. Shen, B. Poad and R. Continetti, Rev. Sci. Instrum. **82** (10), 105105 (2011).
10. R. Otto, A. W. Ray, J. S. Daluz and R. E. Continetti, EPJ Tech. Instrum. **1**, 3 (2014).
11. A. W. Ray, J. Ma, R. Otto, J. Li, H. Guo and R. E. Continetti, Chem. Sci. **8**, 7821-7833 (2017).
12. G. Basnayake, Y. Ranathunga, S. K. Lee and W. Li, J. Phys. B. **55**, 023001 (2022).

# Reaction Dynamics of Organic Radicals and Carbenes

H. Floyd Davis
Dept. of Chem. & Chem. Biology, Cornell University, Ithaca, NY 14853-1301
hfd1@cornell.edu

## I. Program Scope:

This project involves experimental studies of unimolecular and bimolecular reactions of polyatomic free radicals and carbenes using a crossed molecular beams apparatus employing "universal" vacuum ultraviolet (VUV) photoionization and electron impact detection of neutral species. [1,2] A current focus is on the production and characterization of previously-unobserved alkyl-substituted carbenes such as methylcarbene ($CH_3CH$), ethylcarbene ($C_2H_5CH$), and dimethylcarbene ($CH_3CCH_3$). The reactions of radicals and carbenes typically involve multiple reaction intermediates and transition states, leading to competing product channels relevant to atmospheric chemistry, catalysis, combustion, and synthetic chemistry. Our experiments aim to provide key experimental benchmarks against which theoretical models, including the thermochemistry and potential energy barriers for key species and reactions, may be tested.

## II. Recent Progress:

Despite their relative simplicities, alkyl-substituted carbenes have remained remarkably elusive to experimental characterization. Our interest in alkylcarbenes began with our finding that they are produced in the UV photodissociation of alkyl radicals.[3] Lying ~ 300 kJ/mol (~ 3 eV) above their stable ground state alkene isomers, singlet alkylcarbenes, once produced, are subject to rapid isomerization to alkenes via a 1,2-hydrogen atom shift. Most previous attempts at formation of alkylcarbenes involved UV photodissociation of diazoalkanes ($RN_2$), or their cyclic alkyldiazirine isomers. Owing to the high enthalpies of formation and relatively high-lying electronically excited states of these precursors, the photogenerated singlet alkylcarbenes are produced with high internal energies. This leads to extremely short lifetimes, precluding their observation in the laboratory. Consequently, most information about the properties of alkylcarbenes have been derived from theoretical calculations. Following our original studies of ethylidene (methylcarbene), we have produced and studied alkylcarbenes of progressively greater levels of complexity. We have also sought the means to produce these species using precursors that are more easily handled than alkylketenes, many of which spontaneously dimerize at -60°C.

### a) Ethylcarbene vs. Direct Propene Formation in the Near-UV Photodissociation of Ethylketene[4]:

Using a newly-developed in-situ source of monoalkyl ketenes, the competing pathways in the photodissociation of gaseous ethylketene at excitation wavelengths of 320.0, 340.0 and 355.1 nm were studied using photofragment translational energy spectroscopy. The primary dissociation channel was C=C bond fission producing ethylcarbene ($CH_3CH_2CH$; also known as propylidene) and CO. Product translational energy distributions were consistent with theoretical predictions that ground state ethylcarbene lies ~34 kJ/mol higher in energy than its isomer dimethylcarbene ($CH_3CCH_3$). A second dissociation channel involved *direct* formation of propene prior to, or concurrent with, CO elimination. The measured product branching ratios indicate that the effective potential energy barrier for the direct propene channel lies *below* the energetic threshold for ethylcarbene formation. A minor C-C bond fission channel was also observed, leading to $CH_3$ + $CH_2CHCO$ products.

The observed dependence of propene yield on excitation energy for ethylketene photodissociation directly contrasts with that seen recently in our study of dimethylketene photodissociation, where the propene yield relative to dimethylcarbene formation increased sharply with *increasing* photon energy.[5] For dimethylketene photodissociation, we concluded that the potential energy barrier for direct propene formation lies near 300 kJ/mol, ~24 kJ/mol *above* that for C=C bond fission producing CO +

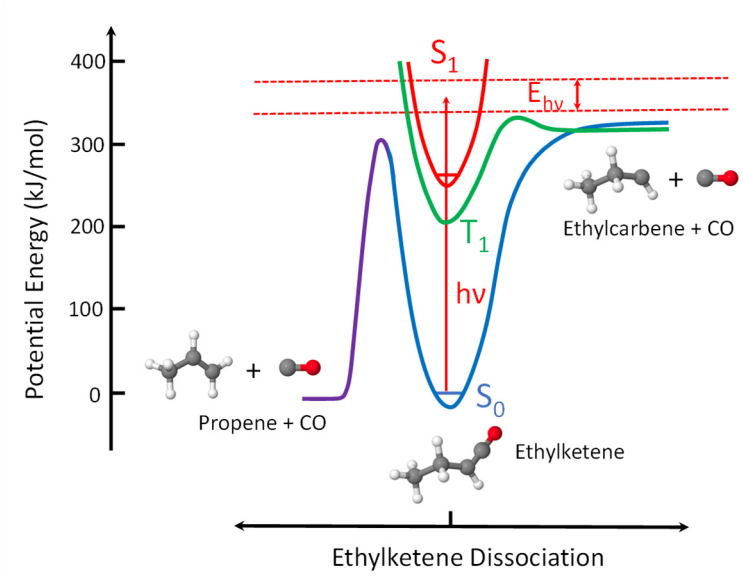


**Fig. 1:** *Potential energy diagram for ethylketene photodissociation producing ethylcarbene + carbon monoxide, via C=C bond cleavage. Alternatively, propene + carbon monoxide can be produced via a direct reaction mechanism, bypassing formation of free ethylcarbene..*

dimethylcarbene.[5] Our finding that direct propene formation plays important roles in both dimethylketene and ethylketene photodissociation, corresponding to systems where the potential energy barriers lie above and below $D_o(C=C)$, respectively, strongly suggests that concerted alkene formation in competition with carbene formation is a *general* feature of alkylketene photodissociation.

b) **Wavelength dependence of the photodissociation of methylketene and propenal (acrolein)[6]**:

Our earlier observations pertaining to the production of ethylidene ($CH_3CH$) were consistent with a high potential energy barrier for isomerization on the triplet surface, rendering triplet ethylidene stable in the absence of collisions.[7] Electronically excited singlet ethylidene was also produced, rapidly undergoing isomerization by a 1,2-hydrogen atom shift after departure of the CO, producing highly vibrationally excited ethylene. The product translational energy distributions, measured at m/e = 28 and 26, verify the theoretically calculated enthalpy of formation of triplet ethylidene, and are consistent with a singlet-triplet energy gap of about 12.5 kJ/mol.

A significant difficulty encountered in our early studies of monoalkyl carbenes such as ethylidene (methylcarbene) and propylidene (ethylcarbene) was that the parent liquid ketenes (methylketene and ethylketene, respectively), produced by pyrolysis of commercially-available acid anhydrides, are stable for no more than about 20-30 minutes, even at -60°C. This instability, due to rapid dimerization via a 2+2 cycloaddition reaction forming involatile lactones, was our motivation for studying the photodissociation of acrolein, the stable "enal" isomer of methylketene. Our studies showed that the ethylidene products from photodissociation of methylketene and acrolein near 355 nm were very similar.[6,7] We concluded that upon electronic excitation near 355 nm, acrolein underwent a rapid 1,3-H atom shift to form methylketene, which subsequently dissociates to produce ethylidene via CO elimination. This is consistent with theoretical calculations indicating that isomerization to ketenes is the lowest-energy pathway for enals. To overcome the difficulty associated with the rapid dimerization of alkylketenes, we developed a new method for production of methylketene involving *continuous in-situ pyrolysis* of propionic anhydride.

Using the in-situ pyrolysis source, we studied methylketene photodissociation at six wavelengths between 320 and 387 nm, for direct comparison to our previous studies of acrolein photodissociation. The results of this experiment are currently under analysis and a publication will be submitted in the near future. The primary conclusion of these studies is that the wavelength dependent photodissociation dynamics of methylketene and acrolein are very similar at all wavelengths studied.

At wavelengths longer than 320 nm, the only products from single photon excitation of methylketene and propenal result from CO elimination producing singlet or triplet ethylidene. The singlet-triplet ethylidene branching ratio is strongly wavelength dependent, with production of ground state triplet ethylidene becoming dominant at wavelengths longer than 360 nm for both isomers. Upon tuning the

excitation laser to wavelengths *longer* than 370 nm for both parent molecules, the photodissociation signals become very weak. A significant potential energy barrier on the triplet methylketene PES, analogous to that for ketene photodissociation, is believed to be responsible. The signals observed in our experiments at long wavelengths largely result from 2-photon excitation (e.g., at the propenal origin band at 386 nm) primarily yielding H atoms and methylketenyl radicals, analogous to that seen in the 193 nm photolysis of propenal. Previous studies of ketene ($CH_2C=O$) photodissociation just above the energetic threshold for formation of triplet methylene revealed that dissociation occurred on timescales as long as several hundred nanoseconds.[8] As noted below, we plan to investigate the timescale for ethylidene production from methylketene and acrolein using nanosecond pump-probe methods.

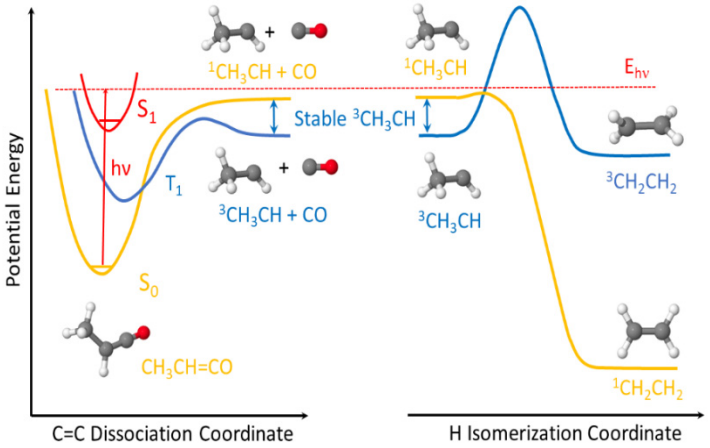


***Fig. 2.*** *Methylketene photodissociation produces ethylidene + carbon monoxide. Triplet ethylidene ($^3CH_3CH$) is stable to intersystem crossing and isomerization if produced with internal energies below the singlet electronically excited state ($^1CH_3CH$).*

## III. Future Plans:

### a) Triplet Ethylidene Formation Near Threshold – Production of Carbene Beams:

We hope to produce molecular beams containing triplet ethylidene by photolysis of methylketene or acrolein, *e*.g., in front of the nozzle in the high- pressure collisional region. This would open up studies of the spectroscopy, photochemistry and bimolecular reaction dynamics of this carbene for the first time. Collisional deactivation through chemical reactions is expected to be the primary mode of decay of triplet ethylidene. Due to the very low barrier for isomerization on the singlet surface, it appears to be unlikely that singlet ethylidene could be prepared in a molecular beam. However, the reactivity of triplet ethylidene is expected to be similar to that of free radicals, which are routinely produced using this approach. One challenge is that the near-UV absorption cross sections for ketenes and enals are relatively small (~5 x $10^{-20}$ $cm^2$). For larger alkylcarbenes such as dimethylcarbene, although the ground state is the highly reactive singlet, a small potential energy barrier for isomerization to propene might allow for molecular beam production.

### b) Carbene Formation from Methacrolein and Crotonaldehyde Photolysis:

As discussed above, we have shown that upon UV excitation, acrolein isomerizes to methylketene via a 1,3 H-atom shift and then dissociates to produce ethylidene + CO. The carbene products from acrolein are nearly indistinguishable from those formed from direct excitation of methylketene. This finding is significant because ethylidene can be readily produced using a commercially-available precursor, acrolein, without the need to synthesize methylketene, which is difficult to handle due to its rapid dimerization to form lactones. The question thus arises about whether or not the analogous isomerization reactions occur following the photolysis of methacrolein, the stable enal isomer of dimethylketene, and crotonaldehyde, the stable enal isomer of ethylketene.

During the past year, we have carried out experiments on methacrolein photodissociation at 352 nm, corresponding to a local peak in the structured absorption spectrum. The photodissociation dynamics appear to be quite different from dimethylketene, which dissociates primarily to form dimethylcarbene + CO.[5]

Since enals such as acrolein and methacrolein have relatively small ($3 \times 10^{-20}$ $cm^2$) absorption cross sections in the near-UV, and van der Waals clusters are typically present, we initially suspected that the observed signals resulted from photodissociation of clusters. Using a heated nozzle, $D_2$ rather than He as the carrier gas, and photolyzing early in the gas pulse, we were able to significantly suppress cluster formation. Yet the dynamics continued to appear quite different from those expected if H atom migration producing dimethylketene followed by carbene formation were operative. We have found that a major channel in methacrolein involves C-C bond fission, producing HCO + $C_3H_5$. Since this channel is energetically closed at these photodissociation wavelengths, this signal must result from two-photon processes. Apparently, near-UV excitation of methacrolein near the band origin produces a long-lived intermediate that readily absorbs a second photon, resulting in formation of higher-energy products.

**c) Time-Resolved Studies of Alkylcarbene Formation:**

We have configured an existing single molecular beam apparatus for nanosecond time-resolved pump-probe studies. The apparatus includes a linear Wiley-McLaren TOF spectrometer employing single photon ionization using tunable light in the 8-10 eV range. First, we plan to study the photodissociation of methylketene and propenal near 370 nm in the vicinity of the potential energy barrier on the triplet methylketene PES. In this energy range, the exclusive products are ground state triplet ethylidene and CO, with dissociation expected to occur on *nanosecond timescales* close to the barrier.[8] By varying the pump-probe delay using a nanosecond digital-delay generator, we will attempt to map out the dissociation timescales directly for triplet ethylidene formation as a function of excitation energy. These studies can be extended to larger systems such as ethylketene and dimethylketene where both the singlet and triplet surfaces likely play important roles near threshold.

**d) Search for Direct Ethylene Formation from Methylketene and Propenal Photolysis:**

As discussed above, propene is formed as a minor concerted channel in both ethylketene and dimethylketene photodissociation, and we believe that direct alkene formation may be a general feature of alkylketene photodissociation. In our earlier study of methylketene/acrolein photodissociation, the analogous channel, involving direct formation of ethylene + CO could not be efficiently probed using 9.9 eV or 8.8 eV photoionization, since ethylene has an ionization energy of 10.5 eV. We therefore plan to search for this channel using 11.0 or 11.9 eV photoionization using the windowless VUV beamline configuration employing custom VUV reflectors developed earlier.

**IV. References (* denotes publications supported by this DOE grant since 2020):**


1. D.R. Albert and H.F. Davis "Experimental Studies of Bimolecular Reaction Dynamics Using Pulsed Tabletop VUV Photoionization Detection", *Phys. Chem. Chem. Phys.* **2013**, 15, 14566-14580.
2.* M. A. Todt, S. Datta, A. Rose, K. Leung, and H. F. Davis, "Subpicosecond HI Elimination in the 266 nm Photodissociation of Branched Iodoalkanes", *Phys. Chem. Chem. Phys.* **2020**, 22, 27338-27347.
3.*.S. Datta, M.A. Todt, and H. F. Davis, "Isomer-Specific C-C Bond Fission in Photoexcited Propyl Radicals Leads to Isomer-Selective Carbene and Radical Products", *J. Phys. Chem. Lett.* **2021**, 12, 11926-11930.
4.* S. Datta and H.F. Davis, "Ethylcarbene vs. Direct Propene Formation in the Near-UV Photodissociation of Ethylketene", *J. Phys. Chem. A.* **2023**, *127, 450-456.*
5*.S. Datta and H.F. Davis, "Dimethylcarbene vs. Direct Propene Formation in Dimethylketene Photodissociation", *J. Phys. Chem. A.* **2021**, *125, 6940-6948.*
6.* S. Datta and H.F. Davis, "Dynamics of Ethylidene Production by Photolysis of Methylketene and Propenal", *manuscript in preparation.*
7*.S. Datta and H.F. Davis, "Direct observation of ethylidene, the elusive high-energy isomer of ethylene", *J. Phys. Chem. Lett.* **2020**, 11, 10476-10481.
8. E.R. Lovejoy, S.K. Kim, and C.B. Moore, "Observation of Transition-State Vibrational Thresholds in the Rate of Dissociation of Ketene", *Science* **1992**, 256, 1541-1544.

**Electronic structure methods and protocols with application to dynamics, kinetics and thermochemistry**

Richard Dawes, dawesr@mst.edu
Missouri University of Science and Technology
400 W. 11th street, Rolla, MO 65409

## I. Program Scope:

**(NOTE – this project is supported jointly through the CTC and GPCP programs and this report will be submitted to both programs)**

Hydrocarbon combustion involves the reaction dynamics of a tremendous number of species beginning with many-component fuel mixtures and proceeding via a complex system of intermediates to form primary and secondary products. Combustion conditions corresponding to new advanced engines and/or alternative fuels rely increasingly on autoignition and low-temperature-combustion chemistry. In these regimes various transient radical species such as $HO_2$, ROO·, ·QOOH, HCO, $NO_2$, HOCO, and Criegee intermediates play important roles in determining the detailed as well as more general dynamics. A clear understanding and accurate representation of these processes is needed for effective modeling. Given the difficulties associated with making reliable experimental measurements of these systems, computation can play an important role in developing these energy technologies.

Accurate calculations have their own challenges since even within the simplest dynamical approximations such as transition state theory, the rates depend exponentially on critical barrier heights and these may be sensitive to the level of quantum chemistry. Moreover, it is well-known that in many cases it is necessary to go beyond statistical theories and consider the dynamics. Quantum tunneling, resonances, radiative transitions, and non-adiabatic effects governed by spin-orbit or derivative coupling can be determining factors in those dynamics.

Building upon progress made during a period of prior support through the *DOE Early Career Program*, this project combines developments in the areas of potential energy surface (PES) fitting and multistate multireference quantum chemistry to allow spectroscopically and dynamically/kinetically accurate investigations of key molecular systems (such as those mentioned above), many of which are radicals with strong multireference character and have the possibility of multiple electronic states contributing to the observed dynamics.

An ongoing area of investigation is to develop general strategies for robustly convergent electronic structure theory for global multichannel reactive surfaces including diabatization of energy and other relevant surfaces such as dipole transition. Combining advances in *ab initio* methods with automated interpolative PES fitting allows the construction of high-quality PESs (incorporating thousands of high-level data) to be done rapidly through parallel processing on high-performance computing (HPC) clusters.

In addition, new methods and approaches to electronic structure theory will be developed and tested through applications. This project will explore limitations in traditional multireference calculations (*e.g.*, MRCI) such as those imposed by internal contraction, lack of high-order correlation treatment and poor scaling. Methods such as DMRG-based extended active-space CASSCF and various Quantum Monte Carlo (QMC) methods will be applied (including VMC/DMC and FCIQMC). Insight into the relative significance of different orbital spaces and the robustness of application of these approaches on leadership class computing architectures will be gained. Synergy with other components of this research program such as automated PES fitting and multireference quantum chemistry will be used to address challenges encountered by the standard approaches to computational thermochemistry (those being single-reference quantum chemistry and perturbative treatments of the anharmonic vibrational energy, which break down for some cases of electronic structure or floppy strongly coupled vibrational modes).

**Recent Progress:** This section describes recent progress achieved along various directions of the project occurring over the past 12 months since the last abstract was provided in May 2022 (start date of this project was 03-01-2019). As this project is coming to an end, some proposed plans with an extension in focus for an upcoming renewal period are mentioned.

Seven articles citing DOE support have appeared so far since 2022[1-7] including one in *Faraday Discussions*.[6] Several other papers are in prep, mostly related to further developments and application of our code to automatically generate PESs suitable for quantum dynamics or spectroscopic studies.

A main thrust mentioned above has been on robust calculation and fitting of energy and property surfaces for strongly coupled and intersecting excited electronic states. In 2021 we reported fitting 22 energies, couplings, and components of properties for $NO_2$ in the Franck-Condon region.[8] We just submitted a paper to JPC A on the temperature dependence of $NO_2$'s electronic absorption spectrum. The effects of rotational and vibrational excitation (thermal and otherwise) were addressed separately by generating predicted electronic absorption spectra for each of hundreds of potentially initially excited states. These individual spectral contributions can be weighted according to a partition function to generate a first-principles prediction at elevated temperatures. In fact, any arbitrary weighting including specifying pure excited states can be applied. All of the data is managed and archived in a Spectral Simulation Tool which performs a variety of processing and analysis tasks and renders various types of plots.

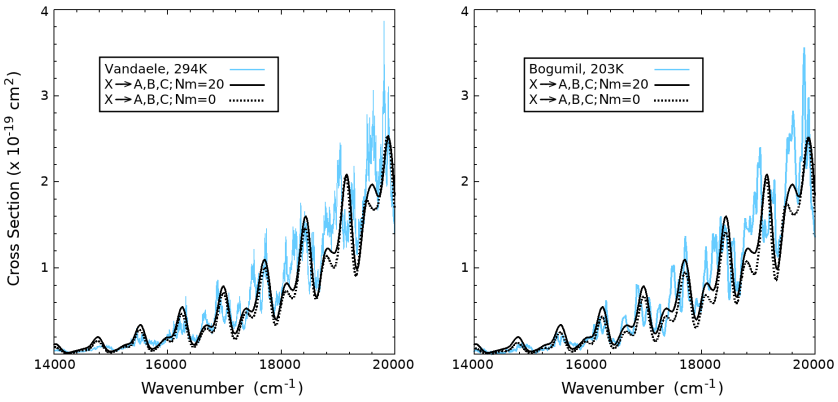


**Figure 1**: (at left) The calculated electronic absorption spectrum weighting rotationally excited initial states at 70 K (up to $N_{Max}$ = 20) improves agreement with the 294 K experimental spectrum of Vandaele *et al.* compared to a 0 K ($N_{Max}$ = 0) calculation. There is also improved agreement between the 70 K calculation and the lower resolution 203 K measurement of Bogumil *et al.* (at right).

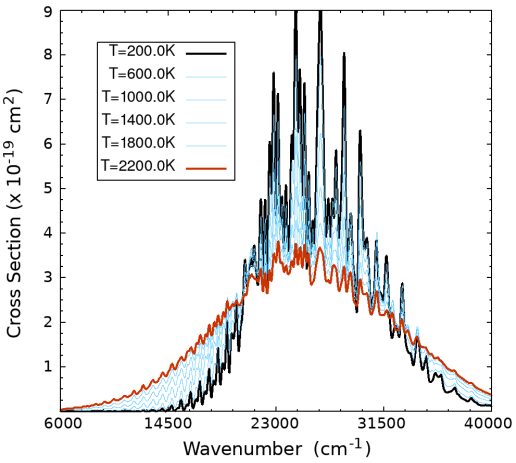


**Figure 2**: The Spectral Simulation Tool is used to yield predicted spectra due to vibrational excitation at a sequence of temperatures.

We have also since greatly extended the coordinate and energy ranges of the fits (globally out to NO + O), generating and processing new data sets. Due to the increased complexity of the data, we developed a visual-based tool for processing and diabatizing data.

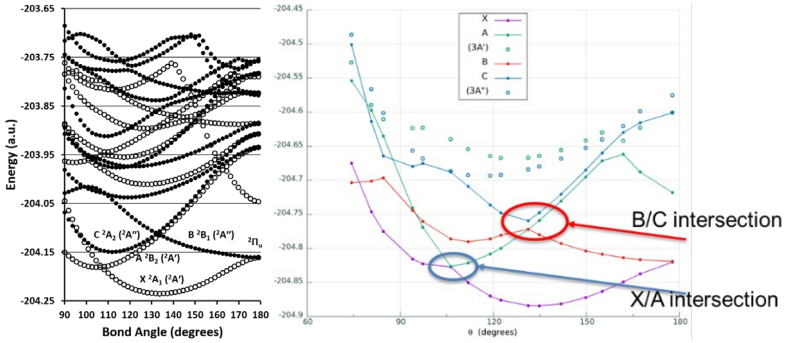


**Figure 3**: (at left) Bend cut through PESs of $NO_2$ at CASSCF level showing rich complexity of electronic states. (at right) Raw data at the MRCI-F12 level showing two intersection regions to be treated by diabatization, but also other crossings at higher energy.

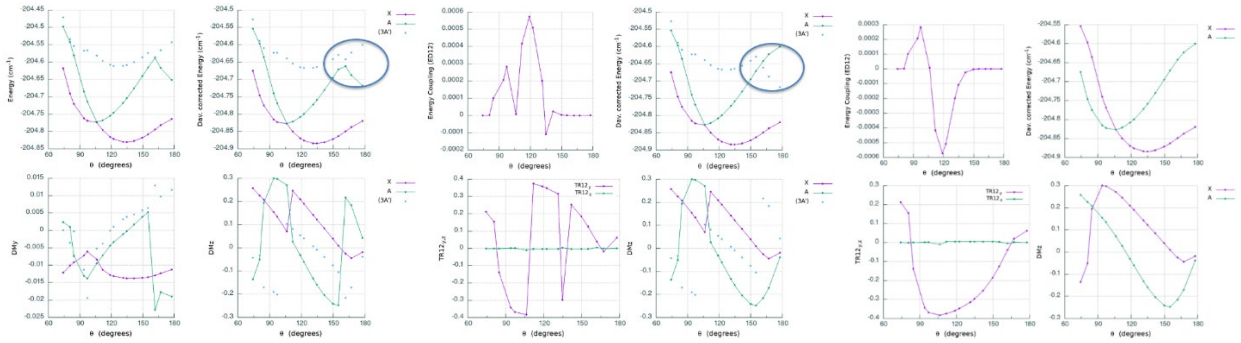

**Figure 4**: The new tool renders plots of various energies, couplings, and properties. Data can be selected to be swapped or removed. Notice how the last three data points for the A-state (circled) have been swapped with those of the 3A' state to extend the A-state diabat, despite that higher crossing not being included in the diabatization. At this stage, the phase is still arbitrary as seen in the coupling and TR12 plots at right. Once a choice of phase convention is specified, each quantity can be verified to be behaving smoothly and accordingly, ready for fitting.

We have developed a flexible Fortran based master code that performs neural network fitting. The parallel code runs hundreds of Matlab processes simultaneously to efficiently explore the effectiveness of various possible network architectures, as well as to assemble the best committee of fits. Permutation symmetry and anti-symmetry are imposed as appropriate (e.g., the two coupling surfaces in $NO_2$ discussed above are anti-symmetric upon exchange of O-atoms). Fitting couplings is considerably more challenging than the related energy diabats, since their topography, phase and dependence on geometry is much more complex. We have found that the region of significant coupling, and even its phase in this system, are often well predicted by the size of the diabatic energy gap and the sign of difference. Adding this quantity to the set of NN inputs dramatically improves the accuracy of fit for the coupling.

The next period of research proposed under a renewal titled "*Time-Dependent Quantum Dynamics and Molecular Control via Shaped Femtosecond Pulses*" leverages developments from this project including construction of accurate surfaces representing coupled electronic states with full dimensional treatment of energies and relevant properties such as dipoles and transition dipoles, as well time-dependent quantum dynamics simulations using the multi-configurational time-dependent Hartree (MCTDH) framework. The next step involves the use of shaped pulses to provide great flexibility in the set of reachable superposition

states that can be prepared. The evolution of these states on multiple coupled potential energy surfaces (PESs), especially in the region of conical intersections, can vary widely in their dynamics, loss of coherence, and energy flow leading to bonding rearrangements. Exploiting coherences and interference effects may drastically affect, for example, reactivity.

$$F_1=(p_{13}+p_{23})$$
$$F_2=(p_{13})^2+(p_{23})^2$$
$$F_3=p_{12}$$
$$F_4=(V_{22}-V_{11})$$

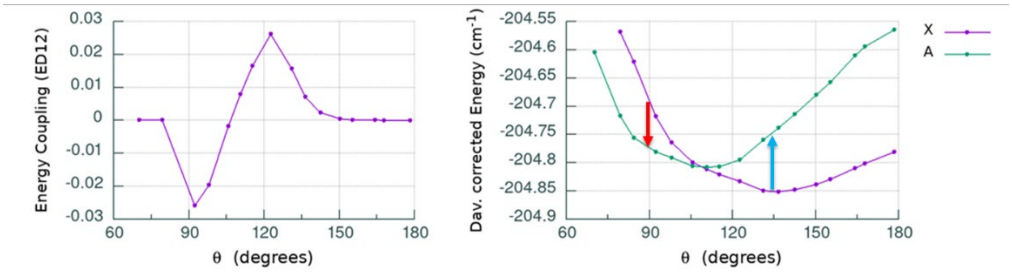


**Figure 5**: The 4 NN inputs used to fit the off-diagonal coupling surface. The first three are Fundamental Invariants (FI) related to the geometry, and used to impose symmetry (anti-symmetry in this case), while the 4th is the energy gap between diabats, the inclusion of which greatly improves the fit since it predicts the location and phase of the coupling.

**Grant Number and Title:** Grant No. DE-SC0019740; Electronic structure methods and protocols with application to dynamics, kinetics and thermochemistry.

[1] Dumouchel, Fabien, Ernesto Quintas-Sánchez, Christian Balança, Richard Dawes, François Lique, and Nicole Feautrier. "Collisional excitation of C2H-by H2: New interaction potential and scattering calculations." *The Journal of Chemical Physics* 158, no. 16 (2023): 164307-164307.
[2] Zadrożny, Adam, Hubert Jóźwiak, Ernesto Quintas-Sánchez, Richard Dawes, and Piotr Wcisło. "Ab initio quantum scattering calculations for the CO–O2 system and a new CO–O2 potential energy surface: O2 and air broadening of the R (0) line in CO." *The Journal of Chemical Physics* 157, no. 17 (2022): 174310.
[3] Denis-Alpizar, Otoniel, Ernesto Quintas-Sánchez, and Richard Dawes. "State-to-state rate coefficients for HCS+ in rotationally inelastic collisions with H2 at low temperatures." *Monthly Notices of the Royal Astronomical Society* 512, no. 4 (2022): 5546-5551.
[4] Dzenis, Karlis, Alexandre Faure, B. A. McGuire, A. J. Remijan, P. J. Dagdigian, C. Rist, Richard Dawes, Ernesto Quintas-Sánchez, François Lique, and M. Hochlaf. "Collisional Excitation and Non-LTE Modeling of Interstellar Chiral Propylene Oxide." *The Astrophysical Journal* 926, no. 1 (2022): 3.
[5] Ajili, Yosra, Ernesto Quintas-Sánchez, Bilel Mehnen, Piotr S. Żuchowski, Filip Brzęk, Nayla El-Kork, Marko Gacesa, Richard Dawes, and Majdi Hochlaf. "Theoretical study of the CO 2–O 2 van der Waals complex: potential energy surface and applications." *Physical Chemistry Chemical Physics* 24, no. 47 (2022): 28984-28993.
[6] Sun, Ge, Shanyu Han, Xianfeng Zheng, Yu Song, Yuan Qin, Richard Dawes, Daiqian Xie, Jingsong Zhang, and Hua Guo. "Unimolecular dissociation dynamics of electronically excited HCO (Ã 2 A′′): rotational control of nonadiabatic decay." *Faraday Discussions* 238 (2022): 236-248.
[7] Ndengué, Steve, Ernesto Quintas-Sánchez, Richard Dawes, Christopher Blackstone and David Osborn. Temperature Dependence of the Electronic Absorption Spectrum of NO2 (submitted to JPC A).
[8] Ndengué, Steve, Ernesto Quintas-Sánchez, Richard Dawes, and David Osborn. "The low-lying electronic states of NO2: Potential energy and dipole surfaces, bound states, and electronic absorption spectrum." *The Journal of Physical Chemistry A* 125, no. 25 (2021): 5519-5533.

# Theoretical and Experimental Studies of Elementary Hydrocarbon Species and Their Reactions (DE-SC0018412)

Gary E. Douberly and Henry F. Schaefer III
University of Georgia, Center for Computational Quantum Chemistry and Department of Chemistry, 1004 Cedar St., Athens, GA 30602-1546
douberly@uga.edu

## Program Scope

New theoretical and experimental methods in chemical physics being developed by the PIs provide great opportunities for the study of molecular species and chemical reactions of fundamental importance in combustion processes. In this research, high level quantum mechanical formalisms are a significant source of critical predictions concerning molecular systems that may be challenging for experiments. Moreover, our helium droplet experiments have opened whole new vistas for the spectroscopic study of molecular species relevant to combustion environments. Theoretical developments proposed herein include a focus on obtaining highly accurate energetics for species pertinent to combustion reactions. Experimental developments focus on strategies to characterize transient combustion intermediates associated with low-temperature hydrocarbon oxidation processes, which have been difficult to probe with other methodologies. The combination of theory and experiment to solve problems inaccessible to either alone is a hallmark of this research.

Nearly all of the proposed non-methodological experimental research will benefit from state-of-the-art molecular electronic structure theory. In some cases, the experimental group needs theoretical predictions prior to beginning a new set of experiments. In other cases, experimental findings are puzzling and need theory for interpretation. We have an abundance of experiences with both sets of problems, and the PIs have already collaborated in several such situations. Some situations where theory-experiment interaction will be particularly important include: (i) the $C_nH_m$ + $O(^3P)$ reactions, where predictions of structures, energetics, and spectroscopic properties of complexes and adducts on both singlet and triplet potential energy surfaces will be required; (ii) the spectroscopic studies of $(NH_2)_2$, NH-($NH_2$), and other pre-reactive radical-radical complexes, where an interpretation will require computations of structures, energetics, and intersystem crossing rates; (iii) the near-IR and mid-IR studies of HOO-alkene complexes and related QOOH species, where computations of the excited state potential energy surface in the vicinity of the exit-channel complex will be essential; and (iv) the mid-IR studies of $\cdot C_nH_{2n+1}$ radicals, where the spectra are complicated by anharmonic and Coriolis resonances to an extent that the interpretation of these spectra will only be achievable through comparisons to effective Hamiltonian computations that employ highly accurate quartic force fields and Coriolis parameters.

## Recent Projects

***Infrared Spectroscopy of Alkyl and Alkyl Peroxy Radicals in Solid para-Hydrogen and Helium Droplets (Experiment/Theory Collaboration)***

King, K.E.; Franke, P.R.; Pullen, G.T.; Schaefer, H.F.; Douberly, G.E. "Helium droplet infrared spectroscopy of the butyl radicals", *Journal of Chemical Physics*, **157**, 084311 (2022). DOI: 10.1063/5.0102287

In this work, we report infrared spectra in the CH stretching region for all four butyl radicals, which include the first experimental spectra in this region for the *s*-butyl radical. These radicals were produced by vacuum pyrolysis, doped into helium nanodroplets, and analyzed with a mass spectrometer and tunable infrared laser. The spectra obtained are relatively well-resolved, revealing a wealth of anharmonic coupling interactions between the CH stretches and overtones and combinations of HCH bending modes. We have predicted the spectra of these radicals with both local mode and VPT2+K [second-order vibrational perturbation theory (VPT) with resonances] effective Hamiltonian methods. These predicted spectra, when combined with the helium droplet spectra, have allowed us to characterize the origins of the anharmonic couplings and assign spectral regions to specific carbon centers. Because of the minimally perturbing helium matrix environment, the results from the model Hamiltonian computations can be compared directly to the butyl radical helium droplet spectra. Indeed, when comparisons to gas-phase spectra are available, vibrational band origin shifts are minimal for molecules solvated in helium droplets.

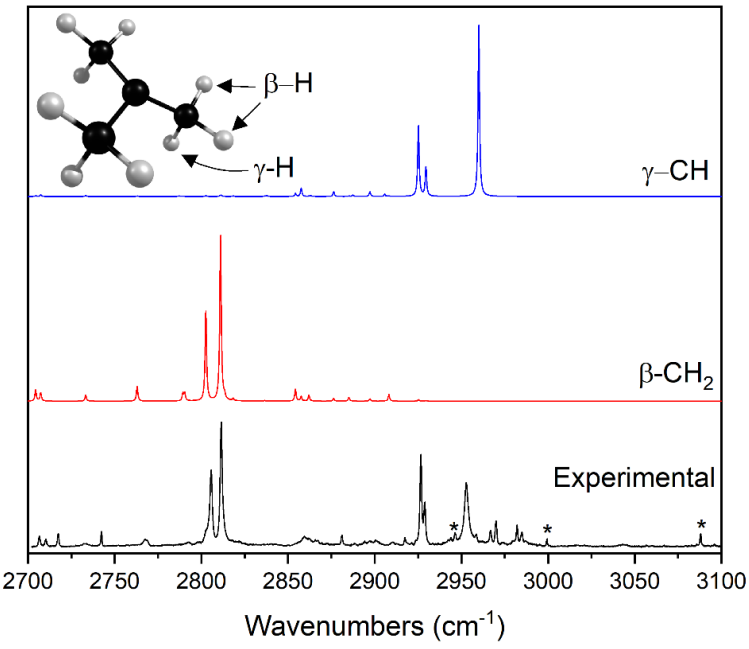


Figure 1: Helium droplet spectra (black) of the tert-butyl radical compared to predictions from a local-mode effective Hamiltonian model (blue and red).

The VPT2+K method has provided a reasonable treatment of alkyl radicals, performing particularly well for the isolated, radical-site CH stretches. Sites directly adjacent to the radical

carbon were not modeled as well, though this tendency was also seen with the local mode method. It is often stated that VPT, based on rectilinear coordinates, cannot accurately describe systems that undergo large amplitude motion. Examples of "hard" problems for VPT are numerous. Consider nitromethane and ethyl radical. It is difficult to say, *a priori*, whether VPT will fail, as the answer depends not only on the nature of the large-amplitude coordinate(s) but on the degree of their coupling to the small-amplitude coordinates. In some cases, VPT may perform poorly for some transitions but very well for others, e.g., the $\alpha$-$CH_X$ stretches of alkyl radicals. Another unresolved question concerns the extensibility of large effective Hamiltonian VPT2+K simulations to the CH stretching spectra of larger saturated hydrocarbons. As molecules become larger and the density of states in this region increases, simulations become more sensitive to accidental resonances and consequently sensitive to the quality of the potential energy surface. To prevent spurious anharmonic mixings, it would be desirable to have diagonal matrix elements accurate to perhaps 1 $cm^{-1}$; however, this is a very difficult standard for molecules of more than a few atoms and is not likely to be achievable on systems like the butyl radical for some time.

A local mode treatment based on an affordable (B3LYP/6-311++G**) quadratic force field yielded predicted spectra qualitatively in line with experimental spectra but did not agree quantitatively for the radical-site CH stretches. This method appears to predict the spectra of the higher-symmetry *i*- and *tert*-butyl radicals more accurately than the straight-chain *n*- and *s*-butyl radicals with multiple conformers. In the case of the *tert*-butyl radical, local mode spectra clearly outperformed the higher-cost VPT2+K computations. We showed that this particular result was mostly fortuitous and related to the high density of vibrational states. When taken in consideration with the local-mode treatments of the propyl and alkylbenzyl radicals, the local mode model appears to be a reliable, low-cost treatment of short-chain alkyl radicals. Spectra for all these species were all obtained using the same fixed scaling and coupling parameters from previous studies, suggesting that these parameters are applicable to a wide range of alkyl radical systems.

***Selection of Theory Projects (no experimental contribution to the work).***

Goodlett, S.M.; Turney, J.M.; Douberly, G.E.; Schaefer, H.F. "The noncovalent interaction between water and the $^3$P ground state of the oxygen atom", Molecular Physics, (2022) DOI: 10.1080/00268976.2022.2086934

By computing the geometries of the water and triplet oxygen complex over several basis sets and high-level treatments of correlation, we have determined an accurate equilibrium geometry that shows little variation as these treatments are further increased. In addition, we have used the focal point approach to predict an accurate dissociation energy of the complex, with De=1.66 kcal $mol^{-1}$ and $D_0$=1.35 kcal $mol^{-1}$. Finally, we report harmonic and anharmonic vibrational frequencies for the complex, in anticipation of expected experimental attempts to detect the system. The experimental procedure we anticipate is a sequential capture of O($^3$P) and $H_2O$ in a helium droplet, followed by infrared laser Stark spectroscopy.

Begley, J.M.; Aroeira, G.J.R.; Turney, J.M.; Douberly, G.E.; Schaefer, H.F. "Enthalpies of formation for Criegee intermediates: A correlation energy convergence study", *Journal of Chemical Physics*, **158**, 034302 (2023). DOI: 10.1063/5.0127588

In this study, high-level coupled cluster techniques were used to compute the enthalpies of formation of various Criegee intermediates. The geometries for formic acid, acetic acid, formaldehyde oxide, *anti*-acetaldehyde oxide, and *syn*-acetaldehyde oxide were optimized at the CCSD(T)/ANO2 level, while the geometries for acetone oxide and propanoic acid were optimized at the CCSD(T)/ANO1 level. The computed energies for each species were extrapolated to the CBS limit and included corrections for the zero-point vibrational energy, the diagonal Born–Oppenheimer correction, the frozen core approximation, relativistic corrections, and higher-order energy corrections. As a cost reduction strategy, energy computations for acetaldehyde oxide conformers and acetic acid were computed with 75% of the optimized virtual orbital space retained, while energy computations for acetone oxide and propanoic acid were computed with 50% of the optimized virtual orbital space retained. Computed enthalpies of formation for formaldehyde oxide, both acetaldehyde oxide conformers, and acetone oxide are reported at these levels.

## Ongoing Experimental Work and Future Plans

### *Sequential Capture of O($^3$P) and Alkenes by Helium Nanodroplets: Infrared Spectroscopy and Ab Initio Computations of the Triplet Biradical Intermediates*

According to Smith *et al*. [Smith, I. W. M.; Sage, A. M.; Donahue, N. M.; Herbst, E.; Quan, D. *Faraday Discuss.* **2006**, 133, 137.], for molecule + radical reactions, the energetic difference between the molecule's ionization energy (IE) and the radical's electron affinity (EA) can provide insight into the nature of the reaction barrier, either *above* or *below* the reactant asymptote. They propose that a difference (IE − EA) greater than 8.75 eV indicates a real barrier above the asymptotic limit, whereas a value below 8.75 eV indicates a submerged barrier. Indeed, this difference for the O($^3$P) + HCN system is 12.2 eV. Accordingly, the barrier to oxygen insertion into the CN π system is ~10 kcal/mol above the reactant asymptote, and a van der Waals complex is observed when these species are brought together in a 0.4 K helium nanodroplet. However, O($^3$P) reactions with *alkenes* are predicted to cross the postulated 8.75 eV threshold as the alkene substitution pattern evolves from ethene (no substitution) to propene (methyl group substitution) to butene (dimethyl substitution, of which there are four different isomers), and this trend was tested by Sabbah *et al.*
[Sabbah, H.; Biennier, L.; Sims, I.R.; Georgievskii, Y.; Klippenstein, S.J.; Smith, I. W. *Science* **2007**, 317, 102.]. Their findings corroborated the behavior predicted by Smith *et al.* The HCN + O($^3$P) results presented recently by us demonstrate the feasibility for analogous alkene + O($^3$P) spectroscopic studies, in which O($^3$P) and alkenes of varying substitution are combined in helium droplets *via* the sequential capture scheme. As the *real* reaction barrier (*i.e.* for the ethene and propene reactions) evolves to being *submerged* below the asymptotic limit (*i.e*. for the butene reactions), one might expect that strongly bound reaction intermediates, such as triplet biradicals, will be observed in helium droplets, rather than van der Waals complexes. Given the fact that a 10,000 atom helium droplet can dissipate 140 kcal/mol, it should be

possible to quench the internal energy of these reaction intermediates and probe them for the first time spectroscopically.

Joseph T. Brice, Peter R. Franke, Gary E. Douberly "Sequential Capture of O($^3$P) and HCN by Helium Nanodroplets: Infrared Spectroscopy and Ab Initio Computations of the $^3\Sigma$ O-HCN Complex" *Journal of Physical Chemistry A,* **121**, 9466-9473 (2017). Published: November 2017.

**Selected Publications acknowledging DOE support (2020-2023):**


1. Mathew M. Davis, Jared D. Weidman, Adam S. Abbott, Gary E. Douberly, Justin M. Turney, Henry F. Schaefer, "Characterization of the 2-Methylvinoxy Radical + $O_2$ Reaction: A Focal Point Analysis and Composite Multireference Study" *Journal of Chemical Physics*, (2019), 151, 124302. DOI: 10.1063/1.5113800. Published: September 2019.

2. Jonathon P. Misiewicz, Kevin B. Moore, Peter R. Franke, W. James Morgan, Justin M. Turney, Gary E. Douberly, and Henry F. Schaefer, "Sulfurous and Sulfonic Acids: Predicting the Infrared Spectrum and Setting the Surface Straight" *Journal of Chemical Physics*, **152**, 024302 (2020). DOI: 10.1063/1.5133954. Published January 2020.

3. Jared D. Weidman, Justin M. Turney, Henry F. Schaefer, "Energetics and Mechanisms for the Acetonyl + $O_2$ Reaction: An Important System for Atmospheric and Combustion Chemistry" Journal of Chemical Physics, 152, 114301 (2020). DOI: 10.1063/1.514859. Published: March 2020.

4. Michael C. Bowman, Alexandra D. Burke, Justin M. Turney, Henry F. Schaefer, "Conclusive Determination of Ethynyl Radical Hydrogen Abstraction Energetics and Kinetics" Molecular Physics, 118 (2020). DOI: 10.1080/00268976.2020.1769214. Published: June 2020.

5. Peter R. Franke, John F. Stanton, Gary E. Douberly, "How to VPT2: Accurate and Intuitive Simulations of CH Stretching Infrared Spectra Using VPT2+K with Large Effective Hamiltonian Resonance Treatments" *Journal of Physical Chemistry A* (Invited Review), **125**, 1301-1324 (2021). DOI: 10.1021/acs.jpca.0c09526. Published January 2021.

6. Matthew G. Christianson, Anna C. Doner, Matthew M. Davis, Alanna L. Koritzke, Justin M. Turney, Henry F. Schaefer, Leonid Sheps, David L. Osborn, Craig A. Taatjes, and Brandon Rotavera. "Reaction Mechanisms of a Cyclic Ether Intermediate: Ethyloxirane" *Int. J. Chem. Kinet.* **53**, 43-59 (2021). DOI: 10.1002/kin.21423. Published: January 2021.

7. Anna C. Doner, Matthew M. Davis, Alanna L. Koritzke, Matthew G. Christianson, Justin M. Turney, Henry F. Schaefer, Leonid Sheps, David L. Osborn, Craig A. Taatjes, Brandon Rotavera, "Isomer-Dependent Reaction Mechanisms of Cyclic Ether

Intermediates: cis-2,3-dimethyloxirane and trans-2,3-dimethyloxirane" *Int. J. Chem. Kinet.* **53**, 127-145 (2021). DOI: 10.1002/kin.21429. Published: January 2021.

8. A. D. Burke, M. C. Bowman, J. M. Turney, and H. F. Schaefer, "Energetics and Kinetics of Various Cyano Radical Hydrogen Abstractions," *Phys. Chem. Chem. Phys.* **23**, 3389-3400 (2021). DOI: 10.1039/D0CP06228F. Published January 2021.

9. Adam S. Abbott, Boyi Z. Abbott, Justin M. Turney, Henry F. Schaefer, "Arbitrary-Order Derivatives of Quantum Chemical Methods via Automatic Differentiation" *J. Phys. Chem. Lett.* **12**, 3232-3239 (2021). DOI: 10.1021/acs.jpclett.1c00607. Published: March 2021.

10. Mull, H.F.; Franke, P.R.; Sargent, C.; Douberly, G.E.; Turney, J.M.; Schaefer, H.F. "Four isomers of $In_2H_2$: a careful comparison between theory and experiment" *Molecular Physics*, **119**, 21-22 (2021). DOI: 10.1080/00268976.2021.1979675. Published: September 2021.

11. Bralick, A.K.; Abbott, B.Z.; Douberly, G.E.; Schaefer, H.F. "The isomerisation of $H_2XY$ to HXYH (X, Y = O, S, and Se)*" *Molecular Physics*, **119**, 17-18 (2021). DOI: 10.1080/00268976.2021.1976429. Published: September 2021.

12. Mull, H.F.; Turney, J.M.; Douberly, G.E.; Schaefer, H.F. "Kinetic stability of pentazole" *Journal of Physical Chemistry A*, **121**, 9092-9098 (2021). DOI: 10.1021/acs.jpca.1c06252. Published: October 2021.

13. Li, G.; Yao, Y.; Lü, S.; Xie, Y.; Douberly, G.E.; Schaefer, H.F. "Potential energy profile for the $Cl + (H_2O)_3 \rightarrow HCl + (H_2O)_2OH$ reaction. A CCSD(T) study" *Physical Chemistry Chemical Physics*, **23**, 26837-26842 (2021). DOI: 10.1039/D1CP04309A. Published: November 2021.

14. Goodlett, S.M.; Turney, J.M.; Douberly, G.E.; Schaefer, H.F. "The noncovalent interaction between water and the $^3P$ ground state of the oxygen atom", Molecular Physics, (2022) DOI: 10.1080/00268976.2022.2086934

15. King, K.E.; Franke, P.R.; Pullen, G.T.; Schaefer, H.F.; Douberly, G.E. "Helium droplet infrared spectroscopy of the butyl radicals", *Journal of Chemical Physics*, **157**, 084311 (2022). DOI: 10.1063/5.0102287

16. Douberly, G.E. (2022). Infrared Spectroscopy of Molecular Radicals and Carbenes in Helium Droplets. In: Slenczka, A., Toennies, J.P. (eds) Molecules in Superfluid Helium Nanodroplets. Topics in Applied Physics, vol 145. Springer, Cham. https://doi.org/10.1007/978-3-030-94896-2_4

17. Begley, J.M.; Aroeira, G.J.R.; Turney, J.M.; Douberly, G.E.; Schaefer, H.F. "Enthalpies of formation for Criegee intermediates: A correlation energy convergence study", *Journal of Chemical Physics*, **158**, 034302 (2023). DOI: 10.1063/5.0127588

# Coordination and Solvation of Actinide Cations Studied with Selected-Ion Infrared Spectroscopy

DOE Award No. DE-SC0018835

Michael A. Duncan
Department of Chemistry, University of Georgia, Athens, Georgia 30602

maduncan@uga.edu

## Program Scope

Actinide metal and metal oxide cation-molecular complexes are studied in the gas phase to investigate their bonding, ligand coordination and solvation. Cation-molecular complexes of the form $M^{n+}(L)_y$, where M = U or Th, n = 1 or 2, and L = small molecules such as $H_2O$, CO, $N_2$, $CO_2$, $CH_3CN$, or benzene are produced in a supersonic molecular beam by pulsed laser vaporization of solid metal targets. Similar methods produce metal oxide complexes. Complexes containing a metal or oxide core ion with a specific number of ligand or solvent molecules are size-selected in a time-of-flight mass spectrometer and studied with different forms of laser photodissociation measurements. Tunable infrared laser spectroscopy reveal the shifts that occur for ligand/solvent vibrations upon binding to these metals and how these vary with the charge state, the number of ligands or solvent molecules present, the geometric and electronic structures of complexes, and the possible occurrence of ligand reactions mediated by the metal center. Additional experiments employ tunable laser UV-visible photodissociation spectroscopy to probe excited states and photodissociation thresholds. Photofragment imaging also investigates cation-molecular bond energies. The experiments are complemented by computational chemistry, with careful attention to relativistic and spin-orbit effects. The goal of these studies is an increased understanding of the fundamental interactions and electronic structure involved in actinide bonding, coordination and solvation.

## Recent Progress

In recent work on this project, we used laser vaporization to produce ion-molecule complexes of uranium and thorium cations with cyclo-octatetraene (COT). These systems were investigated with mass spectrometry and ion photodissociation to explore coordination behavior and possible photochemical reactions that might occur upon ultraviolet excitation. The mass spectra produced are shown in Figure 1a. In the dissociation of these complexes, intact ligand elimination was detected, but also the loss of $C_2H_2$ (presumed to be acetylene) via a photochemical reaction (Figure 1b). A similar reaction was seen previously for transition-metal or lanthanide cation-COT complexes. $U^+(C_5H_5)$ and $U^+(C_3H_3)$ fragment ions were also detected, which we found previously to be fragments from $U^+$(benzene). These unexpected reaction products were missing for thorium ions. Computational studies were done at the DFT/B3LYP level employing the cc-pVTZ-PP basis set, which includes the Stuttgart/Köln

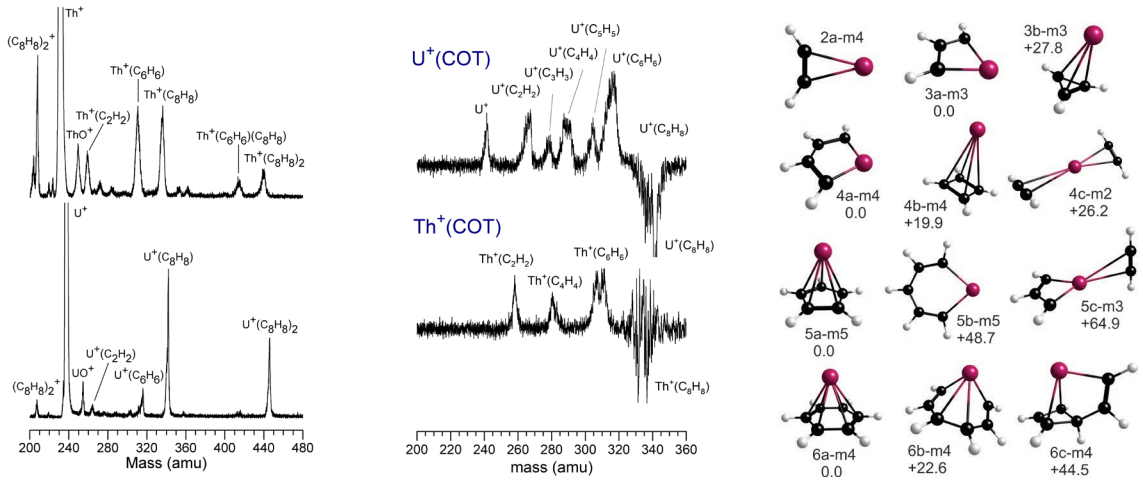


Figure 1. a) Mass spectra of $UO_2^+(acetone)_n$ complexes (left). b) Photodissociation mass spectra of $M^+(COT)$ complexes, showing different ligand fragmentation processes for uranium vs thorium complexes. c) The structures for various $U^+(C_nH_m)$ complexes and fragments from computational studies, including relative energies and multiplicities (m).

fully relativistic 60 electron ECP for uranium. We examined the structures and energetics of all the fragment ions detected to determine the likelihood of sequential versus parallel dissociation processes. The structures for various $U^+(C_nH_m)$ complexes and fragments are shown in Figure 1c.

We continued our studies on the infrared spectroscopy of $U^+(L)_x$ and $UO_n(L)_x^+$ complexes. In the past, we examined the carbonyl complexes of uranium and uranium oxide cations. In more recent work, we have extended these studies to complexes with L = $CO_2$, $N_2$, and water. The N–N stretches of the nitrogen complexes were shifted to lower frequencies compared to the free-$N_2$ stretch (Figure 2a), and the mass spectrum indicated a strong preference for an eight-coordinate complex. The spectrum of the $U^+(N_2)_8$ complex had a single vibrational band, indicating a high-symmetry structure. Uranium-$CO_2$ complexes had complex vibrational structure, indicating the possibility of both metal-$CO_2$ electrostatic complexes and the formation of oxide-carbonyl and/or carbonate reaction products. We were able to obtain infrared spectra for both singly and doubly charged complexes, e.g., $UO^{2+}(CO_2)_{7,8,9}$ in Figure 2b. Computational studies to explain these infrared spectra are ongoing. We have discovered that the cc-pVTZ-PP basis set and the core potential for uranium indicated earlier provide a superior treatment of vibrational spectra compared to the results of previously employed functionals and basis sets. Figure 2c shows the infrared spectrum of $UO_2^+(CO)_5$ compared to the predictions of DFT/PBE/VTZP versus the newer DFT/B3LYP/cc-pVTZ-PP theory. The latter method correctly predicts the direction of the shift in the C–O stretch frequency and its magnitude.

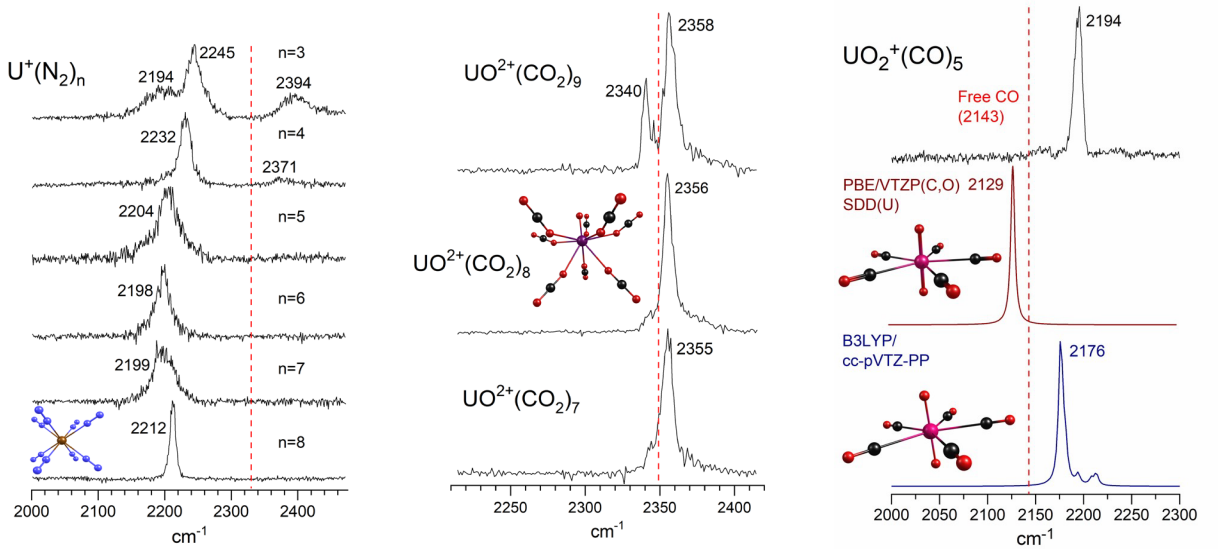


Figure 2. a) (left) IR-PD spectra for $U^+(N_2)_n$ complexes measured via the elimination of $N_2$. The dashed red line shows the frequency of $N_2$. b) IR-PD spectra of $UO^{2+}(CO_2)_{7,8,9}$ showing the blue-shifted asymmetric stretch vibration for the n = 7, 8 complexes and the appearance of a slightly red-shifted $CO_2$ vibration at n = 9 after the coordination is filled at n = 8. c) The infrared spectrum of $UO_2^+(CO)_5$ compared to the predictions of DFT/PBE/VTZP versus DFT/B3LYP/cc-pVTZ-PP theory. The latter predicts the direction and magnitude of the vibrational shift more accurately.

In new work we have extended photodissociation studies to the UV-visible region. For metals like iron and uranium, the density of excited electronic states is so great that $M^+$-L ion-molecule complexes have essentially a continuous absorption spectrum. If this is the case, measurement of the threshold for the appearance of dissociation is equivalent to measuring the bond energy for the complex. We have now measured photodissociation threshold energies to determine the ligand binding energies for $U^+$(benzene) and $UO^+$(benzene). The resulting bond energies are 45.4 and 58.3 kcal/mol, respectively.

## Future Plans

We will continue the infrared spectroscopy experiments by examining uranium-acetylene and uranium-benzene complexes as well as small uranium and thorium carbonyls. Uranium cations have been suggested previously to catalyze the cyclo-trimerization reaction to form benzene, but there is no spectroscopic evidence to confirm this. Infrared measurements will also probe the $U^+(C_nH_m)$ masses produced as fragments from $U^+$(COT). Additional threshold photodissociation experiments in the UV-visible region will be conducted on a variety of $U^+$-L, $UO^+$-L, and $UO_2^+$-L complexes to determine their bond energies.

## BES Supported Publications (2020 – 2023)

1. P. D. Carnegie, J. H. Marks, A. D. Brathwaite, T. B. Ward, M. A. Duncan, "Microsolvation in $V^+(H_2O)_n$ Clusters Studied with Selected-Ion Infrared Spectroscopy," *J. Phys. Chem. A* **124**, 1093−1103 (2020). DOI: 10.1021/acs.jpca.9b11275.

2. J. H. Marks, P. Kahn, M. Vasiliu, D. A. Dixon, M. A. Duncan, "Photodissociation and Theory to Investigate Uranium Oxide Cluster Cations," *J. Phys. Chem. A* **124**, 1940−1953 (2020). DOI: 10.1021/acs.jpca.0c00453.

3. J. H. Marks, T. B. Ward, A. D. Brathwaite, M. A. Duncan, "Infrared Spectroscopy of $Zn(Acetylene)_n^+$ Complexes: Ligand Activation and Nascent Polymerization," *J. Phys. Chem. A* **124**, 4764−4776 (2020). DOI: 10.1021/acs.jpca.0c03358.

4. A. D. Brathwaite, T. B. Ward, J. H. Marks, M. A. Duncan, "Coordination and Solvation in Gas Phase $Ag^+(C_2H_2)_n$ Complexes Studied with Selected-Ion Infrared Spectroscopy," *J. Phys. Chem. A* **124**, 8562−8573 (2020). DOI: 10.1021/acs.jpca.0c08081.

5. B. M. Rittgers, D. Leicht, M. A. Duncan, "Cation-π Complexes of Silver Studied with Photodissociation and Velocity-Map Imaging," *J. Phys. Chem. A* **124**, 9166−9176 (2020). DOI: 10.1021/acs.jpca.0c08498.

6. J. H. Marks, E. Miliordos, M. A. Duncan, "Infrared Spectroscopy of RG-$Co^+(H_2O)$ Complexes (RG = Ar, Ne, He): The Role of Rare Gas "Tag" Atoms," *J. Chem. Phys.* **154**, 064306 (2021). DOI: 10.1063/5.0041069.

7. J. H. Marks, B. M. Rittgers, M. J. van Stipdonk, M. A. Duncan, "Photodissociation and Infrared Spectroscopy of Uranium-Nitrogen Cation Complexes," *J. Phys. Chem. A* **125**, 7278−7288 (2021). (Dan Neumark Festschrift). DOI: 10.1021/acs.jpca.1c05823.

8. N. J. Dynak, B. M. Rittgers, J. E. Colley, *D. J. Kellar*, M. A. Duncan, "Photofragment Imaging of Carbon Cluster Cations: Explosive Ring Rupture," *J. Phys. Chem. Lett*. **13**, 4786−4793 (2022). DOI: 10.1021/acs.jpclett.2c00950.

9. J. H. Marks, A. G. Batchelor, *J. R. C. Blais*, M. A. Duncan, "Cationic Complexes of Uranium and Thorium with Cyclooctatetraene: Photochemistry and Decomposition Products. *J. Phys. Chem. A* **126**, 4230−4240 (2022). DOI: 10.1021/acs.jpca.2c03035.

10. B. M. Rittgers, J. H. Marks, D. J. Kellar, M. A. Duncan, "Photoinduced Charge Transfer in the Zn-Methanol Cation Studied with Selected-Ion Photofragment Imaging," *J. Chem. Phys.* **157**, 114302 (2022). DOI: 10.1063/5.0108467.

# TOWARDS MACHINE LEARNING MOLECULAR DYNAMICS: EFFECT OF DATA PARTITIONING ON MODEL RESULTS

C. Franklin Goldsmith, PI
Brown University

## Program Scope

One of the grand challenges for the Department of Energy is the ability to simulate the complex interactions between fluid mechanics and chemical kinetics for gases at high pressures (e.g. 100 bar). Under these conditions, the ideal gas equation of state is not valid. Although considerable advances have been made regarding real-gas equations of state for thermodynamic properties, the same cannot be said of chemical kinetics under extreme pressures. The standard approach in computational kinetics assumes that reactions occur under isolated conditions. Real-gas behavior can have a profound effect on the chemical source terms in reactive flow simulations. These many-body interactions can change both the rate constants and the product branching fractions.

In this project, we are investigating different methodologies to quantify many-body effects on transition states and thence high-pressure effects on rate constants. The specific aims are: (i) develop chemically accurate surrogate potential energy surfaces for computational kinetics with explicit solvent molecules, and use this surrogate model within molecular dynamics simulations; (ii) quantify the effects of high pressures on rate constants for different reaction families; (iii) determine the pressure at which solvent cage effects will cause the branching fractions in bond-fission reactions to favor molecular elimination products; and (iv) analyze the results for possible trends that can be applied heuristically.

Additionally, we have begun to develop a purely theory-based mechanism for fluorinated compounds to understand the incineration of per- and poly-fluorinated alkyl substances (PFAS).

## Recent Progress

The past year has continued to focus on the development of a machine learning molecular dynamics (MLMD) methodology. The goal is to develop a platform, as close to black box as possible, that will enable us to go from electronic structure calculations to a full-dimensional force-field model for use in molecular dynamics for arbitrary systems.

In order to develop a potential model suitable for MD, we need to provide sufficient sampling in both intramolecular and intermolecular interactions. Our current work uses density functional theory (DFT) to provide the required training data. Preliminary work focused on random sampling within internal-coordinate space as a way of exploring in intramolecular interactions. This approach, while computationally advantageous, did a poor job of covering the regions of phase space that were explored during the MD simulations. Instead, we used ab initio molecular dynamics (AIMD) to generate the training data.

We have submitted our first publication on machine learning molecular dynamics. "High-Dimensional Neural Network Potentials for Accurate Prediction of Equation of State: A Case Study of Methane", Mostafa Abedi, Jörg Behler, and C. Franklin Goldsmith is currently under review at the *Journal of Chemical Theory and Computation*.

The manuscript is notable for two main contributions. First, we considered two different ways of generating the training data. In one case, we planewave basis functions with periodic boundary conditions. This approach, which we call "bulk", is the standard approach used in the community. As an alternative, we also use Gaussian-type orbital basis functions with non-periodic boundary conditions, but instead we specific a repulsive wall to maintain density. This approach, "cluster", is a newer idea, which allows us to use more accurate electronic structure methods that might be better suited for molecular systems (and saddle points). The bulk AIMD was performed in CP2K; the cluster AIMD was performed in ORCA.

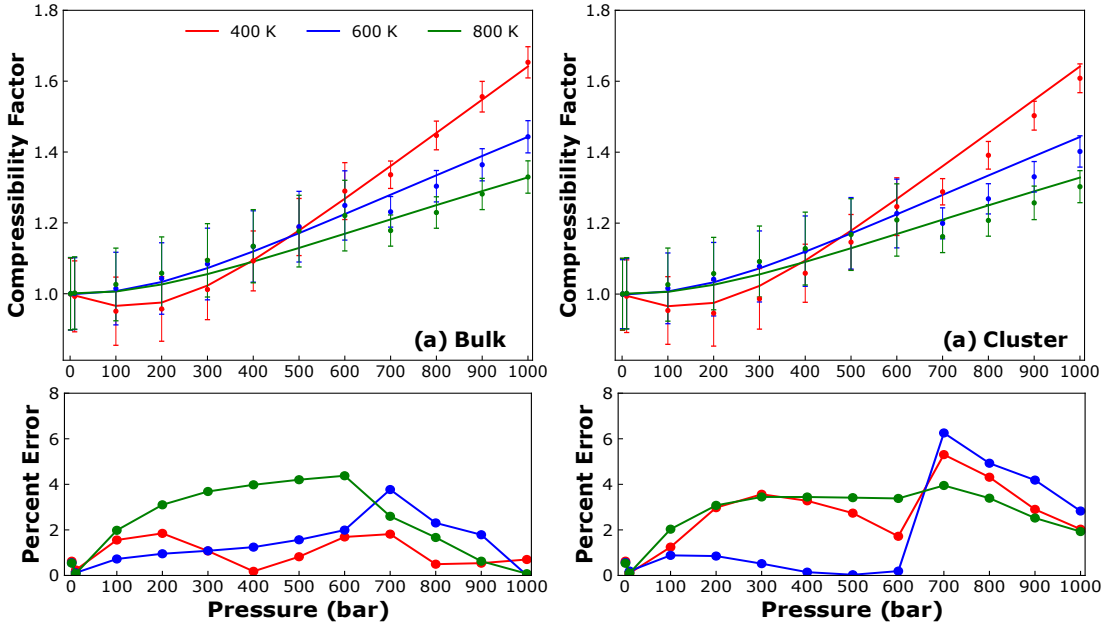


Figure 1: compressibility factor, $Z$, for methane. The solid lines are the reference equation of state, taken from CANTERA. The symbols are the predicted values from our machine learning molecular dynamics approach. The two panes on the left are the bulk data, obtained using periodic boundary conditions and planewave basis functions, and the two panes on the right are the cluster data, which were obtained using non-periodic boundary conditions and GTO basis functions.

The second contribution is the ability to test our model results against previously validated equation of state data. Our model correctly predicts the mass density of methane over a broad range of conditions, from compressed liquids to dense gases to ideal gases. Figure 1 presents the compressibility factor, $Z$, for $CH_4$. Our model correctly predicts the compressibility factor over a broad range of densities. This range includes both conditions where $Z < 1.0$ (indicating that attractive forces dominate, and the density

is decreased relative to that of an ideal gas), and conditions where $Z > 1.0$ (indicating that repulsive forces dominate). For most of these conditions, the error is within ± 4%.

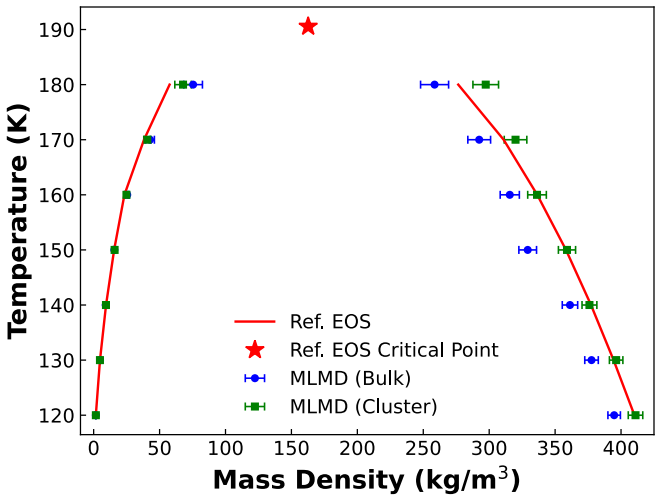


Figure 3: liquid-vapor coexistence curve for methane. The cluster model, shown in green potentially outperforms the bulk model.

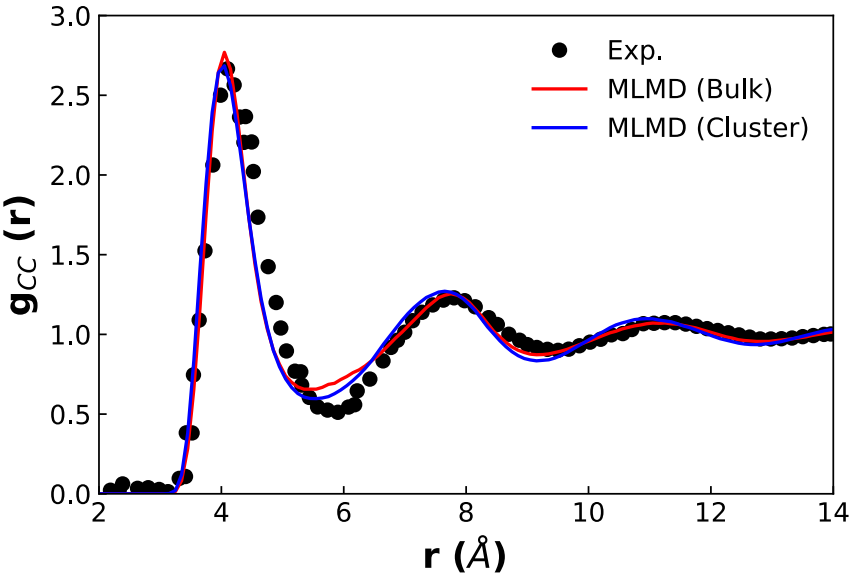


Figure 2: radial distribution function for methane.

In addition to the mass density, we also computed the liquid-vapor coexistence dome, Figure 3, and the radial distribution function, Figure 2. Both methods of generating the training data, bulk and cluster, are in excellent agreement with the experimental data. Arguably, the model generated from the cluster data even outperforms the bulk model, even though it required significantly less time to generate the training data. These results

suggest that the cluster approach is a viable alternative, and it can be relied upon for producing training data for other systems.

Indeed, we have currently moved on to our first application in kinetics. We are using this "cluster" approach to compute a high-dimensional neural network potential for the H abstraction reaction between methanol and hydroperoxyl radical, $CH_3OH + HO_2 \rightleftharpoons CH_2OH + H_2O_2$, in a $N_2$ bath. Our goal is to study the experimental conditions from the recent work of Yiguang Ju and coworkers "Methanol oxidation up to 100 atm in a supercritical pressure jet-stirred reactor", *Proceedings of the Combustion Institute* (2022). Prof. Ju also is supported by the GPCP program, and we have been collaborating on this project.

**Future Plans for MLMD**

Our goal is to compute the change in volume of activation, $\mathbf{\Delta}V^{\ddagger}$, as a function of temperature and pressure. This $\mathbf{\Delta}V^{\ddagger}(T, p)$ will enable us to compute real-gas corrections for rate constants. The internal degrees of freedom of the solute are frozen. As with the EoS results, we first compute the $V(T, p)$ using the *NPT* ensemble. The change in volume of activation is then given by $\mathbf{\Delta}V^{\ddagger}(T, p) = V_{TS}(T, p) - V_{OH}(T, p) - V_{CH3OH}(T, p)$. We have begin computing the individual $V_{TS}(T, p)$, $V_{OH}(T, p)$, and $V_{CH3OH}(T, p)$ at 725K and pressures of 1, 10, 100, and 1000 bar.

**PFAS**

We continue to work on our theory-based mechanism for PFAS incineration. Our first manuscript was recently published: "A Theory-based Mechanism for Fluoromethane Combustion I: Thermochemistry and Abstraction Reactions" Siddha Sharma, Kento Abeywardane, and C. Franklin Goldsmith, *Journal of Physical Chemistry A* (2023). In this manuscript, we extended the ANL0 methodology to include fluorine atoms. We found that the best results were obtained when using $CF_4$ as the reference species. We computed the thermophysical properties for 92 small molecules containing H/C/O/F (all species up to 2 carbon atoms). Additionally, we computed 40+ rate constants for H abstraction, and 30+ rate constants for F abstraction. We are now extending this project to include much larger fluorinated compounds.

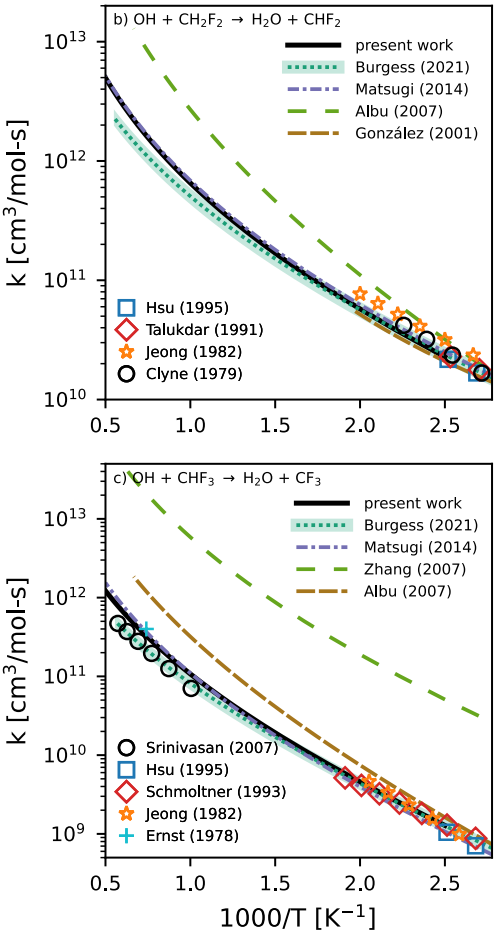


Figure 4: H-abstraction via OH.

**DE-SC0021206: Langevin Dynamics modeling of gas-phase ion-ion recombination**

**Principal Investigator:** Ranganathan Gopalakrishnan, Ph. D., Associate Professor, University of Memphis
Email: rgplkrsh@memphis.edu
Graduate assistants: Mr. Zhibo Liu (MS student), Ms. Mrittika Roy (PhD student)

This project focuses on modeling mutual neutralization reactions of the form $A^+ + B^- + M \rightarrow A + B + M^*$. There are many theoretical models and experimental data available for this kind of reaction for a wide range of pressure and a wide variety of reacting ions[1-3]. Prior work has been aimed at quantifying the effect of temperature, pressure, and concentration on the reaction rate constant $\beta\left(\frac{m^3}{s}\right) = \frac{\alpha}{n_1 n_2}$, where $n_1$ and $n_2$ are the number density of the two species $A^+, B^-$ involved in the elementary collisional reaction (unit: $m^{-3}$), and $\alpha$ is the rate of reaction with unit $m^{-3}s^{-1}$. Our current work focuses on describing recombination between monoatomic ion pairs listed in **Table 1** in specified pressure ranges[4-6]. In addition to modeling specific ion pairs, effort has been aimed at developing a generalized methodology capable of handling any ion pair, and more importantly any type of chemical reaction using Landau-Zener transition state theory. The details of calculating $\beta$ are discussed herein.

| Ion pair (~133 Pa, unless otherwise indicated) |
|---|
| $H^+ + H^-$ |
| $Li^+ + H^-$ |
| $Ne^+ + Cl^-$ |
| $Xe^+ + Cl^-$ |
| $Xe^+ + Br^-$ |
| $Kr^+ + Cl^-$ |
| $He^+ + Cl^-$ |
| $Xe^+ + F^-(\sim 10^4 - 10^5\ Pa)$ |

**Table 1:** Monoatomic pairs modeled using Landau-Zener transition state theory coupled with trajectory simulations.

As the size of the ions are very small, their collision dynamics and chemical transitions, more specifically, electron exchange between an anion and cation, cannot be described using classical physics alone. The electron transfer from the anion to cation starts to happen when the ion pairs are *close enough* for the probability of electron transfer to be non-zero. Our approach has been aimed at addressing three important questions:

1. At what separations between the ions does the electron transfer happen?
2. What is the associated probability of electron transfer at these separations?
3. What is rate the of mutual neutralization for a wide range of pressure given that we know the answers to #1 and #2, considering the effect of background/neutral gas pressure and temperature which influence the rate of transport of the ions towards each other?

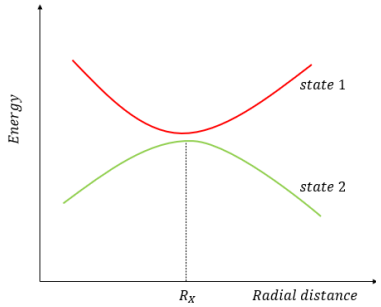


**Figure 1:** Calculating the probability of electron transfer using Landau Zener Transition State Theory between two diabatic states with nearly equal energies.

According to Landau Zener theory, when two diabatic states of a system cross each other, there is a finite probability that the system will have a transition from one state to another at the crossing point (**Figure 1**). The analytic expression for this probability $p$ is:

$$p_{LZ} = \exp\left(\frac{-2\pi H_{12}^2}{\hbar\left|\frac{\partial(E_2 - E_1)}{\partial t}\right|}\right) \ldots (1)$$

Here, $H_{12}$ is the off-diagonal element of a two-state system coupling the bases, $\hbar$ is the reduced Planck's constant, and $E_1$ and $E_2$ are the energy of the two states at the crossing point $R_X$. In 1970, Olson applied Landau Zener theory for a system of two oppositely charged ions and gave a semi-classical theory to calculate their reaction rate[3]. We are following his approach here and using Langevin Dynamics trajectory simulations to efficiently capture the effect of background gas pressure and temperature on the recombination process. For a system of mono atomic ion pairs the denominator of the above expression for probability can be modified and rewritten as:

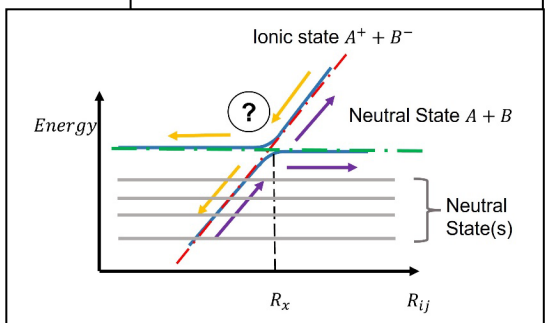


**Figure 2:** Schematic of crossings between an ionic reactant state and neutral product states.

$$p_{LZ} = \exp\left(\frac{-2\pi H_{12}^2}{\hbar\left|\frac{\partial R}{\partial t}\frac{\partial(E_2 - E_1)}{\partial R}\right|}\right) \rightarrow p_{LZ} = \exp\left(\frac{-2\pi H_{12}^2}{\hbar|v_{rad}F|}\right) \ldots (2)$$

Here, $v_{rad}$ and $F$ are the relative radial velocity of two ions and the Coulombic force between them, respectively. In our system, we have oppositely charged ion pairs. By applying Born Oppenheimer approximation to our system, we decouple the electronic and nuclear wave function. So, the potential energy surface can be expressed as a function of the radial distance between the nuclei of the ions. The general structure of a two-dimensional potential energy curve for any ion pair looks like the schematic in **Figure 2**. When the two atoms are in neutral state there is no coulombic force between them. Vander wall force is effective only when they approach each other at very close distances. So, the energy state for two neutral atoms is flat after a small radial distance. These neutral states can be ground state (where both the ions have lowest energy value) or can be excited states (where one or both the ions have greater energy values than their corresponding ground states). But their energy levels are constant over the radial distance. When both the atoms are in ionic state, long range Coulomb force acts between then, making the energy levels vary with radial distance. At distances where this ionic curve crosses any of the excited energy states, there is a finite probability that an electron will jump from the anion to the cation resulting in a system having two neutral atoms. We can draw an imaginary sphere of radius equal to the crossing distance $R_x$ having one of the ions at its center (**Figure 3**). While the two ions approach each other, the second ion enters this sphere. If there is a successful neutralization depends on the state of the second ion while it leaves the sphere of the first ion i.e., the second ion must be in neutral state to assure the occurrence of neutralization. From this argument we can infer that for a successful neutralization event between an ion pair at a crossing point $R_x$ one transition is adiabatic and the other is diabatic. Hence, the probability of electron transfer would be:

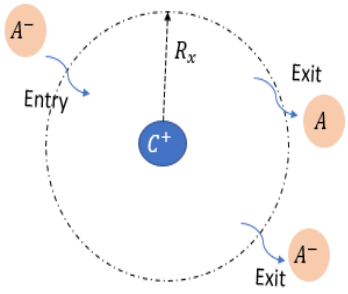


**Figure 3:** Implementation of electron transfer probability using a Monte Carlo approach.

$$p = 2 * p_{LZ}(1 - p_{LZ}) \dots (3)$$

To calculate the Landau Zener probability, we need the radial velocity $v_R$, force between the atoms $F$ and the coupling parameter $H_{12}$. We calculate the radial velocity $v_R$ and the force $F$ from the trajectory simulation as a function of pressure and temperature and charge of the ions. We do ab initio quantum calculations to determine the coupling parameter $H_{12}$ for each ion pair. We use the quantum calculation software *MOLPRO*® to calculate the potential energy curves (PECs).

**Calculation of the Potential Energy Curves (PECs), Crossing distance $R_x$ and Coupling Matrix $H_{ij}$: Figure 4** is the plot of potential energy curves for a system of $H^+$ and $H^-$. The ionic energy state, calculated directly from the spectroscopic data (not doing any quantum calculation), is superimposed with the dissociation energy at very large distance. The dissociation energy is defined as $E_d = IE - EA$, where $IE$ is the ionization energy of the anion and $EA$ is the electron affinity of the cation. The crossing points between the excited states and the ionic state is determined:

$$R_x = \frac{e^2}{4\pi\varepsilon_0(E_d - E_i)} \dots (4)$$

All the solid energy lines are calculated using the MOLPRO software. In the PEC plot the bottom most one is the ground state energy, the next few lines are the excited neutral states of Lithium, and the topmost line is the ionic state. The details of this quantum computation will not be discussed here. But briefly we can state the input parameters of MOLPRO script:

I. Geometry of the two molecules
II. Total number of electrons in the system
III. The wave function symmetry of the system
IV. The total spin of the system
V. Adequate size of active space to include the required energy states.
VI. Size of active space which is not considered during the simulation to save computation expense.

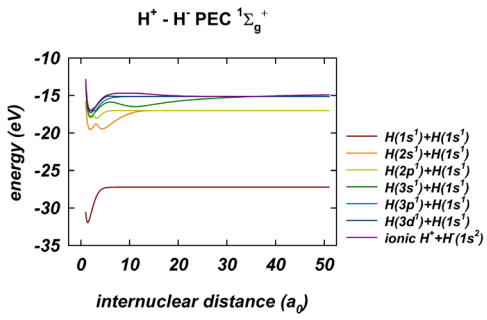


**Figure 4:** Potential energy curve for $H^+ - H^-$.

Inside one DO loop, an MCSCF and MRCI computation are being executed for the current interatomic distance and the interatomic distance is being updated after every calculation. Each MRCI takes the orbitals and the CI vectors from previous MCSCF, and the result, especially energy values for each state are stored in a variable for post analysis. An unrestricted Hartree-Fock (UHF) or a restricted Hartree-Fock (RHF) computation is usually done once before the

looping, serving as the initial guess of the first MCSCF calculation. The nonadiabatic coupling matrix elements (NACMEs) can be calculated using the "DDR" function in MOLPRO, where in this study we use the central difference 3-point method. The NACMEs are calculated in an individual trial using the same separation list values. Based on the NACMEs result, the crossings distances will be determined at where the couplings reach maximum. Combining the result of potential energy curves and the NACMEs, $H_{ij}$ values for each crossing are calculated as $H_{ij} = \frac{E_i - E_j}{2}\Big|_{R_x}$.

## Classical trajectory simulations

**Free Molecular Limit:** The simulation is conducted in a reduced mass reference where the cation A is imposed to the coordinate origin, and the motion of anion B is described as a point mass by Newton's equation of motion with reduced mass, and the position of B as well as the relative position of two nuclei is denoted by $r$. The two potentials present are assumed to be a unscreened Coulombic potential of point charge and a 12-6 Lennard-Jones potential. To mimic the dilute free-molecular system, the anion B is initiated on a plane that is nominally infinitely far away from ion A, which is the origin. The plane is set to be a square plane with the edge length of two times of the critical impact parameter $b_c$ so that all impact parameters that leads to a crossing with the outer most crossing distance are accessible. To evaluate the partial cross-sectional area $\sigma$, ion B is launched with a fixed initial velocity $v_{ini}$ that is perpendicular to the plane of ion A's position, and the initial position of B is chosen on the plane randomly following a uniform probability distribution. The trajectory of B is solved numerically using the generic RK-4 method. Between each two consecutive time steps the nuclei separation is monitored and compared with crossing distances to capture the crossing event. If a crossing event if detected, the instantaneous radial velocity is computed and passed to the Landau-Zener formula to evaluate the diabatic transition probability $p_{LZ}$. Since in this study the general case of electron transfer is considered, so we replace the commonly used theoretical combined probability under free-molecular limit with a set of logical conditioning, the termination of trial due to a successful neutralization reaction is assumed as only when A and B separates as two neutral atoms.

In the simulation, an auxiliary termination conditioning is also used to determine if B has left the region of interest, so the ultimate outcome of each trial will be noted as either an effective neutralization (a "Hit") or an escape from the simulation domain without an effective neutralization (a "Miss"). The evaluation of partial cross-section is done with Monte-Carlo method by:

$$\sigma = 4b_c^2 \frac{N_{Hit}}{N_{Hit} + N_{Miss}} \dots (5)$$

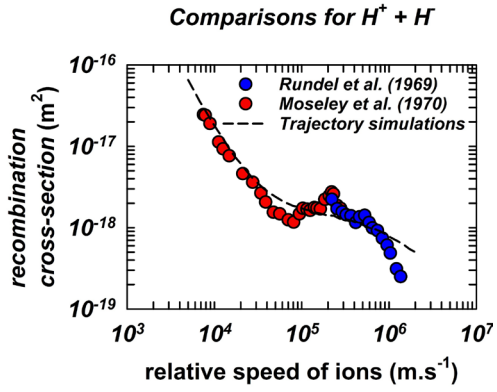


**Figure 5:** Recombination cross-section calculations for $H^+ - H^-$ ion pair.

Where the pre-factor $4b_c^2$ is the area of the plane where B is launched from, and the later term $\frac{N_{Hit}}{N_{Hit}+N_{Miss}}$ is the probability or a measurement of contribution of overall launch plane size. **Figure 5** shows recombination cross-section calculations for $H^+ - H^-$ ion pair as a function of their relative speed. Calculations are compared with experimental data from high energy particle physics experiments[7, 8]. Manuscript under preparation (Liu et al.) describes calculations and comparisons with appropriate experimental data for several monoatomic ion pairs.

**Transition Regime:** In the transition regime and the high-pressure limit, in contrast to free-molecular limit, the motion of each particle is random and stochastic due to either direct collisions or Coulombic collisions between particles. To approximate the effect of neutral gas molecules, the equation of motion of the ions is solved using Langevin Dynamics[9]. During the simulation, we focus on the modification of ion trajectory due to the neutrals or the pressure of the system. Unlike the free-molecular case, one cannot neglect the damping effect of the neutral particles, this damping effect will introduce another pathway for neutralization reaction via forming a pseudo-stable orbiting motion. Unfortunately to study the details of this type of electron transfer a Landau-Zener transition model is not sufficient and it usually would require a full-scale quantum simulation which is out of the scope of the current study. Alternatively, since the rate constant is evaluated by mean first passage time that is commonly in the order of sub millisecond or microsecond due to mainly the transport activity that brings ion pairs to a separation that is favorable for electron transfer, we argue that the time taken for orbit or near-range electron transfer is negligible with respect to

the mean first passage time, which is mainly determined by the thermodynamics of the system. Since the ion concentration is dilute, an interaction of three or more ions is very rare, so we introduce an escape velocity:

$$-\frac{e^2}{4\pi\varepsilon_0}\left(\frac{1}{R_{x\,min}}-\frac{1}{R}\right)-4\varepsilon\left[\left(\frac{\sigma}{R}\right)^{12}-\left(\frac{\sigma}{R}\right)^{6}\right]-\frac{3}{2}k_BT\geq\frac{1}{2}\mu v^2\ldots(10)$$

Here, the left-hand side is the necessary energy for reaching the minimum Landau-Zener crossing distance and the $\frac{3}{2}k_BT$ is the adjustment for the stochastic heating due to Langevin dynamics. The above terms are evaluated at each time steps and once the inequality is satisfied, the probability of reaching the nearest Landau-Zener crossing sphere is closed so the simulation trial is terminated, and a pseudo-stable orbit is noted in the output file. Due to the same dilute ion reasoning, we also consider a crossing event of more than two ions as a rare event and due to the limitation of Landau-Zener theory, so the crossing checking is kept as strictly pair wise. Different from the free-molecular limit, after each neutralization reaction we do not initiate a new trial, the ions involved are then re-initialized following the same procedure as the initialization, and the number of reactions $J_P$ and the current simulation time $t_c$ is recorded. The simulation is usually run until a total 2000 reactions is observed and the reaction rate constant is then obtain using the following equation:

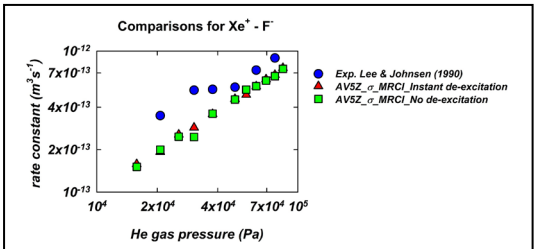


**Figure 5:** Recombination rate constant calculations for $Xe^+ - F^-$ ion pair at pressures $\sim 10^4 - 10^5\ Pa$.

$$\beta=\frac{L^3J_P}{t_c}\frac{4}{N^2}=\frac{L^3}{t_{MFP}}\frac{4}{N^2}\ldots(10)$$

Where $t_{MFP}$ is the mean first passage time. Manuscript under preparation (Liu et al.) describes calculations and comparisons with appropriate experimental data[10-12] for several monoatomic ion pairs at high pressures.

**Next steps in the project include,**

- Extending the approach to reactions involving monoatomic ions and polyatomic ions
- Finding alternative ways to parameterize the electron transfer probability without doing potential energy curve calculations (which are computationally expensive for multi-electron and/or polyatomic species)
- Using first principles to validate approximate electron transfer criteria developed empirically previously and use holistic good agreement between calculations and experimentally measured values of rate constant as a justification for using a simple criterion for electron transfer when two ions approach each other.

**Publications of DOE sponsored research:**

1. Suresh[#], V., Li[#], L., Redmond Go Felipe, J. and Gopalakrishnan, R., Modeling nanoparticle charge distribution in the afterglow of non-thermal plasmas and comparison with measurements. *Journal of Physics D: Applied Physics* 54(27): 275205. https://iopscience.iop.org/article/10.1088/1361-6463/abf70c
2. Suresh*, V. and Gopalakrishnan, R. (***invited*** methods article), Tutorial: Langevin Dynamics methods for aerosol particle trajectory simulations and collision rate constant modeling. *Journal of Aerosol Science* 155: 105476. https://doi.org/10.1016/j.jaerosci.2021.105746

**Manuscripts in preparation of DOE sponsored research:**

1. Liu, Z., Roy, M., Li, L., and Gopalakrishnan, R., Coupling Landau-Zener curve crossing with trajectory simulations to calculate the rate constant for gas-phase ion recombination reactions.

**References**


1. Miller, T.M., et al., The Journal of Chemical Physics, 1994. **100**(12): p. 8841-8848.
2. Shuman, N.S., et al., J Chem Phys, 2014. **140**(4): p. 044304.
3. Olson, R.E., et al., The Journal of Chemical Physics, 1970. **53**(9): p. 3391-3397.
4. Stenrup, M., et al., Physical Review A, 2009. **79**(1).
5. Launoy, T., et al., The Astrophysical Journal, 2019. **883**(1): p. 85.
6. Larson, Å., et al., Physical Review A, 2016. **94**(2).
7. Rundel, R.D., et al., Journal of Physics B: Atomic and Molecular Physics, 1969. **2**(9): p. 954.
8. Moseley, J., et al., Physical Review Letters, 1970. **24**(9): p. 435-439.
9. Suresh, V. and Gopalakrishnan, R., Journal of Aerosol Science, 2021. **155**: p. 105746.
10. Lee, H.S. and Johnsen, R., The Journal of Chemical Physics, 1990. **93**(7): p. 4868-4873.
11. Lee, H.S. and Johnsen, R., The Journal of Chemical Physics, 1989. **90**(11): p. 6328-6334.
12. Jungblut, H., et al., Ieee Transactions on Electrical Insulation, 1989. **24**(2): p. 343-348.

# Enabling Quantitative Predictions of Reacting Gas-Liquid Systems

William H. Green
Department of Chemical Engineering
Massachusetts Institute of Technology
Cambridge, MA 02139
whgreen@mit.edu

## I. Program Scope

Many important systems are complex non-equilibrium mixtures of molecules where multiple reactions are occurring simultaneously; examples include conversion of plastic and agricultural wastes into useful fuels and materials, smog chemistry, biofuel combustion, and $CO_2$ capture. In all of these systems reactions are occurring in both the gas/vapor phase and a liquid phase. The liquid phase affects the reaction rates through solvent effects, and the movement of molecules between the phases affects the overall course of the reactions. At present, many of the models used to understand or improve these systems are oversimplified and not very accurate.

The goal of this project is to use Artificial Intelligence / Machine Learning methods based on chemistry fundamentals and quantum and statistical mechanics to make it possible for scientists and engineers to quickly construct high-fidelity computer models for these reactive systems from first principles. These quantitative simulations would facilitate scientific understanding, better optimization of engineered systems, and faster design of new systems for tackling today's environmental and energy challenges. This project directly addresses DOE BES's Research Priority of **Fundamental Science to Transform Low-Carbon Manufacturing**, as well its priorities in **Artificial Intelligence and Machine Learning** and **Fundamental Science to Enable Clean Energy.** The project is part of the GPCP's research thrust on **Chemical Reactivity**, and is also relevant to that program's efforts to understand **Gas-Particle Interconversions**.

Very recently it has become possible to accurately predict the behavior of some gas-phase reaction systems using rate parameters computed using quantum mechanics. This project is aimed at transforming the way complex gas-liquid chemical systems are treated, by advancing the nascent capability to predict the gas-phase reactions, by computing solvent effects on the liquid-phase reactions, and by combining gas-phase and liquid-phase models into a unified simulation of the coupled gas-liquid system. The project has the potential to both accelerate our development of accurate models for important reaction systems, and to provide a better scientific framework for addressing these systems. This project focuses on two key issues (1) developing computer methods for correctly simulating systems with multiple reactions occurring in both gas and liquid phase, including solvent effects on rates, and (2) computing and measuring the properties of reactions and reactive intermediates which have never been studied in detail before, so we can accurately predict a broader range of systems. Our main focus will be to develop methods for correctly predicting the solvent effects on the rates and energetics, and to develop better understand systems involving heavily unsaturated organics that leading to the formation of molecules with fused cycles, and ultimately to undesirable by-products such as tars. All of the new capabilities will be incorporated into the open-source Reaction Mechanism Generator software suite and associated databases. The accuracy of the predictions of the kinetic models will be validated versus experimental data, both existing data in the literature but also new data measured in our laboratory using laser, mass spectrometry, and two-dimensional gas chromatography techniques.

## II. Recent Results

### A. Fast methods for estimating TS geometries and Reaction Barriers.

A key challenge for this field has been the difficulty of computing reaction rates, largely due to the difficulty of (i) identifying which reactions have low enough barriers that they are worth computing and (ii) providing a good enough guess at the transition state geometry so that the computation will converge.

Automating these calculations would make it feasible to build models with thousands of reactions and also to make it practical for non-experts to make good kinetic models for their systems of interest. We developed a machine learning model to provide high quality initial guess geometries for transition states [14], and computed the transition states of more than 10,000 reactions at high level (CCSD(T)-F12) [8].

We trained a Machine Learning model using the large set of CCSD(T)-F12 barriers we computed, providing a fast estimate of Ea that is about as accurate a good DFT calculation.[9] These large datasets are excellent for building accurate estimation models, but make it even more important to develop high-reliability workflows and automatic tools to help detect any errors, since it is quite tedious for humans to check thousands of numbers.

### B. Methods for computing solvation energies and kinetic solvent effects.

We have developed several different methods for estimating solvation energies (difference of energy of a molecule in gas phase and dilute in a solvent, a.k.a. Henry's Law coefficients) for neutral closed-shell molecules over a wide range of temperatures.[15,16,17] We used the latest versions of COSMO-RS to compute more than a million solute-solvent pairs, used that large data set to train a model, and then calibrated the model using a large set of curated experimental data we and our late collaborator Michael Abraham extracted from the literature. The resulting models are quite accurate, as reliable as many experimental measurements. These solvation energies allow one to compute reaction equilibria in liquid phase, vapor-liquid equilibria, and reverse reaction rates and phase-transfer rates from the forward rates. They provide many of the parameters needed to convert reaction mechanisms into kinetic simulations of reactive gas-liquid systems.

We also have started computing kinetic solvent effects, by using similar methods to compute the solvation free energy of transition states. We have had excellent success predicting kinetic solvent effects for neutral reactions [10], perhaps because there is a large cancellation of errors in the calculated $\Delta\Delta G^{\ddagger}$, but so far we have only found a limited number of experimental data for comparisons.

### C. Developments in computing rates of chemically-activated reactions.

In some sense the problem of pressure-dependence is and chemical-activation is 'solved', due to the excellent work of many in this program in computing and measuring k(E) and/or k(E,J) for many reactions, in the theoretical development of the Chemically Significant Eigenvalues method (e.g. by Georgievskii and Klippenstein), and in theoretical and experimental work on collisional energy and angular momentum transfer (e.g. by Jasper and Mullin). But despite all this excellent work, some issues still remain unresolved. At a practical level, it is still not easy to compute these rates, since there are often many accessible isomers and a large number of possible product channels, so many it can be challenging for a human to remember them all, and it is not unusual to run into numerical problems. We recently developed algorithms and software to try to make the calculations less challenging.[12,13] Also, there are some unresolved conceptual issues (see e.g. comments made at the 2022 Faraday Discussion and in the concluding remarks [10]), in some situations the commonly accepted methods for computing the time evolution disagree significantly from the exact solution of the master equations.[7]

## III. Future Plans

***Upgrading Automated Kinetic Model Construction including Solvation.*** As discussed above, we have recently developed much better ways to estimate reaction barriers, thermochemistry, solvent effects, etc., and ways to automatically spawn quantum chemistry calculations to improve the numerical values. These improved values significantly change the kinetic model predictions compared with models made using Benson-type functional group estimates. We are currently working to extend the work we have done on closed shells to free radicals and ions and their reactions. Preliminary work suggests we can

compute solvation of radicals very accurately, but computing the much larger solvation energies of ions is more challenging. We are using Machine Learning techniques to create fast estimators that emulate the very slow quantum chemistry calculations. We are also developing an automated method for constructing a tree estimator for reactions, and are extending it for radical and molecule properties, for situations where there are not enough data to train a neural net estimator.

***Upgrading Uncertainty Estimates***. We are also examining the many types of errors in today's Machine Learning models, to provide more reliable estimates of the uncertainties in the model predictions (today most published error estimates on ML models are much smaller than the errors you are likely to encounter if you use the models). Next step is to integrate all this into RMG to make it possible to rapidly and automatically improve the kinetic models as they are being constructed, to more accurately represent all the effects of solvation, and to attach reliable uncertainty estimates to RMG's predictions.

**Resolving Discrepancies in Quantum Chemistry Calculations.** For many of the 10,000+ reactions we computed, the CCSD(T) and DFT barrier heights agree within 5 kcal/mole as one might expect. But for hundreds of the reactions the two methods give barriers that differ by more than 10 kcal/mole, and some by more than 20 kcal/mole. We have been investigating the origins of the discrepancies in collaboration with Martin Head-Gordon, and have resolved most of them; we will publish the full story in the coming year.

***Further Analysis of Chemical Activation***. We are examining the mathematics of constructing the reduced models to represent the full master equations, and deriving rigorous error bounds for the difference between the reduced and full models. We hope this will be helpful in developing improved methods, or as a way to alert the user if there is likely to be a problem in a rate predicted using the reduced models.

***Open-Source Software and Databases.*** We are about to release a new version of the Reaction Mechanism Generator software package, and to publish full documentation of the Chemprop (Machine-Learning for Chemistry) package.

## Publications and submitted journal articles supported by DOE BES 2020-2023


1. M.J. Goldman, S. Ono, W.H. Green. Addition to 'Accepted method for computing X+X rates is incorrect, causes large errors in isotope analysis'. *J. Phys. Chem. A* **124,** 257 (2020).
2. C.W. Gao, M. Liu, W.H. Green. Uncertainty Analysis of Correlated Parameters in Automated Reaction Mechanism Generation. *Int. J. Chem. Kinet.* **52**, 266-282 (2020).
3. R.J. Gillis, W.H. Green. Thermochemistry Prediction and Automatic Mechanism Generation for Oxygenated Sulfur Systems: A Case Study of Dimethyl Sulfide Oxidation. *ChemSystemsChem* **2**, e1900051 (2020). http://dx.doi.org/10.1002/syst.201900051
4. W.H. Green. Moving from Postdictive to Predictive Kinetics in Reaction Engineering. *AIChE J.* **66**, e17059 (2020). https://doi.org/10.1002/aic.17059
5. M. Liu, *et al.* RMG 3.0: Advances in Automatic Mechanism Generation. *J. Chem. Inf. Model* **61**, 2686-26969 (2021). https://doi.org/10.1021/acs.jcim.0c01480
6. Y. Liu, C.J. McGill, W.H. Green, P. Deshlara. Effects of Surface Species and Homogeneous Reactions on Rates and Selectivity in Ethane Oxidation on Oxide Catalysts. *AIChE J.* **67,** e17483 (2021). **https://doi.org/10.1002/aic.17483**
7. M. S. Johnson, W.H. Green. Examining the Accuracy of Methods for Obtaining Pressure Dependent Rate Coefficients. *Faraday Discussions* **238**, 380-404 (2022). https://doi.org/10.1039/D2FD00040G
8. K. Spiekermann, L. Pattanaik, W.H. Green. High Accuracy Barrier Heights, Enthalpies, and Rate Coefficients for Chemical Reactions. *Scientific Data* **9**, 417 (2022). https://doi.org/10.1038/s41597-022-01529-6
9. K. Spiekermann, L. Pattanaik, W.H. Green. Fast Predictions of Reaction Barrier Heights:

Towards Coupled-Cluster Accuracy. *J. Phys. Chem. A* **126,** 3976-3986 (2022). https://doi.org/10.1021/acs.jpca.2c02614
10. W.H. Green. Concluding Remarks on Faraday Discussion on Unimolecular Reactions. *Faraday Discussion* **238**, 741-766 (2022). https://doi.org/10.1039/D2FD00136E
11. M.S. Johnson, et al. The RMG Database for Molecular Property Prediction. *J. Chem. Inf. Model* **62**, 4906-4915 (2022). https://doi.org/10.1021/acs.jcim.2c00965
12. M.S. Johnson, A. Grinberg Dana, W.H. Green. A Workflow for Automatic Generation and Efficient Refinement of Pressure Dependent Networks. *Combustion & Flame* (accepted, in press) https://doi.org/10.1016/j.combustflame.2022.112516
13. A. Grinberg Dana et al., Automated reaction kinetics and network exploration (Arkane): A statistical mechanics, thermodynamics, transition state theory, and master equation software. *Int. J. Chem. Kinet.* **55**. 300-323 (2023). **https://doi.org/10.1002/kin.21637**

## Other Literature Cited

14. L. Pattanaik, J.B. Ingraham, C.A. Grambow, W.H. Green. Generating Transition States with Deep Learning. *Phys. Chem. Chem. Phys.* **22**, 23618-23626 (2020). https://doi.org/10.1039/D0CP04670A
15. Y. Chung *et al.* Group Contribution and Machine Learning Approaches to Predict Abraham Solute Parameters, Solvation Free Energy, and Solvation Enthalpy. *J. Chem. Inf. Model.* **62**, 433-446 (2022). https://doi.org/10.1021/acs.jcim.1c01103
16. F.H. Vermeire, W.H. Green. Transfer learning for solvation free energies: from quantum chemistry to experiments. *Chem. Eng. J.* **418**, 129307 (2021). https://doi.org/10.1016/j.cej.2021.129307
17. F.H. Vermeire, Y. Chung, W.H. Green. Predicting Solubility Limits of Organic Solutes for a Wide Range of Solvents and Temperatures. *Journal of the American Chemical Society* **144**, 24, 10785–10797 (2022). https://doi.org/10.1021/jacs.2c01768

# Nonadiabatic Photochemistry

DE-SC0015997

Hua Guo[1], Donald G. Truhlar,[2] and David R. Yarkony[3]

[1]*Department of Chemistry and Chemical Biology, University of New Mexico, Albuquerque, New Mexico 87131.*

[2]*Department of Chemistry, University of Minnesota, Minneapolis, Minnesota 55455*

[3]*Department of Chemistry, Johns Hopkins University, Baltimore, Maryland 21218*

e-mail: hguo@unm.edu; truhlar@umn.edu; yarkony@jhu.edu

## PROGRAM SCOPE

This project involves the development and application of methods for treating electronically nonadiabatic processes both with fitted diabatic potential energy matrices (DPEMs) and by direct dynamics in the adiabatic representation. The project includes both electronic structure theory and dynamics, and the dynamics involves both fully quantal and semiclassical theoretical method development and calculations.

## PROGRESS IN THE LAST YEAR

### Hua Guo

We have collaborated with Jingsong Zhang and Richard Dawes (BES supported) to elucidate the nonadiabatic photodissociation dynamics of HCO in its *A* band.[1] Quantum wave packet calculations on an accurate set of potential energy surfaces (PESs) revealed that the predissociation rate and product distribution are sensitive to the parent rotational quantum numbers. This is due to the fact that the predissociation is facilitated by the Renner-Teller coupling, which is controlled by the projection of the total rotational angular momentum on to the molecular axis. This model satisfactorily explained the experimental observations.

In collaboration with Yarkony, the internal conversion and intersystem crossing in $NH_3$ photodissociation are investigated using a newly constructed diabatic potential energy matrices (DPEMs).[2] This DPEM not only includes coupling between states with the same spin-multiplicity, but also coupling between different spin manifolds. Since a diabatic representation is used, the derivative coupling and spin-orbit coupling can all be represented with smooth functions, paving the road for study internal conversion and intersystem crossing. These DPEMs also enforce the permutation symmetry, which is important for systems with identical atoms. In this study both the molecular ($NH + H_2$) and radical ($NH_2 + H$) channels were studied.

With our collaborators, we have been continuing our investigations of dynamics of bimolecular scattering and reactions. These studies include a full-dimensional quantum scattering calculation for the inelastic scattering between Ar and $H_2O$,[3] which is a prototype for understand ro-vibrational energy transfer. In addition, we have studied the dynamics of the $O + HO_2$ reaction, which has two different pathways leading to the same products.[4] Finally, we have reinvestigated the nonadiabatic quenching of OH(*A*) by $H_2$ using semi-classical methods.[5, 6] In particular, the reactive channel of this prototypical nonadiabatic bimolecular reaction was investigated using an accurate DPEM.[6] The $H_2O$ product was found to possess extensive vibrational excitation, in qualitative agreement with experimental observations. The origin of the vibrational excitation is identified using an extended Sudden Vector Projection model. However, we failed to find significant insertion trajectories which called for further improvement of the DPEM.

**Donald G. Truhlar**

Very often, the computational bottleneck of direct simulations comes from electronic structure theory. For example, at every timestep of a trajectory, nonadiabatic dynamics requires energies and gradients of the potential energy surfaces and the nonadiabatic coupling vector. This difficulty can be alleviated to some extent by employing time derivative coupling, which can be evaluated from overlaps of electronic wave functions of successive timesteps. However, evaluation of overlap integrals is still expensive for large systems. In addition, for electronic structure methods for which the wave functions are not available, putting overlap integrals into nonadiabatic dynamics algorithms becomes an intractable problem. We proposed new nonadiabatic dynamics algorithms that only require energy and gradient information from the electronic structure side. These new methods are named curvature-driven coherent switching with decay of mixing (κCSDM) and curvature-driven trajectory surface hopping (κTSH). We showed how results obtained with these powerful new methods compare to results obtained with previous mixed quantum-classical nonadiabatic dynamics algorithms.[7]

The photoinduced ring-opening reaction of 1,3-cyclohexadiene to produce 1,3,5-hexatriene is a classic electrocyclic reaction and is also a prototype for many reactions of biological and synthetic importance. We simulated the ultrafast nonadiabatic dynamics of the reaction in the manifold of the three lowest valence electronic states by using extended multistate complete-active-space second-order perturbation theory (XMS-CASPT2) combined with the κCSDM method. We obtained an excited state lifetime of 79 fs and a product quantum yield of 40% from 500 trajectories initiated in the first excited singlet state. The obtained lifetime and quantum yield are very close to previously reported experimental and computed values, showing the capability of performing a reasonable nonadiabatic ring-opening dynamics with the κCSDM method that does not require nonadiabatic coupling vectors (NACs), time derivatives, or diabatization. We also optimized the $S_0/S_1$ and $S_1/S_2$ minimum-energy conical intersections (MECIs) by XMS-CASPT2; for $S_1/S_2$, we optimized both an inner and an outer local-minimum-energy conical intersection (LMECI). We provided a potential energy profile along the ring-opening coordinate by joining selected critical points via linear synchronous transit (LST) paths. We found the inner $S_1/S_2$ LMECI to be more crucial than the outer one.[8]

Global potential energy surfaces (PESs) for the $1\ ^2A'$ and $1\ ^2A''$ states of the $C_2N$ system responsible for the $N(^4S_u) + C_2(a\ ^3\Pi_u) \rightarrow CN(X\ ^2\Sigma^+) + C(^3P_g)$ reaction were mapped using compressed-state multistate pair-density functional theory (CMS-PDFT), which is a multi-state version of multiconfiguration pair-density functional theory (MC-PDFT). Calculations were also performed at selected geometries by explicitly correlated multireference configuration interaction with quadruples corrections (MRCI-F12+Q), and the comparison of the two sets of calculations showed that CMS-PDFT describes the global reactive potential energy surfaces well, including the bond-breaking asymptotes. We concluded that CMS-PDFT is an efficient method for constructing potential energy surfaces (PESs) for strongly correlated reactive systems. The potential energy surfaces for producing CN + C were found to be barrierless and to involve intermediate complexes. The CMS-PDFT PESs were fit with a neural network method, and quasiclassical trajectories were computed on the resulting analytic PESs. These trajectories predicted that the reaction produces vibrationally excited CN.[9]

**David R. Yarkony**

Since the *A*-*X* transitions in OH are used to detect this radical, the reactions of $OH(A^2\Sigma^+)$ with $H_2$ are of both practical and didactic consequence. The dynamics of this collisional process involves at least 3 channels:

$OH(A^2\Sigma^+) + H_2 \rightarrow H_2O + H$ R1 reactive nonadiabatic quenching
$\rightarrow OH(X^2P) + H_2$ R2 nonreactive nonadiabatic quenching
$\rightarrow OH(A^2\Sigma^+) + H_2$ R3 nonreactive adiabatic scattering

This prototypical nonadiabatic process was investigated by our DOE funded team using full quantum and semiclassical surface hopping nuclear dynamics.[5, 6, 10] To accomplish this the first task was to construct using accurate multireference electronic wave functions the fully coupled, full dimensional (6 internal coordinates) three-state diabatic potential energy matrix (DPEM),[11] which guides the nuclear motion. We also chose to develop a four-state DPEM so as to better represent the Rydberg region where four states, with $D_{3h}$ and $C_{3v}$ symmetry, are energetically accessible.[12] The dynamics calculations using these DPEMs are discussed above.

In order to test the above suggestion a new four-state DPEM is needed which focuses on (getting to) the Jahn-Teller like Rydberg region. To that end we are developing a new fitting method which extends a procedure of Eisfeld and uses permutation invariant polynomials and neural networks.[13]

Boyed by Lai-Sheng Wang's (BES supported) characterization of our 2011 paper on the photoelectron spectrum (PES) of triazolide (giving the nonadiabatic spectrum of triazolyl) as "an impressive nonadiabatic spectral simulation", Ref. [14] (we have begun a joint effort with the group of Wang to describe the PES of the benzonitrile anion (giving the nonadiabatic spectrum of benzonitrile) which, owing to its detection in the interstellar medium, has recently been discussed in the Proceedings of the National Academy of Science.

## FUTURE PLANS

### Hua Guo

We will explore the internal conversion and intersystem crossing in $H_2CO$ using the recent DPEM from Yarkony. This is an interesting system because of the two possible nonadiabatic routes, via internal conversion to the $S_0$ state and intersystem crossing to the $T_1$ state. The calculated energies and lifetimes can be compared with a large set of experimental data. These nonadiabatic processes are also at the center of the roaming dynamics in the $S_0$ state.

We will also investigate the nonadiabatic dynamics of $SO_2$ photodissociation, motivated by the recent discovery by David Osborn (BES supported) on the existence of the $S + O_2$ channel. We plan to construct a new DPEM for this system and explore the possible dissociation pathways leading to this minor channel.

Finally, we plan to construct a new DPEM for the $HO_2$ system, which is responsible for the $H + O_2 \leftrightarrow OH + O$ reaction. This reaction, which is the second most important reaction in combustion, is strongly affected by conical intersections. The availability of the DPEM will enable accurate quantum mechanical studies of the nonadiabatic dynamics.

### Donald G. Truhlar

We are working on the inclusion of spin-orbit coupling in the κCSDM method. This involves the development of a more convenient method for calculating gradients in the presence of spin-orbit coupling, and we are developing this.

We are completing work on elucidating the photodissociation fingerprint and quantifying the determination of organic hydroperoxides in gas-phase autoxidation.

We are examining the error due to population leaking in trajectory surface hopping due to frustrated hops.

We will use our new diabatic deep neural network (DDNN) method to develop coupled full-dimensional MS-CASPT2 potential energy surfaces for *o*-fluorothiophenol, and we will use

these for semiclassical dynamics calculations to study hydrogen-bonding substituent effects on photodissociation.

We will apply the companion matrix method to develop coupled potential surfaces suitable for photodissociation of methyl radical by the κCSDM method. The combination of the companion matrix method with κCSDM has the potential to allow much more convenient simulation of electronically nonadiabatic processes in the future.

We are developing a new version of the SHARC semiclassical dynamics program with new capabilities, and we will distribute it as part of SHARC 3.0.

**David R. Yarkony**

To understand the benzonitrile photoelectron spectra, we will construct a five-electronic state DPEM where the adiabatic states are coupled by conical intersections. We are currently rewriting our program for fitting nonadiabatic bound states to properly account for point group symmetry. The five-dimensional electronic state space is required owing to the strong coupling between the adiabatic states by conical intersections. We will transform this adiabatic representation to a diabatic representation and then determine the photoelectron spectrum using our version of the well-known Koppel-Domcke-Cederbaum algorithm.

The competition between Intersystem crossing (ISC) [spin nonconserving radiationless decay; spin-orbit coupling] and internal conversion (IC) [spin conserving radiationless decay; conical intersection coupling] is a problem of considerable theoretical and practical importance in photochemistry. Recently we have developed algorithms, organized into two protocols, denoted Pr:X, that enable us to add the dipole interaction Pr:DIP and the spin-orbit coupling interaction Pr:SOC to the Coulomb Hamiltonian (the DPEM). The spin-diabatic Hamiltonian obtained from Pr:SOC will enable us to accurately study ISC, hence IC/ ISC competition. The key issue in building these protocols was to get the dipole and/or spin-orbit interaction into the diabatic state representation eliminating the singularities in the adiabatic representation.

We started with formaldehyde a system exhibiting roaming photodissociation and may also evince ISC., which we treat in the three state ($S_0$, $S_1$ and $T_1$) paradigm which was successfully used in other funded research to describe $NH_3$(A) band photodissociation. We will continue/complete the formaldehyde study in this performance period. For comparison we have initiated a similar study of the sulfur substituted form thioformaldehyde which has been recently studied by Truhlar's group providing another opportunity for comparison.

Our DPEMs and Pr:SOC, Pr:DIP, which are freely available when published, are based exclusively on configuration interaction single and double (MRCISD) wave functions so that both static and dynamic correlation are included. These coupled surfaces, which will provide accurate electronic structure data, will make an important contribution to physical chemistry infrastructure.

**CITED PUBLICATIONS**

(1) Sun, G.; Han, S.; Zheng, X.; Song, Y.; Qin, Y.; Dawes, R.; Xie, D.; Zhang, J.; Guo, H. Unimolecular dissociation dynamics of electronically excited HCO($\tilde{A}^2$A"): rotational control of nonadiabatic decay. *Faraday Discuss.* **2022**, *238*, 236-248.

(2) Wang, Y.; Guo, H.; Yarkony, D. R. Internal conversion and intersystem crossing dynamics based on coupled potential energy surfaces with full geometry-dependent spin–orbit and derivative couplings. Nonadiabatic photodissociation dynamics of $NH^3$(A) leading to the NH($X^3\Sigma^-$, $a^1\Delta$) + $H_2$ channel. *Phys. Chem. Chem. Phys.* **2022**, *24*, 15060-15067.

(3) Yang, D.; Liu, L.; Xie, D.; Guo, H. Full-dimensional quantum studies of vibrational energy transfer dynamics between $H_2O$ and Ar: theory assessing experiment. *Phys. Chem. Chem. Phys.* **2022**, *24*, 13542-13549.
(4) Chen, Q.; Zhang, S.; Hu, X.; Xie, D.; Guo, H. Reaction pathway control via reactant vibrational excitation and impact on product vibrational distributions: The $O + HO_2 \rightarrow OH + O_2$ atmospheric reaction. *J. Phys. Chem. Lett.* **2022**, *13*, 1872-1878.
(5) Han, S.; de Oliveira-Filho, A. G. S.; Shu, Y.; Truhlar, D. G.; Guo, H. Semiclassical trajectory studies of reactive and nonreactive scattering of $OH(A\ ^2\Sigma^+)$ by $H_2$ based on an improved full-dimensional ab initio diabatic potential energy matrix. *ChemPhysChem* **2022**, *23*, e202200039.
(6) Han, S.; Zhao, B.; Conte, R.; Malbon, C. L.; Bowman, J. M.; Yarkony, D. R.; Guo, H. Nonadiabatic reactive quenching of $OH(A^2\Sigma^+)$ by $H_2$: Origin of high vibrational excitation in the $H_2O$ product. *J. Phys. Chem. A* **2022**, *126*, 6944-6952.
(7) Shu, Y.; Zhang, L.; Chen, X.; Sun, S.; Huang, Y.; Truhlar, D. G. Nonadiabatic dynamics algorithms with only potential energies and gradients: Curvature-driven coherent switching with decay of mixing and curvature-driven trajectory surface hopping. *J. Chem. Theory Comput.* **2022**, *18*, 1320-1328.
(8) Zhang, L.; Shu, Y.; Bhaumik, S.; Chen, X.; Sun, S.; Huang, Y.; Truhlar, D. G. Nonadiabatic dynamics of 1,3-cyclohexadiene by curvature-driven coherent switching with decay of mixing. *J. Chem. Theory Comput.* **2022**, *18*, 7073-7081.
(9) Zuo, J.; Zhang, D.; Truhlar, D. G.; Guo, H. Global potential energy surfaces by compressed-state multistate pair-density functional theory: The lowest doublet states responsible for the $N(^4S_u) + C_2(a\ ^3\Pi_u) \rightarrow CN(X\ ^2\Sigma^+) + C(^3P_g)$ reaction. *J. Chem. Theory Comput.* **2022**, *18*, 7121-7131.
(10) Zhao, B.; Han, S.; Malbon, C. L.; Manthe, U.; Yarkony, D. R.; Guo, H. Full-dimensional quantum stereodynamics of the non-adiabatic quenching of $OH(A^2\Sigma^+)$ by $H_2$. *Nat. Chem.* **2021**, *13*, 909-915.
(11) Shu, Y.; Kryven, J.; Sampaio de Oliveira-Filho, A. G.; Zhang, L.; Song, G.-L.; Li, S. L.; Meana-Pañeda, R.; Fu, B.; Bowman, J. M.; Truhlar, D. G. Direct diabatization and analytic representation of coupled potential energy surfaces and couplings for the reactive quenching of the excited $^2\Sigma^+$ state of OH by molecular hydrogen. *J. Chem. Phys.* **2019**, *151*, 104311.
(12) Malbon, C. L.; Zhao, B.; Guo, H.; Yarkony, D. R. On the nonadiabatic collisional quenching of OH(A) by $H_2$: a four coupled quasi-diabatic state description. *Phys. Chem. Chem. Phys.* **2020**, *22*, 13516-13527.
(13) Guan, Y.; Yarkony, D. R.; Zhang, D. H. Permutation invariant polynomial neural network based diabatic ansatz for the (E + A) × (e + a) Jahn–Teller and Pseudo-Jahn–Teller systems. *J. Chem. Phys.* **2022**, *157*, 014110.
(14) Zhang, Y.-R.; Yuan, D.-F.; Wang, L.-S. Probing the strong nonadiabatic interactions in the triazolyl radical using photodetachment spectroscopy and resonant photoelectron imaging of cryogenically cooled anions. *J. Am. Chem. Soc.* **2022**, *144*, 16620-16630.

# Integrated Data-driven Methods for Scientific Discovery of Non-equilibrium Thermochemical Processes in Complex Environments from Ultrafast X-ray Measurements at LCLS

Matthias Ihme, Stanford University (Principal Investigator) mihme@stanford.edu
Eric Darve, Stanford University (Co-Investigator)
Stefano Ermon, Stanford University (Co-Investigator)
Dimosthenis Sokaras, SLAC National Accelerator Laboratory (Co-Investigator)
Jana Thayer, SLAC National Accelerator Laboratory (Co-Investigator)
Adrianus van Duin, Penn State University (Co-Investigator)
Diling Zhu, SLAC National Accelerator Laboratory (Co-Investigator)

## 1 Program Scope

Recent advances achieved with the ultrafast coherent X-ray-Free Electron Laser at the Linac Coherent Light Source (LCLS) and the anticipated LCLS-II upgrade empower us to probe non-equilibrium processes at atomistic scales with femtosecond (fs) temporal resolution. However, despite unprecedented LCLS capabilities, the enormous complexity, data volume (current acquisition rate, 1 GB/s; projected as 200 GB/s with the LCLS-II upgrade), and experimental access constitute major challenges for scientific discovery. The proposed research will directly tackle this urgent issue by developing novel and advanced data-science methods, machine-learning (ML) approaches, and uncertainty-quantification (UQ) techniques to enable ultrafast X-ray Photon Correlation Spectroscopy (XPCS) measurements that are closely supported through tightly coupled atomistic-scale simulations to discover non-equilibrium processes and chemical reactions of fluids at supercritical conditions.

To enable the rapid experimental screening of the complex thermochemical state-space and the efficient exploration of non-equilibrium reaction pathways in systems at supercritical conditions, innovative Bayesian optimization techniques will be developed that combine highly adaptive search strategies and probabilistic models for balancing the exploration of highly uncertain areas and the exploitation of promising ones. To accelerate scientific discovery, novel data-driven assimilation techniques will be developed that integrate XPCS measurements into molecular dynamics (MD) simulations, taking into consideration experimental uncertainties and incomplete models. Novel ML approaches will be developed for directly training MD force-fields from ultrafast XPCS measurements that evolve on comparable spatiotemporal scales, offering powerful new opportunities for improving the predictive accuracy of MD simulations.

These highly complementary data-science methods will be employed for scientific discovery of non-equilibrium processes in mixtures of supercritical fluids that are associated with intermolecular cluster transfer, cage effects, and chemical reactivity. To this end, we seek to examine multicomponent mixtures of relevance to environmental, chemical, and industrial applications. Of particular interest is examining how non-equilibrium cluster transfer, molecular caging, and diffusive transport at ultrafast timescales can be manipulated to affect reaction pathways and thermochemical responses at the macroscopic level.

## 2 Research Progress

### 2.1 Bayesian optimization for rapid state-space exploration

Bayesian Optimization (BO), a global, *black-box*, optimization tool, was developed and applied to Small Angle X-ray Scattering (SAXS) data gathered on supercritical $CO_2$. The goal of the study was to demonstrate the utility for automated experiment and rapid state-space exploration to locate peaks in the SAXS signals and trace the Widom line efficiently and in real-time. By using the Matern kernel and leveraging Gaussian processes, it was found that on average, aided by BO, the peaks are located 35-65% cheaper than traditional methods – this corresponds to 6-10 fewer experiments conducted. Thus, the

technique successfully allows for much more rapid state-space exploration of complex thermodynamic phase spaces. The findings were summarized and presented at the Ultrafast Tracking and Tracking Instrumentation, Methods and Applications Conference (ULITIMA 2023) taking place at SLAC. Furthermore, the results are currently being prepared for submission in the Nuclear Instruments and Methods in Physics Research (NIMA) journal.

To improve the robustness of the BO methodology, a local search-based algorithm was also implemented [Neiswanger et al., 2021]. The purpose of the local BO algorithm was to extend the global approach and locate multiple peaks in the signals, which is hypothesized to take place in the case of binary supercritical mixtures [Mareev et al. 2021]. Such experiments and demonstrations are in-progress, scheduled to take place within the next year.

SAXS experiments involving binary supercritical mixtures are planned to take place in the 2023-2024 cycle, with $CO_2 - CHF_3$ as a candidate mixture. The mixture was chosen due to the strong dipole moment and scattering signal of tri-fluoromethane, hence, it is expected to result in a clear double-peak signal. In addition, the mixture and single-component critical points are similar, allowing for a more direct control over the supercritical state-space. To aid in the exploration, Bayesian optimization, in its local version, will be implemented directly on-the-line, since the binary mixture experiment involves three degrees of freedom: mixture fraction, temperature, and pressure. As a result, unaided by BO, the state space is too vast for manual screening. We expect the findings from the experiment to be the first demonstration of multi-peak SAXS signals, where each peak corresponds to a distinct decay in the correlation length and density fluctuations of each constituent, further highlighting the richness and complexity of the supercritical state space.

## 2.2 MD force-field training and validation (Adri)

Using the I/Xe ReaxFF parameter set developed in the previous reporting period we performed a series of molecular dynamics simulations starting from a 2I-radical/18 Xe system. Using the NVE microcanonical ensemble we saw that the initial temperature of this system (300K) rose to around 950K due to the exothermic $I_2$ formation. The $I_2$ was stable in this system – since it transferred some of its excess kinetic energy directly to the Xe-atoms and remained in a highly excited vibrational state. We have successfully developed analysis tools to evaluate the time-dependent size of the Xe-cluster and to evaluate geminate (i.e. I-I reactions inside a Xe-cluster) vs. non-geminate recombination – where energy transfer between highly vibrationally excited $I_2$ dimers to the Xe matrix is essential for the generation of long-living $I_2$ species. The ReaxFF $I_2$ formation kinetics in supercritical Xe-systems can be directly compared to the experimental results from the Stanford team.

In addition, we developed a ReaxFF description for $CO_2$ using a combination of Density Functional Theory data on $CO_2$ elastic constants for the $CO_2$ crystal and MP2-calculation on $CO_2$ dimers from literature [Tsuzuki et al., 1998]. We performed molecular dynamics simulations using this $CO_2$/ReaxFF description and compared its performance against well-known non-reactive $CO_2$ descriptions like BOMD, TraPPE and MSM and found good agreement between ReaxFF, TraPPE and MSM – with BOMD giving a distinctly higher local $CO_2$ density.

## 2.3 XPCS Experiment to probe Ultrafast Response of Supercritical CO2

We performed split-pulse X-ray Photon Correlation Spectroscopy (XPCS) [Li et al. 2020] of supercritical carbon dioxide (scCO2) to study the dynamics of molecular clusters. The experiment was carried out at the X-ray Pump Probe (XPP) instrument of the Linac Coherent Light Source. The experimental setup is shown in Figure 1. The X-ray pulse

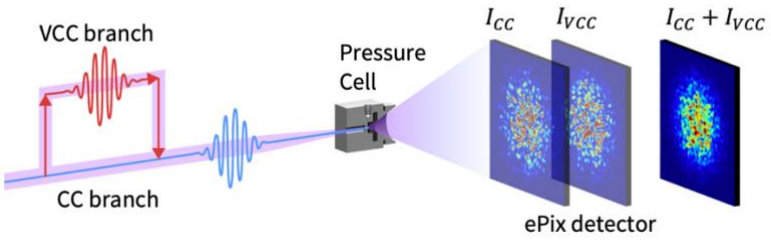


*Figure 1: Experiment setup for split pulse XPCS. The sample is kept in the pressure cell and scattered pattern from scattered X-rays is recorded in the ePix detector for the fixed branch (CC), the delayed branch (VCC) and the two pulses together.*

from the Linac is first monochromatized by the diamond (111) monochromator and then split into a pair of pulses using the compact amplitude-split delay (SD) system [Li et a., 2020]. Studying short lifetime of the molecular clusters [Yoshii and Okazaki, 1997] require ultrafast picosecond time resolution. With that in mind, we chose the time delay $\tau$ between the pulses to be 4 ps, 8 ps and 13 ps. The scattered photons from the sample under study is recorded by a set of four ePix100 detectors [Sikorski et al. 2016]. The experimental setup has a small angle geometry and covers a $Q$ range of 0.01 to 0.1 $Å^{-1}$.

From the detector images, we computed the speckle contrast. The speckle contrast and the intermediate scattering function obtained from the contrast shows a complex dependence on $Q$. We hypothesized that such dependence arises from the presence of clusters. To confirm this hypothesis, we performed molecular dynamics (MD) simulations and developed a theoretical model. The theoretical model represents diffusion within clusters and called intra-cluster diffusion (ICD) model. Figure 2(a) shows the schematic of the model. The timescale obtained from XPCS, MD and the ICD model showed good agreement with each other (Figure 2b). This confirmed that, using XPCS, we successfully measured cluster dynamics, specifically, diffusion dynamics within clusters.

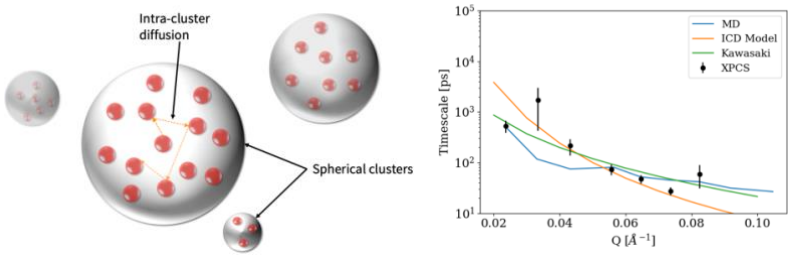


*Figure 2: (a) Schematic of intra-cluster diffusion model. The molecules are constrained inside clusters (cage effect) and undergo multiple collisions. (b) Relaxation timescales obtained from the $f(Q,\tau)$ over various Q values. The results are compared with the diffusion timescale obtained from Kawasaki's theory. Good agreement between XPCS, MD and the ICD model suggests that the cluster dynamics measured by XPCS corresponds to intra-cluster diffusion.*

## 2.4 Core-Shell Ionization in Water with Strong X-ray Laser Pulse from FEL

The core-shell ionization of water induced by high energy photons and its subsequent evolution of the molecular structure, ions and radicals is a key question in many research areas, such as radiation damage [Lomb et al., 2011], radiochemistry [Garrett et al., 2004], and extraterrestrial chemistry [Carlson et al. 1999; Blanc et al. 2015]. The increasing availability of hard x-ray FEL makes it possible to carry out systematic microscopic study of this process.

In general, the inner shell, including the core shell, ionization initiates an ultrafast structural change (<10 fs) in the primary ionization molecules [Jahnke et al., 2021]. In the gas phase, the Coulomb interaction then leads to a rapid response of the ionized molecules. From the trajectory and momentum measurements of the molecule fragments, one can derive the molecule structure evolution after the ionization [Jahnke et al., 2021]. In the liquid phase, for photons with an energy much higher than the core-electron binding energy, Auger decay, secondary electrons and photons start a cascade ionization process and create a large cloud of charged particles and neutral atoms [Garrett et al., 2004]. Depending on the thermodynamic condition and the environment of the inner-shell ionization event, these ionization products transform to a non-thermal mixture of chemically stable species, such as $H_2O$, $H_2$, and $O_2$, through proton and electron transfer (~1 ps). Subsequently, this chemically stable non-thermal mixture relaxes to a local hot spot through regular thermodynamic motion, which eventually dissipates and reaches equilibrium with the bulk environment.

In the gas phase, the ion-mass spectroscopy, ion-ion/electron coincidence and ion-ion-ion triple coincidence measurement provides the most accurate description of the ion production and the initial atomic dynamics within the first 50~fs for each single water molecule [Garrett et al., 2004]. In the liquid phase, the strong interaction among adjacent molecules and the prominent secondary ionization processes makes any microscopic study extremely challenging.

To study of the influence of thermodynamic parameters, such as temperature and pressure, on the microscopic structure dynamics in water induced by high-energy photons, we performed an x-ray pump x-ray probe elastic x-ray scattering measurement at the BL-3 experimental hutch at Spring-8/SACLA. In this experiment, the x-ray photon energy is chosen at 10 keV with an average x-ray pulse energy of 2 $\mu J$ in the pump and probe pulse, respectively. The x-ray beam size on the sample has a radius

of 1 $\mu m$ FWHM, which corresponds to an average pulse intensity of $10^9$ photon/$\mu m^2$ for the pump pulse. The water is maintained in a titanium pressure cell at 340C and 225 bar. As a first order approximation, if one assumes that all absorbed x-ray energy is converted into heat, then the temperature raised by 130K and therefore the sample locally enters the supercritical state, in which according to our theoretical study prominent self-similar structures across several length scales is expected to dominate the microscopic density profile. Therefore, we expect to see a two-stage evolution of the x-ray structure factor *S(Q)* after the strong x-ray pump pulse: the sub-ps ionization and chemically stabilization stage and a slower, 10-to-100 ps, thermalization process where self-similar local structures as a signature of the supercritical fluid gradually develop.

Preliminary experimental results are summarized in Figure 3. It shows the dependence of the structure factor S(Q) normalized to the value at 0.04 $Å^{-1}$ for different x-ray pump energies. The time in **bold** font on the left bottom of each subplot is the relative delay time between the two pulses within each pump-probe pulse pair. We observe that even at a short delay time of 50fs, there is still significant change in the shape of the structure factor. This change is not limited to sub-picosecond time scales. In fact, we observe a change in the structure factor from 50 fs to as long as 100 ps as shown in Figure 4(right). To ensure that the measured phenomena is truly a pump-probe effect, for each delay time, 4000 single pulse scattering patterns were collected to check for accumulated heating effect which would also change the structure factor. After confirming the absence of the accumulated heating effect, 6000 to 8000 diffraction patterns from pulse pairs were obtained to measure the x-ray induced structure dynamics.

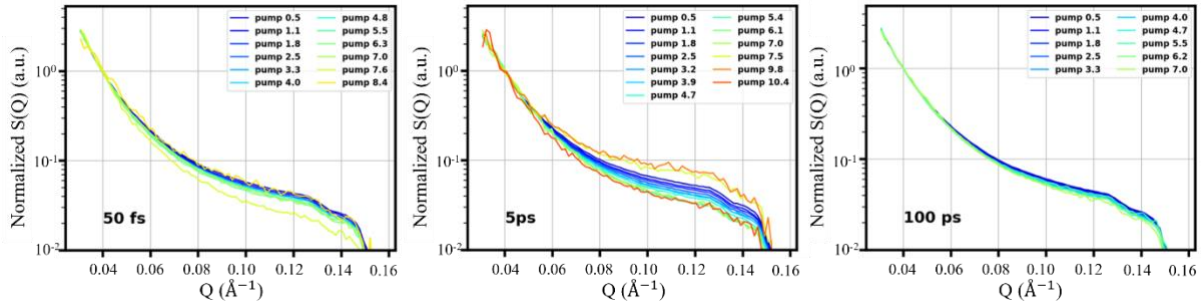


*Figure 3: Normalized structure factor from the pump and probe x-ray pulse pair with different delay time, in bold font in the left bottom corner of each figure, between the pump and probe x-ray pulse. Different color stands for different pump pulse energy in $\mu J$.*

These measurements were performed within a 24-hr beamtime. Therefore, we were not able to change the detector geometry to cover the more interesting and more fundamental high-Q region (1-to-3 $Å^{-1}$). Besides, our pressure cell assembling protocol was incomplete at that time, which introduced significant background to our measured signal. This has stopped us from interpreting results quantitively. Both issues will be addressed in the coming experiment during 5/30 to 6/02 this year.

## 2.5 Machine-learning for scientific discovery

Many state-of-the-art models in machine learning are based on the Transformers neural network architecture. For example, in computer vision and image analysis Transformers are the backbone of supervised (Vision Transformers), self-supervised (Masked auto-encoders, Dino), and generative models of images (for example, diffusion models and MUSE). Similarly, Transformers achieve state-of-the-art results in natural language processing tasks, time series prediction, etc. However, a key challenge of Transfomers is that they struggle with the high-dimensional data (e.g., sequences of images) due to their quadratic cost in sequence length. This is one of the key reasons Transformers have not been widely adopted in scientific applications of machine learning.

We have developed a novel deep neural network architecture called Hyena, specifically designed for handling extremely long sequences. Our proposed Hyena architecture overcomes the key limitation of Transformers by using long convolutions and other signal processing computational primitives, achieving comparable accuracy to Transformers with reduced computational requirements. In particular, we are able to match the performance of Vision Transformers on image classification tasks with significantly reduced computational cost. This approach opens up new opportunities for applying

deep learning techniques to fields with large and complex datasets, such as spatio-temporal data (e.g., XPCS measurements). A research paper detailing the approach ("Hyena Hierarchy: Towards Larger Convolutional Models") has been submitted to the 2023 International Conference on machine Learning.

## 2.5 Accelerating analysis of large-scale data sets using unsupervised learning

The overarching goal of this work is to develop methods for clustering and analyzing high-dimensional large datasets. One approach is to transform data to a low-dimensional space while still retaining relevant physical attributes of the original data.

One technique for achieving this transformation is Principal Component Analysis (PCA). Currently, SLAC requires an online rank adaptive PCA that can process data in a single pass and allow the user to set a target accuracy instead of a target rank. This development was one of the goals of this work. To determine the most promising techniques for the SLAC data, we implemented and benchmarked several online PCA techniques and found that the Incremental PCA (IPCA) and the Frequent Directions (FD) Algorithms were the most effective. However, due to the challenges of estimating the true variance generated by new incoming data during compression, we employed a heuristic approach to estimate and update the rank of the model. One such technique involves computing the reconstruction error of incoming data and increasing the component rank if the error exceeds a threshold. Our initial results suggest that this technique produces comparable error to IPCA or FD with a 2–3 times increase in runtime. We are also investigating other heuristics, such as the ratio of singular values and the percentage of ill-modeled data in a sliding window. Moreover, the FD algorithm has a matrix sketch that can be efficiently combined while preserving error and size guarantees. Therefore, we are exploring the parallelization of our online Rank-Adaptive PCA algorithm by merging FD sketches in a hierarchical tree fashion.

Another area of investigation in this project involved enhancing our understanding of the beam profile through the visualization of the speckle pattern data. To achieve this, we created a data processing pipeline to convert the high-dimensional data into a low-dimensional format. Our first step involved applying PCA to reduce the dimensionality to approximately 10% of its original size. Next, we used the Uniform Manifold Approximation and Projection (UMAP) algorithm to reduce the dimensionality further, since the metrics-based UMAP algorithm struggles with the "dimensionality explosion" issue caused by the high-dimensional original dataset. Finally, we utilized the HDBScan (hierarchical DBSCAN) algorithm to cluster the data. The transformed dataset was then plotted on an interactive dashboard and compared with key features, such as the contrast values of the speckle patterns (see Figure 4, left panel). Along the way, we discovered that Gaussian Mixtures could well approximate the speckle pattern data. Therefore, we are exploring the implementation of Gaussian Mixture Models and related techniques to improve our analysis of the dataset.

Lastly, we are also pursuing a real-time streaming visualization of Speckle Pattern Data to monitor the beam profile and its evolution continuously. Our approach involves using a similar data-compression pipeline (PCA, UMAP, HDBScan) as in the previous section, but with a sliding time window. For this online setup, we use a rank-adaptive PCA. Unfortunately, after our initial literature review, we found that there are no streaming versions of UMAP or HDBScan currently available. Hence, we are currently exploring potential online approaches to UMAP and HDBScan. So, presently, we are applying the Aligned UMAP and standard HDBScan algorithms at each iteration (see Figure 4, right panel). Although the runtime is quite substantial, it remains manageable for benchmarking purposes. Aligned UMAP is a modification of UMAP specifically designed to work with aligned datasets (i.e., datasets partitioned in a sliding window). Additionally, we created a cluster remapping algorithm since HDBScan produces a new set of clusters with different labels at each step. By applying this data analysis, we were able to produce live animations and other visualizations of the speckle pattern data,

demonstrating how the structure of the high-dimensional dataset changes over time.

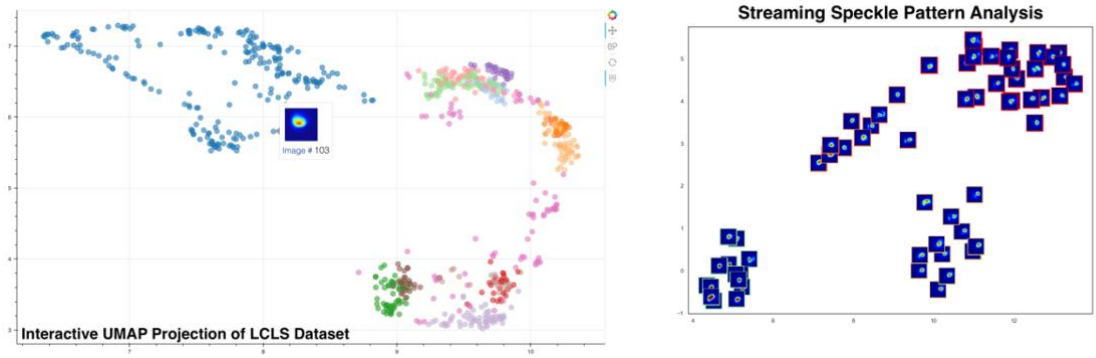


*Figure 4: The figure on the left illustrates an interactive UMAP projection of the LCLS dataset, where the color represents the clusters. When a point is hovered over with the mouse, a thumbnail of the original data sample (an image) is displayed. On the right, the figure shows an instance of streaming analysis with Aligned UMAP where the speckle pattern data is projected onto a low-dimensional space to highlight the similarities and differences between the samples. The samples are spatially grouped by speckle pattern similarity.*

## 3 Planned research

For the core-shell ionization dynamics in water, we plan to perform a systemic experiment study during 5/30 to 6/02 this year at Spring-8/SACLA. We would like to measure the change in the structure factor between 100 C to 400 C at 250 bar after core-shell x-ray ionization. Through this, we would like to study the dependence of the ionization dynamics on the thermodynamics condition and the abundance of the hydrogen bond network.

To address the issues in our preliminary experiment study, we have optimized the experiment geometry to cover Q over 0.1-to-3 Å for a 10 keV hard x-ray pulse. A dedicated imaging system is designed and implemented to facilitate the alignment between the two x-ray pulses. A much more mature and sophisticated pressure cell assembling procedure is established which will greatly reduce the background scattering issue.

For the data interpretation, since the core-shell ionization cannot be described within the conventional molecular dynamics (MD) framework, a combined Monte-Carlo-Molecular-Dynamics (MC/MD) procedure will be developed to simulate the process [Bergh et al. 2004; Inhester et al. 2016]. A Hartree-Fock approach will be used to estimate the water quantum state and then we calculate the quantum state transition probability accordingly. The transition probability is then used in the MC step in the MC/MD simulation to account for all the electron and proton transfer dynamics. Then the atomic dynamics is calculated with the conventional MD simulation technique.

## Publications and visibility from this research


- M. Ihme, W. T. Chung, and A. A. Mishra, “Combustion machine learning: Principles, progress and prospects.” Progress in Energy and Combustion Science, 91, 101010, 2022.
- Ihme, M. “Machine learning methods for reacting flows at macro and micro-scales.” Telluride workshop “Machine Learning and Informatics for Chemistry and Materials” September 2021.
- P. Muhunthan, K. Younes, D. Sokaras, T. Matsui, I. Rajkovic, T. Weiss, and M. Ihme, “Small Angle X-ray Scattering of Supercritical $CO_2$: Comparison with EoS” (submitted)
- K. Younes, M. Poli, P. Muhunthan, S. Ermon, and M. Ihme, “Rapid, online screening of complex phase spaces using Bayesian Optimization for SAXS measurements,” Nuclear Inst. and Methods in Physics Research, A (submitted)
- A. Majumdar, H. Li, Y. Sun, A. Späh, P. Muhunthan, D. Sokaras, D. Zhu and M. Ihme. "Examining molecular cluster dynamics of supercritical $CO_2$ using ultrafast XPCS. " APS March Meeting Abstracts 2023.

- M. Poli, S. Massaroli, E. Nguyen, D. Y. Fu, T. Dao, S. Baccus, Y. Bengio, C. Ré, S. Ermon "Hyena Hierarchy: Towards Larger Convolutional Models". Under review at the International conference on machine learning, 2023

## References


1) Neiswanger, W., Wang, K. A., Ermon, S., Proceedings of the 38th International Conference on Machine Learning, PMLR 139:8005-8015 (2021)
2) Mareev, E.I., Sviridov, A.P., Gordienko, V.M., The Anomalous Behavior of Thermodynamic Parameters in the Three Widom Deltas of Carbon Dioxide-Ethanol Mixture. Int. J. Mol. Sci., 22, no. 9813 (2021)
3) Tsuzuki et al. Journal of Chemical Physics 109 (1998): 2169-2175
4) Lomb L, Barends T R M, Kassemeyer S, et al. Radiation damage in protein serial femtosecond crystallography using an x-ray free-electron laser. Physical Review B, 2011, 84(21): 214111.
5) Garrett B C, Dixon D A, Camaioni D M, et al. Role of water in electron-initiated processes and radical chemistry: Issues and scientific advances. Chemical reviews, 2004, 105(1): 355-390.
6) Carlson R W, Anderson M S, Johnson R E, et al. Hydrogen peroxide on the surface of Europa. Science, 1999, 283(5410): 2062-2064.
7) Blanc M, Andrews D J, Coates A J, et al. Saturn plasma sources and associated transport processes. Space Science Reviews, 2015, 192: 237-283.
8) Jahnke T, Guillemin R, Inhester L, et al. Inner-shell-ionization-induced femtosecond structural dynamics of water molecules imaged at an x-ray free-electron laser. Physical Review X, 2021, 11(4): 041044.
9) Bergh M, Tîmneanu N, van der Spoel D. Model for the dynamics of a water cluster in an x-ray free electron laser beam. Physical Review E, 2004, 70(5): 051904.
10) Inhester L, Hanasaki K, Hao Y, et al. X-ray multiphoton ionization dynamics of a water molecule irradiated by an x-ray free-electron laser pulse. Physical Review A, 2016, 94(2): 023422.
11) H. Li et al., "Design of an amplitude-splitting hard x-ray delay line with subnanoradian stability," Optics letters, vol. 45, no. 7, pp. 2086-2089, 2020.
12) Yoshii, N. and Okazaki, S. "A large-scale and long-time molecular dynamics study of supercritical Lennard-Jones fluid. An analysis of high temperature clusters," The Journal of chemical physics, vol. 107, no. 6, pp. 2020-2033, 1997.
13) Sikorski, M. et al., "Application of an ePix100 detector for coherent scattering using a hard X-ray free-electron laser," Journal of synchrotron radiation, vol. 23, no. 5, pp. 1171-1179, 2016.
14) Kawasaki, K., "Kinetic equations and time correlation functions of critical fluctuations," Annals of Physics, vol. 61, no. 1, pp. 1-56, 1970.

# Probing Supercritical Phase Transition using Ultrafast X-ray Diagnostics

Principal Investigator: Matthias Ihme
Department of Mechanical Engineering, Stanford University
Department of Photon Science, SLAC National Accelerator Laboratory
440 Escondido Mall, Stanford, CA 94305
email: mihme@stanford.edu

Co-Investigator Dimosthenis Sokaras
SLAC National Accelerator Laboratory
2575 Sand Hill Road, Menlo Park, California 94025

## Program Scope

Over recent years, several hypotheses have been put forward to elucidate supercritical transition states. Despite significant progress on the fundamental understanding of fluids at these supercritical conditions, important questions concerning the microstructure and dynamical processes remain [1-5]. A particular research issue is hereby the fundamental understanding of the morphology of the molecular microstructure and its effect on the macroscopic behaviour and thermodynamic response functions. It is widely believed that the supercritical state is homogeneous without structural and dynamic observables to distinguish between a liquid and a vapor. However, recent investigations have identified regions of distinct liquid-like or vapor-like properties even under supercritical conditions [1,5]. Specifically, it was shown that the transition between liquid-like and vapor-like states occurs across an extension to the coexistence line, marked by almost discontinuous changes in fluid properties. This transition was first identified experimentally by Nishikawa and Tanaka [6] and stands in contrast to the classical presentation of the supercritical state space as a featureless, homogeneous domain.

Structurally, the most important properties of supercritical fluids are the dynamic heterogeneities and local density fluctuations that are present within the fluid state at the microscopic level. These inhomogeneities are associated with the formation of molecular clusters of various sizes with liquid-like properties separated by voids of unbound gas-phase molecules which continuously restructure itself at picosecond timescales.

By utilizing ultrafast X-ray Photon Correlation Spectroscopy (XPCS) at the Linac Coherent Light Source (LCLS) and X-ray synchrotron measurements as an experimental probe of these structural changes at the molecular level we seek to elucidate the higher-order phase transition from a liquid-like to a vapor-like state in the region extending the critical point. Open questions we seek to address particularly with XPCS are: (i) the underlying mechanisms responsible for the density fluctuations at supercritical conditions and how these dynamical processes at the molecular level affect the thermodynamic response functions and (ii) on what timescales do dynamical processes evolve that are associated with thermalization, molecular diffusion, and intermolecular cluster transfer.

## Research Progress

### Versatile Pressure Cell for XPCS Measurements of Supercritical Fluids

A direct scientific outcome of this project is the design of a highly versatile pressure cell that meets instrument-specific requirements for X-ray scattering experiments at synchrotron and XFEL sources, specifically targeting Wide/Small Angle X-ray Scattering (W/SAXS) measurements, spectroscopy, and ultrafast scattering experiments with XPCS and X-ray pump-probe. This pressure cell was optimized for dealing with the coherence and brightness of XFELs, optimized X-rays trans- mission, and accommodate a wide range of fluids and operating conditions. By addressing these requirements, we designed a pressure cell, based on previous concepts, which were extended to accommodate specific features, including (i) variable sample thickness, (ii) a metallic seal for high temperature operation, (iii)

thin diamond windows to reduce background scattering, and (iv) peripheral optics for enabling in-situ X-ray beam diagnostics to monitor beam overlap.

The pressure cell was designed to operate at temperature and pressure conditions up to 750 K and 690 bar, respectively, which is necessary to reach conditions for measuring supercritical $H_2O$. To accommodate XFEL-specific requirements, we considered a maximum wavelength of 0.3 nm, corresponding to an equivalent *Q*-range of up to 2.5 1/A at a cone angle of 30 degrees, allowing us to measure the ultrafast dynamics on sub-nanometer length scales.

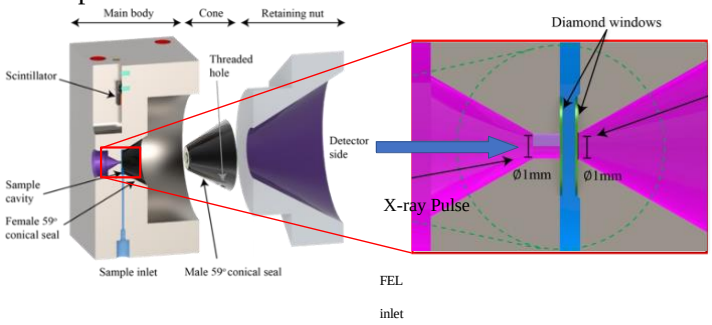


*Figure 1: Pressure cell assembly, consisting of main body, cone section to adjust sample thickness, retaining nut, and scintillator; zoomed view (right) shows the sample cavity with diamond windows*

The pressure cell assembly, shown in Figure 1, consists of three primary com- ponents: the main body holding the upstream X-ray window, a cone supporting the detector-side X-ray window, and a retaining nut. All three components were machined from grade 5 Ti- 6Al-4V titanium alloy, selected for its superior mechanical properties at elevated temperatures and pressures and its proven chemical inertness with supercritical water and supercritical aqueous solutions. A metal-to-metal deformation sealing mechanism was employed to seal the sample cavity at elevated temperatures, where common elastomer sealing mechanisms fails. A total of eight cartridge heaters was installed to control the temperature, which is monitored by a resistance temperature detector and a thermocouple positioned right next to the examined sample fluid, confirming stable temperature conditions within 0.2 K variations around the target temperature.

One general challenge associated with existing XFEL beamlines is the beam pointing stability. Due to the current single-pass lasing mechanism, the beam position and direction of the X-ray pulse from the source fluctuate and drift over a large distance and angle throughout an extended period of time, introducing substantial challenges for enabling accurate XPCS measurements. Therefore, routine monitoring of the beam condition is required. To achieve this, we installed an X-ray scintillator screen (YAG crystal), shown in Figure 4 to facilitate the alignment of the X-ray pulses hitting the sample. In addition, we used a Boron-doped diamond window allowing us to achieve real-time monitoring of the incident beam profile—a task never done before. This was critical for drastically reducing the time needed for the alignment tests, which could occupy up to 25% of the beamtime, thereby allowing us to significantly increase the effective measurement time.

The pressure cell and flow system are fully operational and will be utilized in the proposed re-search. We have successfully employed this pressure cell to perform W/SAXS experiments at SSRL, XPCS experiments at LCLS and the SPring-8 Angstrom Compact Free Electron Laser (SACLA, SPRING-8, Harima Science Garden City, Japan), with the latter two conducted with picosecond time resolution to extract nanometer dynamics in supercritical samples of $CO_2$ and $H_2O$.

## Probing Electronic Structure of Supercritical Fluids using X-ray Raman Spectroscopy

We have performed novel X-ray Raman spectroscopy (XRS) investigations to capture the local electronic structure of $CO_2$ close to the critical point. XRS combines the advantages of a hard X-ray probe (i.e. penetration and bulk information) with the spectral sensitivity of soft XAS. Using this technique, we performed a systematic XRS study under various *p/T* conditions in the vicinity of the $CO_2$ critical point. To overcome the very weak X-ray Raman cross-section, we used the high-throughput 40 crystal SSRL spectrometer.

The experimental study identified spectroscopic fingerprints along the oxygen K-edge XRS spectrum that gradually evolve across the super- critical region of $CO_2$ as exhibiting more liquid-like or gas-like character- istics depending on the density and C-O distance between neighboring molecules in the first coordination shell. We performed MD simulations to extract reliable trajectories of large ensembles of $CO_2$ molecules for the various *p/T* conditions of interest. The resulting molecular trajectories were used for extracting input geometries for hundreds of DFT simulations of XAS spectra using the deMon2K package. Ultimately we calculated an ensemble-averaged theoretical XAS spectrum for each *p/T* condition and directly compared it to the experimental data. Results are presented in Fig. 2. The theoretical DFT calculations closely reproduced the experimental observations and rationalized the spectral fingerprint trends on the basis of the $4s\sigma_g$ Rydberg state hybridization. By plotting the DFT-derived electron densities for the excited states that lie within the energy range of the most prominent spectral changes we were also able to visualize the extended hybridization of the liquid-like phase.

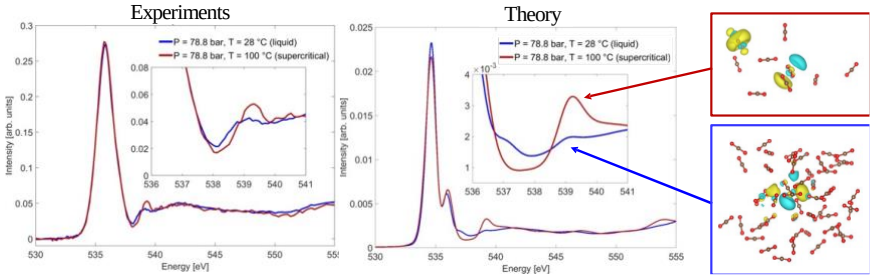


*Figure 2: Experimental and theoretical oxygen K-edge X-ray Raman spectra of CO2 at liquid (78.8bar/28˚C) and supercritical (78.8bar/100˚C) conditions. Electron densities for the excited states within the energy region of interest*

## Molecular-structural Analysis of Supercritical Fluids using SAXS

We performed X-ray scattering experiments at SSRL to examine the molecular structures and short- and long-range correlations in supercritical fluids. These correlations play an important role in relating the microscopic structure of the supercritical state to the macroscopic thermodynamic properties, such as Gibbs' free energy, compressibility, and cluster size. By utilizing the pressure cell developed in this research, we have successfully conducted SAXS experiments on pure $CO_2$, $H_2O$ and Xe, spanning a wide range of temperature and pressure conditions in the supercritical and subcritical regime. These measurements were performed at the SSRL beamline 4-2 (see Fig. 2(a)) through a series of four beamtime experiments; another beamtime with a total of 28 shifts (at 8 hours/shift) was approved the 2023/2024.

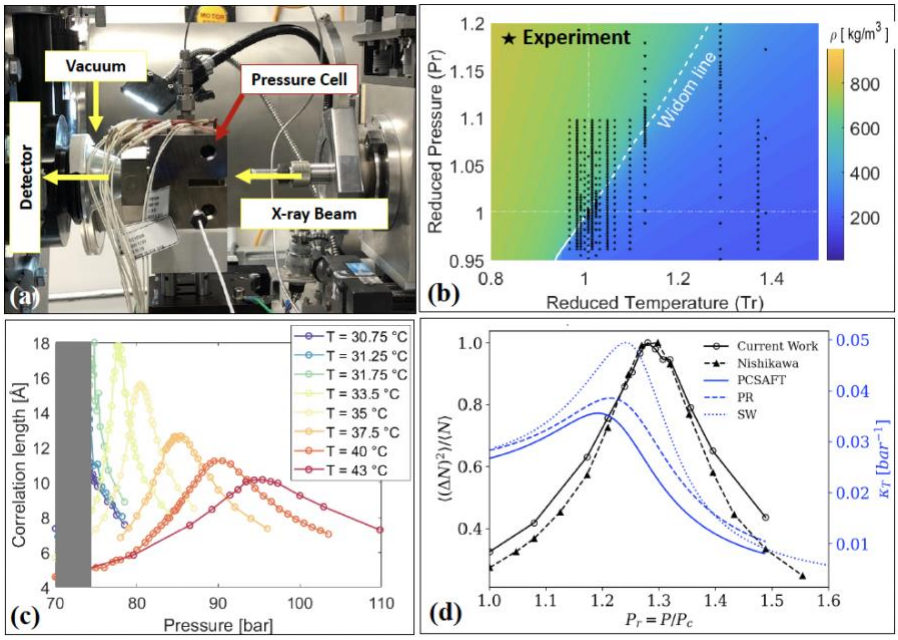


*Figure 2: Experimental and theoretical oxygen K-edge X-ray Raman spectra of CO2 at liquid (78.8bar/28˚C) and supercritical (78.8bar/100˚C) conditions. Electron densities for the excited states within the energy region of interest*

A comprehensive set of data was acquired for $CO_2$ (Fig. 2(b)), consisting of over 250 individual measurements around the critical point and the extended Widom region (Fig. 2(b)). These measurements were analyzed to determine the correlation lengths and density fluctuations, correspond to the variation in the number of molecules in the clusters. Representative experimental results are shown in Fig. 6(c,d). These results highlight the complex nature and interactions present near the Widom line in supercritical fluids. In particular, it can be seen that the curves have a distinct peak that shifts and broadens as we move away from the critical point. In addition, we observe an asymmetric decay on either side of the peak—this is a clear indication of the effects of the liquid-like and gas-like regions in the supercritical state.

To improve the fidelity of current modeling approaches for fluids in the supercritical state, we have examined several prominent equations of state (EoS), namely Peng-Robinson (PR), Span- Wagner (SW), and PC-SAFT, on their predictive capabilities to replicate the SAXS data (Fig. 6(d)). It was found in most cases that the current paradigm of EoS fail to trace peak location and shape of the compressibility, with discrepancies as large as 10% in the near-critical region.

### Theoretical Analysis and Complex Network Behavior of Supercritical Fluids

To connect the structural heterogeneities and cluster behavior to macroscopic thermodynamic properties, we performed theoretical analysis on supercritical fluids. By analyzing MD simulations of H2O in the extended supercritical state space, we discovered self-similarity in the molecular structure and used this finding to show that supercritical fluids behave as complex networks. In this physical network, each molecule represents a node that is connected to several other molecules. To mathematically describe the microscopic structure and dynamics of supercritical fluids, we showed that this complex-network model can predict this behavior in terms of only a few parameters (see Figure 2). In contrast to previous lattice-based models of supercritical fluids, this complex-network model can capture both static and dynamic response of supercritical fluids as evidenced by direct comparison to MD simulations and experiments. We were able to reach the above insight by extending Hill's energy criterion to molecular species, which defined the cluster formation mechanism in supercritical fluids purely via physics-based energy arguments. Moreover, we proposed the Widom self-similarity, *W*, to collapse the supercritical phase space. Finally, we demonstrated that the cluster size and degree distributions can be represented via a complex network model, whose link density can be expressed in terms of experimental observables, *T* and *p*. This model also captures the molecular exchanges among clusters as observed from MD data. These results present new opportunities to connect the microscopic structure of the supercritical phase to thermodynamic and transport properties. The proposed network model can provide the cluster size distribution or the connectivity in the supercritical phase, thereby forming the foundation for developing constitutive models for supercritical fluids.

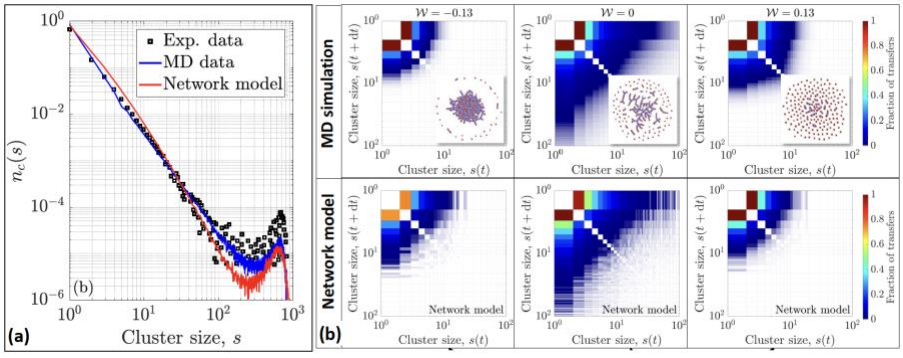


*Figure 2: Supercritical fluids behave as complex networks, showing (a) comparison of static cluster size distribution predicted from the complex network model with MD simulations and experiments and (b) prediction of dynamic cluster transfer, showing overall excellent agreement between our theoretical model and MD results.*

## Publication and Visibility from this research

### Primary research outcome

- Simeski, F. and Ihme, M., "Supercritical fluids behave as complex networks." Nature Communications, 14, 1996, 2023.

- Ly, N. and Ihme, M., “Destabilization of binary mixing layer in supercritical conditions.” Journal of Fluid Mechanics, 945, R2, 2022.
- Ly, N., Majumdar, A., and Ihme, M., “Regimes of evaporation and mixing behaviors of nanodroplets at transcritical conditions.” Fuel, 331, 125870, 2023.
- Guo, J., Yang, X. I. A., and Ihme, M., “Structure of the thermal boundary layer in turbulent channel flows at transcritical conditions.” Journal of Fluid Mechanics, 934, A45, 2022.
- Li, F., Guo, J., Bai, B., and Ihme, M., “Analysis of real-fluid thermodynamic effects on turbulent statistics in transcritical channel flows.” Physical Review Fluids, 8, 024605, 2023.
- Muhunthan, P., Li, H., Vignat, G., Sun, Y., Fulton, J. L., Sokaras, D., and Ihme, M., “A versatile pressure-cell for coherent X-ray scattering measurements of supercritical fluids.” under review in Review of Scientific Instruments, 2023.
- Muhunthan, P., Paredes Mellone, O., Kroll, T., Sokaras, D., and Ihme, M., “The local electronic structure of supercritical CO2 from X-ray Raman spectroscopy and atomistic-scale modeling.” Under review in Journal of Physical Chemistry Letters, 2023.

### Secondary research outcome

- Lin, M.-F., Singh, N., Liang, S., Mo, M., Nunes, P. Ledbetter, K., Yang, J., Kozina, M. Weathersby, S., Shen, X., Cordones-Hahn, A., Wolf, T., Gaffney, K., Pemmaraju, D., Ihme, M., and Wang, X., “Imaging the short-lived hydroxyl-hydronium pair in ionized liquid water.” Science, 374, 6563, 92-95, 2021.
- Rosenberger, P., Dagar, R., Zhang, W., Majumdar, A., Neuhaus, M., Ihme, M., Bergues, B., and Kling, M. F., “Reaction nanoscopy of ion emission from subwavelength propanediol droplets.” Nanophotonics, 2023.

## References

[1] G. G. Simeoni, et al. The Widom line as the crossover between liquid-like and gas-like behaviour in supercritical fluids. Nat. Phys. 6.7 (2010): 503-507
[2] P. F. McMillan and H. E. Stanley. Going supercritical. Nat. Phys. 6.7 (2010): 479-480.
[3] J. Frenkel. Kinetic Theory of Liquids. Dover, 1955.
[4] H. E. Stanley. Introduction to Phase Transitions and Critical Phenomena. International Series of Monographs on Physics. Oxford University Press, 1971.
[5] F. Gorelli, M. Santoro, T. Scopigno, M. Krisch, and G. Ruocco. Liquidlike behavior of supercritical fluids. Phys. Rev. Lett., 97(24):245702, 2006.
[6] L. B. Skinner, M. Galib, J. L. Fulton, C. J. Mundy, J. B. Parise, V.-T. Pham, G. K. Schenter, and C. J. Benmore, "The structure of liquid water up to 360 MPa from x-ray diffraction measurements using a high Q-range and from molecular simulation", J. Chem. Phys. 144, 134504 (2016).

**Tracking the Mechanisms of Catalytic Reactions on Ligand-Protected Gold Nanoclusters**

Christopher J. Johnson
Department of Chemistry
Stony Brook University
100 Nicolls Rd., Stony Brook, NY 11794-3400
chris.johnson@stonybrook.edu

*Program Scope*

This research program focuses on catalytic transformations leveraging atomically-precise nanoclusters as potential designer electrocatalysts. Atomically-precise nanoclusters typically feature a metal or metalloid core of tens to hundreds of atoms surrounded by a stabilizing and solubilizing layer of organic ligands, yielding a nanoparticle with a total diameter of 1-2 nm. They merge desirable qualities of molecular and nanoscale catalysts: they can, in principle, be produced or isolated with exactly specified structures and formulae like molecules, but feature densities of states, redox properties, and compositions more consistent with nanoscale objects or bulk surfaces. Nanoclusters have been extensively pursued as catalysts, showing promise in a number of reactions.[3] We are focusing on the electroreduction of $CO_2$, for which two prototypical nanoclusters in particular have shown enhanced activity that depends their composition.[1, 4] Specifically, we plan:

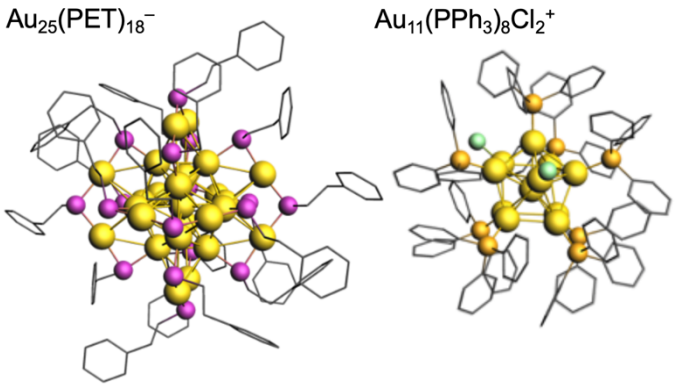


Figure 1: X-ray crystal structures of $Au_{25}(PET)_{18}^-$ (PET = phenylethanthetiol) and $Au_{11}(PPh_3)_8Cl_2^+$ ($PPh_3$ = triphenylphosphine). Here gold = Au, pink = S, orange = P, and green = Cl.[1-2]

1. to determine the active site for electrochemical $CO_2$ reduction by the ubiquitous $Au_{25}(SR)_{18}$ nanocluster,
2. to determine the mechanism of $CO_2$ reduction by $Au_{11}$ nanoclusters,
3. to synthesize nanoclusters with improved catalytic activity by tailoring active sites and optimizing ligand and metal dopant chemistry.

The $Au_{25}(SR)_{18}$ and $Au_{11}(PPh_3)_8Cl_2^+$ nanoclusters, shown in Figure 1, have been shown to be catalytically active towards $CO_2$ and the mechanism has been investigated computationally. Quantum chemical calculations for $Au_{25}(SR)_{18}$ suggest that a ligand dissociates, leaving an undercoordinated Au atom that can take $CO_2$ as a ligand.[5] However, experimentally probing this mechanism directly is made challenging by the inability to isolate the undercoordinated species. We use mass spectrometry as a general approach to produce and isolate this species and compare its activity towards $CO_2$ with that of the intact nanocluster. Mass spectrometry also allows us to track this activity as a function of metal doping and ligand exchange, both of which have been shown to increase activity. Once isolated in the mass spectrometer, we probe key elements of bonding, structure, and the degree of $CO_2$ activation using a combination of common chemical analysis tools adapted for use on mass selected ions. Specifically, electronic spectroscopy yields key energetic information such as relative orbital energies and their dependence on the exact nanocluster composition, while infrared spectroscopy gives insight into structure and small molecule activation. We couple these techniques to variable-temperature ion traps, which give us access to key thermochemical information to characterize the reaction mechanisms driving elementary reactions catalyzed by these nanoclusters. These insights not only inform efforts to synthetically optimize nanoclusters, they also allow us to screen clusters for high activity. Given the difficulty of developing atomically-precise synthetic methods or purification protocols, our ability to propose specific clusters that are likely to be highly catalytically active holds the potential to significantly accelerate developments in this field.

The electrochemically reduced cation $Au_{25}(SR)_{18}^{+}$, formed by two-electron oxidation of $Au_{25}(SR)_{18}^{-}$, is a potential intermediate in the mechanism of $CO_2$ reduction by $Au_{25}$ nanoclusters. In collaboration with Xiaosong Li at University of Washington, we probed the changes to the electronic structure during this process. Given that the anion has a closed 8-superatomic-electron shell, expected the resulting 6-electron cluster to display a reduced HOMO-LUMO gap, and potentially different spin-orbit coupling effects. Indeed, in comparing the spectra of the cation and anion in Figure 2, we found a new transition in the cation spectrum centered around 0.9 eV, a full 0.7 eV lower in energy for than the apparent HOMO-LUMO transition of the anion. This HOMO-LUMO gap is presumably stabilized by a Jahn-Teller-like distortion of the nominally icosahedral $Au_{13}$ core of $Au_{25}$, which we hypothesize to selectively destabilize some of the six S-Au-S-Au-S "staple" ligand motifs protecting its surface. Given that the availability of undercoordinated surface sites is expected to be critical to the catalytic performance of these clusters, such electronic effects may play a key role in their catalytic mechanisms.

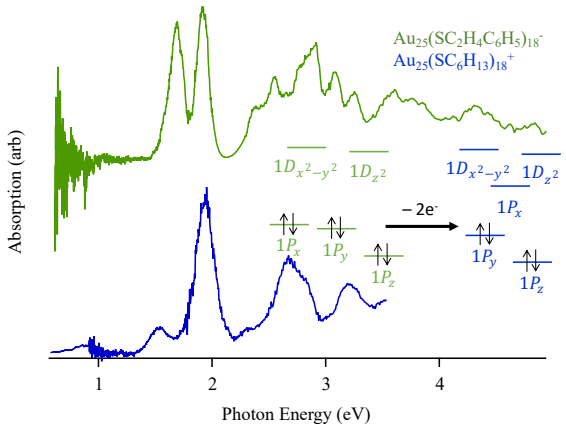


Figure 2: Comparison of the spectra of $Au_{25}(PET)_{18}^{-}$ (top, green) that of $Au_{25}(SC_6H_{13})_{18}^{+}$ (bottom, blue). Note we have previously shown that the spectrum depends minimally on ligand identity, and thus the change in the spectra is dominated by the charge state. Inset is a superatomic orbital diagram to rationalize the change in the energy of the HOMO-LUMO transition.

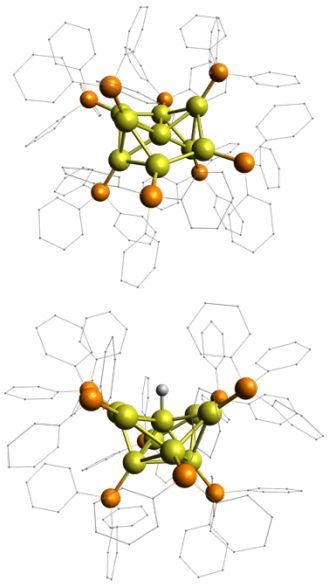

Figure 3: A comparison of the computed structures of $Au_9(PPh_3)_8^{3+}$ (top) and $Au_9(PPh_3)_8H^{2+}$ (bottom). Both structures feature nearly $C_{4v}$ symmetry, but the addition of the hydride induces significant distortions.

The role of surface-bound hydrogen atoms in catalytic mechanisms involving gold nanoclusters has been a topic of recent interest. While hydrogen atoms do not bind well to bulk gold surfaces, gold nanoclusters frequently feature surface-bound hydrogen atoms, typically as formal hydrides. The surface chemistry of these hydrides is rationalized by their ability to donate electrons into the gold superatomic orbitals, a feature of gold clusters known from classic gas phase spectroscopy studies. Therefore, while formally hydrides, it is possible that the electron density in the vicinity of the hydrogen atom is substantially lower, leading to the possibility that they may feature some acidic properties. However, the isolation of hydrogen-enriched nanoclusters in solution is a challenge, impeding further insights into their influence on catalytic and synthetic mechanisms. The mass spectrometry basis of our experimental approaches offers unique opportunities to probe the properties and reactivity of surface-bound hydrogens.

We investigated the prototypical H-atom-containing cluster $Au_9(PPh_3)_8H^{2+}$, derived from the addition of a hydride to the atomically-precise $Au_9(PPh_3)_8^{3+}$ cluster as shown in Figure 3.[6] As a 6-electron superatom, $Au_9(PPh_3)_8^{3+}$ features an unfilled superatomic $P_z$ orbital that is primed to accept two electrons from the hydride to form a closed 8 electron shell. Density functional theory calculations suggest a charge on the hydrogen that ranges from slightly negative to slightly positive, consistent with a weak acid. The doubly-reduced $Au_9(PPh_3)_8^{+}$ cluster has not been observed, suggesting that the overall reactivity of the cluster is not consistent with an acid. We recorded the vibrational spectra of $Au_9(PPh_3)_8^{3+}$, $Au_9(PPh_3)_8H^{2+}$, and

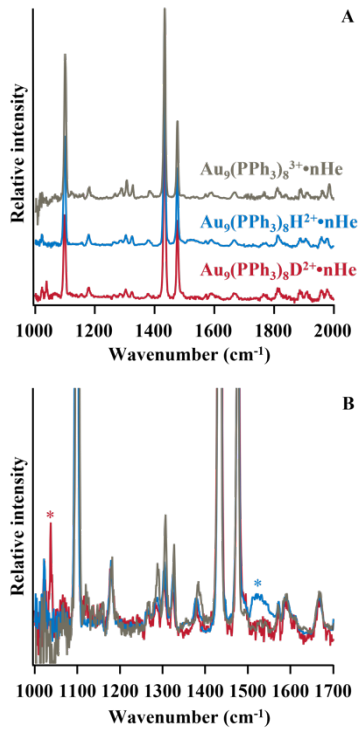


Figure 4: (top) The spectra of $Au_9(PPh_3)_8^{3+}$, $Au_9(PPh_3)_8H^{2+}$and $Au_9(PPh_3)_8D^{2+}$ in the fingerprint region. (bottom) A detailed view of the lower-intensity vibrations associated with Au-H and Au-D stretching, denoted by *.

$Au_9(PPh_3)_8D^{2+}$ to identify the Au-H stretching frequency, which will be key to our studies. Figure 4 compares these spectra, showing an isotope-induced shift of the identified Au-H stretch of 1.47. Given that a purely harmonic oscillator should show no larger of a shift than 1.41, we conclude that the potential governing Au-H motion displays positive anharmonicity indicative of a more "particle-in-a-box-like" bonding arrangement than that of a typical covalent bond. From these vibrational energies, we are able to generate a model quartic potential directly from experimental data, yielding the potential energy curve shown in Figure 5. We collaborated with Rebecca Gieseking at Brandeis University to produce a quantum chemical estimate of the same potential, which also yielded a shape with a significant quartic component, reinforcing this interpretation.

We next sought to characterize the acidity of the hydrogen atom. We hypothesized that complexation of weak bases with the $Au_9(PPh_3)_8H^{2+}$ cluster would yield a red shift of the Au-H vibration, as similar effects are commonly seen in proton-bound hetero- and homodimers.[7] We compared the center of brightness of the Au-H stretching band upon complexation with He and $N_2$, both very weak bases. $N_2$ complexation induced a red shift of 39 $cm^{-1}$, consistent with that expected for a moderate acid. Complexation with stronger bases such as $CO_2$, $H_2O$, or $NH_3$ yielded spectra with no discernable Au-H stretching feature, suggesting that the surface-bound H atom is likely highly reactive. Taken together, these observations suggest a picture in which, when bound to the surface of the cluster, H atoms are likely to react similarly to acidic protons in reaction mechanisms, despite the fact that the conjugate base $Au_9(PPh_3)_8^+$ appears to be unstable, We hypothesize that a series of intermediates in these reactions may exist in which partial proton transfer yields a transient and potentially highly reducing $Au_9(PPh_3)_8^+$ species that acts to donate one or two electrons to nearby or surface-bound reactants. It remains to be seen the extent to which these observations are generalizable to other H-atom-containing gold nanoclusters.

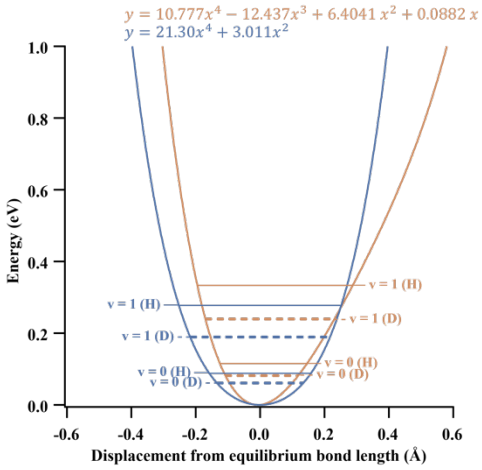


Figure 5: Experimentally-derived (blue) and quantum chemical (orange) potential energy curves for Au-H stretching. At the top are the functional forms of these curves for reference.

*Future Plans*

While gas-phase ion-molecule chemistry is sufficient to form complexes of catalytically-relevant nanoclusters and small molecule reactants, a key to fully exploring their reaction mechanisms is the generation of relevant cluster oxidation states and highly-active undercoordinated sites. To this end, we are finalizing the construction of an electrochemical flow cell integrated into our electrospray ionization source.[8] We have observed electrochemistry spontaneously occurring in the electrospray source, but it is difficult to control for the efficient generation of oxidized or reduced clusters because of the need to balance efficient ion transfer and electrochemistry with a single voltage. The electrochemical flow cell will decouple these parameters, giving us much greater flexibility to use electrochemistry to generate the needed clusters.

We have also recently installed an improved nonlinear crystal for difference frequency generation between 2400 and 800 $cm^{-1}$ (ZGP, replacing $AgGaSe_2$) yielding a 2-4x increase in laser power at the ion target. This spectral range is key for the detection of relatively weak Au-H stretching bands as well as the shifts of $CO_2$ or $O_2$ ranging from unactivated to fully negatively charged. For instance, the vibrational spectra presented in Figure 4 each required approximately one day to record, due primarily to the necessity for significant signal averaging to resolve the weak Au-H stretching band fully from baseline noise. With the improved power, we expect this time to be reduced to 1-2 hours, or minutes for significantly more intense $CO_2$ stretches. This acceleration of data acquisition will enable screening studies for highly-catalytically-active nanoclusters across a range of sizes, ligands and dopants.

*References*


1. Narouz, M. R., et al., N-heterocyclic carbene-functionalized magic-number gold nanoclusters. *Nat. Chem.* **2019**, *11*, 419-425.
2. Heaven, M. W.; Dass, A.; White, P. S.; Holt, K. M.; Murray, R. W., Crystal Structure of the Gold Nanoparticle $[N(C_8H_{17})_4][Au_{25}(SCH_2CH_2Ph)_{18}]$. *J. Am. Chem. Soc.* **2008**, *130*, 3754-3755.
3. Zhao, S.; Jin, R.; Jin, R., Opportunities and Challenges in $CO_2$ Reduction by Gold- and Silver-Based Electrocatalysts: From Bulk Metals to Nanoparticles and Atomically Precise Nanoclusters. *ACS Energy Lett.* **2018**, *3*, 452-462.
4. Alfonso, D. R.; Kauffman, D.; Matranga, C., Active sites of ligand-protected $Au_{25}$ nanoparticle catalysts for $CO_2$ electroreduction to CO. *J. Chem. Phys.* **2016**, *144*, 184705.
5. Kauffman, D. R.; Alfonso, D.; Matranga, C.; Qian, H.; Jin, R., Experimental and Computational Investigation of $Au_{25}$ Clusters and $CO_2$: A Unique Interaction and Enhanced Electrocatalytic Activity. *J. Am. Chem. Soc.* **2012**, *134*, 10237-10243.
6. Takano, S.; Hirai, H.; Muramatsu, S.; Tsukuda, T., Hydride-Doped Gold Superatom $(Au_9H)^{2+}$: Synthesis, Structure, and Transformation. *J. Am. Chem. Soc.* **2018**, *140*, 8380-8383.
7. Roscioli, J. R.; McCunn, L. R.; Johnson, M. A., Quantum Structure of the Intermolecular Proton Bond. *Science* **2007**, *316*, 249-254.
8. Fournier, J. A.; Wolk, A. B.; Johnson, M. A., Integration of Cryogenic Ion Vibrational Predissociation Spectroscopy with a Mass Spectrometric Interface to an Electrochemical Cell. *Anal. Chem.* **2013**, *85*, 7339-7344.

**Studies of non-equilibrium high pressure kinetics at supercritical $H_2O/CO_2$ conditions using a new supercritical jet stirred reactor**

**PI: Yiguang Ju**
Department of Mechanical and Aerospace Engineering, Princeton University, Princeton, NJ 08540
Email: yju@princeton.edu

**Proposal scope:** $CO_2$ emission from burning fossil fuels has caused increasing concerns about climate change. High pressure and low temperature advanced compression ignition engines using biofuels and supercritical $CO_2$ (S-$CO_2$) power cycles have a great potential for higher efficiency and lower carbon emissions. The objectives of this proposal is to develop a new, supercritical pressure jet stirred reactor (SP-JSR) operating up to 200 atm and to advance fundamental understanding of non-equilibrium chemical kinetics via the effects of strong intermolecular force, reactive multi-body reactions, non-equilibrium vibrational energy distribution, and the uncertainty of energy distribution due to collisional broadening on low temperature combustion and $HO_2$ chemistry with $CO_2$ and $H_2O$ dilutions. Non-equilibrium effects via real gas intermolecular force, reactive termolecular reactions involving $HO_2$ and OH, vibrational non-equilibrium energy distribution, and collisional energy broadening at high pressure will be examined. Key $HO_2$ reactions with fuels and radicals will be studied by using microsecond time-resolved mid-IR Faraday rotation spectroscopy (FRS) and high-level quantum chemistry calculations. The obtained high pressure data and the newly measured and computed reaction rates will be used to develop and validate new high pressure combustion models by including non-equilibrium effects. The present studies will advance the fundamental understanding of non-equilibrium chemical kinetics and $HO_2$ chemistry at extreme pressures.

**What was accomplished under these goals?**

1. **A supercritical pressure jet stirred reactor development**: A supercritical pressure jet stirred reactor (SP-JSR) was developed for high pressure kinetics up to 200 atm. SP-JSR is successfully used to examine the high pressure kinetics of small alkanes and oxygenated fuels. The results showed that low temperature chemistry as well as $HO_2$ chemistry are significantly enhanced at high pressure [1-4].

2. **Low- and intermediate-temperature oxidation of propane up to 100 atm:** The low temperature oxidation of propane is investigated by using a SP-JSR with and without 20% $CO_2$ additions at fuel lean and rich conditions at 10 and 100 atm and 500-1000 K (Fig. 1). The experiment shows that different from that of 10 atm, at 100 atm only a weak NTC behavior is observed because of the significant shift of the intermediate temperature $HO_2$ chemistry to lower temperature. In addition, at 100 atm, existing models in literatures can successfully capture the onset temperatures of the low and intermediate chemistry, while under-predict the fuel oxidation quantitatively and fail to capture the NTC behavior between 650-780 K at both fuel lean and rich conditions. Similar discrepancy was observed in studies of n-butane and DME oxidations in literatures, which implying that there exists a large uncertainty in model development of fuels with low temperature chemistry at high pressures [4].

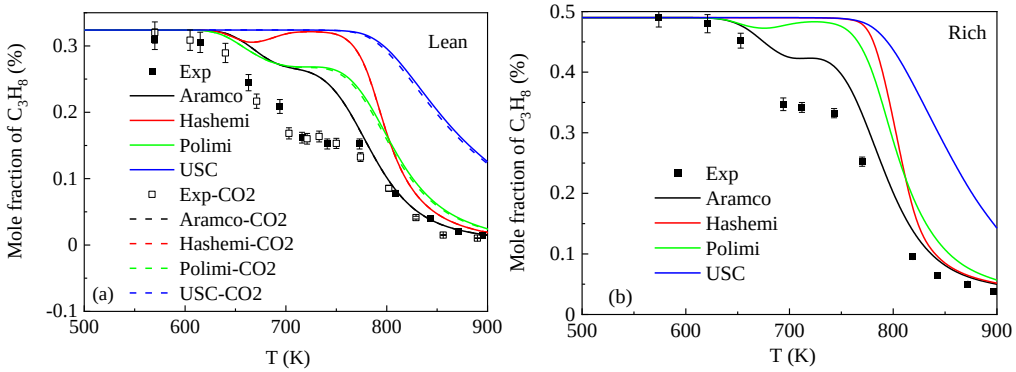


Fig. 1 Temperature evolutions of $C_3H_8$ in the propane oxidation without $CO_2$ at fuel lean conditions, with 20% $CO_2$ at fuel lean conditions, and without $CO_2$ at fuel rich conditions, respectively, at 100 atm.

3. **Methanol oxidation up to 100 atm in a supercritical pressure jet-stirred reactor:** Methanol oxidation was studied using a recently developed supercritical pressure jet-stirred reactor (SP-JSR) at pressures of 10 and 100 atm, at temperatures from 550 to 950 K, and at equivalence ratios of 0.1, 1.0, and 9.0 in experiments and simulations. The experimental results show that the onset temperature of $CH_3OH$ oxidation at 100 atm is around 700 K, which is more than 100 K lower than the onset at 10 atm and this trend cannot be predicted by the existing kinetics models. Furthermore, a negative temperature coefficient (NTC) behavior was clearly observed at 100 atm at fuel rich conditions for methanol for the first time. To understand the observed temperature shift in the reactivity and the NTC effect, we updated some key elementary reaction rates of relevance to high pressure $CH_3OH$ oxidation from the literature and added some new low-temperature reaction pathways such as $CH_2O + HO_2 = HOCH_2O_2$ ($RO_2$), $RO_2 + RO_2 = HOCH_2O$ (RO) + $HOCH_2O$ (RO) + $O_2$, and $CH_3OH + RO_2 = CH_2OH + HOCH_2O_2H$ (ROOH). Although the model with these updates improves the prediction somewhat for the experimental data at 100 atm and reproduces well high-temperature ignition delay times and laminar flame speed data in the literature, discrepancies still exist for some aspects of the 100 atm low-temperature oxidation data. In addition, it was found that the pressure-dependent $HO_2$ chemistry shifts to lower temperature as the pressure increases such that the NTC effect at fuel-lean conditions is suppressed. Therefore, as shown in the experiments, the NTC phenomenon was only observed at the fuel-rich condition where fuel radicals are abundant and the $HO_2$ chemistry at high pressure is weakened by the lack of oxygen resulting in comparatively little $HO_2$ formation.

4. **Repetitive autoignition and extinction of near-limit non-premixed n-dodecane spray cool flames**: Experimental study is performed on autoignition and extinction of non-premixed n- dodecane spray cool flames. A novel phenomenon of repetitive autoignition-extinction instability of near-limit non-premixed spray cool flames is observed (Fig. 2). The repetitive autoignition and extinction cycles are found to be mostly caused by the competition between timescales of low temperature fuel oxidation chemical heat release, and vaporization and heat loss of fuel spray vaporization, where the dynamics of large droplets in polydisperse spray play an important role. It is shown that at the extinction condition, large droplets penetrate the stagnation plane and form a premixed mixture of fuel vapor and oxygen at a higher preheated temperature with a longer flow residence time, leading to an auto-ignited spray cool flame formation. On the other hand, at the cool flame condition, large droplets absorb excessive heat from the flame via vaporization and lower the flame temperature, thus causing flame extinction at the near-limit oxygen concentrations and temperatures. Moreover, experimental results show that with the increase of the oxygen mole fraction, the spray cool flame stabilization time increases, and the cycles of autoignition and extinction become less frequent. The results will contribute to the development of advanced low-temperature combustion engines and spray combustion models.

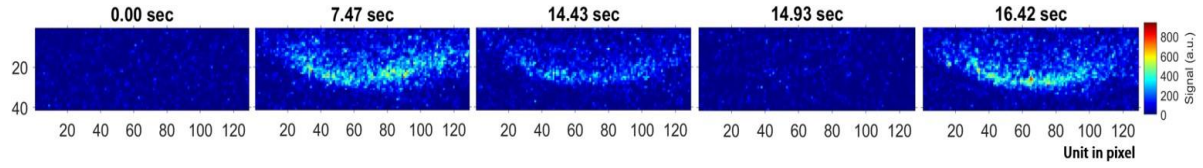


Fig. 2: Formaldehyde chemiluminescence during an autoignition-extinction instability cycle.

5. **Structure, extinction limits, and reactivities of n-dodecane diffusion cool flames at high pressures**: N-dodecane ($nC_{12}H_{26}$) is selected to study its diffusion cool flame dynamics and reactivity in a new high-pressure counterflow burner at pressure up to 10 atm, perhaps for the first time. We investigate the effects of pressure on cool flame extinction limits, structure, radical index, and oxygen concentration dependence in experiments and numerical simulations. The results show that the higher pressure shifts the cool flame to higher strain rates and results in higher cool flame extinction strain rates. By using the concept of density-weighted cool flames, it is shown that the reduced extinction limit is proportional to the square of pressure. A scaling analysis is developed and successfully explained the relationship of the flame structure density-weighted cool flame strain rate and at elevated

pressure. Furthermore, the cool flame structure, heat release rate, and extinction limit as a function of density weighted strain rate. In addition, radical indexes at different pressures are developed by isolating the thermal and transport effects from the chemical contribution to diffusion cool flame extinction. The results show that the low-temperature reactivity increases with pressure (Fig. 3) [5].

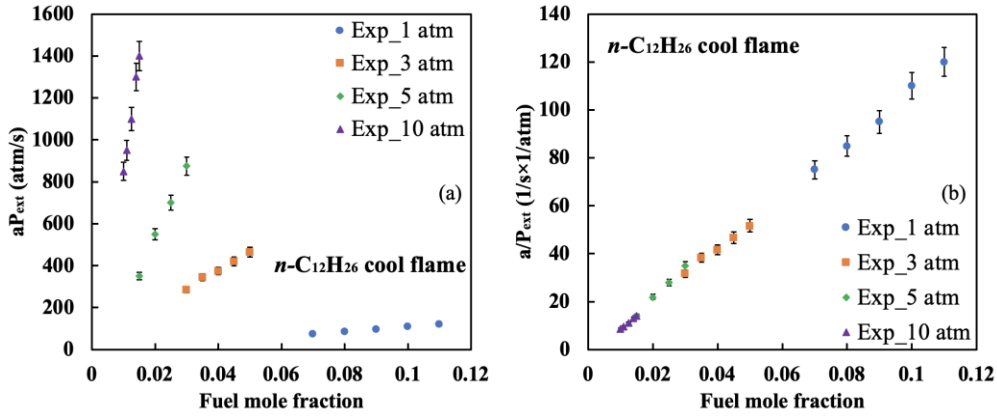


Fig. 3: (a) Pressure-weighted cool flame extinction strain rates and (b) Pressure-rescaled cool flame extinction strain rates versus fuel mole fraction of *n*-$C_{12}H_{26}$

6. **Assessment of the impact of reactor residence time distribution on non-equilibrium product selectivity of polypropylene pyrolysis using reactive molecular dynamics simulations:** Mass residence time distribution (RTD) and non-equilibrium kinetics are considered to be an important factor controlling the product selectivity in the pyrolysis of biomass and plastic wastes along with the pyrolysis chemistry. We introduce a reaction molecular dynamics-based method to examine pyrolysis chemistry and species timescales to assess the impact of RTD on product selectivity and yield. To validate this method, reactive molecular dynamics simulations were conducted for polypropylene pyrolysis and its non-equilibrium product selectivity using 6 different RTDs. We find that the RTD and the reaction chemistry control the peak non-equilibrium product concentrations. The peak monomer ($C_3H_6$) concentration during the pyrolysis can be increased by up to 25% by using a narrow RTD in the case of polypropylene pyrolysis. We also find that product selectivity is strongly affected by the average residence time and RTD. This coupling between the reaction chemistry, RTD, and product selectivity highlights the need to understand detailed reaction chemistry to control RTD and optimize non-equilibrium product selectivity during polymer and biomass pyrolysis. The present method provides a new way to design RTD for reactors to reach maximized product selectivity of plastic waste [7].

7. **Catalyst-free and Far-from-equilibrium Depolymerization of Plastics via Electrified Spatiotemporal Heating:** Depolymerization is a promising strategy for recycling waste plastics into their constituent monomers for subsequent polymerization in another lifecycle. However, many commodity plastics cannot be depolymerized with high selectivity using conventional thermochemical approaches as it is difficult to control the reaction progress and pathway, thereby often leading to a broad spectrum of products. We present a catalyst-free, far-from-equilibrium depolymerization method via electrified spatiotemporal heating and molecular dynamics simulations that enables us to understand non-equilibrium pyrolysis kinetics and to generate monomers from commodity plastics with high yields. Using this approach, we depolymerized polypropylene and polyethylene terephthalate to their monomers with yields of ~36% and ~43%, respectively, which are among the highest compared to conventional thermochemical methods, even those that use catalysts (e.g., ~10–20%) [9].

**Training opportunities**

The research provides opportunities for career training of two graduate students and two postdocs to conduct high pressure low temperature combustion and kinetic studies. In addition, it gives an opportunity for them to have a join mentoring in collaboration with two top chemistry theorists, Drs. Ahren Jasper and Stephen Klippenstein, at Argonne National Laboratory.

**Publications:**


1. Chao Yan, Hao Zhao, Ziyu Wang, Guohui Song, Ying Lin, Clayton R. Mulvihill, Ahren W. Jasper, Stephen J. Klippenstein, Yiguang Ju, Low- and intermediate-temperature oxidation of dimethyl ether up to 100 atm in a supercritical pressure jet-stirred reactor, **Combustion and Flame**, 2022, 112059. https://doi.org/10.1016/j.combustflame.2022.112059
2. Ziyu Wang, Chao Yan, Ying Lin, Mengni Zhou, Bo Jiang, Ning Liu, Hongtao Zhong, Yiguang Ju, Kinetics and Extinction of Non-premixed Cool and Warm Flames of Dimethyl Ether at Elevated Pressure, **Proceedings of the Combustion Institute**, Vol. 39 (2022):1–8. https://doi.org/10.1016/j.proci.2022.06.007
3. Ziyu Wang, Hao Zhao*, Chao Yan, Ying Lin, Aditya D. Lele, Wenbin Xu, Brandon Rotavera, Ahren W. Jasper, Stephen J. Klippenstein, Yiguang Ju, Methanol oxidation up to 100 atm in a supercritical pressure jet-stirred reactor, **Proceedings of the Combustion Institute**, Vol. 39 (2022):1–9. https://doi.org/10.1016/j.proci.2022.07.068
4. Hao Zhao, Chao Yan, Guohui Song, Ziyu Wang, Yiguang Ju, Studies of low and intermediate temperature oxidation of propane up to 100 atm in a supercritical-pressure jet-stirred reactor, **Proceedings of the Combustion Institute**, Vol. 39 (2022):1–9. https://doi.org/10.1016/j.proci.2022.07.086
5. Ziyu Wang, Mengni Zhou, Pascal Diévart, Ying Lin, Ning Liu, Chao Yan, Yiguang Ju, “Study on cool flame radical index and oxygen concentration dependence of oxygenated fuels", **Combustion and Flame**, 112493, 2022, doi.org/10.1016/j.combustflame.2022.112493
6. Ziyu Wang, Chao Yan, Bowen Mei, Ying Lin, Yiguang Ju, Study of Low Temperature Oxidation Kinetics of Diethyl Ether in a Supercritical Pressure Jet-stirred Reactor, **The Journal of Physical Chemistry A**, 2023, 127, 2, 506–516, doi.org/10.1021/acs.jpca.2c06182
7. Aditya Dilip Lele and Yiguang Ju, Assessment of the impact of reactor residence time distribution on non-equilibrium product selectivity of polypropylene pyrolysis using reactive molecular dynamics simulations, **Fuel**, 2023, 338, 127328, https://doi.org/10.1016/j.fuel.2022.127328
8. Andrés Z. Mendiburu, João A. Carvalho Jr., and Yiguang Ju, Flammability Limits: A Comprehensive Review of Theory, Experiments, and Estimation Methods, **Energy & Fuels**, DOI: 10.1021/acs.energyfuels.2c03598
9. Qi Dong, Aditya Dilip Lele, Xinpeng Zhao, Sichao Cheng, Yueqing Wang, Miao Guo, Mingjin Cui, Alexandra H Brozena, Tangyuan Li, Xin Zhang, Ioannis G. Kevrekidis, Jianguo Mei, Xuejun Pan, Dongxia Liu, Yiguang Ju*, Liangbing Hu*, Depolymerization of plastics by means of electrified spatiotemporal heating, **Nature**, 616(7957), pp.488-494, 2023. https://doi.org/10.1038/s41586-023-05845-8


**Future work**

1. Study oxygenated fuels and E-fuels high pressure kinetics and their coupling with $NH_3$.
2. Study non-equilibrium kinetics at supercritical pressure using molecular dynamics modeling.

**Technical Impacts**

1. Extended the high pressure kinetic studies to 100 atm or higher and created a new platform for kinetic studies at extreme pressure.
2. Demonstrated the enhanced competition between $HO_2$ chemistry and low temperature chemistry at extreme pressure and the possibility of new reaction pathways for small alcohols.
3. Developed a molecular dynamic simulation tool to study non-equilibrium kinetics and polymer pyrolysis.

**DoE Impacts**

1. Understanding the low temperature fuel oxidation under engine conditions.
2. Helped to design advanced engines with low carbon emissions.
3. Contributed to the development of biofuels.
4. Contributed to decarbonization and sustainability using plastic recycling.

# Probing the Reaction Dynamics of Hydrogen-Deficient Hydrocarbon Molecules and Radical Intermediates via Crossed Molecular Beams

Ralf I. Kaiser
Department of Chemistry, University of Hawai'i at Manoa, Honolulu, HI 96822
ralfk@hawaii.edu

## 1. Program Scope

The major goals of this project are to explore experimentally by exploiting molecular beams to study the fundamental reaction dynamics and underlying potential energy surfaces (PESs) of hydrocarbon molecules and their corresponding (resonantly free stabilized and aromatic) radical precursors, which are relevant to the formation and molecular growth of polycyclic aromatic hydrocarbons (PAHs). *First*, reactions are initiated in a crossed molecular beams machine under single collision conditions by crossing two supersonic reactant beams containing radicals and/or closed shell species under a well-defined collision energy and intersection angle. By recording angular-resolved time of flight (TOF) spectra, we obtain information on the reaction products, intermediates involved, branching ratios of competing reaction channels, reaction energetics, and on the underlying reaction mechanisms. *Second*, in collaboration with Dr. Musahid Ahmed (Chemical Sciences Division, Lawrence Berkeley Laboratory) and Dr. Patrick Hemberger (Paul Scherrer Institute), reactions are carried out in a chemical micro reactor at well characterized pressure and temperature distributions with reaction products interrogated isomer-selectively by tunable vacuum ultraviolet light (VUV) via photoionization (PI) coupled with a reflectron time of flight mass spectrometer (ReTOF-MS). Merged with electronic structure calculations (Prof. Alexander M. Mebel, Florida International University), these data are of fundamental importance to comprehend the underlying formation mechanisms of two key classes of molecules involved in molecular mass-growth processes leading to carbonaceous nanostructures from the bottom up: resonantly stabilized free radicals (RSFRs) and polycyclic aromatic hydrocarbons (PAHs).

## 2. Recent Progress

*First*, we unraveled fundamental molecular mass growth processes forming the following polycyclic aromatic hydrocarbons carrying up to three rings via radical–radical reactions involving the resonantly stabilized free radicals (RSFRs) propargyl ($C_3H_3$), cyclopentadienyl ($C_5H_5$), phenyl ($C_6H_5$), benzyl ($C_7H_7$), 1-indenyl ($C_9H_7$), and 9-fluorenyl ($C_{13}H_9$): naphthalene (2), indene (3), indenyl (4), anthracene (5), phenanthrene (6), and 9H-fluorene (7) (Figure 1) [**P26, P27, P30, P31**]. Here, the formation of 9H-fluorene ($C_{13}H_{10}$, (7)) is driven by an unconventional mechanism, which first produces diphenylmethane and unexpected 1-(6-methylenecyclohexa-2,4-dienyl)benzene intermediates ($C_{13}H_{12}$) accessed via addition of the phenyl radical to the *ortho* position of the benzyl radical. These findings offer convincing evidence for molecular mass growth processes defying conventional wisdom that radical–radical reactions are initiated through recombination at their radical centers [**P26**]. This unconventional mechanism of a barrierless combination of a resonantly stabilized hydrocarbon radical with an aromatic radical at the carbon atom adjacent to the traditional C1 radical center is also prevalent in the gas phase preparation of anthracene ($C_{14}H_{10}$, (5)) and phenanthrene ($C_{14}H_{10}$, (6)) via spiroaromatic intermediates [**P27**]. Further, the benzyl ($C_7H_7$)–propargyl ($C_3H_3$) system leading to naphthalene ($C_{10}H_8$, (2)) represents a prototype reaction of the novel *Propargyl Addition – BenzAnnulation (PABA)* mechanism coupled via a hydrogen atom assisted isomerization [**P30**]. *Second*, low temperature molecular mass growth processes were discovered leading to racemic [5]- and [6]helicenes ($C_{22}H_{14}$, $C_{26}H_{16}$) [**P22**] along with benzocorannulene ($C_{24}H_{12}$) – a bowl-shaped PAH carrying seven rings. *In silico* studies provided compelling evidence that the benzannulation mechanism can be expanded to pentabenzocorannulene ($C_{40}H_{20}$) followed by successive cyclodehydrogenation to the C40 nanobowl ($C_{40}H_{10}$) – a fundamental building block of buckminsterfullerene ($C_{60}$) [**P29**]. *Third*, we provided testimony on a facile formation of various resonantly stabilized free radicals of $C_4H_5$ and $C_5H_5$ accessed via the bimolecular reactions of atomic carbon with cyclopropane ($C_3H_6$) [**P20**] and the methylidyne (CH) radical with vinylacetylene ($C_4H_4$) [**P23**]; in combustion systems, these isomers can be converted to, e.g., the thermodynamically most stable cyclopentadienyl ($C_5H_5$) isomer through hydrogen assisted isomerization pathways. These

crossed molecular beam studies of elementary reactions of atomic carbon and of the methylidyne radical were expanded to document cyclization reactions leading to cyclooctatetraene ($C_8H_8$) [**P24**] and to the indenyl radical ($C_9H_7$) [**P31**]. *Finally*, we incorporated an ultracompact velocity map imaging spectrometer into our crossed molecular beams machine [**P19, P21**].

### 3. Future Plans

*First*, we are expanding our radical-radical reactions (RRR) exploiting C3-C9 radical reactants to discover new pathways leading to PAHs carrying up to six rings. *Second*, we will work toward a better understanding of reaction mechanisms leading eventually to coronene ($C_{24}H_{12}$) – a fundamental molecular building block of two-dimensional PAHs and graphene nanosheets – involving Hydrogen Abstraction – $C_2H_2$ (acetylene) Addition (HACA), Hydrogen Abstraction – Vinylacetylene Addition (HAVA), and Phenyl Addition – DehydroCyclization (PAC). *Finally*, crossed molecular beam experiments will be carried out to explore the energetics, dynamics, and potential energy surfaces (PESs) of reactions of key resonantly stabilized free radicals (RSFR) such as the phenylethynyl radical ($C_6H_5CC$) to form aromatic molecules carrying two and three rings in the gas phase under single collision conditions.

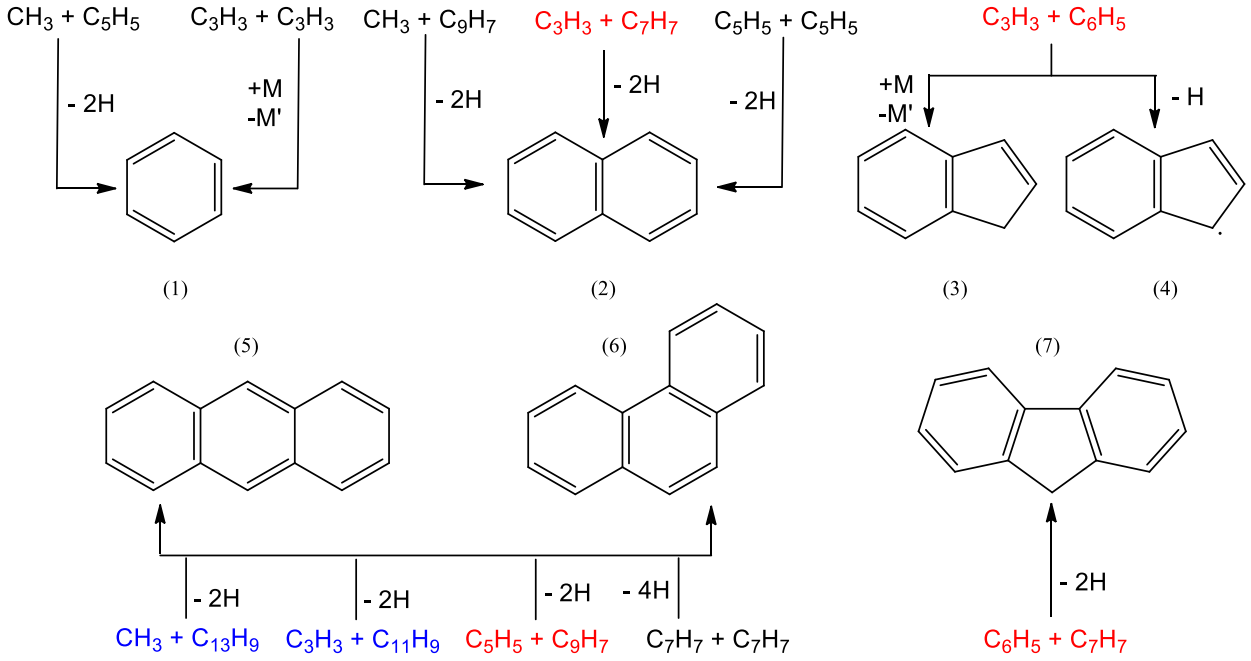


Figure 1: Elucidated pathways to aromatic hydrocarbons carrying one, two, and three rings. Reactants color coded in black, red, and blue indicate systems investigated in the previous funding periods, in the present funding period, and those currently being analyzed, respectively.

### 4. Acknowledgements

This work is supported by US Department of Energy (Basic Energy Sciences; DE-FG02-03-ER15411).

### 5. Publications Acknowledging DE-FG02-03ER15411 (2020–now)

**1** C. He, A. M. Thomas, G. R. Galimova, A. N. Morozov, A. M. Mebel, R. I. Kaiser, Gas-Phase Formation of Fulvenallene ($C_7H_6$) via the Jahn-Teller Distorted Tropyl ($C_7H_7$) Radical Intermediate under Single-Collision Conditions, J. Am. Chem. Soc. 142, 3205-3213 (2020).

**2** L. Zhao, R. I. Kaiser, B. Xu, U. Ablikim, M. Ahmed, M. M. Evseev, E. K. Bashkirov, V. N. Azyazov, A. M. Mebel, A Unified Mechanism on the Formation of Acenes, Helicenes, and Phenacenes in the Gas Phase, Angew. Chem. Int. Ed. 59, 4051-4058 (2020).

**3** C. He, L. Zhao, S. Doddipatla, A. M. Thomas, A. A. Nikolayev, G. R. Galimova, V. N. Azyazov, A. M. Mebel, R. I. Kaiser, Gas-Phase Synthesis of 3-Vinylcyclopropene via the Crossed Beam Reaction of the Methylidyne Radical (CH; $X^2\Pi$) with 1,3-Butadiene ($CH_2CHCHCH_2$; $X^1A_g$), ChemPhysChem 21, 1295-1309 (2020).
**4** L. Zhao, R. I. Kaiser, W. Lu, M. Ahmed, M. M. Evseev, E. K. Bashkirov, V. N. Azyazov, C. Tönshoff, F. Reicherter, H. F. Bettinger, A. M. Mebel, A Free Radical Prompted Barrierless Gas-Phase Synthesis of Pentacene, Angew. Chem. Int. Ed. 59, 11334-11338 (2020).
**5** L. Zhao, R. I. Kaiser, W. Lu, M. Ahmed, A. D. Oleinikov, V. N. Azyazov, A. M. Mebel, A. H. Howlader, S. F. Wnuk, Gas Phase Formation of Phenalene via 10π-Aromatic, Resonantly Stabilized Free Radical Intermediates, Phys. Chem. Chem. Phys. 22, 15381-15388 (2020).
**6** L. Zhao, R. I. Kaiser, W. Lu, O. Kostko, M. Ahmed, M. M. Evseev, E. K. Bashkirov, A. D. Oleinikov, V. N. Azyazov, A. M. Mebel, A. H. Howlader, S. F. Wnuk, Gas Phase Formation of Cyclopentanaphthalene (Benzindene) Isomers via Reactions of 5- and 6-Indenyl Radicals with Vinylacetylene, Phys. Chem. Chem. Phys. 22, 22493-22500 (2020).
**7** A. H. Howlader, K. Diaz, A. M. Mebel, R. I. Kaiser, S. F. Wnuk, Iodoindenes: Synthesis and Application to Cross-Coupling, Tetrahedron Lett., 61, 152427 (2020).
**8** C. He, G. R. Galimova, Y. Luo, L. Zhao, A. K. Eckhardt, R. Sun, A. M. Mebel, R. I. Kaiser, A Chemical Dynamics Study on the Gas-Phase Formation of Triplet and Singlet $C_5H_2$ Carbenes, Proc. Natl. Acad. Sci. U.S.A. 117, 30142-30150 (2020).
**9** S. Doddipatla, G. R. Galimova, H. Wei, A. M. Thomas, C. He, Z. Yang, A. N. Morozov, C. N. Shingledecker, A. M. Mebel, R. I. Kaiser, Low-Temperature Gas-Phase Formation of Indene in the Interstellar Medium, Sci. Adv. 7, eabd4044 (2021).
**10** C. He, A. A. Nikolayev, L. Zhao, A. M. Thomas, S. Doddipatla, G. R. Galimova, V. N. Azyazov, A. M. Mebel, R. I. Kaiser, Gas-Phase Formation of $C_5H_6$ Isomers via the Crossed Molecular Beam Reaction of the Methylidyne Radical (CH; $X^2\Pi$) with 1,2-Butadiene ($CH_3CHCCH_2$; $X^1A'$), J. Phys. Chem. A 125, 126-138 (2021).
**11** L. Zhao, S. Doddipatla, R. I. Kaiser, W. Lu, O. Kostko, M. Ahmed, L. B. Tuli, A. N. Morozov, A. H. Howlader, S. F. Wnuk, A. M. Mebel, V. N. Azyazov, R. K. Mohamed, F. R. Fischer, Gas-Phase Synthesis of Corannulene - A Molecular Building Block of Fullerenes, Phys. Chem. Chem. Phys. 23, 5740-5749 (2021).
**12** L. Zhao, W. Lu, M. Ahmed, M. V. Zagidullin, V. N. Azyazov, A. N. Morozov, A. M. Mebel, R. I. Kaiser, Gas-Phase Synthesis of Benzene via the Propargyl Radical Self-Reaction, Sci. Adv. 7, eabf0360 (2021).
**13** L. Zhao, M. Prendergast, R. I. Kaiser, B. Xu, W. Lu, M. Ahmed, A. H. Howlader, S. F. Wnuk, A. S. Korotchenko, M. M. Evseev, E. K. Bashkirov, V. N. Azyazov, A. M. Mebel, A Molecular Beam and Computational Study on the Barrierless Gas Phase Formation of (Iso)quinoline in Low Temperature Extraterrestrial Environments, Phys. Chem. Chem. Phys. 23, 18495-18505 (2021).
**14** A. A. Nikolayev, V. N. Azyazov, R. I. Kaiser, A. M. Mebel, Theoretical Study of the Reaction of the Methylidyne Radical (CH; $X^2\Pi$) with 1-Butyne ($CH_3CH_2CCH$; $X^1A'$), J. Phys. Chem. A 125, 9536-9547 (2021).
**15** C. He, K. Fujioka, A. A. Nikolayev, L. Zhao, S. Doddipatla, V. N. Azyazov, A. M. Mebel, R. Sun, R. I. Kaiser, A Chemical Dynamics Study of the Reaction of the Methylidyne Radicals (CH, $X^2\Pi$) with Dimethylacetylene ($CH_3CCCH_3$, $X^1A_{1g}$), Phys. Chem. Chem. Phys. 24, 578-593 (2022).
**16** R. I. Kaiser, L. Zhao, W. Lu, M. Ahmed, M. V. Zagidullin, V. N. Azyazov, A. M. Mebel, Formation of Benzene and Naphthalene through Cyclopentadienyl-Mediated Radical−Radical Reactions, J. Phys. Chem. Lett. 13, 208–213 (2022).
**17** R. I. Kaiser, L. Zhao, W. Lu, M. Ahmed, V. S. Krasnoukhov, V. N. Azyazov, A. M. Mebel, Unconventional Excited-State Dynamics in the Concerted Benzyl ($C_7H_7$) Radical Self-Reaction to Anthracene ($C_{14}H_{10}$), Nat. Commun. 13, 786 (2022).

**18** S. J. Goettl, C. He, D. Paul, A. A. Nikolavev, V. N. Azyazov, A. M. Mebel, R. I. Kaiser, Gas-Phase Study of the Elementary Reaction of the D1-Ethynyl Radical ($C_2D$; $X^2\Sigma^+$) with Propylene ($C_3H_6$; $X^1A'$) Under Single-Collision Conditions, J. Phys. Chem. A 126, 1889–1898 (2022).
**19** D. Paul, Z. Yang, S. J. Goettl, A. M. Thomas, C. He, A. G. Suits, D. H. Parker, R. I. Kaiser, Photodissociation Dynamics of Astrophysically Relevant Propyl Derivatives ($C_3H_7X$; X = CN, OH, HCO) at 157 nm Exploiting an Ultracompact Velocity Map Imaging Spectrometer: The (Iso)Propyl Channel, J. Phys. Chem. A 126, 5768-5775 (2022).
**20** G. R. Galimova, A. M. Mebel, S. J. Goettl, Z. Yang, R. I. Kaiser, A Crossed Molecular Beams and Computational Study on the Unusual Reactivity of Banana Bonds of Cyclopropane (c-$C_3H_6$; $X^1A_1'$) through Insertion by Ground State Carbon Atoms ($C(^3P_j)$), Phys. Chem. Chem. Phys. 24, 22453-22463 (2022).
**21** D. Paul, Z. Yang, R. I. Kaiser, Photodissociation Dynamics of Xylene Isomers $C_6H_4(CH_3)_2$ at 157 nm using an Ultracompact Velocity Map Imaging Spectrometer – The $C_7H_7$ Channel, Chem. Phys. Lett. 807, 140064 (2022).
**22** R. I. Kaiser, L. Zhao, W. Lu, M. Ahmed, M. M. Evseev, V. N. Azyazov, A. M. Mebel, R. K. Mohamed, F. R. Fischer, X. Li, Gas-Phase Synthesis of Racemic Helicenes and their Potential Role in the Enantiomeric Enrichment of Sugars and Amino Acids in Meteorites, Phys. Chem. Chem. Phys. 24, 25077-25087 (2022).
**23** C. He, Z. Yang, S. Doddipatla, A. M. Thomas, R. I. Kaiser, G. R. Galimova, A. M. Mebel, K. Fujioka, R. Sun, Directed Gas Phase Preparation of Ethynylallene ($H_2CCCHCCH$; $X_1A'$) via the crossed molecular beam reaction of the methylidyne radical (CH; $X^2\Pi$) with vinylacetylene ($H_2CCHCCH$; $X^1A'$), Phys. Chem. Chem. Phys. 24, 26499-26510 (2022).
**24** Z. Yang, G. R. Galimova, C. He, S. Doddipatla, A. M. Mebel, R. I. Kaiser, Gas Phase Formation of 1,3,5,7-Cyclooctatetraene ($C_8H_8$) through Ring Expansion via the Aromatic 1,3,5-Cyclooctatrien-7-yl Radical ($C_8H_9^{\bullet}$) Transient, J. Am. Chem. Soc. 144, 22470-22478 (2022).
**25** W. Li, L. Zhao, R. I. Kaiser, A Unified Reaction Network on the Formation of Five-Membered Ringed Polycyclic Aromatic Hydrocarbons (PAHs) and their Role in Ring Expansion Processes through Radical–Radical Reactions, Phys. Chem. Chem. Phys. **25**, 4141-4150 (2023).
**26** C. He, R. I. Kaiser, W. Lu, M. Ahmed, P. S. Pivovarov, O. V. Kuznetsov, M. V. Zagidullin, A. M. Mebel, Unconventional Pathway in the Gas-Phase Synthesis of 9H-Fluorene ($C_{13}H_{10}$) via the Radical–Radical Reaction of Benzyl ($C_7H_7$) with Phenyl ($C_6H_5$), Angew. Chem. Int. Ed. 62, e202216972 (2023).
**27** C. He, R. I. Kaiser, W. Lu, M. Ahmed, Y. Reyes, S. F. Wnuk, A. M. Mebel, Exotic Reaction Dynamics in the Gas-Phase Preparation of Anthracene ($C_{14}H_{10}$) via Spiroaromatic Radical Transients in the Indenyl–Cyclopentadienyl Radical–Radical Reaction, J. Am. Chem. Soc. 145, 3084-3091 (2023).
**28** A. M. Mebel, M. Agúndez, J. Cernicharo, R. I. Kaiser, Elucidating the Formation of Ethynylbutatrienylidene (HCCCHCCC; $X^1A'$) in the Taurus Molecular Cloud (TMC-1) via the Gas Phase Reaction of Tricarbon ($C_3$) with the Propargyl Radical ($C_3H_3$). Astrophys. J. Lett. (in press).
**29** L. B. Tuli, S. J. Goettl, A. M. Turner, A. H. Howlader, P. Hemberger, S. F. Wnuk, T. Guo, A. M. Mebel, R. I. Kaiser, Gas Phase Synthesis of the C40 Nano Bowl $C_{40}H_{10}$. Nat. Commun. (in press).
**30** C. He, R. I. Kaiser, W. Lu, M. Ahmed, V. S. Krasnoukhov, P. Pivovarov, V. N. Azyazov, A. N. Morozov, A. M. Mebel, Unconventional Gas Phase Preparation of the Prototype Polycyclic Aromatic Hydrocarbon Naphthalene ($C_{10}H_8$) via the Reaction of Benzyl ($C_7H_7$) and Propargyl ($C_3H_3$) Radicals Coupled with Hydrogen-Atom Assisted Isomerization. (submitted).
**31** Z. Yang, G. R. Galimova, C. He, S. J. Goettl, D. Paul, W. Lu, M. Ahmed, A. M. Mebel, X. Li, R. I. Kaiser, Gas-Phase Formation of the Resonantly Stabilized 1-Indenyl ($C_9H_7$) Radical in the Interstellar Medium. (submitted).
**32** Z. Yang, C. He, S. J. Goettl, R.I. Kaiser, A.M.M. Mebel, B.R.L. Galvão, Low-Temperature Gas-Phase Synthesis of Methylene Amidogen ($H_2CN$) and Cyanomethyl ($H_2CCN$) Radicals and their Role in the Formation of Pyridine and (Iso)quinoline in Hydrocarbon-Rich Atmospheres of Planets and their Moons. (submitted).

# MECHANISTIC INVESTIGATIONS OF GAS-PHASE AND SURFACE-MEDIATED OXIDATIVE COUPLING REACTIONS

Coleman Kronawitter and Ambarish Kulkarni

*Department of Chemical Engineering, University of California, Davis*

*One Shields Ave, Davis, CA 95616*

ckrona@ucdavis.edu, arkulkarni@ucdavis.edu

## PROGRAM SCOPE

In heterogeneous catalytic systems for chemical synthesis and energy conversion, the solid surface plays an essential role in controlling reaction kinetics. As a result, the vast majority of mechanistic investigation in this field is dedicated to the characterization of surfaces and adsorbates. However, it is known that for many reactions, gas phase events critically influence reaction outcomes, as well as dictate the nature of events occurring on surfaces through gas-surface species exchange. Near-surface gas phase composition can additionally serve as a reporter of reactions that solely occur on surfaces.

A core objective of this project is to develop and implement an integrated experiment-theory approach to provide new insights into the interconnected roles of the surface and the near-surface gas phase in heterogeneous catalytic oxidation reactions. This work is enabled by use of (1) new research technologies, originally developed for the field of combustion science, which through recent adaptation now facilitate interrogation of the local, near-surface gas phase above catalyst surfaces in *operando* conditions; (2) site-isolated supported metal catalysts (often atomically dispersed), comprehensively characterized to define active sites and minimize site heterogeneity over length scales of experimental interrogation; (3) density functional theory models to understand the catalysts of (2) and microkinetic models to interpret reaction results from (1) and (2), deriving relationships between specific active site structures and local reaction outcomes. Efforts focus on oxidative conversions of alkanes and alcohols, both of which are critical for production of valuable commodity chemicals. This project strives to bring clarity to the relationship between active site structures on surfaces and the composition of species in the near-surface gas phase during these reactions.

## RECENT PROGRESS

### Surface and near-surface characterization of heterogeneous catalytic systems

We collaborate with Sandia National Laboratories' Combustion Research Facility (SNL-CRF), which involves UC Davis PhD students working alongside Sandia scientific staff. Our project utilizes tools to investigate properties of the near-surface gas phase. This includes near-surface time-of-flight molecular beam mass spectrometry (ns-MBMS) as a primary tool for interrogation of gas phase composition.

*Constraining reaction pathways for methanol oxidation through operando interrogation of both the surface and the near-surface gas phase*

The primary products of heterogeneous reactions – those species that desorb from catalyst surfaces and do not undergo any subsequent chemical transformation on catalyst or reactor wall surfaces – often are not reflected in reactor effluent analyses, even when care is taken to operate in regimes of differential conversion where secondary reactions are minimized. For some reactions, primary products are too reactive or unstable to be detected by conventional analysis tools. In many cases, investigators will be unaware of the presence of reactive or unstable primary products in the gas-phase unless an interrogation tool with the required detection selectivity is applied. We have analyzed both the surface and near-surface gas phase during oxidative conversion of methanol with MgO-supported Pd. Near-surface molecular beam mass spectrometry is used as a universal detector of species at a position 500 μm above the surface of the packed catalyst powder, and diffuse reflectance infrared Fourier transform spectroscopy (DRIFTS) is used to track the vibrational signatures of adsorbates. We show that when the species compositions of the two phases

are correlated, the mechanisms derived from these correlations are uniquely constrained by capture of elusive intermediates in the gas phase.

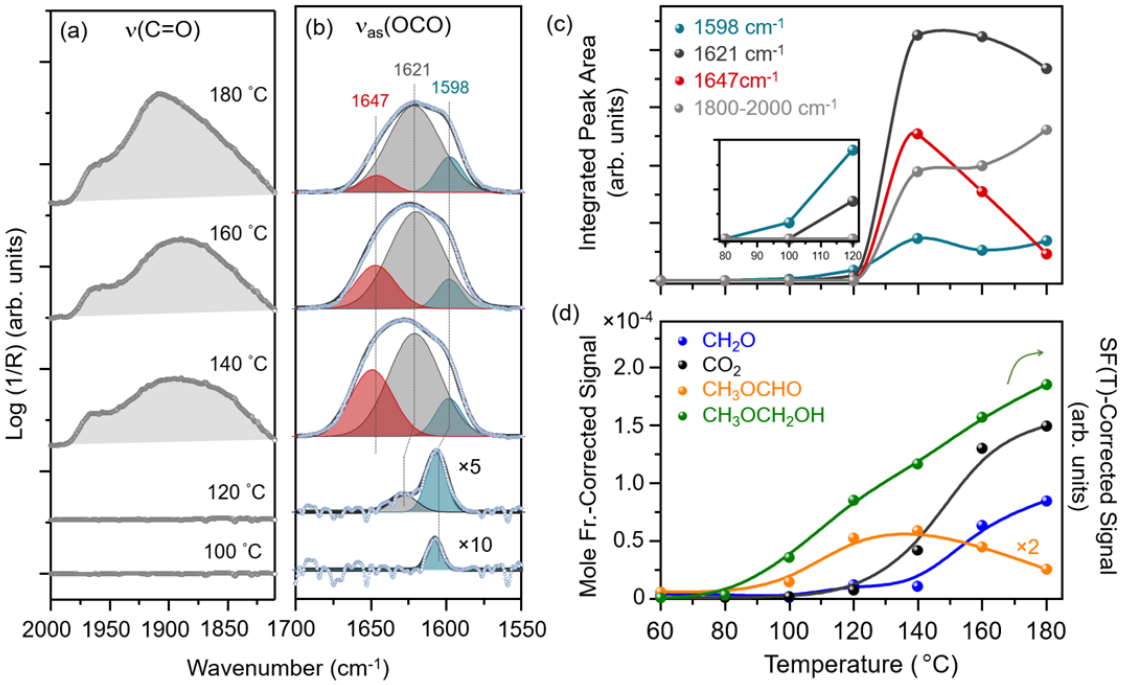


**Figure 1.** Analysis of temperature-dependent surface (DRIFTS) and near-surface (ns-MBMS) data for methanol oxidation catalysis with PdO/MgO; $CH_3OH/O_2$ = 1.5. (a) Magnification of ν(C=O) absorption region. (b) Magnification of $\nu_{as}$(OCO) absorption region with peak deconvolution shown. (c) Integrated intensities of absorption features from (a) and (b) plotted with respect to temperature. (d) ns-MBMS results (500 μm above surface) for products. In (c) and (d) lines are added to guide the eyes.

Figure 1 shows representative results correlating the composition of surface-bound species with that of the near-surface gas phase. Figure 1a,b provides magnifications of the ν(C=O) and $\nu_{as}$(OCO) absorption regions which show features that correspond to surface-bound carbon monoxide and formates (in three different bonding configurations, identifiable by the deconvolution of the $\nu_{as}$(OCO) features). Figure 1c shows the integrated areas of these peaks as a function of temperature and Figure 1d shows the integrated intensities of ns-MBMS signals associated with the indicated near-surface gas phase species (with stable species corrected to quantify mole fraction ratios). In short, analyses of this and other data in this study enabled a comprehensive assessment of the methanol oxidation reaction network with MgO-supported $PdO_x$ catalysts (Figure 2).

The O–$CH_2$–O group within the detected reactive intermediate methoxymethanol supports the assignment of a surface formate in a specific binding configuration as having resulted from spillover of formaldehyde formed at Pd-containing sites. In this way, the interpretation of adsorbate FTIR signatures has been constrained by information that can be uniquely obtained by interrogation of the near-surface gas phase (since methoxymethanol is too reactive to be detected with conventional tools). These results show that further integration of novel near-surface gas-phase interrogation tools, chosen based on their abilities to detect or characterize unstable or reactive intermediates, will yield new essential contributions toward discovering reaction mechanisms of surface-catalyzed reactions as well as transport and chemical events in the gas-phase.

In additional efforts, we have studied the use of $CO_2$ and $N_2O$ as soft oxidants for methane coupling to produce ethylene [*Phys. Chem. Chem. Phys*., **2023**, 25, 9859-9867]. Our ongoing work in this area involves use of ns-MBMS to characterize the reaction network of this catalytic system.

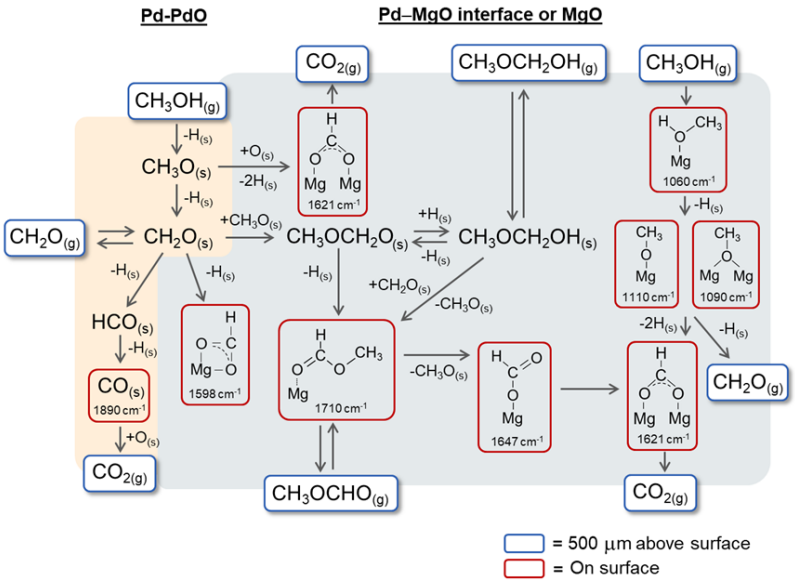


**Figure 2.** Methanol oxidation reaction network implied by DRIFTS and ns-MBMS measurements, derived primarily from observations with PdO/MgO in the context of analysis of the prior literature. The average wavenumbers for observed surface species are noted for reference.

*Near-surface molecular beam photoionization mass spectrometry*

Last year we discovered, through our unique ability to interrogate the near-surface gas phase during catalytic reactions, that methoxymethanol is an intermediate during methanol oxidation with Pd-based catalysts, and investigated its role in the reaction network [*J. Phys. Chem. Lett.,* **2021**, 12, 11252–11258]. Our analysis of that system revealed a notable absence in the literature – neither the experimental ionization energy or photoionization spectrum of methoxymethanol has never been reported. This year, we performed experiments at the Advanced Light Source to record the first photoionization spectrum of this reactive molecule, and performed computational work to interpret the results. In these experiments, heterogeneous catalytic methanol oxidation was used as a tool to generate a steady concentration of gas-phase methoxymethanol.

Figure 3 provides an overview of results from these efforts. It was experimentally determined that the parent cation of methoxymethanol ($C_2H_6O_2^+$, nominal m/z 62) is not detected through photoionization (and electron-impact ionization) molecular beam mass spectrometry. Instead, the ionization is detectable through nominal m/z 61, which corresponds to the composition $C_2H_5O_2^+$, a fragment ion resulting from dissociative ionization of methoxymethanol. Our experimental ionization energy is ca. 10.2 eV, which is consistent with prior computational results in the literature. We used the Gaussian 16 Quantum Chemistry Package to obtain geometries and energetics at the CBS-QB3 level of theory to investigate the energetics of the ionization process and explore the possibility of dissociative ionization. The transition state structure was optimized using the improved Berny algorithm within Gaussian 16. Frequency analysis was used to confirm stationary state structures. An intrinsic rate coordinate (IRC) calculation confirmed the transition state connected to the proposed reactant and product wells. Gibbs free energy, equilibrium constants, and rate constants were calculated under the ideal gas approximation and within transition state theory.

The outcome of this work provided an explanation of experimental observations. Briefly: after ionization, the methoxymethanol cation could dehydrogenate to generate a daughter ion at m/z 61 in a singlet or triplet state. An exploration of the C-H bond strengths for the low-energy methoxymethanol cation conformer reveals that it possesses a weak C-H bond for the carbon bound between both oxygen atoms ($CH_3O\mathbf{CH_2}OH$). Removal of a hydrogen from this carbon atom results in a daughter ion at m/z 61 with a singlet spin state. The transition state for this reaction was determined and confirmed with IRC calculation. The Gibbs free energy under the ideal gas approximation for this reaction is shown in Figure 3. With the presence of a relatively small barrier, 0.36 eV, this reaction occurs rapidly, at ca. 20.5 ns compared to the ca. 13,000 ns time-of-flight of the ionized species within the experimental setup. These calculations

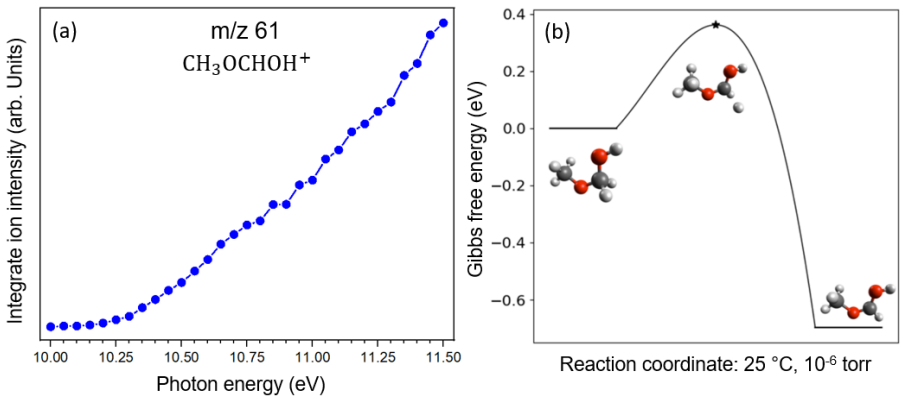


$$CH_3OCH_2OH^{\bullet+} \rightleftharpoons [CH_3OCHOH \cdots H]^+ \rightarrow CH_3OCHOH^+ + H^{\bullet}$$

**Figure 3.** (a) Experimental photoionization spectrum associated with methoxymethanol (represented by the spectrum of fragment ion at m/z 61). (b) Computational determination of Gibbs free energy for removal of a hydrogen from the methoxymethanol parent cation, resulting in a daughter ion at m/z 61 with a singlet spin state. The transition state for this reaction was determined and confirmed with IRC calculation.

demonstrate that the ionization spectrum would be dominated by the daughter ion at m/z 61 due to dissociative ionization of the parent molecule. We are in the process of completing a manuscript for publication of these results.

At the Advanced Light Source, we also detected methyl radicals during oxidative coupling of methane. This was confirmed with measurement of an accurate photoionization spectrum. This measurement is an important milestone for our work with Sandia, since it establishes our ability to track radicals using Sandia's MBMS system.

**Atomically dispersed platinum in sub-surface sites on MgO for catalytic ethylene hydrogenation**

To develop new structure-function relationships for reactions that directly connect the near-surface gas phase composition to specific reaction centers, we aim to use oxide-supported transition metal (TM) catalysts with well-defined active sites. Our prior work established a systematic, theory-led workflow for characterization of atomically dispersed catalysts (QuantEXAFS) [see *J. Am. Chem. Soc.*, **2021**, 143, 20144–20156 and *J. Phys. Chem. Lett.*, **2022**, 13, 3896–3903]. These studies combine, e.g., advanced transmission electron microscopy and synchrotron X-ray absorption spectroscopy with large-scale DFT calculations and automated analyses. The work is in collaboration with Bruce Gates (UC Davis) and Simon Bare (SLAC National Accelerator Lab) and their DOE-funded research efforts. Last year we focused on atomically dispersed Pt cations supported by MgO. To the best of our knowledge, those studies represent the first examples of a well-characterized sub-surface platinum cation stabilized within an MgO lattice.

This year we expanded that work by subjecting the $Pt/MgO_{700}$ sample (700 °C calcination temperature) to a reductive hydrogen treatment at 170°C ($Pt/MgO_{700}$-R). The $Pt/MgO_{700}$-R sample displays increased activity towards ethylene hydrogenation compared to directly reduced catalysts. Extensive experimental characterization of the $Pt/MgO_{700}$-R confirms the structure remains atomically dispersed, but XAS data shows a reduction in the oxidation state of Pt (using XANES) and a decrease in the Pt-O and Pt-Mg coordination number (using EXAFS). Data suggest that Pt remains subsurface and indicates that the reductive treatment may result in additional defect sites. We conducted a large-scale DFT-based combinatorial study of all possible subsurface Pt structures with any combination of 1-4 vacancies in the first coordination shell of Pt (considered both Mg and O vacancies). We used QuantEXAFS to fit each structure to the $Pt/MgO_{700}$-R EXAFS data. This study demonstrated that many classes of defect structures fit the EXAFS data. A primary outcome of this study is that the hydrogen reduction of the $Pt/MgO_{700}$ catalyst introduces additional defects which show favorable activity towards hydrogen dissociation and ethylene hydrogenation. We are in the process of completing a manuscript for publication of these results.

**Reaction screening of atomically dispersed transitions metals in sub-surface sites on MgO**

This year we have expanded the study of transition metals dispersed on MgO supports. Our previous findings established the experimental accessibility of the unique $Pt/MgO_{700}$ site, where Pt resides in the subsurface adjacent to a Mg vacancy. This site has been used in reaction screening to probe the catalytic activity for a family of $TM/MgO_{700}$ (TM includes 3-d 4-d and 5-d series TMs). The reaction screening leverages catalytic activity descriptors that have been determined in the literature for methane activation and ethylene epoxidation. This work is ongoing, and we expect that this study will provide insight into promising reactions to consider for our synthesized catalysts and which new transition metals should be considered in the synthesis of new TM/MgO atomically dispersed catalysts.

**Overcoming barriers in modeling surface-catalyzed reactions**

Computational studies of reactive events on surfaces typically have not reflected experimental observations and trends, and often rely on descriptor-based methods to estimate energetics. We aim to correct this shortcoming by developing a workflow to study surface kinetics at DFT-level accuracy in tandem with microkinetic modeling (MKM). The computational cost for studying a complex reaction network at DFT level is prohibitively expensive, hence our workflow uses active learning-based machine learning (ML)-based potentials to effectively sample reaction coordinates. We have studied methanol partial oxidation on Ag and will next extend this to Pd. Specifically we have built a ML model to study surface diffusion on the (111) facet of Ag and are currently working on calculating adsorbate diffusion barriers through molecular dynamics simulations (at DFT-level accuracy). We are also in parallel building another ML model to compute reaction barriers on Ag that can be tied together with MKM.

Another challenge with the generation of microkinetic models is the tedious and error-prone nature of calculations required to model a reaction network: each elementary step requires exploration of adsorbate configurations and transition states that connect the appropriate reactant and product wells. Automated frameworks are needed to address these challenges and aid in the generation of ML-accelerated MKMs. Based on this challenge, and building off the work of this grant, a graduate student proposal for the (DOE) Office of Science Graduate Student Research (SCGSR) was awarded (Figure 4). This future work will involve using the automated workflow code Pynta and the automated Reaction Mechanism Generator (RMG) to enable the generation of comprehensive MKM of methanol oxidation over a Ag (111) catalyst. This automated toolkit will enable further interrogation of previously observed $C_2$ in the near-surface gas-phase using MBMS. The ML-Pynta-RMG framework for building a comprehensive MKM will be simulated with a stagnation flow model within Cantera to generate a consistent MKM. This model enables direct comparison with stagnation flow experiments conducted at Sandia. This MKM can suggest experimental conditions to maximize specific intermediates for further mechanistic investigation, and those results can be used to test and update the MKM. This powerful feedback loop advances the DOE-funded NSGP project goals of drawing new mechanistic insights into the interconnected roles of the surface and NSGP. This award also deepens and reinforces the value of our collaboration with Sandia-CRF.

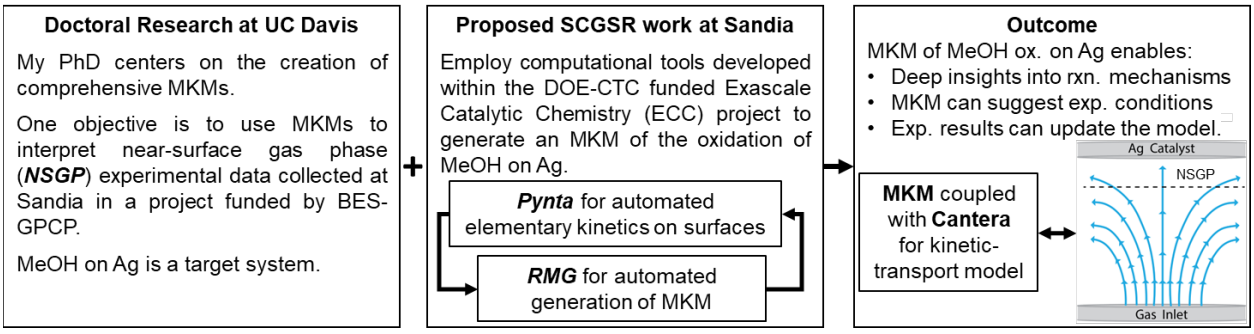


**Figure 4.** Outline of research proposed for SCGSR award for the Ph.D. student supported by our project.

## FUTURE WORK

### Combine all aspects of project to create cohesive, novel workflow for catalysis research

We will apply our integrated experiment-theory approach for studying oxidation reactions with gas- and surface-mediated steps with the use of highly characterized catalysts with well-defined active sites. That is, we seek to correlate catalytic activity for oxidative methanol and methane conversion with the speciation of intermediates in the gas phase and with the atomic-scale structure of supported transition metal active sites. The goal of this work is to derive relationships between local composition/structure of (uniform) active sites and the local gas-phase universal speciation during reaction.

Specially, our current efforts emphasize the evolution of supported Pt catalysts for methane oxidation reactions. We find that we are able stabilize both nanoparticulate and atomically dispersed cationic Pt during reaction, which facilitates study of the structure- and Pt speciation-dependent activity of these systems. This accomplishment was essential because our computational and often experimental XAS (which for low-metal-loading samples often require long spectra acquisition times) analyses assume a well-defined catalyst state. By studying methane (and other alkane) oxidations, we are able to interpret our experimental results in the context of C-H activation results from computational studies.

We also continue to work with SNL-CRF on optimization of experiments to enable study of alkane and alcohol conversions. We synthesize and characterize catalysts and study their activities in reactor studies. Our near-term experimental goals involve optimization of the conditions to track radicals using electron-impact ionization at Sandia. To accomplish this, UC Davis PhD students work alongside Sandia scientists.

### Publications from September 2019 - Present


1. **Supported Metal Pair-Site Catalysts**
   E. Guan, J. Ciston, S.R. Bare, R.C. Runnebaum, A. Katz, A.R. Kulkarni, C.X. Kronawitter, B.C. Gates. *ACS Catalysis*, **2020**, 10, 9065–9085.
2. **Near-Surface Imaging of the Multi-Component Gas Phase above a Silver Catalyst During Partial Oxidation of Methanol**
   B. Zhou, E. Huang, R. Almeida, S. Gurses, A. Ungar, J. Zetterberg, A.R. Kulkarni, C.X. Kronawitter, D.L. Osborn, N. Hansen, J. Frank. *ACS Catalysis*, **2021**, 11, 155−168.
3. **A Theory-Guided X-Ray Absorption Spectroscopy Approach for Identifying Active Sites in Atomically Dispersed Transition Metal Catalysts**
   Y. Chen, R. Rana, T. Sours, F.D. Vila, S. Cao, T. Blum, A.S. Hoffman, C.-Y. Fang, Z. Huang, C. Shang, C. Wang, J. Zeng, M. Chi, C.X. Kronawitter, S.R. Bare, B.C. Gates, A.R. Kulkarni. *J. Am. Chem. Soc.*, **2021**, 143, 20144–20156.
4. **Near-Surface Gas-Phase Methoxymethanol Is Generated by Methanol Oxidation over Pd-Based Catalysts**
   S.M. Gurses, T. Price, A. Zhang, J.H. Frank, N. Hansen, D.L. Osborn, A.R. Kulkarni, C.X. Kronawitter. *J. Phys. Chem. Lett.,* **2021**, 12, 11252–11258.
5. **Atomically Dispersed Platinum in Surface and Subsurface Sites on MgO Have Contrasting Catalytic Properties for CO Oxidation**
   Y. Chen, R. Rana, Z. Huang, F.D. Vila, T. Sours, J.E. Perez-Aguilar, X. Zhao, J. Hong, A.S. Hoffman, X. Li, C. Shang, T. Blum, J. Zeng, M. Chi, M. Salmeron, C.X. Kronawitter, S.R. Bare, A.R. Kulkarni, B.C. Gates. *J. Phys. Chem. Lett*., **2022**, 13, 3896–3903.
6. **Surface basicity controls C–C coupling rates during carbon dioxide-assisted methane coupling over bifunctional Ca/ZnO catalysts**
   L.R. Filardi, F. Yang, J.-H. Guo, C.X. Kronawitter, R.C. Runnebaum. *Phys. Chem. Chem. Phys*., **2023**, 25, 9859-9867.
7. **Constraining Reaction Pathways for Methanol Oxidation with Supported Pd Catalysts through Operando Interrogation of Both the Surface and the Near-Surface Gas Phase**
   S.M. Gursesa, N. Felvey, L.R. Filardi, A.J. Zhang, J. Wood, K. van Benthem, J.H. Frank, D.L. Osborn, N. Hansen, C.X. Kronawitter*, Submitted,* May **2023**.

# Novel Micro-Reactor Development for Fundamental Gas Phase Chemical Kinetics Applications

Nicole J. Labbe,[1] G. Barney Ellison,[2] John W. Daily[1]
[1]Department of Mechanical Engineering
[2]Department of Chemistry
University of Colorado Boulder
UCB 427, 1111 Engineering Drive, Boulder, CO 80301-0427
Nicole.Labbe@colorado.edu, John.Daily@colorado.edu, Barney@jila.colorado.edu

## Program Scope

The Labbe Lab at the University of Colorado Boulder has recently made significant advances in the manufacturing of high aspect ratio, silicon carbide (SiC) reactors for gas phase chemical physics applications. Leveraging these recent advances, this project seeks to reinvent the Chen Nozzle, [1,2] a radical generating micro-reactor, for modern gas phase chemical physics fundamental experiments. In this work, we seek to answer questions regarding the Chen Nozzle (tube reactor), and use that information to create a new suite of reactors for our community's use. In particular, questions we seek to answer are:

- How do reactor material properties such as surface finish, compaction, and thermal conductivity affect the performance of the reactor?
- By adding a nozzle constriction in the reactor, are we able to control pressure within the reactor main body as predicted, and can we leverage that for fall-off regime kinetics studies?
- Can new materials or surface finishes be leveraged to change the reactivity of the reactor itself for oxidation studies or to reduce potential kinetic wall interactions?

Ultimately, the goal of this research project is to understand the influence of materials on reactor design for these small, short-residence time radical sources, and identify how to manipulate materials for targeted kinetics work.

## Recent Progress

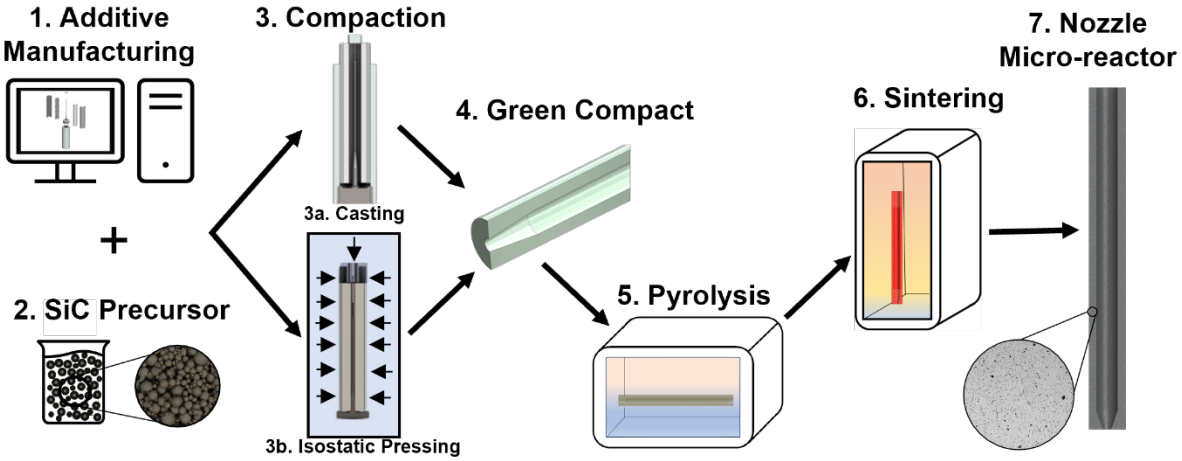


*Figure 1: Process sequence for the digital manufacturing of high aspect ratio SiC components.*

Finalized manufacturing method: A novel, high-throughput, iterative processing route for producing small, high aspect ratio SiC geometries at a low cost was developed through our work. The fabrication sequence integrates a hybrid manufacturing technique that harnesses the rapid

iterability of additive manufacturing, combining it with the existing knowledge base for conventional ceramic processing. The manufacturing sequence for creating high aspect ratio SiC geometries with intricate internal features using digitally manufactured tooling is shown in **Figure 1**. The process involves seven steps. (1.) The process begins with creating a digital design tailored to be manufactured using both polymer and metal additive manufacturing. (2.) A specially formulated SiC precursor is injected into the tooling. (3.) Compaction is achieved either through casting (3a.) or isostatic pressing (3b.) based on the geometric features of the final component and the precursor composition. (5.) The product extracted from the compaction tooling is defined as in the 'green state.' (6.) Post compaction, the component is pyrolyzed at 650°C to enable safe handling. (7.) Final component densification is completed by sintering at 2150°C. (g.) The fully densified component is then post-processed to meet application requirements.

Final reactor material characterization: In order to gage the quality of the material produced with our manufacturing process, a wide range of material characterization studies were conducted. A comparison of the flexural strength and fatigue life was carried out through the Modulus of Rupture (MOR) characterization of samples per ASTM C1161 [3]. A comparison of the MOR results from these tests on eight SiC material systems is presented in **Figure 2**. The results indicate a higher MOR value for the Calix High Strength 2 (HS2) (the material system used in this work) than the Hexoloy material [4] used to fabricate tube reactors in previous works. The superior performance of the Calix HS2 material is linked to the smaller grain size of the α-SiC used in the precursor material and the choice of sintering aids. A higher modulus of rupture translates to better resistive heating characteristics combined with a longer experimental life cycle due to reduced material fatigue. The density of finished components produced using this process and the material system has been measured at 3.18 g/cm$^3$ (almost 98% of the theoretical density limit [5])—the high component density results in finished parts with fewer pores reducing the chance of failure during operation and questions of reactant trapping along the wall lengths. The higher component density achieved using this composition and compaction process is expected to double the usable life cycle in the case of nozzle micro-reactors.

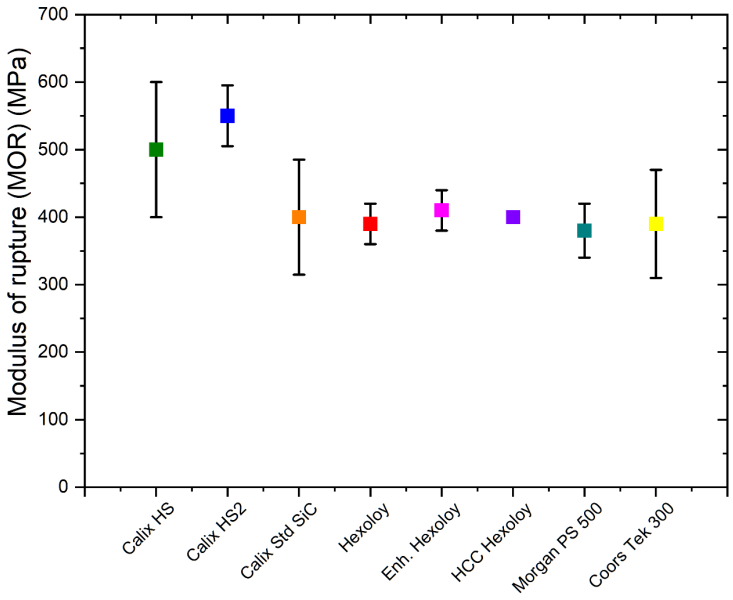


*Figure 2: Modulus of rupture tests on cast rod samples of different SiC grades. The material used in this process is Calix High Strength 2, and the material used in the tube reactor is Hexoloy.*

Initial reactor performance studies: The presence of a nozzle, based on CFD simulations [6] should result in a region of stabilized, elevated pressure and residence time affecting the chemical behavior of the fluid inside the device. Cyclohexene was the molecule chosen for this comparison. The spectra enabled direct observation of molecular signal changes due to the variation in the relative signal of the decomposition of cyclohexene. The thermal decomposition of cyclohexene through a retro Diels-Alder reaction to form 1,3-butadiene and ethylene has been

identified as the primary decomposition reaction [7], [8]. At the higher stabilized pressures of the nozzle reactor (simulated to be 10.2 kPa at 1600 K compared to the estimated unstable pressure profile in a straight tube which reduces from 5.2 kPa to 0.039 kPa at 1600 K), we expect to see higher percentage conversion of cyclohexene to products 1,3-butadiene and ethylene. It is also shown that the increased pressure within the reactor will result in the decomposition reaction beginning at a lower temperature in the nozzle reactor.

Results from the two experimental runs are presented in **Figure 3**. The X-axis represents micro-reactor surface temperature change in increments of 100 K starting at room temperature up to 1800 K. The Y-axis represents the ratio of the normalized signal height of 1,3-butadiene compared to cyclohexene's signal height for a nozzle with an exit diameter of 0.400 mm. The shift in temperature for the onset of decomposition observed can be attributed to the presence of a constriction in the case of the nozzle reactor. This reduction in exit diameter results in a modification in the fluid flow behavior throughout the reactor, resulting in a change in the residence time and pressure of the fluid within the reactor. These alterations make for a more reproducible, consistent flow field, which in turn, makes numerical modeling these reactors more facile, highlighting the value of incorporating this nozzle using this manufacturing method. Prior to the application of this method, such an intricate design change lay outside the fabrication envelope for this material type, both from a cost and time perspective.

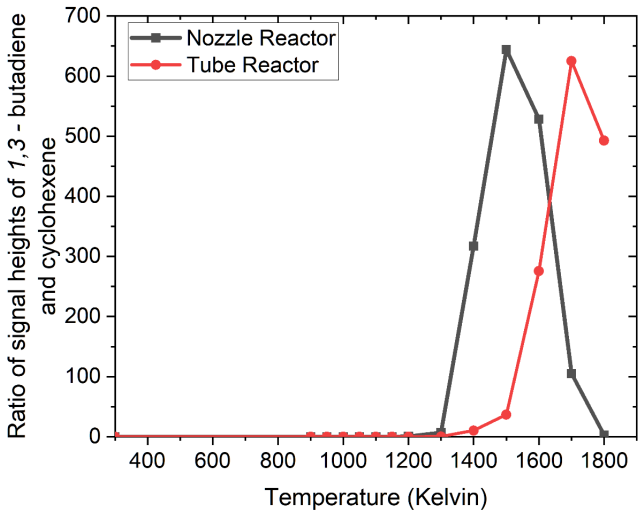


*Figure 3: Ratio of the signal height of butadiene to cyclohexene versus temperature in the nozzle reactor as compared to the tube reactor.*

Extension to alternative materials: In addition to fabricating high aspect ratio geometries using SiC, this manufacturing method has also been extended to other ceramic materials. Designs featuring internal constrictions have been constructed using alumina, yttria-stabilized zirconia, and silicon nitride. These geometries were produced using a process flow and tooling setup identical to the type used for fabricating SiC micro-reactors. No design changes to the mold tooling design were required to make components using these alternate ceramics, highlighting the processing methodology's flexibility. Images of these parts are shown in **Figure 4**. Configurations with other intricate internal features have also been

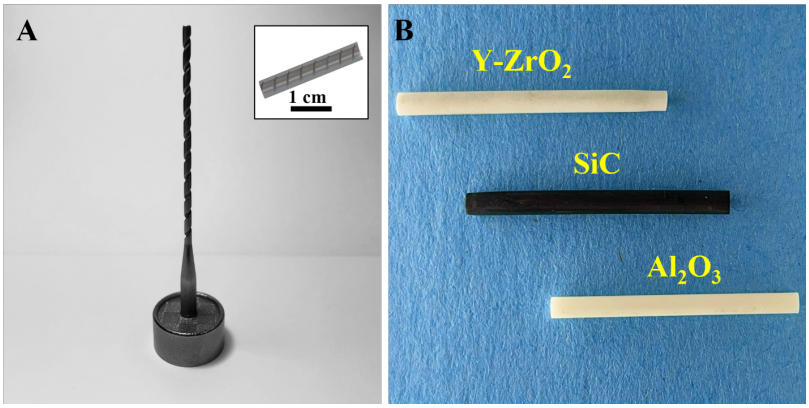


*Figure 4: A.) Image showing the tooling component featuring a helical thread produced using direct metal laser sintering with the inset image showing a rendering of the cross-section of the geometry fabricated using this tooling. B.) SiC, alumina and yttria stabilized zirconia*

demonstrated by applying this technique to produce a helical thread feature on the interior of a tube.

## Future Plans

Our future work centers around further testing the new reactors for use in gas-phase kinetic studies. Our first goal is to determine whether adding a nozzle constriction in the reactor can control pressure within the reactor main body as predicted, and if we can leverage that for fall-off regime kinetics studies. To achieve this, several systems may be considered, including methyl-methyl recombination (has a pressure and temperature dependent swing between recombination and dissociative recombination), $CH_3$ + $HCCCH_2$ (methyl + propargyl reactions have a competition between addition to form 1,3-butadiene versus addition-elimination to form H + $CH_3CHCCH$), and cyclopentadienyl recombination (cyclopentadienyl radicals recombine to form fulvenes, which ultimately isomerize to naphthalene). Additionally, we aim to study how material improvements in the reactor ceramic production may reduce potential secondary wall interactions.

## References


[1] P. Chen, S.D. Colson, W.A. Chupka, J.A. Berson, *Flash pyrolytic production of rotationally cold free radicals in a super sonic jet. Resonant multiphoton spectrum of the $3p^2A_2'' \leftarrow X^2A_2''$ origin band of $CH_3$,* JPC. 90 (1986) 2319-2321

[2] D.W. Kohn, H. Clauberg, P. Chen, *Flash pyrolysis nozzle for generation of radicals in a supersonic jet expansion*, Review of Scientific Instruments 63 (1992)

[3] *Standard Test Method for Flexural Strength of Advanced Ceramics at Ambient Temperature*, https://www.astm.org/c1161-18.html (accessed Nov. 17, 2022).

[4] *Hexoloy SE | SiC Material*, https://www.ceramicsrefractories.saint-gobain.com/materials/silicon-carbide-sic/hexoloy-silicon-carbide-material/hexoloy-se-sic-material (accessed Nov. 17, 2022).

[5] M. Ohyanagi, *Simultaneous transformation and consolidation of stacking-sequence disordered SiC without sintering additives*, in *Spark Plasma Sintering*, G. Cao, C. Estournès, J. Garay, and R. Orrù, Eds. (2019) 127–152.

[6] T. Fan, *Design of a Novel Microreactor to Study Short Residence Time Combustion*, M.S. Thesis, University of Colorado Boulder (2017).

[7] M. Uchiyama, T. Tomioka, A. Amano, *Thermal Decomposition of Cyclohexene*, JPC., 68 (1964) 1878–1881.

[8] W. Tsang, C. M. Rosado-Reyes, *Unimolecular Rate Expression for Cyclohexene Decomposition and Its Use in Chemical Thermometry under Shock Tube Conditions*, J. Phys. Chem. A, 119 (2015) 7155–7162.


## Publications, Presentations, and Submitted Articles Acknowledging This Grant (2019-present)

1. D. E. Couch, Q. L. Nguyen, D. D. Hickstein, H. C. Kapteyn, M. M. Murnane, and N. J. Labbe, "*Detection of the Keto- Enol Tautomerization in Acetaldehyde, Acetone, Cyclohexanone, and Methyl Vinyl Ketone with a Novel VUV Light Source*". Proc. Combust. Inst. (2020), 1737-1744.
2. C. O. Rogers, K. S. Lockwood, Q. L. Nguyen, and N. J. Labbe*, "Diol Isomer Revealed as the Source of Methyl Ketene from Propionic Acid". Int. J. Chem. Kinetics 53 (2021) 12712-1284.*
3. C. O. Rogers, D. Kaczmarek, T. Kasper, and N. J. Labbe, "*Probing the Low-Temperature Chemistry of Methyl Hexanoate: Insights from Oxygenate Intermediates*". Proc. Combust. Inst. 38 (2020), 621-629.
4. K. Lockwood, N. J. Labbe*, "Insights on Keto-Hydroperoxide Formation from O2 Addition to the Beta-Tetrahydrofuran Radical"* Proc. Combust. Inst. (2020), 533-541.
5. J. Sampathkumar, N. Ninos, G. Whiting, N. J. Labbe, *"Rapid Prototyping of High-Resolution Silicon Carbide Devices Using Digital Manufacturing Demonstrated Using Flow Reactors"* Advanced Engineering Materials (Under Review)
6. N.J. Labbe. "*Next Generation Microreactors for Rapid Reaction Speciation Data*," Western States Section of the Combustion Institute Spring Technical Meeting, Stanford, California, March 2022. [Plenary Talk]

**Fundamental Molecular Spectroscopy and Chemical Dynamics**

*Stephen R. Leone and Daniel M. Neumark*
Lawrence Berkeley National Laboratory and Department of Chemistry,
University of California, Berkeley, California 94720
(510) 643-5467 srl@berkeley.edu
510-642-3502 dneumark@berkeley.edu

**Scope of the Project:** Leone and Neumark carry out research within Subtask 1 of the Gas Phase Chemical Physics program at LBNL, focusing on fundamental molecular spectroscopy and chemical dynamics. Decades of research into molecular dynamics, including branching fractions, dissociation dynamics, and energetics, have vastly improved our fundamental understanding of chemical processes. Measurements of radical spectroscopy, ions and excited state time dynamics comprise key goals of this effort, especially the development of new ways to probe excited-state dynamics and photoproducts by the program of Leone and Neumark. The Leone group has pioneered ultrafast time-resolved table-top X-ray spectroscopic investigations of chemical dynamics at sufficiently high photon energies to access the carbon K-edge. Ultrafast X-ray transient absorption spectroscopy based on this methodology investigates transition states and products. Together, Leone and Neumark have developed an attosecond / few-femtosecond X-ray capability based on attosecond pulse technology in the soft X-ray regime up to the carbon K edge. Additionally, Neumark uses slow electron velocity-map imaging of cryogenically cooled anions (cryo-SEVI), a high-resolution variant of photoelectron spectroscopy, to probe the spectroscopy and dynamics of free radicals with a focus on systems that are relevant to combustion.

**Recent Progress:**

***Ultrafast Soft X-ray Transient Absorption Experiments***

Carbon K-edge spectroscopy was used to study pentamethylcyclopentadiene that sheds light on new photodynamics, which is in contrast to other ring systems such as cyclohexadiene. Previous work suggested that rather than undergoing ring opening, a relaxation to the ground electronic state would occur. This mechanism corresponds to the passage through two conical intersections from the initially populated $1B_2$ state and the dark $2A_1$ state and then subsequently to the $1A_1$ state. Probing from the core level has provided unique insights not observed in photoelectron spectroscopy, due to the general ability to selectively probe different atoms within the molecule. It was determined that a dissociation channel corresponding to loss of a hydrogen atom occurs on the timescale of 1 ps. The results mark a clear demonstration of the ability of transient X-ray spectroscopy to resolve radical species to a degree not attainable in traditional experiments such as photoelectron spectroscopy. Aiding in the assignment of this channel are calculations of the X-ray absorption spectra conducted by Martin Head-Gordon's group using density functional theory with the spin-unrestricted Kohn-Sham formalism. Based on the experimental and theorical results it is determined that the photo-induced dynamics following excitation may primarily pass through the $1B_2$ state with a barrier to form the radical.

Recently, the photophysics of hexafluoro-acetylacetone was explored at the carbon K-edge with the aim of determining the influence of electron withdrawing groups on conjugated chromophores. Here a 266 nm pump pulse excites the molecule to the $S_2$ ($\pi\pi^*$) electronic state before undergoing internal conversion to the $S_1$ ($n\pi^*$) electronic state whereupon an intersystem crossing to the $T_1$ ($n\pi^*$) state is observed with a timescale of 1.6 ± 0.2 ps. This is extremely

close to the timescale observed for unsubstituted acetylacetone (1.5 ps), indicating the strongly electron-withdrawing fluorine atoms play only a minor role. However, the fluorine atoms were found to significantly blueshift the X-ray absorption of the terminal carbon atoms, clearly helping to deconvolve the X-ray spectrum and allowing for a cleaner isolation of the dynamics than was possible in acetylacetone. This result demonstrates the possibility that electron withdrawing groups could be strategically added to complex molecules to simplify their X-ray spectra. Additionally, calculations were carried out (in collaboration with the Martin Head-Gordon group) using a square gradient minimization algorithm, which obtains spin-pure restricted open-shell Kohn-Sham energies. These calculations also demonstrate that hexafluoro-acetylacetone undergoes rotamerization along the $T_1$ state, which agrees with a proposed mechanism for the primary dissociation pathway.

Similar to past works on the benzene cation, the soft X-ray probe apparatus has been used to study the open-shell spin coupling of the bromobenzene cation. It was found that the $1s\rightarrow\pi^*$ transition displays a doublet state character arising from spin coupling of the unpaired electron in the partially filled $\pi$ orbital, analogous to what was observed in benzene. The $1s\rightarrow\sigma^*$ transition also displays a doublet state character, however this splitting was determined to originate from several transitions associated with the $\sigma^*$ orbital in addition to vibrational excitations to the C-Br mode following UV ionization. Given a vibrational excitation of the C-Br stretching mode, the most probable location of the bromine atom lies at two different locations as the stretch oscillates. The differing C-Br bond lengths result in different excitation energies from the 1s orbitals resulting in a doublet peak arising solely from the vibrational motion. From this study it was determined that the energy shifts and splitting in the $1s\rightarrow\sigma^*$ transitions demonstrate the influence that the C-Br bond length has on the X-ray spectrum and provide further information on the geometry of bromobenzene as it relaxes. The assignments of both the $1s\rightarrow\pi^*$ and $1s\rightarrow\sigma^*$ transitions were aided through the use of DFT/ROCIS calculations performed by the groups of Anna Krylov and Sonia Coriani.

Additional work with the ultrafast soft X-ray-probe apparatus has been initiated with an extension to a 200 nm pump excitation arm, facilitating the study of a wider range of molecular systems previously inaccessible by X-ray transient absorption techniques. The increased absorption of many organic molecules at 200 nm, relative to 266 nm, and the ability to probe new types of orbitals coupled with the selectivity of X-ray spectroscopy will allow for powerful experiments to be performed. Significant amounts of 200 nm light were generated, corresponding to a maximum energy of 10 μJ with a pulse duration of approximately 150-200 fs and a bandwidth of 1 nm. Preliminary work was conducted on 1,3-butadiene, a prototypical polyene molecule, corresponding to the first transient X-ray measurements at the carbon K-edge with a 200 nm pump excitation, to our knowledge. Here excitation into the $S_2$ ($^1B_u$) bright state was initiated, following which relaxation through a conical intersection to the multireference $S_1$ ($^1A_g$) dark state occurs before passage through a subsequent conical intersection to the ground electronic state.

### *Few-Femtosecond/Attosecond Soft X-ray Transient Absorption Experiments*

With the newly built attosecond / few-femtosecond soft-X-ray apparatus, carbon tetrachloride ($CCl_4$) was excited via a broadband few-femtosecond 800 nm pulse, leading to impulsive stimulated Raman scattering and strong field ionization. For impulsive stimulated Raman of $CCl_4$, the simultaneous observation of the C-Cl symmetric stretching vibration (456 $cm^{-1}$), both at the carbon K-edge (~280-300 eV) and at the chlorine $L_{2,3}$-edge (~195-220 eV), demarcates

the gradient of the core level potential surfaces when viewed through different atoms within the same molecule, providing a new window onto the excited state core level potentials.
Carbon tetrachloride ($CCl_4$) was also excited with a stronger, few-femtosecond 800 nm pulse resulting in strong field ionization, producing $CCl_4^+$. Calculations performed through the collaboration with the Martin Head-Gordon group were carried out with orbital-optimized density functional theory with the SCAN functional, which has been shown to be accurate to within 0.3 eV rms for both closed-shell and open shell species. It was observed that $CCl_4^+$ undergoes symmetry breaking corresponding to a Jahn-teller driven distortion causing the initial tetrahedral $T_d$ structure to become a symmetry broken $C_{2v}$ type structure in a timescale of 6 ± 2 fs. Further dynamics with molecular rearrangement to a non-covalently bonded complex corresponding to a central $C_{3v}$ geometry in 90 ± 10 fs. Here the fourth chlorine atom is weakly coupled with the central carbon atom at roughly 3.38 Angstroms, according to theory. It was observed that this chlorine slowly dissociates to $CCl_3^+$ and Cl in approximately 800 fs, resulting in the final photoproducts.

The observation of Jahn-Teller distortions in $CCl_4^+$ proved that sub-10 fs dynamics can be resolved in the newly built few-femtosecond instrument. A similar experimental configuration was used to measure Jahn-Teller distortions in the methane cation ($CH_4^+$). The molecules are ionized via strong-field ionization by employing a 5 fs 800 nm pump, thereby removing one electron from the triply degenerate HOMO ($1t_2$). Upon ionization, the cation is at the same equilibrium geometry of neutral $CH_4$ ($T_d$). Subsequently, the molecule rapidly breaks its symmetry to remove the degeneracy left by the partially occupied orbital, thus changing its geometry to the more stable $C_{2v}$ configuration. To our knowledge, this is the first time that a direct probe of the Jahn-Teller-driven motion in methane is obtained. This distortion results in a timescale of 10 ± 2 fs, determined by observing the energy shift of the 1s→SOMO transition of the cation at the carbon K-edge. At later times, the 1s→SOMO reveals damped oscillatory behavior with a decay time of 58 ± 15 fs. The frequency of the oscillation is in close agreement with the scissoring vibrational modes of $CH_4^+$ and can be assigned to the motion the molecule has to undergo to reach the $C_{2v}$ from the $T_d$ geometry. The damping of the vibrations is most likely a result of intramolecular vibrational energy redistribution to other vibrational motions, driven by the highly anharmonic potential surface of $CH_4^+$ in the $C_{2v}$ geometry. The experimental results have been corroborated by theory calculations performed by the group of Martin Head-Gordon. Here 256 AIM trajectories of the methane cation were performed in addition to XAS spectrum calculations based on orbital-optimized density functional theory.

Preliminary work on the generation of short ultraviolet pulses with the attosecond instrument has been undertaken resulting in 266 nm pump pulses with an energy of 5 μJ and a Fourier-limited duration of less than 15 fs. The ultraviolet pulses were generated through frequency doubling a portion of broadband compressed 800 nm pump in a nonlinear BBO crystal to generate a short 400 nm pulse. The 400 nm pulse was compressed with chirped mirrors and mixed with the remaining broadband 800 nm pump in a thin BBO crystal inside the vacuum chambers of the soft X-ray instrument, generating 266 nm light. The generation of 266 nm pulses within vacuum limits the dispersion intrinsic to ultraviolet pulses while travelling through glass or air, resulting in a compressed ultraviolet pulse for use in a pump probe experiment.

### *Free radical spectroscopy*

The Neumark group has developed a high resolution (1-2 $cm^{-1}$) variant of anion photoelectron spectroscopy, slow electron velocity-map imaging of cryogenically cooled anions (cryo-

SEVI),and has applied it to the study of reactive free radicals that serve as important intermediates in combustion. Cryo-SEVI yields precise electron affinities and vibrational frequencies for free radicals, and its ability to explore hydrocarbon and related radicals complements the time-resolved experiments carried out with femtosecond and attosecond X-ray sources as described above. The capabilities of this instrument have been improved by new additions to the event-counting and centroiding algorithm that enable centroid analysis of overlapping electron spots, thereby improving the rate of data collection. This improvement was demonstrated in a cryo-SEVI study of the acetyl anion, $CH_3CO^-$, a less stable isomer of the more extensively studied vinoxide anion ($CH_2CHO^-$). The $CH_3CO$ radical is formed from the dissociation of acetone and other ketones. It is an important intermediate in tropospheric hydrocarbon oxidation. The cryo-SEVI spectrum yields a precise electron affinity for the acetyl radical, 0.435 eV, and well-resolved progressions are observed in three vibrational modes of the radical. Franck-Condon analysis indicates a significant change in geometry upon photodetachment primarily in the C-C-O bend angle. The cryo-SEVI spectrum of the vinyl anion ($C_2H_3^-$) has also been measured in order to characterize the vinyl radical, an important intermediate in hydrocarbon combustion, plasma chemistry, and planetary atmospheres. The spectrum shows an irregular peak pattern that is tentatively attributed to large tunnelling splittings in the vicinity of a low energy isomerization barrier with $C_{2v}$ symmetry.

***Future Plans:***

The UV-pump and soft X-ray-probe apparatus will be used to spectroscopically investigate fundamental photochemical processes. Topics such as the decomposition of ketones and the production of diradicals, ring puckering and ring opening dynamics, in addition to the study of cycloaddition reactions, will be a focus for research in the future. Additional investigations, including methyl vinyl ketone, furanone, and norbornadiene, remain exciting possibilities to study such fundamental photochemical processes. To aid in the study of these molecules, compression of the 200 nm pump pulse will be implemented to greatly improve the temporal resolution of the experiment to approach the transform-limited duration of 60 fs corresponding to the FWHM of 1 nm of the successfully produced pulse. Further work in extending the cut-off energy of the soft X-ray probe to improve flux at the nitrogen K-edge (410eV) will be undertaken by further redshifting the driving pulse and optimizing for high harmonic generation. Additionally, the implementation of a waveform synthesizer to create a modified high harmonic generation multi-color driving pulse is planned. By recombining various pulses of differing wavelengths both the efficiency and cut-off energy of the high harmonic generation process can be increased, covering a wider range in the water window. Eventually this methodology can be used to generate isolated attosecond pulses in the soft X-ray region for use in future experiments.

Cryo-SEVI experiments will be carried out on $C_2D_3^-$ to further elucidate the effects of tunneling on the pattern of vibrational energy levels in the vinyl radical. The allyl radical, a benchmark resonantly stabilized radical, will also be investigated by cryo-SEVI. In a new research direction, cryo-SEVI experiments will be performed on anions that have been pre-excited with an infrared laser. This experiment, which will be carried out on the vinyl and allyl anions, represents a novel means to measure infrared spectra of cold, gas phase anions and to simultaneously explore neutral vibrational energy levels and regions of the neutral potential energy surface that are inaccessible via detachment from the anion ground vibrational state.

***Recent Publications Acknowledging DOE GPCP Support (2020-2023):***


- Haugen, E. A; Hait, D.; Scutelnic, V.; Xue, T.; Head-Gordon, M.; Leone, S.R., "Ultrafast X-ray Spectroscopy of Intersystem Crossing in Hexafluoroacetylacetone: Chromophore Photophysics and Spectral Changes in the Face of Electron-Withdrawing Groups". J. Phys. Chem. A. 127,3, 634-644 (**2023**). DOI: 10.1021/acs.jpca.2c06044
- Epshtein, M.; Tenorio, B. N. C.; Vidal, M. L.; Scutelnic, V.; Yang, Z.; Xue, T.; Krylov, A. I.; Coriani, S.; Leone, S. R., "Signatures of the Bromine Atom and Open-Shell Spin Coupling in the X-ray Spectrum of the Bromobenzene Cation". J. Am. Chem. Soc. 145, 6, 3554-3560 (**2023**). DOI: 10.1021/jacs.2c12334
- Popolan-Vaida, D. M.; Eskola, A. J.; Rotavera, B.; Lockyear, J. F.; Wang, Z.; Sarathy, S. M.; Caravan, R. L.; Zador, J.; Sheps, L.; Lucassen A.; Moshammer, K.; Dagaut, P.; Osborn, D. L.; Hansen, N.; Leone S. R.; Taatjes, C.A., "Formation of Organic Acids and Carbonyl Compounds in n-Butane Oxidation via γ-Ketohydroperoxide Decomposition". Angew. Chem. Int. Ed. 61, e202209168 (**2022**). DOI: 10.1002/anie.202209168
- Kobayashi, Y.; Leone, S. R., "Characterizing coherences in chemical dynamics with attosecond time-resolved X-ray absorption spectroscopy". J. Chem. Phys. 157, 1809014 (**2022**). DOI: 10.1063/5.0119942
- Ross, A. D.; Hait, D.; Scutelnic, V.; Haugen, E. A.; Ridente, E.; Balkew, M. B.; Neumark, D. M.; Head-Gordon, M.; Leone, S. R., "Jahn-Teller distortion and dissociation of $CCl_4^+$ by transient X-ray spectroscopy simultaneously at the carbon K- and chlorine L-edge". Chem. Sci., 13, 9310-9320 (**2022**). DOI: 10.1039/D2SC02402K
- DeWitt, M.; Babin, M.C; Lau, J.A.; Solomis, T.; Neumark, D.M., "High Resolution Photoelectron Spectroscopy of the Acetyl Anion" J. Phys. Chem. A, 126, 7962–7970 (**2022**). DOI: 10.1021/acs.jpca.2c06214
- Chang, K. F.; Wang, H.; Poullain, S. M.; Gonzalez-Vazquez, J.; Banares, L.; Prendergast, D.; Neumark, D. M.; Leone, S.R., "Conical intersection and coherent vibrational drnamics in alkyl iodides captured by attosecond transient absorption spectroscopy". J. Chem. Phys. 156, 114304 (**2022**). DOI: 10.1063/5.0086775
- Chambreau, S. D.; Popolan-Vaida, D. M.; Kostko, O.; Lee, J. K.; Zhou, Z.; Brown, T. A.; Jones, P.; Shao, K.; Zhang, J.; Vaghjiani, G.L.; Zare, R. N.; Leone, S.R., "Thermal and Catalytic Decomposition of 2-Hydroxyethylhydrazine and 2-Hydroxyethylhydrazinium Nitrate Ionic Liquid". J. Phys. Chem. A. 126, 373-394 (**2022**). DOI: 10.1021/acs.jpca.1c07408
- Scutelnic, V.; Tsuru, S.; Papai, M.; Yang, Z/; Epshtein, M.; Xue, T.; Haugen, E.; Kobayashi, Y.; Krylov, A. I.; Coriani, S.; Leone, S.R., "X-ray transient absorption reveals the $^1A_u$ ($n\pi^*$) state of pyrazine in electronic relaxation". Nat. Commun. 12, 5003 (**2021**). DOI: 10.1038/s41467-021-25045-0
- Rebholz, M.; Ding, T.; Despre, V.; Aufleger, L.; Hartmann, M.; Meyer, K.; StooB, V.; Magunia, A.; Wachs, D.; Birk, P.; Mi, Y.; Borisova, G. D.; Castanheira, C. C.; Rupprecht, P.; Schmid, G.; Schnorr, K.; Scgriter. C. D.; Moshammer, R.; Loh, Z.; Attar, A. R.; Leone, S.R.; Gaummitz, T.; Worner, H. J.; Roling, S.; Butz, M.; Zacharias, H.; Dusterer. S.; Treush, R.; Brenner, G.; Vester, J.; Kuleff, A. I.; Ott, C.; Pfeifer. T., "All-XUV Pump-Probe Transient Absorption Sepctroscopy of the Structural Molecular Dynamics of Di-iodomethane". Phys. Rev. X. 11, 031001 (**2021**). DOI: 10.1103/PhysRevX.11.031001
- Chang, K. F.; Wang, H.; Poullain, S. M.; Prendergast, D.; Neumark, D. M.; Leone, S.R., "Mapping wave packet difurcation at ta conical intersection in $CH_3I$ by attosecond XUV

transient absorption spectroscopy". J. Chem. Phys. 154, 234301 (**2021**). DOI: 10.1063/5.0056299

- Scutelnic, V.; Leone, S.R., "Elucidation of Molecular Dynamics by Extreme Ultraviolet and Soft X-ray Transient-Absorption Spectroscopy". ACS Symposium Series, Emerging Trends in Chemical Applications of Lasers, 1398, 1-14 **(2021)**. DOI: 10.1021/bk-2021-1398.ch001
- Chang, K. F.; Reduzzi, M.; Wang, H.; M.-Poullain, S.; Kobayashi, Y.; Barreau, L.; Prendergast, D.; Neumark, D. M.; Leone, S. R., "Revealing Electronic State-Switching at Conical Intersections in Alkyl Iodides by Ultrafast XUV Transient Absorption Spectroscopy". Nat. Commun. 11, 4042 **(2020).** DOI: 10.1038/s41467-020-17745-w.
- Epshtein, M.; Scutelnic, V.; Yang, Z.; Xue, T.; Vidal, M. L.; Krylov, A. I.; Coriani, S.; Leone, S. R. "Table-Top X-ray Spectroscopy of Benzene Radical Cation". J. Phys. Chem. A, 124, 9524–9531 **(2020)**. DOI: 10.1021/acs.jpca.0c08736.
- Nichols, B.; Sullivan, E. N.; Neumark, D. M., "Photodissociation Dynamics of the tert-butyl perthiyl Radical". J. Chem. Phys. 152, 244301 **(2020).** DOI: 10.1063/5.0006913.
- Sullivan, E. N.; Saric, S.; Neumark, D. M., "Photodissociation of iso-Propoxy (i-C3H7O) Radical at 248 nm". Phys. Chem. Chem. Phys. 22, 17738-17748 **(2020)**. DOI: 10.1039/d0cp02493g.
- Vidal, M. L.; Epshtein, M.; Scutelnic, V.; Yang, Z.; Xue, T.; Leone, S. R.; Krylov, A. I.; Coriani, S. "Interplay of Open-Shell Spin-Coupling and Jahn–Teller Distortion in Benzene Radical Cation Probed by X-ray Spectroscopy". J. Phys. Chem. A 124, 9532–9541 **(2020)**. DOI: 10.1021/acs.jpca.0c08732.
- Hait, D.; Haugen, E.; Yang, Z.; Oosterbaan, K.; Leone, S. R.; Head-Gordon, M., "Accurate Prediction of Core-Level Spectra of Radicals at Density Functional Theory Cost via Square Gradient Minimization and Recoupling of Mixed Configurations". J. Chem. Phys. 153, 134108 **(2020)**. DOI: 10.1063/5.0018833.
- Barreau, L.; Ross, A. D.; Garg, S.; Kraus, P. M.; Neumark, D. M.; Leone, S. R. "Efficient Table-Top Dual-Wavelength Instrument for Ultrafast Transient Absorption Spectroscopy in the Soft X-ray Region". Sci. Rep. 10, 5773 **(2020)**. DOI: 10.1038/s41598-020-62461-6

# Molecular Reactivity in Complex Systems

Musahid Ahmed (mahmed@lbl.gov), Daniel Neumark (DMNeumark@lbl.gov), Kevin Wilson (krwilson@lbl.gov)

Chemical Sciences Division, LBNL, Berkeley, CA-94720

## Background and Significance

Our effort in molecular reactivity in complex systems targets complex multistep and multiphase chemical transformations built from isolated elementary bimolecular reactions to gas-surface reaction dynamics. The gas phase is central for controlling the multiphase chemistry with additional kinetic processes, playing a key role in governing the overall reactive outcome. Cross-cutting themes of *Chemistry at Complex Interfaces* and *Reaction Pathways in Diverse Environments* are explored, providing valuable insight into microscopic processes relevant to energy generation, storage, and thermal science. Activities in this Subtask drive new theory and simulation, to enrich the molecular level interpretation of experiments. The Gas Phase Chemical Physics program at Berkeley Lab is uniquely placed to conduct this research, with theory and experiment coupled with extensive use of DOE national user facilities such as the Advanced Light Source and NERSC.

## Recent Progress:

***Photoionization Dynamics and Hydrogen Bonding in Clusters:*** Van der Waals and hydrogen bonded clusters provide a template to probe ionization and solvation processes of paramount interest in thermal science, environmental and astrochemical chemistry.[1] We generate such clusters in a continuous supersonic jet expansion and interrogate the neutral species with synchrotron based tunable vacuum ultraviolet (VUV) photoionization mass spectrometry. Photoionization efficiency curves (PIE), fragment mass spectra, and theoretical calculations provide unique insight into the underlying dynamics and chemistry. Experimental results for glycerol water clusters, coupled with theoretical calculations performed by MHG are relevant to radiation-induced chemical processing of alcohol−water ices in the interstellar medium.[2] Confinement and interactions of water with polycyclic aromatic hydrocarbons such as naphthalene and anthracene provide a molecular picture of possible interactions on the icy mantles of dust grains.[3,4] Recently we completed a study on the interaction of naphthalene (N) with carbon dioxide ($CO_2$) clusters. A mechanism emerges, demonstrated previously for exciton charge transfer from excited argon clusters to acetylene[5] and water, where the excited $CO_2$ clusters transfer energy to N leading to its ionization since the excitation energy is higher than N's ionization energy. A survey of the literature reveals that these excited states are probably high-n Rydberg states, and the spectra are very similar to that observed in supercritical $CO_2$ and astrochemical relevant $CO_2$ ices. Moreover, there are red shifts in the order of 10-15 meV as cluster size increases, which provide a picture of how structure changes from the monomer towards the hexamer. This, we believe, is direct experimental evidence of electronic excitation in $CO_2$ clusters and paves a way towards understanding the electronic structure of astrochemical relevant ices. Finally, we completed a combined experimental and theoretical (with MHG) study of protonated water clusters that provides insight into the interactions of the hydronium ion with the hydrogen bond network, and how this evolves as a function of size. The experimental results show unequivocally that $H^+(H_2O)_{21}$ is magic typically corresponding to the largest signal in molecular beam photoionization experiments however $H^+(H_2O)_{14}$ is also magic under certain source conditions. A computational search for the most stable conformer of protonated water clusters from n = 2 to n = 22, using metadynamics methods followed by refinement with DFT methods that are quite accurate for hydrogen-bonded systems was performed. The results show that the n =21 protonated cluster is particularly stable and that the n = 14 cluster also

prominent in experiments emerges as stabilized relative to its neighbors which may contribute to the experimental observations.

***Molecular Beam Experiments on Flat Liquid Jets:*** The gas-liquid interface is a ubiquitous chemical environment in nature. It plays a major role in industrial processes, atmospheric chemistry, and environmental science. Examples include air-fuel mixing in internal combustion engines, acid rain formation, and the uptake of $CO_2$ at the ocean-air interface, where about one third of anthropogenically generated $CO_2$ is absorbed. It is thus desirable to develop a molecular-scale understanding of chemistry at the gas-liquid interface. To this end, an experimental setup for molecular beam scattering from flat liquid sheets has been developed, with the goal of studying reactions at gas-liquid interfaces for volatile liquids. Specifically, a crossed-molecular beam instrument that can measure angular and translational energy distributions of scattered products has been adapted for liquid jet scattering. A microfluidic chip creates a stable flat liquid sheet inside vacuum from which scattering occurs, and both evaporation and scattering from this sheet are characterized by a rotatable mass spectrometer that can measure product time-of-flight distributions. First measurements of evaporation of dodecane and Ne from a Ne-doped dodecane flat jet, as well as scattering of Ne from a flat jet of pure dodecane have been recently published.[6] A manuscript detailing evaporation and polyatomic scattering of $CD_4$ and $D_2O$ from dodecane is currently underway.

Two types of experiments have been carried out: evaporation and scattering. The evaporation of Ne-, $CD_4$-, and $D_2O$-doped dodecane solutions is explored in order to isolate the trapping-desorption (TD) process, which is one of the major channels encountered in scattering experiments, and a detailed understanding of evaporation from a flat jet is key to successfully interpreting scattering experiments. This has allowed for molecular beam scattering experiments of the three gas scattering partners from a dodecane flat jet to be carried out. Measurement of the scattered Ne, $CD_4$, and $D_2O$ velocity and angular distributions enables elucidation of the impulsive scattering (IS) and TD mechanisms. It has been observed that the ratio between the IS and TD mechanistic channels is similar for $CD_4$ and $D_2O$, both being accommodated more readily by the surface compared to Ne. Results as a function of incident and scattering angle are satisfactorily fit to a "soft sphere" model, where a larger energy transfer is observed for both $CD_4$ and $D_2O$ scattering compared to Ne scattering. The measurements reveal that the angular distribution for the IS channel is not specular, as was previously believed, but instead peaks a few degrees further from the surface normal.

***Radical reactions[7-18] & reactivity of large hydrocarbons on nanoparticles***: The growth of polycyclic aromatic hydrocarbons (PAHs) has been explored by Ahmed in collaboration with Ralf Kaiser (Hawaii), and Alex Mebel (FIU). Radical-radical reactions under high pressure and temperature conditions prevalent in the microreactor provides a rich tapestry to understand the underlying reaction dynamics that drive molecular growth in carbonaceous systems. The reaction dynamics of spiro-aromatic radical transients in the gas-phase formation of anthracene in the Indenyl–Cyclopentadienyl radical–radical reaction was elucidated,[7] while an unconventional pathway in the formation of 9H-Fluorene via the radical – radical reaction of benzyl with phenyl was discovered.[8] The formation of naphthalene was deciphered via a H atom assisted isomerization pathway in the reaction of the benzyl with the propargyl radical. Barrier-less, low temperature pathways leading to racemates of [5] and [6] helicene were identified in the reaction of vinylacetylene with helicenyl radicals.[11] A new direction in the collaboration with Kaiser and Mebel is to understand the reactivity of long chain hydrocarbon fuel molecules on nanoparticle surfaces under high temperature and pressure conditions. A study to understand the fundamental bond breaking processes, reaction mechanisms, and kinetics involved in the oxidation of Jet Propellant-10 (JP10; exo-tetrahydrodicyclopentadiene) jet fuel on aluminum oxide nanoparticles was completed using VUV photoionization mass spectrometry. This approach provided an isomer specific, comprehensive inventory of all open and closed shell products along with their

branching ratios related to the decomposition of JP10. Three different temperature regimes, *low* – surface mediated heterogeneous reactions, *medium* – a transition from the heterogeneous to homogenous gas phase reactions, and finally *high*- collisions between helium bath gas and facile gas reactions initiated by H abstraction from JP10 were identified experimentally and verified by theoretical calculations.

***Multiphase Chemistry of Criegee Intermediates (CI):*** Criegee intermediates (CI) are central species in ozonolysis of unsaturated organic compounds; controlling both the formation of small fragmentation reaction products and higher molecular weight oligomeric compounds through competing unimolecular and bimolecular pathways. The reaction of thermalized CI with carboxylic acids (RCOOH) to produce oligomeric α-acyloxyalkyl hydroperoxides is of interest to the chemical transformation of organic compounds in the atmosphere and the environment. In the gas phase, this reaction proceeds at super-collisional rates, consistent with a barrier-less reaction mechanism. However, the rate of this reaction in condensed phases remains uncertain. In a recent publication,[19] we use aerosols to study the ozonolysis of submicron organic aerosol containing mixtures of an internal n-alkene and a saturated acid (RCOOH). The decay of the reactants and formation of reaction products are monitored using an aerosol Atmospheric Pressure Chemical Ionization mass spectrometer. A six fold-decrease in the reaction probability of ozone is observed with increasing acid concentration, consistent with a previous study using alcohol additives.[20] The decay of the saturated acid with ozone exposure shows that it scavenges CI at rates comparable to competing unimolecular pathways involving CI. The multiphase decay kinetics are analyzed to constrain the ratio of the CI + RCOOH and unimolecular CI rate constants. Empirical fitting to this model, combined with theoretical estimates of the unimolecular loss rate, yields a CI + RCOOH rate constant of $1.85 \pm 0.27 \times 10^{-19}$ $cm^3$ $molec^{-1}$ $s^{-1}$, which is six orders of magnitude slower than the expected diffusion limit in a liquid organic matrix. Stochastic kinetic simulations are conducted with different values of the CI + RCOOH rate constant to validate this result, and confirm that the diffusion limited rate is indeed much too rapid to reproduce our experimental results.

***Non-covalent Interaction and Heterogeneous Reaction Probabilities:*** It is well-known in enzyme catalysis that weak interactions (e.g. hydrogen and halogen bonds) can play an important role in altering the energetics of a reaction. Less well known is how these weak interactions can enhance reactivity at gas-liquid interfaces. For example, how weak interactions alter key non-reactive pathways that govern trace gas uptake and reaction at a liquid interface. These non-reactive kinetic steps include gas adsorption/desorption and solvation/desolvation. Building on previous work,[21] we have examined the heterogeneous reaction of chlorine atoms with alkenes, in the presence of $Cl_2$.[22] We observe an unexpectedly large enhancement of reactivity and the predominance of chlorinated reaction products even under high $O_2$ conditions, where Cl atom recycling is expected to be minimal. These observations cannot be explained by known free radical oxidation or cycling mechanisms, but rather we find evidence for the multiphase catalytic coupling of free radical oxidation with electrophilic $Cl_2$ addition. This mechanism is consistent with our previous work,[21] where we showed that oxygenated molecules act as gas-liquid phase transfer catalysts by promoting the accommodation of gas phase $Cl_2$ by the aerosol; thereby enhancing electrophilic addition. We anticipate that this maybe novel example of catalytic coupling of free radical oxidation and electrophilic addition at an aerosol interface.

**Future Plans:**

***Probing non-covalent interactions & gases in confined spaces with laser and synchrotron-based mass spectrometry:*** In addition to our synchrotron-based mass spectrometer, we are developing a lab -based system to probe spectroscopic and time-resolved chemical dynamics involving non-covalent interactions. This system will use 35% of the output from a <300 fs Yb fiber laser for generating the 115 nm (10.9 eV) ninth harmonic by a phase matched process of the third harmonic in a Xenon gas

cell, running at up to 750 kHz. The remaining 65% is used to pump an Optical Parametric Amplifier that covers a tuning range of 210 nm to 16 μm. The resulting wide spectral range allows for direct ionization as well as electronic and vibrational spectroscopy of gas phase systems. The combination with short laser pulses allows for the characterization of fast structural and/or electronic changes upon excitation, ideal for tracking the dynamics of non-covalent systems. We, are interested in the dynamic interactions of water weakly bound to hydrophobic molecular substrates (hydrocarbon with $CO_2$ and $H_2O$ clusters). Despite the cold conditions used to produce such complexes, they still retain large amounts of flexibility. Related are solvent-molecule rearrangements. Solvation can have a strong influence on chemical properties, and particularly their dynamic response to a stimulus, such as photoexcitation. Moreover, this system will enable us to study the processes that occur upon (V)UV absorption, such as dehydrogenation, dissociation, and ionization. We are nearing the completion of constructing this apparatus and have recently acquired initial test mass spectra using it. While the instrument is composed of a molecular beams source, provisions are being made to include aerosol delivery and microfluidics to probe gas-surface and liquid interactions. A new direction will be probe gases in confinement described below.

Porous networks, such as metal-organic frameworks (MOFs), crystalline porous organic salts (CPOSs), hydrogen bonded organic frameworks (HOFs), and hierarchically nanostructured gels (HNGs), offer novel properties compared to their bulk counterparts. Their high internal surface areas are relevant for gas trapping, adsorption, and transport. Gas phase molecules within these confined environments encounter unique forces and dynamics which completely transform their reaction outcomes and have profound and deep implications for the future of energy supply and climate change. However, the fundamental mechanisms that underpin the dynamics that lead to phase changes, and adsorption of gases are still not understood well. We are designing novel reactors[23,24] to probe such dynamics with synchrotron and laser-based mass spectrometry coupled with vibrational spectroscopy. As an example, we will interrogate the dynamics of the gas phase molecules inside a MOF cavity using Raman spectroscopy (50-4000 $cm^{-1}$) allowing access to the lattice dynamics of the MOF cage in the THz regime, and the gas-organic linker functional group information via higher wavelengths. The emanating gas phase molecules will be probed via mass spectrometry. Preliminary results on a Co MOF-74 synthesized within a quartz capillary allowed us to track both the adsorption and desorption kinetics of ambient air upon temperature cycling with our home-made Raman laser system. A particularly exciting direction is that Jin Qian (subtask 3) is developing methods to calculate X-Ray, THz, IR and Raman spectra that will guide interpretation of the experimental results. The successful collaborations of Qian and Ahmed combining theory, Infrared, and Raman Spectroscopies that elucidated the mechanism for crystallization and growth of the metal–organic framework[25] bodes well for future understanding of gas interactions within the confining framework.

***Molecular Beam Experiments on Flat Liquid Jets:*** The immediate goal of this project is to perform scattering experiments off more volatile solvents, with water as the primary target. Preliminary tests have shown that a concentrated LiBr solution can be used to generate a “salty” water flat jet. Such an aqueous solution allows for the exploitation of freezing point depression, reducing the water vapor pressure to ensure that gas–liquid interactions are probed rather than the vapor cloud around the flat jet. Solutions of water with ethylene glycol have also demonstrated the ability to lower the liquid temperature beyond the freezing point of water. Preliminary scattering experiments using rare gas atoms show strong evidence that the scattering is dominated by gas–liquid interactions. We are also working with Acrea 3D to carry out 3D printing of new designs for our microfluidic flat jets in order to optimize their performance in scattering experiments.

Initial experiments would encompass scattering Ne, $CD_4$, $D_2O$, and $ND_3$ from a water-based flat jet to observe how the hydrogen bond network and OH groups affect the characteristics of the surface and subsequent accommodation of the gas scattering partners compared to the dodecane flat jet. Reactive

scattering experiments would then be explored, such as in scattering sulfur trioxide to uncover mechanistic detail behind the formation of acid rain, or by scattering carbon dioxide from an amine-doped water jet in relation to carbon capture efforts.

***Multiphase Chemistry of Criegee Intermediates (CI):*** In ongoing efforts, we will be measuring the temperature dependence of the multiphase ozonolysis of aerosol comprised of an alkene in the presence of a carboxylic acid. This work is focused on elucidating the competition between bimolecular (CI +RCOOH) and unimolecular pathways (decomposition, isomerization) of CI in aerosols. In addition, we are collaborating with Rebecca Caravan's group (ANL) to use small gas phase alkenes to further understand these interconversion pathways between β-$RO_2$ and CI. This will be done using the multiplexed photoionization mass spectrometer (D. Osborn, Sandia) coupled to the tunable VUV output of the Chemical Dynamics Beamline at the ALS.

***Non-covalent Interaction and Heterogeneous Reaction Probabilities:*** We are continuing our work to understand how spectator molecules catalyze heterogeneous reactions. This includes planned experimental studies examining how molecules in the gas phase can adsorb to the aerosol interface to promote or inhibit the electrophilic addition of $Cl_2$ to alkenes. We will be conducting a systematic investigation of a series of gas phase alcohols and alkanes, which differ in their chain length and structure, in order to understand their partitioning to the aerosol interface and their relative catalytic activity. New collaborations are beginning with David Limmer's group (LBNL CPIMS program) to use molecular dynamic simulations to examine how alcohol additives might alter the interfacial solvation energies of $Cl_2$, which could contribute to the overall catalytic mechanism.

## References citing DOE GPCP support(2020-present)[26-33]


1 Ahmed, M. & Kostko, O. From atoms to aerosols: probing clusters and nanoparticles with synchrotron based mass spectrometry and X-ray spectroscopy. *Physical Chemistry Chemical Physics* **22**, 2713-2737, doi:10.1039/c9cp05802h (2020).

2 Lu, W. C., Mackie, C. J., Xu, B., Head-Gordon, M. & Ahmed, M. A Computational and Experimental View of Hydrogen Bonding in Glycerol Water Clusters. *Journal of Physical Chemistry A* **126**, 1701-1710, doi:10.1021/acs.jpca.2c00659 (2022).

3 Zamir, A., Rossich Molina, E., Ahmed, M. & Stein, T. Water confinement in small polycyclic aromatic hydrocarbons. *Phys Chem Chem Phys* **24**, 28788-28793, doi:10.1039/d2cp04773j (2022).

4 Molina, E. R., Xu, B., Kostko, O., Ahmed, M. & Stein, T. A combined theoretical and experimental study of small anthracene-water clusters. *Physical Chemistry Chemical Physics* **24**, 23106-23118, doi:10.1039/d2cp02617a (2022).

5 Lu, W. C., Metz, R. B., Troy, T. P., Kostko, O. & Ahmed, M. Exciton energy transfer reveals spectral signatures of excited states in clusters. *Physical Chemistry Chemical Physics* **22**, 14284-14292, doi:10.1039/d0cp02042g (2020).

6 Lee, C. *et al.* Evaporation and Molecular Beam Scattering from a Flat Liquid Jet. *The Journal of Physical Chemistry A* **126**, 3373-3383, doi:10.1021/acs.jpca.2c01174 (2022).

7 He, C. *et al.* Exotic Reaction Dynamics in the Gas-Phase Preparation of Anthracene (C(14)H(10)) via Spiroaromatic Radical Transients in the Indenyl-Cyclopentadienyl Radical-Radical Reaction. *J Am Chem Soc* **145**, 3084-3091, doi:10.1021/jacs.2c12045 (2023).

8 He, C. *et al.* Unconventional Pathway in the Gas-Phase Synthesis of 9H-Fluorene (C(13) H(10) ) via the Radical-Radical Reaction of Benzyl (C(7) H(7) ) with Phenyl (C(6) H(5) ). *Angew Chem Int Ed Engl* **62**, e202216972, doi:10.1002/anie.202216972 (2023).

9 Kaiser, R. I. *et al.* Unconventional excited-state dynamics in the concerted benzyl (C(7)H(7)) radical self-reaction to anthracene (C(14)H(10)). *Nat Commun* **13**, 786, doi:10.1038/s41467-022-28466-7 (2022).

10 Kaiser, R. I. *et al.* Formation of Benzene and Naphthalene through Cyclopentadienyl-Mediated Radical–Radical Reactions. *The Journal of Physical Chemistry Letters* **13**, 208-213, doi:10.1021/acs.jpclett.1c03733 (2022).

11 Kaiser, R. I. *et al.* Gas-phase synthesis of racemic helicenes and their potential role in the enantiomeric enrichment of sugars and amino acids in meteorites. *Phys Chem Chem Phys* **24**, 25077-25087, doi:10.1039/d2cp03084e (2022).

12 Zhao, L. *et al.* A molecular beam and computational study on the barrierless gas phase formation of (iso)quinoline in low temperature extraterrestrial environments. *Phys Chem Chem Phys* **23**, 18495-18505, doi:10.1039/d1cp02169a (2021).
13 Zhao, L. *et al.* Gas-phase synthesis of benzene via the propargyl radical self-reaction. *Sci Adv* **7**, eabf0360, doi:10.1126/sciadv.abf0360 (2021).
14 Zhao, L. *et al.* Gas-phase synthesis of corannulene - a molecular building block of fullerenes. *Physical Chemistry Chemical Physics* **23**, 5740-5749, doi:10.1039/d0cp06537d (2021).
15 Zhao, L. *et al.* A Unified Mechanism on the Formation of Acenes, Helicenes, and Phenacenes in the Gas Phase. *Angewandte Chemie-International Edition* **59**, 4051-4058, doi:10.1002/anie.201913037 (2020).
16 Zhao, L. *et al.* Gas phase formation of cyclopentanaphthalene (benzindene) isomers via reactions of 5-and 6-indenyl radicals with vinylacetylene. *Physical Chemistry Chemical Physics* **22**, 22493-22500, doi:10.1039/d0cp03846f (2020).
17 Zhao, L. *et al.* Gas phase formation of phenalene via 10 Pi-aromatic, resonantly stabilized free radical intermediates. *Physical Chemistry Chemical Physics* **22**, 15381-15388, doi:10.1039/d0cp02216k (2020).
18 Zhao, L. *et al.* A Free-Radical Prompted Barrierless Gas-Phase Synthesis of Pentacene. *Angewandte Chemie-International Edition* **59**, 11334-11338, doi:10.1002/anie.202003402 (2020).
19 Reynolds, R., Ahmed, M. & Wilson, K. R. Constraining the Reaction Rate of Criegee Intermediates with Carboxylic Acids during the Multiphase Ozonolysis of Aerosolized Alkenes. *ACS Earth and Space Chemistry*, doi:10.1021/acsearthspacechem.3c00026 (2023).
20 Zeng, M. & Wilson, K. R. Efficient Coupling of Reaction Pathways of Criegee Intermediates and Free Radicals in the Heterogeneous Ozonolysis of Alkenes. *The Journal of Physical Chemistry Letters* **11**, 6580-6585, doi:10.1021/acs.jpclett.0c01823 (2020).
21 Zeng, M. & Wilson, K. R. Experimental evidence that halogen bonding catalyzes the heterogeneous chlorination of alkenes in submicron liquid droplets. *Chemical Science* **12**, 10455-10466, doi:10.1039/D1SC02662C (2021).
22 Zeng, M., Liu, C.-L. & Wilson, K. R. Catalytic Coupling of Free Radical Oxidation and Electrophilic Chlorine Addition by Phase-Transfer Intermediates in Liquid Aerosols. *The Journal of Physical Chemistry A* **126**, 2959-2965, doi:10.1021/acs.jpca.2c00291 (2022).
23 Sui, X. *et al.* New Insights into Secondary Organic Aerosol Formation at the Air-Liquid Interface. *Journal of Physical Chemistry Letters* **12**, 324-329, doi:10.1021/acs.jpclett.0c03319 (2021).
24 Komorek, R. *et al.* Probing sulphur clusters in a microfluidic electrochemical cell with synchrotron-based photoionization mass spectrometry. *Physical Chemistry Chemical Physics* **22**, 14449-14453, doi:10.1039/d0cp02472d (2020).
25 Lu, W. *et al.* Probing growth of metal-organic frameworks with X-ray scattering and vibrational spectroscopy. *Phys Chem Chem Phys* **24**, 26102-26110, doi:10.1039/d2cp04375k (2022).
26 Rundel, J. A. *et al.* Production of Aliphatic-Linked Polycyclic Hydrocarbons during Radical-Driven Particle Formation from Propyne and Propene Pyrolysis. *Combustion and Flame*, 112457 (2022).
27 Rundel, J. A. *et al.* Promotion of particle formation by resonance-stabilized radicals during hydrocarbon pyrolysis. *Combustion and Flame* **243**, 111942 (2022).
28 Wilson, K. R. & Qi, F. Probing chemistry at vacuum ultraviolet synchrotron light sources. *Photoionization and Photo‐Induced Processes in Mass Spectrometry: Fundamentals and Applications*, 159-213 (2021).
29 Zeng, M., Heine, N. & Wilson, K. R. Evidence that Criegee intermediates drive autoxidation in unsaturated lipids. *PNAS* **117**, 4486-4490, doi:10.1073/pnas.1920765117 (2020).
30 Pohl, M. N. *et al.* Photoelectron circular dichroism in angle-resolved photoemission from liquid fenchone. *Physical Chemistry Chemical Physics* **24**, 8081-8092, doi:10.1039/D1CP05748K (2022).
31 Thürmer, S. *et al.* Accurate vertical ionization energy and work function determinations of liquid water and aqueous solutions. *Chemical Science* **12**, 10558-10582, doi:10.1039/D1SC01908B (2021).
32 Mason, P. E. *et al.* Spectroscopic evidence for a gold-coloured metallic water solution. *Nature* **595**, 673-676, doi:10.1038/s41586-021-03646-5 (2021).
33 Malerz, S. *et al.* Low-energy constraints on photoelectron spectra measured from liquid water and aqueous solutions. *Physical Chemistry Chemical Physics* **23**, 8246-8260, doi:10.1039/D1CP00430A (2021).

# Theory of Electronic Structure and Chemical Dynamics

*Martin Head-Gordon, Jin Qian, Eric Neuscamman*
Chemical Sciences Division, Lawrence Berkeley National Laboratory, Berkeley, California 94720.
mhead-gordon@lbl.gov, jqian2@lbl.gov, eneuscamman@lbl.gov

**Scope of the Project:** To expand knowledge of transient species such as radicals relevant to combustion chemistry, atmospheric photochemistry, and other areas including catalysis, new theoretical methods are needed for reliable computer-based prediction of their properties. In electronic structure theory, focus centers on the development of new density functional theory methods and new wave function theories. Newly developed theoretical methods, as well as existing approaches, are employed to study prototype radical reactions, often in collaboration with experimental efforts in the related subtasks (see separate LBNL abstracts). These studies help to deepen understanding of the role of reactive intermediates in diverse areas of chemistry. They also sometimes reveal frontiers where new theoretical developments are needed in order to permit better calculations in the future.

**Recent Progress**

Due to length limitations, only a selection of projects can be summarized here.

*High Accuracy Excited States and Monte Carlo Optimization.* Neuscamman and co-workers have continued to develop excited-state-specific methodologies in both quantum chemistry and quantum Monte Carlo (QMC) and to improve QMC wave function optimization techniques. Recent achievements include verifying the stability of excited-state-specific variance optimization (Otis 2023a) and a demonstration showing that excited-state-specific quantum chemistry orbitals can be used without expensive re-optimization to produce accurate QMC excitation energies for valence, charge transfer, and doubly excited states (Otis 2023b). In the context of core excitations, we have shown that excited state mean field theory and its 2nd order perturbation theory can predict oxygen, nitrogen, and carbon K-edges with a mean unsigned error against experiment of just 0.3 eV, which is competitive with the best density functionals (and better than most!) used in ROKS. (Garner 2020b) Using excited-state-specific QMC offers K-edge accuracy in water, ammonia, and methane of about 0.2 eV, and peak separations within 0.07 eV. (Garner 2020a) Very recent work in collaboration with the Leone group has used high-accuracy quantum chemistry to predict and analyze a novel time-dependent XAS feature arising from geometry-dependent 4-electron spin recoupling. This feature offers a new time-resolved spectroscopic handle for ultrafast probes of photochemical processes. Other recent work shows the statistical benefits that arise from executing determinant selection inside QMC optimizations.

*Orbital optimization and regularization to improve MP2 theory.* Coupled with orbital optimization (OO), regularized MP2 provides a direct path to orbitals free of the delocalization error of DFT, and the over-localization and artificial symmetry-breaking errors of mean-field Hartree-Fock. This has proven useful for diagnosing the presence of strong correlation in transition metals (Shee et al, JCP, 2021), and remarkable improvements in the quality of predictions of non-bonded interactions and transition metal chemistry can be obtained relative to MP2 theory (Shee et al, JPCL, 2021; Rettig et al, 2022). Even vibrational frequencies from CCSD(T) for open shell molecules can be significantly improved in this way (Bertels et al, JCTC, 2021).

*Assessing the predictive power of time-dependent DFT for electronic excited states*. A large-scale benchmark assessment of more than 40 popular or recently developed density functionals for the calculation of 463 vertical excitation energies against the large and accurate QuestDB benchmark set was completed by the Head-Gordon group (Liang et al, J. Chem. Theory Comput. 2022). The functionals ωB97X-D and BMK are found to offer the best performance overall with a root-mean square error (RMSE) of around 0.27 eV, better than the computationally more demanding wavefunction-based methods. The Tamm-Dancoff approximation is recommended. These results provide useful updated guidelines for practical TDDFT calculations.

*On-the-fly excited-state nonadiabatic dynamics:* In collaboration with Steve Cotton and Bill Miller, the Head-Gordon group has developed an efficient implementation of the nonadiabatic couplings

between excited states and nuclear forces associated with that same set of excited states via single excitation configuration interaction (CIS), and time-dependent density functional theory (TDDFT) in the Tamm-Dancoff approximation. This is combined with SQC-MM semiclassical non-adiabatic dynamics to enable direct simulations of nonadiabatic photochemistry and photophysics in polyatomic molecules (Talbot et al, Mol. Phys. 2022). A benchmark assessment of branching ratios in photoexcited NaH comparing exact quantum dynamics, Ehrenfest and SQC-MM yielded very encouraging results (Talbot et al, PCCP 2022), with virtually quantitative agreement between SQC-MM and exact dynamics.

*Chemical Applications:* A rich variety of chemical applications have been completed, including a direct collaboration between the Head-Gordon group and Musa Ahmed (LBNL) on glycerol-water complexes, pre- and post-ionization (Lu et al, 2022), and interactions between the Head-Gordon group and members of the Berkeley catalysis group on mechanistic steps associated with CO2 to CO reduction (Wuttig et al, 2021), novel chemistry related to alkyne cyclotrimerization (Witzke et al, 2020), novel iron-I complexes involving N2 (Witzke et al, 2021), and analysis of the importance of Pauli repulsion in gold-I complexes (Wong et al, 2022). Qian and Ahmed (LBNL) successfully combined plane-wave KS-DFT, Infrared, and Raman Spectroscopies to elucidate the mechanism for crystallization and growth of the metal–organic framework (Lu et al, PCCP, 2022), underpinning future collaborations looking at gas phase chemistries in confined space.

**Future Plans**:

*Multi-configurational excitations and accelerated QMC:* Current and future efforts will focus on two areas: (1) development and use of excited-state-specific multi-configurational wave functions for challenging excitations like core and double excitations, and (2) accelerations to QMC algorithms to broaden the scope of applicability of these high-accuracy methods. Towards the first goal, we are developing a combined methodology of excited-state-specific CASSCF and selected configuration interaction that will connect naturally to our existing QMC methods. Early work in this regard has elucidated core excitations in diradicals, while future investigations will extend to strongly correlated doubly excited states. Towards the second goal, we are exploring a real-space embedding scheme for QMC in which long-range coulomb and exchange interactions are approximated through a novel random sampling scheme. Like other embedding schemes, this will lower computational cost and scaling. We are also developing QMC optimization methods that prune unhelpful wave function flexibility in a way that both improves statistics and reduces cost.

*Analytical hessian evaluation for Van der Waals density functionals.* What we believe to be the first analytical theory and implementation of the hessian for VV10-containing density functionals is being completed by the Head-Gordon group, and is being used to assess the quality of vibrational frequency predictions using modern VV10-containing functionals. Both bonded and non-bonded interactions are being considered.

*Non-empirical regularized perturbation theory.* Beginning from a recent proposal to make second order Brillouin-Wigner perturbation theory extensive, the Head-Gordon group has designed a new theory that is also size-consistent. This theory looks quite promising because it is stable in the zero gap limit, without any adjustable parameters (in contrast to the otherwise very appealing regularized MP2 methods developed over the past few years. A full assessment is underway.

*Efficient real-space KS-DFT development:* Key distinctions persist among the dominant practitioners of Kohn Sham-DFT (KS-DFT). On the one hand, quantum chemists favor orbital-like basis sets (usually gaussian type orbitals) and tend to focus their efforts on isolated molecular systems. In contrast, solid-state physicists leverage plane-wave basis sets (usually coupled with periodic boundary conditions) and tend to focus on descriptions of (quasi-) continuous solids and interfacial systems. Qian group is going to explore and develop a different, physics-driven, and robust theoretical methodology that bridges the knowledge gap between molecular and continuum systems. Specifically, our recent development and implementation of Ab-initio Real-space Electronic Structure code (ARES) based on real-space projection and flexible boundary conditions open up new possibilities to investigate states of missing, additional, or displaced (core and valence) charges. The potential applications for this

development involve core excitation predictions for finite systems from small (a few atoms) to large (>10,000 atoms), thermodynamics and kinetics predictions for gas in confined space (Subtask 2 with Musa Ahmed, LBNL).

*"Digital Twin" for XPS, Infrared, and Raman Spectroscopy:* Directly visualizing the trajectories of electronic and nuclear motion can unravel novel insights into the behaviours of catalysts, gas phase reactions, photo-induced dynamics, and building blocks for quantum information processing. The ability to explicitly identify, track, and tag the exchange of electrons, hence the breaking and reforming of chemical bonds, can be best realized through a close coupling of theory and experiment, aka by creating a "Digital Twin" of various spectroscopies. In contrast to the real-space KS-DFT development effort, Qian group will take a data-centric, software development approach. The input of "Digital Twin" will best mimic the real experimental settings, and output of "Digital Twin" will allow direct comparison between theory and experiment in the exact same format, such as XPS, Infrared, or Raman spectra. We envision that this development will facilitate planning of resource-heavy future experiments, interpret the observations on-the-fly, and intelligently guide the execution of subsequent experiments.

*Collaborative chemical applications:* Collaborative applications to understand XAS in glycerol solutions are underway (Head-Gordon, with Musa Ahmed, LBNL), while a joint paper on hydronium clusters has been submitted. Work continues on modelling oxidative chemistry in aerosols of long-chain hydrocarbons (Head-Gordon, with Kevin Wilson, LBNL), where the computational objective is comparing pathways that proceed by radical addition versus abstraction by radicals, as informed by experimental information on kinetics and product distributions. Revisions to a manuscript describing computational modelling of combustion related reactions involving the reactive growth of unsaturated radicals (Head-Gordon with Hope Michelson, Colorado) showing that unimolecular hydrogen ejection processes may compete with abstraction processes. A manuscript on predicting time-resolved XAS features arising from spin recoupling in the quadruply-open-shell states reached by core excitation of diradicals (Leone and Neuscamman) is in the final editing stages. Going forward, we will continue to pursue opportunities to apply Neuscamman group wave function methods and Head-Gordon group ROKS approaches to problems of interest in the Leone and Neumark groups. Qian and Ahmed will continue their studies of $CO_2$ uptake in metal–organic framework adopting the proposed "Digital Twin" approach. Through DFT screening and kinetic modeling, Qian will also collaborate with Seth Snyder (INL) and Yingchao Yang (University of Maine) to look at promising wood-derived activated carbon for Direct Air Capture.

## Recent Publications Citing DOE Support (2020-2023)


- Aljama, H.; Head-Gordon, M.; Bell, A.T., Assessing the stability of Pd-exchanged sites in zeolites with the aid of a high throughput quantum chemistry workflow. Nature Comm. **2022**, *13*, 2910, DOI 10.1038/s41467-022-29505-z.
- Bergman, H.M.; Beattie, D.D.; Handford, R.C.; Rossomme, E.; Suslick, B.A.; Head-Gordon, M.; Cundari, T.R.; Liu, Y.; Tilley, T.D., Copper(III) Metallacyclopentadienes via Zirconocene-Transfer and Reductive Elimination to an Isolable Phenanthrocyclobutadiene. *J. Am. Chem. Soc*. **2022**, *144*, 9853−9858, DOI 10.1021/jacs.2c02581.
- Bertels, L.W.; J. Lee, and M. Head-Gordon, "Polishing the Gold Standard: The Role of Orbital Choice in CCSD(T) Vibrational Frequency Prediction", J. Chem. Theory Comput. 17, 742-755 (2021); doi: 10.1021/acs.jctc.0c00746
- Chang, K.F.; M. Reduzzi, H. Wang, S.M. Poullain, Y. Kobayashi, L. Barreau, D. Prendergast, D.M. Neumark, and S.R. Leone, "Revealing electronic state-switching at conical intersections in alkyl iodides by ultrafast XUV transient absorption spectroscopy", Nat. Commun. 11, 4042 (2020); doi: 10.1038/s41467-020-17745-w
- Epifanovsky, E.; A.T.B. Gilbert, X. Feng, J. Lee, Y. Mao, N. Mardirossian, P. Pokhilko, A.F. White et al, "Software for the frontiers of quantum chemistry: An overview of developments in the Q-Chem 5 package", J. Chem. Phys. 155, 084801 (2021); doi: 10.1063/5.0055522.
- Eriksen, J.; T.A. Anderson, J.E. Deustua, K. Ghanem, D. Hait, M.R. Hoffmann, S. Lee, D. Levine, I. Magoulas, J. Shen, N. Tubman, K.B. Whaley, E. Xu, Y. Yao, N. Zhang, A. Alavi, G. Chan, M. Head-Gordon, W. Liu, P.

Piecuch, S. Sharma, S. Ten-no, C. Umrigar, J. Gauss, “The Ground State Electronic Energy of Benzene”, J. Phys. Chem. Lett. 11, 8922−8929 (2020); doi: 10.1021/acs.jpclett.0c02621
- Garner, S. M.; Neuscamman, E., A variational Monte Carlo approach for core excitations, *J. Chem. Phys.*, **2020**, 153, 144108; doi: 10.1063/5.0020310
- Garner, S. M.; Neuscamman, E., Core Excitations with Excited State Mean Field and Perturbation Theory. *J. Chem. Phys.* **2020**, 153, 154102; doi: 10.1063/5.0020595
- Gobi, S.; Z. Lin, C. Zhu, M. Head-Gordon and R.I. Kaiser, “Oxygen Isotope Exchange Between Carbon Dioxide and Iron Oxides on Mars’ Surface”, J. Phys. Chem. Lett. 13, 2600−2606 (2022); doi: 10.1021/acs.jpclett.2c00289
- Hait, D.; Y.H. Liang, and M. Head-Gordon, "Too big, too small or just right? A benchmark assessment of density functional theory for predicting the spatial extent of the electron density of small chemical systems", J. Chem. Phys. 154, 074109 (2021); doi: 10.1063/5.0038694
- Liang, J.; Feng, X.; Hait, D.; Head-Gordon, M., Revisiting the performance of time-dependent density functional theory for electronic excitations: Assessment of 43 popular and recently developed functionals from rungs one to four. *J. Chem. Theory Comput.* **2022**, *18*, 3460–3473, DOI 10.1021/acs.jctc.2c00160
- Loipersberger, M.; L.W. Bertels, J. Lee, and M. Head-Gordon, “Exploring the Limits of Second- and Third-Order Møller-Plesset Perturbation Theory for Non-Covalent Interactions: Revisiting MP2.5 and Assessing the Importance of Regularization and Reference Orbitals”, J. Chem. Theory Comput. 17, 5582–5599 (2021); doi: 10.1021/acs.jctc.1c00469
- Lu, W.; C.J. Mackie, B. Xu, M. Head-Gordon and M. Ahmed, “A computational and experimental view of hydrogen bonding in glycerol water clusters”, J. Phys. Chem. A 126, 1701−1710 (2022); doi: 10.1021/acs.jpca.2c00659
- Otis, L.; Neuscamman, E., Optimization Stability in Excited-State-Specific Variational Monte Carlo, *J. Chem. Theory Comput.* 19, 767 (2023); doi: 10.1021/acs.jctc.2c00642
- Otis, L.; Neuscamman, E., A promising intersection of excited-state-specific methods from quantum chemistry and quantum Monte Carlo, *WIREs Comput Mol Sci.* e1659 (2023); doi: 10.1002/wcms.1659
- Rettig, A.; D. Hait, and M. Head-Gordon, "Third order Moller-Plesset theory made more useful? The role of density functional theory orbitals", J. Chem. Theory Comput. 16, 7473-7489 (2020); doi: 10.1021/acs.jctc.0c00986
- “Revisiting the Orbital Energy Dependent Regularization of Orbital Optimized Second Order Moller-Plesset Theory”, A. Rettig, J. Shee, J. Lee and M. Head-Gordon, J. Chem. Theory Comput. 18, 9, 5382–5392 (2022); doi: 10.1021/acs.jctc.2c00641
- Shee, J.; M. Loipersberger, D. Hait, J. Lee and M. Head-Gordon, “Revealing the nature of electron correlation in transition metal complexes with symmetry-breaking and chemical intuition”, J. Chem. Phys. 154, 194109 (2021); doi: 10.1063/5.0047386
- Shee, J.; M. Loipersberger, A. Rettig, J. Lee, M. Head-Gordon, “Regularized Second-Order Møller−Plesset Theory: A More Accurate Alternative to Conventional MP2 for Noncovalent Interactions and Transition Metal Thermochemistry for the Same Computational Cost”, J. Phys. Chem. Lett. 12, 12084-12097 (2021); doi: 10.1021/acs.jpclett.1c03468
- Talbot, J.J.; M. Head-Gordon, W.H. Miller and S.J. Cotton, “Dynamic signatures of electronically nonadiabatic coupling in sodium hydride: a rigorous test for the symmetric quasi-classical model applied to realistic, ab initio electronic states in the adiabatic representation”, Phys. Chem. Chem. Phys. 24, 4820–4831 (2022); doi: 10.1039/d1cp04090a
- Talbot, J.J. ; M. Head-Gordon, and S.J. Cotton, “The symmetric quasi-classical model using on-the-fly time-dependent density functional theory within the Tamm-Dancoff approximation”, Mol. Phys. e215376 (2022); doi: 10.1080/00268976.2022.2153761
- Tubman, N.M., C.D. Freeman, D.S. Levine, D. Hait, M. Head-Gordon, K.B. Whaley, “Modern Approaches to Exact Diagonalization and Selected Configuration Interaction with the Adaptive Sampling CI Method”, J. Chem. Theory Comput. 16, 2139-2159 (2020); doi: 10.1021/acs.jctc.8b00536
- Witzke, R.; D. Hait, K. Chakarawet, M. Head-Gordon, and T. D. Tilley, “Bimetallic Mechanism for Alkyne Cyclotrimerization with a Two-Coordinate Fe Precatalyst”, ACS Catal. 10, 7800−7807 (2020); doi: 10.1021/acscatal.0c01828
- Witzke, R.; D. Hait, M. Head-Gordon, T.D. Tilley, “Two-Coordinate Iron(I) Complexes on the Edge of Stability: Influence of Dispersion and Steric Effects”, Organometallics 40, 1758–1764 (2021); doi: 10.1021/acs.organomet.1c00218

- Wong, Z.R.; Schramm, T.K.; Loipersberger, M.; Head-Gordon, M.; Toste, F.D., Revisiting the Bonding Model for Gold(I) Species: The Importance of Pauli Repulsion Revealed in a Gold(I)-Cyclobutadiene Complex. Angew. Chem. **2022**, *61*, e202202019, DOI 10.1002/anie.202202019
- Wuttig, A.; J. Derrick, M. Loipersberger, A. Snider, M. Head-Gordon, C.J. Chang, and F.D. Toste, "Controlled Single Electron Transfer via Metal-Ligand Cooperativity Drives Divergent Nickel Electrocatalyzed Radical Pathways", J. Am. Chem. Soc. 143, 6990-7001 (2021); doi: 10.1021/jacs.1c01487

# SPECTROSCOPY AND DYNAMICS OF REACTION INTERMEDIATES IN COMBUSTION CHEMISTRY

Marsha I. Lester
Department of Chemistry
University of Pennsylvania
Philadelphia, PA 19104-6323
milester@sas.upenn.edu

## I. Program Scope

Our research aims to characterize important, yet often elusive, reaction intermediates in combustion chemistry using novel spectroscopic and dynamical methods. A recent thrust is focused on characterizing hydroperoxyalkyl radical intermediates (•QOOH) containing a carbon radical center (•Q), which are important intermediates in low temperature combustion of hydrocarbon fuels and atmospheric oxidation of volatile organic compounds. In addition, our research continues to focus on carbonyl oxides (Criegee intermediates, $R_1R_2C{=}O^+O^-$) with novel zwitterionic character, which are important intermediates in tropospheric hydrocarbon oxidation and some combustion reactions.

## II. Recent Progress

### A. Infrared spectroscopy and unimolecular dissociation dynamics of •QOOH

A recent focus of our research has centered on the infrared (IR) spectroscopy and unimolecular dissociation dynamics of prototypical hydroperoxyalkyl radical (•QOOH) intermediates. We have characterized the carbon-centered •QOOH radical transiently formed in isobutane oxidation and, most recently, a partially deuterated •QOOD analog.[1,2] $\bullet CH_2(CH_3)_2COOD$ was generated in the laboratory by H-atom abstraction from partially deuterated *tert*-butyl hydroperoxide, $(CH_3)_3COOD$. IR spectral features associated with jet-cooled and isolated •QOOD radicals were observed in the vicinity of the transition state (TS) barrier leading to OD radical and cyclic ether products. The overtone OD stretch ($2\nu_{OD}$) and a combination band ($\nu_{CH_2} + \delta_{HCH}$) of •QOOD were identified by IR action spectroscopy with UV laser-induced fluorescence detection of OD products. Direct time-domain measurement of the unimolecular dissociation rate for •QOOD ($2\nu_{OD}$) extended prior rate measurements for •QOOH. The analogous unimolecular decay rates for •QOOH and •QOOD at similar energies, after accounting for small changes in zero-point energy, demonstrated that the heavy atom tunneling predicted for •QOOH/D is essentially unaffected by deuteration of the hydroperoxy (–OOH/D) group. Comparison of the unimolecular decay rates obtained experimentally with those predicted theoretically for both •QOOH and •QOOD confirm that unimolecular decay is enhanced by heavy-atom tunneling involving simultaneous O-O bond elongation and C-C-O angle contraction along the reaction pathway.

### B. Electronic spectroscopy and photoinitiated dynamics

We continued our investigation of the electronic spectroscopy and photodissociation dynamics of Criegee intermediates ($R_1R_2C{=}O^+O^-$) with different structural motifs, conformations, and conjugation. Specifically, we carried out a systematic laboratory study of substituent effects on the electronic spectroscopy of four-carbon Criegee intermediates (CIs) with methyl-ethyl [$(CH_3)(CH_3CH_2)COO$, MECI] and isopropyl [$(CH_3)_2(H)COO$, IPCI] groups,[3] which are isomers produced in ozonolysis of asymmetric branched alkenes. We separately generated and spectroscopically characterized the jet-cooled CIs on the strong $\pi^* \leftarrow \pi$ transition associated with the carbonyl oxide group utilizing UV-induced depletion of the m/z 88 photoionization signal at 118 nm. The resultant broad and unstructured UV spectral features for MECI and IPCI are peaked at ca. 320 and 330 nm, respectively, with large absorption cross-sections of ca. $10^{-17}$ $cm^2$. Comparisons were made with prior studies of the four-carbon CIs formed in isoprene

ozonolysis, methyl vinyl ketone oxide [$(CH_2=CH)(CH_3)COO$, MVK-oxide] and methacrolein oxide [$(CH_2=C)(CH_3)CHOO$, MACR-oxide], which have the same backbone connectivity as MECI and IPCI, but have extended conjugation across the vinyl and carbonyl groups. A remarkable 50 nm shift of the peak absorption to longer wavelength is observed for MVK-oxide and MACR-oxide, respectively, confirming that the spectral shifts are caused by the extended $\pi$ conjugation in the isoprene-derived CIs.

We also characterized the electronic spectroscopy of 2-butenal oxide [$(CH_3CH=CH)CHOO$], an isomer of the four-carbon CIs derived from isoprene ozonolysis, which differ from one another in the position of the methyl group.[4] Again, the electronic spectrum is recorded using a UV-induced ground state depletion method with photoionization detection on the parent mass (m/z 86). The primary peak of the electronic spectrum, attributed to one or more of its 8 conformation forms, is observed at ca. 375 nm and resembles those of isomeric MVK-oxide and MACR-oxide. The electronic spectrum of 2-butenal oxide extends into the visible region and is shifted to considerably longer wavelength (ca. 50 nm) than $CH_2OO$ or alkyl-substituted CIs.

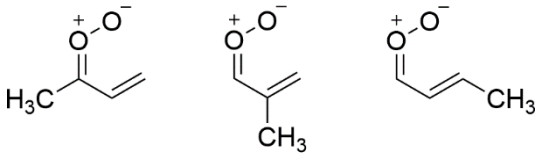


Scheme 1. Chemical structures of structurally similar Criegee intermediates with methyl and vinyl substituents, noting that each has multiple low energy conformers.

Electronic excitation of 2-butenal oxide results in nonadiabatic coupling and rapid dissociation to O ($^1$D) + 2-butenal products, which is observed as anisotropic velocity map images of O ($^1$D) products detected by 2+1 REMPI. The total kinetic energy (TKER) distributions obtained at various excitation wavelengths extend over the full range of energy available. Simulations of the TKER distributions based on a reduced impulsive model that accounts for the geometric coordinates and vibrational modes that change significantly upon dissociation, e.g. C=O, provide a very good representation of the TKER distribution. Notably lower and narrower TKER distributions are obtained for MVK-oxide. Analysis using a reduced impulsive model indicated activation of hindered rotation of the methyl group originating from 60° reorientation of the methyl group from MVK-oxide to MVK, which is distinctly different from the dissociation dynamics of 2-butenal oxide or MACR-oxide.

### C. Photoionization mass spectrometry studies

In the past year, we extended our collaboration with Klippenstein, Caravan, and Taatjes on the thermal unimolecular decay and bimolecular chemistry of Criegee intermediates utilizing the Sandia Multiplexed Photoionization Mass Spectrometer (MPIMS) at the Advanced Light Source. Although unimolecular decay of alkyl-substituted CIs generally proceeds via 1,4 H-atom transfer followed by O-O bond fission that releases OH radicals, we also observe roaming of the separating OH radicals that form stable hydroxycarbonyl products.[5] Specifically, hydroxybutanone (m/z 88) has been detected as exponential rise to a persistent stable product (ca. 7% yield) from roaming in the unimolecular decay of the methyl-ethyl substituted Criegee intermediate (MECI) under thermal flow cell conditions. A weaker methyl vinyl ketone (MVK) signal is attributed to a stable product formed in parallel with the unimolecular decay of MECI. Roaming via reorientation and addition of OH to the vinyl group of the butanonyl co-product is shown to yield hydroxybutanone, and subsequent C-O elongation and H-transfer can lead to MVK. Klippenstein has carried out a comprehensive ab initio kinetic analysis to evaluate minimum energy pathways, rate constants, and branching yields for thermal unimolecular decay of MECI under laboratory and atmospheric conditions, demonstrating a significant yield of roaming products under both conditions.

## III. Ongoing and Future Work

Current and future experiments are expanding our studies from acyclic to cyclic •QOOH radicals. The infrared spectrum and time-resolved unimolecular decay dynamics of a cyclic •QOOH radical formed transiently during cycloalkane oxidation is being investigated using an analogous IR pump-UV probe scheme. The experimental results are then compared with computed anharmonic frequencies and statistical unimolecular decay rates predicted by statistical RRKM theory.

We are also continuing our collaboration with Caravan and Taatjes to examine the rates and products of bimolecular reactions of CIs – with and without extended conjugation – involving key atmospheric species (water vapor, $SO_2$, formic acid, $NO_2$). These bimolecular reactions involve remarkably different types of mechanisms, 1,2 addition, 1,4 addition, and secondary ozonide (SOZ) formation, which form more highly oxygenated products with greater mass.

## IV. References


1. A. S. Hansen, T. Bhagde, K. B. Moore, D. R. Moberg, A. W. Jasper, Y. Georgievskii, M. F. Vansco, S. J. Klippenstein and M. I. Lester, *Science* **373**, 679 (2021).
2. T. Bhagde, A. S. Hansen, S. Chen, P. J. Walsh, S. J. Klippenstein, and M. I. Lester, *Faraday Discuss.* **238**, 575-588 (2022).
3. T. Liu, M. Zou, A. Caracciolo, C. A. Sojdak, and M. I. Lester, *J. Phys. Chem. A* **126**, 6734-6741 (2022).
4. G. Wang, T. Liu, M. Zou, C. A. Sojdak, M. C. Kozlowski, T. Karsili, and M. I. Lester, *J. Phys. Chem. A* **127**, 203-215 (2022).
5. T. Liu, S. N. Elliott, M. Zou, M. F. Vansco, C. A. Sojdak, C. R. Markus, R. Almeida, K. Au, L. Sheps, D. L. Osborn, F. A. F. Winiberg, C.J. Percival, C. A. Taatjes, R. L. Caravan, S. J. Klippenstein, and M. I. Lester, submitted (2023).


## V. Publications supported by this DOE project (2020-present)


1. R. L. Caravan, M. F. Vansco, K. Au, M. A. H. Khan, Y.-L. Li, F. A. F. Winiberg, K. Zuraski, Y.-H. Lin, W. Chao, N. Trongsiriwat, P. J. Walsh, D. L. Osborn, C. J. Percival, J. Jr-M. Lin, D. E. Shallcross, L. Sheps, S. J. Klippenstein, C. A. Taatjes, and M. I. Lester, "Direct kinetic measurements and theoretical predictions of an isoprene-derived Criegee intermediate", *Proc. Natl. Acad. Sci.* **117**, 9733-9740 (2020). https://doi.org/10.1073/pnas.1916711117
2. M. F. Vansco, R. L. Caravan, K. Zuraski, F. A. F. Winiberg, K. Au, N. Trongsiriwat, P. J. Walsh, D. L. Osborn, C. J. Percival, M. A. H. Khan, D. E. Shallcross, C. A. Taatjes, and M. I. Lester, "Experimental evidence of dioxole unimolecular decay pathway for isoprene-derived Criegee intermediates", *J. Phys. Chem. A* **124**, 3542-3554 (2020). https://doi.org/10.1021/acs.jpca.0c02138
3. M. F. Vansco, R. L. Caravan, S. Pandit, K. Zuraski, F. A. F. Winiberg, K. Au, T. Bhagde, N. Trongsiriwat, P. J. Walsh, D. L. Osborn, C. J. Percival, S. J. Klippenstein, C. A. Taatjes, and M. I. Lester, "Formic Acid Catalyzed Isomerization and Adduct Formation of an Isoprene-Derived Criegee Intermediate: Experiment and Theory", *Phys. Chem. Chem. Phys* **22,** 26796-26805 (2020). https://doi.org/10.1039/D0CP05018K
4. R. L. Caravan, M. F. Vansco, and M. I. Lester, "Open questions on the reactivity of Criegee intermediates", *Commun. Chem*. **4**, 44 (2021). https://rdcu.be/chswf
5. V. J. Esposito, T. Liu, G. Wang, A. Caracciolo, M. F. Vansco, B. Marchetti, T. Karsili, and M. I. Lester, "Photodissociation Dynamics of $CH_2OO$ on Multiple Potential Energy Surfaces: Experiment and Theory", *J. Phys. Chem. A* **125**, 6571-6579 (2021). https://doi.org/10.1021/acs.jpca.1c03643
6. A. S. Hansen, T. Bhagde, K. B. Moore III, D. R. Moberg, A. W. Jasper, Y. Georgievskii, M. F. Vansco, S. J. Klippenstein, and M. I. Lester, "Watching a Hydroperoxyalkyl Radical (•QOOH) Dissociate", *Science* **373**, 679-682 (2021).

7. M. F. Vansco, K. Zuraski, F. A. F. Winiberg, K. Au, N. Trongsiriwat, P. J. Walsh, D. L. Osborn, C. J. Percival, S. J. Klippenstein, C. A. Taatjes, M. I. Lester, and R. L. Caravan, "Functionalized Hydroperoxide Formation from the Reaction of Methacrolein-oxide, an Isoprene-Derived Criegee Intermediate, with Formic Acid: Experiment and Theory", *Molecules* **26**, 3058 (2021). https://doi.org/10.3390/molecules26103058
8. G. Wang, T. Liu, A. Caracciolo, M. F. Vansco, N. Trongsiriwat, P. J. Walsh, B. Marchetti, T. Karsili, and M. I. Lester, "Photodissociation Dynamics of Methyl Vinyl Ketone Oxide: A four-carbon unsaturated Criegee intermediate from isoprene ozonolysis", *J. Chem. Phys.* **155**, 174305 (2021). https://doi.org/10.1063/5.0068664
9. M. F. Vansco, M. Zou, I. O. Antonov, K. Ramasesha, B. Rotavera, D. L. Osborn, Y. Georgievski, C. J. Percival, S. J. Klippenstein, C. A. Taatjes, M. I. Lester, and R. L. Caravan, "Dramatic conformer-dependent reactivity of the acetaldehyde oxide Criegee intermediate with dimethylamine via a 1,2-insertion mechanism", *J. Phys. Chem. A* **126**, 710–719 (2022). https://doi.org/10.1021/acs.jpca.1c08941
10. T. Bhagde, A. S. Hansen, S. Chen, P. J. Walsh, S. J. Klippenstein, and M. I. Lester, "Energy-resolved and time-dependent unimolecular dissociation of hydroperoxyalkyl radicals (•QOOH)", *Faraday Discuss.* **238**, 575 – 588 (2022). https://doi.org/10.1039/D2FD00008C
11. T. N. V. Karsili, B. Marchetti, M. I. Lester and M. N. R. Ashfold, "Electronic Absorption Spectroscopy and Photoinitiated Chemistry of Criegee Intermediates", *J. Photochem. Photobiol.* (2022). http://doi.org/10.1111/php.13665
12. V. J. Esposito, T. A. McHenry, and M. I. Lester, "Photoionization energetics and dissociation pathways of hydroperoxyethyl formate produced in the reaction of $CH_3CHOO$ + formic acid", *Chem. Phys. Lett.* **809**, 140179 (2022). https://doi.org/10.1016/j.cplett.2022.140179
13. T. Liu, M. Zou, A. Caracciolo, C. A. Sojdak, and M. I. Lester, "Substituent effects on the electronic spectroscopy of four-carbon Criegee intermediates", *J. Phys. Chem. A* 126, 6734-6741 (2022). https://doi.org/10.1021/acs.jpca.2c05502
14. G. Wang, T. Liu, M. Zou, C. A. Sojdak, M. C. Kozlowski, T. Karsili, and M. I. Lester, "Electronic Spectroscopy and Dissociation Dynamics of Vinyl-Substituted Criegee Intermediates: 2-Butenal Oxide and Comparison with Methyl Vinyl Ketone Oxide and Methacrolein Oxide Isomers", *J. Phys. Chem. A* **127**, 203–215 (2022). https://doi.org/10.1021/acs.jpca.2c08025
15. G. Wang, T. Liu, M. Zou, T. Karsili, and M. I. Lester, "UV Photodissociation Dynamics of the Acetone Oxide Criegee Intermediate: Experiment and Theory", *Phys. Chem. Chem Phys.* **25**, 7453-7465 (2023). https://doi.org/10.1039/D3CP00207A

# Chemistry of Ammonia-Based Fuels

Paul Marshall
Department of Chemistry and Center for Advanced Scientific Computing and Modeling
University of North Texas, 1155 Union Circle #305070, Denton, TX 76203
E-mail marshall@unt.edu

## Program Scope

Ammonia can serve as a carbon-free energy transfer fuel when it is synthesized from green sources of energy such as wind, solar or hydroelectric. Liquid ammonia is relatively easily transported (by comparison to liquid hydrogen) and can be catalytically decomposed to release hydrogen for use in fuel cells, or directly burned for energy release, for example, as a substitute for diesel fuel. There are indications that ammonia's ignition and engine properties are improved by mixing with conventional fuel. This study is aimed at understanding the combustion chemistry of ammonia alone and in conjunction with hydrocarbons, so that with a reliable chemical mechanism, engines can be modified or designed intelligently.

Species to be considered are ammonia ($NH_3$) and the primary product of radical attack, amino radicals ($NH_2$). Recombination of a pair of $NH_2$ radicals leads to hydrazine ($N_2H_4$). Oxidation of $NH_2$ leads to nitrogen oxide intermediates and species such as $NH_2O$ and $NH_3O$. Cross reactions with hydrocarbons, such as recombination of $NH_2$ and $CH_3$, will form amines (and perhaps unsaturated imines) and subsequent chemistry of the exemplar methylamine ($CH_3NH_2$) and related species will be investigated. Key radicals in high-temperature combustion are H and OH, where the rapid diffusion of atomic hydrogen in particular influences flame speed. In the ignition regime, below 1000 K, hydroperoxy ($HO_2$) radicals have important roles in determining ignition delay. Reactions with $O_2$ allow for initial attack on fuel molecules and radical formation, and can provide chain-branching at high temperatures. These systems will be studied both by theory and experiments, in the context of isolated elementary reactions and in multireaction systems, to gain fundamental insight into nitrogen chemistry, to permit detailed comparisons with theory, and to create a quantitative mechanism for combustion of ammonia/hydrocarbon mixtures.

## Recent progress

Laser-photolysis laser-induced fluorescence is applied to measure radical kinetics under conditions (low concentration and short time) where single elementary reactions dominate the measured species profiles. Exploration of $NH_2$ chemistry is the first experimental target, and the rate constant $k_1$ for

$$NH_2 + N_2H_4 \rightarrow \text{products} \quad (1)$$

was measured at room temperature. We obtained the temperature dependence via Multistructural Improved Canonical Variational Transition State Theory with Small Curvature Tunneling, with geometries and scaled frequencies obtained with M06-2X/6-311+G(2df,2p) theory, and single-point energies from CCSD(T)-F12b/cc-pVTZ-F12 theory, plus a term to correct approximately for electron correlation through CCSDT(Q). Theory and experiment matched with a -2.8 kJ $mol^{-1}$ correction to the calculated barrier height.

Figure 1 shows good accord with the empirical estimate of Dean and Bozzelli, but our $k_1$ is much larger than the only other quantum chemistry work, by Li and Zhang, and much smaller than that measured by Gehring et al. Modeling their reaction conditions indicates low sensitivity to reaction 1. Modeling of hydrazine decomposition experiments in shock tubes by Michel and Wagner showed sensitivity to reaction 1, behind N-N bond dissociation, although the half-life was underpredicted by up to

a factor of 3. Further analysis of $N_2H_4$ dissociation with Glarborg and Troe has been accepted for publication.

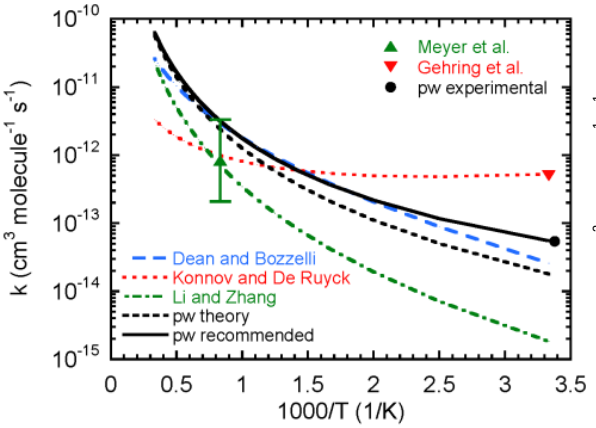


**Figure 1.** LP-LIF measurement and calculation for $NH_2 + N_2H_4$ and literature data.

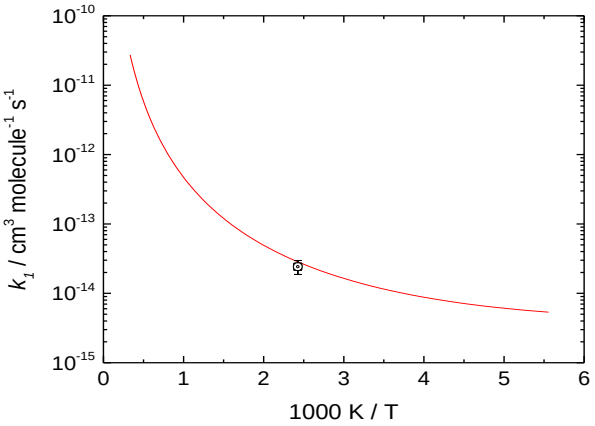


**Figure 2.** LP-LIF measurement and calculation for $NH_2 + H_2O_2$.

A similar strategy of measurements combined with calculations and analysis has been applied to

$$NH_2 + H_2O_2 \rightarrow NH_3 + HO_2 \quad (2)$$

and the results are shown in Fig. 2. There are no other experiments for comparison, but we note that for the reverse reaction (relevant to $HO_2$ chemistry connected to ignition delay) our results agree well with the 1000 K value obtained by Cavalotti et al. with EStokTP.

Our measurements over 290 – 640 K, plotted in Fig. 3, for

$$NH_2 + CH_2O \rightarrow \text{products} \quad (3)$$

indicate an activation energy $E_a$ of ca. 19 kJ mol$^{-1}$, by contrast to computational predictions by Barone and coworkers of a barrierless path to $H + HCONH_2$. We agree that computationally this channel to formamide is more favorable than direct formation of $NH_3 + HCO$, as seen in our PES below, but not with a zero barrier. Barriers from W1Usc and CCSD(T)-F12 theory are in accord with the measured $E_a$.

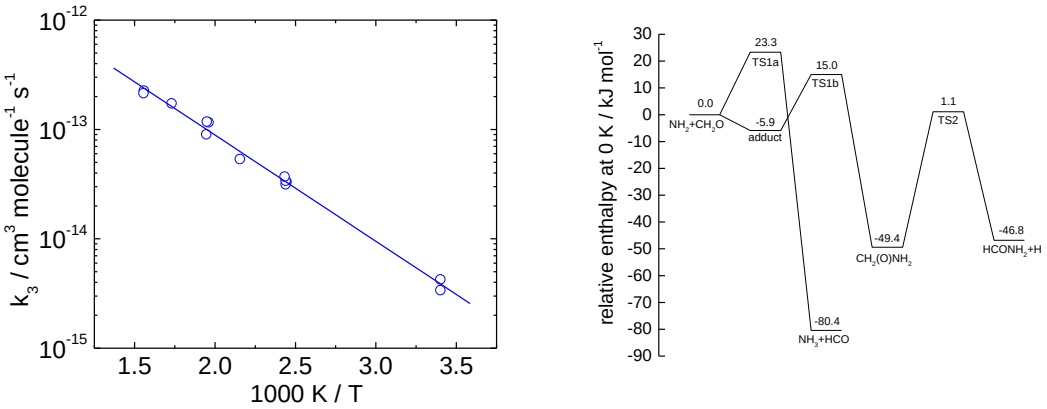


**Figure 3.** Arrhenius plot of LP-LIF measurements for $NH_2 + CH_2O$ (left) and the W1Usc PE diagram (right).

Further chemistry of $NH_2$ has been explored computationally, again based on M06-2X density functional and the 6-311++G(2df,2p) basis set for geometries and, after scaling, for zero-point vibrational energy and for fundamental frequencies used in partition functions. Relative enthalpies are obtained via direct extrapolation of coupled cluster CCSD(T) energies to the complete basis set limit, and the CBS-APNO approximation. A contribution was made to mechanistic interpretation of dimethyl ether (DME,

$CH_3OCH_3$) co-combustion with $NH_3$, probed via ignition delays measured in a rapid Compression Machine at the University of Groningen. Kinetics for

$$NH_2 + CH_3OCH_3 \rightarrow NH_3 + CH_2OCH_3 \quad (4)$$

and the thermochemistry and bond strengths in $CH_3OCH_2NH_2$ were computed.

Mechanistic interpretation of experiments at Technical University of Braunschweig on ammonia/methanol mixtures was assisted by evaluation of $k_{5a}$ and $k_{5b}$ for

$$NH_2 + CH_3OH \rightarrow NH_3 + CH_2OH \quad (5a)$$

$$\rightarrow NH_3 + CH_3O \quad (5b)$$

based on Canonical Variational Transition State Theory with internal torsions treated as uncoupled 1-D rotors. Tunneling was assessed from the curvature at the top of the vibrationally adiabatic barrier and the Eckart model. It is planned to return to these processes using MS-CVT at a later date. Modeling indicated that addition of methanol to ammonia fuel speeds ignition through increased [$HO_2$] and [OH] while recycling $NH_2$ back to $NH_3$ via reaction 5.

A recent theory/modeling study focused on the sometimes-included reaction $NH_2 + NH_3 \rightleftarrows N_2H_3 + H_2$ with the conclusion that there is no moderate barrier direct pathway or via an $N_2H_5$ intermediate, and that for several scenarios multireaction modeling can match observations without assuming this process.

There has been some question about the high-pressure limit for

$$NH_3 + M \rightleftarrows NH_2 + H + M \quad (6)$$

with shock-tube experiments interpreted to yield $k_{-6,\infty}$ values for $NH_2 + H$ recombination of $2 \times 10^{12}$ to $2 \times 10^{14}$ $cm^3$ $mol^{-1}$ $s^{-1}$. Searches with multireference CASSCF-MP2 theory revealed no tight transition state and classical capture theory based on long-range dispersion interactions yielded $k_{-6,\infty} \approx 6.5 \times 10^{14}$ $cm^3$ $mol^{-1}$ $s^{-1}$ at 298 K and proportional to $T^{1/6}$. This result supports the idea that most experiments are at the low-pressure limit for reaction 6 and a mechanism for ammonia pyrolysis that incorporates a recommended $k_{-6,\infty} = (4 \pm 2) \times 10^{14}$ $cm^3$ $mol^{-1}$ $s^{-1}$ has been published. A collaboration with Troe is to explore the possibility of dissociation via triplet pathways.

Potential energy surfaces for the reaction of $CH_3NH_3$, and its subsequent products, with molecular $O_2$ have been investigated. Derived reaction enthalpies showed a rms error below 2 kJ $mol^{-1}$ when compared to data from the Active Thermochemical Tables. Rate constants were derived with simple Canonical Transition State Theory for the following processes:

$$CH_3NH_2 + O_2 \rightarrow HO_2 + CH_2NH_2 \text{ and } CH_3NH \quad (7)$$

$$CH_2NH_2 \text{ and } CH_3NH + O_2 \rightarrow HO_2 + CH_2NH \quad (8)$$

$$CH_2NH + O_2 \rightarrow HO_2 + HCNH \text{ and } H_2CN \quad (9)$$

The associated process

$$CH_2NH_2 \rightleftarrows CH_3NH \quad \text{(high-pressure limit)} \quad (10)$$

was also characterized. Some of these reactions have been investigated before in the context of atmospheric chemistry. Thermochemistry and kinetics were derived for high-temperatures, and incorporated into a mechanism that successfully rationalized explosion limits for $CH_3NH_2$ and its oxidation in a fast flow reactor. Work remains to reach quantitative agreement with flame speeds and oxidation in the presence of high NO concentrations.

The high pressures and high $NH_3$ concentrations that arise with use of $NH_3$ as a fuel, rather than as a model for a fuel-nitrogen source of $NO_x$, mean that diamine formation may be important. Our published study focused on diazene (HNNH), emphasizing reactions of the Z (*cis*) isomer, as well as the more usually studied and more stable E (*trans*) isomer. There is also the higher energy *ipso* $H_2NN$ isomer. Pathways that interconvert the isomers, and formation and consumption reactions, were addressed, and low-pressure, falloff and high-pressure behaviors were quantified. One observation is that Z HNNH dissociation to H + NNH is almost two orders of magnitude faster than for the E isomer at atmospheric pressure. There are substantial barriers to E $\rightleftarrows$ Z for both bending and twisting pathways, so at low, ignition temperatures they may need to be treated as distinct species, while at high temperatures interconversion is fast and partial equilibrium may be attained.

Details of the current quantitative mechanism for oxidation and pyrolysis of $NH_3$, $N_2H_4$ and related compounds developed to date are contained in publications 4, 7 and 8 below.

**Future Plans**

Experiments with resonance fluorescence detection of H atoms will be applied to the kinetics of H + $CH_3NH_2$. Theory will help assess H-abstraction from C-H vs N-H, and possible pathways to $CH_4$ + $NH_2$ and $CH_3$ + $NH_3$. Proposed extensions of $NH_2$ chemistry include its kinetics with biofuels and diesel surrogates. Product studies of H and O-atom reactions with $N_2O$, a greenhouse gas potentially formed during ammonia oxidation, are aimed at improving understanding of these processes that destroy $N_2O$ in flames. These product studies will include ca. 1 atm pressure discharge-flow experiments. In preliminary work we found a microwave plasma hard to sustain at such pressures, and we are presently constructing an inductively-coupled plasma apparatus with an on-hand radio frequency generator.

Our UV photolysis cell with FT-IR detection will be modified for high-temperature photochemistry, to investigate the reactivity and product formation for $NH_3$ and $CH_3NH_2$ reactions, initially with O atoms. Computationally, the unimolecular reactions of methylamine and ethylamine will be examined because the reverse of C-N bond breaking couples regular hydrocarbon chemistry and ammonia chemistry. Theoretical work is on-going for HN=NH, while experiments are planned on a stable imine, $(CF_3)_2C$=NH, to compare with calculations. Mechanism development in collaboration with Glarborg will continue, and species for further evaluation include $NH_2O$.

**DOE Sponsored Publications from current grant 2020-2023**


1. "Oxidation of Methylamine" P. Glarborg, C.S. Andreasen, H. Hashemi, R. Qian and P. Marshall, Int. J. Chem. Kinet., 52, 893-906 (2020).
2. "Ignition Delay Times of $NH_3$/DME Blends at High Pressure and Low DME fraction: RCM Experiments and Simulations" L. Dai, H. Hashemi, P. Glarborg, S. Gersen, P. Marshall, A. Mokhov and H. Levinsky, Combust. Flame, 227, 120-134 (2021).
3. "New Reactions of Diazene and Related Species for Modeling Combustion of Amine Fuels" P. Marshall, G. Rawling and P. Glarborg, Mol. Phys., 119, e1979674 (2021).
4. "Challenges in Kinetic Modeling of Ammonia Pyrolysis" P. Glarborg, H. Hamid and P. Marshall, Fuel Commun., 10, 100049 (2022).
5. "An Experimental and Modeling Study on Auto-Ignition Kinetics of Ammonia/Methanol Mixtures at Intermediate Temperature and High Pressure" M. Li, X. He, H. Hashemi, P. Glarborg, V.M. Lowe, P. Marshall, R. Fernandes and B. Shu, Combust. Flame, 242, 112160 (2022).
6. "Experimental and Computational Studies of the Kinetics of the Reaction of Hydrogen Peroxide with the Amidogen Radical" I.M. Alecu, Y. Gao and P. Marshall, J. Chem. Phys., 157, 014304 (2022).
7. "Reactions of Hydrazine with the Amidogen Radical and Atomic Hydrogen" Y. Gao, I.M. Alecu, H. Hashemi, P. Glarborg and P. Marshall, Proc. Combust. Inst., in press DOI 10.1016/ j.proci.2022.07.045
8. "Re-Evaluation of Rate Constants for the Reaction $N_2H_4$ (+ M) ⇄ $NH_2$ + $NH_2$ (+ M)" C.J. Cobos, P. Glarborg, P. Marshall and J. Troe, Combust. Flame, in press DOI 10.1016/ j.combustflame.2022.112374
9. "Probing high-temperature amine chemistry: Is the reaction $NH_3$ + $NH_2$ = $N_2H_3$ + $H_2$ important?" P. Marshall and P. Glarborg, J. Phys. Chem. A, 127, 2601-2607 (2023)

# Electronic Structure, Spectroscopy, and Bond Dissociation Energies of Small Actinide Molecules

*Michael D. Morse, Principal Investigator*

Department of Chemistry, University of Utah, Salt Lake City, UT morse@chem.utah.edu
Graduate Students: Dakota Merriles, Kim Tomchak, Joshua Ewigleben, Tommy Kawagoe

*Overall research goals:* This work is focused on obtaining detailed, precise information concerning the electronic structure, spectroscopy, and bond dissociation energies of small thorium and uranium molecules, with the goal of providing precise data that can be used to assess the approximations employed in quantum chemical calculations on these species. Ultimately, it is our hope that the precise data we obtain will be useful in benchmarking quantum computational methods for the 5*f* elements, allowing efficient and accurate methods to be developed for application to the transuranic elements.

*Significant achievements during 2021- 2023:*

In recent years, the Morse group has established that an effective means of precisely measuring bond dissociation energies (BDEs) in small open shell *d*- and *f*-block molecules is through the measurement of sharp predissociation thresholds in a congested, quasicontinuous vibronic spectrum.[1] For these types of molecules, the extremely large density of electronic states present at the ground separated atom limit causes rapid predissociation to set in as soon as the bond dissociation energy is exceeded. In our resonant two-photon ionization (R2PI) spectroscopic studies, the predissociation threshold is readily identified by a sharp drop in ion signal to baseline as the BDE is exceeded.

**Table 1. Bond dissociation energies measured by the onset of predissociation**

| Molecule | BDE (eV) | Status | Molecule | BDE (eV) | Status |
|---|---|---|---|---|---|
| ThSe | 5.484(12) | Preliminary | USe | 4.609(9) | Finalized |
| UC | 4.304(3) | Finalized | URh | 5.472(3) | Finalized |
| US | 5.25(5) | Preliminary | UIr | 5.647(13) | Preliminary |
| SU-S | 4.96(2) | Preliminary | | | |

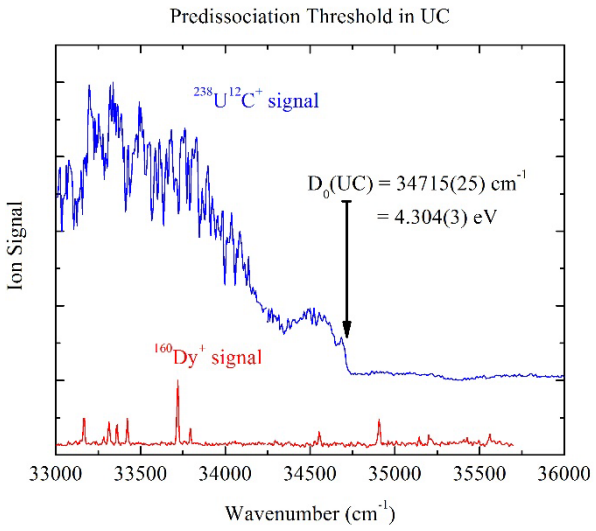


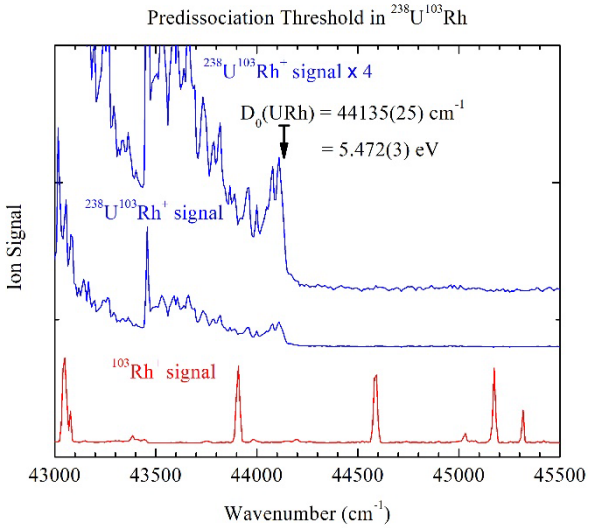


Figs 1 and 2. Sharp predissociation thresholds in the R2PI spectra of UC and URh provide precise values of their bond dissociation energies, as reported in Table 1 above.

In other work, we have collaborated with Prof. Tim Steimle to study ThC. He has used the locations of the ThC vibronic bands that we have measured in low resolution to obtain high resolution LIF and dispersed fluorescence spectra. The rotational analysis is ongoing, but the ThC $X^3\Sigma^+$ ground state vibrational interval, $\Delta G_{1/2}$, has been measured as 798 $cm^{-1}$.

We are also completing the construction of a cryo-cooled ion photodissociation instrument that will allow us to extend these BDE measurements to mass-selected cations. During the 2021-2023 period, we have designed, modeled, and assembled the laser ablation source region of this instrument. This includes the laser ablation ion source itself, an ion funnel to collect the cations, a hexapole preliminary trap that can be used to ligate the cooled ions with stable molecules, and an octupole ion guide to transport the ions to a quadrupole mass filter for mass selection. The remainder of the instrument was built prior to this period and employs a quadrupole bender, a cryo-cooled linear quadrupole ion trap, a second quadrupole mass filter set to the mass of the expected fragment, and a conversion dynode for counting fragment ions. The cryo-cooled linear quadrupole trap is constructed so that two collimated laser beams can be sent through the cell from opposite directions, allowing photodissociation-based probes of the trapped ions. At this point in time, construction is complete but we are still working to obtain the rf power supplies that are needed to operate the ion funnel, hexapole trap, and octopole ion guide. When those are in hand, the system will be complete.

*Science objectives for 2023- 2025:*

During the next two years, we plan to finalize the preliminary BDEs listed above and measure BDEs of additional small neutral molecules such as UB, U-$B_2$, UN, ThB, Th-$B_2$, ThN, and ThS. We will also measure the BDEs of additional actinide-metal molecules such as URu, UPt, ThRu, ThRh, ThIr, and ThPt. We will collaborate with computational chemists to understand the electronic structure of these species. We will also measure the BDEs of the actinide dimers $Th_2$ and $U_2$. A precise BDE for $U_2$ will be particularly useful as a benchmark for quantum chemical calculations. We will complete the rotational analysis of ThC and work to collect rotationally resolved spectra of UC to measure its bond length and identify its ground electronic state experimentally. We also plan to record vibrationally resolved spectra of $UO_2$ and other species in the near-infrared region using an R2PI scheme employing two tunable OPO lasers. One will scan in the near-infrared region while the second is used to provide a fixed wavelength ionization source. This method will provide very useful means of investigating the calculated low-energy electronic states of $UO_2$. Once successfully demonstrated on $UO_2$, I anticipate using this method for other actinide species as well, fleshing out our knowledge of their electronic states in the near infrared region.

The nearly-completed cryo-cooled ion photodissociation spectrometer will be used to provide precise BDEs of $UF^+$, $UO^+$, and $UO_2^+$ using a resonant two-photon dissociation scheme. In NSF-funded work, a similar method has been quite successful in measuring ionization energies of neutral molecules like RuB, RhB, OsB, IrB, and PtB.[2] The BDEs of multiply-ligated cations will be more readily measured than for the corresponding neutrals, allowing BDEs of a series of species such as $UF_2^+$, $UF_3^+$, $UF_4^+$, *etc.* to be measured.

*Publications supported by this project 2021-2023*

None as of yet.

*References:*


[1] Morse, M. D. "Predissociation Measurements of Bond Dissociation Energies" *Acc. Chem. Res.,* **2019**, *52*, 119-126, DOI: http://dx.doi.org/10.1021/acs.accounts.8b00526.

[2] Merriles, D. M.; Morse, M. D. "Ionization energies and cationic bond dissociation energies of RuB, RhB, OsB, IrB, and PtB" *J. Chem. Phys.,* **2022**, *157*, 074303, DOI: https://doi.org/10.1063/5.0107086.

**Spectroscopy, Kinetics, and Dynamics of Highly Reactive Species**

**JILA/NIST/Department of Chemistry/Department of Physics**
**University of Colorado, Boulder 80309**
**David. J. Nesbitt (djn@jila.colorado.edu)**

Our DOE research program involves experimental and theoretical study of transient chemical species relevant to fundamental chemical processes. The work focuses on spectroscopy and unimolecular/bimolecular dynamics of highly reactive radical intermediates, combining i) high-resolution direct IR laser absorption methods with quantum shot noise limited detection, ii) high densities ($10^{12}$-$10^{14}$ #/cm$^3$) of jet-cooled hydrocarbon radicals and molecular ions in slit supersonic discharge expansions, accompanied by iii) high-level *ab initio* potential surface and multidimensional quantum mechanics calculations. Over the past year, our group has utilized and further developed ultrasensitive high resolution spectroscopy methods to achieve detailed characterization of a number of atmospherically and astronomically important species, with selected highlights described below. 1) Direct absorption IR spectroscopy is used to detect and analyze high resolution spectra of supersonically cooled trans formic acid (HCOOH) in the OH stretch region, the analysis of which has been stymied for decades by heavy spectral congestion at room temperature and strong intramolecular vibrational coupling effects.[1-2] These studies follow naturally from previous detection of cis-formic acid in the slit discharge, a highly energetic but metastable rotamer of the normal trans formic acid known to form in copious quantities in the interstellar medium. 2) These slit jet studies have been extended to probe and analyze gas phase $C_4$ (cyclobutyl) and $C_5$ (cyclopentyl) cycloalkyl radicals for the first time, which, despite an increasingly large number of atoms continues to exhibit remarkably sharp and high-resolution spectra with little indication of spectral fragmentation due to intramolecular vibrational redistribution (IVR).[3] 3) We have combined broad band mid-IR frequency combs with high finesse (Q = 10,000) optical build up cavities for buffer gas cooled laser spectroscopy and optical saturation dynamics of $C_{60}$, which represents the first quantum state-to-state rotational and vibrational collisional energy transfer studies in a molecule of this size (N = 60), mass (960 amu), and complexity.[4] These studies have identified novel intramolecular rotational coupling effects in $C_{60}$ due to transitions between ergodic and non-ergodic behavior that are facilitated by the high icosahedral symmetry and rigidity of the molecular structure.[5] We have further utilized these IR frequency comb methods for detection of small molecule components in human breath samples at < 100 ppt (parts per trillion) sensitivities, which in combination with machine testing/learning algorithms has in preliminary trials allowed us to successfully diagnose pulmonary disease states such as COVID infection with high accuracy (AUC = 85%).[6] 4) Laser absorption spectroscopic sensitivity with difference frequency generation methods is currently limited by quantum shot noise due to photon arrival on the detectors, which provides a powerful incentive for implementation of higher cw laser power sources. In such laser development, we have designed and successfully built a JILA cw high resolution light source based on optical parametric oscillation in a singly resonant compact bow tie PPLN cavity resonant on the OPO signal, which yields MHz resolution idler power output at > 1Watt levels and tunable over the 2.7-4 micron region. In the interests of space, highlights from 3 of these topics are briefly discussed below, with opportunities for more detailed in-person discussions at the contractors meeting itself.

**A. High-resolution infrared spectroscopy of gas-phase cyclobutyl radical in the α-CH stretch region: Surprisingly low barrier puckering dynamics.** Cyclopropyl by necessity has a planar CCC geometry and a π radical, whereas cyclopentyl is known from high resolution gas phase spectroscopy in a slit discharge to be strongly puckered. What is not known and indeed not easy to predict is the equilibrium structure of cyclobutyl radical, which is formed with a relatively strained 4-membered CCCC ring. Gas-phase cyclobutyl radical (*c*-$C_4H_7$) is generated at a rotational temperature of 25.6 ± 1.4 K in a slit-jet discharge mixture of 70% Ne/30% He and 0.5-0.6% cyclobromobutane (*c*-$C_4H_7Br$). The fully rovibrationally resolved absorption spectrum of the α-CH stretch fundamental band between 3062.9 $cm^{-1}$ to 3075.7 $cm^{-1}$ is obtained and analyzed, yielding the first precision structural information for this radical species. The α-CH stretch fundamental band origin is determined to be 3068.7887(4) $cm^{-1}$, which from previous infrared spectroscopic studies of cyclobutyl radicals in droplets implies a 0.8 $cm^{-1}$ blue shift due to the presence of liquid helium. This value is also in good agreement with high-level *ab initio* calculations, which predicts an anharmonic frequency of 3076.4 $cm^{-1}$ from second-order vibrational perturbation theory (VPT2). The 1D potential energy surface along the ring puckering coordinate computed at CCSD(T) level of theory shows double minima in $C_s$ puckered geometry and a $C_{2v}$ transition state, with a remarkably low barrier height of < 0.8 $cm^{-1}$ calculated at the highest CCSD(T)/ANO2 basis set level. Eigenvalues and eigenfunctions for this 1D double minimum potential are solved using Numerov-Cooley method. With calculated zero-point energy of the ground state above the interconversion barrier, a vibrationally averaged $C_{2v}$ structure is predicted. Intensity alternation in the experimental spectrum due to nuclear spin statistics upon exchanging 3 pairs of identical fermionic hydrogen atoms ($I_H$ = ½) matches the predicted $K_a + K_c$ = even : odd = 36:28 for a $C_{2v}$ structure, providing the first experimental confirmation of the planar CCCC cyclobutyl radical ground state transition geometry. The persistence of fully resolved high resolution infrared spectroscopy for such large cyclic polyatomic radicals ($C_4$ and $C_5$ radicals) at high vibrational state densities suggests a "*deceleration*" of IVR for a cycloalkane ring topology, much as low frequency torsion/methyl rotation degrees of freedom have demonstrated a corresponding "*acceleration*" of IVR processes in linear hydrocarbons. The results continue to suggest successful applications of high-resolution infrared spectroscopy for even larger polyaromatic ring radical systems.

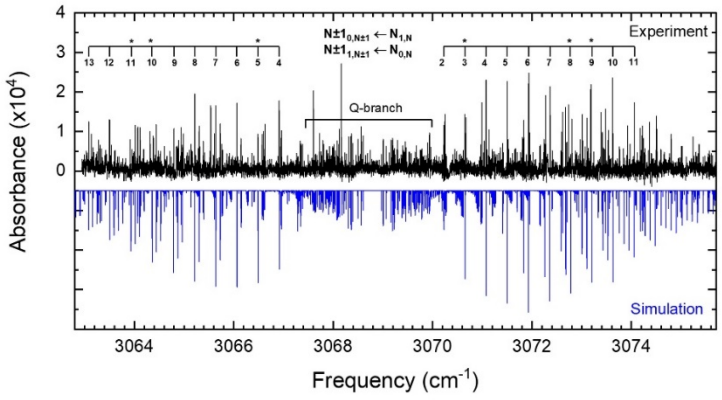


**B. Ergodicity breaking in rapidly rotating $C_{60}$ fullerenes.** Large buckminsterfullerene molecules with 5 dozen identical $^{12}C$ atoms offer completely novel opportunities for long lived quantum control in many body spin systems, establishing a gas-phase molecular platform in principle capable of representing a 60-qubit entangled state with potential applications in quantum computation. As a preliminary step in this direction, quantum state-resolved

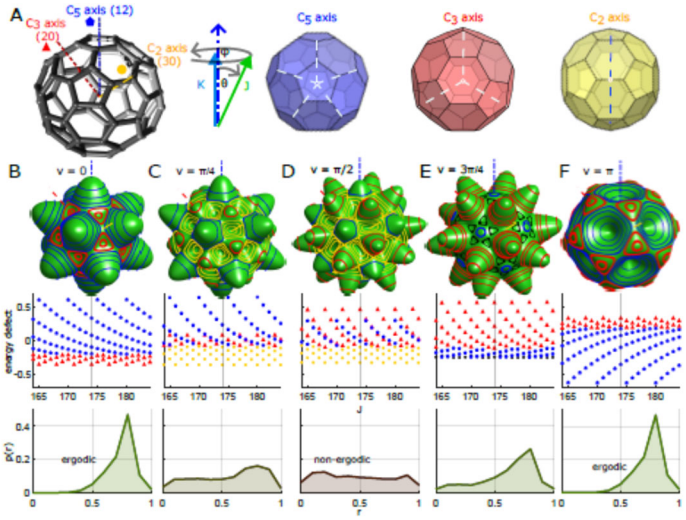


spectroscopy has been recently achieved in a Nesbitt/Ye group collaboration for gas phase $C_{60}$ molecules when cooled by buffer gas collisions and probed with a mid-infrared frequency comb. These results establish a novel route towards quantum state control for creating quantum entanglement in a new class of unprecedentedly large gas phase molecules. The high resolution of this buffer gas absorption spectroscopy for such fullerenes with unprecedented size, rigidity, and icosahedral symmetry allows for first access to novel rotational physics of intramolecular energy flow. Specifically, ergodicity, the central tenet of statistical mechanics, predicts that an isolated system will explore all of energetically available phase space. Mechanisms for violating ergodicity are of great interest for probing non-equilibrium matter and protecting quantum coherence in complex systems. For decades, polyatomic molecules have served as an intriguing and challenging platform for probing ergodicity breaking in vibrational energy transport, particularly in the context of controlling chemical reactions. This work reports the observation of rotational ergodicity breaking in an unprecedentedly large and symmetric molecule, $^{12}C_{60}$. This is facilitated by the first ever observation of icosahedral rovibrational fine structure in any physical system, first predicted for $^{12}C_{60}$ in 1986. The ergodicity breaking exhibits several surprising features: 1) there are multiple transitions between ergodic and non-ergodic regimes as the total angular momentum is increased, and 2) they occur well below the traditional vibrational ergodicity threshold. These peculiar dynamics result from the interplay of the molecules' unique combination of symmetry, size, and rigidity, highlighting the potential of fullerenes to discover emergent phenomena in mesoscopic quantum systems.

**C. High Power, Single mode cw mid-infrared Optical Parametric Oscillators.** Due to its wide wavelength tunability and narrow linewidth, cw-OPOs in the mid-infrared wavelength regions are attractive light sources for high-resolution molecular spectroscopic applications. Among all OPO configurations, singly resonant optical parametric oscillators (SROs), where only the signal wavelength is resonated within the cavity, are of particular interest. Even though SROs require higher oscillation thresholds, they offer superior amplitude and spectral stability and simple wavelength tuning algorithms. A JILA continuous-wave singly resonant optical parametric oscillator in the mid-infrared region has been built, generating tunable cw output (1W) over broad 2.7 − 4.0 μm spectral region and will be used to study the CH and OH stretch rovibrational bands of radicals and molecular ions that are relevant to fundamental chemistry processes. Our home-built cw-OPO has a four-mirror bowtie ring cavity design, consisting of two curved mirrors with a radius of curvature of 100 mm and two flat mirrors (*FSR* ~ 600 MHz) and undoped-YAG (diameter of 0.5 inch and thickness of 3 mm) used as the mirror substrate.

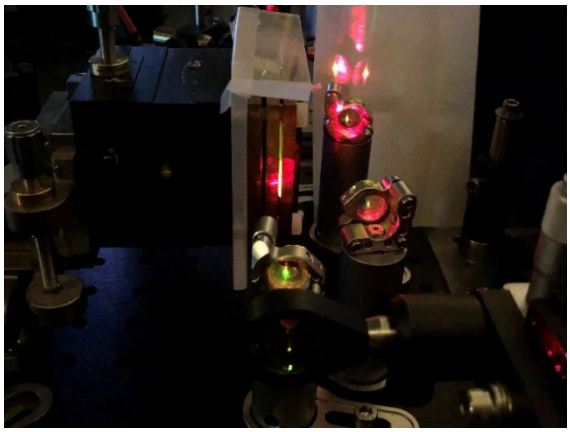

Each mirror has a highly reflective coating R > 99.5% for the signal wavelength (1420 – 1750 nm) and highly transmissive coating T > 97% and T > 95% for the pump wavelength (1064 nm) and idler wavelength (2700 – 4000 nm), respectively. No output coupler is used to reduce oscillation threshold. A 50 mm long, 1 mm thick, 5 mol.% magnesium oxide doped periodically-poled lithium niobate (MgO:PPLN), with poling periods from 28.7 – 32.2 μm in a fanout design (HC Photonics), is used as a nonlinear material. The crystal is placed in an oven (50 °C) between the two curved mirrors. The back surfaces of the mirrors and input/output faces of MgO:PPLN have anti-reflection coating for all three wavelengths. The pump laser used in our cw-OPO consists of a fiber seed laser and a fiber amplifier that can deliver up to 15 W of continuous-wave single-frequency radiation at 1064 nm with a narrow linewidth of < 20 kHz and a good beam quality of $M^2 < 1.05$ (NKT Photonics). A 75 mm focal length lens is used to focus the pump to a ~65 μm beam waist at the center of the nonlinear crystal to be mode-matched with the OPO cavity. Wavelength tuning can be accomplished by mode-hop free tuning of the pump laser frequency over 6 $cm^{-1}$. When the pump power exceeds the oscillation threshold, the signal and idler waves are efficiently produced. In addition, the intracavity signal power is high enough to generate parasitic oscillation from the second harmonics of the signal wavelength, resulting in the appearance of red to orange light. The pump, signal, and idler frequencies are measured by a wavemeter. Currently, >1 W of idler cw power across the 2.7 − 4.0 μm spectral range is achieved, with oscillation thresholds between 4 – 10 W. We are now working on signal frequency stabilization and automatic wavelength scanning algorithms.


1. Doney, K. D.; Kortyna, A.; Chan, Y. C.; Nesbitt, D. J., Formation and detection of metastable formic acid in a supersonic expansion: High resolution infrared spectroscopy of the jet-cooled cis-HCOOH conformer. *J. Chem. Phys.* **2022**, *156*, 9, 10.1063/5.0093401.
2. Chan, Y. C.; Nesbitt, D. J., High-resolution rovibrational spectroscopy of trans-formic acid in the v(1) OH stretching fundamental: Dark state coupling and evidence for charge delocalization dynamics. *J. Mol. Spec.* **2023**, *392*, 11, 10.1016/j.jms.2023.111743.
3. Chan, Y. C.; Nesbitt, D. J., High-resolution infrared spectroscopy of gas-phase cyclobutyl radical in the α-CH stretch region: Structural and dynamical insights. *J. Chem. Phys.* **in prep**
4. Liu, L. R.; Changala, P. B.; Weichman, M. L.; Liang, Q. Z.; Toscano, J.; Klos, J.; Kotochigova, S.; Nesbitt, D. J.; Ye, J., Collision-induced $C_{60}$ rovibrational relaxation probed by state-resolved nonlinear spectroscopy. *PRX Quantum* **2022**, *3*, 16, 10.1103/PRXQuantum.3.030332.
5. Liu, L. R.; Rosenberg, D.; Changala, P. B.; Crowley, P. J. D.; Nesbitt, D. J.; Yao, N. Y.; Tscherbul, T.; Ye, J., Ergodicity breaking in rapidly rotating $C_{60}$ fullerenes. *Science* **submitted, 2023**
6. Liang, Q. Z.; Chan, Y. C.; Toscano, J.; Bjorkman, K. K.; Leinwand, L. A.; Parker, R.; Nozik, E. S.; Nesbitt, D. J.; Ye, J., Breath analysis by ultra-sensitive broadband laser spectroscopy detects SARS-CoV-2 infection. *J. Breath Res.* **2023**, *17*, 10, 10.1088/1752-7163/acc6e4.

## State-to-State Molecular Reactions in the Ultracold Regime

Kang-Kuen Ni
Department of Chemistry and Chemical Biology, Harvard University
12 Oxford St., Cambridge, MA 02138
ni@chemistry.harvard.edu

**Research Scope**:
We aim to experimentally probe the AB + CD and AB + C types of reactions with state-to-state resolution, which can be compared to advanced theoretical calculations to help elucidate the role of quantum mechanics in the processes of bond breakage and formation. Our approach uses reactants that are prepared at ultracold temperatures ($< 1\,\mu K$) such that the quantum effects of translational motion are an important factor. Specific example reactions, including the potassium-rubidium metathesis reaction KRb + KRb $\rightarrow$ $K_2$ + $Rb_2$ as well as the atom exchange reaction Rb + KRb $\rightarrow$ $Rb_2$ + K, are chosen because the technology of quantum internal and motional state control of these types of molecules is particularly advanced. For the majority of this grant, we have constructed a quantum degenerate gas apparatus that integrates ion detection and velocity map imaging capabilities, allowing us to explore the KRb + KRb $\rightarrow$ $K_2$ + $Rb_2$ bimolecular reaction in detail. In this work, we mapped out the complete product state distribution, which was compared to a state-counting model based on statistical theory. Our results show an overall agreement with the statistical state counting model, but also reveal several deviating state-pairs. An exact quantum calculation for molecule-molecule collisions, that is needed to understand these deviations, is however beyond the current state-of-the-art. We then explored the more theoretically tractable Rb + KRb reaction, which is endothermic. Surprisingly, we observed an exceedingly long-lived $KRb_2^*$ collisional complexes, with our experimentally measured complex lifetime deviating from conventional theoretical calculations by five orders of magnitude. This discrepancy has motivated many explorations of possible underlying causes, though no model yet captures this phenomenon completely. In the final grant period, we extend upon these atom-molecule collision experiments to explore the origin of the long-lived $KRb_2^*$ complex lifetime and develop means to control the outcome of the reaction complex.

**Recent Progress**:
The advent of ultracold chemistry (T $<$ 1 mK) has facilitated the exploration of bimolecular reactions in detail long sought after. Such studies are made possible by the exquisite control over the states of molecules produced in this regime, owing to the coherent and state-selective optical process by which they are formed. The ability to completely specify the initial states of the reactants, when coupled with state-specific detection methods, allows for the complete mapping of state-to-state dynamics in these reactions. We have previously harnessed these capabilities to study the model KRb + KRb system to great effect, mapping the full product state distribution and determining that the reaction intermediate lives for sufficiently long times ($>$100 ns) to be probed and controlled.

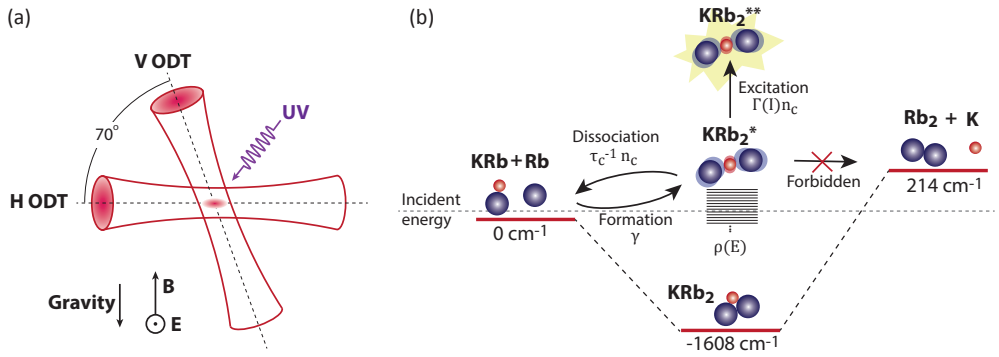


Figure 1: KRb + Rb collision dynamics in an optical dipole trap (ODT). (a) The ODT configuration used to confine the mixture of KRb molecules and Rb atoms. The purple arrow represents the UV ionization laser pulse, used for photoionization detection of $KRb_2^*$ complexes. (b) Illustration of the KRb + Rb collision dynamics. The incident energy of one free electronic ground state Rb atom and one free KRb molecule in its rovibronic ground state is defined as the zero of energy.

These studies have proven foundational to our understanding of chemistry in this regime, and in the final funding period, we focus on building upon this early work to establish a means to *control* the outcome of ultracold reactions. The focus of this work is the Rb + KRb reaction, selected for its relative simplicity compared to molecule-molecule reactions while still displaying rich chemical dynamics. The facile manipulation of atomic states enables us to explore reactions where the reactants have a wide array of internal energies, spanning $10^{-4}$ to $10^{4}$ cm$^{-1}$. Such studies have allowed us to systematically explore the unimolecular dissociation reaction of the $KRb_2$ collisional complex, arising from the endothermic Rb + KRb reaction, as exit channels are opened or closed, dramatically changing its dissociation rate. Further, we find the appearance of rotationally excited molecules and de-excited atoms when KRb is reacted with Rb atoms in the $|F,m_F\rangle = |2,2\rangle$ electronically excited state. Together, these findings demonstrate control over the unimolecular dissociation process of the $KRb_2^*$ collisional complex, the first steps towards a regime of fully-controlled chemical reactions.

At sub-microkelvin temperatures, the chemical reaction between Rb and KRb is energetically forbidden, though the loss-rate of molecules is increased dramatically when atoms are introduced. Here we investigate the origin of this loss by directly observing the collisional complex dynamics. As before, our reactants are held in a 1064 nm crossed optical dipole trap (ODT), see Figure 1(a), in which they stochastically begin reacting with one another. Importantly, we have found that any reaction complex formed is photoexcited and lost by the trapping light. Thus, by applying a square-wave modulation to the intensity of our trapping light such that the time-averaged power is constant, we can maintain trapping of our species while setting a clean time-zero for which the population of these complexes build up and react. The population of complex or products of the $KRb_2^* \rightarrow$ KRb + Rb reaction, see Figure 1(b), are then probed using a pulse of ionizing UV radiation in the ODT-off portion of the square wave in tandem with ion imaging.

We observe that the $KRb_2^*$ complex lifetime is sensitive to the initial atomic state: when atoms are prepared in the $F = 2$ state, lying 6.8 GHz above the ground state, we observe no $KRb_2^*$ complex

signal. However, the observed loss rate of KRb (with atoms prepared in $F = 2$) does not deviate from that observed when atoms are prepared in various $m_F$ levels of the $F = 1$ state, for which we observe 10s of counts per experimental cycle. Notably, though we do not observe the $KRb_2^*$ collisional complex, 1+1' REMPI measurements reveal that the product KRb molecules are translationally hot and distributed among their first two rotationally-excite states, KRb ($N$ = 0-2), while the product Rb atoms populate the lower-lying $F = 1$ manifold, see Figure 2(b). Such a process occurs as the excited $|F, m_F\rangle = |2,2\rangle$ state is sufficiently high-lying to open the rotationally-excited exit channels in the $KRb_2^* \rightarrow$ KRb + Rb reaction. Recent theoretical work from our collaborator Timur Tscherbul (University of Nevada, Reno) suggests a strong coupling of atomic hyperfine, $F$, and molecular rotational, $N$, angular momenta occurs in the short-range region of the reactive potential energy surface. Our measurement, to our knowledge, is the first direct detection of spin-rotation reaction in the ultracold regime. Finally, with careful state-dependent ion count calibration underway, our measurement of the branching ratio of the rotationally-excited products will determine whether the distribution conforms to the expected chaotic behavior that results from a random mixing of states within the complex, Figure 2(c). (Our preliminary data leans toward a non-statistical behavior.) Together, these results provide new insight into the fundamental mechanism by which unimolecular dissociation proceeds.

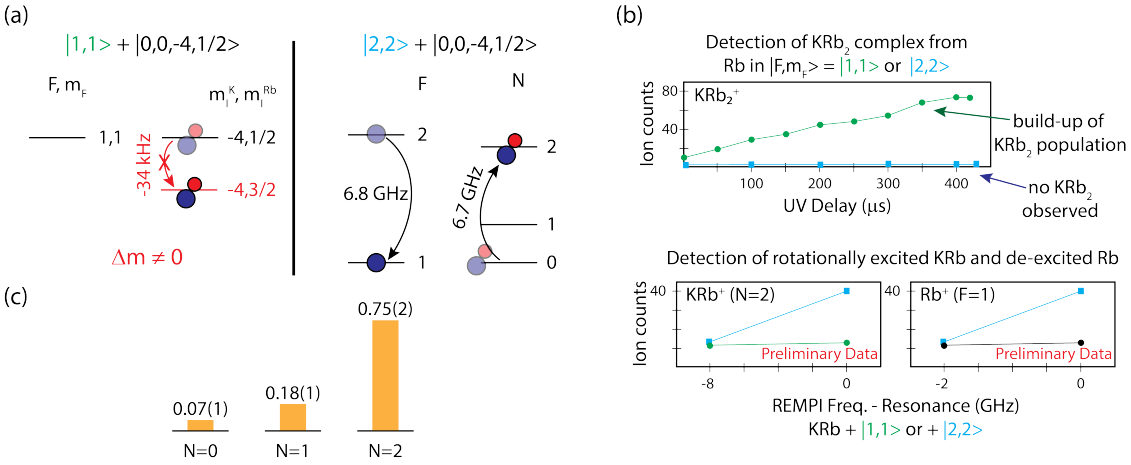


Figure 2: Observations from the reaction of KRb + Rb in the $|2,2\rangle$ state. (a) Energy level diagram for the reaction as well as that for the lower-lying $|1,1\rangle$ state outlining the opening of rotationally-excited KRb ($N$ = 0-2) channels. (b) Complex lifetime observations showing the disappearance of the $KRb_2^*$ collisional complex when atoms are in the $|2,2\rangle$. Commensurate with this is the observation of rotationally excited KRb and de-excited Rb atoms. (c) Measured branching ratio of rotationally-excited KRb.

We have also explored the impact on the complex lifetime of the $m_F$ level within the $F = 1$ manifold. Here, the rotationally-excited exit channels are closed and we observed long-lived complexes. The $m_F$ levels are split by 0.7 MHz/G, allowing us to explore the role of both the atomic state and energy by preparing atoms in various $m_F$ levels and at different magnetic fields. Under constant magnetic field, we find that the complex lifetime drops by a factor of two when the Rb atoms are promoted from their ground $|1,1\rangle$ state, but is otherwise independent of the $m_F$ level or the nuclear hyperfine level of KRb, see Figure 3(a). Importantly, however, we find that when the magnetic field is varied, the complex lifetime can be continuously varied by a factor of five, with the lifetime

saturating at higher fields, Figure 3(b). Counter to the expectations from statistical theories, the complex lifetime increases with higher field, and thus higher initial state energy. Developing a full understanding of this may enable further control over this unimolecular dissociation process and provide a blueprint for controlled-chemistry.

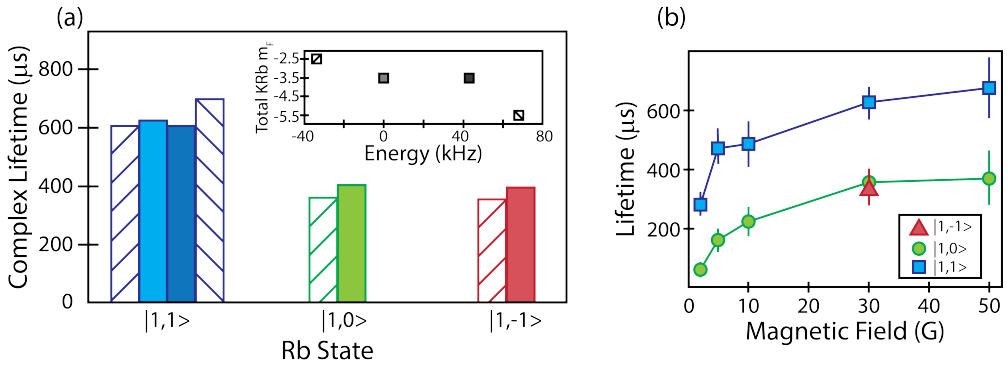


Figure 3: $KRb_2^*$ Complex lifetime measurements (preliminary). (a) Measured complex lifetime as a function of Rb state, $|F, m_F\rangle$, and molecular nuclear hyperfine state, $|m_I^K, m_I^{Rb}\rangle$. Inset: KRb hyperfine level spacing. (b) Complex lifetime as a function of magnetic field for various Rb $|F, m_F\rangle$ + KRb $|-4, 1/2\rangle$ state-pair combinations.

**Future Plans**:
Controlling the lifetime of the $KRb_2^*$ collisional complex is an exciting step towards an era of controlled chemistry, for which we aim to lay a foundation using atom-molecule reactions. As can be seen from our preliminary data, there are many surprising observations in ultracold atom-molecule reactions. We plan to finalize the preliminary measurements presented above and develop models in tandem with theorists to enable further experiments on chemical control.

**References to publications of DOE sponsored research 2020-2023**:
1. Y. Liu, K.-K. Ni. Bimolecular chemistry in the ultracold regime. *Annu. Rev. Phys. Chem.*, 73:73-96, 2022.
2. M. A. Nichols, Y.-X. Liu, L. Zhu, M.-G. Hu, Y. Liu, and K.-K. Ni. Detection of long-lived complexes in ultracold atom-molecule collisions. *Phys. Rev. X*, 12, 011029, 2022.
3. G. Quéméner, M.-G. Hu, Y. Liu, M. A. Nichols, L. Zhu, and K.-K. Ni. Model for nuclear spin product-state distributions of ultracold chemical reactions in magnetic fields. *Phys. Rev. A*, 201, 052817, 2021. 4. Y. Liu, M.-G. Hu, M. A. Nichols, D. Yang, D. Xie, H. Guo, and K.-K. Ni. Precision test of statistical dynamics with state-to-state ultracold chemistry. *Nature*, 593, 379-384, 2021.
5. M.-G. Hu, Y. Liu, M. A. Nichols, L. Zhu, Goulven Quemener, O. Dulieu, and K.-K. Ni. Nuclear spin conservation enables state-to-state control of ultracold molecular reactions. *Nat. Chem*, 13, 435-440, 2021.
6. Y. Liu, M.-G. Hu, M. A. Nichols, D. D. Grimes, T. Karman, H. Gua, and K.-K. Ni. Photo-excitation of long-lived transient intermediates in ultracold reactions. *Nat. Physics*, 16, 1132-1136, 2020.
7. Y. Liu, D. D. Grimes, M.-G. Hu, and K.-K. Ni. Probing Ultracold Chemistry using Ion Spectrometry. *Phys. Chem. Chem. Phys.*, 22, 4861-4874, 2020.

# Mechanistic Understanding of the Criegee Intermediates Reaction Network in Atmospheric and Combustion Systems

Denisia M. Popolan-Vaida
Department of Chemistry, University of Central Florida, Orlando, FL 32816
denisia.popolan-vaida@ucf.edu

## Program scope

The reaction networks that describe the complex chemical processes involved in atmospheric and combustion systems are typically dominated by reactive intermediates that usually occur in small concentrations. Identification and quantification of these reactive species within complex reactive mixtures are key for the development of a fundamental, chemically accurate description of complex atmospheric and combustion systems. The objective of this program is to generate new mechanistic understanding of the reaction network of Criegee intermediates (CIs), which are important species formed during the ozonolysis of unsaturated organic compounds and have been linked to the formation of secondary organic aerosols (SOA). In addition, our research also aims to find the pathways by which CIs can drive the formation of high-molecular-weight, lower volatility precursors that can lead to SOA, and eventually detect and identify the size and composition of SOA. To assess the role of resonance stabilization induced by the competition between collisional stabilization and unimolecular reaction of the energy-rich CIs, the ozone-assisted oxidation reaction of selected acyclic and endocyclic alkenes is investigated as a function of alkene structure and carbon number. The key questions this program will answer are: (1) How does the mechanism of ozone-assisted oxidation change as a function of alkene carbon-number and structure? (2) Is there a specific carbon-number that corresponds to a crossover between the radical production and secondary ozonide (SOZ) stabilization in the case of endocyclic alkenes? (3) What is the role of CIs in gas-particle interconversion? and (4) Does high carbon-number facilitate the formation of organic particles.

## Research progress

***Identification of acetaldehyde oxide and glyoxal oxide CIs reaction network in the ozone-assisted oxidation of crotonaldehyde:*** An atmospheric pressure jet stirred reactor in conjunction with molecular beam high-resolution mass spectrometry and tunable synchrotron single-photon ionization have been used to investigate the reaction network of two Criegee intermediates, $CH_3CHOO$ and CHOCHOO, formed in the ozone-assisted oxidation reaction of crotonaldehyde. While the reaction pathway of $CH_3CHOO$ have been investigated before, including studies in our laboratory,[1, 2 and refs. therein] the experimental literature on CHOCHOO reactions is sparse and limited to its unimolecular reaction pathways. Therefore, our investigations focused on (i) understanding

the reaction network of CHOCHOO, (ii) understanding the reaction network of $CH_3CHOO$ when both the primary ozonide (POZ) precursor and the reaction environment are changed, and (iii) exploring the CIs induced oligomerization in a system where two CIs with different functionality are simultaneously reacting.

Temperature dependent measurements performed in this research program revealed that the presence of ozone triggers the oxidation of crotonaldehyde at lower temperatures than in the presence of oxygen alone. A network of CI reactions was identified below 600 K characterized by addition of CIs to species like aldehydes, alkenes, ketones, and carboxylic acids. Experimental photoionization efficiency scans and *ab initio* threshold energy calculation performed by our collaborator Dr. Jasper, lead to identification and quantification of previously elusive intermediates, such as ketohydroperoxide (KHP) and hydroperoxide species. For instance, $C_4H_6O + O_3$ adduct was identified as a 2-hydroperoxy-3-oxobutanal KHP, while hydroxyacetaldehyde formation was attributed to unimolecular isomerization of $CH_3CHOO$. Despite of the fact that the product mass spectra is characterized by the formation of high-molecular-weight products with *m/z* above 150 amu, no direct evidence for CI induced oligomerization was observed. A possible explanation is that these products are energetically unstable and will immediately decompose upon formation.

***Molecular weight growth observed in the ozone-assisted oxidation reaction of cyclopentene:*** The ozone-assisted oxidation reactions of C5 endocyclic and acyclic alkenes, cyclopentene and *trans*-2-pentene, were investigated to assess the changes induced on the products distribution by various alkene structures while keeping a constant carbon number. The ozone-assisted oxidation reaction of cyclopentene is expected to lead to the formation of a long-chain CI. Therefore, the bimolecular reactions of CIs formed in the ozone assisted-oxidation reaction of C5 endocyclic alkene are expected to lead to higher molecular weight products that in the case of the acyclic alkene. Indeed, preliminary studied reveled that the product mass spectra recorded after ozonolysis of cyclopentene are characterized by the presence of high-molecular-weight species at *m/z* that are indicative of reaction of the long-chain CI with species like alkenes and aldehydes. Theoretical calculations are in progress to determine the chemical identity of these products. Addition ongoing investigations are focusing on connecting the onset of particle phase products observed in these studies with the observed high molecular weight gas-phase products.

**Future work**

Structural differences between the acyclic and endocyclic alkenes as well as the differences in the carbon number are predicted to produce different high energy intermediates and thus have different reaction kinetics. In addition, subtle changes around the C=C double bond of alkenes can have dramatic effect on OH formation yields. At some critical size (carbon number), ozonolysis of acyclic and endocyclic alkenes is expected to switch from a pathway directed toward preferential

formation of OH radicals, to a pathway routed through the SOZ, presumably devoid of OH radical production but potentially very efficient in the formation of SOA. In addition, to continuing the exploration of ozonolysis reactions of C5 acyclic endocyclic alkenes at different alkene concentration, future investigations will focus on the impact of resonance-stabilization of CIs induced by a progressive increase the carbon number of the alkene, on the CI reaction network. A series of acyclic alkenes, such as trans-3-hexene, and trans-3-heptene – as well as endocyclic alkenes, like cyclopentene, 3,5-dymethylcyclopentene, cyclohexene, 4,5-dimethylcyclohexene, cycloheptene, and 4,5-dymethylcycloheptene, that have a common characteristic, i.e. only one C=C double bond, but different structures and carbon numbers will be investigated.

As the alkene concentration is increased in the reaction mixture, radical-radical reactions will be enhanced. In particular, the reactions of the resonance-stabilized species will increase, which will be evident due to the formation of carbon-rich products. Therefore, changes in the initial alkene concentration will be employed to reveal the effects of resonance stabilization for all alkenes proposed to be investigated in this project. Finally, by following the changes in the gas- and particle-phase mass spectra as a function of alkene concentration, we plan to corelate the formation of high-molecular-weight compounds with the onset of the organic particles.

**Publications supported by this DOE project (2022-present)**

- Alec C. DeCecco, Alan R. Conrad, Nath-Eddy Moddy, Ahren W. Jasper, Nils Hansen, Philippe Dagaut, and Denisia M. Popolan-Vaida, "*Identification of acetaldehyde oxide and glyoxal oxide CIs reaction network in the ozone assisted oxidation of crotonaldehyde*", submitted 2023.

**References**


1. Conrad, A. R.; Hansen, N.; Jasper, A. W.; Thomason, N. K.; Hidaldo-Rodrigues, L.; Treshock, S. P.; Popolan-Vaida, D. M., Identification of the acetaldehyde oxide Criegee intermediate reaction network in the ozone-assisted low-temperature oxidation of trans-2-butene. *Phy. Chem. Chem. Phys.* **2021,** *23*, 23554-23566.
2. Osborn, D. L.; Taatjes, C. A., The physical chemistry of Criegee intermediates in the gas phase. *Int. Rev. Phys. Chem.* **2015,** *34*, 309-360.

# Ultrafast Transient Absorption Spectroscopy of Hydrocarbon Radicals

Melanie Reber
Department of Chemistry, University of Georgia, Athens, GA 30602
mreber@uga.edu

## Project Scope

We aim to complete an ultrafast cavity-enhanced transient absorption spectrometer and incorporate two sources of radicals in molecular beams and study the excited state dynamics of vinyl radical and allyl radical. The spectrometer consists of a home-built Ytterbium fiber laser frequency comb and Ytterbium fiber chirped-pulse amplification system that will generate ultrafast (about 100 fs pulse duration) pulses across much of the visible region. This light will be split into pump and probe beams and coupled into enhancement cavities housed in a vacuum chamber. Lock-in detection and noise subtraction techniques will be used during signal detection. With the increase in signal-to-noise with these techniques, it will be possible to perform ultrafast transient absorption spectroscopy in the visible and near-IR spectral regions of radical intermediates in molecular beams.

The overarching goal of this project is to study the excited state dynamics of vinyl, $C_2H_3$, and allyl, $C_3H_5$, radicals. The first excited state of allyl radical exhibits a broad absorption and is thought to connect to the ground state through several conical intersections. The upper state lifetime is less than 5 ps and excitation of this state results in the release of a hydrogen atom. Direct, time-resolved absorption spectroscopy could elucidate this mechanism. Similarly, the first excited state of vinyl radical has picosecond lifetimes, with a decrease in lifetimes with higher vibrational excitation. The frequency-resolved spectroscopy has the signature of ultrafast predissociation from the ground state. We hope to gain insight into these processes in vinyl radical with ultrafast transient absorption spectroscopy. This work will advance our knowledge of excited state processes in combustion intermediates and reactive species.

The first step of this project is to demonstrate the ability to take ultrafast transient absorption spectroscopy of the electronically excited states of radical intermediates. Specifically, there are three components of this goal. (i) The first part is to finish testing the new cavity-enhanced transient absorption spectrometer. (ii) The second part was to complete and test the differential pumping and vacuum system. (iii) The third part entails a proof-of-principle that we can study radicals with this spectrometer, which includes generating radicals with the Excimer laser in our new differential pumping setup.

## Recent Progress

The cavity-enhanced transient absorption spectrometer begins with a home-built Ytterbium fiber laser. General mode-locked ytterbium fiber lasers have always had slightly uncontrollable and irreproducible output spectra. By including an optical bandpass interference filter in the laser cavity, we are able to control the output spectra. The cutoff wavelength of the filter can be tuned slightly by rotating the filter and changing the incident angle, thus allowing us to see trends with cutoff frequency of the filter. Figure 1 shows how an intracavity edgepass filters can push the laser spectrum to the red, including further red than the laser usually lases.

Figure 1: Comparison of Yb:fiber laser with intracavity filter (A and B) and the same filter placed outside the cavity (C and D). Rotation of the angle of incidence (AOI) on the filter tunes the cutoff frequency.

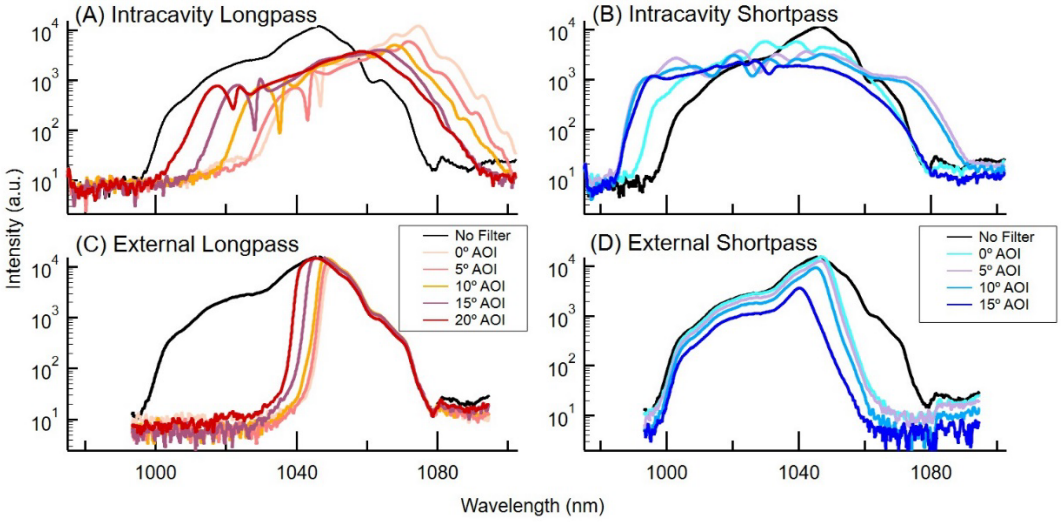


With a shortpass filter at certain cutoff wavelengths, we are able to broaden the overall spectrum. With a double-pass transmission grating compressor setup outside the laser cavity, we compressed the pulse and measured the pulse duration with a GRENOUILLE (SwampOptics). The broader laser spectra resulted in shorter pulse durations, see Figure 2, with pulse durations below 45 fs routinely achievable even under slightly different mode-locking conditions. With the addition of the filter, the output spectrum is more reproducible, spans most of the available gain bandwidth, and short pulses are easily achievable. There are wings on the side of the pulse at the shortest pulse durations and they disappear as the pulse is stretched slightly. The work on these improvements to the ytterbium fiber laser were published this year.

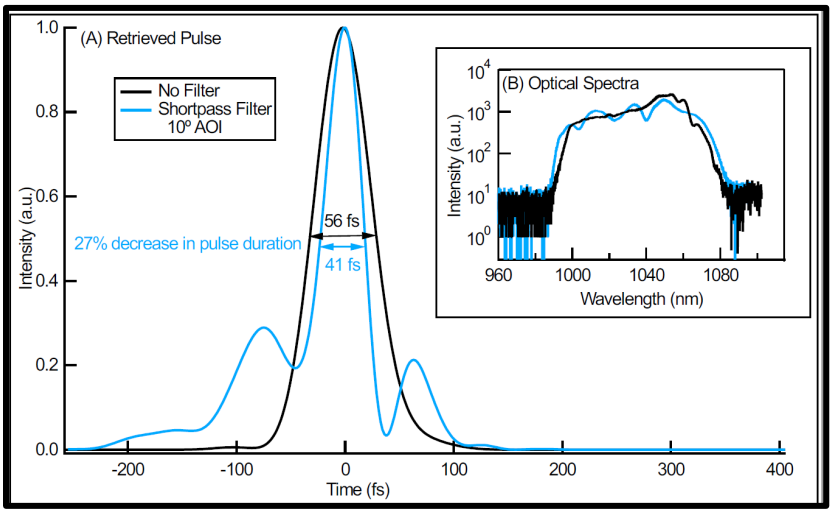


Figure 2: (A) Retrieved pulse: Sample pulse characterization using the shortpass filter at a 10° angle on incidence (blue) and the laser with no filter (black) using a commercial frequency-resolved optical gating pulse measurement (GRENOUILLE system, Swamp Optics). (B) Corresponding optical spectra.

The laser is the start of the ultrafast cavity-enhanced transient absorption spectrometer. The spectrometer is now set up and we have the probe enhancement cavity locking. We are currently working to improve the cavity lock and decrease the noise levels.

The second step of this project is to complete and test the differential pumping system. The differential pumping system is now constructed and we currently can operate with two orders of magnitude pressure differential between the two regions. The molecular beam is installed as a simple pinhole nozzle and easily interchangeable. Figure 3 shows a cutaway of the CAD drawing of the vacuum chamber. The cavity optics are in a high vacuum region, ideally < $10^{-6}$ Torr to cut down on the effects of dispersion, keep optics clean, and reduce cavity noise. The molecular beam is in a region pumped by a Roots blower to accommodate the high flow rates of the nozzle. The cavity beams pass between the two regions through small slits, cut just large enough for the beams to pass through.

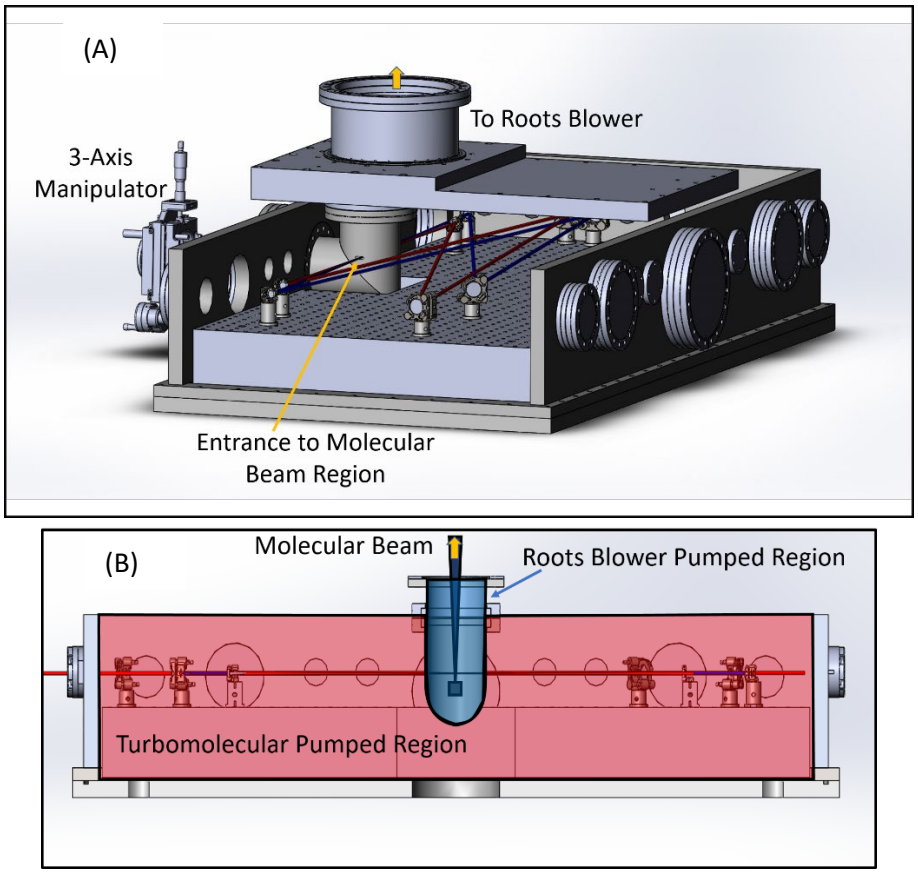


Figure 3: (A) Cutaway view of the vacuum chamber showing the enhancement cavities on a breadboard in the chamber and the entrance to the molecular beam region. (B) Side view of chamber. The pink section is pumped by a turbomolecular pump and the blue region is pumped by a Roots blower.

## Future Plans

Now that the spectrometer and vacuum system is setup, we are ready to study systems in molecular beams with the transient absorption spectrometer. We have plans to study a stable molecule, azulene, with visible pump - visible probe and UV pump - visible probe transient absorption spectroscopy as the final test of the spectrometer before making radicals.

The radicals will initially be generated through photolysis with an excimer laser, with a pyrolysis nozzle added eventually. Photolysis will be carried out with an Excimer laser, already installed, that is sent through the differential pumping slit and through the molecular beam. To incorporate photolysis into the ultrafast transient absorption spectrometer, a gated integration data acquisition program is being implemented. We will then start with studying the time-resolved excited state spectroscopy of vinyl and allyl radical. Experiments with a wide range of combustion radicals are planned for the future as well as increasing the spectral range of the spectrometer to include the infrared and mid-infrared region.

## Publications

Nicholas D. Cooper, Uyen M. Ta, and Melanie A. R. Reber, "Spectral shaping of an ultrafast ytterbium fiber laser via a passive intracavity optical filter: a simple and reliable route to sub-45 fs pulses," Appl. Opt. 62, 2195-2199 (2023)

# Photoinitiated Reactions of Molecules and Radicals in Molecular Beams

Hanna Reisler
Department of Chemistry, University of Southern California
Los Angeles, CA 90089-0482
reisler@usc.edu

## Program Scope

The UV photochemistry of organic molecules is a fundamental process that governs reactions in the atmosphere, synthetic chemistry, organic aerosols, and biological damage in living tissues. The ensuing dynamics usually involve pathways that are in competition, such as direct dissociation on excited states, couplings to lower potential energy surfaces, isomerization, and secondary dissociation of products. The current project is focused on the photochemistry of alpha-keto carboxylic acids, a group of acids implicated in aerosol formation and biological processes, which can also be a source of hydroxycarbenes. Another important class of molecules are the azines, such as pyridine and pyrazine, benchmarks for vibronic and spin-orbit couplings. Understanding their complex photophysical and photochemical behavior requires multiple experimental approaches and close cooperation between experiment and theory.

## Recent Progress

### The photophysics of pyrazine and 2-picoline on multiple potential energy surfaces

The azines and diazines have been the subject of intense spectroscopic research. These N-substituted aromatic molecules serve as components of nucleic acids (DNA and RNA) and fundamental understanding of their photophysics and photochemistry in the gas phase and in aqueous solutions is important. We initially attempted to characterize complexes of pyrazine with water but encountered issues that led us to realize that our understanding of the photophysics of these molecules is still incomplete.

The azines/diazines are isoelectronic with benzene, but the substitutions of CH groups with N atoms change their spectra relative to benzene and create new vibronic coupling pathways. The lone-pair electrons on nitrogen give rise to $n\pi^*$ transitions in the near UV region, whose vibronic bands have been assigned under room temperature and jet-cooled conditions. Not much higher in energy lie the much stronger $\pi\pi^*$ transitions, which are diffuse and not well characterized. Several "dark" states exist lower in energy, such as triplet states and the $^1$Au state.

The complexity of the spectral analysis arises because the $n\pi^*$ and $\pi\pi^*$ transitions are close in energy, and their upper states are known to interact and then further couple to the triplet and the ground state. The situation with the short lived $\pi\pi^*$ transition is particularly complicated, as its upper state, commonly known as $S_2$, decays in less than a picosecond, giving rise to lifetime broadening and loss of spectral features. The time evolution of the $S_2$ state has been studied with ultrafast lasers (<100 fs), but the quantum state-specific details of this decay remain unknown. At 300 K, substituted pyridines and pyrazines exhibit rather similar absorption spectra with two main systems assigned as $n\pi^*$ and $\pi\pi^*$ transitions, the former showing distinct vibronic levels, while the latter displaying only broad features. The detailed decay pathways, however, depend on factors such as symmetry, energy proximity of other electronic states, the location and type of conical

intersections, etc. High level theory together with detailed experiments carried out in the time and energy domain are required to answer the open questions.

Prof. Anna Krylov and I have initiated a collaborative experimental-theoretical project to elucidate the decay of the $S_2$ states of two prototype molecules, pyrazine (a diazine) and 2-picoline (an azine) and below we report preliminary results. The experimental studies on pyrazine (described last year) showed that the $S_2$ state, which lives only for about 20 fs, is not amenable to REMPI detection with nanosecond lasers. Our theoretical calculations, now in progress, are aimed at setting up detailed vibronic Hamiltonians for the pyrazine states that are expected to couple, $S_1(^1B_{3u})$, $S_2(^1B_{2u})$, and $^1A_u$.[1] The role of the dark $^1A_u$ state is still not clear, but the most recent work supports its involvement.[1] This is a challenging task, which we plan to accomplish with the help of Prof. John Stanton. The initial effort included calculations of Franck-Condon (FC) factors and preliminary analysis of vibronic interactions. We have identified the FC-active modes and the modes that are most likely to play a role in vibronic couplings of the electronic states (shaded in Figure 1). Currently, we are working on setting up a vibronic Hamiltonian based on EOM-EE-CCSD parameterization. Once completed, our results will provide benchmarks for future computational studies of other systems and will help validate more approximate models. The theoretical results will be compared to experimental findings.

| Mode No | Symmetry | Frequency ($cm^{-1}$) | Note |
|---|---|---|---|
| 0 | $a_u$ | 359.59 | |
| 1 | $b_{1u}$ | 434.35 | N out of plane |
| 2 | $a_g$ | 611.34 | N along y-axis |
| 3 | $b_{1g}$ | 718.33 | |
| 4 | $b_{3g}$ | 776.12 | |
| 5 | $b_{1u}$ | 821.18 | CH out of plane |
| 6 | $b_{2g}$ | 960.38 | CH out of plane |
| 7 | $b_{3g}$ | 999.24 | CH out of plane |
| 8 | $a_u$ | 1010.05 | CH out of plane |
| 9 | $b_{2u}$ | 1047.61 | |
| 10 | $a_g$ | 1051.70 | |
| 11 | $b_{3u}$ | 1098.16 | |
| 12 | $b_{3u}$ | 1145.23 | |
| 13 | $b_{2u}$ | 1175.98 | |
| 14 | $a_g$ | 1266.48 | CH in plane |
| 15 | $b_{1g}$ | 1385.05 | CH in plane |
| 16 | $b_{3u}$ | 1457.14 | CH in plane |
| 17 | $b_{2u}$ | 1537.21 | |
| 18 | $b_{1g}$ | 1612.79 | |
| 19 | $a_g$ | 1661.24 | |
| 20 | $b_{1g}$ | 3195.18 | CH stretch |
| 21 | $b_{2u}$ | 3196.70 | CH stretch |
| 22 | $b_{3u}$ | 3212.90 | CH stretch |
| 23 | $a_g$ | 3218.03 | CH stretch |

**Figure 1:** Pyrazine's ground state normal modes, their symmetries (Q-Chem convention) and frequencies, CCSD/aug-cc-pVTZ. The grey shading highlights modes likely involved in vibronic coupling between the three lowest excited states ($B_{1u}$, $B_{3u}$, and $A_u$) that will be included in the vibronic Hamiltonian.

For the experimental study, we chose 2-picoline (methyl substituted pyridine) because (i) the reported lifetime of its $S_2$ state (nearly 1 ps) was longer than that of pyrazine,[2] making it amenable to REMPI spectroscopy with nanosecond lasers; and (ii) its $S_1$ and $S_2$ states are close in energy, separated by only 2900 $cm^{-1}$, which should allow us to record the full spectral region between $S_1$ and $S_2$, in search of evidence of vibronic couplings. The origin of the $S_1$ state is at 34,766 $cm^{-1}$.[3,4] The corresponding value for $S_2$ is not well established and has been estimated at 37,620 $cm^{-1}$, from the first clear broad peak in the 300 K absorption spectrum seen in Figure 2(b).[5] The ionization energy is 72,371 $cm^{-1}$.[4] and two-photon excitation in a one-color experiment reaches above the adiabatic ionization threshold at photon energies > 36,185 $cm^{-1}$. We note that the symmetry of 2-picoline ($C_s$) is lower than that of pyridine and pyrazine due to the

methyl group, and the density of states is expected to be higher.

Referring to Figure 2, REMPI spectra of 2-picoline were recorded under molecular beam conditions. Mixtures of 2-picoline kept at 300 K in 1-2 atm He were expanded using a pulsed valve (200 μs opening time) and collimated using a skimmer. The picoline partial pressure and the delay between the laser and pulsed valve firings were adjusted to minimize contributions from clusters. The REMPI spectrum near the nπ* origin band is similar to that of jet cooled measurements reported earlier.[4] We extended the previous measurements to shorter wavelengths where nπ* absorption features overlap with the onset of the ππ* transition. Part of the spectrum is displayed in Figure 2(c). At wavelengths close to the nπ* origin, the vibronic bands are narrow and isolated, but as the wavelength decreases, some of the bands are broadened, and a featureless background signal appears, whose intensity increases gradually as the wavelength decreases. As described before,[4] some of the observed bands are not allowed in $C_s$ symmetry. These can gain intensity via vibronic interaction with $S_2$, which is of A' symmetry. We recognize that $C_s$ symmetry may be approximate, as it depends on the orientation of the methyl group relative to the aromatic ring. When symmetry is reduced to $C_1$ all vibronic transitions are allowed.

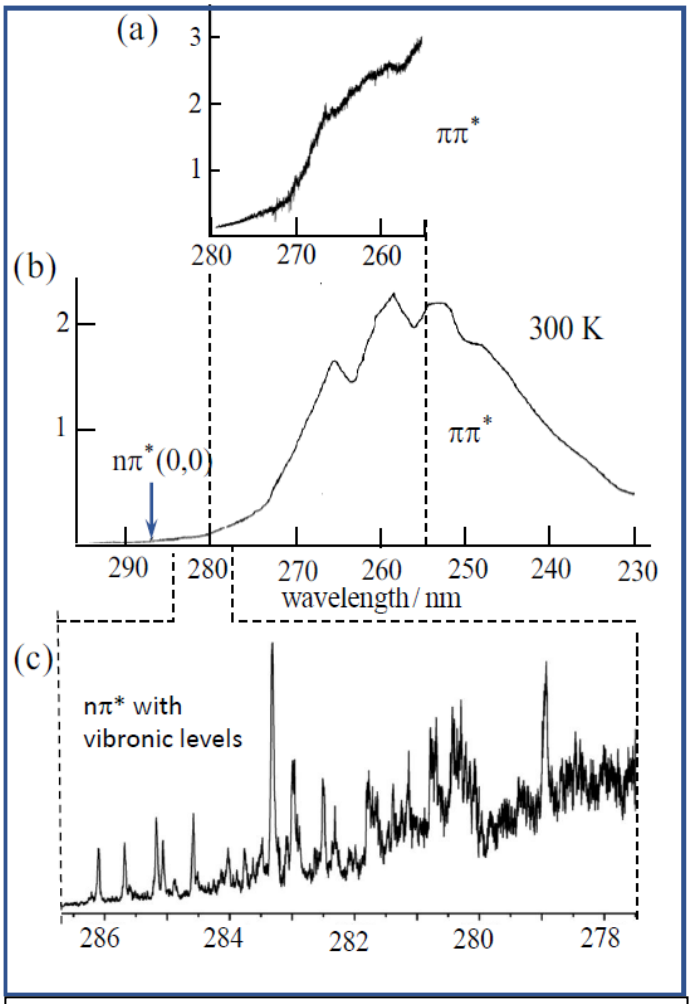


**Figure 2.** REMPI spectra of jet cooled 2-picoline are compared to its 300 K absorption spectrum shown in (b). Entry (a) is a portion of the ππ* system. Entry (c) shows the transition between the nπ* and ππ* systems. Intensity scales are arbitrary and do not reflect populations.

As the excitation wavelength further decreases, the sharp peaks disappear and the broad signal due to the ππ* transition dominates. Figure 2(a) shows a section of the jet cooled REMPI spectrum up to the maximum of the 300 K absorption spectrum shown in Figure 2(b). Only a few shallow features are observed. This is the first report of a jet cooled spectrum involving the $S_2$ state of the azines using a nanosecond laser. We are now extending the measurements to include the wavelength region beyond the maximum of the ππ* absorption system. We plan to carry out the spectral analysis, bearing in mind that a REMPI spectrum is an action spectrum in which we observe a signal only when excitation leads to the molecular ion. We will further explore the lifetime and decay mechanisms(s) with the help of theoretical calculations.

Evidently, the lack of structure in the jet cooled ππ*REMPI spectrum points to an $S_2$ lifetime shorter than the previously reported 900 fs.[2]

## Future work

We plan to continue the theoretical work on the vibronic Hamiltonian for the excited states of pyrazine. Prof. Krylov's student (Pawel Wojcik) will visit Prof. Stanton in the summer for two weeks to set up the Vibronic Hamiltonian model. We envision that our results will provide a benchmark for future computational studies of other systems and will help validate more approximate models. The REMPI spectroscopy of the picolines in the region of the nπ* and ππ* transitions will continue and extended from 2-picoline to 3- and 4-picoline, focusing on the wavelength regions where the transition from the nπ* to the ππ* absorption system occurs.

## References


1. V. Scutelnic, S. Tsuru, M. Pápai, Z. Yang, M. Epshtein, T. Xue, E. Haugen, Y. Kobayashi, A.I. Krylov, K.B. Møller, S. Coriani, and S.R. Leone. Nat. Commun. **12**, 5003 (2021).
2. B. Abulimiti, R. Zhu, J. Long, Y. Xu, Y. Liu, A. Y. Ghazal, M. Yang, and B. Zhang, J. Chem. Phys. **134**, 234301 (2011).
3. J.H.; Rush and H. Sponer, H. J. Chem. Phys. **20**, 1847 (1954)
4. N. Helle, S. Kruger and J. Grotemeyer, Current Phys. Chem. **8**, 58 (2018).
5. W. Roebke, J. Phys. Chem, **74**, 4198 (1970).


## Publications 2019-2022


1. S. Sutradhar, B.R. Samanta, R. Fernando, and H. Reisler, "Spectroscopy and two-photon dissociation of jet-cooled pyruvic acid", J. Phys. Chem. A **123**, 5906-5917(2019).
2. B.R. Samanta, R. Fernando, D. Rösch, H. Reisler, and D.L. Osborn, "Looking at the bigger picture: Identifying the photoproducts of pyruvic acid at 193 nm", J. Chem. Phys. **153**, 074307 (2020).
3. B. R. Samanta, R. Fernando, D. Rösch, H. Reisler, and D.L. Osborn, "Primary photodissociation mechanisms of pyruvic acid on $S_1$: observation of methylhydroxycarbene and its chemical reaction in the gas phase", Phys. Chem. Chem. Phys. **23**, 4107-4119 (2021).

# FUNCTIONAL GROUP EFFECTS ON UNIMOLECULAR QOOH REACTIONS AT HIGH PRESSURE USING HIGH-RESOLUTION ELECTRONIC ABSORPTION SPECTROSCOPY

Brandon Rotavera
*College of Engineering | Department of Chemistry*
*University of Georgia*
*Athens, GA 30602*

*rotavera@uga.edu* | (rotavera.uga.edu)

## Program Scope

The primary goal of this research program is to produce new fundamental knowledge on connections between molecular structure of hydroperoxy-substituted carbon-centered radicals (ȮOOH) and selectivity towards specific unimolecular reaction pathways (**Figure 1**). This knowledge is derived in part from combustion experiments using a jet-stirred reactor that is employed to measure isomer-resolved species concentration profiles of multi-functional intermediates derived from ȮOOH formed via oxidation of the C4 species in **Figure 2**. As a primary outcome, this research program expands gas-phase chemical kinetics knowledge on the effects of functional groups on chemical reactivity that is necessary to refine computational combustion models that support ongoing efforts to incorporate biofuels in current and future combustion systems. Additionally, owing to the complex combustion behavior of functionalized molecules, this program focuses on identifying new reaction pathways that are studied in greater detail using theoretical chemical kinetics computations, including potential energy surfaces and rate calculations. In addition, a primary focus of the program is to utilize experiments and chemical kinetics modeling to understand the effect of oxygen concentration on competing reactions of ȮOOH radicals formed from the species in **Figure 2**. In particular, experiments are conducted to specifically examine product formation from unimolecular reactions versus from the second-$O_2$-addition step. The red-highlighted text in Figure 1 indicates the classes of species produced via the former reaction type, which involve both constitutional isomers as well as stereoisomers and are important due to the connection to specific ȮOOH radicals that govern reactivity.

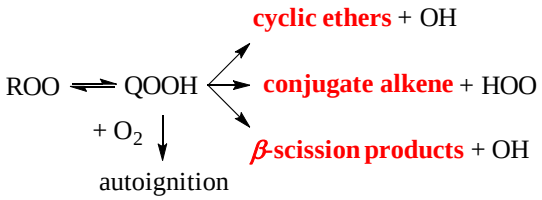


**Figure 1**. *Reaction mechanisms of ȮOOH radicals are central to understanding and developing modeling capabilities for hydrocarbon and biofuel oxidation. Accurately quantifying product formation from ȮOOH reflects the balance of chain-branching reactions (downward-pointing arrow) to chain-propagation and chain-inhibiting reactions (arrows pointing towards the right), each of which can produce an abundance of isomers.*

*Direct measurements of such isomers, e.g. cyclic ethers, provide stringent benchmarks of ȮOOH chemistry and are therefore central to the development of robust chemical kinetics mechanisms. This program bridges knowledge gaps between molecular structure and ȮOOH reactivity for C4 molecules, namely the balance of unimolecular decomposition vs. bimolecular reaction with $O_2$.*

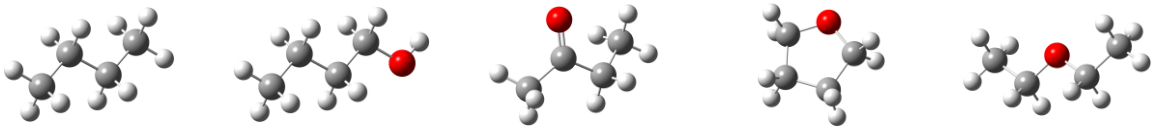

**Figure 2**. *Molecular structure of C4 species studied in this program (left to right): n-butane, 1-butanol, butanone, tetrahydrofuran, and diethyl ether*.

## Recent Progress

***Speciation experiments in a jet-stirred reactor***: The jet-stirred reactor (JSR) at the University of Georgia is capable of experiments at pressures up to 50 atm and operates with a well-characterized temperature profile. Particular attention is paid to quantifying spatial temperature uncertainty in the sampling region as well as in species quantification. Complete temperature characterization was accomplished using a systematic series of experiments conducted at residence times up to 4000 ms over a range of temperatures controlled independently in two distinct heating regions of the JSR, the reactor region and the pre-heating region. In all cases, owing to a custom-built, woven Inconel and ceramic insulation heating system, $1\sigma$ deviations in temperature are <1% of the reaction temperature (up to 1200 K) over a 3-cm sampling distance. Species quantification is accomplished with an uncertainty of ~10% in all cases and is achieved via tandem gas chromatography measurements via two independent detection methods (Figure 3). The first uses electron-impact (EI) mass spectrometry (Figure 3a). The second uses vacuum ultraviolet absorption spectroscopy (Figure 3b). The unique aspect of the tandem approach is that for each retention time, two molecular signatures are produced, an EI mass spectrum and an absorption spectrum measured from 5.167 – 9.920 eV, which enables resolution of both constitutional isomers and stereoisomers. An example of the latter is shown in **Figure 3** and is important due to stereochemical-dependent reaction chemistry [3-5].

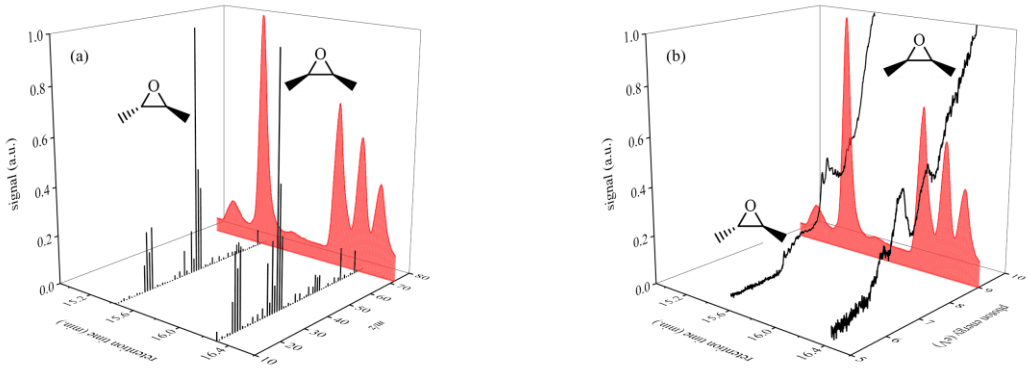


**Figure 3**. *EI mass spectra (a) and VUV absorption spectra (b) of 2,3-dimethyloxirane isomers.*

To examine the influence of temperature and oxygen concentration on intermediates from 1-butanol, similar to *n*-butane [6] and tetrahydrofuran [7], isomer-resolved speciation measurements were conducted at 810 Torr in a jet-stirred reactor (JSR) from 500 – 1000 K. **Figure 4** shows representative experimental results for the type of competing chemical pathways probed quantitatively. The main objective of these experiments is to provide specific, quantitative targets for modeling ȮOOH-mediated chemistry over a range of oxygen concentration to interrogate the chemistry depicted in Figure 1, particularly species that are uniquely formed via the unimolecular step including, in the case of alcohols, Waddington pathways and water-elimination, as well as the existence of cyclic ethers. Similar experiments were conducted for diethyl ether and butanone.

Despite low-lying channels on potential energy surfaces computed for peroxy radicals derived from 1-butanol, and in spite of our spectroscopic capability to detect 1-butanol-derived cyclic ethers [1, 2], none were detected in our experiments at 1 atm. This suggests that the pathway of ȮOOH → cyclic ether + ȮH, which is conventional to alkane oxidation as well as other, functionalized molecules, is unimportant. Instead, products of from alternative ȮOOH-mediated pathways, specifically Waddington (**Figure 4a**) and water-elimination were detected in significant quantities at 1 atm along with butanal from HOO-elimination. The inability to detect cyclic ethers has been an open question and ascribed, in the case of photoionization experiments, to cation instability. Because our spectroscopy technique probes absorption of ground-state neutrals, rather than relying on stable cations, we have the capability to detect these species and do not (at 1 atm).

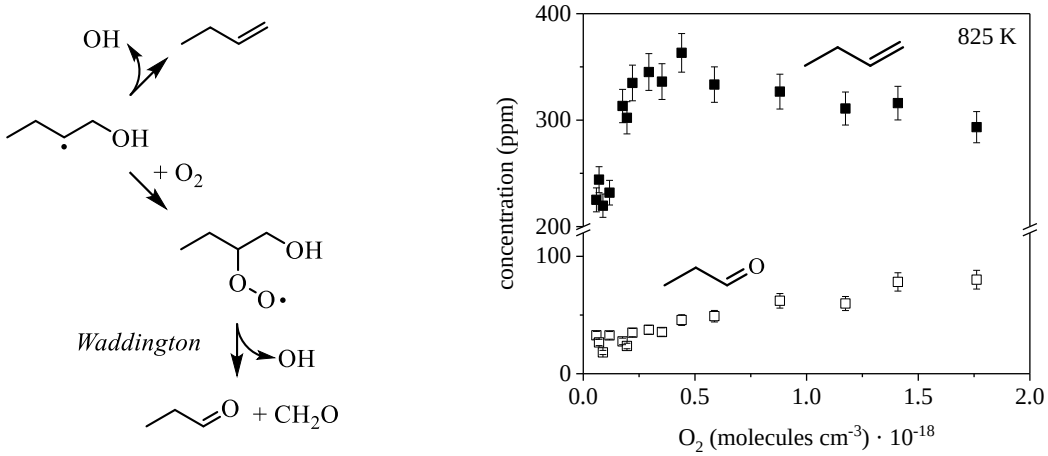


**Figure 4**. *(a) Chain-propagation reactions of 1-hydroxybut-2-yl via C–O β-scission yielding 1-butene and via the Waddington mechanism yielding propanal and $CH_2O$.*

## Machine Learning

Vacuum ultraviolet (VUV) absorption spectroscopy measurements conducted under x were utilized to construct machine learning models [8]. The motivation for this venture was to develop new statistical modeling capabilities to extract molecular structure information from VUV absorption spectra in order to determine the identity of species for cases where isolated, reference measurements are not possible. An example of this occurred in *n*-butane experiments of Hartness et al. [6] on hydroperoxybutyl reactions, wherein absorption signal detected at *m/z* 90 likely indicates an ROOH species yet it remains unclear what constitutional isomer is being detected (i.e. either 1-butylhydroperoxyde or 2-butylhydroperoxyde). The applicability of the basic hypothesis that we could use our spectroscopy database to build predictive machine learning models was tested in order to show proof-of-concept in Doner et al. [8]. Briefly, machine learning methods were applied in combination with measurements from the differential VUV-absorption spectra in the region 5.167 – 9.920 eV. Principal component analysis (PCA) was conducted for exploratory purposes to assist in identifying important spectral features that account for a large amount of the variance. Partial least-squares discriminant analysis (PLS-DA) was then applied to the raw spectral data and to data produced using pre-processing methods, such as functional transformations and stacking additional regression data. Our ML models provided binary assignments of certain molecular structure details with minimized statistical uncertainties. Five types of species were defined and, for modeling purposes were classified as: (1) alkane, (2) conjugation with oxygen (e.g. diacetyl), (3) non-conjugated alkene (e.g. 1,4-cyclohexadiene), (4) oxygen-containing (e.g. 1-butanol), or (5) cyclic (e.g. cyclohexanone). The latter classification excluded cyclic ethers. We utilized three quantitative metrics for assessing ML model performance: accuracy (percentage of species that are correctly identified), precision (percentage of species identified as being in a given class that actually belong to that class), and recall (percentage of species in a given class that are identified as belonging to that class).

## Future Work

***High-pressure jet-stirred reactor experiments***: A high-pressure control system is currently being implemented into the JSR for operation up to 50 atm. Temperature profile measurements are also being conducted to quantify temperature gradients and uncertainty as a function of reaction pressure in the combustion experiments, which is important due to changes in diffusion rates with pressure. Quantification of measurement uncertainties will be completed over the full range of experimental variables, namely temperature, pressure, and residence time.

***Rate computations***: Species for which new reaction pathways are identified, such as those proposed in Hartness et al. [4] and Koritzke et al. [5], will require rate computations and, in some cases, thermochemistry to include in chemical kinetics mechanisms to assess the impact on combustion model predictions. This will be accomplished using KinBot software and the MESS code in collaboration with both Sandia National Laboratories and Argonne National Laboratory.

***Refining chemical kinetics mechanisms***: The efforts above combine to achieve one of the primary goals of the program, which is increasing the quantitative prediction capabilities of chemical kinetics mechanisms by (i) providing new, benchmark experimental data, (ii) identifying new reaction pathways that may hold relevance to increasing the accuracy of modeling combustion, and (iii) computing theoretical rates. Future work on this topic will involve using existing mechanisms from the literature on the five species in **Figure 1** and refining via a combination of the efforts above.

**Publications/Presentations Acknowledging Support from the Gas-Phase Chemical Physics Program, 2020 – Present**:

1. (*invited seminar*, February 2023) **Combustion for Sustainable Transportation**, *University of Illinois*, Chicago, Illinois.
2. (*invited seminar*, March 2022) 7th Irvin Glassman Young Investigator Award Lecture, **The Importance of Reaction Mechanisms in Combustion**, *Spring Meeting of the Eastern States Section of the Combustion Institute*, Orlando, Florida.
3. **Simulation of the VUV Absorption Spectra of Oxygenates and Hydrocarbons: A Joint Theoretical-Experimental Study**, A. K. Bralick, E. C. Mitchell, A. C. Doner, A. R. Webb, M. G. Christianson, J. M. Turney, B. Rotavera, H. F. Schaefer III, *Journal of Physical Chemistry A* (Krishnan Raghavachari Festschrift), 2023.
4. **Probing $O_2$-Dependence of Hydroperoxy-Butyl Reactions via Isomer-Resolved Speciation**, S. W. Hartness, N. S. Dewey, M. G. Christianson, A. L. Koritzke, A. C. Doner, A. R. Webb, B. Rotavera, *Proceedings of the Combustion Institute*, Vol. 39, 2023.
5. **Machine Learning Models for Binary Molecular Classification using VUV Absorption Spectra**, A. C. Doner, H. A. Moran, A. R. Webb, M. G. Christianson, A. L. Koritzke, G. D. Smith, B. Rotavera, *Journal of Quantitative Spectroscopy & Radiative Transfer*, Vol. 297, 2023.
6. **Probing $O_2$-Dependence of Tetrahydrofuranyl Reactions via Isomer-Resolved Speciation**, A. L. Koritzke, M. G. Christianson, S. W. Hartness, N. S. Dewey, A. C. Doner, A. R. Webb, B. Rotavera, *Combustion and Flame (Special Issue in Honor of Jim Miller)*, 2023.
7. **Vacuum-Ultraviolet Absorption Cross-Sections of Functionalized Four-Carbon Species,** A. C. Doner, M. G. Christianson, A. L. Koritzke, A. Larsson, K. Frandsen, B. Rotavera, *Journal of Quantitative Spectroscopy & Radiative Transfer*, Vol. 292, 2022.
8. **Influence of Functional Groups on Low-Temperature Combustion Chemistry of Biofuels,** B. Rotavera and C. A. Taatjes, *Progress in Energy and Combustion Science*, Vol. 86, pp. 1-96, 2021.
9. **Vacuum-Ultraviolet Absorption Cross-Sections of Functionalized Cyclic Hydrocarbons: Five-Membered Rings,** M. G. Christianson, A. C. Doner, A. L. Koritzke, K. Frandsen, B. Rotavera, *Journal of Quantitative Spectroscopy & Radiative Transfer* Vol. 258, 2020.
10. (*invited seminar*, March 2021) "Influence of Functional Groups on Low-Temperature Combustion Chemistry of Biofuels", *Princeton/Georgia Tech Combustion Seminar Series*.

## References


[1] M.G. Christianson, et al., *J. Quant. Spec. Rad. Trans.*, 258 (2021) 107274.
[2] A.C. Doner, et al., *J. Quant. Spec. Rad. Trans.*, 292 (2022) 108346.
[3] A.C. Doner, et al., *Int. J. Chem. Kin.*, 53 (2021) 127-145.
[4] A.D. Danilack, et al., *J. Phys. Chem. A*, 125 (2021) 8064-8073.
[5] A.C. Doner, et al., *Faraday Discuss*, 238 (2022) 295-319.
[6] S.W. Hartness, et al., *Proc. Combust. Inst.*, 39 (2022).
[7] A.L. Koritzke, et al., *Combust. Flame*, (2022).
[8] A.C. Doner, et al., *J. Quant. Spec. Rad. Trans.*, 297 (2023) 108438.

**Coordinated Interrogation and Modeling in Ammonia Oxidation Catalysis**

William F. Schneider and Jason C. Hicks
Department of Chemical and Biomolecular Engineering, 250 Nieuwland Science Hall, Notre Dame, Indiana, 46556
wschneider@nd.edu, jhicks@nd.edu

## Program Scope

The overarching goal of this project, joint between GPCP and Catalysis Science, is to establish the potential for plasma stimulation to modify the behavior of a catalytic system, through application of plasma stimulation to well-defined and well-characterized thermal catalytic systems, chosen for reaction features that are amenable to careful experimental and computational interrogation. While the theory and practice of thermal heterogeneous catalysis is well established and design rules well understood, the same cannot be said of catalysis in the presence of external stimulus. Electrocatalysis and photocatalysis are two familiar examples of stimulated catalysis, but plasma-promoted catalysis is emerging as a third, high potential alternative. Plasmas are easy to generate and have the distinctive feature of creating non-equilibrium energy distributions within the plasma phase. By appropriately coupling this non-equilibrium behavior with a catalytic surface, we hypothesize that it is possible to carry out otherwise difficult or impossible chemical transformations, to do so at high efficiency, to take advantage of renewable electricity to drive chemistry, and to do so at smaller scales than those possible thermally.

This project combines careful synthesis and interrogation of catalytic materials and chemistry under plasma stimulation with first-principles-based microkinetic modeling to both elucidate and guide experiment. Its primary output will be fundamental insights transferable across this space. The project focuses on the catalytic chemistry of nitrogen. Nitrogen reductions and oxidations are of great economic value and critical to environmental protection, thermal catalytic chemistry is well understood, and relevant reactions are simple enough to be readily probed but complex enough to provide non-trivial insights. In particular, we focus on the reduction of $N_2$ (ammonia synthesis) and oxidation of $N_2$ (an alternative to the Ostwald process).

## Recent Progress

Ammonia synthesis: Ample literature evidence from our group and others indicates that ammonia can be formed at or near ambient conditions in a dielectric barrier discharge (non-thermal) plasma integrated with a catalytic surface. Our prior work (*Nature Catal.* **2018**, doi:10.1038/s41929-018-0045-1; *ACS Catal.* **2020**, doi:10.1021/acscatal.0c00684) reveals that at least one mode of action of the plasma is to decrease the demands on the catalytic surface to dissociate nitrogen. Recently published work (*ACS Sus. Chem. Eng.* **2021**, doi:10.1021/acssuschemeng.1c02713) highlights the potential for competing contributions of radical and vibrational excitations to influence ammonia production.

To provide more clarity into the influence of plasma on mechanisms of $NH_3$ synthesis on a catalytic material, we performed experiments at the Spallation Neutron Source at Oak Ridge National Laboratory and density functional perturbation theory to probe the relationship between exposure of a catalytic Ni surface to $N_2$ and/or $H_2$ plasma and the formed surface species. Both experiments and models highlight the appearance of chemisorbed hydrogen and of partially to fully hydrogenated nitrogen in the $N_2/H_2$ plasma, in contrast to a plasma-free control. Further, we

find that a sequential exposure to $N_2$ plasma and to $H_2$ without plasma leads to the same surface intermediates, highlighting the role of $N_2$ excitations specifically on ammonia synthesis. This work was published last year (*ACS Energy Lett.* **2021**, doi:10.1021/acsenergylett.1c00643).

The INS experiments provide compelling evidence that plasma activation of $N_2$ allows it to adsorb and dissociate on an otherwise unreactive catalytic surface. These findings motivated a series of sequential dosing experiments to decouple the plasma phase reactions from surface catalyzed pathways. Recently, we performed systematic plasma-assisted temperature programmed ammonia synthesis reactions (plasma-TPRxn) using this sequential $N_2$ plasma-catalyst stimulation followed by thermal hydrogen treatment. During the hydrogen treatment, the temperature was ramped to facilitate surface hydrogenation reactions. This approach avoids the influence of plasma-phase reactions and allows for the direct evaluation of the plasma activated nitrogen and the active surface of supported transition metal catalysts. These experiments confirm INS results that show plasma generated surface nitrogen can be converted to $NH_3$ through surface catalyzed pathways. Peak ammonia desorption temperatures vary with transition metal catalysts (Fe, Co, Ni, and Pt), reflecting differences in the hydrogenation ability of the catalysts as opposed to the ability to adsorb $N_2$, with Pt desorbing $NH_3$ at the lowest temperature. Unsteady state microkinetic models that incorporate nitrogen surface coverage dependency were developed and verified ammonia desorption trends across the metal catalysts. This work was published in *ACS Sustainable Chemistry & Engineering (ACS Sus. Chem. Eng.* **2022**, https://doi.org/10.1021/acssuschemeng.2c04217).

Nitrogen oxidation: Nitrogen oxidation to NO is an alternative route to nitrogen fixation that, because it is endothermic, is particularly well suited to plasma promotion. Nitrogen oxidation in thermal plasmas has a long history, and recent evidence indicates that the same is possible in non-thermal plasmas. We have developed a modeling framework to assess the potential for plasma-catalyst combinations to promote nitrogen oxidation over a metal catalyst, based on a reduced model for plasma-phase chemistry and DFT-predicted results for surface catalytic chemistry. The models highlight the sensitivity of NO productivity to plasma conditions (radical density, vibrational temperature, and mixing ratio) and reveal plasma regimes well suited to catalytic promotion of NO production (*J. Phys. D: Appl. Phys*. **2021**, doi:10.1088/1361-6463/ac1bd1). Experiments performed by collaborators at the Dutch Institute for Fundamental Energy Research (DIFFER) agree well with model predictions. The work is particularly significant in that it demonstrates quantitatively a plasma-catalytic coupling at conditions at which intrinsic plasma and catalytic contributions alone are negligible and which produces NO at concentrations that exceed thermal equilibrium (*Nat. Comm.* **2022**, doi:10.1038/s41467-021-27912-2). Current efforts focus on extending the models to incorporate coupled electro- and plasma-catalysis (see doi:10.1021/acsenergylett.0c02349 for motivation). In this configuration, only N2 passes through plasma, avoiding undesired plasma-phase $N_2/O_2$ reactions and potentially improving energy and atom efficiency.

The complexity of coupled plasma-phase reactions and plasma-surface reactions is reflected in the fact that most reports exploring the effect of catalytic materials are largely empirical. Although Edisonian-type exploration can lead to practical advances, they typically provide limited information on the fundamental elementary processes occurring at the plasma-catalyst interface. We developed an alternative design for a plasma-transmission IR cell capable of surface-sensitive, in situ/operando measurements under a wide range of plasma conditions. The design and function of the cell are comparable to commonly used dielectric barrier discharge

(DBD) plasma-catalytic reactors, and can easily be adopted as a widespread tool for rapidly obtaining large volumes of in situ plasma-catalysis data. The effectiveness of the cell was demonstrated using (1) plasma-oxidation of amine-functionalized SBA-15 to establish plasma-surface contact and (2) low-temperature nitrogen oxidation over a $Pt/SiO_2$ catalyst to provide an example of plasma-catalyst interactions. This work appeared in *ACS Engineering Au* (*ACS Eng. Au* **2022,** doi:10.1021/acsengineeringau.2c00026).

Our inelastic neutron scattering (INS) experiments provide evidence that plasma can activate molecular nitrogen to produce surface N intermediates that are reactive with separately dosed H2 to yield. $NH_3$. We hypothesized that these intermediates could also be available to other reactive pathways (e.g., oxidation). We demonstrated this possibility through carefully designed sequential experiments that initially expose a catalyst surface to a plasma stimulated nitrogen environment followed by a temperature programmed reaction with an oxygen feed. In the past year, we have focused on identifying the surface reactivity of Pt and Au under this sequential dosing approach. These metals were selected for their varying range of nitrogen and oxygen affinities to investigate how these parameters affect product formation and selectivity. We observe that the metals are indeed able to facilitate the reaction of plasma-activated nitrogen to produce multiple oxide species (NO, $N_2O$), with the product selectivity dependent on the metal selected. A manuscript highlighting these findings is in preparation.

Microkinetic modeling: Microkinetic models are the bridge between experimental observations and atomistic models. The treatment of adsorbate coverage continues to be a gap in current modeling approaches. We published a set of kinetic Monte Carlo (kMC) simulations probing the consequences of adsorbate interactions on observed rates, which appeared in the Michel Boudart special issue of *Journal of Catalysis* (*J. Catal.* **2022**, doi:10.1016/j.jcat.2021.12.005). In a manuscript submitted recently to the same, we extended this work to explore the ability of a mean-field model to capture kMC results. Mean-field models are less expensive to execute and more readily amenable to analysis (e.g., degree of rate control). By fitting kMC results to mean field equations, we show that it is possible to recover kMC rates and sensitivities, and further show that the optimal parameterization differs from conventions commonly employed by the community.

Lastly, as a side-product of our on-going interactions with the DIFFER team, we applied these coverage-dependent binding concepts to rationalize surprising experimental observations of the large and surprisingly temperature-dependent performance of a NiTi alloy towards the hydrogen evolution reaction. This work is in preparation for publication.

## Future Plans

Work to-date is refining our understanding of how plasma properties, reactor configuration, and material selection interplay to determine the productivity of plasma-catalyst combinations. Further progress depends on improved understanding of the mechanisms of reaction at the catalyst surface. We plan to continue to exploit in situ spectroscopy and transient product analysis to provide these mechanistic insights across a range of metal catalysts, using ammonia synthesis and nitrogen oxidation as our two model reactions. Computational models will be extended to encompass this wider material range. Our modeling strategy will follow two streams, one aimed at capturing trends with variation in material and ambient pressure plasma and the other aimed at quantitative predictions for precisely defined and low pressure plasmas.

## Publications Acknowledging DE-SC0021107


Clarke, R.; Hicks, J.C.; "Interrogation of the Plasma-Catalyst Interface via In Situ/Operando Transmission Infrared Spectroscopy", *ACS Eng. Au* **2022**, 2, 6, 535–546. https://doi.org/10.1021/acsengineeringau.2c00026

Barboun P.; Otor, H.; Ma, H.; Goswami, A.; Schneider, W. F.; Hicks, J. C.; "Plasma-Catalyst Reactivity Control of Surface Nitrogen Species through Plasma-Temperature Programmed Hydrogenation to Ammonia," *ACS Sus. Chem. Eng.* **2022**, *10*, 15741–15748. https://doi.org/10.1021/acssuschemeng.2c04217

Ma, H.; Sharma, R. K.; Welzel, S.; van de Sanden, M. C. M.; Tsampas, M. N.; Schneider, W. F. Observation and Rationalization of Nitrogen Oxidation Enabled Only by Coupled Plasma and Catalyst. *Nat Commun.* **2022**, *13*, 402. https://doi.org/10.1038/s41467-021-27912-2.

Goswami, A.; Ma, H.; Schneider, W. F. Consequences of Adsorbate-Adsorbate Interactions for Apparent Kinetics of Surface Catalytic Reactions. *Journal of Catalysis* **2022**, *405*, 410–418. https://doi.org/10.1016/j.jcat.2021.12.005.

Waitt, C.; Miles, A. R.; Schneider, W. F. Adsorbate Free Energies from DFT-Derived Translational Energy Landscapes. *J. Phys. Chem. C* **2021**, *125*, 20331–20342. https://doi.org/10.1021/acs.jpcc.1c05917.

Nematollahi, P.; Ma, H.; Schneider, W. F.; Neyts, E. C. DFT and Microkinetic Comparison of Ru-Doped Porphyrin-like Graphene and Nanotubes toward Catalytic Formic Acid Decomposition and Formation. *J. Phys. Chem. C* **2021**, *125*, 18673–18683. https://doi.org/10.1021/acs.jpcc.1c03914.

Ma, H.; Schneider, W. F. Plasma-Catalyst Modeling for Materials Selection: Challenges and Opportunities in Nitrogen Oxidation. *Journal of Physics D: Applied Physics* **2021**, *54*, 454004. https://doi.org/10.1088/1361-6463/ac1bd1.

Engelmann, Y.; van 't Veer, K.; Gorbanev, Y.; Neyts, E. C.; Schneider, W. F.; Bogaerts, A. Plasma Catalysis for Ammonia Synthesis: A Microkinetic Modeling Study on the Contributions of Eley–Rideal Reactions. *ACS Sustainable Chem. Eng.* **2021**, *9*, 13151–13163. https://doi.org/10.1021/acssuschemeng.1c02713.

Barboun, P.; Daemon L., Waitt, C.; Wu, Z.; Schneider, W.F.; and Hicks, J.C., "Inelastic Neutron Scattering Observation of Plasma-Promoted Nitrogen Reduction Intermediates on Ni/ɣ-$Al_2O_3$", *ACS Energy Letters,* **2021**, *6*, 2048–2053. https://doi.org/10.1021/acsenergylett.1c00643

Bogaerts, A.; Tu, X.; Whitehead, J. C.; Centi, G.; Lefferts, L.; Guaitella, O.; Azzolina-Jury, F.; Kim, H.-H.; Murphy, A. B.; Schneider, W. F.; Nozaki, T.; Hicks, J. C.; Rousseau, A.; Thevenet, F.; Khacef, A.; Carreon, M. The 2020 Plasma Catalysis Roadmap. *J. Phys. D: Appl. Phys.* **2020**, 53, 443001. https://doi.org/10.1088/1361-6463/ab9048

# ADVANCED DIAGNOSTICS

David W. Chandler, Jonathan H. Frank, Nils Hansen, Christopher J. Kliewer, Habib N. Najm, David L. Osborn, Krupa Ramasesha, Leonid Sheps, Craig A. Taatjes, Timothy S. Zwier
Combustion Research Facility, Sandia National Laboratories, MS 9055, Livermore, CA 94551-0969
chand@sandia.gov, jhfrank@sandia.gov, nhansen@sandia.gov, cjkliew@sandia.gov, hnnajm@sandia.gov, dlosbor@sandia.gov, kramase@sandia.gov, lsheps@sandia.gov, cataatj@sandia.gov, tszwier@sandia.gov

## PROGRAM SCOPE

The Gas Phase Chemical Physics Program at Sandia National Laboratories has a long history of innovation in Advanced Diagnostics that illuminate the hidden world of molecules and molecular transformations. In this subtask, Basic Energy Sciences funding has enabled numerous breakthrough technologies that impact chemical physics broadly, including: ion imaging, Frequency-Resolved Optical Gating (FROG), femtosecond molecular-frame photoelectron spectroscopy, single-shot 2-dimensional Coherent Anti-Stokes Raman (CARS) imaging, 4-dimensional tomographic Laser-Induced Fluorescence (LIF) imaging, Multiplexed Photoionization Mass Spectrometry (MPIMS), and time-resolved Photoelectron Photoion Coincidence Spectroscopy (PEPICO). These approaches include *in situ* laser and light source-based techniques that directly probe reacting environments, and *ex situ* techniques that extract species from reactive environments before implementing diagnostics that would be impossible under the native conditions of the chemically reacting system. Our recent work in optimal experimental design adds a new dimension to the coupling between experiment and theory, providing a feedback loop to optimize an experiment, thereby maximizing extracted information and quantifying uncertainty. As these advanced diagnostics mature, we implement them as new tools in the other subtasks of our Gas Phase Chemical Physics program at Sandia. Although our commitment to innovation is unchanged, going forward we will develop the next generation of diagnostics within each scientific subtask where they will be used. This year therefore marks the end of our Advanced Diagnostics subtask. This abstract contains a progress report summarizing past work. For proposed work on diagnostics developments, please see the other scientific subtasks of the Gas Phase Chemical Physics program at Sandia National Laboratories.

## RECENT PROGRESS

***Bayesian Optimal Experimental Design, Application to Time-of-Flight Mass Spectrometry*** We continued our work on applying Bayesian optimal experimental design (BOED) in a high-pressure photoionization mass spectrometry apparatus (HP-PIMS). We developed a Bayesian calibrated probabilistic model of the HP-PIMS experiment in the pre-photolysis phase, quantifying both parametric and model uncertainties. Using multi-level partitioning of the spectrum enabled us to efficiently perform calibration of the instrument model parameters, model error, on a TOF-MS data set with over $10^6$ measurements.[2] A sample of the calibrated model error correction performance is shown in Fig. 1. In addition to representing the pre-photolysis mass spectrum with uncertainty, calibrating the mass spectrometer model with model error revealed key deficiencies in the prior modelling assumptions. These included missing physics (e.g., high-harmonic ionization of $O_2$ or incomplete gas renewal between photolysis pulses) and poorly estimated model parameters (e.g., TOF calibration of the mass spectrum).

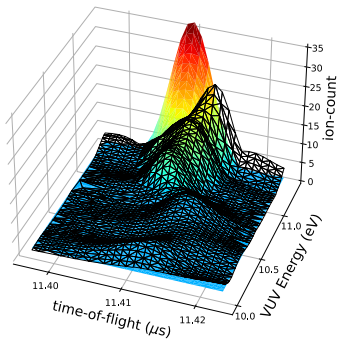


***Figure 1.*** *Comparison between predicted surfaces in the TOF region associated with m/z=34, without (colored surface) and with (mesh surface) model error. The latter better matches the experimental mass peak drift with varying VUV ionization energy.*

In general, due to its nested Monte Carlo (MC) estimation steps, BOED becomes computationally intractable for complex physics-based models due to costly simulation

times, and large number of model parameters and outputs. We addressed these challenges for BOED in high-dimensional models, utilizing both global sensitivity analysis and projection-based dimensionality reduction. We demonstrated this framework on the full HP-PIMS computational model, which includes 1146 uncertain reaction rate parameters and over half a billion model outputs representing the time- and energy-varying mass spectrum measured by the experiment. Our objective was to find design conditions that will most improve our estimate of specific sets of rate parameters. Including a variance-based global sensitivity analysis allows the method to identify the model parameters which are most-influential at each design. To reduce simulation time, we constructed surrogate models of the low-dimensional representation of the mass spectrum. Our BOED framework utilizes these low-dimensional surrogate models to compute the expected information gain (EIG) of an experiment. We marginalized over all nuisance parameters, i.e., parameters not of interest, to find the expected improvement for specific reactions of interest. We employed Bayesian optimization to maximize this EIG over the operating conditions of the apparatus (reactor temperature, pressure, initial concentration of radicals and oxygen). A manuscript is in-progress to report these results.

***Characterizing the Time-Resolved Photoelectron Photoion Coincidence Spectrometer*** Our time-resolved PEPICO spectrometer is now operational, and its capabilities using non-synchrotron vacuum ultraviolet radiation are documented in a recent publication .[1] Envisioned as the successor to our low-pressure Multiplexed Photoionization Mass Spectrometer, it provides velocity map imaging of both cations and electrons from user-selectable sources, including a hard supersonic expansion (pulsed or cw) and a side-sampled reactor tube for kinetics studies. We achieve mass resolution m/Δm = 4,000 when using the reactor tube and m/Δm = 11,000 with the hard supersonic expansion. The multiplexed capabilities of this apparatus provide a uniquely powerful instrument for the interrogation of chemical dynamics and kinetics of complex mixtures. We sort reactants, intermediates, and products in multiple dimensions: by m/z ratio, by kinetic time relative to an initiating event (e.g., a photolysis laser pulse), by photoionization spectrum, by mass-selected photoelectron spectrum, and by cation kinetic energy release. Figure 1 shows an example of these multidimensional capabilities for $SO_2$ photodissociation at λ = 193 nm with ionization radiation at 16.85 eV. The time-resolved photoelectron spectrum of m/z = 48 ($SO^+$ ions) in panel B can be projected onto either an energy or time axis (panels A and C), while the mass spectrum (panel D) shows a clear distinction between the daughter ions from $SO_2$ neutral (broad, red) and the narrow feature (yellow) representing parent ions of SO neutral. In future work

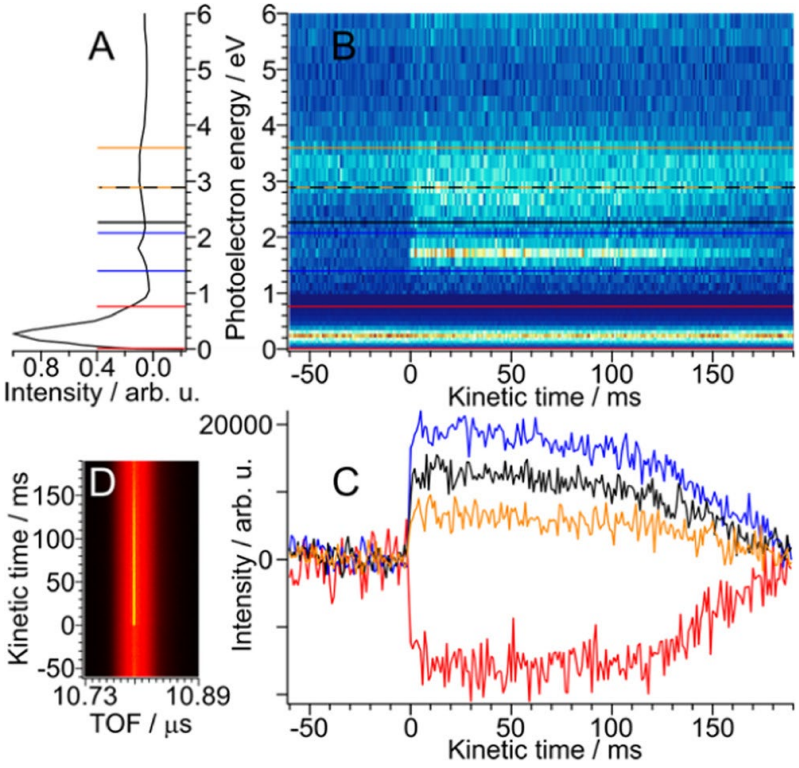


*Figure 2: Time-resolved PEPICO data of m/z = 48 ($SO^+$) from photodissociation of $SO_2$, ionized at 16.85 eV. The panels show different projections of the data as detailed in the text.*

we will implement the chamber for scientific goals in the Kinetics, Dynamics, and Ultrafast Chemical Physics subtasks.

***Broadband Microwave Spectroscopy for Isomer-specific Detection of Transient Intermediates*** Broadband microwave spectroscopy experiments of transient intermediates will be carried out in one of two vacuum chambers. A 3D rendering of the supersonic expansion-based CP-FTMW instrument is shown in Fig. 3. When structural characterization of the reactive intermediates/free radicals is the primary goal, one of several pulsed sources for creating them can be used, including flash pyrolysis, pulsed electric discharge, or photolysis. In collaboration, we have incorporated the unique high *P*/high *T* source[79] designed by Sheps, so that microwave detection of its effluent is possible. This is an exciting development, because the high *P* conditions can be used to prepare high concentrations of specific intermediates that are hard to prepare otherwise (e.g., ROO radicals), thus affording a unique source for spectroscopic interrogation. Since this source is continuous, we will collect FIDs every 20 μs, equivalent to a signal averaging rate of 50 kHz so that 1M shot averages will take just 20 seconds to record.

Over the past two years, we have also designed and nearly completed construction of a cryo-cooled buffer gas cell (CBGC) shown in Fig. 3a, which will enable complementary experiments to those the supersonic expansion. In this case, a Pulse Tube cooler will be used to cool He buffer gas in the cell, and the gas mixture of interest will be injected into this cell where the molecules are interrogated with broadband microwave pulses. The longer residence time of the molecules in the buffer gas cell (10–20 ms anticipated) will enable interrogation at 50 kHz, albeit at the expense of somewhat higher rotational temperatures (~4–6 K). Cooling the low-noise amplifier to 5 K will drop the noise floor of the experiment by about a factor of 8 relative to room temperature.

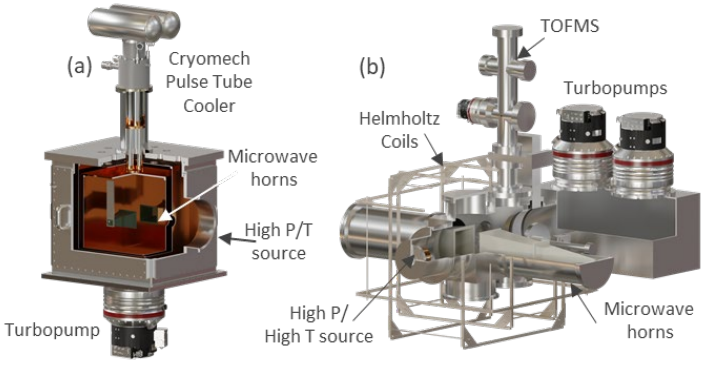


***Figure 3****. 3D rendering of the vacuum chambers that incorporate (a) a cryo-cooled buffer gas cell and (b) a supersonic expansion as the means of cooling. The chamber in (b) also possesses a TOFMS for PIMS analysis.*

***Detection of spatially resolved reaction products near a surface using REMPI and ion imaging*** Improved instrumentation for monitoring the location and kinetics of chemically or catalytically active domains on an arbitrary surface is an attractive and potentially transformative goal as detailed understanding of catalytic activity requires one to understand exactly what features (step, plateau, crack, grain boundary, particular exposed surface) on a catalytic material are responsible for the observed bulk reactivity. This past year we demonstrated a new approach for imaging the local gas phase distribution over an active catalyst in the near-surface region, a velocity-selected spatial map ion imaging (VSSMII) spectrometer. The concept is depicted in Figure 4; velocity mapped ion imaging (VMII) is combined with spatial map ion imaging (SMII) simultaneously to substantially reduce the spatial blur that is inherent in a spatial image of REMPI cations projected to an ion detector. This blur is caused by the significant thermal translational velocity distribution of the parent molecules.

First, a velocity-mapped image is formed at a plane within the instrument. At this location, regardless of the starting spatial position of the ions, ions of the same velocity vector are mapped to the same spatial position. Differing positions correspond to differing velocities. It is analogous to the optical imaging

Fourier plane. At this location in the current instrument, an electrically grounded pinhole is mounted in the time-of-flight portion of the instrument. As this pinhole is placed at the velocity-mapped image plane, only a small subset of initial molecular velocities is allowed to pass through. Cations only within this narrow subset of velocity space are allowed to expand forming the spatial image on the ion detector. The velocity selected ions that pass through the pinhole continue toward the detector and spread. One can think of this as a pinhole camera. In this experiment, the pinhole is placed in the center of the velocity distribution (that is, nominally 0 m/s lateral projection) and thus only those molecules that are moving perpendicular to the surface are projected onto the detector. Thus, the image maps the concentration of product molecules over the surface.

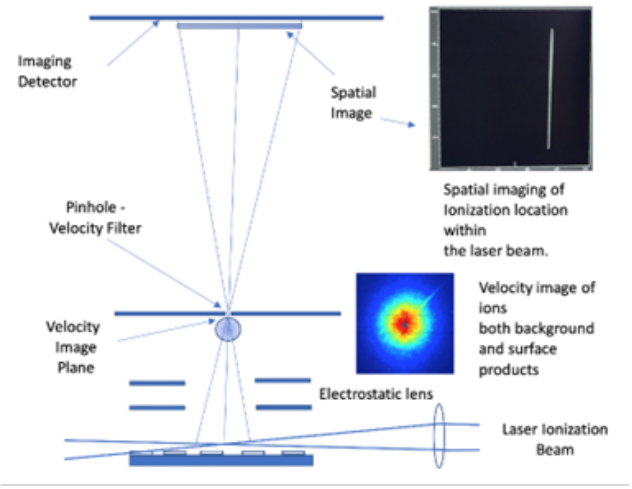


***Figure 4.*** *Schematic of apparatus. A laser beam skims the surface of a patterned catalytic electrode that repels the cations that are formed by the focused laser beam. Electrostatic lenses focus the ions onto a pinhole in a metal plate thereby velocity selecting the ions that will pass through to the imaging detector. A line image of the laser focus is formed.*

The resolution of the current instrument was determined. First, the movement of the imaged ionizing laser line across the phosphor screen was tracked while moving a micrometer controlling the laser position over the sample, allowing us to determine that the dispersion was 13 micrometer/pixel on the camera. As shown in Figure 4 (top right), the FWHM of the image of the focused laser beam was evaluated to be ~60 micrometer. Given that the laser focus is smaller than this, it is an upper limit to the resolution with a 50 micrometer pinhole. Our image is slightly blurred by such things as the point spread function of a single ion strike and the fact that our image is not a point source of ions. Thus, the resolution of the system is demonstrated to be set primarily by the pinhole size. So for this camera the pixel resolution will not limit the VSSMII until we utilize a pinhole of ~15 microns or smaller.

Finally, we tested the instrument over a patterned sample of Pt deposited on Au. The hypothesis is that one may observe an increased HD production rate over the Pt strips when dosing the surface with $H_2$ and $D_2$ from molecular beams. Figure 5 shows a significantly enhanced production of HD over one of the Pt strips. The width of the strip is denoted by the blue line in the plot. We plan future work using this instrument in the Multiphase Interactions subtask of our program to study local catalytic processes related to water redox reactions.

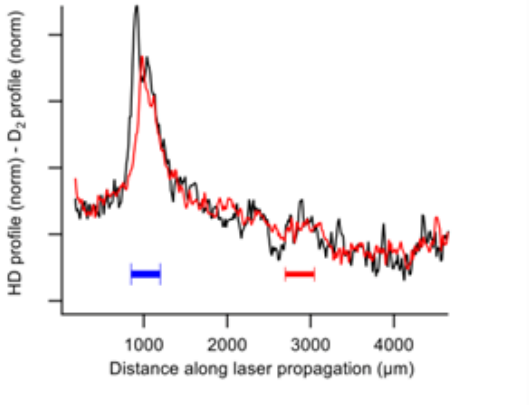


***Figure 5.*** *Imaged intensity profile from the HD (J=3) REMPI line along the laser beam. The laser was first tuned to the two-photon E,F transition from J=2 $D_2$ to provide an image normalization profile. The experiment was reproduced (black and red lines). The blue strip indicates the width of a single Pt strip on the sample. The red strip indicates where the next Pt strip would be on the patterned sample.*

## BES-sponsored publications, 2020 – present


1. D. Rösch, R. Almeida, B. Sztaray, and D. L. Osborn, High-Resolution Double Velocity Map Imaging Photoelectron Photoion Coincidence Spectrometer for Gas-Phase Reaction Kinetics, *J. Phys. Chem. A* **2022**, 126, 1761.
2. J. Oreluk, L. Sheps, and H. Najm, Bayesian model calibration for vacuum-ultraviolet photoionization mass spectrometry. *Combustion Theory and Modelling* **2022**, 26, 513.
3. B. Zhou, J. H. Frank, B. Coriton, Z. Li, X-S. Bai, M. Alden, Experimental Perspective and Challenges. In: N. Swaminathan, X-S. Bai, C. Fureby, N. E. L. Haugen, G. Brethouwer editors. Turbulent Combustion Physics: Cambridge University Press; **2022**.
4. D. Rösch, R. L. Caravan, C. A. Taatjes, K. Au, R. Almeida, and D. L. Osborn, Absolute Photoionization Cross Section of the Simplest Enol, Vinyl Alcohol, *J. Phys. Chem. A* **2021**, 125, 7920.
5. J. H. Frank, Advances in imaging of chemically reacting flows, *J. Chem. Phys.* **2021**, 154 (4), 040901.
6. S. M. Fritz, P. Mishra, J. Wullenkord, P. G. Fugazzi, K. Kohse-Höinghaus, T. S. Zwier, N. Hansen, Detecting Combustion Intermediates Via Broadband Chirped-Pulse Microwave Spectroscopy, *Proceedings of the Combustion Institute* **2021,** 38, 1761.
7. P. Mishra, S.M. Fritz, S. Herbers, A.M. Mebel, T.S. Zwier, Gas-phase pyrolysis of *trans* 3-pentenenitrile: Competition between Direct and Isomerization-directed Dissociation, *Phys. Chem. Chem. Phys.* **2021**, 23, 6462.
8. B. Zhou, T. Li, J. H. Frank, A. Dreizler, B. Bohm, Simultaneous 10 kHz three-dimensional CH2O and tomographic PIV measurements in a lifted partially-premixed jet flame, *Proceedings of the Combustion Institute* **2021,** 38, 1675.
9. B. Zhou, J. H. Frank, Experimental study of vorticity-strain interactions in turbulent premixed counterflow flames, *Proceedings of the Combustion Institute* **2021,** 38, 2909.
10. T. Li, B. Zhou, J. H. Frank, A. Dreizler, B. Böhm, High-speed volumetric imaging of formaldehyde in a lifted turbulent jet flame using an acousto-optic deflector, *Exp. Fluids* **2020**, 61 (4), 112.

# CHEMICAL DYNAMICS METHODS AND APPLICATIONS

David W. Chandler, Laura M. McCaslin, David L. Osborn, Judit Zádor, Christopher Kliewer, Timothy S. Zwier
Sandia National Laboratories, MS 9051, Livermore, CA 94551-0969
chand@sandia.gov, lmmccas@sandia.gov, dlosbor@sandia.gov,
jzador@sandia.gov, cjkliew@sandia.gov, tszwier@sandia.gov

## PROGRAM SCOPE

This program focuses on unraveling the mechanisms and timescales of dynamical processes in molecular systems via multiplexed experimental and theoretical techniques. These studies employ high-level electronic structure and dynamics theory alongside time-resolved spectroscopic tools to investigate rotational, vibrational, electronic, and reaction dynamics in molecular systems. The work reported here relates closely to studies performed in the Ultrafast Physics, Ultrafast Chemistry, Advanced Diagnostics, Multiphase Interactions, and Electron-Driven Chemistry tasks, all of which encompass studies of energy flow within molecules, correlations between nuclear and electronic motion, and development of advanced optical techniques.

Highlights from our program include photoelectron photoion coincidence studies of the 193 nm photodissociation of $SO_2$, broadband microwave spectroscopy of tunneling dynamics, site-specific photochemistry mapped by IR spectra in the excited state, and studies of electronic energy transfer between remote, near-degenerate chromophores.

## RECENT PROGRESS

### *$SO_2$ Photodissociation: Unexpected Formation of S+$O_2$ (Osborn)*

The photodissociation dynamics of $SO_2$ at $\lambda$ = 193 nm, exciting the $\tilde{C}(^1B_2)$ state, have been well studied for decades. The only product channel reported in the literature is formation of $O(^3P)$ + SO ($^3S^-$). There is experimental evidence for both internal conversion and intersystem crossing in the predissociation mechanism of the bound initially excited $\tilde{C}(^1B_2)$ state. We chose photodissociation of $SO_2$ as a simple test case for validating the capabilities of the new Time-Resolved PhotoElectron PhotoIon Coincidence Spectrometer (TR-PEPICO), and in the process discovered clear evidence for a minor photodissociation channel producing $S(^3P)$ + $O_2(^3S_g^-)$. We observe photodissociation of $SO_2$ and production of all four photoproducts, confirmed by their photoionization and photoelectron spectra. Our experiments quantify the branching fraction for this channel of 2 – 4%, based on different literature photoionization cross sections of $S(^3P)$ and confirm that this new product channel results from single photon excitation. Together with MRCI calculations of the ground and excited state singlet and triplet surfaces (collaboration with Xixi Hu and Hua Guo), we conclude that this product channel can occur only after internal conversion to the ground electronic state. Quasi-classical trajectory calculations show that the mechanism involves isomerization to a transient SOO intermediate followed by dissociation. This unexpected photodissociation pathway may help reconcile discrepancies in sulfur mass-independent fractionation mechanisms in Earth's geologic history, which shape our understanding of the Archean atmosphere and the Great Oxygenation Event that occurred 2.4 billion years ago in Earth's evolution.

### *An OH in Fluorine's Clothing: Tunneling Dynamics in Perfluorophenol [7] (Zwier)*

Tunneling is a quintessential quantum mechanical process with important implications for such wide-ranging areas as quantum control and reaction kinetics. We have begun a project that uses chirped-pulse Fourier Transform microwave (CP-FTMW) methods to probe molecules with unusual tunneling pathways, multiple tunneling pathways, or free radicals where tunneling occurs in the presence of an unpaired electron. We are presently writing up a study of OH tunneling in perfluorophenol ($C_6F_5OH$, PFP), a close analog of hexafluorobenzene ($C_6F_6$), with one fluorine atom (19 amu) replaced by a hydroxyl group (17 amu). This

substitution has a threefold effect: it provides a permanent dipole moment, the molecule remains very close to the oblate symmetric top limit, and intramolecular H-bonds between the OH and adjacent fluorine atoms are formed. These factors result in the unusual case of a polar, tunneling, near-symmetric top. We have recorded and analyzed the broadband rotational spectrum of perfluorophenol between 7.5 and 17.5 GHz. Transitions between the split torsional states were observed only for a-type rotational transitions due to the sign change of $\mu_a$ upon internal rotation of the OH group. The energy difference between the split $0^+$ and $0^-$ torsional states was established to be 24.850 MHz while the calculated barrier to internal rotation ($V_2$) is 1210 $cm^{-1}$. This observed energy splitting is much lower than might be expected for this barrier height when compared to other phenolic derivatives due to the larger heavy-atom motions associated with the tunneling event that breaks and re-forms H-bonds.

### *Site- and Conformer-specific Photochemistry along a Protonated Peptide Scaffold[18] (Zwier)*

Photoexcitation is a powerful means for initiating chemistry, yet the outcome of such excited state processes becomes harder to predict as the size and chemical complexity of the reactants grows. We are presently using a multi-stage mass spectrometer outfitted with a cryo-cooled octopole ion trap to explore photochemistry of large, conformationally complex ions with multiple competing product channels. In particular, IR-UV double resonance spectroscopy was used to study the photophysics and photochemistry of single conformations of protonated Leu-enkephalin (Tyrosine-Glycine-Glycine-Phenylalanine-Leucine, YGGFL) and its chromophore-swapped analog FGGYL (**Figure 1**) under cryo-cooled conditions in the gas phase. UV-IR gain spectra recorded as a function of delay between UV and IR pulses revealed unique IR signatures for the Tyr OH stretch in the first excited singlet ($S_1$) produced by photoexcitation and the triplet states ($T_n$(v)) formed by intersystem crossing.

The detected photochemical pathways include intersystem crossing to the triplet manifold, proton transfer leading to backbone fragmentation, electron transfer from the aromatic ring to the $NH_3^+$ group leading to loss of neutral $NH_3$, and excited state loss of the tyrosyl radical side chain. The loss of neutral $NH_3$ following electron transfer is selectively present in Conformer A of YGGFL, which incorporates a π H-bond between the N-terminal protonated amine ($NH_3^+$) and the π cloud of Tyr. The single observed conformer for FGGYL was proven to be identical to that of conformer A of YGGFL, but the site-specific swap of Tyr for Phe moves the Tyr chromophore further away from the $NH_3^+$ group, preventing electron transfer over this longer distance.

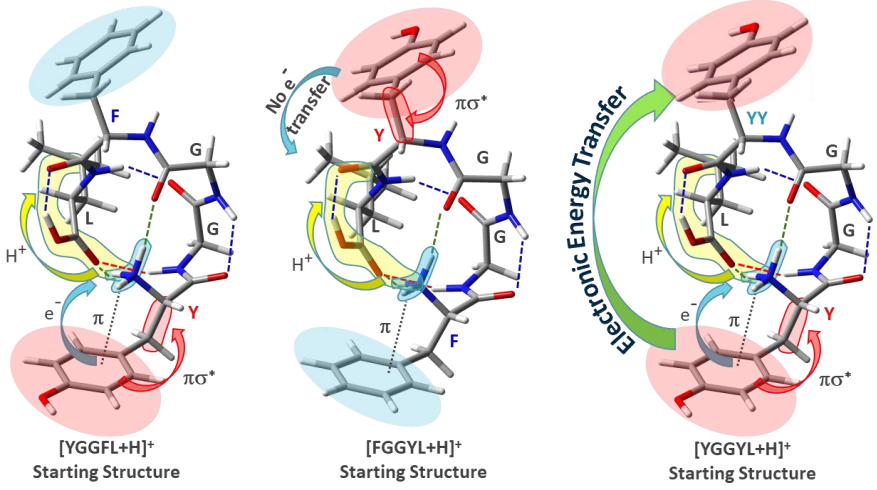


*Fig. 1: The dominant conformations of protonated YGGFL, FGGYL, and the bichromophore YGGYL.*

***Site-Directed Electronic Energy Transfer and its Photochemical Implications[19] (Zwier)***

Building off the studies of YGGFL and FGGYL, we have used similar methods to study the photophysics and photochemistry of YGGYL, with its two Tyr chromophores in unique local environments, separated from one another by 11 Å (**Figure 1**). These studies are the first steps towards proposed work involving more complex chromophore arrays in which site-directed electronic energy transfer can be used to control the photochemical pathways available to large multi- chromophores. We used IR-UV gain spectroscopy to prove that the structure of YGGYL is the same one as in YGGFL and FGGYL (**Figure 1**), and then recorded UV-IR gain spectra as a function of delay between IR and UV lasers to map out the excited state dynamics and determine the photochemical pathways that are enhanced by IR excitation in the excited state. We have mapped out the time profiles for each chromophore site, with $S_1$ lifetimes that differ by almost a factor of two between the two Tyr sites. Notably, there is no evidence for the electron transfer (ET) pathway leading to loss of neutral $NH_3$ following excitation of Y(1), even though this pathway dominates in YGGFL. This shut-off of ET arises because electronic energy transfer (EET) from Y(1) to Y(4) out-competes ET. This is an example of EET turning off ET rather than facilitating it.

**FUTURE WORK**

***Super Rotor Dynamics (Kliewer, Osborn, McCaslin)***

In order to develop our program's study of non-equilibrium systems, experiments involving highly rotationally excited molecules will be performed. While the effects of highly excited translational and vibrational states on chemical reactions are well-characterized, the effects of highly rotationally excited molecules are not as well understood. During the past year, the laser-based molecular optical centrifuge has been finished and demonstrated under the Ultrafast Physics section of our program. This year we plan to begin work on the photodissociation dynamics of $N_2O$ super-rotors. We will expand $N_2O$ in a supersonic jet to cool the rotational distribution to only the lowest few J states. This distribution will be accelerated to super-rotor states. We will dissociate $N_2O$ at ~203 nm and observe the $O(^1D)$ and the $N_2$ fragments via resonance-enhanced multi-photon ionization coupled with VMI imaging. Beyond this direct observation of photodissociation dynamics from an unexplored position on the PES, this will allow a direct test if rotation-to-vibration coherence transfer as recently observed for $CO_2$ super-rotors is a ubiquitous phenomenon. Furthermore, to better understand the reactions of super-rotors and atoms, we will react rotationally excited $N_2O$ and $O(^1D)$ to form NO, monitoring via VMI.

***Tunneling dynamics (Zwier, Zádor)***

Our studies of OH tunneling in perfluorophenol highlight the extraordinary sensitivity of microwave spectra to tunneling dynamics. We propose to expand this work in three directions. First, we will explore the spectroscopic consequences for OH tunneling of a remote substitution that breaks the symmetry of the above and below plane tunneling pathways for OH internal rotation. Second, we will probe the effects of an unpaired spin on the OH tunneling barrier by studying the microwave spectroscopy of *o*-, *m*-, and *p*-hydroxy phenoxy radicals. Third, we will study tunneling in a series of molecules containing multiple, coupled tunneling pathways (e.g., $CH_3$ and OH internal rotations).

***Excited state photochemistry (Zwier, McCaslin)***

In our cryo-cooled ion spectroscopy/dynamics experiments, we will extend our studies of photochemistry in YGGYL by ring-deuteration of one of the Tyr (Y) chromophores. This will enable us to mass-selectively distinguish between two photochemical channels that are indistinguishable from one another in YGGYL; namely, the loss of the Tyr side-chain, $\dot{C}H_2$-PhOH or Tyr(d4) side chain, $\dot{C}H_2$-Ph(d4)OH. Since this side-chain loss is unique to UV-excited Tyr, it is a marker of where electronic excitation resides, giving us a mass spectral diagnosis of the efficiency of electronic energy transfer (EET). This will provide a clean mechanism to vary the energy difference $\Delta E$ between the two excitation sites, and hence understand how the vibronic coupling, EET, and competition between photochemical pathways depend on this energy difference. Second, we will substitute a non-natural amino acid with a nitrile substituted phenyl ring (PhCN) in place of one of the Tyr amino acids in YGGYL. When substituted in the Y(4) position to form

YGG(PhCN)-L, we anticipate a reversal in the energy ordering of the two excited states. Thus, compared to YGGYL, we hope to reverse the direction of EET to enhance the dissociative electron transfer reaction, exerting a degree of control over the photochemistry.

***High-Resolution Molecular Scattering (Chandler)***

In the past there has been much success in testing the potential energy surfaces associated with bimolecular reaction of diatomic molecules with rare gas atoms. Velocity Mapped Ion Imaging enabled measurements of the differential cross section of a single quantum state of the scattered molecule. The image so obtained was of a single Newton sphere, as the rare gas had no internal quantum states that could be populated by the collision energy. Attempts at performing molecule-molecule scattering such that one can investigate ever more complex potential energy surfaces has been hampered by two issues: (i) even in a molecular beam several quantum states of the molecules are often populated, and (ii) the velocity spreads in the molecular beam can obscure/blur the Newton spheres for individual rotational product states of the collision partner. Recently the Meerakker group in the Netherlands has implemented a creative solution by utilizing a Stark decelerator to pick a single quantum state from a molecular beam and then selectively slow a narrow velocity distribution of that selected molecule to use as a scattering partner. However, the ability to Stark decelerate the collision partner(s) limits which molecules can be studied, and the technique, while a tour de force, is expensive. We propose to investigate an alternative technique that is simpler and more universal. With the advent of extremely high-resolution infrared quantum cascade lasers we intend to demonstrate that we can selectively excite a narrow velocity group in a molecular beam to the first vibrational level (as the resolution of the laser is much smaller than the Doppler profile of the molecular beam) and scatter this single quantum state from a molecular partner and thus resolve the correlated scattering differential cross sections for all energetically possible product channels. We will begin with the scattering of NO(v=1 J=1.5) from $O_2$.

***Vibrational spectroscopy and Dynamics (McCaslin)***

Recent progress in development of mixed quantum-classical (MQC) dynamics methods for predicting vibrational spectra has enabled quantification of the underlying molecular motion corresponding to each spectral feature. More specifically, when spectral features are broad, these techniques can identify how the underlying molecular motion changes across the feature, providing detailed theoretical insight into the physical underpinnings of spectral broadening. In this framework we can assign a particular nuclear displacement coordinate for each discrete frequency in the Fourier transform. With these techniques in mind alongside recent developments in machine learned (ML) potentials for attaining CCSD(T) accuracy at force field cost, we propose development of low-cost hybrid ML-density functional theory (DFT) approaches to computing IR spectra. One of the major drawbacks of these ML force fields is the poor representation of dipole moments, resulting in unreliable IR intensities when spectra are predicted from MQC dynamics. To overcome these issues, we propose computing the energies and gradients involved in MQC dynamics with newly developed ML force fields. Vibrational densities of state will be computed from the autocorrelation function of the velocities. IR intensities will be computed from DFT only in the spectral region of interest via computation of dipole derivatives along molecular coordinates associated with the discrete frequency. We propose to use these low cost methods to obtain low-cost dynamics with higher accuracy IR intensities to study the vibrational structure of strongly coupled and anharmonic systems such as molecules that exhibit proton-coupled electron transfer (PCET).

**BES-SPONSORED PUBLICATIONS (SINCE 2020)**

1) D. Rosch, Y. Xu, H. Guo, X. Hu, and D. L. Osborn, $SO_2$ Photodissociation at 193 nm Directly Forms $S(^3P) + O_2(^3\Sigma_g^-)$: Implications for the Archean Atmosphere on Earth, *J. Phys. Chem. Lett.* **2023**, 14, 3084, DOI: 10.1021/acs.jpclett.3c00077

2) J. D. Savee, B. Sztaray, P. Hemberger, J. Zador, A. Bodi, and D. L. Osborn, Unimolecular Isomerization of 1,5-Hexadiyne Observed by Threshold Photoelectron Photoion Coincidence Spectroscopy, Faraday Discussions, 2022, DOI: 10.1039/D2FD00028H
3) J. D. Savee, B. Sztaray, O. Welz, C.A. Taatjes, D. L. Osborn, Valence Photoionization and Autoionization of the Formyl Radical, *J. Phys. Chem. A* **2021**, 125, 3874. DOI:10.1021/acs.jpca. 1c01775
4) J.L. Fischer, K.M. Blodgett, C.P. Harrilal, P.S. Walsh, S.H. Choi, and T.S. Zwier, Conformer-specific Spectroscopy and IR-induced Isomerization of a Model γ-peptide: Ac-$\gamma^4$-Phe-NHMe, J. Phys. Chem. A **126**, 1837 (2022). DOI: 10.1021/acs.jpca.2c00112
5) John T. Lawler, Christopher P. Harrilal, Andrew F. DeBlase, Edwin L. Sibert III, Scott A. McLuckey, and Timothy S. Zwier, "Single-conformation Spectroscopy of Cold, Protonated $^{D}$PG-containing peptides: Switching β-turn types and Formation of a Sequential Type II/II' Double β-turn", Phys. Chem. Chem. Phys. **24**, 2095-2109 (2022). DOI: 10.1039/D1CP04852J
6) Edwin L. Sibert III, Karl N. Blodgett, and Timothy S. Zwier, Spectroscopic Manifestations of Indirect Vibrational State Mixing: Novel Anharmonic effects on a pre-reactive H-atom transfer surface, J. Phys. Chem. A **125** 7313 (2021). DOI: 10.1021/acs.jpca.1c04264
7) Christopher Harrilal, Andrew DeBlase, Scott McLuckey, and Timothy S. Zwier, 2-Color IRMPD Applied to Conformationally Complex Ions: Probing Cold Ion Structure and Hot Ion Unfolding", J. Phys. Chem. A **125**, 9394 (2021). DOI: 10.1021/acs.jpca.1c08388
8) A.O. Hernandez-Castillo, Camilla Calabrese, Sean M. Fritz, Iciar Uriarte, Emilio J. Cocinero, and Timothy S. Zwier, "Bond Length Alternation and Internal Dynamics in Model Aromatic Substituents of Lignin", ChemPhysChem **23** (in press). DOI: 10.1002/cphc.202100808
9) Alignment and Dissociation of Electronically-Excited Molecular Hydrogen With Intense Laser Fields, M. Fournier, G.V. Lopez, A.K. Spiliotis, T.A. Casey, T.P. Rakitzis, D.W. Chandler, Mol. Phys. **119**, 1 (2020). DOI: 10.1080/00268976.2020.1778200

# Chemical Kinetics for Complex Systems

*Jacqueline H. Chen, Nils Hansen, Habib N. Najm, David L. Osborn, Leonid Sheps, Craig A. Taatjes, Judit Zádor, and Timothy S. Zwier*
*Sandia National Laboratories, MS 9055, Livermore, CA 94551-0969*
jhchen@sandia.gov, nhansen@sandia.gov, hnnajm@sandia.gov, dlosbor@sandia.gov, lsheps@sandia.gov, cataatj@sandia.gov, jzador@sandia.gov, tszwier@sandia.gov

## Program Scope

We employ experiment and theory to elucidate mechanisms of elementary chemical reactions, which impacts the research theme of Reaction Pathways in Diverse Environments. This task extends the high-resolution view of Sandia's "Chemical Dynamics" task to encompass complex interactions in collisional environments, and it provides a basis for the interface studies in Sandia's "Multiphase Interactions" subtask. Analytical tools that use tunable vacuum ultraviolet light from the Advanced Light Source synchrotron at Lawrence Berkeley National Laboratory and chirped pulse microwave spectroscopy enable sensitive and isomer-specific detection of reactant and product molecules sampled from chemical reactions. These individual reaction studies are linked to controlled measurements of more complex reaction systems as found in well-defined laboratory scale zero- and one-dimensional reactors. Alongside, we use master equation frameworks based on automated potential energy surface (PES) exploration tools, and approaches to study stochastic and nonthermal effects at the mesoscale.

## Recent progress

***Recent developments in automated kinetics***[1] In our JPCA Feature Article we have shown how our automated kinetics workflow code, KinBot, can explore and characterize in a kinetically relevant manner reaction pathways for autoxidation and hydrocarbon chemistry. We studied the room-temperature oxidation pathways of limonene using multi-conformer transition-state theory, where KinBot was able to handle geometrically difficult reaction searches for these large radical species. The kinetics and branching fractions along with uncertainties for a nitrogen-containing heterocycle, pyrrolidine, were calculated, demonstrating how our workflow can facilitate better experiment–theory comparisons in the future. The kinetics of a simple KHP was studied, and we pointed out the importance of dynamic effects. On the $C_5H_5$ and $C_6H_6$ PESs we found numerous new pathways, and we illustrated the difficulties in the context of automation when the stationary points are weakly bound, and how it might lead to ambiguities in the graph representing the connections between species. Our work highlighted important outstanding shortcomings in most automated kinetics workflow tools setting goals for further research.

***The fate and role of ketohydroperoxides in autoxidation systems through theory and experiment***[5] A crucial chain-branching step in autoignition is the homolytic decomposition of ketohydroperoxides (KHPs), but it competes with the "Korcek" dissociation reaction. In a collaborative work with Popolan-Vaida (UCF) and Leone (Berkeley)[5] we characterized the formation of a γ-KHP and its decomposition to formic acid + acetone in jet-stirred reactor measurements and in laser-initiated oxidation experiments during *n*-butane oxidation. Modeling the time-resolved production of formic acid provides an estimated upper limit of 2 $s^{-1}$ for the rate coefficient of KHP decomposition to formic acid + acetone.

***Elucidating the photodissociation fingerprint and quantifying the determination of organic hydroperoxides in gas-phase autoxidation***[44] In this work, we developed a mild and method for the synthesis of alkyl hydroperoxides (ROOH) with various structures, and we systematically measured the absolute photoionization cross-sections of the ROOHs using synchrotron vacuum ultraviolet-photoionization mass spectrometry. We found that organic hydroperoxide cations are largely dissociated by loss of OOH. This fingerprint was used for the identification and accurate quantification of the organic peroxides and it can therefore be used to improve models for autoxidation chemistry.

***Kinetics in complex environments***[22-24] In this work we performed a collaborative study with Pitsch (RWTH Aachen, Germany) to explore the oxidation chemistry of 1,3-dioxane and 1,3-dioxolane. [22] Using our jet-

stirred reactor (JSR)-MBMS instrument, we found that 1,3-dioxane is more reactive in the low-temperature regime compared to 1,3-dioxolane. An explanation is the difference in the C-O bond dissociation energies, which leads to different dissociation pathways, i.e., 1,3-dioxane favors low-temperature chain branching pathways to form keto-hydroperoxides and other oxygenates weakening the adjacent C-O and C-C bond before ring-opening. In contrast, direct ring-opening is the dominant pathway for 1,3-dioxolane due to lower C-O bond dissociation energies. The experimental work that allowed for the identification of the key intermediates during low-temperature oxidation was followed by a theoretical exploration of the reaction pathways of 1,3-dioxane oxidation. [24] In similar experiments, we investigated the low-temperature oxidation chemistry of 2- and 3-pentanone in a collaboration with Yang (Tsinghua University, China). [23] These ketones are interesting to study because the ROO radicals tend to produce resonance-stabilized QOOH radical structures. The intramolecular hydrogen migration reactions are slowed down in the presence of the carbonyl functional group, which makes the low-temperature reactivity of the two C5 ketones lower than that of *n*-pentane.

***Conformer-dependent chemistry in the OH-initiated oxidation of vinyl alcohol***[45] Two theoretical investigations reached opposing conclusions of the dominant branching pathway in the OH-initiated oxidation of vinyl alcohol, namely whether glycolaldehyde + $HO_2$ or formaldehyde + formic acid + OH is dominant. Our experiments show that the glycolaldehyde:formic acid branching ratio is 3.6:1.0, supporting the former theoretical prediction. Interestingly, the *syn*-VA conformer, which is estimated to be 82% of the VA population at 298 K, forms mostly the glycolaldehyde product channel, whereas the minor conformer, *anti*-VA leads to the formic acid product channel. This reaction demonstrates the importance of reactant conformation on branching and highlights the need for conformer-specific probes of chemical reactions.

***Fundamental studies of the reactivity of Criegee intermediates***[15] We investigated the reaction of acetaldehyde oxide ($CH_3CHOO$), which has two conformers depending on whether the OO group is oriented towards (*syn*) or away from (*anti*) the methyl group, with dimethylamine (DMA) in a collaboration spearheaded by Caravan (ANL), with Klippenstein (ANL) and Lester (U. Penn). This reaction proceeds via a 1,2 insertion of the carbonyl oxide into the N-H bond of DMA. Experiments showed an extremely rapid reaction of the *anti*-$CH_3CHOO$ with DMA but a negligible reaction for the *syn* conformer. Theoretical kinetics from ANL showed that a pre-reactive complex in the entrance channel for the *syn*-$CH_3CHOO$ reaction presents a submerged barrier that reduces the rate coefficient by a predicted factor of 34,000 relative to the reaction of *anti*-$CH_3CHOO$.

***OH ($X^2\Pi$) + cyc-$C_5H_6$: Oxygenated resonance-stabilized radical formation***[33] In collaboration with Goulay (UWV), we studied the OH + cyc-$C_5H_6$ reaction using MPIMS. From the time-resolved photoionization spectra we conclude that only the 5-hydroxycyclopent-2-en-1-yl (*cyc*-$C_5H_6OH$) resonance-stabilized radical is formed. CCSD(T)-level stationary points we calculated on PES suggest that the reaction mechanism involves formation of a pre-reactive van der Waals complex that isomerizes over a submerged barrier to the deep well of 5-hydroxycyclopent-2-en-1-yl. Our master equation calculations predict that this stabilization product remains the only outcome up to $T = 500$ K, and should be favorable even at very low temperatures, which shows the impact this fundamental chemistry investigation could have on.

***Stiff chemical systems***[36] Chemical kinetic systems are commonly modeled as dynamical systems which satisfy requisite mass/enthalpy conservation laws by construction. Moreover, for stiff systems, the associated reduced chemical models involve differential algebraic equations. Employing local state perturbations is inconsistent with the implicit constraints. We explored the consequences of these constraint violations for homogeneous ignition of $H_2$/air and $CH_4$/air systems. [36] Using eigen-analysis of system Jacobians, we showed that it is critical for accuracy to identify the correct dynamical partitioning of the state variables, which can be done using computational singular perturbation methods.

***Non-thermal chemistry/termolecular reactions***[19, 40] The impact of non-thermal reaction chemistry on the propagation of combustion fronts (from deflagration waves transitioning to detonations) was studied using direct numerical simulation (DNS) for a $H_2$-$CH_4$ fuel mixture burning in air in a bounded domain, representing compression ignition in an idealized engine cylinder. [19] Inclusion of non-thermal termolecular

reactions in the DNS influences chemical reaction fluxes during high-pressure $H_2$-$CH_4$ combustion and the manner of transition from deflagration to detonation fronts. In particular, H + $O_2$ forms long-lived excited-state intermediates, $H_2O$* and $HO_2$*, that react with H, O, OH, and $O_2$ *before* undergoing collisional stabilization. The effects of radical-molecule association and radical-radical recombination induced nonthermal reactivity on the initiation, propagation and structure of wedge-stabilized oblique detonation waves were studied.[40] Results show that non-thermal reactivity leads to a higher mean heat release rate due to the contribution of two termolecular reactions to mean exothermicity, exceeding many of the baseline thermal reactions, resulting in a shorter initiation length and larger detonation cell size.

**Proposed Work**

***The role of singlet and triplet PESs in bimolecular reactions***. In the next year, we propose to conduct experimental and computational studies to elucidate the mechanisms of ROO self-reactions and the role of ISC in determining the branching among the possible product channels. We will focus on small model systems with alkyl and oxygenated R. We will quantify RO, ROOH, and ROOR using PIMS by measuring the observed product yields as a function of [$O_2$]. We hypothesize that systematic variation of [$O_2$] will allow us to constrain the yields of ROO, RO, ROOH, and ROOR from the overall C atom balance. We will also probe the ROO self-reactions at elevated temperatures where ROOH and ROOR become thermally unstable, providing additional constraints on speciation measurements and on the mechanism. The proposed experiments will be closely coupled to calculations for kinetics and branching on $^3$RO-OR and $^1$RO-OR PESs as well as ROO + $HO_2$ and ROO + R kinetics. We will first establish the methods by which these complicated reactions can be systematically and effectively studied and implement these developments in our automated kinetics workflow code, KinBot, to allow us to then extend the calculations more easily to larger, more complex systems, and understand how for instance the structure of R influences the kinetics.

***Stereoisomer-specific kinetics*** Our goal is to experimentally determine the *nascent* branching fractions for formation of diastereomeric forms for peroxy radicals formed from a series of cyclic organic precursors using chirped pulse Fourier transform microwave (CP-FTMW) spectroscopy coupled to a cryo-cooled buffer gas cell or a supersonic expansion as the means of cooling along with TOFMS for PIMS analysis. The broadband microwave spectra will be used for structure identification and to quantify the abundances of products using computed dipole moments that determine the intensities of rotational transitions. The aim of the experiments is to determine the branching for intuitive interpretation, and to serve as a benchmark and advance calculations. VRC-TST is an accurate theoretical framework, which, when applied correctly, can yield errors in the 10-20% range for total rate coefficients. However, for larger systems, theory needs to make compromises in things like basis set and number of sampled points. Moreover, the branching fractions can be sensitive to the location of the dividing surfaces and to dynamic effect.

***Criegee chemistry*** We will continue to explore the chemistry of carbonyl oxide CIs, focusing on questions where mechanistic information is available via the powerful capability of synchrotron PIMS to characterize product channels. This part of the program will include continued collaboration on work led by Rebecca Caravan (ANL), Klippenstein (ANL) and Lester (Penn). We will be extending the work our groups have performed on the oligomerization reactions of CIs, reactions in which several CI additions can occur in succession. We will also explore detection of products with the new photoelectron photoion coincidence (PEPICO) machine to take advantage of the higher specificity of photoelectron spectra, and we will investigate the role of water as a chaperone (or catalyst) for bimolecular reactions of CIs with other species.

***Mechanism and kinetics of carbene reactions*** Our 2021 publication on the 351-nm photodissociation of pyruvic acid (PA, $CH_3C(O)C(O)OH$) showed that singlet-methylhydroxycarbene (MHC, $CH_3$-C-OH) is a primary photodissociation product. That work provided evidence for the first known observation of a bimolecular reaction of MHC, namely MHC + PA $\rightarrow$ $C_4H_8O_2$ + $CO_2$. This work opened the door to the direct study of reactions of MHC, which we will pursue in the next year. We will measure the kinetics of reactions of MHC and their isomer-resolved product distribution. We will also develop a master equation

treatment of the reaction kinetics and product branching to predict not only the room temperature results to compare with our experiments and provide rate coefficients in a much broader temperature range.

***Data-science driven saddle-point geometry prediction*** In recent years, KinBot has generated tens of thousands of saddle points for various organic molecules. We propose to build a database and to use the already available saddle point structures to improve our saddle point guess generation, reducing the cost and failure rate of the search using atomic environment vectors (AEVs) to fingerprint the reactions. We will also explore the possibility of using constrained generative adversarial networks (CGANs) to provide a generative engine for candidate geometries in an interpolative regime.

***Bayesian optimal experimental design*** We will continue working on Bayesian optimal experimental design (BOED) for the HP-PIMS apparatus. This is work that was originally part of the "Advanced diagnostics" subtask of Sandia. We are currently in an operational mode in this setting, where, starting from available HP-PIMS data, we are using BOED to propose new experimental conditions in the pursuit of increased estimated expected information gain on targeted reaction rates, proceeding to take measurements at these conditions, and iterating on this loop. Based on preliminary data from this activity, we are enhancing the modeling framework with an *embedded* model error construction, aside from the already implemented additive model error setup, which will be useful in better informing uncertainty on measured rates at each step.

We will also pursue the application of BOED for optimizing performance of the PEPICO spectrometer for time-resolved reaction kinetics. The key output of the instrument is a set of mass-selected photoelectron spectra that are obtained from the time and positions of photoelectrons/photoions incident at the detectors. The main goal of BOED here is to minimize peak widths in photoelectron spectra.

***Nonthermal processes in heterogeneous environments*** We plan to use DNS with the termolecular phenomenological modeling approach and DNS with a multi-temperature formulation to study non-equilibrium reaction systems behind a planar detonation wave and a high-Mach turbulent shear layer triggered by a Kelvin–Helmholtz instability between streams of $H_2/O_2/N_2$ and $H_2$/air. Both methods will be informed by DSMC simulations performed at a molecular level in SPARTA for similar flow configurations. We will assess the effect of non-thermal termolecular and thermo-chemical non-equilibrium on planar detonation waves, particularly focusing on initiation length and detonation cell structure.

We plan to assess the effect of non-equilibrium in key reactions of the latter mechanism, by means of QCT calculations performed using existing potential energy surfaces (PES) data currently available. Moreover, we will compare DNS with the phenomenological termolecular chemistry model and the multi-temperature DNS/DSMC approach applied to study chemical non-equilibrium effects on detonation wave structure and dynamics. We will improve on a commonly used model in DSMC, the Quantum-Kinetic (QK) model, to include non-equilibrium effects. While the QK model has been shown to be robust for dissociation and exchange reactions for near-equilibrium conditions, it doesn't account for state-specific reaction rate coefficients, important for non-equilibrium conditions. Hence, we plan to include QCT-informed chemistry models in DSMC to represent state-specific reaction cross-sections.

## BES-sponsored publications, 2020–present


**1.** Zádor, J.; Martí, C.; Van de Vijver, R.; Johansen, S. L.; Yang, Y.; Michelsen, H. A.; Najm, H. N., Automated reaction kinetics of gas-phase organic species over multiwell potential energy surfaces. *J. Phys. Chem. A* **2023**.

**2.** Sheps, L.; Dewyer, A. L.; Demireva, M.; Zádor, J., Quantitative detection of products and radical intermediates in low-temperature oxidation of cyclopentane. *J. Phys. Chem. A* **2021,** *125* (20), 4467-4479.

**3.** Demireva, M.; Oreluk, J.; Dewyer, A. L.; Zádor, J.; Sheps, L., Genetic algorithm optimization of a master equation cyclopentane oxidation model against time-resolved speciation experiments. *Combust. Flame* **2022**, 112506.

**4.** Doner, A. C.; Zádor, J.; Rotavera, B., Stereoisomer-dependent unimolecular kinetics of 2,4-dimethyloxetanyl peroxy radicals. *Faraday Discuss.* **2022,** *238* (0), 295-319.

**5.** Popolan-Vaida, D. M.; Eskola, A. J.; Rotavera, B.; Lockyear, J. F.; Wang, Z.; Sarathy, S. M.; Caravan, R. L.; Zádor, J.; Sheps, L.; Lucassen, A.; Moshammer, K.; Dagaut, P.; Osborn, D. L.; Hansen, N.; Leone, S. R.; Taatjes, C. A., Formation of organic acids and carbonyl compounds in n-butane oxidation via γ-ketohydroperoxide decomposition. *Angew. Chem. Int. Ed.* **2022,** *61* (42), e202209168.

**6.** Chen, B.; Ilies, D. B.; Hansen, N.; Pitsch, H.; Sarathy, S. M., Simultaneous production of ketohydroperoxides from low temperature oxidation of a gasoline primary reference fuel mixture. *Fuel* **2021,** *288*, 119737.
**7.** Ramasesha, K.; Savee, J. D.; Zádor, J.; Osborn, D. L., A new pathway for intersystem crossing: Unexpected products in the O(3P) + cyclopentene reaction. *J. Phys. Chem. A* **2021,** *125* (45), 9785-9801.
**8.** Liao, H.; Tao, T.; Sun, W.; Hansen, N.; Yang, B., Isomer-specific speciation behaviors probed from premixed flames fueled by acetone and propanal. *Proc. Combust. Inst.* **2021,** *38* (2), 2441-2448.
**9.** Bierkandt, T.; Hoener, M.; Gaiser, N.; Hansen, N.; Köhler, M.; Kasper, T., Experimental flat flame study of monoterpenes: Insights into the combustion kinetics of α-pinene, β-pinene, and myrcene. *Proc. Combust. Inst.* **2021,** *38* (2), 2431-2440.
**10.** Braun-Unkhoff, M.; Hansen, N.; Dietrich, M.; Methling, T.; Moshammer, K.; Yang, B., Entanglement of n-heptane and iso-butanol chemistries in flames fueled by their mixtures. *Proc. Combust. Inst.* **2021,** *38* (2), 2387-2395.
**11.** Chen, B.; Kruse, S.; Schmid, R.; Cai, L.; Hansen, N.; Pitsch, H., Oxygenated pah formation chemistry investigation in anisole jet stirred reactor oxidation by a thermodynamic approach. *Energ. Fuel.* **2021,** *35* (2), 1535-1545.
**12.** Terracciano, A. C.; Neupane, S.; Popolan-Vaida, D. M.; Blair, R. G.; Hansen, N.; Vaghjiani, G. L.; Vasu, S. S., Elucidating the differences in oxidation of high-performance α- and β- diisobutylene biofuels via synchrotron photoionization mass spectrometry. *Sci. Rep.* **2020,** *10* (1), 21776.
**13.** Rieth, M.; Gruber, A.; Williams, F. A.; Chen, J. H., Enhanced burning rates in hydrogen-enriched turbulent premixed flames by diffusion of molecular and atomic hydrogen. *Combust. Flame* **2022,** *239*, 111740.
**14.** Taatjes, C. A.; Caravan, R. L.; Winiberg, F. A. F.; Zuraski, K.; Au, K.; Sheps, L.; Osborn, D. L.; Vereecken, L.; Percival, C. J., Insertion products in the reaction of carbonyl oxide Criegee intermediates with acids: Chloro(hydroperoxy)methane formation from reaction of CH2OO with HCl and DCl. *Mol. Phys.* **2021,** *119* (17-18), e1975199.
**15.** Vansco, M. F.; Zou, M.; Antonov, I. O.; Ramasesha, K.; Rotavera, B.; Osborn, D. L.; Georgievskii, Y.; Percival, C. J.; Klippenstein, S. J.; Taatjes, C. A.; Lester, M. I.; Caravan, R. L., Dramatic conformer-dependent reactivity of the acetaldehyde oxide Criegee intermediate with dimethylamine via a 1,2-insertion mechanism. *J. Phys. Chem. A* **2022,** *126* (5), 710-719.
**16.** Vansco, M. F.; Zuraski, K.; Winiberg, F. A. F.; Au, K.; Trongsiriwat, N.; Walsh, P. J.; Osborn, D. L.; Percival, C. J.; Klippenstein, S. J.; Taatjes, C. A.; Lester, M. I.; Caravan, R. L., Functionalized hydroperoxide formation from the reaction of methacrolein-oxide, an isoprene-derived Criegee intermediate, with formic acid: Experiment and theory. *Molecules* **2021,** *26* (10), 3058.
**17.** Vansco, M. F.; Caravan, R. L.; Pandit, S.; Zuraski, K.; Winiberg, F. A. F.; Au, K.; Bhagde, T.; Trongsiriwat, N.; Walsh, P. J.; Osborn, D. L.; Percival, C. J.; Klippenstein, S. J.; Taatjes, C. A.; Lester, M. I., Formic acid catalyzed isomerization and adduct formation of an isoprene-derived Criegee intermediate: Experiment and theory. *Phys. Chem. Chem. Phys.* **2020,** *22* (46), 26796-26805.
**18.** Miller, J. A.; Sivaramakrishnan, R.; Tao, Y.; Goldsmith, C. F.; Burke, M. P.; Jasper, A. W.; Hansen, N.; Labbe, N. J.; Glarborg, P.; Zádor, J., Combustion chemistry in the twenty-first century: Developing theory-informed chemical kinetics models. *Prog. Energy Combust. Sci.* **2021,** *83*, 100886.
**19.** Desai, S.; Tao, Y.; Sivaramakrishnan, R.; Wu, Y.; Lu, T.; Chen, J. H., Effects of non-thermal termolecular reactions on detonation development in hydrogen (H2)/methane (CH4) - air mixtures. *Combust. Flame* **2022,** *244*, 112277.
**20.** Huang, C.; Zhou, Z.; Li, S.; Tao, T.; Zhang, F.; Hansen, N.; Law, C. K.; Yang, B., From inherent correlation to constrained measurement: Model-assisted calibration in mbms experiments. *Proc. Combust. Inst.* **2021,** *38* (1), 1071-1079.
**21.** Doner, A. C.; Zádor, J.; Rotavera, B., Unimolecular reactions of 2,4-dimethyloxetanyl radicals. *J. Phys. Chem. A* **2023,** *127* (11), 2591–2600.
**22.** Hellmuth, M.; Chen, B.; Bariki, C.; Cai, L.; Cameron, F.; Wildenberg, A.; Huang, C.; Faller, S.; Ren, Y.; Beeckmann, J.; Leonhard, K.; Heufer, K. A.; Hansen, N.; Pitsch, H., A comparative study on the combustion chemistry of two bio-hybrid fuels: 1,3-dioxane and 1,3-dioxolane. *J. Phys. Chem. A* **2023,** *127* (1), 286-299.
**23.** Kang, S.; Liao, W.; Sun, W.; Lin, K.; Liao, H.; Moshammer, K.; Dagaut, P.; Hansen, N.; Yang, B., Exploring low-temperature oxidation chemistry of 2- and 3-pentanone. *Combust. Flame* **2022**, 112561.
**24.** Huang, C.; Zhao, Y.; Roy, I. S.; Chen, B.; Hansen, N.; Pitsch, H.; Leonhard, K., Pathway exploration in low-temperature oxidation of a new-generation bio-hybrid fuel 1,3-dioxane. *Proc. Combust. Inst.* **2022**.
**25.** Fan, X.; Sun, W.; Gao, Y.; Hansen, N.; Chen, B.; Pitsch, H.; Yang, B., Chemical insights into the multi-regime low-temperature oxidation of di-n-propyl ether: Jet-stirred reactor experiments and kinetic modeling. *Combust. Flame* **2021,** *233*, 111592.
**26.** Ruwe, L.; Cai, L.; Wullenkord, J.; Schmitt, S. C.; Felsmann, D.; Baroncelli, M.; Chen, B.; Moshammer, K.; Hansen, N.; Pitsch, H.; Kohse-Höinghaus, K., Low- and high-temperature study of n-heptane combustion chemistry. *Proc. Combust. Inst.* **2021,** *38* (1), 405-413.
**27.** Wang, Z.; Hansen, N.; Jasper, A. W.; Chen, B.; Popolan-Vaida, D. M.; Yalamanchi, K. K.; Najjar, A.; Dagaut, P.; Sarathy, S. M., Cool flame chemistry of diesel surrogate compounds: N-decane, 2-methylnonane, 2,7-dimethyloctane, and n-butylcyclohexane. *Combust. Flame* **2020,** *219*, 384-392.
**28.** Chen, B.; Ilies, B. D.; Chen, W.; Xu, Q.; Li, Y.; Xing, L.; Yang, J.; Wei, L.; Hansen, N.; Pitsch, H.; Sarathy, S. M.; Wang, Z., Exploring low temperature oxidation of 1-butene in jet-stirred reactors. *Combust. Flame* **2020,** *222*, 259-271.
**29.** He, X.; Hansen, N.; Moshammer, K., Molecular-weight growth in ozone-initiated low-temperature oxidation of methyl crotonate. *J. Phys. Chem. A* **2020,** *124* (39), 7881-7892.
**30.** Rousso, A. C.; Jasper, A. W.; Ju, Y.; Hansen, N., Extreme low-temperature combustion chemistry: Ozone-initiated oxidation of methyl hexanoate. *J. Phys. Chem. A* **2020,** *124* (48), 9897-9914.

**31.** Liao, H.; Kang, S.; Hansen, N.; Zhang, F.; Yang, B., Influence of ozone addition on the low-temperature oxidation of dimethyl ether in a jet-stirred reactor. *Combust. Flame* **2020,** *214*, 277-286.
**32.** Conrad, A. R.; Hansen, N.; Jasper, A. W.; Thomason, N. K.; Hidaldo-Rodrigues, L.; Treshock, S. P.; Popolan-Vaida, D. M., Identification of the acetaldehyde oxide Criegee intermediate reaction network in the ozone-assisted low-temperature oxidation of trans-2-butene. *Phys. Chem. Chem. Phys.* **2021,** *23* (41), 23554-23566.
**33.** Caster, K. L.; Lee, J.; Donnellan, Z.; Selby, T. M.; Osborn, D. L.; Goulay, F., Formation of a resonance-stabilized radical intermediate by hydroxyl radical addition to cyclopentadiene. *J. Phys. Chem. A* **2022,** *126* (48), 9031-9041.
**34.** Caster, K. L.; Selby, T. M.; Osborn, D. L.; Le Picard, S. D.; Goulay, F., Product detection of the CH(X2Π) radical reaction with cyclopentadiene: A novel route to benzene. *J. Phys. Chem. A* **2021,** *125* (32), 6927-6939.
**35.** Shiels, O. J.; Prendergast, M. B.; Savee, J. D.; Osborn, D. L.; Taatjes, C. A.; Blanksby, S. J.; da Silva, G.; Trevitt, A. J., Five vs. six membered-ring pah products from reaction of o-methylphenyl radical and two c3h4 isomers. *Phys. Chem. Chem. Phys* **2021,** *23* (27), 14913-14924.
**36.** Valorani, M.; Malpica Galassi, R.; Ciottoli, P. P.; Najm, H.; Paolucci, S., The spectral characterisation of reduced order models in chemical kinetic systems. *Combust. Theory Model.* **2022,** *26* (7), 1185-1216.
**37.** Han, X.; Najm, H. N., Modeling fast diffusion processes in time integration of stiff stochastic differential equations. *Comm. App. Math. Comp. Sci.* **2022,** *4* (4), 1457-1493.
**38.** Casey, T. A.; Khalil, M.; Najm, H. N., Inference and combination of missing data sets for the determination of H2O2 thermal decomposition rate uncertainty. *Combust. Flame* **2021,** *232*, 111507.
**39.** Chen, B.; Liu, P.; Li, Z.; Hansen, N.; Roberts, W.L.; Pitsch, H. Furan formation pathways exploration in low-temperature oxidation of 1,3-butadiene, trans-2-butene, and cis-2-butene. *Combust. Flame* **2021**, *232*, 111519.
**40.** Desai, S.; Tao, Y.; Sivaramakrishnan, R.; Chen, J. H., Effects of non-thermal termolecular reactions on wedge-induced oblique detonation wave. *Combust. Flame* **2023,** *doi:10.1016/j.combustflame.2023.112681*.
**41.** Rieth, M.; Gruber, A.; Chen, J. H., The effect of pressure on lean premixed hydrogen-air flames. *Combust. Flame* **2023,** *250*, 112514.
**42.** Rieth, M.; Gruber, A.; Chen, J. H., A direct numerical simulation study on NO and n2o formation in turbulent premixed ammonia/hydrogen/nitrogen-air flames. *Proc. Combust. Inst.* **2023**.
**43.** Im, H.; Chen, J. H.; Apsden, A., Direct numerical simulation perspective. In *Turbulent combustion physics*, Swaminathan, N. B., X.-S.; Fureby, C.; Haugen, N. E. L.; Brethouwer, G., Ed. Cambridge University Press: 2022.
**44.** Hu, Z.; Di, Q.; Liu, B.; Li, Y.; He, Y.; Zhu, Q.; Xu, Q.; Dagaut, P.; Hansen, N.; Sarathy, S. M.; Xing, L.; Truhlar, D. G.; Wang, Z., Elucidating the photodissociation fingerprint and quantifying the determination of organic hydroperoxides in gas-phase autoxidation. *Proc. Nat. Acad. Sci.* **2023,** *120* (10), e2220131120.
**45.** Rösch, D.; Jones, G. H.; Almeida, R.; Caravan, R. L.; Hui, A.; Ray, A. W.; Percival, C. J.; Sander, P. S.; Smarte, M. D.; Winiberg, F. A. F.; Okumura, M.; Osborn, D. L., Conformer-dependent chemistry: Experimental product branching of the vinyl alcohol + OH + O2 reaction. *J. Phys. Chem. A.* **2023,** *127* (14), 3221–3230.
**46.** Hansen, N.; Kukkadapu, G.; Chen, B.; Dong, S.; Curran, H. J.; Taatjes, C. A.; Eskola, A. J.; Osborn, D. L.; Sheps, L.; Pitz, W. J.; Moshammer, K.; Jasper, A. W.; Chen, W.; Yang, J.; Wang, Z., The impact of the third O2 addition reaction network on ignition delay times of neo-pentane. *Proc. Combust. Inst.* **2021,** *38* (1), 299-307.
**47.** Vansco, M. F.; Caravan, R. L.; Zuraski, K.; Winiberg, F. A. F.; Au, K.; Trongsiriwat, N.; Walsh, P. J.; Osborn, D. L.; Percival, C. J.; Khan, M. A. H.; Shallcross, D. E.; Taatjes, C. A.; Lester, M. I., Experimental evidence of dioxole unimolecular decay pathway for isoprene-derived Criegee intermediates. *J. Phys. Chem. A* **2020,** *124* (18), 3542-3554.
**48.** Caravan, R. L.; Vansco, M. F.; Au, K.; Khan, M. A. H.; Li, Y.-L.; Winiberg, F. A. F.; Zuraski, K.; Lin, Y.-H.; Chao, W.; Trongsiriwat, N.; Walsh, P. J.; Osborn, D. L.; Percival, C. J.; Lin, J. J.-M.; Shallcross, D. E.; Sheps, L.; Klippenstein, S. J.; Taatjes, C. A.; Lester, M. I., Direct kinetic measurements and theoretical predictions of an isoprene-derived Criegee intermediate. *Proc. Natl. Acas. Sci.* **2020,** *117* (18), 9733-9740.
**49.** Doner, A. C.; Davis, M. M.; Koritzke, A. L.; Christianson, M. G.; Turney, J. M.; Schaefer Iii, H. F.; Sheps, L.; Osborn, D. L.; Taatjes, C. A.; Rotavera, B., Isomer-dependent reaction mechanisms of cyclic ether intermediates: Cis-2,3-dimethyloxirane and trans-2,3-dimethyloxirane. *Int. J. Chem. Kinet.* **2021,** *53* (1), 127-145.
**50.** Christianson, M. G.; Doner, A. C.; Davis, M. M.; Koritzke, A. L.; Turney, J. M.; Schaefer Iii, H. F.; Sheps, L.; Osborn, D. L.; Taatjes, C. A.; Rotavera, B., Reaction mechanisms of a cyclic ether intermediate: Ethyloxirane. *Int. J. Chem. Kinet.* **2021,** *53* (1), 43-59.
**51.** Van de Vijver, R.; Zádor, J., KinBot: Automated stationary point search on potential energy surfaces. *Comp. Phys. Comm.* **2020,** *248*, 106947.
**52.** Kohse-Höinghaus, K.; Ferris, A.M.; Zetterberg, J.; Lacoste, D. A.; Fjodorow, P.; Wagner, S.; Cai, L.; Rudolph, C.; Zádor, J.; Li, Y.; Ruwe, L.; Gaiser, N.; Wang, Z.; Geigle, K., P., *Chemistry diagnostics for monitoring.* In Combustion Chemistry and the Carbon Neutral Future: What will the next 25 years of research require?" Elsevier, **2023**.
**53.** Schmitt, S.; Wick, M.; Wouters, C.; Ruwe, L.; Graf, I.; Andert, J.; Hansen, N.; Pischinger, S.; Kohse-Höinghaus, K., Effects of water addition on the combustion of iso-octane investigated in laminar flames, low-temperature reactors, and an HCCI engine. *Combust. Flame* **2020**, *212*, 433-447.

# ELECTRON-DRIVEN CHEMISTRY

David W. Chandler, Jonathan H. Frank, Laura M. McCaslin, Krupa Ramasesha, Tim Zwier
Sandia National Laboratories, MS 9051, Livermore, CA 94551-0969
chand@sandia.gov, jhfrank@sandia.gov, lmmccas@sandia.gov, kramase@sandia.gov, tszwier@sandia.gov

## PROGRAM SCOPE

Electron-driven chemistry, which we define as chemical transformations driven by an initial charge separation or addition, underpins many areas of interest to the DOE. The goal of this program is to deepen understanding of reactivity that is driven by motion of charges. We will apply a combination of sophisticated experimental and theoretical methodologies to provide detailed time- and state-resolved views of complex charge-transfer processes. These investigations will illuminate phenomena that defy the common simplifying assumptions of the Hartree-Fock and Born-Oppenheimer approximations and will aid in developing more sophisticated descriptions of coupled electron and nuclear motion. This work extends the research we have done on neutral processes, using quantum state-resolved experiments that provide detailed information about molecular potential energy landscapes and the dynamics involving coupled potential energy surfaces. We pursue experiments that include: 1) induced charge separation in an isolated molecule, 2) dynamics following attachment of a free electron to a neutral molecule or cluster, and 3) coupled chemical and physical evolution of a laser-induced plasma. In each area, we apply advanced techniques, including techniques presently being developed, to provide a new and deeper understanding of chemical physics processes. This effort complements research being performed in the Solar Photochemistry and Condensed-Phase and Interfacial Molecular Sciences programs and addresses BES Grand Challenges associated with the study of the nature of excited electronic states and the breakdown of the Born-Oppenheimer approximation. This research is closely tied to other work in our program. The study of ultrafast intramolecular charge transfer dynamics of large conjugated systems has strong connections to the ultrafast non-adiabatic dynamics and the detection schemes being developed in the Ultrafast Chemistry and Physics subtask. Research described in this subtask extends the work performed under the Chemical Dynamics subtask to investigate inelastic collisions of electrons with molecules and charge transfer and reaction after photoexcitation of a molecule.

## RECENT PROGRESS

### *New diagnostic for studying plasmas with Velocity Mapped Imaging of electrons and ions*

Our recently developed VMI apparatuses for high-resolution electron scattering and excited-state dissociative electron attachment (DEA) has also enabled studies of the dynamics of laser-initiated plasmas and plasma-induced chemistry in well-controlled, field-free conditions. We generate distributions of electrons and cations by laser photoionization of atoms and molecules in a pulsed supersonic beam. These charge distributions evolve into a plasma when the photocation density produces a potential well that matches or exceeds the photoelectron energy and traps the electrons. For photoelectron energies that exceed ~100 $cm^{-1}$, recombination with atomic cations is improbable resulting in a simple, collisionless, self-similar plasma expansion into vacuum for an initially spherical gaussian charge distribution. We selected a 2+1 REMPI Kr plasma to demonstrate the utility of our plasma VMI spectrometers by extracting kinetic and dynamical data on the evolving electron distribution across a multiple μs interval with ns time resolution.

We generate the plasma by focusing 80 μJ of 214.7 nm radiation into a pulsed supersonic beam of pure Kr or 20% Kr in He. Hydrodynamic calculations predict 2.3E19 $m^{-3}$ for the density of pure Kr at the interaction region. Density matrix rate equations calculations suggest that ~11% of the beam is ionized by the 0.2 $cm^{-1}$ laser bandwidth. A beam profiling camera and an assumed gaussian transverse profile of the skimmed supersonic beam are used to estimate the REMPI excitation volume as 2.4E-11 $m^3$. The energy scale in the VMI images is calibrated by assigning the radius of an Abel-inverted image of low-power 2+1 Kr REMPI with the expected 3.32 eV photoelectron energy.

Figure 1 demonstrates the extraction of plasma kinetic information by monitoring the total intensity of VMI images as a function of extraction time. For both pure Kr and 20% Kr in He, the extracted electron signal decays with two timescales. We associate the fast timescale (τ~20 ns) with REMPI electrons that escape to produce a net-positive charge distribution with a potential well that traps the 3.32 eV photoelectrons. The resulting electron trapping fractions are 31% for the Kr/ He mixture and 56% for pure Kr.

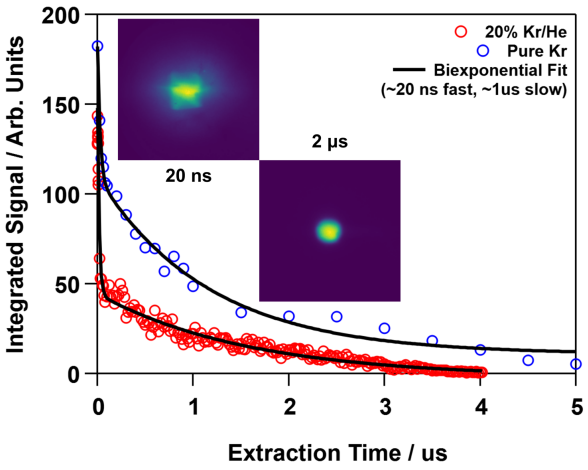


Fig. 1: Variation in the total extracted electron signal from a 2+1 REMPI Kr plasma as a function of extraction time obtained by integrating velocity mapped images. Inset: Velocity mapped images for 20% Kr/He at different extraction times.

As shown in Fig. 2, the temporal evolution of electron distributions for this plasma are captured with 0.5 µs increments, although the diagnostic is capable of nanosecond resolution. After the contribution from escaping electrons decays away, velocity mapped images of the extracted plasma electrons are approximately isotropic with an intensity maximum at image center (see inset of Fig. 1). A 1D velocity distribution is obtained by integrating velocity mapped images perpendicular to an axis that passes through image center. From gas-kinetic theory, a Maxwell-Boltzmann velocity distribution characterized by a single temperature is associated with a gaussian distribution in any cartesian direction. Effective electron temperatures are derived from the FWHM of the 1D velocity distributions shown in Fig. 2. The monotonic contraction of the 1D velocity distributions is a result of evaporation from the high-energy tail of the velocity distribution of the trapped electrons. This electron evaporation, identified as the slow timescale (τ~1 µs) in Fig. 1, is controlled by the decrease of the cation Coulomb potential as the plasma expands in vacuum.

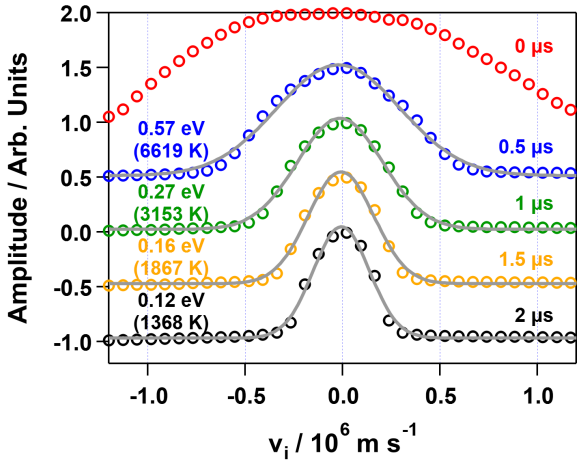


Fig. 2: Experimental 1D velocity distributions from a pure Kr supersonic beam at extraction times of 0 to 2 µs. All spectra are peak normalized and offset for clarity. Effective electron temperatures are derived from the FWHM of each 1D velocity distribution. Gray lines indicate curve fits to gaussian lineshapes.

This study demonstrated a new method to determine the energy distribution of electrons within a plasma, even if that distribution is not described by a single temperature. We have used this new capability to observe the trapping and cooling of 3 eV electrons from REMPI of Kr. A manuscript describing these first results has been submitted for publication.

***NO/$SF_6$ plasmas: formation of $SF_6^-$ in Rydberg collisions, from free electrons and in plasmas***

Experiments that characterize ultracold plasma dynamics with chemical or reactive degrees of freedom are relatively few despite their potential as a perturbative probe and a means of tuning or manipulating plasma properties. For example, introducing a molecule that can attach electrons to form stable or metastable anions should dramatically reduce the ambipolar expansion rate and limit electron driven relaxation processes like dissociative recombination and three-body recombination that have an impact on plasma lifetime, temperature, and coupling strength.[1] To develop this capability, we investigated the behavior of two-color ($\omega_1 + \omega_2$) excited NO in an ~100 $cm^{-1}$ window that includes the lowest energy ground state ionization potential ($IP_{NIST}$) with and without the presence of an electron acceptor. For the electron acceptor, we selected $SF_6$, which has an electron affinity of 0.97 eV. With the internal state cooling that accompanies

preparation of $SF_6$ and NO in a pulsed molecular beam, the formation of $SF_6^-$ dominates over dissociative electron attachment products like $SF_5^-$ and $F^-$ by a factor of approximately $10^4$.[2]

Figure 3 plots the electrons extracted 200 ns after two-color excitation of NO in a pulsed supersonic beam of 10% NO in He with no electron acceptor present. Extracted electrons are a result of adiabatic field ionization of Rydberg states or plasma formation initiated either by a sufficient density of Rydberg states or by trapping electrons with a photocation potential that exceeds the photoelectron energy. When the frequency of $\omega_1$ is tuned to the A←X $Q_1(0.5)$ transition of NO, selection rules and Rydberg lifetimes favor accessing a rotationally excited *f* Rydberg series that converges to the second rotational state of the cation, which has 12 $cm^{-1}$ higher energy than $IP_{NIST}$ ionization potential. We refer to this secondary Rydberg limit as $IP_{Rydberg}$. Rydberg peaks lose their definition when $\omega_2$ is near 30495 $cm^{-1}$ where a broad continuum grows due to mixing with background Rydberg states.

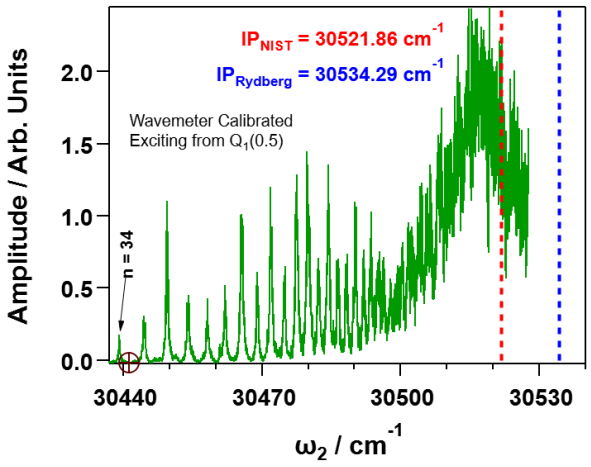


Fig. 3: Electron signal extracted from a supersonic expansion of 10% NO in He 200 ns after two-color ($\omega_1 + \omega_2$) excitation of NO. The frequency of $\omega_1$ is tuned to the A←X $Q_1(0.5)$ transition of NO. The left vertical dashed line marks the location of the ground state ionization potential of NO. The right vertical dashed line marks the N = 2 convergence limit of the f Rydberg series of NO.

In contrast, a similar experiment in a molecular beam containing 20% NO in $SF_6$ produces a very different spectrum, as shown in Fig. 4. For extraction times between 200 ns and 2 μs, no discrete Rydberg peaks are observed in the extracted electron spectrum. Instead, electrons are only detected at $\omega_2$ energies above a threshold of ~30511$cm^{-1}$. The extracted electron signal is highest between $IP_{NIST}$ and $IP_{Rydberg}$ and reasonably constant from 0 to ~50 $cm^{-1}$ above $IP_{Rydberg}$, where only free electrons are formed by the lasers. Features in the extracted electron spectrum are independent of extraction time, extraction voltage, and laser power. In addition to the electron signal, a single anion peak is observed on extraction and identified as $SF_6^-$. The $SF_6^-$ signal grows before and abruptly falls after each IP. Kinetics traces following $SF_6^-$ signal as a function of extraction time show a monotonic increase with extraction time.

The extraction-time independent position and lineshape of the $SF_6^-$ signal near each IP is strong evidence that these anions are formed by direct Rydberg electron transfer.[3] Associating anion production with direct Rydberg electron transfer is supported by the differences in the $SF_6^-$ and electron spectra in Fig. 4: For example, the ratio of the $SF_6^-$ signals near the IPs is $SF_6^-$ ($IP_{NIST}$)/$SF_6^-$($IP_{Rydberg}$) ~ 3.3, whereas for the electrons it is $e^-$($IP_{NIST}$)/$e^-$($IP_{Rydberg}$) ~ 1.3, and the ratios of the two signals, $SF_6^-$($\omega_2$)/$e^-$($\omega_2$), varies strongly below, between, and above $IP_{NIST}$ and $IP_{Rydberg}$. In Fig. 4, the electron signal above $IP_{Rydberg}$ at an extraction time of 0.5 μs is unambiguous proof that a free electron plasma is formed. Thus, the data in Fig. 4 suggest that direct Rydberg electron transfer is more efficient than free-electron attachment in an ultracold plasma (perhaps due to competing processes like three body recombination). The sharp progression of Rydberg

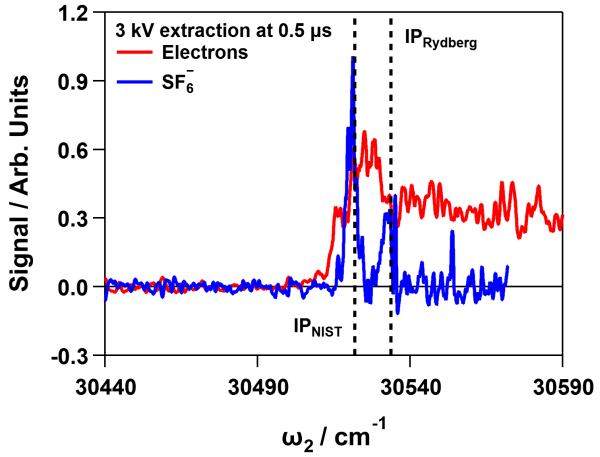


Figure 4. Electrons and $SF_6^-$ extracted from a pulsed molecular beam of 20% NO in $SF_6$ after two-color ($\omega_1 + \omega_2$) excitation of NO. The frequency of $\omega_1$ is tuned to the A←X $Q_1(0.5)$ transition of NO and the pulse energy is adjusted to saturate the transition. The left vertical dashed line marks the location of the ground state ionization potential of NO. The right vertical dashed line marks the N=2 convergence limit of the f Rydberg series of NO. Data are smoothed and background subtracted for clarity.

states observed in the extracted electron spectra of pure NO/He are not observed in the electron spectra of $NO/SF_6$ at extraction times as low as 200 ns. Figure 4 demonstrates that this absence is not a result of extractable $SF_6^-$ formation. However, Coulombic interactions between ions formed by Rydberg electron transfer are known to increase with decreasing principal quantum number and decreasing Rydberg size. The data indicate that although we are exciting the NO Rydberg states with the laser, we see neither electrons nor $SF_6^-$ for all lower discrete Rydberg states under these conditions. A likely explanation is that when these Rydberg excited NO molecules donate an electron to an $SF_6$ molecule the resulting cation/anion pair do not separate and we are blind to them in our experiment. We see $SF_6^-$ formed from the highest Rydberg states indicating that larger Rydberg states can donate an electron at a distance that does not necessarily capture the formed anion and a free $SF_6^-$ is born that we detect. For these anions formed from high Rydberg states, we observe a growth in the detected $SF_6^-$ with increasing delay times up to 2.5 μs. Along with the formation of $SF6^-$ we observe several anions of nitrogen and oxygen species. This will be the subject of future studies.

These investigations demonstrate the utility of being able to monitor in real time the kinetics of anionic species production in these plasmas and the timescale over which high lying Rydberg states can continue to create anions. A manuscript describing the dynamics of $SF6^-$ formation in an NO Rydberg gas is in preparation. Future work will explore these interesting Rydberg-state-specific dynamics. We will study ion pair formation in ultracold plasmas, modify the beam conditions to encourage the formation of DEA products, increase the fraction of anions made, and attempt to quantify a reduction in the plasma expansion velocity with a 2D position-sensitive detector.

## FUTURE WORK

### *Laser-produced plasma initiation dynamics*

The combination of VMI with well-controlled laser-generated plasmas opens many opportunities for detailed studies of chemical reactions of molecules in plasmas with tunable electron energy distributions. In the next year, our plasma-chemistry studies will focus on nitric oxide (NO), which can be used both to generate the plasma and to study plasma chemistry.

We will form plasmas either through excitation of NO Rydberg states or by laser ionization of NO molecules. This is done by first exciting the NO(A) state, which has a 200 ns lifetime. A second laser then excites from the A state either a long-lived Rydberg that evolves into a plasma or excites the NO(A) with sufficient energy to directly ionize it. After the plasma forms and is thermalized (tens of nanoseconds), we will send in another laser pulse to generate more Rydberg state molecules or add electrons of a known energy within the plasma as we do not deplete the NO(A) state population when we form the plasma. These perturbations will be monitored by imaging the electrons.

There are several interesting processes that are thought to happen within the early times of these plasmas that generate neutral N and O atoms. One process is the electron capture of some of the electrons by $NO^+$ cations forming an excited dissociative state of NO. A second mechanism is the Penning ionization that occurs when two Rydberg excited NO molecules (denoted as NO(R)) collide and one NO(R) generates a cation-electron pair and the second NO(R) is deactivated and dissociates. Both processes can be studied and differentiated by laser ionization of the N and O atoms and velocity imaging them. In this manner, the quantum state populations of the fragments will be determined. These processes are expected to be Rydberg number dependent as the size and velocity of the electrons may contribute to these processes. For instance, large Rydberg state molecules, high N, require only a small amount of energy transfer to ionize and they are much more likely to encounter either a free electron and ionize or another Rydberg and Penning ionize. This physics will be directly measured and quantified.

### *Dynamics following attachment of a free electron to a neutral molecule: Experimental studies*

Detailed insights into the fundamental chemical interactions that occur in charge distributions such as plasmas can be obtained by investigating the dynamics following attachment of free electrons to isolated molecules or clusters. For these studies, our electron scattering apparatus has two characteristics that we

are taking advantage of. One is the high energy resolution of the electrons dictated by the frequency spread of the laser beam. This allows us to scan the frequency of the laser and thereby scan the energy of the electrons with approximately 0.5 $cm^{-1}$ (0.06 meV) resolution. This feature is essential for resolving narrow low energy resonances. In the next year, these studies will focus on DEA of nitric oxide and sulfur dioxide.

To better understand dynamics of electron attachment to ground state NO followed by detachment, we will scan the energy of the electrons through low energy resonances of NO. We will then use 1+1 REMPI to detect the formation of vibrationally excited NO. In this manner, we will measure the natural linewidth of the resonances associated with production of vibrationally excited ground state transient ions and determine the lifetime of the transient anions. We will also take advantage of the time resolution of using pulsed lasers to produce the electrons. The electrons traverse the molecular beam in a time that is shorter than the laser pulse duration. Therefore, all transient anions will be formed during the 5-ns laser pulse as the electrons encounter molecules in the molecular beam. As we have control over the time of the electron generation, we can excite a molecule in the molecular beam prior to the electron production. In this manner, we will study the production of transient anions from electronically excited states of NO and $SO_2$.

Dissociative electron attachment to nitric oxide exhibits significant changes in dissociative electron attachment to the ground and electronically excited states that require a more detailed understanding. DEA to ground state NO requires a minimum electron energy of approximately 7.5eV. In contrast, DEA to electronically excited NO in the $A^2\Sigma^+$ state (5.48 eV) is exothermic by 0.45eV, and the DEA cross sections are three orders of magnitude larger for the electronically excited state.[4] This extraordinary enhancement in the cross section is associated with a Feshbach resonance. The dissociation channel in the excited state also differs from that of ground state NO. DEA to ground state NO primarily produces $N(^2D) + O^-(^2P)$, and DEA to electronically excited NO(A) produces $N(^4S) + O^-(^2P)$.[5] The sensitivity of the DEA enhancement and branching of dissociation channels to varying levels of vibronic excitation are not well established. We plan to investigate the enhancement and branching ratios of DEA to excited-state NO by selective laser excitation to different vibronic states prior to electron attachment.

Electronic excitation of sulfur dioxide, $SO_2$, has profound effects on the dissociation channels following electron attachment, resulting in nearly complete suppression in the production of some ionic fragments. For DEA to $SO_2$ in the excited electronic state ($\tilde{B}^1B_1$), the cross sections for formation of products $O^-$ and $SO^-$ are enhanced by factors of 6 and 1.5, respectively, while the formation of $S^-$ is almost entirely suppressed.[6] Previous studies of these effects of DEA to excited state $SO_2$ primarily focused on using time-of-flight mass spectrometry (TOFMS) and included limited investigation into the sensitivity of cross sections and product channels to different levels of excitation. We will conduct a series of detailed studies of DEA to $SO_2$ using velocity mapped imaging to provide mass selective detection of the kinetic energy and angular distribution of the DEA fragments following laser excitation of the parent molecule.

***Dynamics following attachment of a free electron to a neutral molecule: Theoretical studies***

We will pair experimental studies with theoretical investigations of the DEA processes in excited-state molecules. In order to probe the underlying dynamics and electronic structure involved in the vibrational- and electronic-state dependence of reactions such as $SO_2 + e^-$, non-adiabatic mixed quantum-classical (NA-MQC) dynamics calculations will be performed. Though these are relatively small systems, the electronic structure is quite difficult to describe due to the multiconfigurational nature of the wavefunctions. Electronic structure methods such as equation-of-motion coupled cluster in its electron-attachment variant (EOM-EA-CCSD) will be benchmarked against methods that incorporate treatments of both static and dynamic electron correlation such as MRCI in order to identify methods with an appropriate balance of accuracy and computational efficiency for employment in dynamics calculations.

***Intramolecular charge transfer dynamics in gas phase donor-bridge-acceptor systems***

Over the next year, we will begin studies focusing on excited-state dynamics in large, conjugated molecules with extended $\pi$-orbitals. These dynamics are governed by the molecular structure, the nature of participating valence orbitals, the interactions among electronic states, and the surrounding environment.

Donor-bridge-acceptor (DBA) molecules are a class of π-conjugated systems, where large amplitude changes to molecular structure are coupled to intramolecular charge transfer (ICT). Given the known sensitivity of ICT to external electric fields and solvent interactions, we propose to first study the charge transfer dynamics in isolated gas phase DBA molecules in cold molecular beams, free from interaction with the environment. The system we will first study is *p*-nitroaniline (PNA), which has an electron-acceptor –$NO_2$ group and an electron-donor –$NH_2$ group. Following electronic excitation to the locally excited singlet state, excited state evolution to the twisted ICT state and to triplet states via intersystem crossing are expected to compete. Our experiments will study excited state dynamics in jet-cooled PNA using ultrafast core-level X-ray absorption following electronic excitation to the locally excited state. Core-level spectroscopy near the O and N K-edges will serve as site-specific probes of ICT dynamics, and to this end, we have submitted a user proposal for beam time at the LCLS. In order to guide interpretation of results from these experiments, we calculated the nitrogen and oxygen K-edge transitions at the core-valence separation ADC(2) level of theory with a 6-31G* basis of ground-state PNA. The nitrogen 1s core-to-valence transition energies of ground state PNA, shown in Fig. 5, demonstrates that transitions from the $NH_2$ and $NO_2$ moieties of PNA are sufficiently separated in energy to be experimentally distinguished. In the planned experiments, we will detect valence excitation and charge transfer-induced changes in the electronic structure in the vicinity of the $NH_2$ and $NO_2$ groups, reflected in shifts of these core-to-valence transition energies and intensities. These results will be compared with theoretical predictions of electronically excited PNA, which will involve both non-adiabatic excited state dynamics simulations and predictions of core-level spectra of valence-excited PNA.

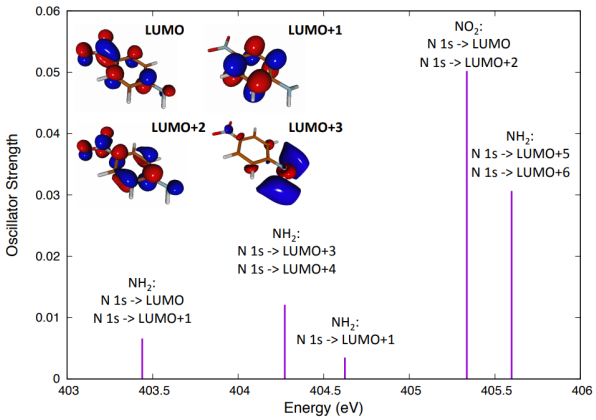

Fig. 5: The calculated lowest-energy core nitrogen K-edge transitions in ground state PNA, originating from the nitrogen atoms in the $NH_2$ and $NO_2$ moieties.

**References**


(1) Killian, T. C.; Pattard, T.; Pohl, T.; Rost, J. M. Ultracold neutral plasmas. *Phys. Rep.* **2007**, *449* (4), 77-130. DOI: https://doi.org/10.1016/j.physrep.2007.04.007.

(2) Braun, M.; Barsotti, S.; Marienfeld, S.; Leber, E.; Weber, J. M.; Ruf, M. W.; Hotop, H. High resolution study of anion formation in low-energy electron attachment to SF6 molecules in a seeded supersonic beam. *Eur. Phys. J. D* **2005**, *35* (2), 177-191. DOI: 10.1140/epjd/e2005-00230-6.

(3) Klar, D.; Ruf, M. W.; Hotop, H. A tunable laser-atomic beam photoelectron source with sub-milli-electron-volt resolution: design, operation and application to threshold electron attachment studies. *Meas. Sci. Technol.* **1994**, *5* (10), 1248. DOI: 10.1088/0957-0233/5/10/010.

(4) Kuo, C. T.; Hardwick, J. L.; Moseley, J. T. Low-energy-electron attachment to excited nitric oxide. *J. Chem. Phys.* **1994**, *101* (12), 11084-11085, Note. DOI: 10.1063/1.467797.

(5) Kuo, C. T.; Ono, Y.; Hardwick, J. L.; Moseley, J. T. Dissociative attachment of electrons to the A $^2\Sigma^+$ state of nitric oxide. *J. Phys. Chem.* **1988**, *92* (18), 5072-5074, Letter. DOI: 10.1021/j100329a002.

(6) Krishnakumar, E.; Kumar, S. V. K.; Rangwala, S. A.; Mitra, S. K. Dissociative-attachment cross sections for excited and ground electronic states of $SO_2$. *Phys. Rev. A* **1997**, *56* (3), 1945-1953, Article. DOI: 10.1103/PhysRevA.56.1945.

# IMAGING THE NEAR-SURFACE GAS PHASE: A NEW APPROACH TO COUPLED GAS-SURFACE CHEMISTRY

Jonathan H. Frank, Farid El Gabaly, Nils Hansen, Christopher J. Kliewer, David L. Osborn
*Sandia National Laboratories, Livermore, CA*
jhfrank@sandia.gov, felgaba@sandia.gov, nhansen@sandia.gov, cjkliew@sandia.gov, dlosbor@sandia.gov
Coleman Kronawitter and Ambarish Kulkarni
*Department of Chemical Engineering, University of California, Davis*
ckrona@ucdavis.edu, arkulkarni@ucdavis.edu

## PROGRAM SCOPE

The chemical reactivity of gases with solid surfaces is ubiquitous in natural and industrial energy transformation. Cooperative effects that couple gas phase chemistry with surface chemistry are critical for foundational understanding but challenging to probe experimentally and theoretically. Heterogeneous catalysis is an ideal field to expose and isolate the fundamental chemical physics of these cooperative effects. Our program seeks to characterize gas-surface coupling through chemically specific, temporally, and spatially resolved probes of both reacting surfaces and the near-surface gas phase. The program combines optical spectroscopy with mass spectrometry and photoelectron spectroscopy of both gas phase and surface species. The long-term goal is to elucidate the fundamental mechanisms of cooperative gas-surface chemistry, influencing DOE mission research in catalysis, synthesis, and energy transformation.

This program comprises two interrelated thrusts that are distinguished by the physical mechanism of gas-surface coupling – transport or reaction – and employ differing degrees of chemical complexity and control over the model catalyst surface. The first thrust explores how molecular transport in the gas phase may mediate coupling between different domains on a surface without gas-phase chemical reactions. It employs well-controlled reactions on atomically cleaned crystalline and polycrystalline surfaces prepared under ultra-high vacuum (UHV) conditions, with reactivity studied under pressures of $10^{-6}$ to 760 Torr. The second thrust adds the complexity of reactive coupling, with bond breaking and formation among intermediates occurring in the gas phase as well as on the surface. Thrust 2 utilizes both polycrystalline films and more complex surfaces (e.g., doped metal oxides, and bifunctional supported catalysts), with reactivity studied at elevated temperatures (400 - 1250 K) and pressures of 1 - 1500 Torr.

## RECENT PROGRESS

**Near-surface imaging of H atom during catalytic dehydrogenation of alkanes to alkenes: surface-catalyzed emission of reactive species into the gas phase** One of the foundational hypotheses of this research project is that it is possible, even likely, that chemically reactive intermediates generated at a catalytic surface are emitted into the gas phase. In such cases, to fully describe the cooperative gas-surface chemical reaction necessitates a coupled gas and surface chemical kinetic model where reaction steps activated at a catalytic surface go on to do further chemistry in the gas phase. As a test of this hypothesis, we carried out a series of experiments on the catalytic dehydrogenation of ethane to form ethylene over Pt-based catalysts. Olefins are of significant practical importance, and the catalytic dehydrogenation of alkanes to alkenes has received significant attention. The current state-of-the-art unfortunately involves energy-intensive steam cracking, and thus catalytic alternatives are sought both by industry and DOE.

The conventional approach to monitoring heterogenous catalysis involves the analysis of downstream products using approaches such as gas chromatography. However, such approaches are blind to both short-lived intermediates ejected into the gas phase as well as the natural heterogeneity of practical catalysts. In this work,[1] we sought to extend the ideas of local, near-surface, probing of the gas phase to the study of alkane dehydrogenation.

We measured near-surface H-atom concentrations using femtosecond 3-photon LIF using 40 μJ pulses at 307 nm. Because this is a multi-photon absorption, the inherent 5 nm bandwidth of the pulse was not a limitation when hitting the narrow atomic transition, as many frequency pairs within the pulse bandwidth compensate for the detuning of the other photons, and strong signal levels were achieved for the detection of H-atom down to concentrations ~$10^{15}$ atoms $cm^{-3}$. The laser beam skimmed the catalyst surface to within 50 μm of the surface without damaging the surface. Samples included smooth quartz and platinum–manganese bimetallic nanoparticles supported on silica with nominal 2 wt % Pt loading (PtMn). H-atom fluorescence was collected at 656 nm. The fluorescence signal was quantified by calibration to a methane/air flame placed at the experimental probe volume. Furthermore, Kr gas was used in the cell with known fluorescence cross section and concentration for quantification.

On both edges of the sample, the H-atom signal disappears, providing evidence that the H-atom is being generated at the surface and emitted into the gas phase. The possibility of photolytically produced H-atom signals was ruled out by experiments in a gas-filled cell. Furthermore, as Figure 1 demonstrates, the H-atom signal obtained decreased with time as the catalyst deactivated through surface coking, with H-atom evolution ceasing upon complete deactivation. This provides unambiguous proof that the H-atoms were catalytically produced at the catalyst surface and emitted into the gas phase.

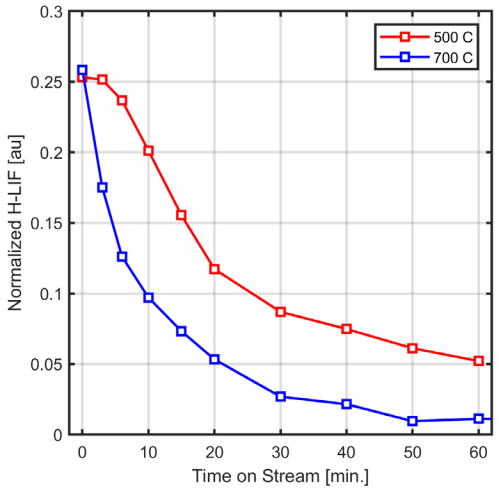


***Figure 1.*** *H-atom LIF as a function of reaction time on stream for two sample temperatures during exposure to a flow of ethane. As the catalyst deactivated through coking, the gas-phase H-atom concentration reached undetectable levels.*

**Correlating the Evolution of Surface Atomic Steps with the Initial Stages of Ordered Hydrogen Phases Adsorbed on Palladium using LEEM and PEEM** Gas/surface interactions are often initiated at defect sites, including ubiquitous surface steps, and these features evolve as reactions proceed. The equations of motion of single steps in simple environments are by now very well known. However, step evolution (including creation and annihilation) is a complex cooperative situation that depends upon the surrounding configuration. These dynamics are an important aspect of how a surface will interact with reactive gas. To address the question of what determines the time of relaxation to equilibrium after a temperature or pressure change, we used low energy electron microscopy (LEEM) to follow the evolution in real time of individual steps on the [111] surface of Pd from 730 - 800°C. Understanding how the global step structure evolves requires considering many steps simultaneously. What has not been considered in depth is a type of morphology often observed on single crystal surfaces: random arrangements of "hillocks" or "mesas" consisting of three-dimensional stacks of two-dimensional islands. This type of configuration is, for example, usually seen after the etching and annealing cycles used to clean surfaces. We examined with LEEM the temperature dependence of steps decay in Pd(111). We reveal that the stability of step hillocks is a complex and a cooperative process. We created a surface diffusion model that takes into account three factors: 1) atomic fluxes on the terraces, 2) detachment/attachment barrier, and 3) step-step interactions. Our simulation model together with LEEM experiments reveal that there is a well-defined time during which step nucleation takes place at the surface of mesa structures. Moreover, we rationalize the mass transport kinetics explaining how step detachments depend upon slope changes of the island structure by monitoring oscillations in electron reflectivity. Finally, we have demonstrated that the external flux of atoms outward from the island to the environment determines the overall decay rate of hillock structures, unravelling the mechanisms that control nanoscale smoothing on metal surfaces.

**Surface Sum Frequency Generation Vibrational Spectroscopy – Interference of the Free Induction Decay** An important component of our experimental arsenal for evaluating coupled gas-surface chemical

reactions is surface sum-frequency vibrational spectroscopy (SFG-VS), providing vibrational spectra of interfacial molecules, including orientation and vibrational lifetime. Our unique laser sources additionally offer femtosecond excitation of the vibrational modes of adsorbed molecules with wavelengths from 2-15 μm, enabling direct probing of molecular backbone stretches in addition to the C-H and O-H stretching regions. Recently we evaluated an important interference to surface sum-frequency generation vibrational spectroscopy at Torr pressures or higher. When a gas-phase molecule absorbs an infrared photon, it generates a coherent polarization. At some time later, this polarization emits radiation in the form of an infrared photon (with $\pi/2$ phase shift) at the same frequency and into the same spatial mode as the incoming laser pulse. If the original driving field and these $\pi$-shifted photons strike an integrating detector, it gives rise to the well-known linear absorption in the IR spectrum. As the coherent polarization of the gas-phase molecules decays, a free-induction decay (FID) is generated. When this IR pulse, with trailing FID radiation, strikes the interface of interest, and generates SFG, the FID train gets upconverted by the probe pulse, generating apparent SFG resonances that are purely real (no imaginary component) from the perspective of the sample itself. However, this is a case when SFG-VS is not surface-specific, as the observed spectrum is the result of gas-phase FID upconverting upon the Au(111) surface. Particularly insidious, the polarization analysis appears as a surface SFG signal that obeys conventional expectations, S-polarized IR light yields no resonant signal because the signal generated is indeed second-order SFG from the gold surface. We are presently evaluating the physics behind why the coherence decays observed in these SFG signals is so much shorter than what would be predicted by gas-phase transition linewidths at these pressures, as the decay is orders of magnitude faster than would be predicted. However, at a more general level, these considerations must be considered in all gas-phase SFG, as well as infrared transient absorption experiments and is the subject of a manuscript near completion.

**Diagnostic for Near-Surface Imaging of Methyl** To better capture the thermochemical state of the gas phase above different catalytic systems, we are expanding our diagnostics suite to include *in situ* 2D LIF imaging of key intermediate species. We have demonstrated for the first time *in situ* imaging of the methyl radical in the near-surface region of an operating catalyst. We initially detected $CH_3$ above a catalyst surface using MBMS, and our new capability enables complementary laser-based imaging of the spatial distribution

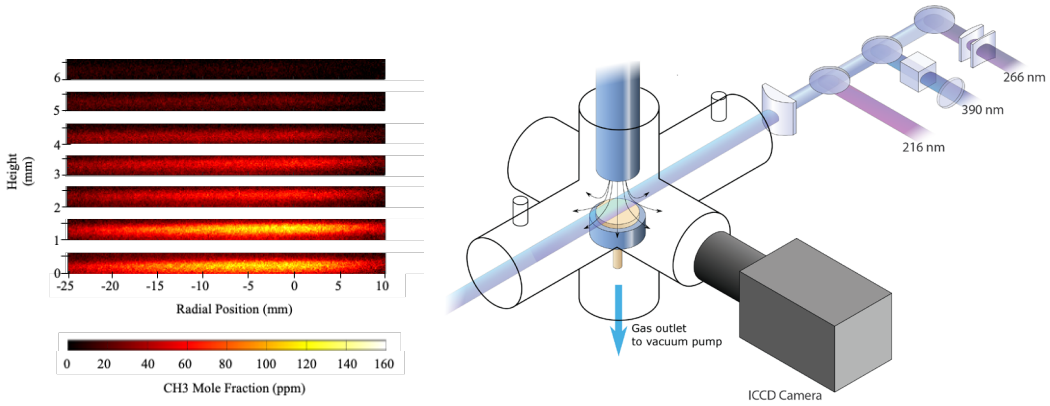


*(a)* *(b)*

***Figure 2.*** *(a) Photofragmentation LIF images of methyl mole fraction as a function of height above silver catalyst surface during partial oxidation of methanol. (b) Experimental configuration for 2D photofragmentation LIF imaging of $CH_3$ in catalytic partial oxidation of methanol over silver.*

of methyl. $CH_3$ imaging is challenging because it cannot be directly detected by LIF due to strong pre-dissociation of electronically excited states. We used photofragmentation laser-induced fluorescence (PF-LIF) to detect methyl during partial oxidation of methanol over a silver catalyst. Photofragmentation LIF is a pump-probe technique in which the pump laser (e.g. 2$^{nd}$ harmonic of a Nd:YAG-pumped dye laser at 216 nm) photo-dissociates methyl to form CH($X^2\Pi$) fragments. The probe laser near 390 nm excites laser-induced fluorescence of CH and fluorescence emission from the A-X and B-X(0,1) bands is detected at 420-440 nm. We performed $CH_3$ PF-LIF imaging in our newly implemented stagnation flow configuration

(Fig. 2b). $CH_3OH$, $O_2$, and $N_2$ create a laminar stagnation flow across a packed surface of $Ag/SiO_2$ powder, which is mounted on a button heater. We calibrate the PF-LIF signal by generating a known number density of $CH_3$ by photodissociation of acetone with a third laser (at 266 nm).

Figure 2a shows quantitative imaging measurements of methyl mole fraction performed at different heights above the $Ag/SiO_2$ catalyst during partial oxidation of methanol at a chamber pressure of 60 Torr. With sufficient laser fluence the laser sheet can be expanded in the vertical direction to capture the entire 2D methyl distribution in a single image. This diagnostic capability enables investigations of the spatiotemporal evolution of methyl in a wide range of catalytic systems.

**Methanol Oxidation with Supported Pd Catalysts through Operando Interrogation of Both the Surface and the Near-Surface Gas Phase** We studied the mechanisms of oxidative conversion of methanol with MgO-supported Pd catalysts using a unique approach based on combined application, during reaction at atmospheric pressure, of near-surface molecular beam mass spectrometry and surface-sensitive FTIR spectroscopy. We compared experiments using a pre-oxidized catalyst (PdO/MgO, containing $Pd^{2+}$), a pre-oxidized-and-reduced catalyst (Pd-PdO/MgO, containing $Pd^0$ and $Pd^{2+}$), and the pure MgO support. In all cases, the surface-sensitive FTIR spectra reflect mainly the adsorbate composition on the MgO surface, consistent with a system where spillover events from Pd-containing sites are central to the mechanism. To constrain the mechanism, we correlated adsorbate compositions of the catalyst surfaces with the composition of the near-surface gas phase. It yielded both clearly differentiated oxygenate adsorption configurations in FTIR spectra and staged desorption of species during temperature ramps. The results showed that when the system is operating at low temperatures, with 100% selectivity to $C_2$ products, adsorbed methoxy is oxidized to adsorbed formaldehyde, a portion of which participates in coupling events to produce methoxymethanol and methyl formate, and a portion of which spills over at the Pd–MgO interface. The $O\text{-}CH_2\text{-}O$ group within the detected reactive intermediate methoxymethanol supports the assignment of a surface formate in a specific binding configuration to an artifact originating from spillover of formaldehyde formed at Pd-containing sites. In this way, the interpretation of adsorbate FTIR signatures has been constrained by information uniquely obtained by interrogation of the near-surface gas phase. A manuscript reporting on these results is currently in preparation and will be submitted soon.

## FUTURE PLANS

**Hydrogen oxidation over Pt and Rh– a simple gas-surface reaction with rich dynamics and many open questions** One of the simplest, and oldest known gas-surface catalytic reactions is $H_2 + O_2$ over Pt and Rh. Over Pt(111), recent velocity-resolved kinetics work demonstrated that, within currently accepted microkinetic models, we either do not yet consider the appropriate reaction site for H (s) + O (s) → OH (s), or there must be an as-of-yet unconsidered reactive intermediate pathway to the formation of $H_2O$ (s). In our ongoing work, we have employed imaging AP-XPS and have found evidence of both OH (s) and $H_2O$ (s) in the O(1s) XPS spectral range. In our initial work, we compared two single crystals mounted together- Pt(111) and Pt(557) - to elucidate the effect of step-density. Our hypothesis is that if defects, or steps, provide a near-barrierless route to H (s) and O (s) combination, then surfaces with higher step density should yield more observed OH (s) or $H_2O$ (s). We propose to expand this work in several directions. We will first incorporate a curved Pt crystal that continuously increases the density of steps. This will allow our imaging approaches to sample a range of step densities under identical conditions simultaneously. We will incorporate H, OH, and O atom femtosecond LIF in the near-surface gas phase to monitor for these related intermediates. Heterodyne SFG-VS will be used to monitor the OH stretching region for surface adsorbed species/moieties. We have discovered a new PF-LIF approach for measuring near-surface $H_2O$ with high sensitivity. Our gas-phase and surface diagnostics will reveal the role of steps and defects on $H_2O$ formation rate as well as monitor the surface and near-surface gas phase for unexpected intermediates.

On Rh foil polycrystals the kinetic picture becomes significantly more complex. $H_2$ oxidation of Rh polycrystals has been shown to follow time-varying kinetics and kinetic oscillations that clearly depend on the local crystallographic termination and grain boundaries. The reaction rate follows oscillatory behavior between active and inactive states, and it is thought that the feedback mechanism is related to the formation

and depletion of subsurface oxygen. The mechanism of communication and diffusion between domains remains unclear, and certainly a correlated measurement of localized product desorption and surface oxidation state remains elusive. We will attack this problem with our suite of correlated near-surface gas phase and surface-specific imaging probes to elucidate the mechanism of kinetic oscillation, unambiguously identify the more active state, and begin to understand communication between catalytic domains.

**Correlated Measurements of Surface Oxidation State and Gas-Phase Structure using AP-XPS and Optical Spectroscopy** To date, more than two dozen catalytic reactions have been reported to demonstrate nonlinear oscillatory and spatially inhomogeneous kinetics from UHV to atmospheric pressure conditions, and more reports are made nearly every year. Although many plausible kinetic models can create time-varying oscillations in agreement with macroscopic experiments, incisive experimental tests of these theories require coupling local measurements of the surface and gas-phase over different domains of a catalyst. Our powerful combination of new and developed optical approaches will simultaneously probe the local gas-phase composition, surface intermediates, and surface oxidation state. We will first probe CO oxidation catalyzed by Pd and Ru catalysts. The catalytic oxidation of CO has been studied extensively over transition-metal catalysts due to the industrial relevance of catalytic treatments of automobile exhaust streams as well as the rich dynamics induced by this reaction over many surfaces and scientific debate over the origins of kinetic nonlinearities and oscillations. For instance, while catalytic oscillations have been observed for CO oxidation over Pd(110), the exact mechanisms are still debated, and it is not certain whether metallic Pd or PdO is the phase of higher reactivity for CO oxidation. In part, this depends on which mechanism is invoked to explain the time-dependent kinetics. Kinetic oscillations may result from subsurface oxygen, switching between stable solutions of the Langmuir-Hinshelwood equations, or a Mars-van Krevelen mechanism in which the reaction proceeds through two cycles. This sort of literature disagreement highlights the need for our novel experimental approach. By combining spatially resolved imaging of gas-phase products and reactants, in this case CO, $O_2$, and $CO_2$ with correlated AP-XPS imaging measurements of the surface oxidation state, we can close the kinetic loop with clear evidence for which oxidation states are present and correspond to a given catalytic activity. **The key to this breakthrough in mechanistic understanding is the combination of correlated surface and gas-phase imaging diagnostics.**

**Probing Chemical Mechanisms Through Photolysis Perturbation** One approach to deciphering the chemical mechanisms and complex interactions of catalytic and gas-phase reactions is to introduce perturbations to the chemistry in a well-controlled manner and monitor the response. We propose to develop an apparatus for *in situ* measurements of the temporal response of an *operando* catalytic reactor to a transient perturbation of the gas composition using laser photolysis of a precursor molecule to generate a pulse of reactive species at a prescribed distance from the catalytic surface.

In preliminary work, we demonstrated the transient addition of $CH_3$ radicals by laser photodissociation of acetone vapor diluted in $N_2$ in the near-surface region above a vanadium pentoxide ($V_2O_5$) catalyst using the stagnation flow reactor operated at 10 Torr (Fig. 3). Catalytic reactions of $CH_3$ with $V_2O_5$ are known to produce methanol and formaldehyde. We combine methyl PF-LIF and formaldehyde LIF imaging to monitor the transient response of both reactants and products in this catalytic system (Fig. 3). To differentiate between gas-phase and surface-mediated reactions that impact the consumption of the laser-generated methyl and the production of formaldehyde, we compare the response of these species using the $V_2O_5$ catalyst and a significantly more inert surface: fused silica. In both experiments, the two materials are at the same temperature. At 300K, the rate of $CH_3$ consumption and $CH_2O$ production are very similar with the two different materials (Fig. 3). However, when the surfaces are heated to 500K, a clear difference is observed between the two materials with the rates of $CH_3$ consumption and $CH_2O$ production significantly enhanced by the presence of the heated $V_2O_5$ catalyst. Although the complete chemistry of this system is unclear at present, this enhanced chemical activity provides a measure of the impact of surface-mediated reactions with $V_2O_5$.

We propose using this experimental approach of laser-induced perturbations to the near-surface composition in combination with time-dependent simulations by Olaf Deutschmann's group to provide mechanistic insights into the transient response of gas-surface interactions in catalytic systems.

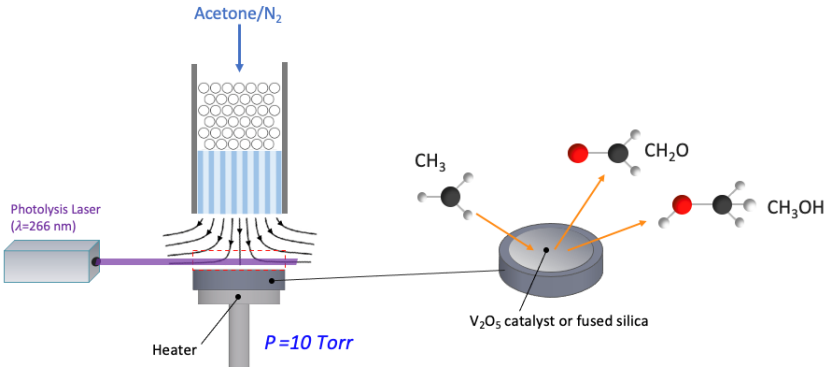


***Figure 3.*** *Experimental configuration for studying transient response of catalytic systems to laser perturbation of the near-surface composition.*

We will also consider other transient perturbations beyond methyl. For example, we can generate additional OH radicals by photodissociation of a precursor (e.g., added $H_2O_2$) at a time (10 ns precision) and place (10s of μm precision) of our choosing. A probe laser will then monitor the chemical response by laser-induced fluorescence measurements at different time delays relative to the photolysis pulse. Separate MBMS experiments in the same chamber will quantify $CH_4$ conversion and C2 selectivity. Finally, our approach enables new, incisive methods to *perturb* mechanisms. **Monitoring of transient, spatial response to a pulse of OH radicals via PLIF and MBMS will provide new critical tests of proposed mechanisms.**

**Oxidative Coupling of Methane with Soft Oxidants** Oxidative coupling of methane (OCM) is a potentially transformative catalytic process for production of valuable C2 species, such as ethane and ethylene. However, the selectivity of OCM towards C2 products is limited by over-oxidation as the desired C2 products react with $O_2$ to form CO and $CO_2$. One approach to improving the selectivity is to replace $O_2$ with "softer" oxidants, such as $N_2O$ that moderate the degree of oxidation. Previous work has shown that compared to $O_2$, $N_2O$ results in larger conversion rates and improved selectivity. However, the use of such alternative oxidants in OCM is much less studied than the use of $O_2$, and significant gaps remain in the mechanistic understanding of the improved selectivity afforded by other oxidants. For example, the role of the gas phase after surface activation of $N_2O$ is not clear. We propose fundamental studies of OCM with $N_2O$ using complementary MBMS and laser imaging diagnostics. These results build on those from the Kronawitter lab that focus on co-upgrading $CO_2$ and alkanes, including through $CO_2$-OCM.

The use of $N_2O$ in OCM impacts the formation or oxidation of methyl. We propose to investigate the different pathways of methyl consumption using laser imaging diagnostics to probe the near-surface gas phase above OCM catalysts with $N_2O$ or $O_2$ as the oxidizer. We will measure the methyl distributions using photofragmentation LIF and detect distributions of products OH, $CH_2O$, $CH_3O$ using LIF imaging. Using these measurements in a series of studies with different catalysts and operating conditions combined with chemical kinetic simulations, we will provide mechanistic insights into the enhanced selectivity of OCM with $N_2O$ as an oxidant. Quantitative $N_2O$-OCM reactor experiments will be performed in the Kronawitter lab at UC Davis to complement data from the near-surface.

## BES-sponsored publications, 2020 – present


1) S. A. Steinmetz, A. T. DeLaRiva, C. Riley, P. Schrader, A. Datye, E. D. Spoerke, and C. J. Kliewer, Gas-Phase Hydrogen-Atom Measurement above Catalytic and Noncatalytic Materials during Ethane Dehydrogenation, *J. Phys. Chem. C* **126**, 3054 (2022).
2) S. M. Gurses, T. Price, A. Zhang, J. H. Frank, N. Hansen, D. L. Osborn, A. Kulkarni, and C. X. Kronawitter, Near-Surface Gas-Phase Methoxymethanol is Generated by Methanol Oxidation over Pd-Based Catalysts, *J. Phys. Chem. Lett.*, **12**, 11252 (2021).
3) B. Zhou, E. Huang, R. Almeida, S. Gurses, A. Ungar, J. Zetterberg, A. Kulkarni, C. X. Kronawitter, D. L. Osborn, N. Hansen, and J. H. Frank, Near-Surface Imaging of the Multicomponent Gas Phase above a Silver Catalyst during Partial Oxidation of Methanol, *ACS Catalysis* **11**, 155 (2021).

# Machine Learning for Understanding Heavy Hydrocarbon Clustering

*Habib Najm*[*1], *Judit Zádor*[1], *Michael Eldred*[2], *Hope Michelsen*[3]
[1]*Sandia National Laboratories, Livermore, CA*
[2]*Sandia National Laboratories, Albuquerque, NM*
[3]*University of Colorado, Boulder, CO*

## Program Scope

The goal of this program is to use machine learning (ML) to advance the state of the art in understanding of reactions relevant in heavy hydrocarbon clustering leading to particle formation in high-temperature environments, e.g., combustion and pyrolysis. We do this by building neural network (NN) potential energy surface (PES) representations for a class of hydrocarbon molecules, and using these to explore reactions among a set of species relevant in flames. Our objective is to identify reactions that dominate hydrocarbon clustering, and explore the role of resonantly stabilized radicals in this process. Our training data comes from quantum chemistry computations at a range of levels of theory, and we use the information thus gained from models of different fidelities in a multifidelity formalism to efficiently attain requisite NNPES test accuracy. We rely on active learning to identify conditions for which additional *ab initio* computations provide maximal expected information gain. We use KinBot [12] for exploration of the PES for generating geometries for training, and for exploring the trained NNPES to estimate reaction rate coefficients. We also work on experimental validation using models built with computed rates.

## Recent Progress

We have made progress on several fronts this year, as outlined in the following.

***Theoretical Chemical Kinetics for Multiwell PESs Relevant for Chemical Clustering:*** In addition to the previously explored $C_5H_5$ PES, we studied two important PESs in the last period. In our Feature Article in J. Phys. Chem. A [1], we described isomerization and dissociation pathways for low-energy $C_5H_5$ and $C_6H_6$ species using our automated workflow tool, KinBot [12]. The recombination reaction of propargyl radicals is thought to play a central role in the formation of soot as it is a key reaction that leads to the formation of the first aromatic ring during combustion. The reaction takes place on the ground $C_6H_6$ PES, which is an extraordinarily complex surface with at least 215 stable isomers. Similarly, the $C_5H_5$ PES is central to clustering, as it features the resonantly stabilized cyclopentadienyl and vinyl-propargyl radicals. Both PESs have been the subject of many prior studies, both experimental and theoretical. Our work, nevertheless, has shown the power of automation even for these well-studied systems. In both cases we found many new pathways and reevaluated some of the previously described channels. We submit that the lack of three-member ring structures in manually explored PESs of $C_5H_5$ points to possible biases experts might introduce when searching for saddle points. In fact, such structures were recently included on another $C_5H_5$ PES explored using more expensive molecular dynamics approaches [13]. We have illustrated the difficulties in the context of automation when the stationary points are weakly bound, and how this might lead to ambiguities in the graph representing the connections between species.

As a natural continuation [2], and to connect to experimental work on this project (see below), we undertook an even more detailed investigation, this time on the $C_7H_7$ PES. In this study, besides exploring the PES, we also constructed and solved the master equation (ME). This was a significant undertaking; our PES contained about 130 minima (reduced to about 70 for the purposes of the ME solution). We determined the main regions of the PES, and showed how these regions can be still connected through bimolecular reactions on the same PES. The automated search was able to uncover the pathways from the literature. In addition, three important new routes were discovered: a lower-energy pathway connecting benzyl with

[*] Principal Investigator. Address: P.O. Box 969, MS 9051, Livermore, CA 94551; Email: hnnajm@sandia.gov

vinylcyclopentadienyl, a decomposition mechanism from benzyl that results in side-chain hydrogen atom loss to produce fulvenallene + H, and shorter and lower energy routes to the dimethylene-cyclopentenyl intermediates. We developed and implemented a new visualization approach for such large PESs, and developed a strategy to grow them more efficiently. We also simulated concentration profiles and calculated branching fractions from the important entry points to provide an interpretation of this important chemical landscape. We compared our results to all suitable experimental data from the literature on elementary rate coefficients, and either found good agreement, or provided alternative explanation for the observations. Our rate coefficients were also included in the model that was used to interpret the experimental data on particle formation [11] in the validation component of the project, below. Recently we also included Sella [14] in KinBot as a code-agnostic geometry optimizer (developed by some of us on a different DOE-supported project), and coupled it to the NN PES, with which we generated reactive energy landscapes and rate coefficients for the $C_5H_5$ system. We also implemented a new, graph-based, visualization approach to handle the complexity of the landscapes.

***Machine Learning of Reactive PESs:*** We have enhanced our ML capabilities in terms of both performance and accuracy. Using physically informed molecule-specific offsets for potential energy data, we reduced the effective disparities of energy-data of different molecules in the NN training phase, resulting in great enhancement in the convergence rate of the training error, and thus similarly speeding up NN training. Further, with this effective rescaling of the data, we were able to train significantly smaller NNs to fit the full PES of $C_5H_5$. We suspect that the rescaling may result in reduced complexity of the loss landscape, which might explain this result. Moreover, with these smaller trained NNs, we found significant reduction in the test error, and have been able to demonstrate chemical accuracy on test predictions for the $C_5H_5$ PES.

***Multifidelity NN PES*:** We have investigated multiple multifidelity (MF) NN PES formulations for integrating data from differing levels of electronic structure theory, easing reliance on the most expensive calculations. The goal in our study in [3] was to explore the effectiveness of MF NN PES constructions for hydrocarbons. Multifidelity constructions are a crucial technology for enabling NN PES representations of larger molecular structures, particularly when relying on computationally expensive electronic structure calculations at high levels of theory. This work presented results with a particular chemical system and electronic structure model hierarchy, allowing more comprehensive exploration of the performance of MF methods in this context. In particular, we explored a range of MF NN PES formulations spanning sequential and discrepancy-based approaches, hybrid input augmentation strategies, activation function selections, learning rate adaptations, and decoupled versus all-at-once training. For the typical case of limited access to high-fidelity training data, our computational results demonstrate that this MF NN PES construction can achieve up to an order of magnitude improvement (Figure 1), either in terms of reduction in error for equivalent total cost or reduction in total cost for equivalent error. This can significantly reduce the reliance on the highest levels of theory, making accurate predictions of molecular energies much more affordable.

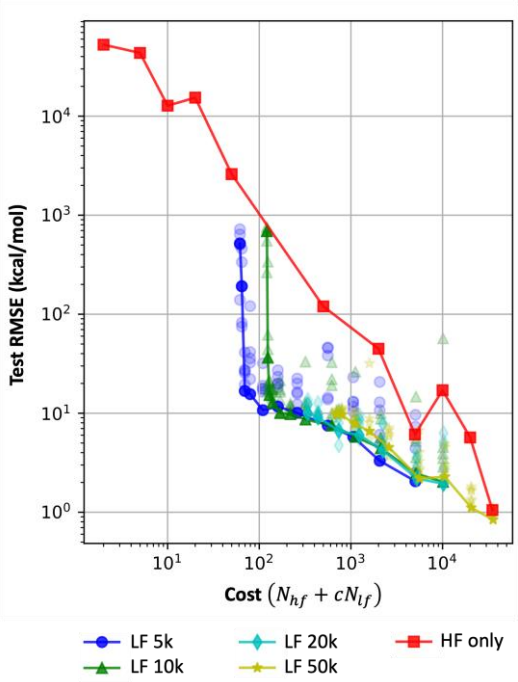


Figure 1. Test RMS error vs. total simulation cost, in terms of equivalent no. of high-fidelity (HF) runs, varying both low-fidelity (LF) & HF run counts. Colors indicate amounts of LF data while HF data is varied from two up to 35k points for each of the five cases.

***Experimental Validation and Modeling:*** Our work in the analysis of experimental data is largely focused on driving and validating the theoretical advances through complementing comprehensive models with newly calculated rate coefficients to advance our understanding of particle-inception processes. This portion of the work was directly coupled with the work focused on quantum chemistry, chemical kinetics, and KinBot development. In this project, we identified isomers of $C_7H_7$ produced during particle formation under combustion and pyrolysis conditions [11]. We compared the observed isomers with a chemical kinetic model that included the rate coefficients calculated as described above [2]. The work demonstrated the power of the advances made with KinBot in the automation of theoretical calculations and the impact these advances can have on transforming the understanding of complex chemical reaction networks. As noted above, KinBot was able to find new low-energy pathways involving $C_7H_7$ isomers. This project provided deeper insight into the chemistry of resonance-stabilized radical reactions, dispelling longheld misunderstandings of the importance of other $C_7H_7$ isomers besides benzyl during combustion and pyrolysis. It has also highlighted similar complexity in the chemistry of these isomers in astrochemistry, an example of which was recently published in Nature Astronomy [15].

We performed two studies focused on testing the theory that resonance-stabilized radicals (RSRs) initiate and drive radical-chain reactions that may be responsible for hydrocarbon clustering and particle formation at high temperatures. This theory is known as the Clustering of Hydrocarbons by Radical Chain Reactions (CHRCR) mechanism [16]. These studies provided strong evidence to support the CHRCR theory. Last year, we performed a study in which we formed particles during the pyrolysis of ethylene and indene (a direct precursor to the RSR indenyl) [6]. Particles were formed at lower temperatures for indene than for ethylene, suggesting that particles were formed more readily with the RSR precursor. In addition, when we added a small amount of indene to ethylene, particles were formed at the same temperature as for pure indene, indicating that clustering only required a small amount of the RSR initiator/driver. In addition, under these pyrolysis conditions, no acetylene was available for molecular-weight growth by the Hydrogen Abstraction $C_2H_2$ Addition (HACA) mechanism, demonstrating particle formation without HACA involvement.

This year we performed a follow-up study of two other direct precursors to RSRs, propene, which forms allyl, and propyne, which forms propargyl [9]. Propyne formed particles at temperatures lower than those observed in the previous study, and propene formed particles at temperatures higher than observed for indene but lower than those for ethylene. In addition, the larger species produced by propyne and propene pyrolysis had more hydrogen content than expected for peri-condensed polycyclic aromatic hydrocarbons (PAHs) at the lowest particle-formation temperatures, suggesting significant aliphatic content for these particles, an observation that supports the CHRCR theory.

## Proposed Work

Going forward, there are numerous lines of development/inquiry that we propose to work on.

***Theoretical Chemical Kinetics for Multiwell PESs Relevant for Chemical Clustering:*** The key effort proposed for the next period is to carry out rate coefficient calculations for several $C_mH_n$ PESs using trained NN PESs. We will begin with the $C_5H_5$ PES, which forms the basis of the current NN PES construction, to assess the accuracy and efficiency of this approach in comparison to *ab initio* calculations. This will be followed by tests to assess ability of the NN PES to extrapolate/generalize to larger species, such as $C_7H_7$, as outlined in the following ML text, along with augmenting and expanding the database with systems beyond $C_5H_5$. If successful, we will start calculating rate coefficients for a large number of reaction systems that are potentially relevant for molecular weight growth and clustering moving from smaller and well-known systems to larger ones. The outcome of this activity will be a database of NN PES rate coefficients that can be used to assemble detailed molecular weight growth and clustering models. We will connect with the experimental validation and modeling effort on this project to establish the most important reaction classes and species to study. Also, in collaboration with the experimental validation and modeling efforts,

we will run KinBot for reactions relevant to indenyl and indenyl dimer chemistry under pyrolytic conditions. This activity, besides connecting to the modeling work, will provide further training and validation data for the ML work.

***Machine Learning of Reactive PESs:*** On the ML front, as already indicated, we plan to evaluate the trained $C_5H_5$ NN PES against direct use of *ab initio* computations for tasks involving PES exploration using KinBot, and calculation of reaction rate coefficients for all the relevant reactions. We will also explore the generalizability of this trained NN for representing the PES of other radical systems, such as $C_7H_7$ and $C_9H_7$. This is a key investigation that allows the determination of the utility of these ML constructions for extrapolation tasks. It is understood that larger errors are expected as we extend the use of the trained PES to successively more complex molecules. While this has been explored [17] for molecules in their minimum energy state with observable controlled growth of the error, *i.e.*, where the extrapolation error can be reduced by enlarging the simpler molecule training data set, it is not known whether this is indeed the case away from the stable minima, and particularly at transition states or for open-shell systems. Along this same vein, we will also explore the utility of transfer learning [18] as well as multifidelity methods for climbing the ladder of complexity. We envision multiple paths in this context. One option is to use the trained $C_5H_5$ NN as a low-fidelity predictor for the $C_7H_7$ PES, allowing us to train a well-fitted NN for the latter using a small number of high-fidelity, and a larger number of low-fidelity, $C_7H_7$ *ab initio* computations, along with many minimal-cost evaluations of the trained $C_5H_5$ NN. This can similarly be done starting with the $C_5H_5$-trained MF NN PES, adding both low and high-fidelity $C_7H_7$ data, and retraining the NN to either represent the $C_7H_7$ PES exclusively or to accurately represent *both* molecules. Given that we already have extensive *ab initio* computations of the $C_7H_7$ PES, as has been mentioned above, we will be able to easily validate and compare these paths to higher complexity. This framework will then be similarly applied to target training NN PESs for more complex molecules, always leveraging the previous highest-complexity trained model as a starting point to provide efficient learning of the next level of molecule size while targeting chemical accuracy relative to coupled cluster computations. Demonstrations on indenyl, and beyond, will provide a stringent test on the effectiveness of the construction.

We also plan extensive improvements of the ML toolkit to facilitate extending utilization of the framework to training on larger hydrocarbons, including molecules in the $C_{20}$–$C_{30}$ range, where significantly larger data sizes are expected, both because of the need to cover higher-dimensional PES domains and the larger size AEV representation of any given structure. Planned developments include enabling multi-GPU utilization for training on data sizes that are incompatible with single-GPU memory constraints. They also include improved parallelization and C++ refactoring of our force-training code, to accelerate force-training tasks. We also plan open-source release of both our database and NN PES software products.

***Multifidelity NN PES*:** Looking forward, we envision several essential refinements to the MF NN PES formulations in [3]. First, we expect to apply procedures for the adaptive determination of training set refinements using a multifidelity active learning procedure, as motivated by previous work in greedy adaptive refinement for MF surrogates [19-21]. Second, we expect to expand beyond bi-fidelity to integrate additional low-fidelity models, enabling greater flexibility in ensemble selection and greater optimality within the adaptive resource allocation problem. Third, it will be essential to assess the performance of these MF NN PES approaches when generalizing to other chemical systems, including the integration of molecule families via the AEV, and involving additional modeling alternatives. For well-correlated hierarchies, we expect that the hybrid input/all-at-once training augmentation of the classical $\Delta$-learning architecture will remain effective, while the hybrid-sequential approach is expected to become more competitive in generalized cases where low-to-high fidelity mappings become more complex and nonlinear. In terms of additional modeling alternatives, we plan to expand our model hierarchy to include coupled cluster models as our new high-fidelity reference, with costs for $C_5H_5$ increasing to $\sim 50k$ CPU sec per simulation, extending the present high-fidelity cost by another factor of $\sim 40$. With additional cost separation and the

expectation of no significant increase in mapping complexity, additional multifidelity performance gains will be possible. Ultimately, our goal is to make use of MF NN methods to integrate data from multiple hydrocarbon molecules at multiple levels of theory to facilitate prediction of heavier molecules at previously unaffordable levels of theory.

***Experimental Validation and Modeling:*** In the next phase of this work, we will extend our studies on RSR chemistry, testing and validating new developments in automated PES construction and chemical kinetics calculations. Our study on the $C_7H_7$ reaction network suggested that more work was required to identify potential missing loss pathways for benzyl and/or formation pathways for vinylcyclopentadienyl, tropyl, and ortho-tolyl. There is growing evidence that this reaction network is an important key RSR reaction network in the formation of soot and interstellar dust. How and which isomers are formed under high-temperature conditions could lead to important insights into the formation of particles and other potentially high-value condensed-phase materials.

We will similarly extend our work on the $C_5H_5$ and $C_6H_6$ reaction systems driven by the experimental results obtained in the study of propyne and propene pyrolysis. Of particular scientific importance is developing an understanding of the unexpected preferential production of aliphatically linked aromatics during particle formation, rather than the production of more stable PAHs via extensively studied molecular-weight growth mechanisms.

**Publications supported by this project 2020-2023**


1. Judit Zádor, Carles Martí, Ruben Van de Vijver, Sommer L. Johansen, Yoona Yang, Hope A. Michelsen, and Habib N. Najm. Automated reaction kinetics of gas-phase organic species over multiwell potential energy surfaces (Feature Article and also cover page for Issue 5, 2023). *The Journal of Physical Chemistry A*, 127(3):565–588, 2023. doi:10.1021/acs.jpca.2c06558.
2. Carles Martí, Hope A. Michelsen, Habib N. Najm, and Judit Zádor. Comprehensive kinetics on the $C_7H_7$ potential energy surface under combustion conditions. *The Journal of Physical Chemistry A*, 127:1941–1959, 2023. doi:10.1021/acs.jpca.2c08035.
3. Yoona Yang, Michael S. Eldred, Judit Zádor, and Habib N. Najm. Multifidelity neural network formulations for prediction of reactive molecular potential energy surfaces. *Journal of Chemical Information and Modeling*. 63, 8, 2281-2295, doi:10.1021/acs.jcim.2c01617
4. H. A. Michelsen, M. B. Colket, P.-E. Bengtsson, A. D'Anna, P. Desgroux, B. S. Haynes, J. H. Miller, G. J. Nathan, H. Pitsch, H. Wang, A Review of Terminology Used to Describe Soot Formation and Evolution Under Combustion and Pyrolytic Conditions, *ACS Nano*, **14** 12470-12490 (2020). doi:10.1021/acsnano.0c06226.
5. H. A. Michelsen, Effects of Maturity and Temperature on Soot Density and Specific Heat, *Proc. Combust. Inst.*, **38** 1197-1205 (2021) doi:10.1016/j.proci.2020.06.383. Distinguished Paper Award.
6. J. A. Rundel, C. M. Thomas, P. E. Schrader, K. R. Wilson, K. O. Johansson, R. P. Bambha, and H. A. Michelsen, "Promotion of Particle Formation by Resonance-Stabilized Radicals During Hydrocarbon Pyrolysis", *Combustion and Flame*, **243**, 111942 (2021) doi:10.1016/j.combustflame.2021.111942.
7. H. A. Michelsen, M. F. Campbell, I. C. Tran, K. O. Johansson, P. E. Schrader, R. P. Bambha, J. A. Hammons, E. Schaible, C. Zhu, and A. van Buuren, "Distinguishing gas-phase and nanoparticle contributions to small-angle X-ray scattering in reacting aerosol flows", *J. Phys. Chem. A*, **126**, 3015-3026 (2022) doi:10.1021/acs.jpca.2c00454. Chosen by ALS to highlight as a brief.
8. H. A. Michelsen, M. F. Campbell, K. O. Johansson, I. C. Tran, P. E. Schrader, R. P. Bambha, E. Cenker, J. A. Hammons, E. Schaible, C. Zhu, and A. van Buuren, "Soot particle core-shell and fractal structures from small-angle X-ray scattering measurements in a flame", *Carbon*, **196**, 440-456 (2022) doi:10.1016/j.carbon.2022.05.009.

9. J. A. Rundel, K. O. Johansson, P. E. Schrader, R. P. Bambha, K. R. Wilson, J. Zádor, G. B. Ellison, and H. A. Michelsen, "Production of aliphatic-linked polycyclic hydrocarbons during radical-driven particle formation from propyne and propene pyrolysis", *Combust. Flame*, in press, 112457 (2022) doi:10.1016/j.combustflame.2022.112457.
10. H. A. Michelsen, E. Boigné, P. E. Schrader, K. O. Johansson, M. F. Campbell, R. P. Bambha, and M. Ihme, "Jet-entrainment sampling: A new method for extracting particles from flames", *Proc. Combust. Inst.*, **39**, in press (2022) doi:10.1016/j.proci.2022.07.140.
11. J. A. Rundel, C. Martí, J. Zádor, P. E. Schrader, K. O. Johansson, R. P. Bambha, G. T. Buckingham, J. P. Porterfield, O. Kostko, and H. A. Michelsen,"The identity and chemistry of $C_7H_7$ radicals observed during soot formation", *J. Phys. Chem. A*, **127**(13), 3000-3019 (2023) doi:10.1021/acs.jpca.2c08949.

**References**

12. KinBot. https://www.github.com/zadorlab/kinbot.
13. Chao He, Zhenghai Yang, Srinivas Doddipatla, Aaron M. Thomas, Ralf I. Kaiser, Galiya R. Galimova, Alexander M. Mebel, Kazuumi Fujioka, and Rui Sun. Directed gas phase preparation of ethynylallene ($H_2CCCHCCH$; $X^1A'$) via the crossed molecular beam reaction of the methylidyne radical (CH; $X^2\Pi$) with vinylacetylene ($H_2CCHCCH$; $X^1A'$). *Physical Chemistry Chemical Physics*, 24(43):26499–26510, 2022.
14. Sella. https://www.github.com/zadorlab/sella.
15. J. Bouwman, M. N. McCabe, C. N. Shingledecker, J. Wandishin, V. Jarvis, E. Reusch, P. Hemberger, and A. Bodi. " Five-membered ring compounds from the *ortho*-benzyne + methyl radical reaction under interstellar conditions" *Nature Astron.*, **7**, 423-430 (2023) DOI: 10.1038/s41550-023-01893-2.
16. K. O. Johansson, M. P. Head-Gordon, P. E. Schrader, K. R. Wilson, and H. A. Michelsen, "Resonance-stabilized hydrocarbon radical chain reactions may explain soot inception and growth", *Science*, **361**, 997-1000 (2018) DOI: 10.1126/science.aat3417.
17. J. S. Smith, O. Isayev, and A. E. Roitberg. "ANI-1: an extensible neural network potential with DFT accuracy at force field computational cost". *Chem. Sci.*, 8:3192–3203, 2017.
18. Silvan Käser, Eric D. Boittier, Meenu Upadhyay, and Markus Meuwly. "Transfer Learning to CCSD(T): Accurate Anharmonic Frequencies from Machine Learning Models". *J. Chem. Theo. Comput.*, 17(6):3687–3699, 2021. PMID: 33960787.
19. Michael S. Eldred, Alex A. Gorodetsky, Gianluca Geraci, John D. Jakeman, and Teresa Portone. "Recent advances in adaptive refinement of multifidelity surrogates for UQ". In *SIAM Conference on Computational Science and Engineering (CSE21)*, 2021.
20. John D. Jakeman, Michael S. Eldred, Gianluca Geraci, and Alex Gorodetsky. "Adaptive multi-index collocation for uncertainty quantification and sensitivity analysis". *Int. J. Num. Meth. Eng.*, 121(6):1314–1343, 2019.
21. John D. Jakeman, Sam Friedman, Michael S. Eldred, Lorenzo Tamellini, Alex A. Gorodetsky, and Doug Allaire. "Adaptive experimental design for multi-fidelity surrogate modeling of multi-disciplinary systems". *Int. J. Num. Meth. Eng.*, 123(12):2760–2790, 2022.

## GAS PHASE INTERACTIONS WITH OTHER PHASES

David W. Chandler, Nils Hansen, Christopher J. Kliewer, Laura M. McCaslin,
Habib N. Najm, David L. Osborn, Leonid Sheps, Craig A. Taatjes, Timothy S. Zwier
Combustion Research Facility, Sandia National Labs, Livermore, CA 94550

chand@sandia.gov, nhansen@sandia.gov, cjkliew@sandia.gov, lmmccas@sandia.gov,
hnnajm@sandia.gov, dlosbor@sandia.gov, lsheps@sandia.gov, cataatj@sandia.gov, tszwier@sandia.gov

### PROGRAM SCOPE

This research program encompasses experimental and computational investigations of a wide range of multiphase phenomena, investigating the formation of particulates in gas-phase reaction systems, measuring and modeling the gas-phase processes at reactive interfaces and probing the physical and chemical interactions between phases. Understanding reactions that lead to particle formation and calculating surface reactions draw on work in the Sandia "Chemical Kinetics for Complex Systems" task, and experiments employ innovations from the "Ultrafast Physics: Nonlinear Optical Spectroscopy and Diagnostics" and "Advanced Mass Spectrometry and X-Ray Diagnostics" tasks. Recent emphasis is on chemically controlled gas-to-particle conversion; proposed new directions will extend work into understanding the interactions of gas-phase molecules with liquid and solid surfaces. These initiatives complement the catalytic surface investigations in Sandia's "Imaging the Near-Surface Gas Phase" program.

### RECENT PROGRESS

***Ion imaging above reactive surfaces*** Recent progress on spatially resolved imaging above a catalytic surface employing velocity-selected, spatial-map ion-imaging (VSSMII) microscope is described in the report on the "Advanced Diagnostics" subtask of this program. Quantum-state-resolved laser ionization of a product (HD, v=0, J=3) of a catalytic $H_2$ + $D_2$ reaction has been imaged above the catalytic surface (a platinum strip at 500 K) with a spatial resolution currently measured to be better than 60 micrometer but expected to be ~15 micrometer with improvements detailed below. This capability will be further developed and applied under this subtask (see proposed work below).

***Molecular weight growth and particle formation*** Soot nucleation in flames is extremely challenging to model on a fundamental basis, and chain reactions may contribute to the formation of nucleation initiators. Several years ago, work in this program (Johansson et al., *Science* **361**, 997 (2018)) proposed that radical-radical chain reactions provide a route to rapid hydrocarbon growth in both low- and high-temperature environments in a mechanism termed CHRCR (clustering of hydrocarbons by radical chain reactions). We continue to investigate the scope of hydrocarbon molecular-weight growth through radical-radical chain reactions, focusing on the role of initial adduct stabilization and well-skipping pathways in radical-radical reactions at ambient to high temperatures.

In our work, we used two complementary experimental approaches: controlled pyrolysis in a SiC microreactor in combination with molecular-beam mass spectrometry, and multiplexed photoionization mass spectrometry with a temperature-controlled reactor. Following work reported in last year's abstract where we employed the SiC microreactor to investigate well-skipping channels in the benzyl + phenyl and phenyl + propargyl reactions, in the past year we also studied the recombination reaction of phenyl and cyclopentadienyl radicals by dilute pyrolysis at low pressure near 30 Torr and intermediate temperatures of 800-1600 K. We showed that the adduct, $C_6H_5$-$C_5H_5$, is the most abundant product below 1600 K, but

radical pathways emerge with elevated temperature. The radical $C_6H_5$-$C_5H_4$ is observed across a wide range of temperatures, and calculations indicate that the well-skipping route is responsible for this radical at low pressure. Decomposition of this radical by three pathways is observed: loss of H atom, acetylene, or propargyl radical. Calculations of the potential energy surface (by Ahren W. Jasper, Argonne National Laboratory) revealed that all three of these pathways occur by a ring-opening reaction and have similar highest-barrier transition states and thus would be expected to all compete at high temperatures.

To complement these high-temperature studies in a SiC microreactor, we also performed a study of the phenyl + propargyl reaction in the multiplexed photoionization mass spectrometer, at approximately constant density from T = 300 K / p = 4 Torr to T = 1000 K / p = 10 Torr. These time-resolved experiments use tunable photoionization spectroscopy to distinguish isomers. At the lower temperatures of this study, the reaction is dominated by stabilization to $C_9H_8$, although at 800 – 1000 K we see non-negligible amounts of the $C_9H_7$ + H product channel. At 300 K only the direct adducts (3-phenyl-1-propargyl, and 1-phenyl-1,2-propadiene) from radical-radical addition are observed, with good agreement between the experimental isomer ratio and variable reaction coordinate transition state theory calculations of this barrierless process. As the temperature is increased to 1000 K we observe two additional isomers, including indene, the two-ring PAH that is the most stable $C_9H_8$ isomer. However, our master equation results predict significantly less indene than we observe experimentally. From additional calculations and experimental evidence, we conclude that the most likely cause of this discrepancy is the contribution of H-atom assisted isomerization that converts less-stable $C_9H_8$ isomers into indene. This study highlights that especially at low pressures typical of the most detailed laboratory investigations, H-atom assisted isomerization needs to be considered. Nevertheless, the experimental observation of indene demonstrates that the phenyl + propargyl react leads, either directly or by H-atom assisted isomerization, to a 2-ring PAH.

***Cluster models for reactions at environmental air-water interfaces*** The reactions of $N_2O_5$ with $Cl^-$ and $H_2O$ at the surface of sea spray aerosols have been of great recent scientific interest due to their outsized influence on global levels of ozone, methane, and $NO_x$ species, as well as their underlying unique mechanisms that resemble $S_N2$ reactions. To understand the competition between $Cl^-$ substitution and hydrolysis of $N_2O_5$, we performed electronic structure and mixed quantum-classical (MQC) dynamics calculations of $N_2O_5/Cl^-/nH_2O$ (n=2-5) clusters. In all clusters, we find that barriers to $Cl^-$ substitution are lower than barriers to direct hydrolysis, indicating that when $Cl^-$ is close to $N_2O_5$, $Cl^-$ substitution to form $ClNO_2$ occurs more quickly than hydrolysis to form $HNO_3$. Two hydrolysis mechanisms are identified, including direct $H_2O$ attack of $N_2O_5$ (one-step) and via a $ClNO_2$ intermediate (two-step). We find that barriers to one-step hydrolysis are lower than that of two-step hydrolysis, indicating that when $Cl^-$ is not close to $N_2O_5$, the one-step hydrolysis mechanism is likely.

## PROPOSED WORK

***Kinetic Monte Carlo for stiff surface kinetics*** Kinetic Monte Carlo (KMC) methods provide means for mesoscopic studies of chemical processes at surfaces. By focusing on accounting for rare processes, and ignoring fast molecular vibrations, KMC enables simulation at timescales that are not feasible with detailed atomistic simulations. At the same time, by accounting for local surface structure and coverage effects, the method retains superior accuracy relative to mean field theory computations of surface kinetics. However, notwithstanding these advantages, KMC simulations can be adversely affected by the presence of a wide range of time scales in the system response. Fast processes that are effectively equilibrated end up slowing the overall progress of the time integration and wasting computational resources in back-and-forth state transitions at small time steps, while slow processes that occur much more rarely, are in fact the key factors affecting system performance. There is, therefore, significant incentive for accelerating time integration of KMC simulations of surface kinetics. There is, indeed, an extensive literature on the acceleration of KMC, with a wide variety of approaches targeting the amelioration of the fast-processes bottleneck. This includes both exact and heuristic methods, with varying degrees of success, and a slew of computational challenges,

particularly for systems with many species and thus a very complex state landscape. This is an active area of research.

We have done preliminary work on examining the performance of the "tau-leap" method, which is an approximate stochastic simulation algorithm that models the cumulative effect of fast processes over slow time scales, originally developed for gas phase chemistry, and subsequently used in surface kinetics. Going forward, we propose to continue this work, targeting advances in the state of the art having to do with the adaptive choice of the slow time step according to active system dynamics. We will also examine the performance of tau-leap in comparison with accelerated superbasin KMC methods, which, while involving costly linear algebra, have been found to provide significant acceleration in specific situations. Finally, and as a third leg, we will examine the utility of projective time integration methods in this regard, relative to these other two methods. Projective time integration has been demonstrated with KMC for surface kinetics, but there have not been extensive studies of its performance relative to other KMC acceleration methods.

***Spatial imaging of gas phase reaction products above reactive surfaces*** We propose to develop our new VSSMII microscope to eventually study the photocatalytic production of $H_2$ and $O_2$ from $H_2O$. To achieve our goal, we will first improve the existing apparatus of the existing spatially resolved ion microscope. This will mostly entail performing a more precise detection of the position of the ions when they strike the detector by centroiding the signal from individual ion strikes. This will eliminate both pulse height distribution issues as a single ion count will be recorded for each strike and the position of that strike can be determined to better accuracy than the camera resolution. This will increase our resolution by about a factor of two. In addition, we need to improve the velocity filtering (size of the pinhole) and the way in which we position the pinhole to obtain the best image. Being able to move the pinhole will allow us to also map out the velocity distribution of products originating from a single particle. As we will be able to begin the reaction with a laser pulse and detect the products with a second laser pulse, we will have the ability to measure the appearance kinetics of products after excitation with nanosecond time resolution.

***Molecular weight growth and particle inception*** Previous work has highlighted the importance of aliphatically substituted PAHs for the formation of pericondensed ring structures. We hypothesize that because of the interplay of aliphatically substituted propargyl (R-CHCCH or R-$CCCH_2$) radicals and 5-membered ring structures, the reaction of phenyl ($C_6H_5$) and propargyl ($C_3H_3$) is well suited to investigate the role of aliphatically substituted PAHs for the formation of five-membered ring structures that contribute to particle formation.

Previous experimental work of this reaction in a fast pyrolysis reactor has shown that this radical-radical reaction can at low pressures provide a chain-propagating pathway for the formation of polycyclic radicals implicated in soot nucleation (described above). However, these measurements used mass spectrometry detection in combination with electron ionization and do not allow the distinction of the important isomers at *m/z* 116 ($C_9H_8$) and 115 ($C_9H_7$). To understand the reactivity of aliphatically substituted PAHs, we will study the phenyl + propargyl reactions at high temperatures using $i^2$PEPICO spectroscopy with tunable vacuum-ultraviolet (VUV) synchrotron radiation at the Swiss Light Source. By measuring the temperature-dependent product yields of $C_9H_8$ at $m/z$ = 116 and of $C_9H_7$ isomers at $m/z$ = 115, the experiment aims to clarify the role of phenyl-substituted propargyl radicals in the formation of five-membered ring structures like indene and indenyl. For this work, the isomer-resolving capabilities of the $i^2$PEPICO endstation are necessary to allow for distinction between the different isomers by measuring mass-selected photoelectron spectra as a function of temperature. The findings of this work can be extrapolated to similar reactions of larger aromatics with propargyl radicals and are therefore relevant for developing a better chemical kinetics understanding of the formation of larger aromatic ring structures that appear in particle formation processes in flames, in interstellar medium, and in industrial reactors.

The cyclopentadienyl radical is known to have a multifaceted chemistry. For example, the recombination of two $C_5H_5$ radicals and its potential to form naphthalene has been the focus of numerous works. This route would in fact allow to bypass the formation of single-ring aromatic species by directly forming naphthalene,

the simplest PAH. A recently performed pressure-dependence analysis by Long *et al.* (*Combust. Flame* **187**, 247-256 (2018)) summarizes the most promising pathways for high and low temperatures. Along with the most-investigated pathways of the cyclopentadienyl radical with $CH_3$ and $C_2H_2$, the reactions $C_5H_5$ + $C_3H_3$ and $C_5H_5$ + $C_3H_5$ ⇄ $C_8H_8$ + $H_2$ forming styrene have been proposed. However, experimental datasets which could be useful to discriminate the most relevant reactions are still scarce. Further questions remain such as, are these reactions important for molecular-weight growth by bypassing benzene formation and can we find experimental conditions that allow us to prove this importance.

Following our approaches for studying radical-radical reactions in microtubular pyrolysis reactors followed by mass spectrometric analysis of the intermediates and products, we propose to study the $C_5H_5$+$C_3H_3$ and $C_5H_5$+$C_3H_5$ reactions. Mass spectra will be taken as a function of the reactor temperature and we will follow the transition from the initial $C_5H_5$-$C_3H_3$ and $C_5H_5$-$C_3H_5$ adducts to the six-membered styrene ($C_6H_5$-$C_2H_3$) and ethylbenzene ($C_6H_5$-$C_2H_5$) and styrene+$H_2$, respectively. While the EI-/PI-mass spectrometric approaches will allow for evaluating the importance of these reactions in the complex network of reactions, tandem mass spectrometry will provide more information about the respective intermediates that occur along the reaction pathways. The experiment is expected to provide the necessary details to understand this ring-enlargement reaction in more detail.

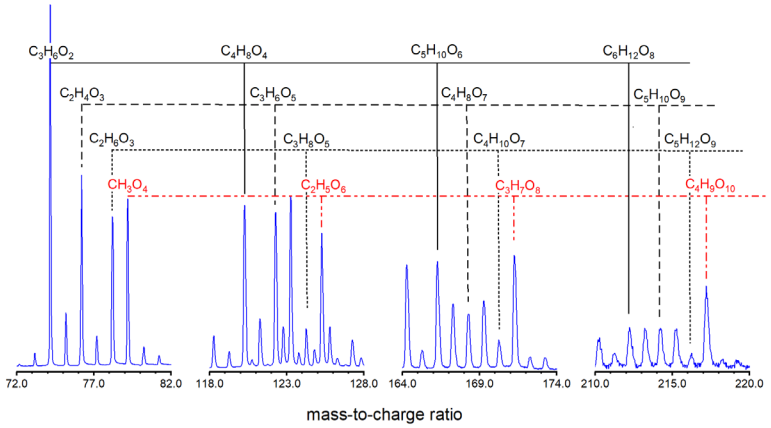


*Section of mass spectrum showing the Criegee intermediate insertion reaction sequences.*

***Particle formation from Criegee intermediate reactions*** Following our successful approach of initiating the oligomerization reactions of the Criegee intermediates in an atmospheric pressure jet-stirred reactor, we performed experiments in collaboration with K.R. Wilson (Lawrence Berkeley National Laboratory), in which we connected our reactor chamber to Wilson's aerosol mass spectrometer. Portions of an aerosol mass spectrum accumulated after ethylene ozonolysis are provided in the figure below, in which mass peaks are indicated that potentially originate from sequential addition of CI to ketene ($C_2H_2O$), acetaldehyde ($C_2H_4O$), ethanol ($C_2H_6O$), and methylhydroperoxide ($CH_4O_2$). As can be seen, highly oxygenated species, containing 7-8 oxygen atoms, are formed. An interesting observation is the occurrence of radical species at m/z = 183 and 185 in the mass spectra and obvious questions to ask are: Are these radical species involved in the chemistry of molecular-weight growth and particle inception or are they formed through the flash pyrolysis and/or the photoionization process? In the next year we will carry out a coordinated effort combining direct experimental measurements and theoretical characterization of elementary Criegee intermediate reactions (see the "Chemical Kinetics for Complex Systems" task), continuing our collaboration with Rebecca Caravan (Argonne), Marsha Lester (Penn) and Stephen Klippenstein (Argonne), with modeling of the oligomerization kinetics that leads to particle formation.

***Nano-Confinement: The Spectroscopy of Ions in Molecular Cages*** Intermolecular interactions and bimolecular reactions in the gas phase typically occur between two unconstrained partners that are free to enter and exit their interaction in unencumbered fashion. The dividing line between phases tends to blur when the compartment in which intermolecular interactions occur is molecular in size, a type of nanoconfinement. When one or more of the partners are ions, the effects of nanoconfinement are important to DOE mission areas such as heavy metal sequestration, $CO_2$ capture, catalysis, and charge transport.

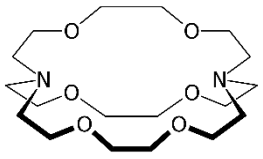

[2.2.2]cryptand

Supramolecular chemistry has its genesis in 3D molecular cages such as cryptands that are designed to selectively trap ions by size, charge state, and binding geometry. [2.2.2]cryptand has six ether oxygens and two capping tertiary nitrogens that bind to cations in aqueous solution, placing them in nanoconfinement. A principal motivation for this work is to understand the spectroscopic implications of nanoconfinement under gas-phase conditions in which the ion and cage are both free of interfering effects from solvent or crystal packing. By removing the solvent, the infrared spectrum can be recorded without interference that often masks or shifts the infrared absorptions due to the ion-cage complex. The spectroscopic manifestations of nanoconfinement in the gas phase are largely unexplored, motivating this work.

In the past year, we have carried out preliminary studies of alkali and alkaline earth cations bound inside [2.2.2]-benzocryptand. The phenyl ring serves as UV chromophore for IR-UV double resonance. Single-conformation IR spectra in the alkyl CH stretch region are surprisingly sensitive to the complexing ion and are diagnostic of the cage structure taken up by the ion-cryptand complex in the gas phase. Our collaborator Ned Sibert at UW-Madison has developed a local mode anharmonic model of the alkyl CH stretch region that he recently extended to these strong-binding circumstances.

In the coming year, we plan to study the protonated and di-protonated forms of benzocryptand; that is, the structures formed when the tertiary amine sites are either singly or doubly protonated. The $N\text{-}H^+$ groups will be good IR chromophores, reporting directly on the proton binding to the oxygens.These cryptand cages can also be used to trap a +2 charged cation to which a singly charged anion can be bound, enabling studies of cage-separated (as opposed to solvent-separated) cation-anion pairs.

***Non-adiabatic dynamics of photosensitizing reactions at environmental air-water interfaces*** In the coming year we aim to unravel the non-adiabatic photochemical mechanisms and timescales of photosensitizing reactions of fatty acids at environmental air-water interfaces. Photosensitizers are molecules that absorb light and undergo electronic excitation; internal conversion and intersystem crossing processes may occur before energy transfer from the photosensitizer to a nearby acceptor molecule. Recent work has unraveled that there are two classes mechanisms for photosensitization of fatty acids at environmental air-water interfaces: external photosensitizing and self photosensitizing reactions. External photosensitizing processes involve UV-Vis excitation of a photosensitizing molecule such as 4-benzoylbenzoic acid (4-BBA) and subsequent internal conversion before excited energy transfer to a nearby fatty acid molecule. Self photosensitizing reactions involve direct UV-Vis excitation of a fatty acid molecule and subsequent internal conversion or intersystem crossing before excited energy transfer to a second, nearby fatty acid molecule. In both cases, energy transfer from the photosensitizer to fatty acid can cause $H^+$ or $e^-$ transfer. The details of these photosensitizing processes of fatty acids are largely unknown, including the electronic states involved, competition between internal conversion and intersystem crossing, and timescales of photosensitizing. Furthermore, the effects of relative molecular orientation, degree of solvation, and fatty acid chain length on these mechanisms are unknown. Using the non-adiabatic MQC methods used recently in work described in the Ultrafast Chemistry subtask abstract, we will investigate these mechanisms and timescales of photosensitizing reactions of fatty acids at air-water interfaces.

## Publications acknowledging support from this project 2020 – 2023


1. L. M. McCaslin, A. W. Götz, M. A. Johnson, R. B. Gerber, "Effects of Microhydration on the Mechanisms of Hydrolysis and Cl− Substitution in Reactions of $N_2O_5$ and Seawater", *ChemPhysChem*, e202200819. doi:10.1002/cphc.202200819. (2023).
2. D. E. Couch, G. Kukkadapu, A. J. Zhang, A. W. Jasper, C. A. Taatjes, N. Hansen, "The role of radical-radical chain-propagating pathways in the phenyl + propargyl reaction", *Proc. Combust. Inst.*, doi:10.1016/j.proci.2022.09.01 (2022).
3. N. Hansen, B. Yang, M. Braun-Unkhoff, G. Kukkadapu, "Molecular-Growth Pathways in Premixed Flames of Benzene and Toluene doped with Propyne", *Combust. Flame,* **243**, 112075 doi:10.1016/j.combustflame.2022.112075 (2022).
4. H. A. Michelsen, M. F. Campbell, K. O. Johansson, I. C. Tran, P. E. Schrader, R. P. Bambha, E. Cenker, J. A. Hammons, C. H. Zhu, E. Schaible, A. van Buuren, "Soot-particle core-shell and fractal structures from small-angle X-ray scattering measurements in a flame", *Carbon* **196**, 440-456. doi:10.1016/j.carbon.2022.05.009. (2022).
5. K. C. Kalvakala, P. Pal, J. P. Gonzalez, C. P. Kolodziej, G. Kukkadapu, S. Wagnon, R. Whitesides, N. Hansen, S. K. Aggarwal, "Numerical Analysis of Soot Emissions from Gasoline-Ethanol and Gasoline-Butanol Blends under Gasoline Compression Ignition Conditions", *Fuel* **319**, 123740 doi:10.1016/j.fuel.2022.123740 (2022).
6. H. A. Michelsen, M. F. Campbell, I. C. Tran, K. O. Johansson, P. E. Schrader, R. P. Bambha, J. A. Hammons, E. Schaible, C. H. Zhu, A. van Buuren, "Distinguishing Gas-Phase and Nanoparticle Contributions to Small-Angle X-ray Scattering in Reacting Aerosol Flows", *J. Phys. Chem. A* **126**, 3015-3026. (2022).
7. D. E. Couch, A. W. Jasper, G. Kukkadapu, M. M. San Marchi, A. J. Zhang, C. A. Taatjes, N. Hansen, "Molecular weight growth by the phenyl + cyclopentadienyl reaction: Well-skipping, ring-opening, and dissociation", *Combust. Flame*, 112439, doi: 10.1016/j.combustflame.2022.112439 (2022).
8. H. Michelsen, E. Boigné, P. E. Schrader, K. O. Johansson, M. F. Campbell, R. P. Bambha, M. Ihme, "Jet-entrainment sampling: A new method for extracting particles from flames," *Proc. Combust. Inst.*, doi:10.1016/j.proci.2022.07.140 (2022).
9. B. Yang, W. Sun, K. Moshammer, N. Hansen, "Review of the Influence of Oxygenated Additives on the Combustion Chemistry of Hydrocarbons", *Energy Fuels* **35**, 13550-13568 doi:10.1021/acs.energyfuels.1c01841 (2021).
10. J. A. Rundel, C. M. Thomas, P. E. Schrader, K. R. Wilson, K. O. Johansson, R. P. Bambha, H. A. Michelsen, "Promotion of particle formation by resonance-stabilized radicals during hydrocarbon pyrolysis," *Combust. Flame* **243***,* 111942 doi:10.1016/j.combustflame.2021.111942 (2022).
11. R. I. Kaiser, N. Hansen, "An Aromatic Universe", *J. Phys. Chem. A* **125**, 3628-3840 (invited Perspective Paper) doi:10.1021/acs.jpca.1c00606 (2021).
12. M.G. Vazquez de Vasquez, K.A. Carter-Fenk, L.M. McCaslin, E.E. Beasley, J.B. Clark, H.C. Allen, "Hydration and Hydrogen Bond Order of Octadecanoic Acid and Octadecanol Films on Water at 21 and 1°C", *J. Phys. Chem. A* **125**, 10065 (2021).
13. M. Baroncelli, Q. Mao, N. Hansen, H. Pitsch, "Effects of $C_1$-$C_3$ Hydrocarbon Blending on Aromatics Formation in 1-Butene Counterflow Flames", *Combust. Flame* **230**, 111427 doi:10.1016/j.combustflame.2021.111427 (2021).
14. D. E. Couch, A. J. Zhang, C. A. Taatjes, N. Hansen, "Experimental Observation of Hydrocarbon Growth by Resonance Stabilized Radical-Radical Chain Reaction", *Angew. Chem. Int. Ed.* **60**, 27230-27235 (2021).
15. G. Kukkadapu, S. W. Wagnon, W. J. Pitz, N. Hansen, "Identification of the Molecular-Weight Growth Reaction Network in Counterflow Flames of the $C_3H_4$ Isomers Allene and Propyne", *Proc. Combust. Inst.* **38**, 1477-1485 doi:10.1016/j.proci.2020.07.130 (2021).
16. S. Mitra, N. Yang, L. M. McCaslin, R. B. Gerber, M. A. Johnson, "Size-Dependent Onset of Nitric Acid Dissociation in $Cs^+(HNO_3)(H_2O)_{n=0-11}$ Clusters at 20K", *J. Phys. Chem. Lett.*, 12, 3335 (2021).
17. M. Baroncelli, Q. Mao, S. Galle, N. Hansen, H. Pitsch, "Role of Ring-Enlargement Reactions in the Formation of Aromatic Hydrocarbons", *Phys. Chem. Chem. Phys.* **22**, 4699-4714 doi:10.1039/c9CP05854K2020 (2020).
18. N. Hansen, B. D. Adamson, S. A. Skeen, M. Ahmed, "Nucleation of Soot: Experimental Assessment of the Role of Polycyclic Aromatic Hydrocarbon (PAH) Dimers", *Z. Phys. Chem.* **234**, 1295-1310 (2020).

# ULTRAFAST CHEMISTRY: EXCITED STATE DYNAMICS IN GAS-PHASE MOLECULES

Krupa Ramasesha, Laura M. McCaslin, Christopher J. Kliewer
Combustion Research Facility, Mail Stop 9055; Sandia National Laboratories, Livermore, CA 94550
kramase@sandia.gov, lmmcas@sandia.gov, cjkliew@sandia.gov

## I. Program Scope

This program aims to apply ultrafast techniques and theoretical calculations to investigate fundamental gas-phase chemical dynamics. Our research uses diverse experimental probing techniques to follow coupled electronic and nuclear motion on femtosecond to picosecond timescales in gas-phase molecules, as well as advanced quantum chemical calculations to investigate these dynamics and predict experimental observables. The coupling of electronic and nuclear degrees of freedom, representing a breakdown of the Born-Oppenheimer approximation, gives rise to complex pathways for non-radiative energy dissipation in electronically excited molecules, often involving participation of multiple electronic states. Identifying the motions that couple electronic states, the timescales and dynamics of excited state population relaxation, and the role of coupled vibrational modes of a molecule in guiding energy flow is crucial to our understanding of non-equilibrium dynamics, and it forms the mainstay of this program. The work in this task has strong connections to the laser spectroscopy investigated under the "Ultrafast Physics: Nonlinear Optical Spectroscopy and Diagnostics" task, and the high photon-energy techniques developed in the "Advanced Diagnostics" task. This task extends the "Chemical Dynamics Methods and Applications" work down to the fundamental timescales of vibrational and electronic motion. *Ultrafast Chemistry* is one of the synergistic research themes of CSGB and this work addresses two key aspects of the Grand Challenges for Basic Energy Sciences: (1) investigating the nature of electronic excited states, and (2) exploring the breakdown of the Born-Oppenheimer approximation.

## II. Recent Progress

***Excited state dynamics during primary C–I dissociation in acetyl iodide*** Acetyl halides [$CH_3$–C(O)–X; X=halogen atom], are a unique class of molecules that contain both the $n\sigma^*_{C\text{-}X}$ and the $n\pi^*_{C=O}$ chromophores. In acetyl iodide [$CH_3$–C(O)–I, AcI], both these chromophores are excited by 266 nm, leading to complex excited state dynamics prior to the primary dissociation of the C–I bond. The goal of our work is to characterize these valence excited states and non-adiabatic dynamics prior to C–I bond dissociation in AcI. To this end, we performed ultrafast XUV transient absorption spectroscopy by probing the I 4d-to-valence transitions, and Martin Head-Gordon's group employed electronic structure theory based on EOM-CCSD and TDDFT to characterize the valence excited states and predict core-level spectra. Theoretical characterization of the valence excited states of AcI reveal significant spin-orbit coupling, resulting in valence states of strongly mixed singlet-triplet character. Our experimental results (Figure 1) show fast formation of both ground state and spin-orbit excited I atoms (I*:I ratio of 1:1.9) following 266 nm excitation, seen as transitions due to ground state I at 46.1 eV ($^2P_{3/2}\rightarrow{}^2D_{5/2}$), at 47.8 eV ($^2P_{3/2}\rightarrow{}^2D_{3/2}$), at 55.5 eV and at 57 eV (4d→6p), and due to spin-orbit excited I* at 46.8 eV ($^2P_{1/2}\rightarrow{}^2D_{3/2}$). In addition, short-lived features at 47.1 eV and near 55.5 eV evolve with <100 fs time constants, arising from excited state wavepacket

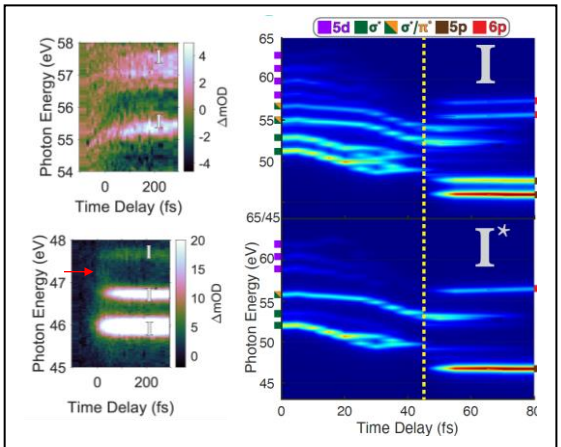


**Figure 1**: (Left) Experimental I N-edge transient absorption spectra after 266 nm excitation of AcI, revealing short-lived features. (Right) Theoretical I N-edge spectra calculated along non-adiabatic *ab initio* molecular dynamics simulation trajectory.

evolution in AcI prior to C-I bond dissociation. Non-adiabatic AIMD simulations performed by the Head-Gordon group suggest rapid C–I bond dissociation, and time-dependent core-level spectra calculated from these AIMD trajectories assign the spectral features giving rise to the short-time dynamics seen in experiments. We will also perform ultrafast soft X-ray transient absorption at the C K-edge to monitor both the primary and the predicted anomalously fast[1] secondary dissociation of the acetyl radical after 266 nm excitation of AcI.

***Ultrafast XUV absorption spectroscopy of excited state dynamics in $Fe(CO)_5$*** To directly monitor the excited state dynamics governing $Fe(CO)_5$ (IP) photodissociation, we applied ultrafast XUV transient absorption spectroscopy near the Fe $M_{2,3}$-edge (3p-to-valence transitions) as a probe of local electronic structure evolution in the vicinity of the Fe atom. Theoretical work by Martin Head-Gordon's group involved valence electronic structure calculations and core level spectral predictions to help interpret experimental results. Figure 2 displays the evolution of the transient XUV absorption spectra following 266-nm excitation of IP, showing time-dependent induced absorption features centered at 65 eV, 59 eV, and 54 eV, in addition to the bleach at 61 eV due to depletion of ground state IP. The 65 eV feature narrows on a 120-fs timescale, whereas the features at 54 and 59 eV evolve with a 3-ps timescale. TDDFT and CCSD calculations of valence excited states and potential energy cuts, and electron affinity TDDFT (EA-TDDFT) calculations of core-level absorption spectra of valence-excited IP and $Fe(CO)_x$ were used to interpret these results. Our work revealed that excitation at 266 nm populates the $9^{th}$, $10^{th}$, and $11^{th}$ singlet excited states of MLCT character. Following <100 fs internal conversion to doubly-degenerate lowest lying open-shell singlet states of metal-centered character, the first CO loss begins either from the axial or the equatorial positions; however, elongations of either the axial or the equatorial Fe-CO bond results in the wavepacket reaching a minimum energy crossing point (MECP) in the $C_{2v}$ geometry with the closed-shell singlet excited state along the dissociation coordinate. Dissociation of the first CO thus leads to the formation of a closed-shell singlet excited $Fe(CO)_4$ in primarily the $C_{2v}$ geometry with minority of the population in $C_{3v}$ geometry. Comparison of experimental and predicted core-level absorption spectra (Figure 2) reveals that at early time delays (~100 fs), closed-shell singlet excited state of $Fe(CO)_4$ in the $C_{2v}$ geometry majorly contributes to the experimental XUV spectrum, with minor contribution from $Fe(CO)_4$ in the $C_{3v}$ geometry. We assigned the 120 fs evolution of the 65 eV feature to structural dynamics in $Fe(CO)_4$ while reaching the asymptotic $C_{2v}$:$C_{3v}$ population ratio. The 3 ps evolution of the core-level absorption spectra arises from the second CO loss that leads to the formation of $Fe(CO)_3$ in its closed-shell singlet excited state in mostly the non-planar $C_s$ geometry. This body of work has provided a comprehensive description, backed by direct spectroscopic evidence, of the femtosecond to picosecond valence electronic and structural dynamics underlying multi-body dissociation of UV-excited IP. These studies also established that orbital relaxation effects–usually considered important for L- and K-edge spectra of transition metals–significantly influence M-edge spectra of $Fe(CO)_x$, necessitating the implementation of EA-TDDFT, which uses core-ionized reference states for accurate spectral predictions.

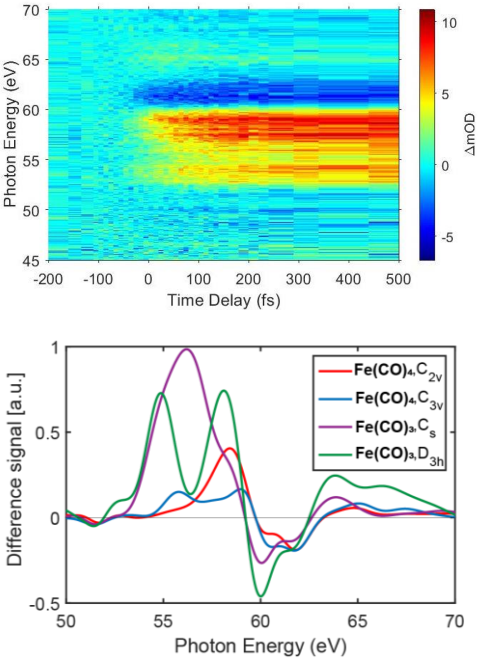


**Figure 2:** (Top) Experimental transient XUV absorption spectra at the Fe M-edge following 266 nm excitation of $Fe(CO)_5$. (Bottom) EA-TDDFT predicted core-level absorption spectra of $Fe(CO)_x$ in the indicated geometries.

***Excited state dynamics of $Fe(CO)_5$ following 200 nm excitation*** We also recently performed ultrafast XUV transient absorption spectroscopy of IP after 200 nm excitation to unravel the excited state dynamics governing multi-body dissociation at this wavelength as well as the role of intersystem crossing (ISC), which was suggested by our previous ultrafast IR studies. Dynamics involving 200 nm excitation in transition metal carbonyls are particularly difficult to theoretically describe due to the very large density of electronic states accessible at this wavelength and the myriad excited state pathways available. Based on the UV absorption spectrum of IP, 200 nm excitation likely populates a high-lying MLCT state, following which, rapid internal conversion could place population in the low-lying dissociative metal-centered states with very large excess energy that can open multiple pathways to dissociation. Our experimental transient XUV absorption spectra show a prompt bleach at 61 eV indicating loss of ground state IP. At time delays less than 100 fs, an induced absorption centered at 59 eV is present, which over the next ~200 fs intensifies, shifts, and broadens to lower energies to ultimately be centered near 58 eV; this feature ceases to evolve past a delay 300 fs. On the other hand, a weak induced absorption centered at 54 eV evolves minimally in the first few hundred femtoseconds, after which it dramatically intensifies on a picosecond timescale. To provide insights into these dynamics and spectroscopy, we are continuing our collaboration with Martin Head-Gordon's group, who are working on predicting singlet excited state and triplet ground state XUV absorption spectra of $Fe(CO)_3$ and $Fe(CO)_2$ for comparison with experiment.

***Competing pathways in the ultrafast photodissociation of dimethyl disulfide*** Dimethyl disulfide (DMDS, $CH_3$–S–S–$CH_3$) is the simplest model system for the disulfide (S–S) bond, an important moiety in protein structure. Despite its central role in maintaining the structural integrity of proteins, the disulfide bond is photolabile with several electronic excited states proposed to be dissociative along the S–S and C–S bonds. Photodissociation studies on the first excited state, $S_1(n_S\sigma^*_{S\text{-}S})$, of DMDS have found exclusive S–S bond fission.[2] However, little work has been done on the photochemistry of the higher lying electronic excited states near the DMDS absorption maximum at 195 nm, where early nanosecond experiments suggested cleavage of both C–S and S–S bonds.[3] We performed ultrafast electron diffraction (UED) at the SLAC MeV-UED facility to probe the competing pathways in the ultrafast photodissociation of DMDS following 200 nm excitation. Our theoretical work has revealed that 200 nm populates the 5$^{th}$ singlet excited state that is characterized by transitions from $n_S$ to primarily Rydberg orbitals, with minor contribution from transitions to $\sigma^*_{C\text{-}S}$. Following this excitation, experimental results show prompt appearance of negative signal at 2 Å and 3 Å interatomic distances (Figure 4), corresponding to the loss of C–S/S–S distances and the second-nearest neighbor C---S distances, respectively. This prompt response is followed by subtle evolution on a 1.5 ps timescale at interatomic distances between 2 and 3 Å. Genetic algorithm fitting of the diffraction data suggests the presence of both S–S and C–S bond dissociations. To provide a spectroscopic complement to these diffraction measurements, we collaborated with Vasilios Stavros' group (University of Birmingham) for performing ultrafast photofragment velocity-mapped ion imaging of the $CH_3$ fragment; these results also show evidence for C–S and S–S bond dissociations, with possible existence of a second, slower C-S dissociation channel.

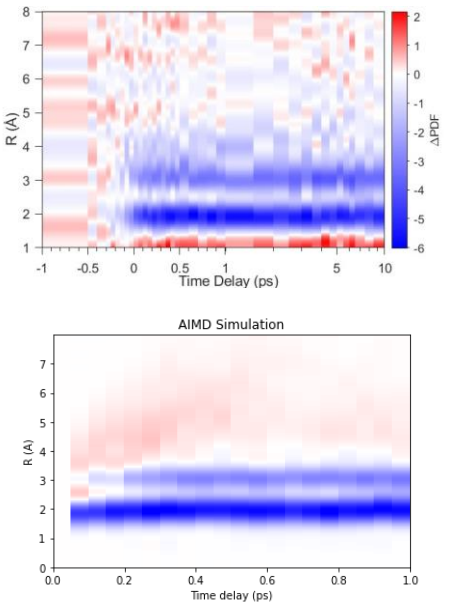


**Figure 3:** Evolution of the pair distribution function with respect to pump-probe time delay and interatomic distance following 200 nm excitation of dimethyl disulfide. Experiment (top), AIMD (bottom).

We performed high-level electronic structure theory employing EOM-CCSD and TDDFT to help interpret experimental results. To this end, we assessed several theoretical methods and basis sets by

extensively benchmarking their accuracies in reproducing the experimental UV absorption spectrum, allowing us to converge on EOM-CCSD/aug-cc-pVTZ and TDDFT CAM-B3LYP/aug-cc-pVDZ as the best-suited methods for characterizing the excited states of this molecule. One-dimensional cuts through the ground and excited singlet and triplet state potential energy surfaces along the S–S and C–S dissociation coordinates characterized the energetics, and TDDFT-based non-adiabatic AIMD simulations using the SHARC[4, 5] program are being performed to understand the electronic and structural dynamics following electronic excitation. Preliminary results from these simulations show both S–S and C–S bond dissociations, revealing numerous dynamical pathways, including (1) fast (~300 fs) S-S cleavage in the singlet manifold, (2) slow (~1.5 ps) S-S bond cleavage after ISC, and (3) a $CH_3$ roaming mechanism to form a $CH_3SCH_3$. Also, long-lived (>1 ps) complexes observed in calculations support experimental observations. Pair distribution functions extracted from these simulations show excellent agreement with experimental results (Figure 3).

***Core spectroscopy of ground-state oxazole*** Oxazole ($C_3H_3NO$) is a five-membered aromatic heterocycle with O and N substitutions in the 1 and 3 positions, respectively. It is a model biochromophore whose excited state dynamics we will explore using ultrafast core-level spectroscopy, as described under Future Work. To this end, we collaborated with Anja Röder, Piero Decleva and Marcello Coreno on a theory-led investigation by Sonia Coriani's group on the core-level spectroscopy of this molecule in its ground electronic state to form the foundation for future work on core-level spectroscopy of valance excited state dynamics. This study measured the X-ray absorption spectra, valence and X-ray photoelectron spectra, and Auger-Meitner electron spectra of oxazole at the carbon, nitrogen, and oxygen K-edges at the Elletra synchrotron in Trieste, Italy. High-level electronic structure theories using coupled cluster, restricted complete active space second order perturbation theory, and time dependent density functional theory were used to calculate these experimental observables to determine which methods best agree with the core-level spectra. This joint theory-experiment study assigned the spectral features present in the ground state X-ray absorption spectra at the C, N, and O K-edges.

## III. Future Work

***Ultrafast soft X-ray transient absorption spectroscopy of excited state dynamics in the dissociation of dimethyl disulfide*** Our non-adiabatic AIMD calculations that accompanied the ultrafast electron diffraction and photofragment VMI experiments on DMDS suggest complex valence excited state dynamics, particularly on picosecond timescales, when involvement of low-lying triplet states appear to lead to slower S–S and C–S bond dissociations. We will experimentally study the valence excited state dynamics of DMDS photodissociation, with particular emphasis on picosecond dynamics, using ultrafast soft X-ray transient absorption spectroscopy near the S L-edge and C K-edge following 200 nm excitation of DMDS. The experiment will use an ultrafast 200 nm excitation pulse and table-top high-harmonic-generated soft X-ray pulses to probe the evolution of sulfur 2s-to-valence transitions at ~230 eV, sulfur 2p-to-valence transitions at ~160 eV, and carbon 1s-to-valence transitions at ~285 eV, simultaneously. 200 nm excitation is characterized by the promotion of an electron from the one of the two non-bonding orbitals of sulfur to Rydberg and $\sigma^*_{CS}$ orbitals as determined by our ongoing work. Immediately following this excitation, we expect new and strong pre-edge features near the S L-edge arising from transitions out of the S 2s and 2p orbitals to the now-partially-occupied localized non-bonding orbital of sulfur, as well as reduction in intensity of the S and C core level transitions to the newly populated $\sigma^*_{CS}$ and Rydberg orbitals. As the molecule relaxes through singlet and triplet excited states characterized by transitions out of the two non-bonding sulfur orbitals to $\sigma^*_{SS}$, $\sigma^*_{CS}$ and Rydberg states, the time-dependent evolution of corresponding transitions from the S 2s and 2p core orbitals to $n_{S1}$, $n_{S2}$, $\sigma^*_{SS}$, $\sigma^*_{CS}$, Rydberg orbitals and the C 1s core orbital to $\sigma^*_{CS}$ and Rydberg orbitals will report on the relaxation dynamics prior to dissociation. Finally, C–S and S–S bond dissociations will result in a red-shift to the core level transitions due to the increase in electron density on the S and C atoms and the corresponding decrease in core binding energies. Given the sensitivity of X-ray absorption spectroscopy to the nature of valence excited states, these experiments will

thus be a direct test of the results from our ongoing AIMD simulations. In parallel, core-level absorption spectra of the sulfur 2s-to-valence, 2p-to-valence and carbon 1s-to-valence transitions, using either EA-TDDFT or EOM-CVS-CCSD, will be calculated for valence excited state configurations predicted by our NA-MQC dynamics trajectories of DMDS.

***Photoisomerization and ring-opening in 1,3,5-triazine*** Knowledge of the photochemistry of aromatic heterocycles, such as pyridine and pyrimidine, is crucial to a bottom-up understanding of the photostability of these fundamental building blocks of life. In particular, the role of conical intersections (CIs) in the non-adiabatic dynamics of these heterocyclic rings has been the subject of intense study for several decades. While the photochemistry of pyridine and pyrimidine has been well studied, the related system 1,3,5-triazine (*c*-$C_3H_3N_3$, *sym*-triazine, ST) has received less attention. ST is both an important model biochromophore and is a prototypical example of three-body dissociation dynamics. Photodissociation of ST only occurs following internal conversion (IC) to the ground electronic state, with conflicting evidence for synchronous *vs*. asynchronous concerted three-body dissociation mechanisms. Also, there is limited information on the ST structural changes that accompany IC. The only time-resolved study of ST used mass spectrometry to follow the evolution of $ST^+$ yield after photoexcitation at 277 nm.[6] This study reported decay time constants of <200 fs and ~100 ps, implying rapid excited state isomerization, with no experimental evidence for the structural evolution presented. Subsequent computational work on ST has instead suggested a ring-open pathway to return to the ground electronic state.[7] Conversely, recent MeV-UED work[8] on the related system pyridine has suggested a ring-pucker CI, which facilitates excited state population transfer back to the ground electronic state. To understand the excited state structural dynamics and the role of photoisomerization versus ring-open intermediates in ST, we have been awarded beam time at SLAC's MeV-UED facility to perform ultrafast electron diffraction following 266 nm excitation. Our preliminary predicted differential scattering intensities and pair distribution functions suggest that the ring-closed intermediates (Hückel, Dewar and ring-puckered structures) can be clearly distinguished from the ring-open intermediate and the three-body dissociation products.

***Treatment of Intersystem Crossing in Systems with a High Density of Electronic States*** Accurately treating intersystem crossing in molecular dynamics involving a dense manifold of electronic states is a well-known problem in chemical theory. In mixed quantum-classical (MQC) dynamics, a molecular system's energy and nuclear forces are calculated on ground and excited state BO surfaces using quantum chemistry methods and the nuclear dynamics are propagated using Newton's equations of motion. One of the premiere codes for computing non-adiabatic MQC dynamics, SHARC[4, 5], employs the fewest-switches surface hopping (FSSH)[9] algorithm for both internal conversion and intersystem crossing events. Numerous studies have assessed the suitability of FSSH for internal conversion processes and developed corrections (e.g. decoherence corrections) such that FSSH samples from the electronic state populations computed in a fully quantum dynamics treatment.[10-12] However, far fewer comparisons have been made between SHARC's FSSH approach for ISC and a full quantum dynamics treatment. Benchmarks that have been performed have been done on small molecules like $SO_2$ with relatively localized spin-orbit coupling.[13] We will perform further benchmarking of ISC timescales between mixed quantum-classical and quantum dynamics on systems with a greater delocalization of spin-orbit coupling, such as along the dissociation pathways of dimethyl disulfide. We will compare quantum state populations to those computed with FSSH in SHARC and assess decoherence corrections in ISC timescales and mechanisms. We will compare our techniques with high-accuracy quantum dynamics simulations to test the limits of this hybrid approach, including how to combine surfaces and their weighting schemes.

***Photoinduced ring-opening in oxazole*** Organic heterocycles serve as building blocks in a variety of biological systems. Ultraviolet excitation to a $\pi\pi^*$ state in these systems is typically followed either by a deformation of the ring structure (ring puckering) as the molecule relaxes back to the ground electronic state, or ring-opening via bond cleavage following non-adiabatic passage to an $n\sigma^*$ state. Ultrafast photoelectron spectroscopy and accompanying theory[14] on oxazole (*c*-$C_3H_3NO$) suggested <100 fs ring

opening and several picosecond timescale ring puckering; however, this experiment could not detect photoproducts, and unambiguous assignment of experimental spectra to specific non-adiabatic processes was not achieved. In collaboration with Anja Röder and Sonia Coriani, we propose to study the excited state dynamics of oxazole using near-edge X-ray absorption spectroscopy that allows site-specific probing at the C, N and O K-edges following 200 nm photoexcitation, both using in-house transient absorption instrumentation as well as at SLAC/LCLS through a future user proposal. This study will build upon our recent thorough characterization of the core level spectra of ground-state oxazole.

## IV. BES-sponsored publications (2020-present)


1. Cole-Filipiak, N. C.; Troß, J.; Schrader, P. E.; McCaslin, L. M.; Ramasesha, K., Ultraviolet Photodissociation of Gas-Phase Iron Pentacarbonyl Probed with Ultrafast Infrared Spectroscopy, *Journal of Chemical Physics*, **2021**, *154* (13), 134308
2. Cole-Filipiak, N. C.; Troß, J.; Schrader, P. E.; McCaslin, L. M.; Ramasesha, K., Ultrafast Infrared Transient Absorption Spectroscopy of Gas-Phase $Ni(CO)_4$ Photodissociation at 261 nm, *Journal of Chemical Physics*, **2022**, *156* (14), 144306
3. Schnack-Petersen, A. K.; Tenorio, B. N. C; Coriani, S.; Decleva, P.; Troß, J.; Ramasesha, K.; Coreno, M.; Totani, R; Röder, A, Core Spectroscopy of Oxazole, *Journal of Chemical Physics*, **2022**, *157* (21), 214305
4. Troß, J.; Carter-Fenk, K.; Cole-Filipiak, N. C.; Schrader, P. E.; Word, M.; McCaslin, L. M.; Head-Gordon, M.; Ramasesha, K., Excited State Dynamics during Primary C-I homolysis in Acetyl Iodide Revealed by Ultrafast Core-Level Spectroscopy, *Journal of Physical Chemistry A*, **2023**, 10.1021/acs.jpca.3c01414


## V. References


(1) Kroger, P. M.; Riley, S. J. Dynamics of three-body half collisions. I. Secondary product decomposition in the photodissociation of acetyl iodide. *The Journal of Chemical Physics* **1977**, *67* (10), 4483-4490.
(2) Schnorr, K.; Bhattacherjee, A.; Oosterbaan, K. J.; Delcey, M. G.; Yang, Z.; Xue, T.; Attar, A. R.; Chatterley, A. S.; Head-Gordon, M.; Leone, S. R. Tracing the 267 nm-induced radical formation in dimethyl disulfide using time-resolved x-ray absorption spectroscopy. *The journal of physical chemistry letters* **2019**, *10* (6), 1382-1387.
(3) Nourbakhsh, S.; Liao, C. L.; Ng, C. A 193 nm laser photofragmentation time-of-flight mass spectrometric study of CH3SSCH3, SSCH3, and SCH3. *The Journal of chemical physics* **1990**, *92* (11), 6587-6593.
(4) Richter, M.; Marquetand, P.; González-Vázquez, J.; Sola, I.; González, L. SHARC: ab initio molecular dynamics with surface hopping in the adiabatic representation including arbitrary couplings. *Journal of chemical theory and computation* **2011**, *7* (5), 1253-1258.
(5) Mai, S.; Marquetand, P.; González, L. Nonadiabatic dynamics: The SHARC approach. *Wiley Interdisciplinary Reviews: Computational Molecular Science* **2018**, *8* (6), e1370.
(6) Zhong, D.; Diau, E. W.-G.; Bernhardt, T. M.; De Feyter, S.; Roberts, J. D.; Zewail, A. H. Femtosecond dynamics of valence-bond isomers of azines: transition states and conical intersections. *Chemical physics letters* **1998**, *298* (1-3), 129-140.
(7) Dyakov, Y.; Mebel, A.; Lin, S.; Lee, Y.; Ni, C.-K. Photodissociation of 1, 3, 5-triazine: An ab initio and RRKM study. *The Journal of Physical Chemistry A* **2007**, *111* (38), 9591-9599.
(8) Yang, J.; Zhu, X.; F. Nunes, J. P.; Yu, J. K.; Parrish, R. M.; Wolf, T. J.; Centurion, M.; Gühr, M.; Li, R.; Liu, Y. Simultaneous observation of nuclear and electronic dynamics by ultrafast electron diffraction. *Science* **2020**, *368* (6493), 885-889.
(9) Tully, J. C. Molecular dynamics with electronic transitions. *The Journal of Chemical Physics* **1990**, *93* (2), 1061-1071.
(10) Subotnik, J. E.; Shenvi, N. A new approach to decoherence and momentum rescaling in the surface hopping algorithm. *The Journal of Chemical Physics* **2011**, *134* (2), 024105. DOI: 10.1063/1.3506779 (acccessed 4/26/2023).
(11) Subotnik, J. E. Fewest-Switches Surface Hopping and Decoherence in Multiple Dimensions. *The Journal of Physical Chemistry A* **2011**, *115* (44), 12083-12096. DOI: 10.1021/jp206557h.
(12) Falk, M. J.; Landry, B. R.; Subotnik, J. E. Can Surface Hopping sans Decoherence Recover Marcus Theory? Understanding the Role of Friction in a Surface Hopping View of Electron Transfer. *The Journal of Physical Chemistry B* **2014**, *118* (28), 8108-8117. DOI: 10.1021/jp5011346.
(13) Mai, S.; Marquetand, P.; González, L. Non-adiabatic and intersystem crossing dynamics in SO2. II. The role of triplet states in the bound state dynamics studied by surface-hopping simulations. *The Journal of Chemical Physics* **2014**, *140* (20), 204302. DOI: 10.1063/1.4875036 (acccessed 4/26/2023).
(14) Geng, T.; Ehrmaier, J.; Schalk, O.; Richings, G. W.; Hansson, T.; Worth, G.; Thomas, R. D. Time-Resolved Photoelectron Spectroscopy Studies of Isoxazole and Oxazole. *The Journal of Physical Chemistry A* **2020**, *124* (20), 3984-3992.

# ULTRAFAST PHYSICS: NONLINEAR OPTICAL SPECTROSCOPY AND DIAGNOSTICS

Christopher J. Kliewer, Laura McCaslin, David L. Osborn, Krupa Ramasesha, David W. Chandler
Sandia National Laboratories, MS 9051, Livermore, CA 94551-0969
cjkliew@sandia.gov, chand@sandia.gov, kramase@sandia.gov, jhfrank@sandia.gov

## Program Scope

The interaction of intense pulsed laser fields with atoms, molecules, and surfaces induces a coherent response in the material. At especially high intensities, the material response becomes nonlinear and gives rise to a wealth of approaches to both *control* and to *probe* molecular processes in gas-phase and interfacial chemical physics, even processes very far from chemical equilibrium. In this program, our goal is to develop ultrafast optical methods to both measure and control matter at the molecular level and on molecular timescales. On the measurement side, ultrafast nonlinear approaches are advanced for the detection of transient reactive molecular species. In addition, broadband approaches enable the sampling of many spectroscopic transitions at once, allowing for the assessment of instantaneous molecular energy partitioning and energy transfer. A critical aspect of our research includes the study of fundamental spectroscopy, energy transfer, molecular dynamics, and photochemical processes. This aspect of the research is essential to the development of accurate models and quantitative application of techniques to complex environments. We are uniquely positioned to study molecular systems driven far from equilibrium, as well as relaxation rates and pathways. Time-resolved collisional dephasing measurements provide insight into the local chemical environment as well as inform spectroscopic models for quantitative interpretation.

## Recent Progress

***Development of the molecular optical centrifuge and novel probing methods.*** The selective control of population in the various degrees of freedom in molecules has opened the possibility for unprecedented understanding of reactive potential energy surfaces in gas phase chemical physics. While significant work has been dedicated to understanding, and controlling, the vibrational and translational degrees of molecular freedom, far less attention has been paid to the direct control of molecular rotational energy. In part, this is due to the quantum mechanical selection rules that govern rotational excitation. Only small changes in angular momentum are allowed during an optical absorption or Raman process. In recent years, however, pioneering work has established a method for spinning molecules into very high angular momentum states. Like adiabatic passage methods for vibrational ladder climbing, passage up the rotational ladder has now been demonstrated on several molecules. The first experimental demonstration of the optical centrifuge technique, by Corkum and coworkers,[1] was performed on $Cl_2$. Rotationally induced dissociation was observed through mass spectrometry for $Cl_2$ molecules driven to nuclear angular momentum states up to J ~ 420. Due to the ability to induce such high rotational excitation, optical centrifuges have been used to investigate these so-called "super-rotors" and their collisional dynamics and energy transfer.[2-5]

We have recently constructed an ultrafast optical centrifuge at Sandia with the aim to study complex nonequilibrium collisional and intramolecular energy transfer, as well as to provide a new testbed for studying the interaction of high angular momentum states with chemical transformations during photodissociation and bimolecular collision experiments. The instrument heavily builds upon the expertise acquired in this lab over the past several review periods in ultrafast Raman spectroscopy. As discussed later, to effectively laser trap molecules for acceleration at the probe volume, significant pulse energy is required (~10-30 mJ / pulse in the femtosecond beam). This requirement was beyond the output of our commercial high-power femtosecond amplifiers. Thus, we designed and constructed a home-built 10 Hz repetition rate, 7-pass bow-tie amplifier for the femtosecond pulses, which could produce at least 20 mJ per pulse. Similar to previous implementations of the optical centrifuge, this pulse entered a pair of home-built pulse shapers that created two chirped arms of light fanning outward from 800 nm in time. One arm is chirped to the blue,

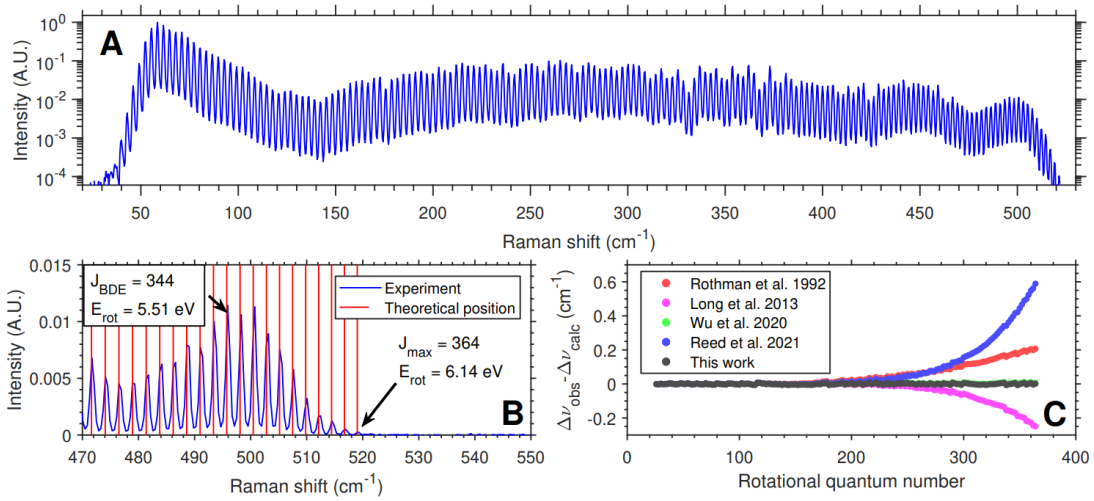


**Figure 1.** Optically centrifuged $CO_2$ beyond the C-O bond dissociation energy. (A) Coherent Raman spectrum of centrifuged $CO_2$ showing the simultaneous detection of J=24 to J=364. (B) Zoom in of the high J cut-off. Rotational energies as high as 6.14 eV, well beyond the ground state C-O bond energy. (C) New centrifugal distortion constants for $CO_2$ have been determined from this work, resolving disagreements within the literature.

while the other arm is chirped to the red. The two arms are converted to left- and right- circularly polarized light and superimposed on the sample, creating a linear polarization which rotates and accelerates with time. The difference in frequency between the two arms drives successively higher rotational Raman transitions in the target molecule. The acceleration of the trap must be tailored to the molecule of interest, and we have been able to accelerate $N_2$, $O_2$, CO and $CO_2$ thus far. Because the rotational centrifuge prepares molecules coherently, a rotational wavepacket is launched that can be probed through nonlinear mixing. We take advantage here of our capabilities in fs/ps CARS to scatter a time-resolved ps or ns probe pulse from this coherence and read out the full distribution of populated rotational levels simultaneously.

Figure 1 displays results from the angular acceleration of $CO_2$ to extreme rotational states. In its ground state, $CO_2$ has a C-O bond dissociation energy of 5.51 eV. Demonstrated here, we have driven an ensemble of $CO_2$ to rotational energies of 6.14 eV. While the molecules are left with more than enough energy to dissociate, there is an angular barrier to dissociation which prevents the molecules from being spun apart in this case, which is just over 7 eV. However, the molecules have been driven to very high levels of centrifugal distortion. Given that our approach simultaneously detects all populated levels, this yielded an opportunity to revisit the literature accepted values for the nonlinear centrifugal distortion constants for $CO_2$. As can be seen in Figure 1C, several high-resolution studies have been reported in recent years with conflicting molecular parameters. The reason for the disagreement was not caused by a lack of frequency resolution, but rather by the difficulty of fitting the nonlinear function to $J < 100$. We report new centrifugal constants, resolving the discrepancy in the literature. At the highest J, we do not see evidence of dissociation, however, if dissociation proceeded after full dephasing of the coherence we would not be sensitive to this channel.

***Direct observations of coherence transfer and rotation-to-vibration energy transfer.*** In Figure 2B, the coherent scattering spectrum of centrifuged $CO_2$ is shown for 200 ps and 500 ps probe delays. As the optical centrifuge pulse had ended by 150 ps, this corresponds to evolution of the molecular ensemble in a field-free environment. At 500 ps, new odd-degeneracy peaks are seen to form as shoulders off the pure rotational transitions. These are caused by population in the bending mode of $CO_2$. To verify that this was indeed a collisional energy transfer process populating the vibrational quanta, pressure dependent studies are shown

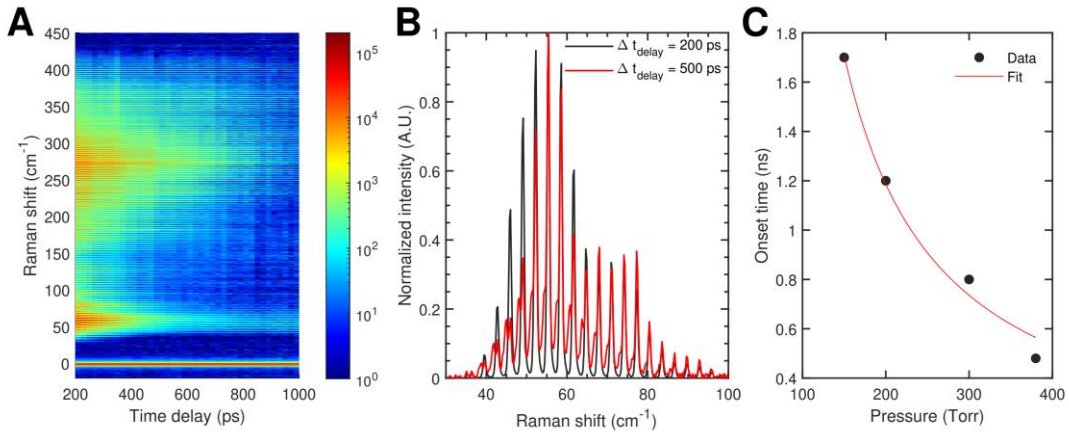


**Figure 2.** (A) Probe delay scan of centrifuged $CO_2$ coherence at 380 Torr. (B) Appearance of vibrationally excited $CO_2$ hot bands at a 500 ps probe delay for centrifuged $CO_2$ at 380 Torr. (C) Onset times for the hot band appearance as a function of pressure and fit by a 1/P function.

in Figure 2C. The onset time for population growth in vibrational bending mode follows a 1/P pressure dependence, verifying it to be caused by collisional energy transfer. The transfer of coherence from vibrational ground state rotors to rotors with bending vibration is a remarkable observation, as it implies that these molecules undergo an energy exchanging collision, picking up vibrational angular momentum via the bend excitation, yet the rotational state remains phase-locked with the originally prepared ensemble of coherent molecules. This is the first such observation of rotational coherence transfer. But beyond this, these measurements track the flow of rotational energy to vibrational energy across the entire manifold of rotors. Collaborator Ahren Jasper at Argonne National Laboratories carried out semiclassical trajectory calculations for a $CO_2$ ensemble for which the initial distribution state was matched to our experimental data. Qualitative trends were observed to be in agreement with our measurements. We find that there is an optimal J-range for rotation-vibration energy exchange, which agreed with the SCT calculations, with as high as 25% probability of undergoing such transformation during a collision. By cutting bandwidth within the centrifuge pulse, we were able to adjust the total level of rotational excitation and track the reduction in vibrational population with time. This showed us that as much as 30 quanta of angular momentum are lost per collision with the super-rotors.

## Future Work

***Optical centrifuge of $N_2O$ for photodissociation dynamics studies*** In the coming year, planned work at Sandia involves the study of the photodissociation of $N_2O$ super-rotors. This work is described in the "Chemical Dynamics" abstract of the Sandia Gas-Phase Chemical Physics program. To enable these studies, we need to tailor our optical centrifuge for efficient centrifuging of the $N_2O$ molecule. In order to efficiently trap target molecules, the optical centrifuge must be tailored to the molecular system such that $8\pi\delta/E^2 < \Delta\alpha/I$, where $\delta$ is the rate of optical acceleration, $E^2$ is the laser intensity, $\Delta\alpha$ is the molecular polarizability anisotropy, and I is the molecular moment of inertia. Thus, for each new molecule studied, the pulse shaper must be once again optimized. An important aspect of the design is the effective turn-on time for the optical centrifuge pulse. Prior to interaction with the laser pulse, the gas-phase ensemble of molecules will be isotropically oriented about the laboratory coordinate. As the optical centrifuge turns on, it will begin exerting an aligning force on these molecules. If the turn-on time is too fast, the molecule will not have time to respond and become adiabatically trapped within the potential well created by the laser. In angular coordinates, the laser must cover $\pi$ radians during the turn-on period to effectively trap all orientations. If the turn-on is too slow, the angular frequency will be too fast by the time the pulse is at full intensity and will not be able to retain the molecules, i.e. the kinetic energy of the molecules gained during

centrifuge turn-on must be always less than the current potential well depth induced by the laser pulse. Spanner and Ivanov [6] have proposed a method to derive these upper and lower limits, and have found that $(2\pi/\delta)^{\wedge}.5 < t_{on} < (U_0/[I\delta^2])$ allows for molecules to be effectively coupled into the centrifuge. Here, again, $\delta$ is the angular acceleration rate of the trap, $t_{on}$ is the pulse turn-on time, $U_0$ is the potential well depth felt by the molecule from the laser, and I is the molecular moment of inertia. This year we will demonstrate efficient driving of $N_2O$ to J > 150.

***Study of coherence and rotation-to-vibration transfer of $N_2O$*** Our recent work has demonstrated the unique finding that molecules can undergo rotation-to-vibration collisional energy transfer without disrupting the phase of the rotations of the molecule that gains vibrational energy. This is the mechanism by which the hot-bands appear Figure 2B. This behavior was unexpected, as traditionally collisional energy transfer has been assumed to disrupt the phase or an ensemble of prepared rotors, and therefore those molecules are removed from the coherence and contribute to collisional coherence dephasing. However, this finding opens the possibility for detailed studies of energy relaxation across the entire populated manifold in other nonequilibrium systems using the same approach. We will study the centrifugation and relaxation pathways first for $N_2O$. It has been previously found during measurements of centrifuged $N_2O$ that one quanta of bending vibration is likely excited during relaxation of the high angular momentum excitation. But this measurement was made over a limited range of populated rotational levels, and the multiplex approach demonstrated in our lab will provide more complete relaxation information. This information will first serve to validate whether coherence transfer during rotation-to-vibration energy exchange is a ubiquitous finding or unique to the particular case of $CO_2$. Laura McCaslin will further perform quantum chemical calculations to study how rotational phase disruption follows from rotation-to-vibration energy transfer for comparison to our results for both $CO_2$ and $N_2O$. These results will be compared to semi-classical trajectory calculations from collaborator Ahren Jasper (Argonne National Laboratories). Further, the understanding of energy transfer pathways and timescales for $N_2O$ will be critical foundational understanding leading into the superrotor photodissociation and bimolecular collision experiments proposed in the Chemical Dynamics subtask. $N_2O$ has been previously shown to undergo some level of rotation-to-vibration energy exchange, but only limited portions of the manifold could be studied. Implementing our VIPA-CARS detected optical centrifuge approach, the full picture of nonequilibrium energy transfer will be followed. Following experiments with $N_2O$, we plan similar studies on more molecules, such as OCS, $H_2S$, and $SO_2$.

***Direct detection and quantification of the reactive singlet delta $O_2$ using hybrid time and frequency domain methods.*** There is strong evidence that $O_2$ molecules it the first electronically excited state, $O_2$ ($a^1\Delta_g$), dramatically enhance hydrocarbon oxidation reaction rates [7] in the gas phase. Because the excitation energy from the ground state is only 0.98 eV nearly all oxygen containing plasmas generate significant concentrations of $O_2$ ($a^1\Delta_g$) and the enhanced reaction rates may be useful in many potential gas-phase and interfacial processes such as plasma assisted catalysis and combustion. The radiative lifetime of the excited state is long, 1000's of seconds, because relaxation to the ground state is spin forbidden. However, the quantitative detection of $O_2$ ($a^1\Delta_g$) is a difficult task because of small cross-sections for absorption. Off-axis integrated cavity enhanced absorption[8] has been demonstrated on the (1,0) band of the weak $b^1\Sigma_g^+$-$a^1\Delta_g$ system for

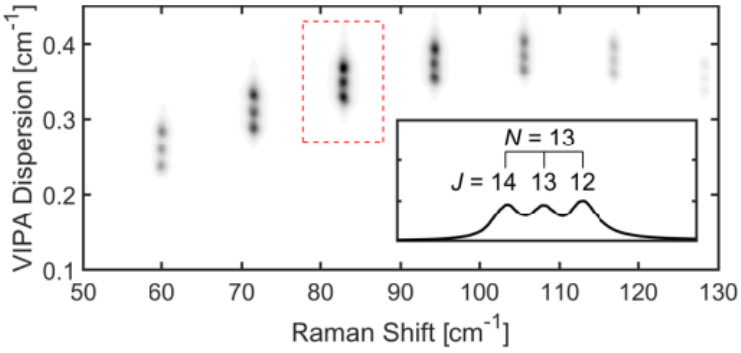


Figure 3. VIPA-CARS spectrum of the triplet ground state rotational transitions of molecular $O_2$ resolving the hyper-fine splitting of the lines.

quantitative detection, yet this multi-pass approach necessarily yields both poor spatial and time resolution, because of the significant averaging required. Such an approach precludes the capability to follow time-dependent concentrations in kinetics experiments or spatially evolving concentrations. For molecular beam studies, single photon dissociation of $O_2$ followed by REMPI and VMI of the O atoms can resolve $O_2$ ($a^1\Delta_g$), however, this is limited to low-pressure investigations where REMPI probes can be inserted.

We will explore a new method using ultrafast Raman spectroscopy for the quantitative, spatially resolved detection of $O_2$ ($a^1\Delta_g$) that should generate enough signal level such that single-laser-shot implementation will be possible. The pure-rotational coherent Raman spectrum of ground state (triplet) $O_2$ consists of a series of rotational lines with hyperfine splitting caused by coupling between electronic spin and nuclear angular momentum with splitting as low as 480 MHz. We have resolved these lines in using our recently developed VIPA-CARS spectrometer, as shown in Fig. 3. The rotational constant for excited $O_2$ ($a^1\Delta_g$) shifts the pure-rotational transitions a significant fraction of a wavenumber to the red, yielding easily directly resolved spectral lines with the new capability.

In order to generate the $O_2$ ($a^1\Delta_g$) for validation experiments, we will use a well-established method of UV photolysis of ozone with a 266-nm laser, which yields 90% in the product channel $O_2$ ($a^1\Delta_g$) + $O(^1D)$[9]. We will build a photolysis cell with cross-beam access to perform the fs/ns pure-rotational CARS experiment. We will determine the ultimate single-laser-shot detection sensitivity for $O_2$ ($a^1\Delta_g$), which we expect to be around 500 ppm based on scaling from our current fs/ps experiments on ground state $O_2$.

***Coherence Lifetime Imaging through Structured Illumination***

Coherence dephasing times are often governed by intermolecular interactions. In gas-phase systems, collisional energy transfer is the dominant source of rotational and vibrational coherence dephasing. Thus measuring the coherence decay rate allows for the in-situ mapping of collisional energy transfer rates, which are highly dependent on collision partner, number density, and collision energy. In condensed phase samples, the coherence lifetime gives an indication of the coupling of individual vibrational states to the surrounding environment. In microscopy applications, coherence lifetime would provide a novel imaging contrast mechanism sensitive subtle changes in local chemical environment. In previous work, we demonstrated the ability to measure coherence lifetimes within a single laser shot in the gas phase by separating the probe pulse into four separate weak probe pulses, each with a different phase matching angle. We propose here to develop a 2D coherence lifetime imaging approach which can have impact in both gas-phase chemistry applications as well as in condensed phase fields. Similarly to fluorescence lifetime imaging, the coherence lifetime image will provide information on the chemical coupling and energy transfer to the local environment.

In order to realize single-shot coherence lifetime imaging, we will combine our recently developed 2D-CARS approach, with the structured illumination approach developed by our colleagues at Lund University. More specifically, the probed molecules will be excited with a pump/Stokes femtosecond laser sheet. The probe beam, however, will be separated via beam-splitters into four separate beams. Each of these beams will propagate through a time-of-flight optical delay stage and then be passed through a transmission grating. These gratings will be designed to optimize the +/- 1 orders. The position of the grating will be relay imaged to the experiment. In this way, each of the four probe beams gets imprinted with a fringe pattern at a controllable angle. The CARS beams will then be recombined into a single beam and scattered from the sample. The resulting image will contain four separate probe delays, with independent spatial frequencies, which can be extracted through spatial Fourier transform. In gas phase chemistry applications such as combustion, or coupled gas-surface chemistry, such an approach would enable simultaneous speciation, measurement of energy distributions, as well as provide an assessment of the degree of coupling to other molecules or the surface.

**Journal publications supported solely by this BES project (2020-2022)**

1. T.Y. Chen, B.M. Goldberg, B.D. Patterson, E. Kolemen, Y. Ju, and C.J. Kliewer*, "1-D imaging of rotation-vibration non-equilibrium from pure rotational ultrafast coherent anti-Stokes Raman scattering" Opt. Lett. **45**, 15, 4252-4255 (2020)
2. T.Y. Chen, C.J. Kliewer*, B.M. Goldberg, E Kolemen, and Y Ju, "Time-domain modelling and thermometry of the $CH_4$ Q-branch using hybrid femtosecond/picosecond coherent anti-Stokes Raman scattering" Combustion and Flame **224**, 183-195 (2021)
3. M. Linne, N.T. Mecker, C.J. Kliewer, D. Escofet-Martin, B. Peterson, "Revisiting $N_2$-$N_2$ collisional linewidth models for S-branch rotational Raman scattering" Combustion and Flame https://doi.org/10.1016/j.combustflame.2021.111928, (2021)
4. S.A. Steinmetz, C.J. Kliewer*, "Gas detection sensitivity of hybrid fs/ps and fs/ns CARS" Opt. Lett. **47**, 1470-1473 (2022)
5. T.Y. Chen, N. Liu, C.J. Kliewer, A. Dogariu, E. Kolemen, Y Ju, "Simultaneous single-shot rotation-vibration non-equilibrium thermomemtry using pure rotational fs/ps CARS coherence beating" Opt. Lett. **47**, 1351-1354 (2022) *Highlighted as an "Editor's Pick" article
6. T.Y. Chen, C.J. Kliewer*, "Numerical study of pure rotational fs/ps CARS coherence beating at high pressure and for multi-species rotation-vibration non-equilibrium thermometry" J. Chem. Phys. 157, 16, 164201 (2022)
7. S.A. Steinmetz, T.Y. Chen, B.M. Goldberg, C.M. Limbach, C.J. Kliewer*, "Resolved rotation–vibration non-equilibrium with rotational VIPA-CARS" Opt. Lett, 47, 20, 5429-5432 (2022)

***corresponding author**

**References**


1. Villeneuve, D. M.; Aseyev, S. A.; Dietrich, P.; Spanner, M.; Ivanov, M. Y.; Corkum, P. B., Forced molecular rotation in an optical centrifuge. *Phys. Rev. Lett.* **2000,** *85* (3), 542-545.
2. Yuan, L. W.; Teitelbaum, S. W.; Robinson, A.; Mullin, A. S., Dynamics of molecules in extreme rotational states. *Proc. Natl. Acad. Sci. U. S. A.* **2011,** *108* (17), 6872-6877.
3. Korobenko, A.; Milner, A. A.; Milner, V., Direct Observation, Study, and Control of Molecular Superrotors. *Phys. Rev. Lett.* **2014,** *112* (11), 5.
4. Milner, A. A.; Korobenko, A.; Hepburn, J. W.; Milner, V., Effects of Ultrafast Molecular Rotation on Collisional Decoherence. *Phys. Rev. Lett.* **2014,** *113* (4), 5.
5. Steinitz, U.; Khodorkovsky, Y.; Hartmann, J. M.; Averbukh, I. S., Dynamics and Hydrodynamics of Molecular Superrotors. *ChemPhysChem* **2016,** *17* (22), 3795-3810.
6. Spanner, M.; Ivanov, M. Y., Angular trapping and rotational dissociation of a diatomic molecule in an optical centrifuge. *J. Chem. Phys.* **2001,** *114* (8), 3456-3464.
7. Ombrello, T.; Won, S. H.; Ju, Y. G.; Williams, S., Flame propagation enhancement by plasma excitation of oxygen. Part II: Effects of O-2(a(1)Delta(g)). *Combust. Flame* **2010,** *157* (10), 1916-1928.
8. Williams, S.; Gupta, M.; Owano, T.; Baer, D. S.; O'Keefe, A.; Yarkony, D. R.; Matsika, S., Quantitative detection of singlet O-2 by cavity-enhanced absorption. *Optics Letters* **2004,** *29* (10), 1066-1068.
9. Torbin, A. P.; Pershin, A. A.; Mebel, A. M.; Zagidullin, M. V.; Heaven, M. C.; Azyazov, V. N., Collisional relaxation of O-2(a(1) Delta, upsilon=1, 2, 3) by CO2. *Chem. Phys. Lett.* **2018,** *691*, 456-461.

# Quantum Chemistry of Radicals and Reactive Intermediates

John F. Stanton
Quantum Theory Project
Departments of Chemistry and Physics
University of Florida
Gainesville, FL 32611
johnstanton@ufl.edu

**Scope of Research**

My research group works in the area of theoretical chemical physics, especially on the thermodynamics, spectroscopy and chemistry of organic radicals and other reactive intermediates. This research follows a number of paths, including first-principles calculation of bond energies and other thermochemical information (as well as development of methodology needed for such calculations), methods for the simulation and analysis of molecular spectra (especially those relevant to experiments that can be used to glean thermochemical information), the development of *ab initio* quantum chemical methods needed for the accurate treatment of fundamental aspects of electronic structure and potential energy surfaces, and computational kinetics including semiclassical transition state theory and master equation modeling of chemical reactions.

**Summary of Selected Recent Accomplishments and Future Plans**

• A debate centering around the assignment of low-lying vibrational levels of the nitrate radical continues. This uncertainty, which has its roots in how one assigns the fundamental degenerate stretching mode ($\nu_3$). Originally reported by Hirota and coworkers[1] and assigned to a strong infrared feature at 1492 cm$^{-1}$, the location of this fundamental mode has been a topic of spirited debate for the last fifteen years. Although one might regard the issue as settled – both theory[2] and experiment[3] agree that this fundamental is near 1050 cm$^{-1}$ – differing points of view can still be found in the literature. While simulations of the infrared, negative ion photoelectron, and ($\tilde{B} \rightarrow \tilde{X}$) dispersed fluorescence spectra based on Hamiltonians ranging from illustrative[4] to state-of-the-art[5] have supported the reassignment

[1]K. Kawaguchi, E. Hirota, T. Ishiwata and I. Tanaka *J. Chem. Phys.* 93, 951 (1990); T. Ishiwata, I. Tanaka, K. Kawaguchi and E. Hirota *J. Chem. Phys.* 82, 2196 (1985).

[2]C.S. Simmons, T. Ichino and J.F. Stanton *J. Phys. Chem. Lett.* 3, 1946 (2012)

[3]M.C. Babin, J.A. DeVine, M. DeWitt, J.F. Stanton and D.M. Neumark *J. Phys. Chem. Lett.* 11, 395 (2020).

[4]B. Kim, P.L. Hunter and H.S. Johnston *J. Chem. Phys.* 96, 4057 (1992).

[5]M. Fukushima *J. Mol. Spect.* 387, 111646 (2022).

of $\nu_3$, a high-level simulation of the dispersed fluorescence spectrum had not been carried out. Motivated by recent, and quite impressive, high resolution experiments by Fukushima (which were argued to support the original assignment of $\nu_3$ to 1492 cm$^{-1}$ in the published work), a three-state vibronic Hamiltonian based on the equation-of-motion coupled cluster method known as EOMIP-CCSDT was used to simulate the spectrum. The results, which are reproduced here, show excellent agreement with the impressively resolved [6] experimental spectrum, and further support the reassignment of $\nu_3$ to a level more than 400 cm$^{-1}$ below the position of its original assignment. This issue can now be clearly regarded as settled, and it is hoped that this will lead to a greater understanding of the vibrational levels of this molecule up to 3000 cm$^{-1}$. It is believed that this should be regarded as a goal of spectroscopy, as $NO_3$ has become something of a benchmark molecule for studied of vibronic coupling effects.

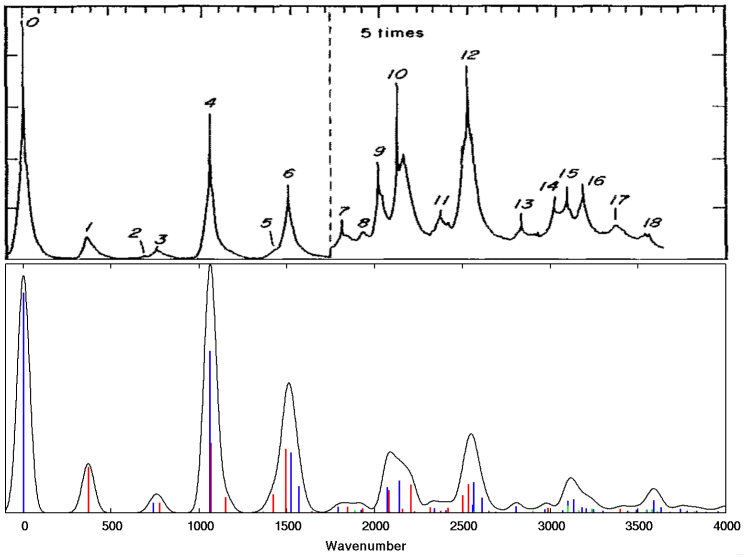


Observed simulated dispersed X-B fluorescence spectrum of the $NO_3$ radical (top trace) and the simulated spectrum (lower trace). The region of controversy are those near 1500 and 1050 cm$^{-1}$, the former corresponding to the traditional assignment of the $\nu_3$ fundamental, and the latter to the newer assignment that has been supported by a number of recent theoretical and computational studies. The two bands seen near 1050 cm$^{-1}$ in the simulation correspond to the $\nu_1$ fundamental (blue) and the controversial $\nu_3$ (red). The experimental spectrum shown here is that of Kim *et al* (see footnote 4).

• As a part of our ongoing collaboration with Ruscic (Argonne) on the Active Thermochemical Tables (ATcT) project, we have been investigating the intriguing carbonic acid molecule ($H_2CO_3$) that has largely avoided being seen in isolated form in the gas phase. In the process of working out the thermochemistry of this molecule, species that lay nearby on a thermochemical network become relevant. Amongst these is the $HOCO_2$ radical, which is related to the notorious formyloxy ($HCO_2$) and substituted formyloxy radicals. These species have well-known and profound vibronicv coupling effects, with $HCO_2$ having been the target of several theoretical studies in the past fifty years. The electron affinity of $HOCO_2$ was measured some time ago, but the identification of the origin in the negative ion photodetachment spectrum might be regarded as problematic. In the course of studying both the neutral radical and this spectrum, we discovered that the very well-known "symmetry-breaking"[7] of the ($C_{2v}$ symmetric) $RCO_2$ radicals manifests here as an insidious problem involving the exaggerated localization of spin density on one of the two putative radical centers in this

[6] In the spectrum of Fukushima, the two peaks near 1050 cm$^{-1}$ are clearly resolved, with an intensity ration very similar to that seen in the simulation. The spectrum shown at the top of the simulation is that from Kim *et al.*, as a full set of data over this range was not given in the more recent paper.

[7] The term here refers to the orbitals in the self-consistent field wavefunction.

molecule. It turns out that this causes significant problems involving consistency of the reference function choice in various aspects of the high-level thermochemical calculations. A full investigation of this "symmetry breaking in the absence of symmetry" effect was carried out with an excellent undergraduate student, and published. This permitted us to continue with the analysis of the thermochemical network involving carbonic acid and various important and intriguing radicals and ions of the type $H_iCO_j$.

• With collaborators on two different continents, we have participated in a combined theoretical and experimental investigation of the classic cyclopropyl radical ($C_3H_4$) and its cation. The latter is particularly interesting and its electronic behavior is in rather stark contrast to that of the neutral species. Specifically, both disrotatory and conrotatory ring opening of the former are forbidden by Woodward-Hoffman rules, while disrotatory ring opening path of the cation is allowed:

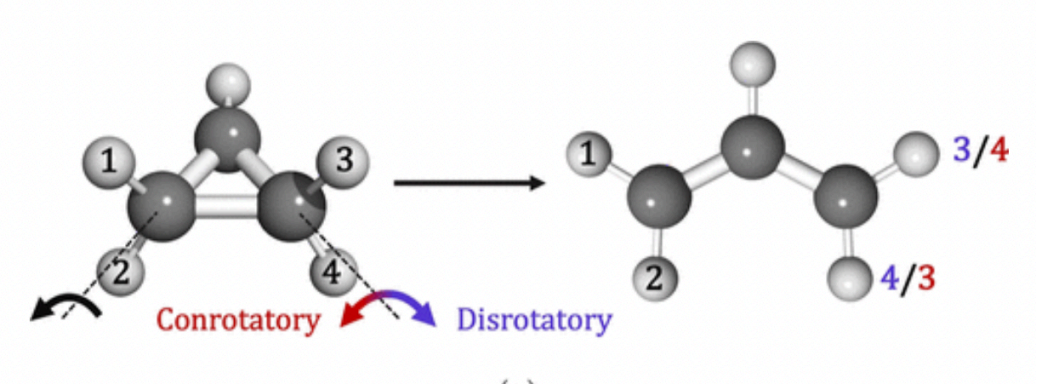


Consequently, vertical ionization of the neutral terminates near a transition state on the upper surface, a situation that leads to challenges in spectral analysis. Using a recently developed time-dependent approach well-suited to such cases, we were able to faithfully recreate all important features of the laboratory spectrum. In addition, this led to some insight regarding the transition state region (as viewed from a phase space perspective) and added important information to the Active Thermochemical Tables.

• In ongoing work, my excellent and energetic postdoctoral associate Peter Franke (a graduate of U. Georgia where he worked with Gary Douberly of our program) has extended the extrapolated model chemistry ideas that underlie most modern computational thermochemistry protocols to the realm of both equilibrium molecular structures and ro-vibrational spectroscopy. Viewed appropriately as a way of generalizing strategies used in such thermochemical methods to the calculation of structural and spectroscopic parameters has led to a suite of approaches that represent efficient and useful schemes at the bottom end, and a (very expensive and very accurate) approach at the top end. Benchmarking of these ideas is well-underway, and much of this work should be reported before the end of this calendar year. In addition to this, Dr. Franke has been working on application of fourth-order vibrational perturbation theory to problems other than the calculation of vibrational energy levels. These include higher-order corrections to centrifugal distortion constants (largely complete, with two publications near the submission stage) and rotation-vibrational interaction constants that are quadratic in $(n + \frac{1}{2})$. While I have long wanted to move my research program in rovibrational theory to such problems, it is hard to find those capable of carrying out this difficult work.

**Students and Postdoctoral Supported:**
J.T. Thorpe (student)
M.B. Bentley (student)
P.R. Franke (postdoc)

# References from 3/2022-3/2023 citing BES-GPCP grant


J.F. Stanton Simulation of the Dispersed Fluorescence Spectrum of the NO3 B-X Origin Band J. Mol. Spect. 389, 111690 (2022).

N. Genossar, P.B. Changala, B. Gans, J.-C. Loison, S. Hartweg, M.-A. Martin-Drumel, G.A. Garcia, J.F. Stanton, B. Ruscic and J.H. Baraban Ring Opening Dynamics of the Cyclopropyl Radical and Cation: The Transition State Nature of the Cyclopropyl Cation J. Amer. Chem. Soc. 144, 18418 (2022).

R. Rana, J.H. Thorpe and J.F. Stanton An Interesting Case of Symmetry Breaking in the Absence of Symmetry: The Bicarbonate Radical (HOCO2) Mol. Phys. e2144518, 2022.

D. Feller, J.F. Stanton and E.R. Davidson Atomic Isotropic Hyperfine Properties for Second Row Elements (Al  Cl) J. Chem. Phys. 157, 126101 (2022).

H.A. Bunn, B.J. Esselman, S. Kougias, P.R. Franke, R.C. Woods, R.J. McMahon and S. Widicus Weaver Millimeter/Submillimeter Wave Spectroscopy and Semi-Experimental Structure of 1H-1,2,4-Triazole(C2N3H3) J. Phys. Chem A 126, 8196 (2022).

L.T. Nguyen and J.F. Stanton The Reaction of HO2 and CH3O2: CH3OOH Formed from The Singlet Electronic State Surface Atmosphere 19, 1397 (2022).

D.A. Arbagio, Q.Y. Cheng, R.C. Fortenberry, J.F. Stanton and N.J. DeYonker Theoretical Rovibrational Spectroscopy of Magnesium Tricarbide-Multireference Character Thwarts a Full Analysis of All Isomers J. Phys. Chem. A 126, 4132 (2022).

L.T. Nguyen, D.H. Bross, B. Ruscic, G.B. Ellison and J.F. Stanton Mechanism, Thermochemistry, and Kinetics of the Reversible Reactions C2H3 + H2  C2H4 + H  C2H5 Faraday Discussions 238, 405 (2022).

# Universal and State-Resolved Imaging Studies of Chemical Dynamics

Arthur G. Suits
*Department of Chemistry, University of Missouri, Columbia MO 65211*
*suitsa@missouri.edu*

## 1. Program Scope

The focus of this program is on combining universal ion imaging probes providing global insight with high-resolution state-resolved probes providing quantum mechanical detail, to develop a molecular-level understanding of chemical phenomena. Particular emphasis is placed upon elementary reactions involving transient species and in revealing new aspects of reaction mechanisms and the dynamical behavior of molecules. Much of the current effort here is in generalizing the lessons from simple systems as we investigate the behavior of larger polyatomic molecules and radical-molecule reactions. This research is conducted using state-of-the-art molecular beam machines, photodissociation, reactive scattering, and vacuum ultraviolet lasers in conjunction with velocity map ion imaging and other techniques we develop. One focus of our effort remains crossed-beam reactive scattering of polyatomic molecules. In addition, new directions in ultrafast time-resolved studies of photochemical processes are also underway.

## 2. Recent Progress

### *2.1 Crossed Beam Scattering*

We continue our ongoing studies of bimolecular reaction dynamics using crossed-beam velocity map imaging with single-photon 157 nm detection. We devoted some effort to hot H atom reactions with alkanes, but the background interference from photochemistry precluded obtaining any imaging results. However, we have uncovered some fascinating chemistry involving ground state sulfur atoms that we have been studying in collaboration with J. Zádor at Sandia. We report these results in some detail in the following.

### *S($^3$P) reactions with conjugated hydrocarbons.*

Sulfur, chiefly as $SO_2$, is a common pollutant both as a by-product of fossil fuel combustion and from volcanic emissions. It has been proposed as part of a geoengineering approach – stratospheric aerosol injection – to increase the Earth's albedo and mitigate global warming. UV photodissociation of $SO_2$ has recently been found to give $S(^3P)+O_2$ directly, with significant implications for the early atmosphere of Earth. Very recently, $SO_2$ has been detected in the atmosphere of the exoplanet WASP-39b, while organic sulfur species, particularly thiophenes, have also recently been detected on Mars, stimulating speculation about possible association with biological processes there. Detailed dynamics studies of sulfur atom reactions are thus a matter of keen current interest.

The reaction dynamics of atomic sulfur have indeed been examined both by theory and experiment in recent years, but the focus has exclusively been on the metastable singlet state and in particular its reaction with molecular hydrogen and its isotopologues. To our knowledge there have been no fundamental studies of the reaction dynamics of ground state sulfur atoms using modern methods. However, kinetics and product branching for $S(^3P)$ reactions were examined in an extensive series of papers by Gunning and Strausz at the University of Alberta beginning in 1962. In one study,

Gunning and coworkers examined S($^3$P) reaction with C4 olefins including 1,3-butadiene (13BD) with detection by GC-MS. The 13BD reaction, conducted at room temperature and 200-600 Torr total pressure, gave rise mainly to vinyl thiacyclopropane (VTCP), thiophene and $H_2$. Much of the thiophene was attributed to subsequent photodissociation of the VTCP product, but a yield of 9% was ascribed to a primary reaction giving thiophene + $H_2$.

Here we show crossed molecular beam imaging of S($^3$P) reactions, focusing on the conjugated dienes 13BD, isoprene (2-methyl-1,3-butadiene) and others. The results have been interpreted with the aid of ab initio calculations of the initially accessed triplet PES and the singlet PES that leads to products, and by RRKM calculations of the branching, from J. Zádor. The results are in striking contrast to the behavior of the analogous O($^3$P) + 13BD system, and the differences allow for an investigation and discussion of their origin.

Fig. 1a shows the reactive scattering image of the H-loss product at m/z=85 resulting from S($^3$P) addition to 13BD with the Newton diagram superimposed. Ground state sulfur atoms are produced by 193 nm photodissociation of $CS_2$ in the presence of $H_2$ or $CO_2$ to quench any S($^1$D). This product mass appears just at the center of mass velocity, confirming its origin in reaction of sulfur atoms with 13BD. The small size of the scattering image is consistent with H loss, leaving the detected heavy fragment with low recoil velocity. The total translational energy distribution, shown in Fig. 1b, peaks at zero and extends to ~10 kcal/mol, consistent with a statistical, barrierless decay of an energized complex. No other masses are detected using the 157 nm probe. Theory suggests, however, that the dominant product is thiophene, with thioketene also a favored pathway. These are all found to occur on the singlet state following intersystem crossing. The detected H loss is found to be a minor channel but one that also results following cyclization on the singlet surface. The radical H-loss product identified in theory is 2-H-thiophen-5-yl.

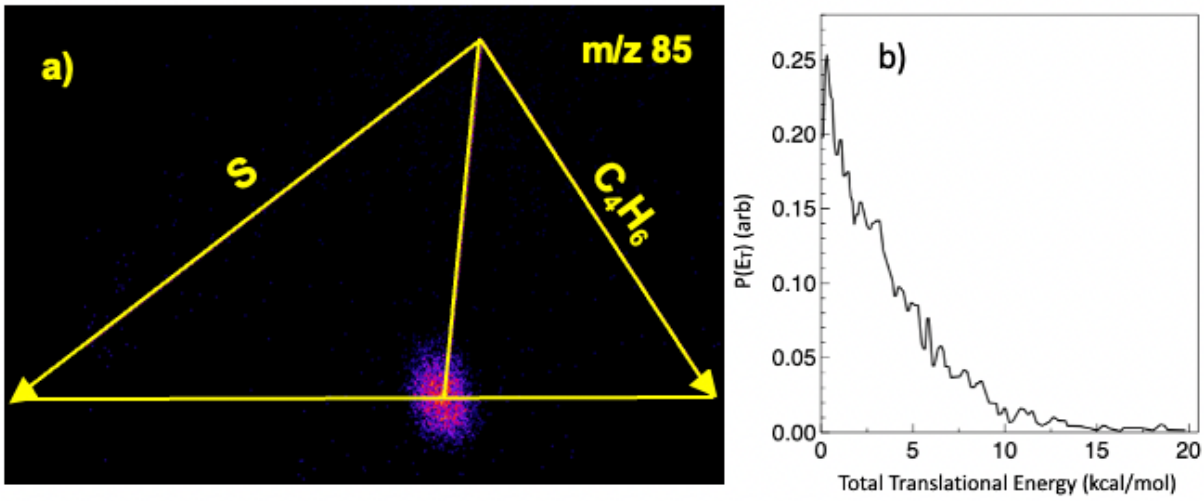


**Figure 1.** a) Velocity map image of the 85 u product ($C_4H_5S$ ) of the crossed-beam reaction of S($^3$P) with 1,3-butadiene at 13.6 kcal/mol collision energy. The most probable Newton diagram is superimposed on the image showing the beam velocities and the center-of-mass velocity of the system. b) Total translational energy distribution determined for the S + 13BD → $C_4H_5S$ + H reaction based on the measured recoil velocity distribution in the image.

We also performed the analogous experiment for S($^3$P) reaction with isoprene and the results are shown in Fig. 2. We find an H loss channel giving the corresponding methyl-substituted radical, and methyl loss again giving 2-H-thiophen-5-yl at m/z=85. The H loss product is again confined to the center of mass velocity, but the methyl loss channel has significant recoil velocity and the angular distribution sows forward-backward symmetry as expected for the long-lived singlet intermediate formed by ISC. Theory suggests other products including methyl thiophene + $H_2$ as well as thioformaldehyde + 13BD, methyl thioketene + ethene and thioketene + propene. We are planning to use our chirped-pulse mm-wave apparatus "CPUF" to look for these and the products for the 13BD reaction which are not detectable using our 157 nm probe. We have already documented formation of thioketene in the 13BD reaction and we are currently modifying our mm-wave spectrometer to detect other products.

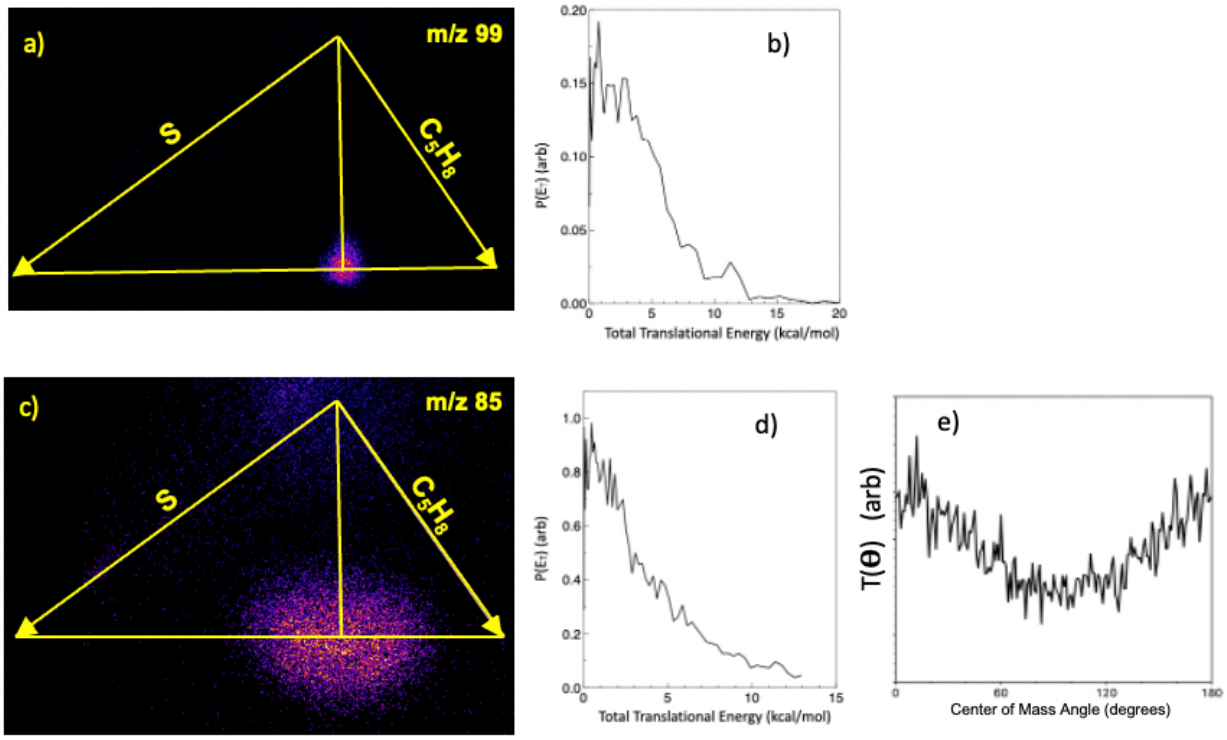


**Figure 2.** a) Velocity map image of the m/z = 99 product, $C_5H_7S$, from the reaction of S($^3$P) with isoprene at 15 kcal/mol collision energy with most probable Newton diagram superimposed. Total translational energy (b) distribution for the S + isoprene → $C_5H_7S$ + H reaction extracted from the image in (a). c) Velocity map image of the m/z = 85 product, $C_4H_5S$ from the same reaction. Total translational energy (d) and angular (e) distributions for the S + isoprene → $C_4H_5S$ + $CH_3$ reaction extracted from the image in (c).

### *2.2 Ultrafast Experiments*

#### *Coulomb Explosion Imaging*

In favorable cases, molecular structure and dissociation dynamics can be inferred from the ionic fragments' momentum images recorded in a Coulomb Explosion Imaging (CEI) experiment when multiple electrons are rapidly removed from a molecule. Advanced momentum imaging methods such as those we have at our disposal allow recording multiple ionic fragment channels in coincidence, which is key to making such measurements. We have demonstrated this in two

systems as reported in last years' abstract. In the past year we have been addressing some challenges in the laser system and improving our data acquisition throughput, and expect to have new CEI results soon.

## 3. Future Plans

*S($^3$P) reactions.* In the next year we plan to begin a systematic investigation of S($^3$P) reactions with unsaturated hydrocarbons. We will examine reactions with styrene, phenyl acetylene and various. Terpenes. We will combine our VUV imaging approach with "universal" mmwave spectroscopy of the reactions in a low temperature flow, from which we can derive product branching for comparison to theory.

*Time-resolved CEI.* Our success with static Coulomb Explosion Imaging shows that we are now in a position to use this for time-dependent dynamics studies. We are working to identify an optimal system for our first such investigations. We will begin with di-iodobenzene (DIB). Previous Coulomb explosion work on the para-isomer observed the recoil of two iodine atoms in opposing directions after three-body fragmentation, which suggests that it should be possible to observe distinct two- and three-body covariance patterns from 1,2-DIB.

## 4. DOE Publications 2020-present


H. Li and A. G. Suits, "Universal Crossed Beam Imaging Studies of Polyatomic Reaction Dynamics," *Phys Chem Chem Phys.* (2020) **22**, 11126-11138 DOI: 10.1039/D0CP00522C.

H. Li, D. Troya and A. G. Suits, "Multichannel dynamics in the OH + n-butane reaction revealed by crossed-beam slice imaging and quasiclassical trajectory calculations," *J. Chem. Phys.* (2020) 153, 104302. DOI: 10.1063/5.0013585.

G. A. Cooper, S. T. Alavi, W. Li, S.-K. Lee, and A. G. Suits, "Coulomb Explosion Dynamics of Chlorocarbonylsulfenyl Chloride," *J. Phys. Chem. A.* (2021) **125**, 5481-5489. DOI: 10.1021/acs.jpca.1c02332.

S. Tahereh Alavi, Graham A. Cooper and Arthur G. Suits "Coulomb Explosion Dynamics of Methoxycarbonylsulfenyl Chloride by 3D Multimass Imaging," Mol. Phys. (2021) DOI: 10.1080/00268976.2021.1988170.

R. W. Field and A. G. Suits, "Modern Techniques, Modern Concepts, and Molecules Doing Stuff" in "*Emerging Trends in Chemical Applications of Lasers*," M. Berman, L. Young, H.L. Dai, Eds., **ACS Symposium Series.** (2021) Chapter 15, 333-361. DOI: 10.1021/bk-2021-1398.ch015

# Curvature Formation During TCD for Activity Regeneration by Partial Oxidation for Maintaining Autocatalytic Activity

Mpila Nkiawete[1], Randy Vander Wal[1,2], Adri van Duin[2] and Margaret Kowalik[2]
[1]The EMS Energy Institute and [2]The Dept. of Mechanical Engineering
Penn State University
University Park, PA 16802
Emails: ruv12@psu.edu, acv13@psu.edu

## I. Program Scope

### *Motivation for Thermo-catalytic Decomposition*

Hydrogen is envisioned as the energy carrier (fuel) of the future and is a crucial feedstock for various manufacturing industries. Thermo-catalytic decomposition (TCD) of methane can produce $CO_X$-free hydrogen for PEM fuel cells, oil refineries, ammonia and methanol production [1]. Recent research has focused on enhancing the production of hydrogen by the direct thermo-catalytic decomposition of methane to form elemental carbon and hydrogen as an attractive alternative to the conventional steam reforming process [2].

Carbon as a catalyst has many advantages compared to other catalytic materials: a) fuel flexibility, b) insensitivity to sulfur poisoning and c) high temperature resistance. TCD offers 100% carbon capture with the solid, high purity carbon useful as electrode material for energy storage [3]. Despite these advantages, carbon as a catalyst also problematically deactivates. Ideally the deposited carbon would be autocatalytic but all studies with methane find that *the deposited carbon is not as active a catalyst as the original carbon.*

### *Addressing TCD and Regeneration Research Needs*

High fidelity parallels exist between TCD and soot processes. The TCD rate may be viewed as equivalent to a soot particle growth rate. Both reactions add mass via heterogenous radical-driven reactions. In a flame environment, variables affecting growth are highly coupled. In TCD these factors may be disentangled, and their contributions resolved. Of particular interest are the relationships between nanostructure, active sites and growth rate. These same connections apply to TCD. Nanostructure governs active site number. In turn, active sites determine kinetic rates. Additionally, deposition conditions determine nanostructure and thus kinetic rates.

The proposed TCD measurements provide direct measures of each of these parameters, resolved by species, parametric with temperature and differentiated by nanostructure of nascent carbon. As detailed objectives,

1. Quantified nanostructure, time-resolved and correlated with TCD rate tests the dependence of rate on initial nanostructure and its time-variation.
2. Similarly, the TCD dependence on active sites tests the correlation between active sites and kinetic rates.
3. Correlation between nanostructure and active sites throughout TCD tests continuity of dependence.
4. Ties between experiments and atomistic- plus continuum-scale simulations include a) capturing the evolving nanostructure of the carbon deposit under TCD and soot relevant conditions, b) resolving nanostructure impact on regeneration and connecting to (renewed) activity in TCD and c) active site identification.

Active sites are related to nanostructure by comparison of simulations to experimental chemical kinetic rates and nanostructure metrics. Sequential rate measurements are made along the course of TCD and regeneration reactions. At the same corresponding points nanostructure are observed and quantified by HRTEM and image analyses, enabling development of the hypothesized correlations. The overall project goal is to connect active sites, nanostructure and deposition rates in concert with reactive force field (ReaxFF) based modeling.

## II. Recent Progress

### *Packed Bed*

The principal advantage of the packed bed is its scale enables monitoring reaction kinetics by reaction products with standard instrumentation. Product analyses furnish reaction metrics of yield, (product) selectivity and (catalyst) stability. Particular parameters of interest include reaction selectivity, yield and stability.

The challenge in determining each of these metrics lies in the intermediate regime where both the initial carbon catalyst and evolving TCD carbon both contribute to the overall reaction/conversion. Depending upon the relative reactivity of the two different carbons, varied time behaviors can be observed for the reaction rate and conversion yield with time. At longer durations it can be safely assumed that only the deposited carbon is contributing to the observed activity – due to complete coverage of the initial catalyst and asymptotic behavior of the observed reaction rate.

***Approach***

Starting carbon catalyst(s) are placed in a U-shaped quartz tube held in a vertical reactor. Mass flow controllers regulate the flow mixtures consisting of a mixture of inert carrier and hydrocarbon gas or mixture for TCD or inert plus oxidizer, such as $CO_2$, $H_2O$ or $O_2$ for regeneration. Oxidation levels are gauged initially by matching in situ regeneration conditions to corresponding TGA data for the same carbons and RGN conditions. (GC calibration will, in the future, enable real-time determination of oxidation level by mass balance). Presently a thermal conductivity detector is being used for monitoring reaction progress in TCD and regeneration (RGN).

***Nanostructure Comparisons: Sugar Char versus Carbon Black***

Given the mixed contributions from the initial and depositing carbon, two regimes are of particular interest. The first is where the initial catalyst dominates, governing the observed rate. Here direct dependence of rate upon nanostructure can be made by direct comparisons across different carbon nanostructures using methane.

The first comparison is between a char and a conductive carbon black. The TCD curves for each appear in **Fig. 1**. Onset temperatures for the char are different, approximately 650 ℃ for the char and 750 ℃ for the carbon black. Peak conversions are also quite different ~ 33% versus ~ 52% for the char and carbon black respectively. Most significant are the recovery to asymptotic levels where the TCD carbon is governing deposition. The char is minimally active, ~ 3% at long durations while the carbon black supported TCD carbon maintains a relative activity of 30%.

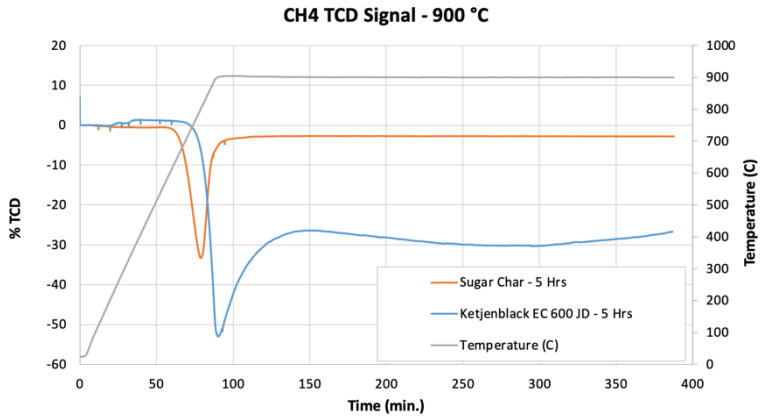


**Figure 1**. TCD conversion rates for a char and conductive carbon black as a function of time. The temperature ramp is illustrated by the dashed curve, plotted on the 2nd y-axis.

These different behaviors are relatable to nanostructure. At short reaction times the conversion is due to the initial carbon activity but at long durations, it depends on the TCD carbon activity. From **Fig. 1** the different onsets and peak conversions are attributed to the different lamellae nanostructure between the char and carbon black.

As the TEM images in **Fig. 2** show, the former is nearly amorphous while the latter presents extended lamellae with proportionally fewer edge sites. One might expect an amorphous carbon with aromatic clusters for lamellae to host more active sites than a carbon formed by high temperature pyrolysis (specifically acetylene pyrolysis for the conductive black). However, the opposite appears to be the case. Formed at a low temperature, 600 ℃, the early char behavior is attributed to annealing under the reducing TCD environment. Thereafter TCD carbon controls the deposition rate. Both carbons support irregular carbon graphenic stacks as shown in **Fig. 3** for the sugar char. The annealing is apparent by the visible lattice fringes forming shells, capsules and stacks. Either this annealing provides fewer TCD growth sites and/or the resulting TCD carbon is less active than that on the conductive carbon. This latter possibility seems unlikely given the

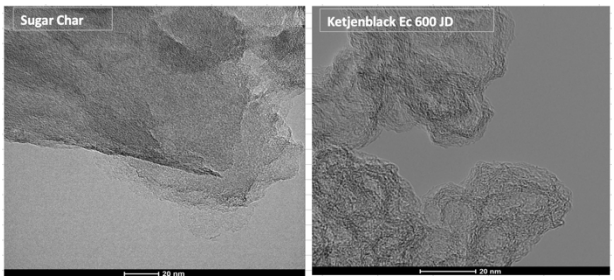


**Figure 2**. TEM images of nascent sugar char and the conductive carbon black.

similarity of the TCD carbon forms on both carbon. By XPS analysis, chemisorbed oxygen content, as a measure of active sites was < 1 at.% for the conductive black while 3.4 at.% for the char. While the initial onsets and rates correlate with active sites, the activity of the TCD carbon anti-correlates, demonstrating a complex relation between deposit nanostructure versus that of the nascent carbon. Further tests are on-going.

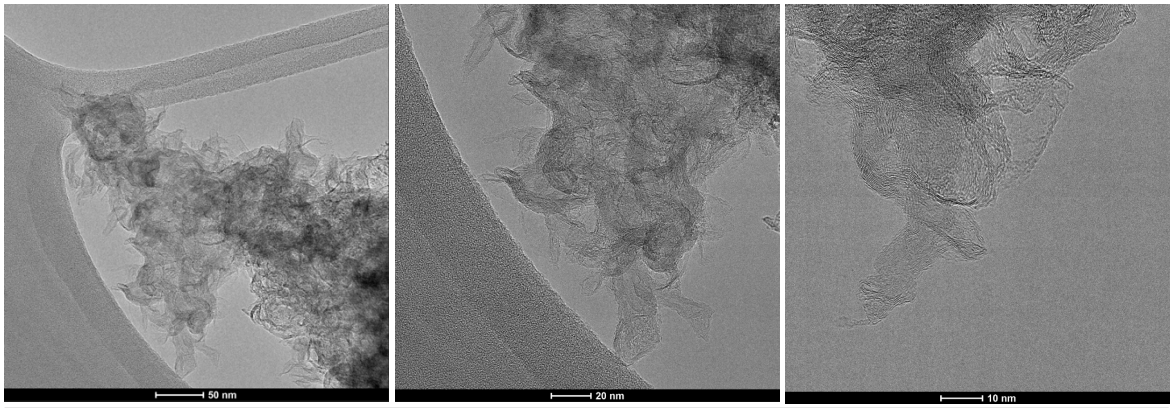


**Figure 3**. Post-TCD TEM images, post TCD of the sugar char with TCD carbon evident as graphenic outgrowths from the char. Similar TCD carbon "outgrowths" were observed on the conductive carbon. Annealing of the char is apparent relative to its nascent form as shown in Fig. 2.

***Regeneration Comparison: Nascent versus Partially Oxidized Carbon Catalyst***

**Figure 4** shows the conversion level with time for TCD using methane and R250, an ordinary carbon black as the starting catalyst. From the rate versus temperature curve, the onset of $CH_4$ conversion begins at 700 ℃, steeply increasing thereafter. In contrast the partially oxidized form exhibits an earlier onset, faster initial rates but a lower conversion level at long durations. Notably the peak conversion for each carbon does not last long, thereafter the conversion level and rate decrease, approaching an asymptotic limit of ~ 40% and 50% of peak conversion long-term for the partially oxidized and nascent forms, respectively. This behavior and limiting rates at long durations are attributed to the deposited carbon governing the overall reaction rate, as the initial carbon is covered and deactivated. Based on this premise, the different asymptotic rates suggest that the TCD carbon nanostructure is dependent upon the initial nanostructure of the original carbon catalyst. As the low temperature (500 ℃) partial oxidation is expected to break up lamellae and otherwise shorten lamellae by edge-site oxidation, the activity of the TCD carbon appears inversely related to the disorder of the nascent carbon given that the TCD carbon on the partially oxidized carbon is less active. TEM reveals different particle size, as expected, but preliminary fringe analysis suggest the partial oxidation increased the lamellae length distribution, thus decreasing the number of active sites and potential carry-over into the TCD carbon, as rationalization for its lower activity. In addition to serving as a comparison for nanostructure-based activity, these measurements provide a baseline for gauging the effect of partial oxidation (RGN) which presumably should increase the active sites (and corresponding change in nanostructure).

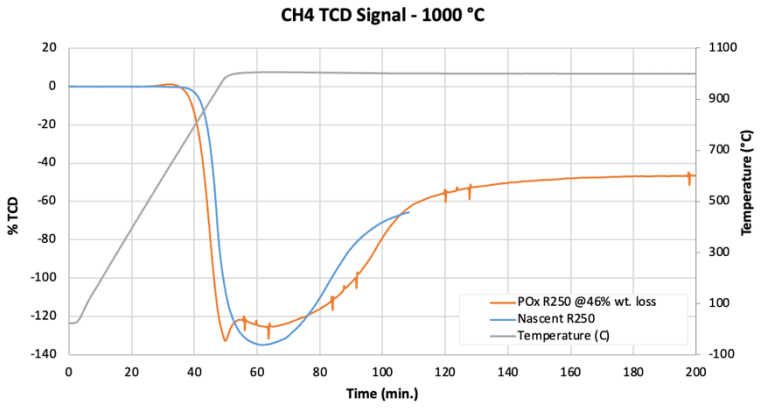


**Figure 4**. TCD plots corresponding to conversion of methane into carbon and hydrogen.

***Activation Energy Analysis***

Activation energies were extracted from the TCD rates, analogous to the leading edge analysis in thermal desorption spectroscopy [4] or the single ramp rate method used in TGA analysis [5]. With the approximation that there is little deposited carbon on the initial catalyst during the ramp to operating temperature, (hence the initial catalyst yet governs the deposition rate), rates can be

extracted by analyzing the TCD rate. Following an Arrhenius analysis for the activation energy, the TCD activation energy with nascent R250 was 281 kJ/mol but decreased to 133 kJ/mol for the partially oxidized R250. This dramatic decrease confirms the regeneration / re-creation of active sites by partial oxidation and moreover, that sites formed by oxidation are active towards deposition. Notably the earlier onset temperature is consistent with the lower activation energy value for the partially oxidized carbon.

**III. Future Plans**

Reactive force-field (ReaxFF) based simulations will be used to gauge evolution of deposition carbon structure during both TCD and RGN reactions as well as probe the dependence of initial deposition upon the underlying carbon nanostructure. It should be noted that these simulations begin with a structural model and need benchmarks for comparison during development. We anticipate that active sites at different reaction stages coupled with TCD and RGN rates will serve as such.

In the coming year we also plan to connect active sites and kinetic rates as the data sets for each grow. In situ experiments are planned in the packed bed reactor for mapping active sites across TCD and RGN reaction durations and for pairing TCD with RGN in a cyclic, iterative manner to test the equivalency of active sites between RGN and TCD. Pulsed chemisorption is planned for active site determination with potential mass spectrometer detection if thermal conductivity detection proves inadequate.

**IV. Publications and Presentations Acknowledging DOE_BES Support (2021-2023)**

Mpila Nkiawete, Randy Vander Wal Thermo-catalytic Decomposition of Methane to Produce hydrogen Using Carbon as Catalyst. Paper M4.444. Session: Industrial Decarbonization: CCS & Hydrogen. Monday, June 19th. TechConnect World Innovation Conference, National Harbor, MD, USA. June 19-21, 2023.

Mpila Nkiawete, Randy Vander Wal Carbon Catalyzed Thermo-catalytic Decomposition of Methane: Connecting Nanostructure to Deposition Conditions and Rates. Session: Industrial Decarbonization – Posters. Paper M8.521. Monday, June 19th. TechConnect World Innovation Conference, National Harbor, MD, USA. June 19-21, 2023.

Mpila Nkiawete, Randy Vander Wal Clean Hydrogen Production By Decarbonizing Natural Gas By Carbon-Catalyzed Thermal Decomposition. Session: Hydrogen. The 47th International Technical Conference on Clean Energy. Sheraton Sand Key, Clearwater, Florida, USA July 23 to 27, 2023.

Nkiawete, M., and Vander Wal, R. L., Thermo-catalytic Decomposition of Methane: Connecting Deposition Rates, Nanostructure, and Active Sites. Division: Division of Energy and Fuels. Symposium: Advances in Energy and Fuel. Session: Thermal Catalysis for Natural Gas and $CO_2$ Conversions. Paper ID: 3821924. ACS Spring 2023 – Crossroads of Chemistry. Indianapolis, IN March 26-30, 2023. Oral-Virtual.

Nkiawete, M., and Vander Wal, R., Thermo-catalytic decomposition of methane: Focus on nanostructure
Session/Paper 2A15: 149NEC-0118. 2022 Spring Technical Meeting, Eastern States Sections of The Combustion Institute, University of Central Florida Orlando, Florida March 6-9, 2022.

**V. References**


1. Muradov N. (2002). Thermo-catalytic $CO_2$-free production of hydrogen from hydrocarbon fuels. U.S. DOE Hydrogen Program Review. U.S.: Department of Energy (DOE); NREL/CP-610-32405.
2. Ahmed, S., Aitani, A., Rahman, F., Al-Dawood, A., and Al-Muhaish, F. (2009). Decomposition of hydrocarbons to hydrogen and carbon. *Applied Catalysis A: General*, ***359***(1), 1-24.
3. De Falco, M., Basile, A. (Eds.). (2015). *Enriched Methane: The First Step Towards the Hydrogen Economy*. Springer.
4. Redhead, P.A. (1962). Thermal desorption of gases. *Vacuum*, **12** (4): 203–211.
5. Chen, R. (1976). Methods for kinetic analysis of thermally stimulated processes. *Journal of Materials Science*, ***11***, 1521-1541.

# Probing Nonvalence Excited States of Anions Using Photodetachment and Photoelectron Spectroscopy

Lai-Sheng Wang
Department of Chemistry, Brown University, Providence, RI 02912
Email: lai-sheng_wang@brown.edu

## Program Scope

This program is aimed at obtaining energetic, electronic, and vibrational information of molecules and radicals important in combustion or the atmosphere, such as polycyclic aromatic hydrocarbons (PAHs), using new anion spectroscopic techniques. Negative ions do not possess Rydberg states, but highly-diffuse nonvalence states can exist in anions as a special class of electronic excited states due to the long-range forces between the extra electron and the neutral molecular cores. Valence-bound anions may possess such nonvalence excited states just below the detachment threshold, analogous to Rydberg states of neutral molecules. The objective of this program is to probe the nonvalence excited states that exist in anions of PAH or functionalized PAH species and to utilize the nonvalence excited states as a new window to obtain energetic and spectroscopic information of the underlying neutral PAH radicals and molecules. The PI's lab has built a high-resolution electrospray photoelectron imaging apparatus equipped with a cryogenically-cooled ion trap, which is essential to probe this class of nonvalence anionic excited states. Photodetachment spectroscopy is used to search for the nonvalence excited states of PAH anions via resonant two-photon detachment or vibrational autodetachment. The autodetachment process is investigated by resonantly-enhanced photoelectron spectroscopy. The combination of photodetachment spectroscopy and resonant photoelectron spectroscopy can yield rich energetic, electronic, and vibrational information about the underlying neutral species, as well as information about vibronic coupling leading to autodetachment.

## Recent Progress

***Probing the Strong Nonadiabatic Interactions in the Triazolyl Radical Using Photodetachment Spectroscopy and Resonant Photoelectron Imaging of Cryogenically-Cooled Anions.***[13] While the adiabatic potential energy surfaces defined by the Born-Oppenheimer approximation are the cornerstones for understanding the electronic structure and spectroscopy of molecular systems, nonadiabatic effects due to the coupling of electronic states by nuclear motions are common in complex molecular systems. The nonadiabatic effects are so strong in the 1,2,3-triazolyl radical ($C_2H_2N_3$) that the photoelectron spectrum of the triazolide anion was rendered unassignable. Using photodetachment spectroscopy and resonant photoelectron imaging of cryogenically-cooled anions, we are able to completely unravel the complex vibronic levels of the triazolyl radical. Photodetachment spectroscopy reveals a dipole-bound state for the triazolide anion at 172 $cm^{-1}$ below the detachment threshold and thirty-one vibrational Feshbach resonances. Resonant photoelectron imaging is conducted by tuning the detachment laser to each of the Feshbach resonances. Combining the photodetachment spectrum and the resonant photoelectron spectra, we are able to assign all twenty-eight vibronic peaks resolved for the triazolyl radical. Fundamental frequencies for twelve vibrational modes of the ground state of the triazolyl radical are measured experimentally. This study provides unprecedented experimental vibronic information, which will be valuable to verify theoretical models to treat nonadiabatic effects involving multiple electronic states.

***Dipole-Bound State, Photodetachment Spectroscopy, and Resonant Photoelectron Imaging of Cryogenically-Cooled 2-Cyanopyrrolide.***[14] Because of the similarity in geometry and vibrational frequencies between the dipole-bound states (DBSs) and the corresponding neutrals, DBSs have been exploited as intermediate states to conduct resonant photoelectron spectroscopy (PES), resulting in highly non-Franck-Condon photoelectron spectra via vibrational autodetachment and providing much richer vibrational information than conventional PES. We have conducted a photodetachment and high-resolution photoelectron imaging study of the 2-cyanopyrrolide anion, cooled in a cryogenic ion trap. The electron affinity of the 2-cyanopyrrolyl radical is measured to be 3.0981 ± 0.0006 eV (24988 ± 5 $cm^{-1}$). A DBS is observed for 2-cyanopyrrolide at 240 $cm^{-1}$ below its detachment threshold using photodetachment spectroscopy. Twenty-three above-threshold vibrational resonances (Feshbach resonances) of the DBS are observed. Resonant PES is conducted at each Feshbach resonance, yielding a wealth of vibrational information about the 2-cyanopyrrolyl radical. Resonant two-photon PES confirms the *s*-like dipole-bound orbital and reveals a relatively long lifetime of the bound zero-point level of the DBS. Fundamental frequencies for nineteen vibrational modes (out of a total of 24) are obtained for the cyanopyrrolyl radical, including six out-of-plane modes. This work provides important spectroscopic information about 2-cyanopyrrolyl, which should be valuable for the study of this radical in combustion or astronomical environments.

***Investigation of the Electronic and Vibrational Structures of the 2-Furanyloxy Radical using Photoelectron Imaging and Photodetachment Spectroscopy via the Dipole-Bound State of the 2-Furanyloxide Anion.***[15] The 2-furanyloxy radical is an important chemical reaction intermediate in the combustion of biofuels and aromatic compounds. We have investigated its electronic and vibrational structures using photoelectron and photodetachment spectroscopy, and resonant photoelectron imaging (PEI) of cryogenically-cooled 2-furanyloxide anion. The electron affinity of 2-furanyloxy is measured to be 1.7573(8) eV. Two excited electronic states are observed at excitation energies of 2.14 eV and 2.82 eV above the ground state. Photodetachment spectroscopy reveals a DBS 0.0143 eV below the detachment threshold and twenty-five vibrational Feshbach resonances for the 2-furanyloxide anion. The combination of photodetachment spectroscopy and resonant PEI yields frequencies for eighteen out of a total of twenty-one vibrational modes for the 2-furanyloxy radical, including all six of its bending modes. The rich electronic and vibrational information will be valuable for further understanding the role of 2-furanyloxy as a key reaction intermediate of combustion and atmospheric interests.

***Observation of A Polarization-Assisted Dipole-Bound State.***[16] The critical dipole moment to bind an electron was empirically determined to be 2.5 Debye, even though smaller values were predicted theoretically. We have observed the first polarization-assisted DBS for a molecule with a dipole moment below 2.5 Debye. Photoelectron and photodetachment spectroscopy are conducted for cryogenically-cooled indolide anion, where the neutral indolyl radical has a dipole moment of 2.4 Debye. Photodetachment experiment reveals a DBS only 6 $cm^{-1}$ below the detachment threshold along with sharp vibrational Feshbach resonances (**Fig. 1**). Rotational profiles are observed for all the Feshbach resonances, which are found to have surprisingly narrow linewidths and long autodetachment lifetimes attributed to weak coupling between vibrational motions and the nearly free dipole-bound electron. Calculations suggest that the observed DBS has π symmetry stabilized by the strong anisotropic polarizability of indolyl.

***Cryogenic Photodetachment Spectroscopy and High-Resolution Resonant Photoelectron Imaging of Cold para-Ethylphenolate Anions.***[17] DBSs can be systematically searched using photodetachment spectroscopy (PDS), which can yield the binding energies of

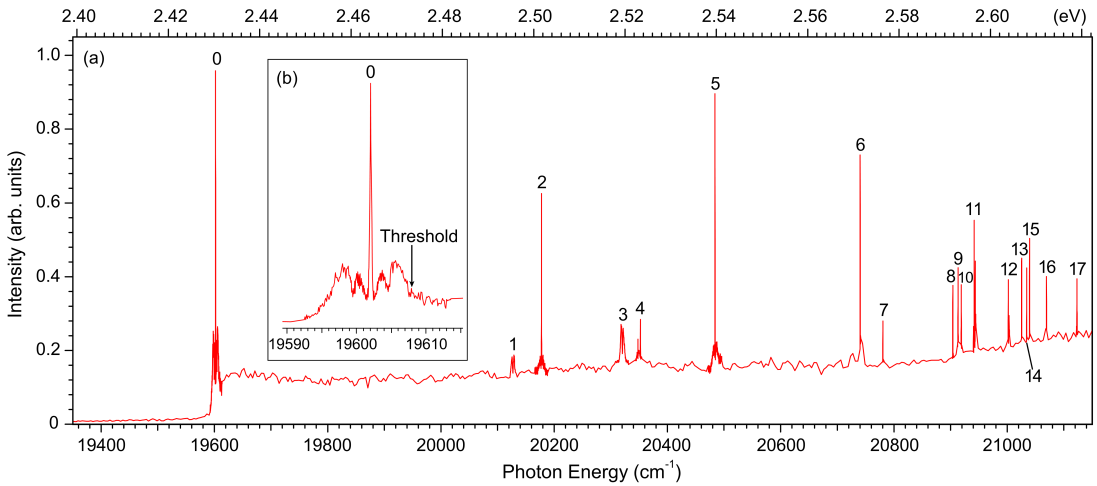


**Fig. 1.** Photodetachment spectrum of indolide by measuring the total electron yield as a function of photon energy. (a) The full spectrum. (b) The insert shows the rotational profile of peak 0. The arrow indicates the detachment threshold at 19608 $cm^{-1}$ (2.4311 eV).

the DBSs, the electron detachment threshold of the anion, and above-threshold vibrational levels of the DBSs (Feshbach resonances). We have shown that the combination of PDS and resonant photoelectron spectroscopy (rPES) at the Feshbach resonances is a powerful approach to obtain rich vibrational information for complex molecular radicals. A prerequisite for this technique is to produce vibrationally cold anions, made possible by a cryogenically-controlled Paul trap. We have conducted a PDS and rPES study of cold *para*-ethylphenolate anions (*p*-$EP^-$). The electron affinity of the *p*-EP radical is measured to be17425 ± 3 $cm^{-1}$ (2.1604 ± 0.0004 eV); and a DBS is found at 145 $cm^{-1}$ below the detachment threshold of *p*-$EP^-$. Thirty-four vibrational levels are observed for the DBS, including two bound levels and thirty-two Feshbach resonances. Frequencies for seventeen vibrational modes of the *p*-EP radical are measured from the combination of PDS and rPES, including six symmetry-forbidden modes with A" symmetry. This study confirms again the power of combining cryogenic ion cooling with PDS and high-resolution rPES to obtain spectroscopic information of complex molecular radicals.

## Future Plans

Experiments on dipole-bound excited states will be continued on O- and N-containing PAH anions. We have found recently that N-containing 5-memebered ring systems have rich spectroscopy and complicated vibronic couplings, which can be effectively interrogated using our cryogenic ion trap and high-resolution photoelectron imaging.[10,11,13,14] We will continue this effort on 5-membered ring systems with different substituents. We will further extent work to other N-containing heteroring PAHs and begin studies on larger PAH species.

## Publications resulted from the BES-GPCP sponsored research (2020-2023)

1. D. F. Yuan, Y. Liu, C. H. Qian, Y. R. Zhang, B. M. Rubenstein, and L. S. Wang. Observation of a $\pi$-Type Dipole-Bound State in Molecular Anions. *Phys. Rev. Lett.* **125**, 073003 (2020). DOI: 10.1103/PhysRevLett.125.073003.
2. C. H. Qian, G. Z. Zhu, and L. S. Wang. Photodetachment Spectroscopy and Resonant Photoelectron Imaging of the 2-Naphthoxide Anion via Dipole-Bound Excited States. *J. Chem. Phys*. **152**, 214307 (13 pages) (2020). DOI: 10.1063/5.0011234.

3. Y. T. Wang, C. G. Ning, H. T. Liu, and L. S. Wang. High-Resolution Photoelectron Imaging and Photodetachment Spectroscopy of Cryogenically-Cooled $IO^-$. *J. Phys. Chem. A* **124**, 5720-5726 (2020). DOI: 10.1021/acs.jpca.0c04080.
4. D. F. Yuan, Y. Liu, C. H. Qian, G. S. Kocheril, Y. R. Zhang, B. M. Rubenstein, and L. S. Wang. Polarization of Valence Orbitals by the Intramolecular Electric Field from a Diffuse Dipole-Bound Electron. *J. Phys. Chem. Lett*. **11**, 7914-7919 (2020). DOI: 10.1021/acs.jpclett.0c02514
5. Y. Liu, G. Z. Zhu, D. F. Yuan, C. H. Qian, Y. R. Zhang, B. M. Rubenstein, and L. S. Wang. Observation of a Symmetry-Forbidden Excited Quadrupole-Bound State. *J. Am. Chem. Soc*. **142**, 20240-20246 (2020). DOI: 10.1021/jacs.0c10552
6. C. H. Qian, Y. R. Zhang, D. F. Yuan, and L. S. Wang. Photodetachment Spectroscopy and Resonant Photoelectron Imaging of Cryogenically-Cooled 1-Pyrenolate. *J. Chem. Phys*. **154**, 094308 (2021). DOI: 10.1063/5.0043932
7. D. F. Yuan, Y. R. Zhang, C. H. Qian, Y. Liu, and L. S. Wang. Probing the Dipole-Bound State in the 9-Phenanthrolate Anion by Photodetachment Spectroscopy, Resonant Two-Photon Photoelectron Imaging, and Resonant Photoelectron Spectroscopy. *J. Phys. Chem. A* **125**, 2967-2976 (2021). DOI: 10.1021/acs.jpca.1c01563
8. "Observation of A Dipole-Bound Excited State in 4-Ethynylphenoxide and Comparison with the Quadrupole-Bound Excited State in the Isoelectronic 4-Cyanophenoxide" (Y. R. Zhang, D. F. Yuan, C. H. Qian, and L. S. Wang), *J. Chem. Phys*. **155**, 124305 (2021). DOI:10.1063/5.0065510
9. "Resonant Two-Photon Photoelectron Imaging and Adiabatic Detachment Processes from Bound Vibrational Levels of Dipole-Bound States" (D. F. Yuan, Y. R. Zhang, C. H. Qian, and L. S. Wang), *Phys. Chem. Chem. Phys*. **24**, 1380-1389 (2022). DOI: 10.1039/D1CP05219E
10. "Observation of Core-Excited Dipole-Bound States" (Y. R. Zhang, D. F. Yuan, and L. S. Wang), *J. Phys. Chem. Lett*. **13**, 2124-2129 (2022). DOI: 10.1021/acs.jpclett.2c00275
11. "Probing the Electronic Structure and Spectroscopy of the Pyrrolyl and Imidazolyl Radicals using High Resolution Photoelectron Imaging of Cryogenically-Cooled Anions" (Y. R. Zhang, D. F. Yuan, and L. S. Wang), *Phys. Chem. Chem. Phys*. **24**, 6505–6514 (2022).
DOI: 10.1039/D2CP00189F
12. "Probing the Electronic Structure and Bond Dissociation of $SO_3$ and $SO_3^-$ using High-Resolution Cryogenic Photoelectron Imaging" (D. F. Yuan, T. Trabelsi, Y. R. Zhang, J. S. Francisco, and L. S. Wang), *J. Am. Chem. Soc*. **144**, 13740-13747 (2022). DOI: 10.1021/jacs.2c04698
13. "Probing the Strong Nonadiabatic Interactions in the Triazolyl Radical Using Photodetachment Spectroscopy and Resonant Photoelectron Imaging of Cryogenically-Cooled Anions" (Y. R. Zhang, D. F. Yuan, and L. S. Wang), *J. Am. Chem. Soc*. **144**, 16620-16630 (2022). DOI: 10.1021/jacs.2c07167
14. "Dipole-Bound State, Photodetachment Spectroscopy, and Resonant Photoelectron Imaging of Cryogenically-Cooled 2-Cyanopyrrolide" (D. F. Yuan, Y. R. Zhang, and L. S. Wang), *J. Phys. Chem. A* **126**, 6416-6428 (2022). DOI: 10.1021/acs.jpca.2c04405
15. "Investigation of the Electronic and Vibrational Structures of the 2-Furanyloxy Radical using Photoelectron Imaging and Photodetachment Spectroscopy via the Dipole-Bound State of the 2-Furanyloxide Anion" (Y. R. Zhang, D. F. Yuan, and L. S. Wang), *J. Phys. Chem. Lett*. **13**, 11481-11488 (2022). DOI:10.1021/acs.jpclett.2c03382
16. "Observation of a Polarization-Assisted Dipole-Bound State" (D. F. Yuan, Y. Liu, Y. R. Zhang, and L. S. Wang), *J. Am. Chem. Soc*. **145**, 5512-5522 (2023). DOI: 10.1021/jacs.3c00246
17. "Cryogenic Photodetachment Spectroscopy and High-Resolution Resonant Photoelectron Imaging of Cold *para*-Ethylphenolate Anions" (D. F. Yuan, Y. R. Zhang, C. H. Qian, G. Z. Zhu, and L. S. Wang), *Precis. Chem*. **1**, online (2023). DOI: 10.1021/prechem.2c00012

**Experimental and Computational Study of Quantum Nuclear and Many-Body Effects in Water Network Formation and Water-Surface Interaction in PAH-Water Cluster Ions**

J. Mathias Weber[1,2] and Joel D. Eaves[2]
[1]JILA, University of Colorado Boulder, 440 UCB, Boulder, CO 80309-0440
[2]Department of Chemistry, University of Colorado Boulder, 215 UCB, Boulder, CO 80309-0215
weberjm@jila.colorado.edu; joel.eaves@colorado.edu

**Program Scope –** This research program employs a combined experimental and theoretical approach to probe interactions between water molecules and aromatic hydrocarbons (PAHs). We study the interaction of water molecules with charged PAHs in mass selected cluster ions of the form $PAH^-\cdot(H_2O)_n$, employing infrared (IR) photodissociation spectroscopy, and comparing the experimental results with theoretical predictions.

Clusters offer a unique opportunity to systematically add molecular complexity, thus offering a robust and accurate predictive framework for aqueous interactions with charged hydrocarbons, generally. PAHs are important in many areas of chemistry, such as soot formation, astrochemistry, and materials chemistry, where they are valuable model systems for both neutral and doped graphene and their chemical derivatives.

Using hydrated PAH cluster ions circumvents many of the problems associated with complex condensed phase environments that can obscure or "cancel out" important parts of intermolecular interactions. Experimental IR spectroscopy in the region of the OH stretch informs on molecular details of water-water and water-hydrocarbon interactions and their dynamics, offering a direct probe of hydrogen bonding structure and dynamics. From a theoretical and computational point of view, current water-carbon model potentials are not robust, particularly in interfacial phenomena. Changes in the minimum energy of the van der Waals potential between water and graphitic carbon atoms that are on the 0.5 $k_BT$ at room temperature can mean the difference in hydrophobicity between superhydrophobic and complete wetting. We aim to obtain a detailed theoretical description of water-PAH interactions, which will be the basis of a cost-effective computational models transferable between cluster and condensed phase systems.

**Recent Progress –** In the past year, we have successfully prepared a range of $PAH^-\cdot(H_2O)_n$ cluster ions by supersonic entrainment of PAH and water vapors into a pulsed supersonic expansion of Ar (Figure 1). For pyrene (Pyr) and perylene (Per), we prepared cluster ions with and without Ar messenger tags, $PAH^-\cdot(H_2O)_n\cdot Ar_m$ ($m$ = 0-2) while only the bare hydrated cluster ions, $PAH^-\cdot(H_2O)_n$, have been prepared so far for tetracene (Tet). Target ions were injected into a tandem time-of-flight mass spectrometer (TOF-MS, Figure 1). After mass-selection in the first space focus of the TOF-MS, the ions were irradiated with the output of a tunable, pulsed IR light source. With Ar-tagged target ions, we monitored the photoinduced loss of Ar according to

$$PAH^-\cdot(H_2O)_n\cdot Ar_m + h\nu \rightarrow PAH^-\cdot(H_2O)_I + m\ Ar, \quad (1)$$

as a function of IR frequency to measure their photodissociation spectra. For species without Ar tagging, we used instead the loss of water molecules in the process

$$PAH^-\cdot(H_2O)_n + h\nu \rightarrow PAH^-\cdot(H_2O)_{n-1} + H_2O. \quad (2)$$

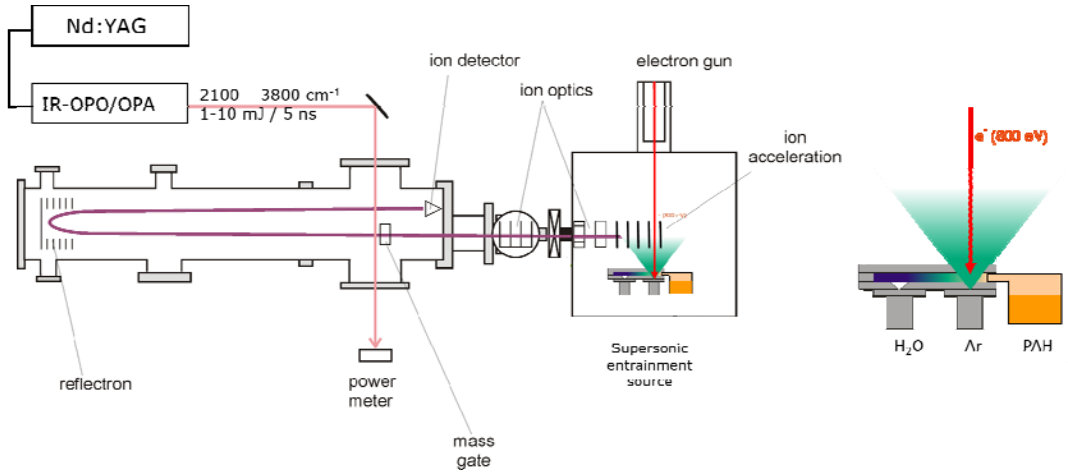


**Figure 1.** Schematic of the experimental setup used (left) with detail of the supersonic entrainment ion source (right).

Fragment ions are separated from the undissociated parent ions using a reflectron, and the fragment ion intensity is monitored on a dual microchannel plate as the light source is tuned.

Figure 2 shows the IR photodissociation spectra for $Pyr^{-}\cdot(H_2O)_n\cdot Ar_2$ ($n = 0 – 4$), which contain the signatures of the CH stretching modes (2850 – 3100 $cm^{-1}$) of the pyrene anion as well as the OH stretching signatures of the water molecules (3300 – 3750 $cm^{-1}$). The signatures of the water molecules encode information on the interaction of the water molecules with the PAH surface, the structure of the water sub-clusters (for $n \geq 2$), and the dynamics of the cluster.

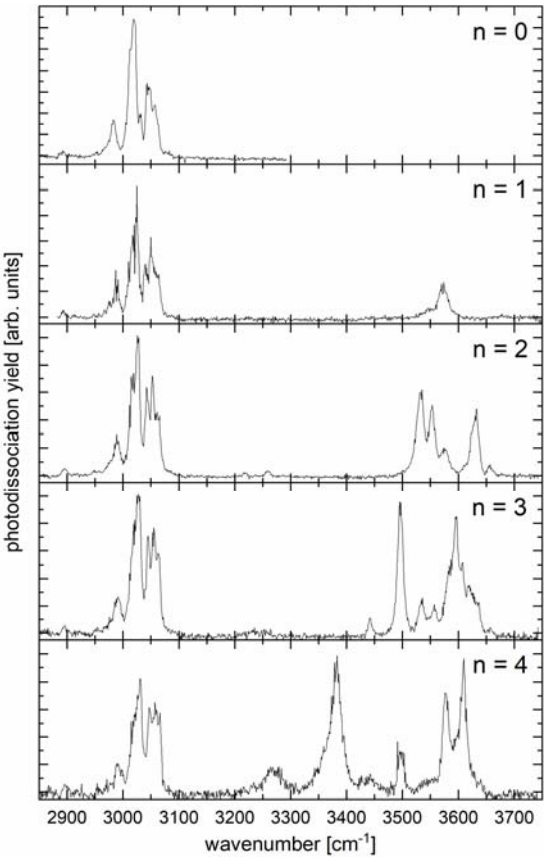


**Figure 2.** Infrared photodissociation spectra of $Pyr^{-}\cdot(H_2O)_n\cdot Ar_2$ ($n = 0$-4, indicated in each panel.

We draw structural information from the comparison of the experimental IR spectra with computed spectra based on density functional theory (DFT, ωB97XD/def2-TZVPP). The lowest energy structures of the different sizes are shown in Figure 3.

The monohydrate is characterized by a very flat potential energy landscape, connecting several basins, in which the water molecule moves across the PAH surface. In general, both of its OH groups interact with the π system of the PAH, which accommodates the excess electron of the cluster anion. Consistent with simple electrostatic considerations, the water molecules preferentially position themselves at the rim of the carbon frame, and mostly at the rings on the long axis of the molecule. One OH group is closer to the PAH than the other by ca. 25 pm, forming a weak hydrogen bond (H-bond) with the π system (OHC

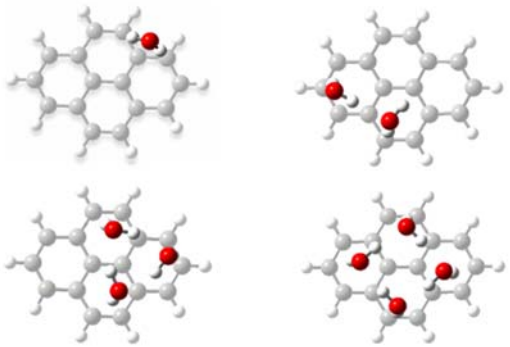

**Figure 3.** Lowest energy structures of $Pyr^{-}\cdot(H_2O)_n$ cluster ions ($n$ = 1-4).

angle ca. 160°), while the second is binding even less strongly (OHC angle ca. 130°). As a result, the symmetry of the water molecule is broken. We assign the dominant peak in the OH stretching region (3573 $cm^{-1}$) to the symmetric OH stretching mode, the more strongly H-bonded OH group having a larger amplitude than the other. A shoulder around 3542 $cm^{-1}$ is due to a vibrational hot band originating in the v=1 state of the water rocking mode. With this hot band, we estimate the cluster temperature to be (78 ± 9) K. The antisymmetric stretching mode is only detectable as a broad, overall weak signature, with a maximum at ca. 3679 $cm^{-1}$. Both features are slightly red-shifted from their positions in free water (3657 and 3756 $cm^{-1}$, respectively) due to their interactions with the negatively charged π system.

In the dihydrate, the two water molecules form a water dimer. The overall mode of interaction with the PAH is similar to that in the monohydrate, as each water molecule forms one H-bond to the π system. One water molecule acts as a double H-bond donor (DD), donating a proton into a H-bond with the second water molecule, the other can be characterized as a donor/acceptor (DA). There are two structural families for this cluster size, which differ in the orientation of the dimeric sub-cluster on the pyrene surface. The two structures are distinguishable from their calculated IR signatures, and they both contribute to the experimentally observed spectrum.

The trihydrate preferentially forms a three-membered ring with each water molecule having DA character. However, at least one chain-like conformer also contributes to the observed spectrum. Similarly, the tetrahydrate has a four-membered ring conformer as its lowest energy structure, and it is the main active conformer.

Photodissociation without Ar messenger tagging, i.e., exploiting the loss of a water molecule from $Pyr^{-}\cdot(H_2O)_n$ clusters, result in similar spectra as those shown in Figure 2, but with broadened bands due to higher temperature (lower limit estimate from the hot band in the monohydrate spectrum ca. 100 K).

To model the spectra of small PAH anionic hydrated clusters, we developed a water and simulation model that allows us to systematically test how intramolecular anharmonicity, kinetic frustration, computational nonergodicity, and structural fluctuations influence calculations of the vibrational spectra. Using linear response theory in concert with classical molecular dynamics (MD) simulations rather than, for example, parameterized vibrational exciton models, allows for a comparatively unbiased computational strategy for computing IR spectra of hydrated PAH clusters. Our results indicate that intramolecular flexibility is vital, and that common intramolecular harmonic potentials do not reproduce experimentally observed spectra. A minimal model consists of a modified TIP4P/2005 water model and a Dreiding potential for the PAH. To capture the bond vibrations, we combine parameters from Reimers & Watts (1984) with the TIP4P/2005 model, using a Morse bond potential to capture the anharmonic motions in the OH

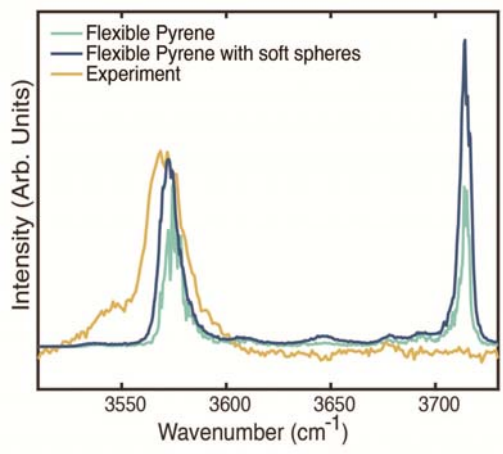


**Figure 4.** Comparison of different classical MD methods at 50 K for modeling the OH stretching peak of $Py^{-}\cdot H_2O$ in comparison to experimental IR spectrum. The symmetric stretch occurs around 3575 $cm^{-1}$ and the antisymmetric stretch occurs around 3715 $cm^{-1}$.

bonds and a harmonic potential in the bending coordinate. The charge assignments for the PAH were generated from DFT optimizations with the $\omega$B97XD functional and the 6-31+G (2d,p) basis set. The spectra come from an average over the time autocorrelation function of the dipole moment. Single water-PAH systems have few degrees of freedom and are slow to equilibrate in the microcanonical ensemble, with rampant temperature fluctuations. As experiments show, and our simulations predict, the linewidth increases significantly when the temperatures increases by tens of Kelvin. To dampen temperature fluctuations during the MD simulations, we imitate a buffer gas by inserting a bath of inert soft spheres which only interacts repulsively. The soft sphere bath brings the system closer to the thermodynamic limit. Parallel tempering has proven an effective way to sample the (surprisingly) complex intermolecular potential energy surface in hydrated-PAH clusters.

The simulations reproduce the asymmetry of the observed line shape of the OH symmetric stretch. The asymmetry is dynamical—we assign it to non-Gaussian spectral diffusion and not to the component spectra of stable intermolecular structures (Figure 4). This asymmetry does not occur for a rigid PAH structure or in the absence of soft spheres, where lineshapes are qualitatively incorrect and overstructured. While the computed lineshape is comparable to the experimental one in shape and width, it is curious that increasing the vibrational density of states by including flexible pyrene and/or soft spheres leads to intensity in the antisymmetric OH stretching mode. This is not observed experimentally.

**Future Plans –** For the coming year, we plan to extend our current experiments on perylene and tetracene, as well as studying analogous clusters with anthracene. While Born-Oppenheimer molecular dynamics (BOMD) simulations are presumably the gold standard for accuracy, they are slow to converge and may be cost-prohibitive for future investigations. We will continue to evaluate BOMD and develop methods to improve convergence, particularly for larger clusters $Py^{-}\cdot(H_2O)_n$ ($n > 1$).

We intend to publish several articles on the work done so far, the first one focusing on the binary $Py^{-}\cdot H_2O$ complex, highlighting how the different theoretical and computational approaches fare in describing this conceptually simple system. A second manuscript describing the experiments and calculations on "cold" $Py^{-}\cdot(H_2O)_n\cdot Ar_2$ clusters ($n = 0 – 4$) will follow, and a third article will concentrate on a comparison with the "warmer" cluster ions in the absence of Ar tags.

**Fundamental chemical kinetics of siloxane and silicon compounds**

DOE BES Grant #18SC503179
Margaret S. Wooldridge (PI)
*University of Michigan, Department of Mechanical Engineering, 2350 Hayward St., Ann Arbor, MI, 48109-2125, mswool@umich.edu*
Andrew B. Mansfield
*Eastern Michigan University, College of Engineering and Technology, Ypsilanti, MI, 48197, amansfi3@emich.edu,*
Robert S. Tranter
*Chemical Sciences and Engineering Division, Argonne National Laboratory, Argonne, IL, 60439, tranter@anl.gov*

## Program Scope

Siloxanes and other silicon compounds play significant roles as impurities in land-fill gas and as primary feedstock materials for high-value and large-volume products, yet the fundamental reaction chemistry of gas-phase silicon compounds remains largely unexplored. This research program integrates two complementary experimental efforts to significantly advance the science of gas-phase silicon reaction chemistry. The primary research focus is on the elementary thermal reactions of siloxanes and their decomposition products with a progression in the chemical structure of the compounds studied to elucidate the effects of bond structure. An additional area of interest is the interaction of gas-phase species with silica nanoparticles that are formed naturally as products of the thermal reactions of siloxanes and during oxidation.

## Recent Progress

*Experimental Approach:* The experimental approach leverages the strengths of the University of Michigan (UM) rapid compression facility (RCF) and atmospheric burner and the diaphragmless shock tube (DFST) and the high-repetition rate shock tube (HRRST) at Argonne National Laboratory for advancing understanding of siloxane chemistry. The combination of experimental approaches allows a broad and complementary range of state conditions to be studied with temperatures in the range of 700-2000 K and pressures of 0.1-50 bar. Work on this project has included RCF experiments where we measured time-histories of OH radicals using continuous-wave, narrow-line laser absorption during ignition of $H_2$ and CO with and without the addition of trace amounts of trimethylsilanol (TMSO), **Figure 1**. OH is the radical chain carrier in these ignition systems and the impact of trimethylsilanol on OH provides insight into the reaction pathways active during silanol oxidation. This past year, we expanded on the OH studies including additional analysis and experiments spanning a broader range of mixtures and state conditions. We also completed the analysis of the experiments conducted last year at Argonne using the facilities of the Advanced Photon Source (APS), and we completed another series of complementary experiments at the APS. Specifically,

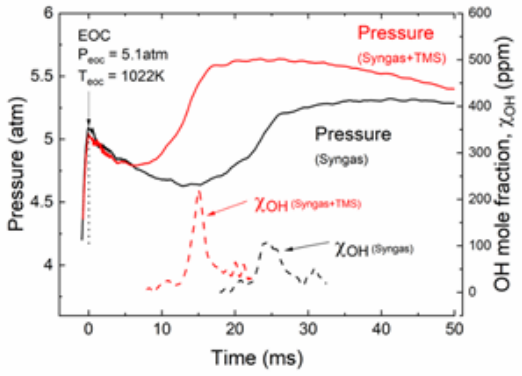


**Figure 1.** Comparison of OH time-histories obtained during RCF $H_2$ and CO ignition experiments at T = 1050 K, P = 5 atm with and without TMSO (100 ppm).

the studies focused on measurements of mixing and temperature fields via krypton x-ray fluorescence of a Hencken, multi-element diffusion (MEDB), burner equipped with a central fuel tube for introducing nanoparticle precursors such as siloxanes. Brief summaries of these efforts are provided here. Additional details can be found in the associated references.

*RCF OH absorption studies:* **Figure 1** shows a comparison of the pressure and OH time histories between two ignition experiments of $H_2$ and CO mixtures with and without the addition of 100 ppm of TMSO. The addition of even this small amount of TMSO has a marked effect on the ignition process, reducing the ignition delay time from approximately 25 ms to 14 ms and increasing the peak pressure by about 15%. Furthermore, the OH time history is significantly affected by the addition of TMSO. As expected, the OH concentrations in both experiments increase along with their respective pressure profiles at the point of ignition. However, the addition of TMSO appears to generate a much faster increase in the OH population. At this point it is not clear why TMSO has such a profound effect on the OH concentration and this is a focus of ongoing work. Ignition delay times have been measured with and without 100 ppm of TMSO over approximately 1010 K to 1075 K, **Figure 2**. Over this range TMSO consistently accelerated ignition of the mixtures as determined from the pressure and OH measurements.

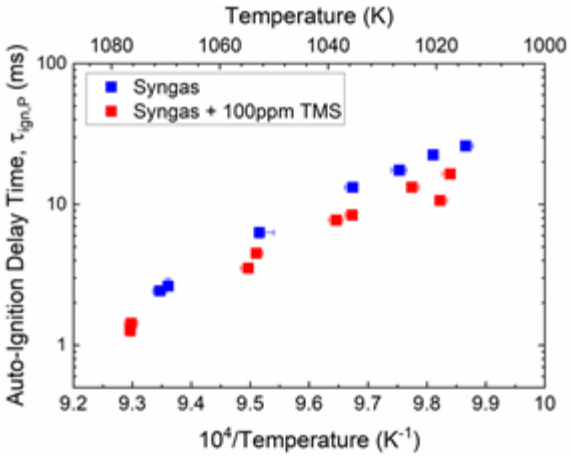


**Figure 2.** Comparison of ignition delay time measurements for $H_2$ and CO mixtures with and without TMSO.

In addition to OH-absorption and pressure measurements, high-speed imaging has been used to examine the impact of the TMSO concentration on the ignition time and the homogeneity of the ignition event. In these studies, the endwall of the RCF was replaced with a quartz window allowing the whole of the reaction chamber to be viewed. **Figure 3** shows high-speed imaging results as a function of the amount of TMSO which was varied between 100 – 5000 ppm. For TMSO <=1000 ppm the ignition events are

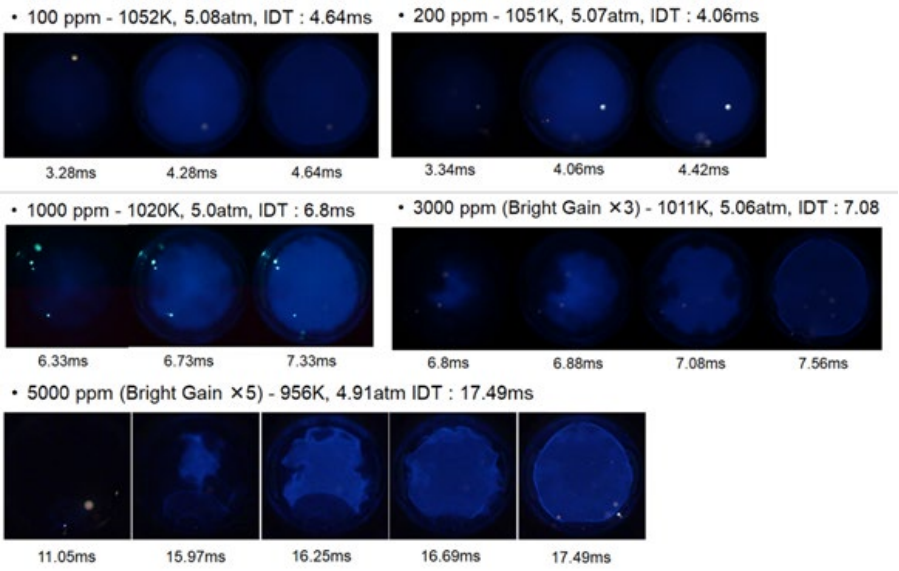


**Figure 3.** High-speed imaging of ignition behavior with increasing TMSO in the initial reactant mixture. Higher concentrations of TMSO exhibit higher sensitivity to the test state conditions, indicated by spatial non-uniformities. The bright spots are artifacts and are not related to the ignition process.

homogenous, whereas above 3000 ppm spatial inhomogeneities become significant and are especially severe with 5000 ppm TMSO. This transition in homogeneity of the ignition regime is indicative of a change in the sensitivity of the reaction chemistry to thermal gradients in the experiments. Current work includes additional analysis and interrogation of the data to understand the impact of TMSO on syngas ignition.

*X-ray fluorescence imaging of flames for nanoparticle formation:* As described last year, we employed an x-ray fluorescence (XRF) technique with krypton as the fluorescence agent at the APS [1,2,3]. In these experiments Kr-Kα fluorescence photons are produced by core-shell ionization of Kr atoms seeded into the flame gases. The photons are collected and the signal intensity is proportional to the number density of Kr atoms, see for example **Figure 4**. The number density is inversely proportional to the local temperature of the volume from where the photons were collected. Thus, by measuring the number density of Kr atoms throughout the flame, a temperature map is obtained. The incident x-ray beam is focused to a small cross section and a polycapillary optic (100 mm focal length) samples photons from a small length of the x-ray beam. The measurement volume is 6 x 4 x 325 μm. In the majority of the experiments, 2D raster scans are made, and these are substituted with higher resolution 1D horizontal and vertical scans as necessary. The initial XRF studies were performed without nanoparticle precursors and provided reference measurements for lean (ϕ=0.8) methane/air flames. In a second experimental campaign,

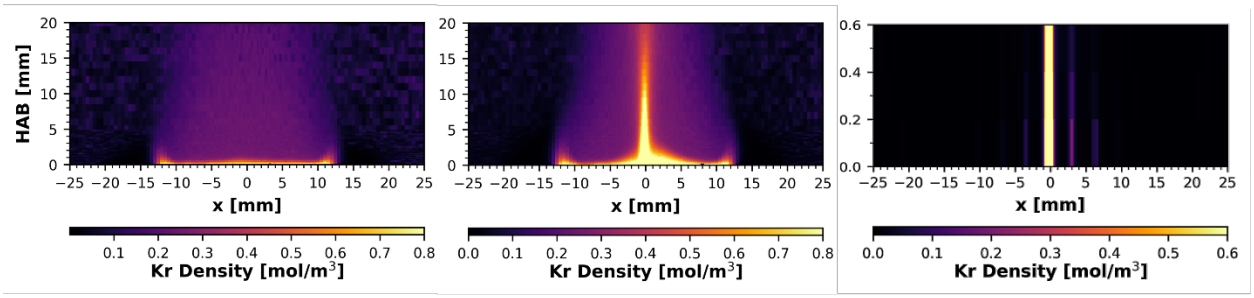


**Figure 4.** XRF results from 2D raster scans of ϕ=0.8 methane/air flames doped with 3% Kr. Left: no flow through the central jet. Middle: 3% Kr /$N_2$ added to the central jet. Note the 'wings' at HAB < 3mm that extend serval mm sideways from the central jet. Right: No fuel or oxidizer in the main burner. Only 3% Kr/$N_2$ in the central jet. The faint vertical lines at x>0 mm are due to leakage from the central tube into the oxidizer plenum.

described below, the flames were doped with HMDSO and TMSO via the central jet. The MEDB used in these experiments has been previously well documented at UM [4] for nanoparticle production from silane. Details of the APS study can be found in Meng et al. [5]. Briefly, the data show that rapid mixing occurred near the exit-plane of the burner and increased spatial uniformity was achieved from 0.1 mm to 0.5 mm above the surface of the burner. An unexpected benefit of the XRF method was that it facilitated identification of a minor leakage from the central fuel tube into the oxidizer plenum. This would have been challenging to see otherwise. In the right-hand panel of **Figure 4**, the MEDB was operated with only 3% Kr in $N_2$ flowing through the central jet i.e., no fuel or oxidizer flows in the main burner. The faint signals either side of the bright line at

x = 0 mm are due to the leaking gases. This effectively introduced extra krypton into the main burner flow and produced the 'wings' on either side of the central jet in the middle panel of **Figure 4**. In **Figure 5,** temperatures calculated from the fluorescence measurements in the left and center panel in **Figure 4** along the center line (x = 0 mm) are compared with simulations of the centerline flame temperature using the GRIMech 3.0 reaction mechanism. For the case without the central flow, there is excellent agreement between the XRF measurements and the simulations. The data also show that the temperature within the jet is low and even at HAB = 10.0 mm, has only increased to around 500 K despite the surrounding flame reaching ~1600 K by HAB = 2.0 mm.

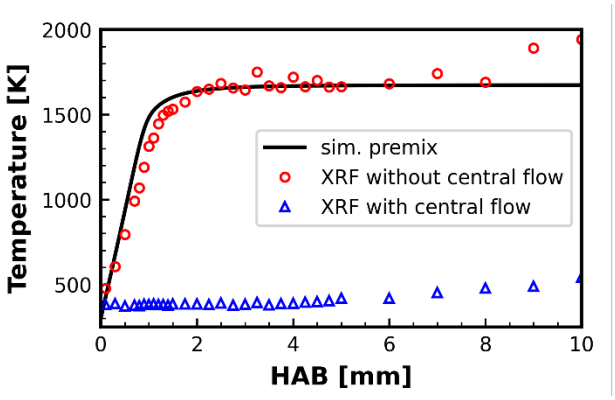


**Figure 5.** Comparison of temperatures measured by Kr-XRF and simulations. Note that within the central jet flow the temperature remains very low relative to the surrounding flame.

In a second experimental campaign earlier this year, HMDSO and TMSO nanoparticle precursors were introduced into the flame via the central jet. In these studies, three flames with stoichiometries of 0.8, 1.0 and 1.22 were used with the lean flame being the same as studied in the first experimental campaign. The addition of TMSO and HMDSO produced opaque plumes of silica nanoparticles. However, similar to earlier XRF studies in heavily sooting flames [6], the nanoparticles did not impede the XRF measurements. In **Figure 6**, 2D plots of the temperature fields derived from XRF measurements from each flame with HMDSO are shown. Note that the central jet does not have 'wings' at low HAB. In this set of experiments, a different MEDB without a leaky central tube was used. In the lower part of **Figure 6**, vertical traces at x=0 mm (centerline) and x=5 mm and 9 mm are shown. The temperatures from the two off-centerline locations are in very good agreement, showing the expected uniformity in the flames. Whereas the centerline temperature is initially very low compared with the x=5 mm location, but within several millimeters becomes the same as the x=5 mm temperature. This contrasts with the results in **Figure 5**, where without HMDSO the centerline temperature remained very low. This suggests that HMDSO is decomposing and reacting within the jet. As noted above, the undoped jet temperatures are too low to initiate pyrolysis of HMDSO. Currently, we hypothesize that H-atoms from the flame are traversing the jet and initiating reaction. Testing this hypothesis will be future work. The apparently very high temperatures that start at x= +/- 9 mm and HAB = 10 mm in **Figure 6** are regions outside the flame boundaries where the Kr number density is very low. These are essentially artifacts of the data processing routine, and a new algorithm has recently been developed that correctly identifies the flame boundaries.

**Future Plans**

The planned work will follow two tracks. We will expand our RCF studies of doping $H_2$/CO mixtures with HMDSO and TMSO. We will also add trimethyl silane (TMS) to the studies. HMDSO and TMS have chemical structures that when compared with TMSO can provide

hierarchal understanding of this class of compounds. Additionally, HMDSO and TMS have direct relevance to semiconductor and other materials manufacturing and biogas systems. We will also probe the source of reaction in the MEDB jets. To test our hypothesis regarding H-atoms initiating reaction we will collaborate with Kulatilaka at Texas A&M to measure H-atom concentrations within the jet. This is critical to accurately simulating nanoparticle production. Another key aspect of this project is providing opportunities for graduate students to expand their portfolios and connections. Consequently, our plans continue to include UM graduate students working with Tranter on shock tube studies, and we will expand our collaboration to include experiments at the Advanced Light Source at LBNL in May 2023. This past year, UM doctoral students, Qinghui Meng and John Kim and PI Margaret Wooldridge conducted the APS experiments with Tranter and APS scientist Alan Kastengren at Argonne. Graduate students Meng and Kim will also help with the planned ALS experiments in May 2023.

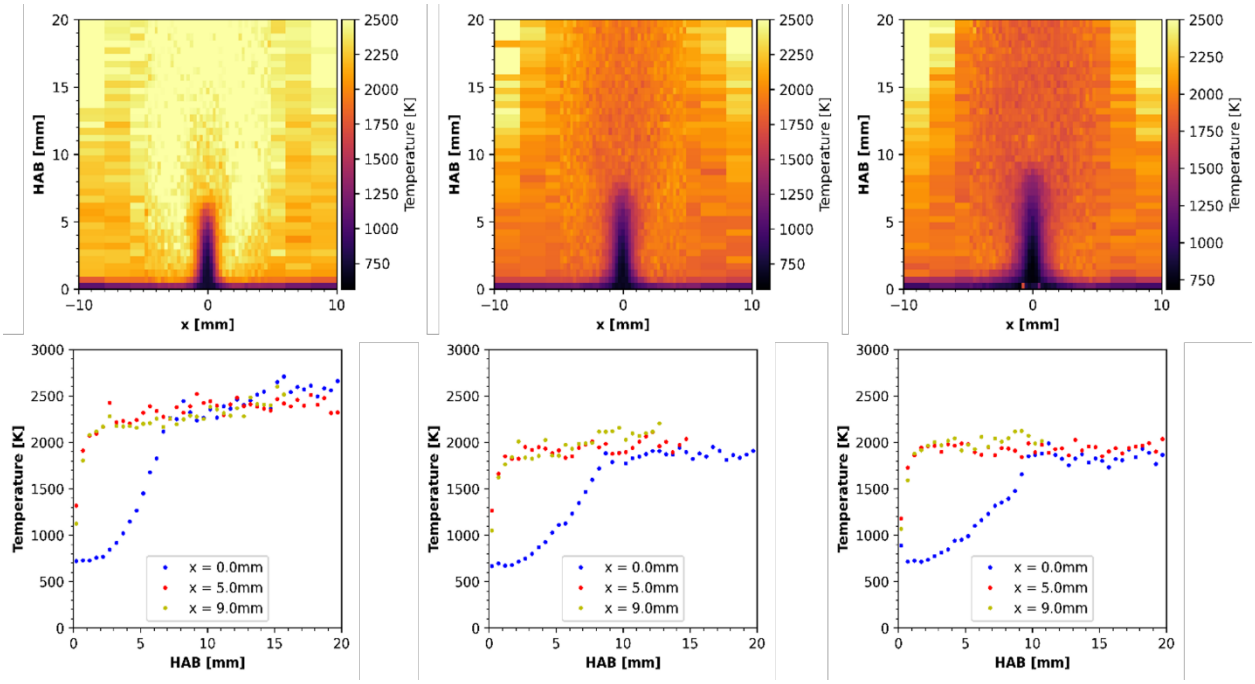


**Figure 6.** HMDSO central flame 2D (top panels) and 1D (bottom panels) distributions at fuel lean (left panel, $\phi = 0.83$), stoichiometric (central panel, $\phi = 1.0$), and fuel rich (right panel, $\phi = 1.22$) conditions.

## DOE publications supported by this project


Kim, J. H., Mansfield, A. B., Burnett, M. A., Wooldridge, M. S. (2022), "A Study of OH Measurements during Auto-ignition of Syngas and Siloxane Mixtures," 2022 Spring Technical Meeting of The Central States Section of the Combustion Institute, May 15–17, 2021, Detroit, Michigan.

Kim, J. H., Mansfield, A. B., Burnett, M. A., Wooldridge, M. S., (2021) "An Experimental Study of OH During Auto-Ignition of Syngas with Trace Trimethylsilanol," 12th National Meeting of the U.S. Sections of the Combustion Institute.

Kim, J. H., Banyon, C., Kim, K., Wooldridge, M. S., Tranter, R. S., (2023) "A shock- tube laser-schlieren study of iso-propanol pyrolysis," 13th U. S. National Combustion Meeting, Organized by the Central States Section of the Combustion Institute, March 19–22, 2023, College Station,

Texas.
Mansfield, A.B. Wooldridge, M.S. “The effect of impurities on syngas combustion,” Combust. Flame 162 (2015) 2286-2295.
Meng, Q., Banyon, C., Kastengren, A. L., Wooldridge, M. S., Tranter, R. S., (2022) “Experimental Measurement of the Rapid Mixing of Fuel and Air in a Multi-Element Diffusion (Hencken) Burner,” 2022 Spring Technical Meeting of The Central States Section of the Combustion Institute, May 15–17, 2021, Detroit, Michigan
Meng, Q., Banyon, C., Kastengren, A. L, Wooldridge, M. S., Tranter, R. S., (2023) “Experimental Measurement of the Rapid Mixing of Fuel and Air in a Multi-Element Diffusion (Hencken) Burner,” Combustion and Flame, 251, 112686 https://doi.org/10.1016/j.combustflame.2023.112686.
Meng, Q., Banyon, C., Kim, K., Kim, J., Kastengren, A. L, Wooldridge, M. S., Tranter, R. S., (2023) “X-ray Fluorescence Measurements of Methane Flames with Trimethylsilanol and Hexamethyldisiloxane Dopants in a Multi-Element Diffusion Burner,” 13th U. S. National Combustion Meeting, Organized by the Central States Section of the Combustion Institute, March 19–22, 2023, College Station, Texas.
Schwind, R. A., 2019, *Understanding the Combustion Chemistry of Siloxanes: Reaction Kinetics and Fuel Interactions*, Ph.D. Thesis, University of Michigan, Ann Arbor.
Schwind, R., Wooldridge, M. S., (2019) “Effects of Organic Silicon Compounds on Syngas Auto-ignition Behavior,” *Combustion and Flame*, 212 pp. 234-241.
Schwind, R. A., Wooldridge, M. S., Sivaramakrishnan, R., (2019) “Understanding Siloxane Combustion Chemistry: Computational and Experimental Studies of Hexamethyldisiloxane (HMDSO),” 11th National Meeting of the U.S. Sections of the Combustion Institute, Paper No. 1A18, Pasadena, CA.

## References

1. Hansen, N., Tranter, R. S., Moshammer, K., Randazzo, J. B., Lockhart, J. P. A., Fugazzi, P. G., Tao, T., Kastengren, A. L. (2017) “2D-imaging of sampling-probe perturbations in laminar premixed flames using Kr x-ray fluorescence,” *Combust. Flame* 181:214-224.
2. Hansen, N., Tranter, R. S., Randazzo, J. B., Lockhart, J. P. A., Kastengren, A. L. (2019) “Investigation of sampling-probe distorted temperature fields with x-ray fluorescence spectroscopy,” *Proc. Combust. Inst.* 37:1401-1408.
3. Tranter, R. S., Kastengren, A. L., Porterfield, J. P., Randazzo, J. B., Lockhart, J. P. A., Baraban, J. H., Ellison, G. B. (2017) “Measuring flow profiles in heated miniature reactors with x-ray fluorescence spectroscopy,” *Proc. Combust. Inst.* 36:4603-4610.
4. Donovan, M. T., Hall, D. L., Torek, P. V., Schrock, C. R., Wooldridge, M. S. (2003) “OH absorption measurements in $SiH_4/H_2/O_2$/Ar flames,” *Proc. Combust. Inst.* 29:2635-2643.
5. Meng, Q., Banyon, C., Kastengren, A. L, Wooldridge, M. S., Tranter, R. S., (2023) “Experimental Measurement of the Rapid Mixing of Fuel and Air in a Multi-Element Diffusion (Hencken) Burner,” *Combustion and Flame*, 251, 112686 https://doi.org/10.1016/j.combustflame.2023.112686.
6. Montgomery, M. J., Kwon, H., Kastengren, A. L., Pfefferle, L. D., Sikes, T., Tranter, R. S., Xuan, Y.. McEnally, C. S., (2022) “In situ temperature measurements in sooting methane/air flames using synchrotron x-ray fluorescence o seeded krypton atoms,” *Sci. Adv.* 8, eabm7947 10.1126/sciadv.abm7947.

# Spectroscopic and Computational Studies of Spin-Orbit Coupling of Lanthanide Oxides

Dong-Sheng Yang, University of Kentucky (Principal Investigator)
Mark S. Gordon, Iowa State University and Ames Laboratory (Co-Principal Investigator)
dyang0@uky.edu, mark@si.msg.chem.iastate.edu

## Program Scope

Spin-orbit (SO) coupling makes it possible for spin forbidden transitions or reactions within non-relativistic quantum theory feasible. Thus, quantification of such interactions has important implications in photophysics and chemical catalysis. This work aims to quantify SO interactions using lanthanide (Ln) oxides as target molecular systems. Through these systems, we examine the impact on the SO coupling by electron configurations and 4f orbital occupancies of Ln elements and sizes of the metal oxides. By examining these factors, we explore how SO coupling is affected by the number of Ln 4f electrons for a given size of molecules and if the Ln 4f orbitals remain atomic in nature in these small clusters. Ln oxides are produced in laser ablation molecular beams, identified with time-of-fight mass spectrometry, and characterized with laser spectroscopy and relativistic quantum chemical computations. Spectroscopic measurements include mass-analyzed threshold ionization (MATI), zero electron kinetic energy, and slow electron velocity-map imaging spectroscopies. Relativistic computations treat scalar relativistic corrections, electron correlations, and SO interactions. The main results are SO terms and energies of the neutral molecules and singly charged cations, ionization energies of the neutral species, metal-metal and metal-oxygen vibrational frequencies of the ions and, in some cases, neutrals as well, and charge effects on the bonding and structures.

## Recent Progress

We have investigated electron correlations and SO coupling of the 4f electrons in diatomic Ln oxides[1-3] and small Ln cluster oxides.[4] The Ln elements include La, Ce, Pr, and Lu. These Ln elements have the ground electron configurations of $5d^16s^2$(La), $4f^15d^16s^2$ (Ce), $4f^36s^2$ (Pr), and $4f^{14}5d^26s^1$ (Lu) and fewer 4f electrons or holes than those in the middle of the Ln series. The measured adiabatic IEs are two-fold improvements over previously reported values where the comparison is available and are used to evaluate literature reaction enthalpies of chemical ionization reactions. The IE of the neutral molecule and vibrational frequencies in the neutral and ionized states quantify the charge effects on the metal-oxygen bonding. The SO terms and energies quantify the extent and strength of electron spin and spatial orbital mixing. In comparing with the measured spectroscopic constants, SO-second-order multiconfiguration quasi-degenerate perturbation (SO-MCQDPT2) computations yield reasonable agreements for the ground and very low-lying excited states ($\leq 500$ $cm^{-1}$) of the neutral and ionized molecules.

### 1. Ionization Energies, SO Coupling, and Vibrational Frequencies of Ln Diatomic Oxides

Table 1 summarizes the spectroscopic and computational results for four LnO (Ln =La, Ce, Pr, and Lu) and their singly charged cations.[1-3] The spectroscopic results are from MATI measurements, which have a typical uncertainty of ~ 5 $cm^{-1}$. The theoretical results are from CCSD(T) calculations for $LaO/LaO^+$, MCQDPT2 for $LuO/LuO^+$, and SO-MCQDPT for $CeO/CeO^+$ and $PrO/PrO^+$. The ground electron configurations are $6s/6s^0$ for $LaO/LaO^+$ and

LuO/$LuO^+$, 4f6s/4f for CeO/$CeO^+$, and $4f^2$6s/4f for PrO/$PrO^+$. These configurations are formed by transferring two electrons from Ln to O in forming the Ln oxides. Electronic energies and vibrational frequencies reported in the table are all associated with the ground electron configurations except for LuO/$LuO^+$. Values in parentheses are the adiabatic IEs of the molecules.

**Table 1.** LS terms, electronic energies ($T_{00}$, $cm^{-1}$) and Ln-O vibrational frequencies ($\nu$, $cm^{-1}$) of LnO and $LnO^+$ (Ln = La, Ce, Pr, Lu) from MATI spectroscopic measurements and theoretical calculations.

| Molecule | LS term (>10%) | $T_{00}$(MATI) | $T_{00}$ (Calc) | $\nu$ (MATI) | $\nu$ (Calc) |
|---|---|---|---|---|---|
| LaO (6s) | $X^2\Sigma^+(100)$ | 0 | 0 | 810 | 808 |
| $LaO^+(6s^0)$ | $X^1\Sigma^+(100)$ | 0(42300) | 0(42908) | 877 | 871 |
| | | | | | |
| CeO(4f6s) | $X^3\Phi(92)$ | 0 | 0 | 819.0 | 822 |
| | $A^3\Phi(52)$, $^1\Phi(38)$, | 88 | 92 | 821.9 | |
| | $B^3\Delta(88)$ | 819 | 920 | | |
| | $C^3\Delta(50)$, $^1\Delta(34)$, $^3\Pi(15)$ | 912 | 1014 | | |
| | $D^3\Pi(63)$, $^3\Sigma^+(37)$ | 1675 | 1700 | 817 | |
| | $E^3\Sigma^+(44)$, $^1\Pi(21)$, $^3\Pi(34)$ | 1873 | 1876 | 815 | |
| | $F^3\Pi(77)$, $\Sigma^+$ (23), | 1920 | 1977 | 817 | |
| | $G^3\Phi(100)$ | 2048 | 2051 | 817 | |
| | $a^1\Phi(52)$, $^3\Phi(46)$ | 2144 | 2178 | 818 | |
| | $b^1\Delta(87)$, $^1\Phi(11)$ | 2626 | 2757 | 832 | |
| | $c^1\Delta(50)$, $^3\Delta(41)$ | 2771 | 2906 | 826 | |
| $CeO^+$(4f) | $X^2\Phi(89)$, $^2\Delta(11)$ | 0(43015) | 0(42992) | 887 | 887 |
| | $A^2\Delta(87)$, $^2\Pi(13)$ | 665 | 794 | | |
| | | | | | |
| PrO($4f^2$6s) | $X^4H_{7/2}$ (95) | 0 | 0 | 835 | 830 |
| | $a^2H_{9/2}(55)$, $^4H_{9/2}(39)$ | 218 | 179 | 835 | |
| | $b^2\Gamma_{7/2}$ (42), $^4\Gamma_{7/2}$(35), $\Phi_{7/2}$(16) | 1784 | 1982 | | |
| | $D^4H_{9/2}(55)$, $^2H_{11/2}(39)$ | 2071 | 2116 | | |
| $PrO^+(4f^2)$ | $X^3H_4$ (92) | 0(43600) | 0(43203) | 909 | 930 |
| | | | | | |
| LuO(6p/5d)$\sigma$ | $C^2\Sigma^+(100)$ | 0 | 0 | 750 | 770 |
| $LuO^+$ (6p$\pi$) | $a^3\Pi$ (100) | 0(44699) | 0(47430) | 761 | 654 |

Several important conclusions emerge from the table. First, adiabatic IEs of LnO are lower than those of free Ln atoms (44980, 44672, and 44142 $cm^{-1}$ for La, Ce, and Pr, respectively) and increase from LaO to PrO even though the IEs of the Ln atoms decrease from La to Pr. This observation suggests that the charge effect on the Ln-O bonding decreases from La to Pr. LuO does not fit into the trend as ionization of LuO removes an O 2p electron, while ionization of the other three LnO oxides removes a 6s electron. Second, significant SO coupling between different spin states is identified in CeO and PrO. The spin-mixing arises from the existence of both 4f and 6s electron in the molecules. Third, Ln-O vibrational frequencies are quite similar among the low-lying SO coupled electronic states with the same electron configuration (e.g., CeO and PrO).

Fourth, predicted SO term energies and vibrational frequencies are generally in reasonable agreement wit the experimental values, except for the Lu-O vibrational frequency of the $a^3\Pi$ exited ion.

## 2. Implications of Well-Defined LnO IEs

Precise IEs of LnO obtained in this work can be used to assess the reaction enthalpies of the Ln + O → Ln O + $e^-$ chemi-ionization. Chemi-ionization reactions in the form of Ln + O → LnO + $e^-$ have recently received considerable interest in gas-phase chemistry. The interest arises largely from the hypothesis that these reactions may be used to mitigate natural fluctuations of the electron density and to stabilize the radio wave transmission in the ionosphere atmospheric region by creating a localized enhanced plasma. The IE of PrO measured in this work is 5.4061(6) eV, which is about 0.5 eV higher than the literature value [4.90(10) eV] from electron impact ionization. There are also discrepancies in the literature about the reaction enthalpy of the Pr + O → $PrO^+$ + $e^-$ chemi-ionization, where $\Delta H_0$ values were reported in the range of (-2.06)-(-3.1) eV. With the refined IE of PrO [5.4061(6)] eV in this work and $D_0$(PrO) = 7.76(10), 7.63(13), and 7.74(13) eV in the literature, we have obtained revised $\Delta H_0$ values of -2.36(10), -2.22(13), and -2.33(13) eV by using $\Delta H_0$ = IE(PrO)-$D_0$(PrO). The $\Delta H_0$ value of -2.22(13) eV has the best match with $\Delta H_0$ = -2.15(9) eV obtained by using $\Delta H_0$ = IE(Pr)- $D_0$ ($PrO^+$), where IE (Pr) =5.473 eV and $D_0(PrO^+)$= 7.62(9) eV. Because $\Delta H_0$ = -2.22 (13) and -2.15(9) eV are obtained from two different methods, we believe that these values are reasonable and propose their average -2.18(13) eV as the enthalpy of the chemi-ionization reaction.

## 3. Empirical Prediction of LnO IEs

For free Ln atoms, the ground electron configurations are $4f^n5d6s^2$ for La, Ce, Gd, and Lu; and $4f^{n+2}6s^2$ for all others, where n = 0 for the first member (La) and n = 14 for the last member (Lu) of the Ln series. To form LnO, two electrons in the free Ln atom are promoted to 5d orbitals to form the Ln $4f^n5d^26s$ configuration. To form $LnO^+$, the outermost 6s electron is removed to form the $Ln^+$ $4f^n5d^2$ configuration. Thus, the IE of LnO may be approximated as the energy difference between the $Ln^+$ $4f^n5d^2$ and Ln $4f^n5d^26s$ configurations. Figure 1 shows the thermodynamic cycle used for predicting the IE(LnO), where E(Ln*) is the lowest energy of the Ln $4f^n5d^26s$ configuration, E($Ln^+$*) the lowest energy of the $Ln^+$ $4f^n5d^2$ configuration, IE(Ln) the atomic IE, and IE(LnO) the energy difference between the excited states of $Ln^+$*($4f^n5d^2$) and Ln*($4f^n5d^26s$). Table 1 summarizes the IE(LnO) values calculated using the empirical formula IE(LnO) = IE(Ln) + E($Ln^+$*)-E(Ln*). Because the values are considered to be approximate, only two significant figures are used for each IE from the empirical calculations. IEs of four LnO molecules (PmO, SmO, HoO, and TmO) are not calculated because atomic excited energies are not available (NA) for Ln or $Ln^+$ or both Ln and $Ln^+$. For LnO (Ln = La, Ce, Pr, Nd,

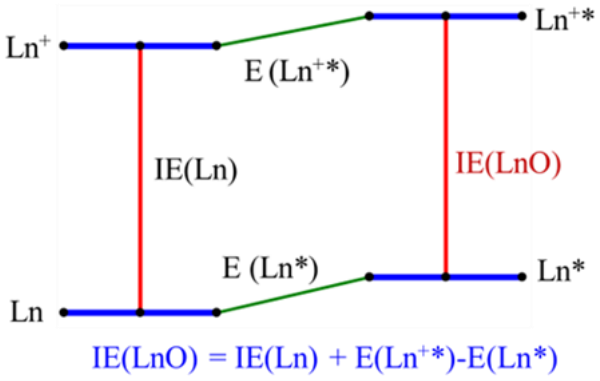


**Figure 1.** Thermodynamic cycle for predicting IE(LnO) from Ln and $Ln^+$ atomic electronic parameters.

and TmO), the measured values are well defined from MATI, zero electron kinetic energy, or resonant two-photon ionization spectroscopic measurements, and the calculated IEs from the empirical formula agree well with the experimental values, with the largest error of -0.08 eV. For other LnO molecules, the literature IEs are less defined. Nevertheless, the predicted values are within the range of the reported IEs except for YbO. For YbO, the reported IE is in the range of 6.5-6.7 eV, while the predicted value is 7.20 eV. The reason for this discrepancy is not clear. But the ytterbium atom has a closed $4f^{14}$ subshell in the neutral and ionic ground states. Excitation of an electron from a closed $4f^{14}$ subshell to a 5d orbital requires a considerably higher energy than that from an incomplete 4f subshell. This makes the assignment of the Yb($4f^{14}5d^{2}6s$) or $Yb^{+}$($4f^{14}5d^{2}$) configuration more difficult. Nevertheless, more accurate experimental IE values of LnO (Ln = Eu-Lu) would be helpful to validate the empirical calculations for these LnO molecules.

**Table 2.** Ionization energies (IEs) of Ln and LnO and electronic energies of the Ln* ($4f^{n}5d^{2}6s$) [E(Ln*)] and $Ln^{+}$* ($4f^{n}5d^{2}$) [E($Ln^{+}$*)] excited states relative to the energies of the ground states of Ln and $Ln^{+}$. All energies are in units of eV.

| Ln | Ln ground configuration | IE(Ln) | E($5d^{2}6s$) | $Ln^{+}$ ground configuration | E($5d^{2}$) | IE(LnO) experiment | IE(LnO) Empirical |
|---|---|---|---|---|---|---|---|
| La | $5d6s^{2}$ | 5.5769 | 0.3308 | $5d^{2}$ | 0 | 5.2446(6) | 5.25 |
| Ce | $4f5d6s^{2}$ | 5.5387 | 0.2937 | $4f5d^{2}$ | 0 | 5.3332(6) | 5.25 |
| Pr | $4f^{3}6s^{2}$ | 5.473 | 0.8325 | $4f^{3}6s$ | 0.7259 | 5.4059(6) | 5.37 |
| Nd | $4f^{4}6s^{2}$ | 5.5250 | 1.0911 | $4f^{4}6s$ | 0.9932 | 5.5083(2) | 5.43 |
| Pm | $4f^{5}6s^{2}$ | 5.582 | NA | $4f^{5}6s$ | NA | 5.2(2) | NA |
| Sm | $4f^{6}6s^{2}$ | 5.6437 | 2.8325 | $4f^{6}6s$ | NA | 5.7427(6) | NA |
| Eu | $4f^{7}6s^{2}$ | 5.6704 | 3.8689 | $4f^{7}6s$ | 4.6295 | 6.3(8) | 6.43 |
| Gd | $4f^{7}5d6s^{2}$ | 6.1498 | 0.7908 | $4f^{7}5d6s$ | 0.4993 | 6.5(10) | 5.86 |
| Tb | $4f^{9}6s^{2}$ | 5.8638 | 1.0155 | $4f^{9}6s$ | 1.1040 | 5.8(5) | 5.95 |
| Dy | $4f^{10}6s^{2}$ | 5.9389 | 2.2905 | $4f^{10}6s$ | 2.4169 | 6.1(1) | 6.07 |
| Ho | $4f^{11}6s^{2}$ | 6.0215 | 2.5006 | $4f^{11}6s$ | NA | 6.2(5) | NA |
| Er | $4f^{12}6s^{2}$ | 6.1077 | 2.5004 | $4f^{12}6s$ | 2.7055 | 6.2(5) | 6.31 |
| Tm | $4f^{13}6s^{2}$ | 6.1843 | NA | $4f^{13}6s$ | 3.8241 | 6.56(2) | NA |
| Yb | $4f^{14}6s^{2}$ | 6.2542 | 4.6392 | $4f^{14}6s$ | 5.5812 | 6.6(1) | 7.20 |
| Lu | $4f^{14}5d6s^{2}$ | 5.4259 | 2.3374 | $4f^{14}6s^{2}$ | 3.6462 | 7.0(10) | 6.73 |

## 4. Coupling of unpaired electrons on separate Ln atoms in $Ln_2O_2$

For molecules containing two or more Ln atoms, an important question is if the unpaired electrons ($4f^{n}6s$) on separated Ln atoms would couple to each other. It is possible that some of the low-lying molecular excited states would be practically degenerate if the distances between Ln atoms are relatively long and spin correlation is negligible for the electrons localized on the separated Ln atoms. The MATI spectrum of $Pr_2O_2$ is shown in Figure 2. $Pr_2O_2$ has a rhombic $D_{2h}$ structure. Bands 1-4 are the origin bands of transitions from the low-lying SO coupled states (X, A, B, and C) of the neutral molecule to the two nearly degenerate SO states ($1^{6}E_{1/2}$ and $2E_{1/2}$) of the ion, and bands 5-6 are the origin bands of transitions from the neutral ground (X) state to the ion $3E_{1/2}$ and $4E_{1/2}$ states, respectively. The energy of the band 4 (38045 $cm^{-1}$) corresponds to the adiabatic IE of the molecule. The Pr-Pr stretching frequency of the ion is measured as 236 $cm^{-1}$

from the three transitions (bands 4-6), while the Pr-O stretching frequency of the ion is 616 $cm^{-1}$ from the two transitions (bands 3-4). All of these observed SO coupled terms are mixtures of multiple spin states except for the septet neutral C state and the sextet ion $1^6E_{1/2}$ state. The extent of the spin mixing differs among the various states. For the neutral molecule the predicted LS terms are 32% singlet + 49% triplet + 18% quintet for the X state; 44% triplet + 48% quintet for the A state; and 76% quintet + 24% septet for the B state. For the ion, the LS terms are 49% doublet + 40% quartet + 11% sextet for the $2E_{1/2}$ state, 17% doublet + 53% quartet + 30% sextet for the $3E_{1/2}$ state, and 38% quartet + 62% sextet for the $4E_{1/2}$ state. A strong coupling between the $4f^26s$ electrons on the separate Pr atoms is evident by comparing the MATI-measured SO splittings of PrO and $Pr_2O_2$. the two-lowest SO coupled terms are separated by 218 $cm^{-1}$ in PrO, whereas the separations of four low-lying SO states are 157, 339, and 438 $cm^{-1}$ in $Pr_2O_2$. The coupling of the $4f^26s$ electrons on two separated Pr atom is interesting because the Pr-Pr distance (3.270 Å) in $Pr_2O_2$ is much longer than that in $Ce_2$ (2.582-2.604 Å) where no coupling was predicted between the two Ce atoms.

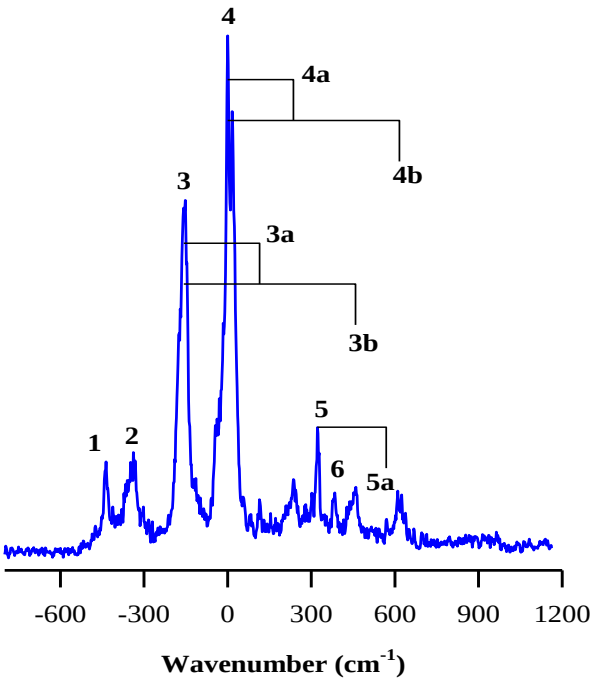


**Figure 2**. MATI spectrum of $Pr_2O_2$

## 5. Software development

To meet the needs of this project, we have implemented several new features in the GAMESS code originally developed in our group. These new developments include, but are not limited to, (1) support for relativistic integrals involving h and i functions for spin-orbit calculations. This is in addition to the support for scalar relativistic methods that was previously implemented. (2) a special case for diatomic molecules in the numerical Hessian code that reduces the number of energy evaluations from 108 to 4. This approach rotates the coordinates to realign the molecule along the principal axes after each displacement, thus preserving symmetry. This has the two-fold advantage of reducing the number of energy evaluations needed based on symmetry constraints while simultaneously allowing for the use of symmetry to aid in the optimization of excited states. (3) a special case for diatomic molecules that allows for the use of symmetry when computing excited states with the vibrational self-consistent field method. (4) parallelization of the computation of the transition density matrix in the spin-orbit code. (5) expanding support for the density-based bonding analysis to allow for the use of the graphical unitary group approach-based multireference methods. Previously, this functionality was limited to use of the occupation restricted multiple active space method. (6) support for effective core potentials (ECPs) that use a h-ul potential with a coefficient of zero. This allows for the use of the Stuttgart-Dresden ECPs and by extension the correlation consistent pseudopotential-based basis sets. The h-ul potential provides an upper limit (ul) for the angular momentum as well as a reference point for difference

potentials that are computed based on the s, p, d, f, and g potentials provided in the input file. (7) support for the generation of valence virtual orbitals when using model core potentials.

## Future Plans

We will set up resonant two-photon MATI experiments and attempt to measure the IEs of other LnO oxides for which accurate IE values are not yet available in the literature. These measurements will serve as benchmarks for the empirical and SO-MCQDPT2 calculations. We will investigate other Ln oxide clusters containing two or more Ln atoms and various numbers of oxygen atoms. Experimental measurements will be focused on searching for vibronic spectra of the clusters of interest, and theoretical computations will be performed in coordination with the experiments. The theoretical treatment of Ln cluster oxides is more challenging due to the larger size of the systems and the possible coupling of the $4f^n6s$ electrons on separated Ln atoms. We thus will implement new functionalities in the GAMESS code to accomplish the task as specific needs become apparent in the course of this work.

## Publications Supported by the BES-GPCP Program


1. W. J. Cao, Y. C. Zhang, L. Wu, and D. -S. Yang, "Threshold Ionization Spectroscopy and Theoretical Calculations of LnO (Ln = La and Ce)," J. Phys. Chem. A **125**, 194 (2021). DOI: 10.1021/acs.jpca.1c00533.

2. Y. C. Zhang, T. Nakamura, W. J. Cao, L. Wu, M. Roudjane, M. S. Gordon, and D. -S. Yang, "Spectroscopy and Electronic States of Praseodymium Oxide and its Singly charged Cation," J. Chem. Phys. **157**, 114304 (2022). DOI: 10.1063/5.0113741.

3. L. Wu, G. Schoendorff, Y. Zhang, M. Roudjane, M. S. Gordon, and D. -S. Yang, "Excited States of Lutetium Oxide and its Singly Charged Cation," *J. Chem. Phys.* **156**, 084303 (2022). DOI: 10.1063/5.0084483.

4. L. Wu, T. Nakamura, B. Dangi, Y. Zhang, G. Schoendorff, M. S. Gordon, and D. -S. Yang, "Probing Spin-Orbit Coupling in Praseodymium Cluster Oxides," *J. Chem. Phys.*(to be submitted).